NASA CONTRACTOR REPORT 159032

(NASA-CR-159032) DATA REDUCTION AND ANALYSIS OF GRAPHITE FIBER RELEASE EXPERIMENTS (TRW Defense and Space Systems Group) 362 p HC A16/MF A01 CSCL 01C

N80-19048

Unclas
G3/03 14869

DATA REDUCTION AND ANALYSIS OF GRAPHITE FIBER RELEASE EXPERIMENTS

P. Lieberman, A. R. Chovit,
B. Sussholz, and H. F. Korman

TRW Defense and Space Systems Group
Redondo Beach, CA 90278

CONTRACT NAS 1-15465
July 1979

National Aeronautics and
Space Administration

Langley Research Center
Hampton, Virginia 23665
AC 804 827 3966

CONTENTS

CONTENTS

TABLES

FIGURES

FIGURES

FIGURES

FIGURES

FIGURES

FIGURES

DATA REDUCTION AND ANALYSIS OF GRAPHITE FIBER RELEASE EXPERIMENTS

Paul Lieberman, Albert R. Chovit, Benjamin Sussholz
and Howard F. Korman

TRW Defense and Space Systems Group

SUMMARY

A series of burn and explode tests and burn-only tests have been performed for plate, barrel, spoiler and cockpit samples containing various amounts of carbon fiber composite material. Measurements of the fiber concentrations and deposition characteristics were made by means of active and passive instrumentation supplemented by photographic and meteorological data.

Results of burning the plate and barrel samples over hot propane burner for 20 minutes and subsequently exploding the post-burn residue indicated that the material was projected to heights of almost 100 feet, and that concentrations of 10^3 fibers per cubic meter and exposures of 10^4 fiber-seconds per cubic meter had developed within a range of 300 feet of the explosion for fibers in 3 to 20 mm length intervals. The length interval is of importance to the electric hazards potential.

Higher concentrations and exposures were measured when the fiber lengths in the range of 1 to 3 mm were included. However, these lengths are of lesser electrical hazards potential. The Thornel 300 carbon fibers from the plate tests formed single fibers and clumps. The largest number of fibers generated were in the 1 - 2 mm length interval and about 1-ply in diameter, with the next largest numbers also in the range of 1 - 2 mm length about 1 fiber (5-10μ) diameter. In the 1 - 20 mm length interval measurement, the average fiber length was between 2 and 3 mm. The fraction of mass of the initial plate that was emitted as single fibers with lengths between 1 and 20 mm was between 0.005 to 0.015% mass based upon integration of the mass deposited in the ground footprint. The barrel samples composed of Hercules AS carbon fiber also resulted in the greatest number of single fibers being measured in the range of 1 - 2 mm lengths, and also in the emission of clusters of fibers that formed feather-like structures which were easily carried by the wind to 3000 ft ranges and beyond.

The intermediate size 20-ft by 20-ft JP-5 fire was used to burn the barrel sample in one test where only movies were taken. The fire burned for 3 minutes and then 6 minutes. The same size fire was used again to burn and then explode the barrel. This fire burned for 5 minutes but the explosion took place during the early portion of the burn. Limited data was taken and the burn and burn/explode test techniques were formulated in these two tests. These high fire and smoke plumes resulted in barrel feathers being lofted and blown downrange to distances of 1000 ft. One strip was 10" by 1" at the 1000 ft range. Results of burning the aircraft spoiler over a 40 ft by 60 ft JP-5 jet fuel pool fire for 4 minutes without any explosion during one test; a 7-minute burn and explode in the next test; and a 6-minute burn-only on an aircraft cockpit structure in the next test indicated that the plume rose 4000 ft in altitude and that carbon fiber strips were being generated that were floated 6000 ft downrange. The

single fiber environment as measured by bridal veil sensors showed several orders of magnitude lower exposures in the 300 ft from ground zero from the 40 ft by 60 ft fire as compared to the propane burner tests. The rapid and sudden heating of the few ply aircraft structures quickly delaminated the composites and sent the individual lamina strips up into the plume for deposition 1000 - 3000 ft downrange.

The carbon fibers imbedded in the 40 ply structure of the plate did not experience the oxidation that the thin ply structures of the barrel, spoilers and cockpit did. The latter three structures had their fibers experience a 30 percent decrease in diameter on the average. Subsequent TRW laboratory tests indicated two important trends. First, carbon fibers react with sufficient rapidity at 2000F temperatures that even a few minutes exposure will cause measurable mass loss. Second, the presence of the resin acts as a catalyst, so that even lower temperatures achieve the same mass loss in a few minutes.

In the case of burn-only for the aircraft spoiler and cockpit samples within a jet fuel pool fire resulted in a plume of about 4000 ft height, and essentially benign local environments with regard to single fibers but the deposition of large scale carbon fiber composite strips of about 1 ply thickness over a range of 1000 to 3000 ft.

Previous tests of this nature relied solely on passive instrumentation for fiber deposition distributions. A number of unique innovations in measurement techniques were introduced in the present program such as namely; light emitting diode instruments, microwave gages, ladar, infrared imaging camera, LC deposition history gage and flame velocimeter. The total spectrum of instrumentation including passive as well as existing and newly developed active elements permitted the measurement of concentration histories and fiber distributions, and yielded considerable data regarding the fiber cloud dynamics during the course of propagation over the instrumentation network.

It was possible to differentiate between the family of smaller fiber clouds that comprised the overall fiber cloud and to separate the detonation product gases from the rapidly falling fiber cloud. In addition, the infrared camera permitted tracking the flying debris inside the smoke plume.

Correlations were established by means of empirical equations relating the meteorological data and plume measurements.

Use of commercial products or names of manufacturers in this report does not constitute official endorsement of such products or manufacturers, either expressed or implied, by the National Aeronautics and Spa e Administration.

1. INTRODUCTION

The introduction of carbon/graphite composite material structures for aircraft structures is increasing for both military aircraft and for commercial aircraft. The use of this composite material results in considerable weight savings and thus in increased aircraft performance and/or eventual decreased operating costs. Unfortunately, with these advantages there also arises a disadvantage not ever experienced with metal structures. Namely, when a composite structure burns and the resulting char is jostled, a cloud of airborne conductive fibers is released which will cause damage to electrical facilities downwind of the fire. The military has been investigating the carbon fiber problem for over the past six years. NASA has been involved in investigations concerning commercial aircraft for over the past year.

Under an Air Force contract, TRW has studied the burn and burn/explode effects on aircraft structures in a series of fifteen outdoor tests. The tests were conducted by TRW at the TRW Capistrano Test Site, San Clemente, California and at the Naval Weapon Center, China Like, California during the period November 1977 through May 1978. The purpose of the tests was 1) to verify the results obtained in previous burn and explode tests of carbon/graphite composite samples conducted in a closed chamber at the Naval Surface Weapon Center, Dahlgren, Virginia and 2) to simulate aircraft accident scenarios in which carbon/graphite fibers would be released.

The primary effects that were to be investigated in these tests were the amount and size distribution of the conductive fibers released from the composite structures, and how these various sizes of fibers were transported downwind. The structures included plates, barrels, aircraft spoilers and a cockpit. The heat sources included a propane gas burner and 20-ft by 20-ft and 40-ft by 60-ft JP-5 pool fires. (The 40-ft by 60-ft size JP-5 pool fire was selected to simulate an aircraft accident incident which occurred in January 1978 at an Air Force installation.) The passive instrumentation included sticky paper and sticky bridal veil over an area 6000 ft downwind and 3000 ft crosswind. The active instrumentation included instrumented meteorological towers, movies, infrared imaging cameras, LADAR, high voltage ball gages, light emitting diode gages, microwave gages and flame velocimeter.

This instrumentation provided data that when reduced and analyzed would yield 1) fiber deposition, concentration and exposure information over the regions of the test site which were instrumented, 2) the characteristics of the fire and explosion plumes and 3) the ambient atmospheric conditions existing during the tests.

The data acquired in these tests was reduced and analyzed by TRW under the subject NASA sponsored program. The results obtained in this program are reported in this document.

The data reduction and analysis was performed during the period July 1978 through February 1979 and included the use of 1) laboratory techniques to analyze the characteristics of the composite samples and released material; 2) systematic

data reduction techniques of the raw field data obtained by the passive and active instruments and 3) analytic evaluations of the data reduction results to provide qualitative and quantitative descriptions of the accidental release threat parameters.

This data reduction and analysis was conducted for thirteen of the fifteen tests; the last two tests at NWC were not included as part of this contracted effort.

This report has been organized into the following sections:

Section No.	Description
1	Introduction
2	List of Symbols
3	Description of Test Program
4	Passive Instrumentation: Data Reduction and Analysis
5	Active Instrumentation: Data Reduction and Analysis
6	Photographic and Meteorological Instrumentation: Data Reduction and Analysis
7	Results and Analyses
8	Conclusions

The introduction presents the background and overview of the program. The list of symbols permits a ready access to acronyms and symbols. The description of the test program gives a complete background of the overall program to permit the reader to interpret and use the data, an overview of the test program at the two test sites, a description of the two test sites, the test matrix of the test samples and test conditions, and a description of the instrumentation. The passive instrumentation section describes the data reduction methodology and equipment; site layout; photographs of typical raw data to show types of fiber clusters emitted; number and mass single fibers per length interval measured at a station; particles per unit area as a function of down range distance and of cross-range distance and of vertical height; the relative occurrence of single, double, triple fibers per particle; mass fraction of single fibers emitted; deposition footprint; width and length of strips in the deposition footprint; and oxidation rate of the carbon fibers. The active instrumentation describes the arrival time and duration of the concentration and mass flux of the fiber cloud at specific stations, the lengths of the fibers in the cloud, and flame parameters. The photographic and meteorological data describes the fire plume, smoke plume, fiber cloud, and speed, wind direction, and temperature gradients measured according to test. The results and analyses section summarizes the overall test program. The conclusion section indicates the significant trends in the results.

2. LIST OF SYMBOLS

A	cross sectional area of sampling volume normal to wind direction, m^2
$C_n(t)$	number concentration history, fibers/m^3
$C_m(t)$	mass concentration history, gm/m^3
D	width of sampling volume
$\bar{l}_i$	average fiber length, mm
L	length of sampling volume
m	mass of single fibers, gm
$\dot{M}(t)/A$	mass flux history, gm/m^2-sec
$\dot{N}(t)$	number history per unit time, fibers/sec
N_i	number of fibers of length, l_i
P_c	fiducial point for photographic data analysis
R	radial distance
t	time
U	wind velocity, mps
X_c	horizontal displacement of puff center
X_m	horizontal displacement of puff maxima
Z_c	height of puff center
Z_m	height of puff maxima
θ	plume leading edge angle with horizontal

DEFINITIONS

concentration	mass or fiber density
deposition	mass deposited per unit area
exposure	integral of concentration over time
Jacob's ladder	rope mesh laden with bridal veil vugraphs
mass flux	rate of passage of mass through a unit area
spoiler	long narrow plate along upper surface of an airplane wing that may be raised for reducing lift and increasing drag

CONVERSIONS

1 ft	0.305 m
1 in	2.54 cm

ABBREVIATIONS

BRL	Ballistic Research Laboratory
cm	centimeter
E	East
Fastax	fast action
fps	feet per second
ft	ft
gm	gram
H	horizontal
IR	infrared
in	inch
kg	kilogram
LADAR	laser detecting and ranging device
LC	inductance - capacitance
LED	light emitting diode
m	meter
met	meteorological
mm	millimeter
mps	meters per second
N	North
NWC	Naval Weapon Center at China Lake, CA
pst	Pacific Standard Time
S	South
sec	seconds
T.C.	thermocouple
TGA	termal gravimetric analysis
USA BRL	United States Army Ballistic Research Laboratory
V	vertical
W	West
μgm	microgram
μ	micrometer - micron

3. DESCRIPTION OF TEST PROGRAM

The test data that were reduced and analyzed in the program reported herein were obtained in a test program conducted under an Air Force contract. A review of this program is presented in Ref. 1. Portions of that document are used in this section. The tests were conducted by TRW at the TRW Capistrano Test Site, San Clemente, California and at the Naval Weapon Center (NWC), China Lake, California during the period November 1977 through May 1978. The purpose of the tests was 1) to verify the results obtained in previous burn and explode tests of carbon/graphite composite samples conducted in a closed chamber at the Naval Surface Weapon Center (NSWC/DL), Dahlgren, Virginia and 2) to simulate aircraft accident scenarios in which carbon/graphite fibers would be released.

In order to provide background information which is pertinent for the complete interpretation and utilization of the results presented in this document, this section presents an overview description of the test program, a description of the test sites, a description of the fielded instrumentation that acquired the test data, and a detailed listing of the conditions of each test.

TEST PROGRAM OVERVIEW

A major objective in conducting the accidental release simulation field tests was to obtain fundamental emperical data which would permit characterization of the carbon fiber threat. These data when reduced, analyzed and formatted would have formed the data bank to support analytic source and transport model development efforts. Therefore, the field test results would ultimately guide the structuring of the model algorithms, provide many of the emperical functional relationships in the models and form the basis for checkout and validation of the models.

In order to assure that at the completion of the field tests sufficient appropriate data of the proper quality would be available, a thorough analysis was made of the threat characteristics as they relate to the modeling requirements and accident scenario variables. The results of this analysis impacted all aspects of the test program; the test plan, the test matrix, the test site configuration, and most important, the selection of both the active and passive instrumentation types and deployment.

In this threat/model requirements analysis, the carbon release threat characteristics were divided into five categories as shown in Table 3.1. The first two categories, source description and initiation mechanism, relate to the accidental release scenarios that were simulated. The last three categories, hazard or material type release, propagation phenomenology and threat definition parameters, all relate directly to the source/transport model requirements.

Table 3.1 Threat Characteristics

SOURCE DESCRIPTION

- Material Quantity
- Composite Type
- Structural Configuration

INITIATION MECHANISM

- Burn
- Burn/Impact
- Burn/Explode

HAZARD RELEASE

- Single Fibers
- Multiple Fibers
- Clusters
- Composite Strips

PROPAGATION PHENOMENOLOGY

- Plume Lofting
- Cloud Transport
- Fallout Pattern

THREAT DEFINITION

- Concentration History
- Deposition
- Size Distribution
- Electrical Conductivity

The scenario related threat characteristics were translated into the test requirements for excitation sources and test sample types. Major constraints in specifying these requirements were 1) the necessity for adhering as closely as possible to the test conditions of the NSWC/DL closed chamber tests to attempt to verify those test results under outdoor field conditions, 2) the availability of test samples and 3) test range limitations on the total amount of carbon/graphite composite material that could be tested.

Selected carbon/graphite composite samples were burned in either of two modes; a propane/air generated flame or JP-5 pool fire. Both "cool" (~1900°F) and "hot" (~2600°F) propane flame tests were conducted and two sizes of pool fires were used, 20 ft x 20 ft and 40 ft x 60 ft. Subsequent to the sample propane burns, the burned sample was exploded (after a one-half to one hour delay). In the case of the JP-5 fire tests of the barrels and spoilers, the sample residue from a JP fire burn was replaced over a replenished JP-5 pool, the JP fuel ignited and after the fire stabilized (approximately 40 to 60 seconds), a C-4 explosive charge was detonated under the sample. The fire was configured to continue to burn minutes after the explosion. Data was collected downwind

after both the burn and the burn/explode phases of these JP fire tests.

Carbon composite plates with dimensions of 1 ft x 1 ft x 1/4 in thickness were tested utilizing propane burns followed by an explode phase. Experimentally fabricated composite barrels were tested under both propane burn and JP-5 pool fire conditions with subsequent explosion phases. Finally, tests were conducted with aircraft spoilers and a F-16 cockpit which were burned in JP-5 pool fires and in the case of the spoiler test, subsequently exploded in a JP-5 pool fire.

The threat characteristics shown in Table 3.1 that relate to the modeling requirements, are listed in the first column Table 3.2. In the second column, each of the threat characteristics is translated into the set of parameters that define the threat characteristic. These are the parameters that were required to be measured and for which instrumentation had to be selected which would acquire the appropriate data. Listed in the third column are the measurement techniques or instruments which were selected for determining each corresponding set of parameters. These instruments provided the raw field data that when appropriately processed and analyzed would quantify each parameter for supporting the source/transport modeling activities.

Table 3.2 Selected Measurement Techniques

THREAT CHARACTERISTICS	PARAMETERS TO BE MEASURED	SELECTED MEASUREMENT TECHNIQUES
Plume Lofting	Plume Gas Velocities Horizontal Air Entrainment Velocities	Flame Velocimeter Movies IR Scanning Camera
Plume Lofting Cloud Transport	Time To Ignition Time to Combustion Completion	Thermocouples Movies
Plume Lofting Cloud Transport	Detonation/Combustion Cloud Rise Transport Properties	Flame Velocimeter Movies IR Scanning Camera Meteorological Sensors
Cloud Transport Concentration Histories Size Distritution	Cloud Trajectories Growth Envelope Concentration Histories As Function of Released Fiber Sizes	All Fielded Active Sensors Millipore Tuna Cans Jacob's Ladder
Fallout Pattern Deposition	Deposition Densities As Function of Cloud Footprint and Released Fiber Sizes	Sticky Paper Bridal Veil Frames Pad Collection Sweep Brigades

Table 3.2 Selected Measurement Techniques (Cont.)

THREAT CHARACTERISTICS	PARAMETERS TO BE MEASURED	SELECTED MEASUREMENT TECHNIQUES
Hazard Release	Mass Fraction Released as Function of Release Fiber Sizes	All Passive collectors Supplemented by Active sensors

The parameters for the first three groups of threat characteristics (which include plume lofting and cloud transport) were measured by the sole use of active instruments. These instruments included standard photographic and temperature sensing techniques; a relatively complex IR scanning and associated data reduction system; and a flame velocimeter, an instrument devised from existing laboratory equipment specifically for measuring the flame velocities in the JP pool fires.

All of the active sensors in the field which also included LED gages, ball gages, microwave gages and LADAR, were used to measure the parameters relating to the fourth group of threat characteristics (cloud transport, concentration histories and released material size distribution). Although the measurement of these parameters was best accomplished by the active instruments, it was necessary to augment the active instruments with a millipore vacuum system, bridal veil on tuna cans and a 90 ft x 90 ft "Jacob's Ladder" array with over 300 bridal veil collectors. This passive instrumentation provided data sampling to the vertical heights and over the large site areas that the limited number of expensive active instruments could not cover.

The released material fallout and deposition patterns were measured by the sole use of passive instruments or collection techniques. These passive collection techniques were employed over extensive site arrays ranging from ground zero to 6000 ft down range and up to 1500 ft on either side of the site centerline.

Finally, the data required to measure the mass fraction and size distribution of the released material were obtained by all of the fielded passive collectors. In this case, the passively collected data was supplemented by data obtained by many of the active measurement techniques.

A total of fifteen field tests were conducted in the program, three at the TRW Capistrano Test Site (CTS) and twelve at the Naval Weapon Center (NWC) Test Site. In all, four different sample types were tested. A summary Test Matrix is given in Table 3.3. (A more complete description of each test is given in the section entitled Test Conditions.)

This test matrix evolved adaptively in that the selection of test conditions for each subsequent test was based on the observations and results obtained from the prior tests. As each test was conducted, an evaluation was made taking into consideration information from 1) field observations relating both to the

Table 3.3. Summary Test Matrix

TEST NO.	SAMPLE COMPONENT	SITE	EXCITATION					
			BURN			EXPLODE		
			PROPANE	HOT PROPANE	JP-5	DELAYED EXPLODE	NO DELAY EXPLODE	EXPLODE IN PLUME
1	FLAT PLATE	CTS	●			●		
2	FLAT PLATE	CTS		●		●		
3	FLAT PLATE	CTS		●		●		
4	FLAT PLATE	NWC	●			●		
5	FLAT PLATE	NWC		●		●		
6	FLAT PLATE	NWC		●		●		
7	NONE	NWC					●	
8	BARREL	NWC		●		●		
9	HALF BARREL	NWC			●			
10	HALF BARREL & #9 DEBRIS	NWC			●			●
11	SPOILERS	NWC			●			
12	#11 DEBRIS	NWC			●			●
13	COCKPIT	NWC			●			
14	FLAT PLATE	NWC		●		●		
15	FLAT PLATE	NWC		●		●		

characteristics of the fiber release and the performance of the fielded instrumentation, 2) "quick look" data analyses performed on the acquired active and passive data, 3) the results of pre-test and post-test laboratory analyses, 4) the data requirements necessary for ultimately defining the threat characteristics, 5) guidelines imposed by range safety and scheduling constraints and 6) the overall program objectives and interim DoD program concerns and directives.

All of the tests employed both active and passive instrumentation. The amount of instrumentation, the type of instruments employed in each test and the layout of the instruments on the test site were based on pre-test predictions of the extent and density of the released fiber material.

Of the fifteen tests, eight were conducted for 1 ft x 1 ft x 1/4 in carbon fiber composite flat plates. In all of these tests, the plate sample first was burned and subsequently exploded by a C-4 explosive charge. The flame temperature and the explosion characteristics were systematically varied from test-to-test.

Three tests were conducted on 2 ft dia x 3 ft carbon composite barrels. In the first of thest tests a barrel was burned in a propane flame and subsequently exploded. In the second test a half barrel was exposed to heating from a 20 ft x 20 ft JP-5 fire plume. The burned debris remaining from the second barrel test was combined with an unburned half barrel segment. Then both samples were burned for several minutes and exploded within the fire plume of a JP-5 fire.

Test Numbers 11 and 12 involved three aircraft spoilers constructed of carbon fiber composite material. In Test Number 11, the three spoilers were burned within a 40 ft x 60 ft JP-5 fire plume. The burned debris was then used in Test Number 12. The debris was placed over the replenished JP fuel pool, the fuel ignited and permitted to burn for approximately 40 seconds until ignition was complete and the fire plume stabilized. At this point, an explosive charge was detonated under the debris sample with the fire continuing to burn for approximately five minutes.

The last test that employed an aircraft component was Test Number 13 in which an F-16 cockpit partially fabricated of carbon fiber composite material was burned. This test again used the 40 ft x 60 ft JP-5 fuel configuration and the total burn time was approximately six minutes. Due to a combination of subsequent adverse meteorological conditions and test schedule constraints, no opportunity was available to follow-up with a burn and explode test of the burned cockpit debris.

The data acquired in Test Nos. 1 through 13 in this test program provided the starting point for the data reduction and analysis tasks performed under the subject NASA program and reported in this document. (Reduction and analysis of the data from Test Nos. 14 and 15 was not included in this contracted effort). The data reduction and analysis performed in this NASA sponsored program included the use of laboratory techniques such as thermo-graviametric analyses (TGA), oven tests, chemical tests, a scanning electron microscope, et al, to analyze the characteristics of the composite samples. These analyses were performed on the pre-burned samples, the sample debris after burn and the sample debris after

burn/explode. Also, the data collected in the field (from each instrument type) for each test was systematically reduced; analyses of the reduced data were performed to yield both a qualitative and quantitative evaluation of the simulated accidental release threat parameters to the extent the field data permitted.

TEST SITE CONFIGURATIONS

The test program was conducted at two test sites: the TRW Capistrano Test Site (CTS), San Clemente, California and the Naval Weapon Center (NWC), China Lake, California. The initial three tests of the test series were conducted by TRW at CTS during the months of November and December 1977. All twelve subsequent tests were conducted by TRW at NWC during the months January through May 1978.

CAPISTRANO TEST SITE

The Capistrano Test Site was selected for conducting the initial tests of the series on the basis of several factors. First, the proximity to TRW Space Park and the availability of the test site permitted an approximately two and one-half month earlier implementation of the test series than otherwise would have been possible due to unavoidable schedule constraints at the NWC test site. These early tests, therefore, were accomplished without incurring any schedule slippage of the tests at NWC. Second, information obtained from these early tests and the nature of the test facility configuration would provide quantitative and qualitative data that could be utilized to better plan and structure the relatively more expensive and extensive tests at NWC. This information included the fraction of material released from the material samples under several test conditions, and qualitative descriptions of the released material mass, size, form and distribution on the test pad. Third, these early tests permitted the verification of test objectives, test plans and procedures that would later be employed in the NWC tests.

Finally, the CTS tests provided timely field experience to aid in the development of:

- data collection and cataloging procedures
- data reduction and interpretation techniques
- instrumentation/data recording operating methods
- safety and security requirements

The test pad facility at CTS consisted of an approximately 15 ft x 15 ft x 15 ft structure constructed of light structural steel members, Figure 3.1. This structure was completely covered on all sides and top by fiberglass screening with a mesh size of approximately 1 mm x 1 mm. The structure was constructed on an existing concrete pad. The burn and explode tests were conducted in the center of this enclosure.

The enclosing screen served three purposes: 1) it assured that essentially all hazardous fibers that were released (greater than 1 mm) would be completely contained thus safeguarding sensitive equipment and instruments that were located at the site for other TRW program purposes, 2) the screening eliminated blast

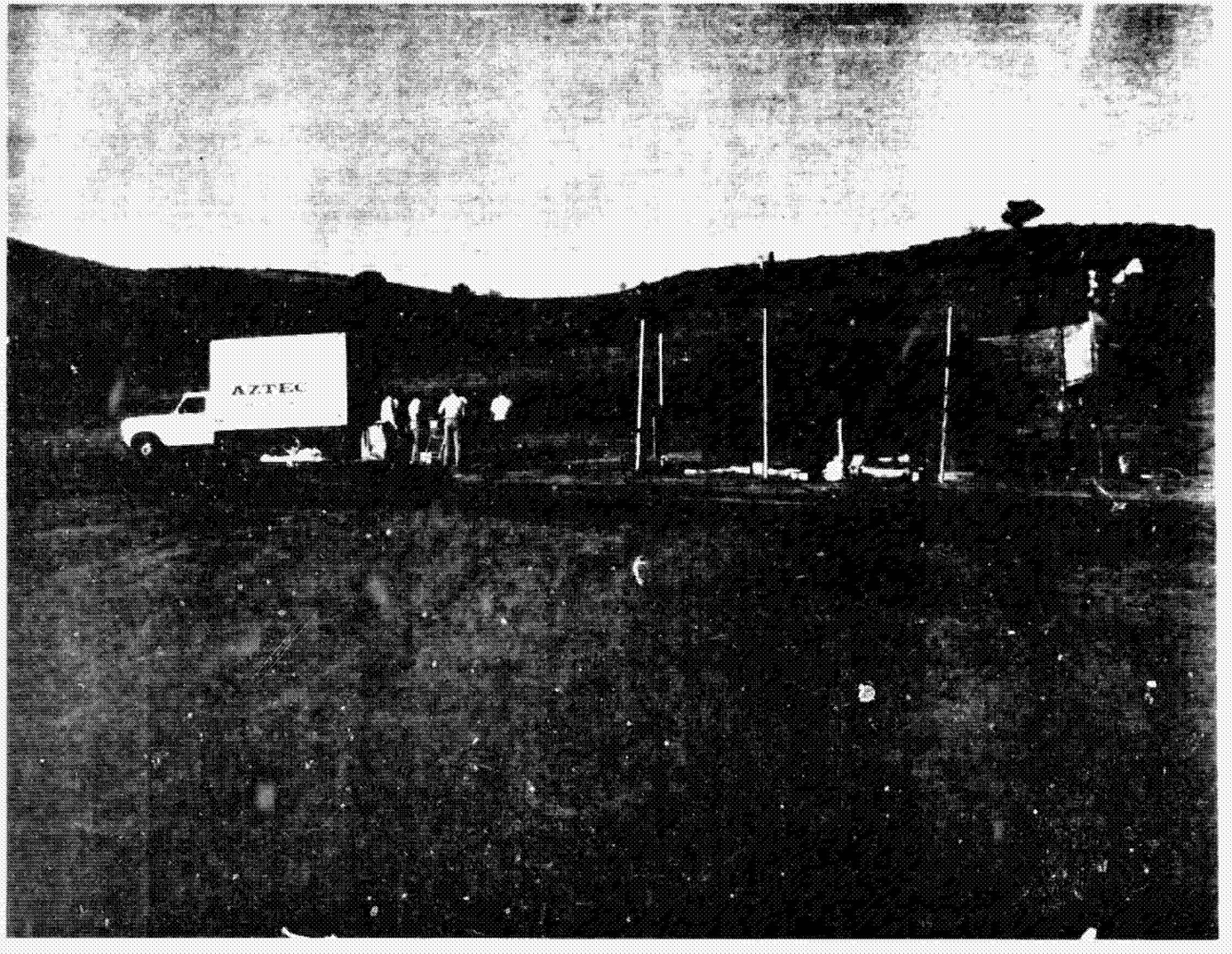

Figure 3.1. CTS Test Site

wave reflections during the explode test phase thus preserving the required ambient outdoor test conditions, and 3) all material released in the tests (greater than 1 mm) would be contained within the relatively small enclosure and thus, an accurate accounting of the amount and type of material could be made.

The instrumentation used for the CTS tests included sticky paper, petri dishes, bridal veil tuna cans, millipore filters, flame and sample thermocouples, LED gages, ball gages, a microwave gage, pyrometer, and still and motion picture cameras, both 16 fps and high speed.

NAVAL WEAPON CENTER TEST SITE

An aerial view of the field test site at the Naval Weapon Center at China Lake, California is shown in Figure 3.2. The asphalt portion of the pad has dimensions of approximately 300 ft x 300 ft and is roughly hexagon shape. Within the upwind end of the asphalt pad (right side in the photograph) is located a 50 ft x 50 ft concrete pad, the center of which is designated "ground zero." All propane tests and the 20 ft x 20 ft JP-5 pool fire tests were centered on the concrete pad. The center of the 40 ft x 60 ft pool fires was located approximately 45 ft upwind (to the right) of the edge of the asphalt pad.

Figure 3.3 shows the dimensions of the asphalt test pad as well as some of the semi-permanent facilities and instrumentation on the test site.

The control center was located approximately 500 ft upwind of the asphalt pad and consisted of three structures; the test control building which also served as a safety barricade, an instrumentation trailer for data acquisition for the active instruments, and a meteorological instrumentation van

The test site was oriented to take advantage of the usually prevailing south winds (which would blow from right to left in Figure 3.2.)

Limitations on cable lengths for the active instrumentation confined the placement of this instrumentation primarily on the asphalt pad with some units located on the desert floor approximately 300 ft downwind from ground zero. In addition, a vast number of passive collectors were placed in crosswind arrays both on the asphalt pad and on the desert floor. The passive collectors were located as far downwind as 6000 ft from the pad and ranged crosswind 1500 ft on either side of the north-south site center line.

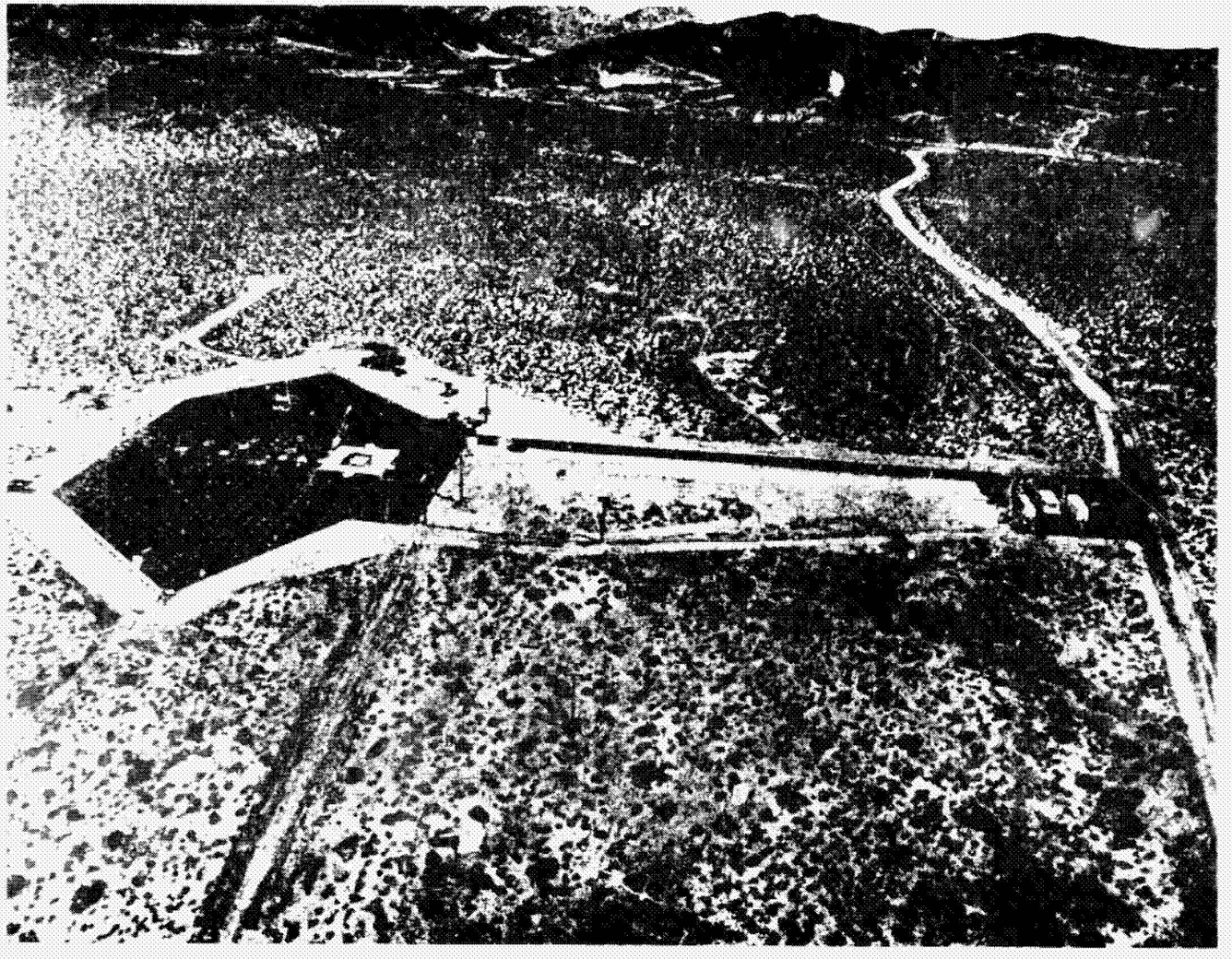

Figure 3.2. Naval Weapon Center Test Site

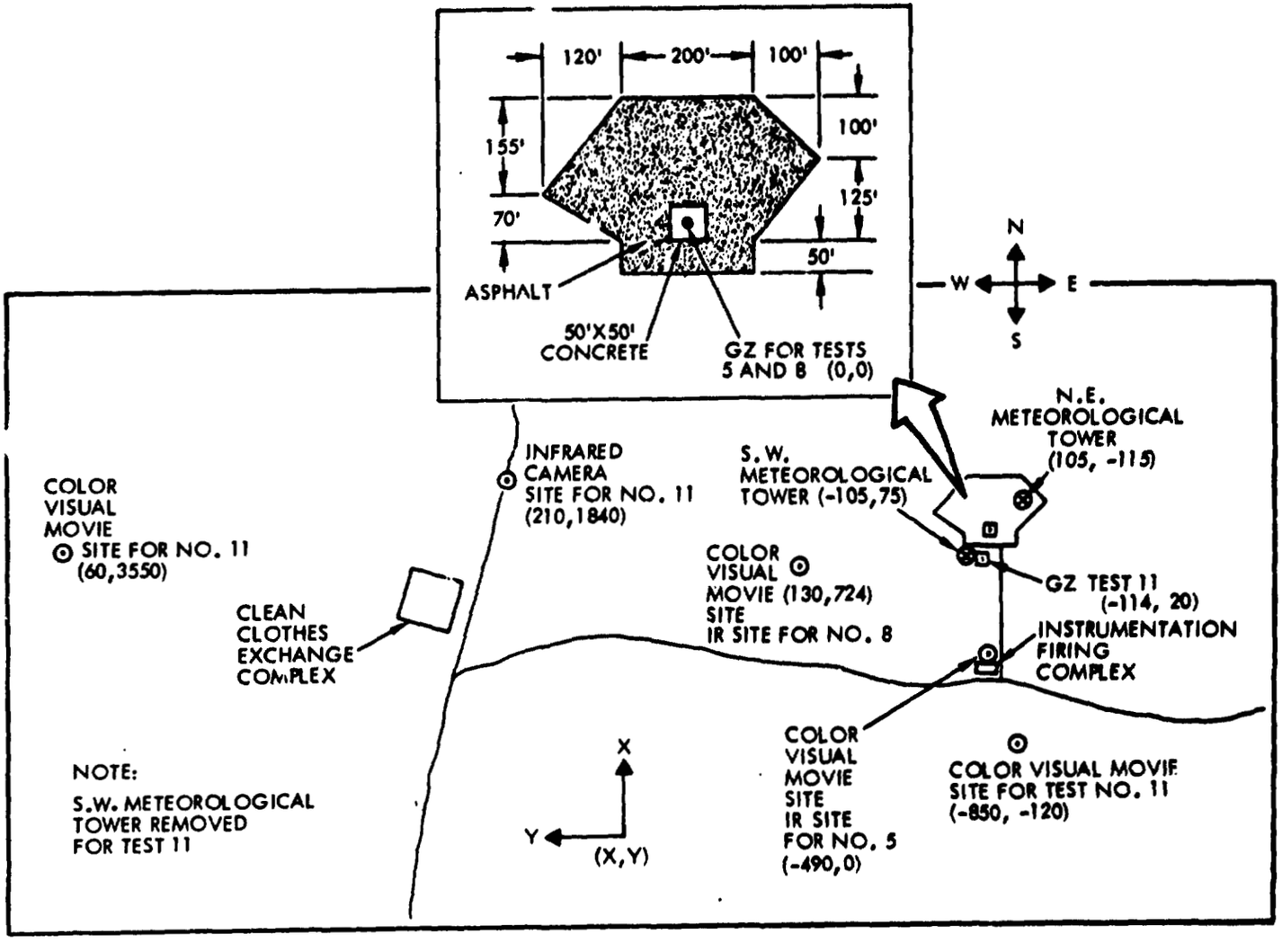

Figure 3.3. NWC Test Site Layout

TEST INSTRUMENTATION

For the purposes of classification, the instrumentation used in the CTS and NWC tests fall into four categories: 1) passive, 2) active, 3) photograhic and 4) meteorological. The different sensors or instruments in each of these categories are listed below

Category 1 Passive

- Sticky paper stands
- Sticky paper strips
- Sticky paper rolls
- Bridal veil tuna cans
- Bridal veil vu graphs
- Bridal veil frames
- Bridal veil ladder vu graphs
- Millipore collectors
- Pad collection
- Sweep brigades

Category 2 Active

- LED
- Microwave
- Ball
- LADAR
- Thermocouple-sample
- Thermocouple-flame
- Flame velocimeter

Category 3 Photographic

- Infrared imaging
- Movies-visual and IR

Category 4 Meteorological

- Thermocouples
- Vanes
- Anemometers
- Smoke puff generator
- Captive balloons
- Free balloons

The primary sensor system was the passive instrumentation. Data from the passive sensors yield the fiber deposition per unit area at downwind and cross-wind locations, for various fiber length intervals and fiber diameter intervals. The passive sensor is a simple, cheap and reliable device (sticky paper, sticky bridal veil, filter paper/vacuum system, etc.) which can be distributed over great areas with the spacing between sensors varied to suit the specific test condition. There has been frequent use of these passive systems in past

experiments. Passive sensors are the corner-stone of the tests discussed in this document.

Although active sensors were used in earlier tests, they were calibrated only for single fibers. In support of this test program, they were successfully calibrated for multiple fibers and fiber clusters. However, the active sensors are considerably more costly to purchase and install than passive sensors, and therefore, were used in smaller numbers.

All of the active instruments used in the test series required that their data output be transmitted via land lines to recorders located in an instrumentation van. As such, their use was restricted to locations within two or three hundred meters from the instrumentation van. These sensors obtain time histories of the fiber cloud concentration for aid in mathematical modeling of the air transport and deposition of the fibers. The active sensors also have the capability of studying the overhead cloud that overshoots the field of passive sensors at ground level.

The photographic instruments were used to record continuous time histories of the fire plume and fiber cloud during each test. Reduction of the recorded photographic data provides the information required for the plume and carbon fiber cloud transport modeling.

The meteorological instruments have a two-fold purpose. First, they provide the data that characterize the atmospheric conditions under which the tests are conducted (again, these data are required for the transport modeling). Second, the instruments provide wind velocity data that is observed during the test in real time to assure that the test is conducted within the specified range safety criteria and within the areal deployment of the fielded instrumentation.

PASSIVE INSTRUMENTATION

Sticky Paper is a term used to identify an adhesive coated paper that was used to collect the carbon fibers deposited during the tests. The particular paper used in the tests was manufactured by the Con-tact Paper Co. (part no. 2263) and was obtained in rolls 18 in. wide and 37.5 ft. in length. This paper is medium-weight stock, white in color and coated with a pressure sensitive type adhesive that does not dry out or loose its sticky properties with time, temperature or dew. This paper is manufactured with a protective cover-paper over the adhesive coating. When the tests were ready to commence, the sticky surface was activated by merely pulling off the cover-paper. At the conclusion of the test, clear acetate sheets are applied to the sticky coating. This preserves the data and prevents the adhesive from coming in contact with other sheets when stacked and stored.

Sticky Paper Stands are 2-foot high wooden platforms that support 8 in x 10 in sheets of sticky paper. These portable stands primarily were deployed in arrays on the asphalt test pad and 50 to 75 ft downwind of the asphalt pad.

Sticky Paper Strips are strips of sticky paper cut 6 inches wide and 8 feet

long. These strips were stapled to wood planks that were placed in arrays approximately 300 feet to 3000 feet downwind from ground zero and up to 1500 feet east and west of the test site center line. At each sensor location for stations 300 to 600 feet downwind of ground zero, two 8-foot wood planks were used. These planks were joined in a portable "T" configuration and provided with wooden block feet which raised the sensor platform 2 to 3 inches off the ground. For each sensor location at the 1000, 1500, 2000 and 3000-foot downwind stations a single 8-foot board was used for the sticky paper strips. These boards were placed directly on the ground surface. For some of the tests, 8-foot sticky paper lengths were stapled to both sides of these boards. At the conclusion of one test, the exposed sticky paper was covered with acetate and collected. At the same time, the board was turned over and the paper backing stripped from the remaining sticky paper. Thus, a second test could be conducted with a minimum of turn-around time.

Sticky Paper Rolls are long strips of sticky paper, 6 inches wide and 200 feet long. These strips were fastened to narrow, 10-foot long wood planks that were layed end-to-end in radial patterns on the asphalt pad. The 200-foot long radial strips extended out downwind from near-ground zero every 5 to 10 degrees on either side of the site north-south centerline. The boards were supported on stands two feet high to prevent reintrained fibers off the pad from depositing on the sticky paper strips.

Bridal Veil is a fine nylon netting sometimes called tulle. This fabric was used in several passive sensor configurations. The bridal veil has openings or a mesh size approximately 1 mm by 1mm and is available in bolts 180 inches wide by 50 yards long. Prior to a test, a sticky adhesive is either brushed or sprayed on the bridal veil. This adhesive is a pressure sensitive adhesive consisting of an acrylic emulsion made by Rohm and Haas Co., part no. RHOPLEX N-619. This adhesive has the unique property of remaining tacky for several days under all of the encountered ambient conditions of wind, temperature, dew and solar radiation. As in the case of the sticky paper, the bridal veil is covered with a clear acetate sheet before it is collected and stored.

Bridal Veil Tuna Cans describe the form of passive sensor that is made from a tin can (typical tuna can size) which has both ends removed and covered with a fine nylon netting over the upwind end. The bridal veil netting is held in position over the tuna can opening by a rubber band. Seven tuna cans were fastened three feet apart to vertical aluminum poles 21 feet high, Figure 3.4. Crosswind arrays of nine to eleven poles were deployed at stations ranging from 200 to 275 feet downwind of ground zero. The bridal veil end of the tuna can faced into the wind.

Bridal Veil Vugraphs are those passive collectors made by fastening bridal veil netting on a standard vugraph frame. These passive sensors were deployed facing into the wind approximately three feet off the ground, approximately ten feet apart around the downwind periphery of the asphalt pad. These vugraph sensors were also used to determine the vertical and horizontal fiber depositions in the vicinity of the active instruments (LED, ball and microwave gages) in order to verify the calibrations of the active instruments.

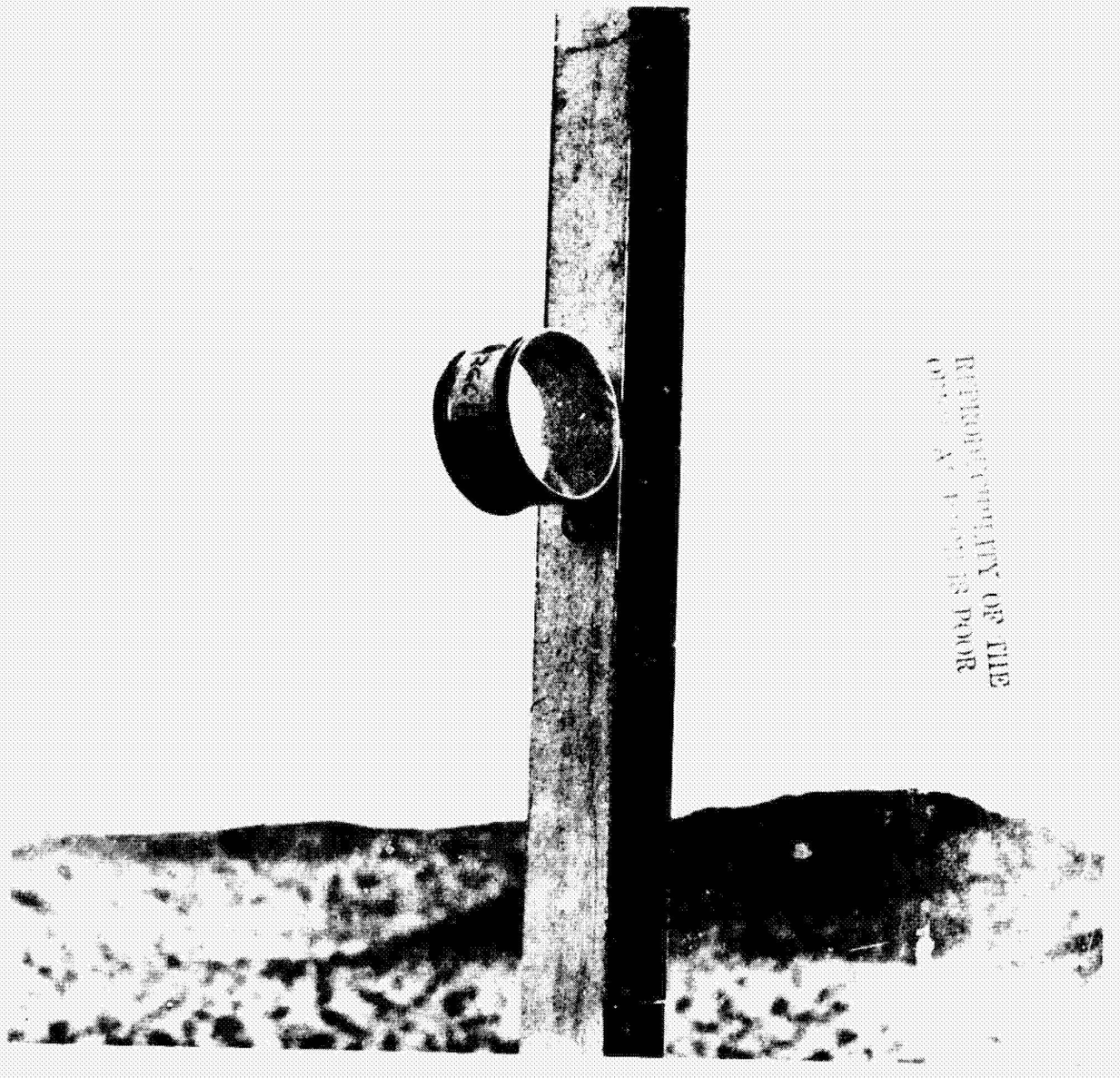

Figure 3.4. Bridal Veil Tuna Can Sensors

Bridal Veil Frames are large horizontally oriented frames constructed from 2 by 4 lumber over which bridal veil netting was stretched and fastened with staples. These frames were 9 feet by 10 feet in size and were raised three feet off the ground surface by 2 by 4 legs. The bridal veil frames were deployed at the 6000-foot downwind station, spaced 100 feet apart and extending crosswind 1500 feet on either side of the test site centerline.

Bridal Veil Ladder Vugraphs (Jacob's Ladder) were used to provide fiber exposure data by intercepting a vertical, crosswind cross section of the fiber cloud with an array of bridal veil vugraphs. The Jacob's Ladder was constructed of vertical and horizontal strands of nylon rope spaced five feet apart that formed a "screen" with a five-foot by five-foot mesh size. Each intersection of the horizontal and vertical strands of rope was tied securely. Two cranes were located on the pad 70 to 80 feet on either side of the test site centerline and approximately 180 feet downwind of ground zero. Each of the ends of the upper horizontal strand of rope was attached to the crane hoisting cables. By raising and lowering the crane cables simultaneously, the ladder could be raised and lowered. As the ladder was raised a crew of test personnel clipped on adhesive sprayed vugraphs at each of the rope intersections. After the ladder was raised to its fullest height (90 ft), the bottom of the ladder was fastened to the ground at several points. (See Figure 3.5 and 3.6.) The ladder was 90 feet wide and 90 feet high resulting in 342 intersections (19 rows horizontally and 18 rows vertically) with a vugraph at each intersection. After the test, the cranes lowered the ladder and the vugraphs were removed, covered with an acetate sheet and stored for future data reduction.

The Jacob's Ladder was first used for Test No. 11 and then for all subsequent tests.

Millipore Collectors are cylindrical plastic holders into which a disc shaped filter paper 37mm in diameter is inserted. Air sampling tests are accomplished by drawing air through the open end of the holder by a vacuum pump. Air flow (volume) is controlled by a precision-metered orifice connected ahead of the filter holder. Particulate matter is collected on the surface of the disc filters as the air is drawn through the filters. The filter paper is a membrane with a pore size of 0.8 micron, thus, particulates larger than 0.8 micron will not pass through the filter but will be collected on the surface.

The millipore filters were mounted on an instrument pole 30 feet high with five, six-foot crossarms. Three filters were mounted on each crossarm for a total of 15 millipore filters per pole. Six poles were fielded for a total of 90 millipore filters. The poles were arrayed crosswind nine feet apart at the 200 foot station downwind of ground zero.

Pad Collection was a procedure whereby after each test, test personnel manually collected all relatively large fiber clusters and strips from the asphalt pad. This collection was done by pad sections and the collected material was placed in plastic bags, sealed and marked by test number and pad section location.

Sweep Brigade was a procedure of manual fiber strip collecting in which 30 plus

Figure 3.5. Jacob's Ladder at NWC Test Site

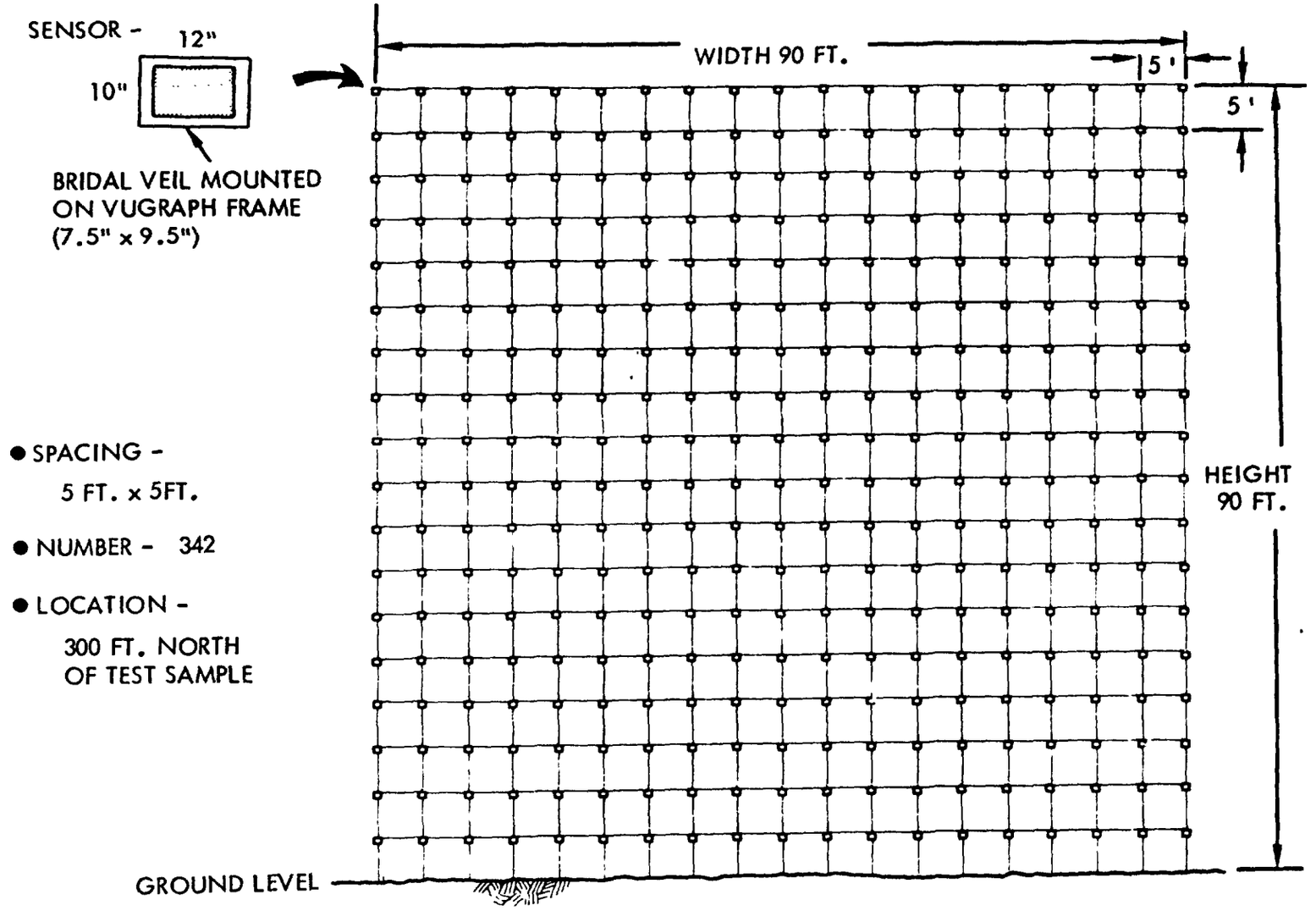

Figure 3.6. Jacob's Ladder Configuration

test site personnel were deployed in a crosswind array out past the 6000-foot station after Test Nos. 10, 11 and 13. This brigade then "swept" over the entire deposition footprint from the 6000 plus-foot station back to the asphalt pad. All observed carbon fiber strips were collected and the approximate fallout location of each strip and its size were tabulated. In some cases, the sweep was repeated up to four times in order to obtain a statistical estimate of the percentage of total strip fallout that was collected. These repeated sweeps also had the effect of "decontaminating" the range, i.e., minimized and also quantified the probability that strips collected in subsequent tests were actually fallout from previous tests.

ACTIVE INSTRUMENTATION

LED is a term which identifies the Light Emitting Diode Source/Detector instrument used to measure the near ground level rarefied fiber cloud concentration histories at 75 to 300 foot ranges. It consists of a collimated LED light source, focusing lens, neutral density and band pass filters and a silicon pin diode detector.

The LED measures number rate of particles passing through its light beam and causing a shadow on the detector. The number rate can be converted to a concentration by introducing the wind velocity, LED beam length and LED beam diameter. For cloud chambers where all particles are single fibers with the same length, the mass flux history is readily obtained from the concentration history by using the mass of each particle. For outdoor tests it is necessary to use a relationship relating the fiber statistical orientation during fall through the LED beam and size distribution of fibers obtained from sticky paper next to the LED to obtain mass flux history from the concentration history. The mass flux history allows comparison of the LED sensor data to microwave sensor data. Figure 3.7 shows a fielded LED instrument.

Microwave refers to microwave sensors specifically developed to measure the mass flux of clusters and clumps of fibers, as well as dense clouds of single fibers. The system atop the five-foot platform shown in Figure 3.8 contains a 12 gigahertz source, transmitter horn and collimator lens in one column; and a lens, receiver horn and detector/amplifier in the other column. The air gap between the columns permits the fiber cloud to pass through it for mass flux measurement. During passage of the fiber cloud, the received energy is reduced in proportion to the mass of fibers in the beam path.

The microwave system is installed in locations close to the source where the other active systems have the likelihood of being saturated by the dense fiber clouds.

Ball Gage is an instrument that not only can detect the presence of a single carbon fiber, but also can measure its length with the aid of a multi-channel analyzer system. The count rate is porportional to the fiber concentration; the amplitude of each count is proportional to the fiber length. The ball gage is unique in that it can yield concentration histories for different groups of single fiber lengths. The ball gage does not detect fibers under 4mm in length because the signal falls within the electrical noise level, but with modified

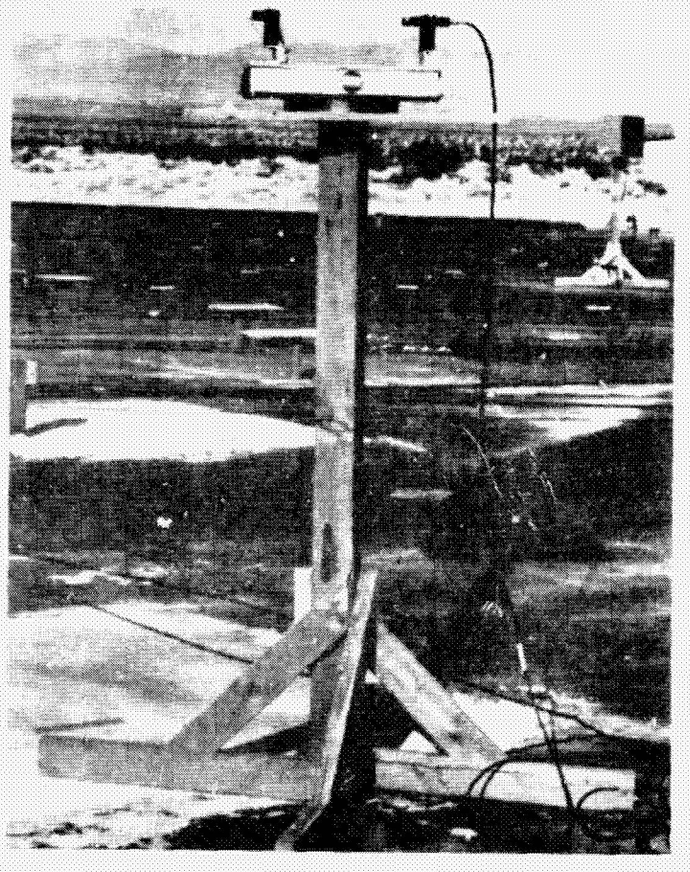

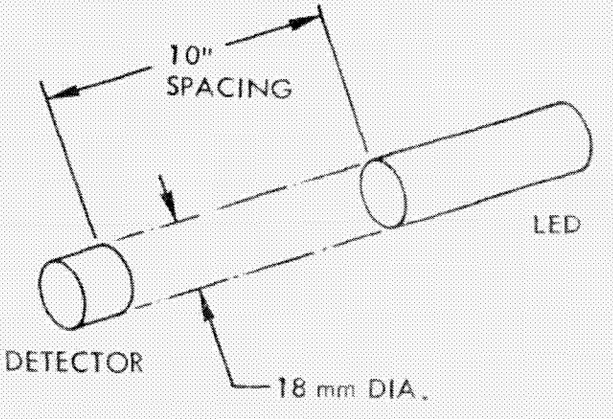

Figure 3.7. LED Particle Detecting System

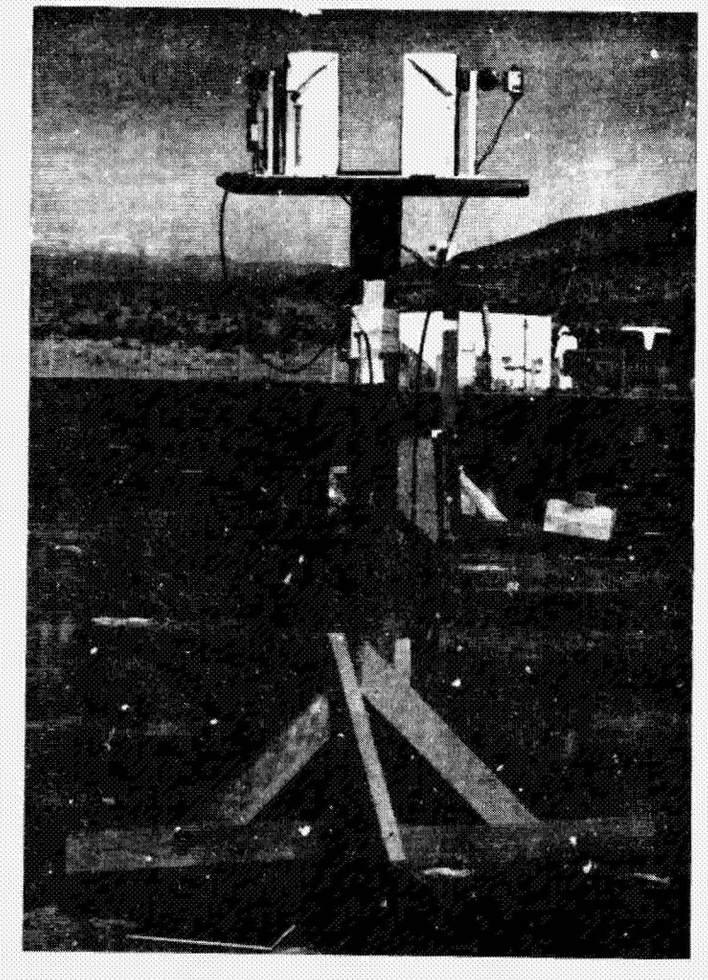

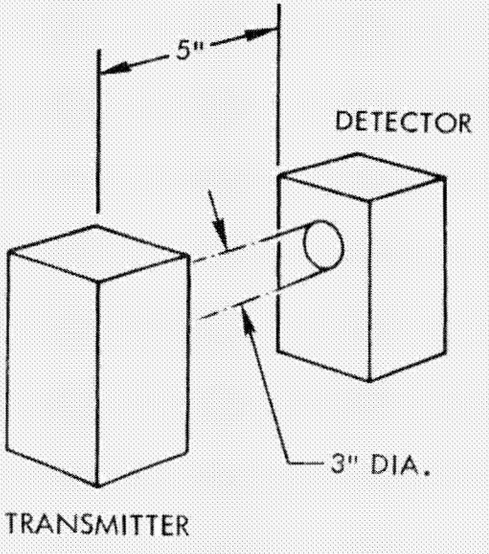

Figure 3.8. Microwave Gauge System

circuitry can measure shorter fiber lengths. The high voltage ball shown in Figure 3.9, charged to 2000 volts, has a sphere of influence several times its own ball diameter.

LADAR refers to Laser Detection and Ranging System. This system is used to measure the relative distribution in space of particulate cloud densities at successive times. The principle involves projecting a short 3 nanosecond pulse of visible ruby laser light along a path where cloud material is expected to pass. then observing the diffuse and pseudo-specular reflection signals from a photomultiplier detector along side the laser. The photomultiplier signal is monitored by photographing a fast oscilloscope trace. The horizontal sweep speed is calibrated in time so that the progress of the laser light pulse reflected return can be related to distance along the light path. The vertical displacement of the oscilloscope sweep is proportional to the fiber concentration of material reflecting the light at the determined location.

In initial tests, the LADAR pulses were projected horizontally and eastward at approximately 225 feet downwind from ground zero.

In later tests a mirror was used to deflect the horizontal beam upward to sample the fiber cloud concentration as a function of height.

Thermocouple-Sample is a system using several thermocouples for measuring the temperature history at various depths within and locations on the test material during the burn phase of the test.

Thermocouple-Flame is a system of thermocouples used for measuring the temperture of the flame at various locations during the burn phase of the test.

Flame-Velocimeter is an electro-optical instrument developed to validate the model of the fire plume and to scan the pool fire and track hot spots and particles within the fire. The principle of operation is depicted in Figure 3.10. A grid mask placed over a detector series with spacing $\Delta S'$ views the fire with a grid spacing ΔS. When a given hot spot in the fire plume rises past the grid, the hot spot appears at the successive grid detectors in a time interval Δt. The grid spacing and time interval between hot spot arrivals at successive grids, yield the vertical velocity of the hot spot.

The inset photograph shows the telescope, grid system, infrared detectors, amplifier and power supply all housed in a portable system.

Infrared Imaging systems consisted of two thermovision IR scanning cameras that were used to obtain histories of the fire plume and carbon cloud envelopes and to track the trajectories of hot particulate within the cloud. Both cameras were modified AGA Corp., Model 661. Various optics were used to obtain narrow and wide fields of view. One camera was sensitive to the light wavelength 2 to 5 microns; the other was sensitive to 8 to 12 microns. Pictures were displayed on a TV monitor and recorded on video tape for later play back and data reduction.

Movies-Visual and IR systems were used to obtain histories of the fire and

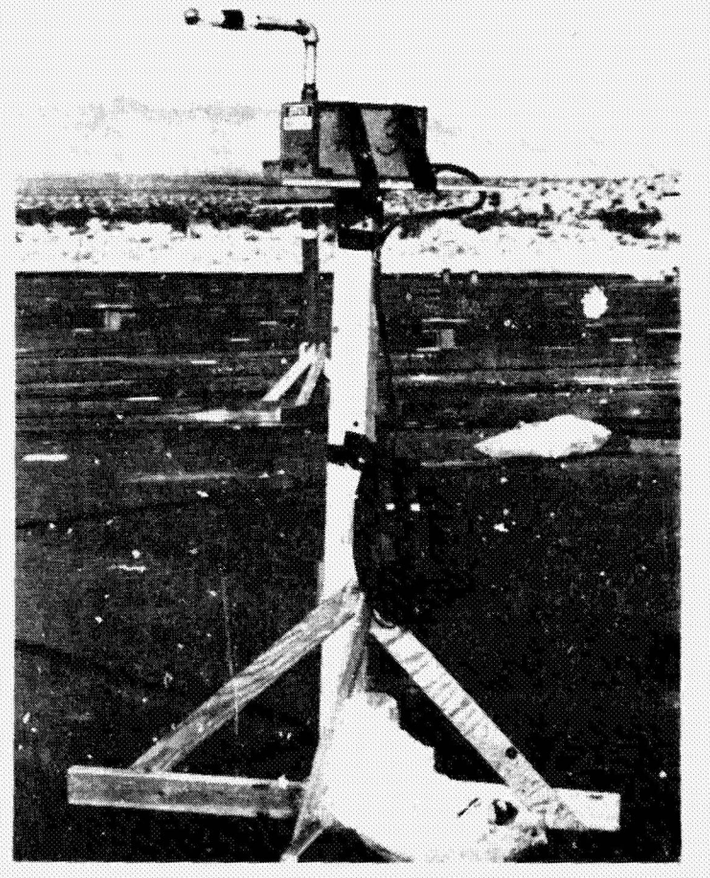

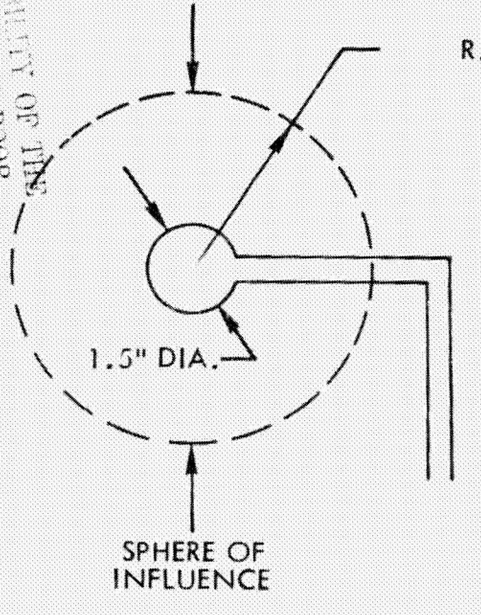

Figure 3.9. Ball Gauge Installation

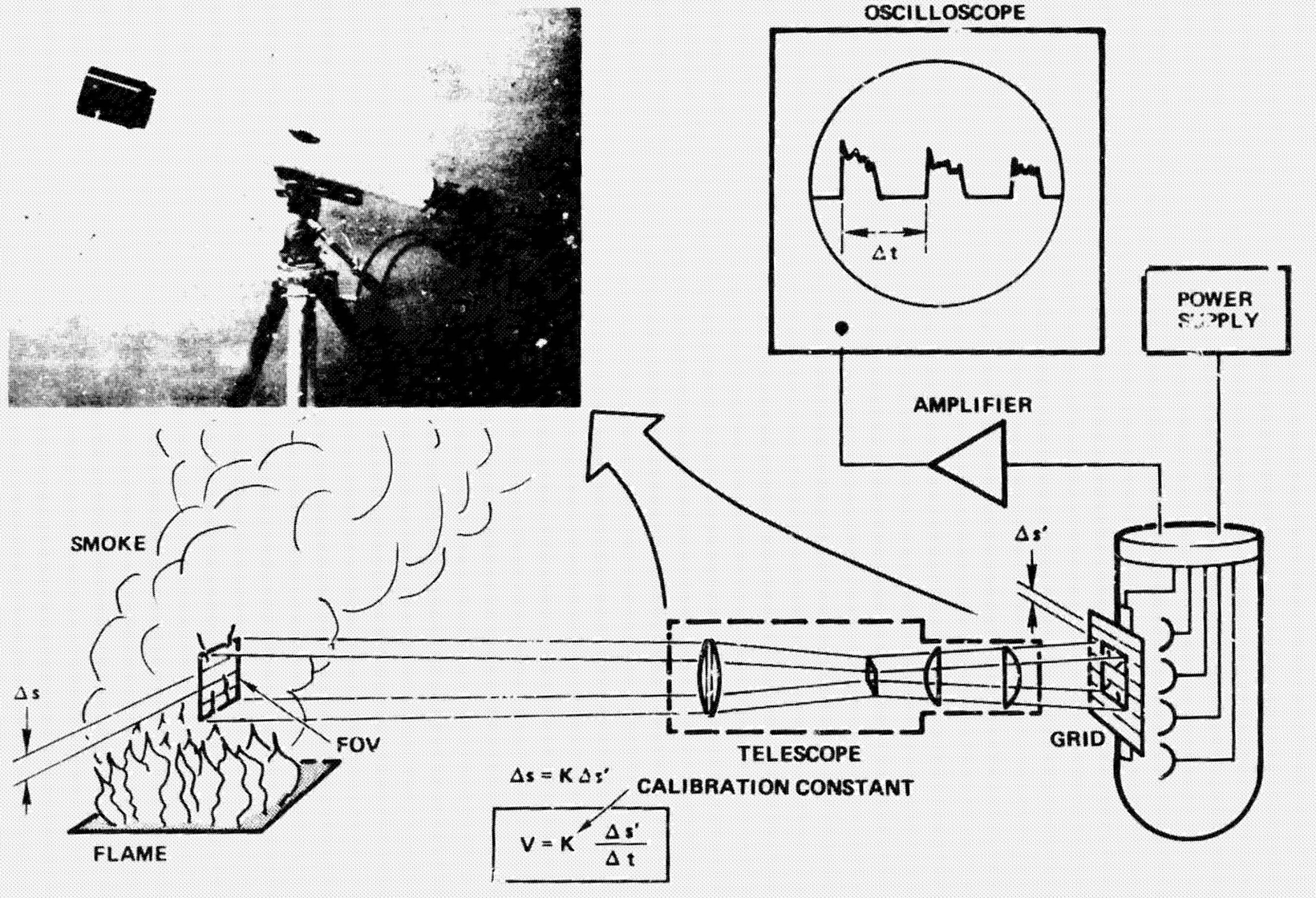

Figure 3.10. Flame-Smoke Velocimeter

and explode events. Several professional 35mm Mitchell movie cameras were used in various locations for each test. High speed cameras were also employed on several tests. Primarily, color motion picture film was used, however, on several tests, film sensitive to the near IR spectrum was also used. The processed film was subsequently data reduced to obtain the characteristics of the fire plume and fiber cloud for later use as a data base in modeling.

METEOROLOGICAL INSTRUMENTS

Thermocouple, Vane and Anemometer systems were mounted on two towers, one erected on the asphalt test pad and one near the southwest corner of the pad. At each of three vertical locations on each tower a system of one vane and one anemometer was mounted together with temperature bulbs that provided a reference ambient air temperature and the temperature differences from this reference temperature at three tower heights. These data (wind velocities and temperatures) were recorded on strip recorders continuously, 24 hours a day, during the test series. The information obtained from those instruments was required to determine wind direction and speed, wind shear, and atmospheric inversion characteristics. This information was used to permit conduct of the tests within range safety constraints and instrumentation limits and for subsequent data reduction for modeling data base purposes. The data from these instruments were also digitized at one minute intervals and recorded on tape.

Smoke Puff Generator was used to monitor the ground level wind direction on the asphalt pad just prior to test initiation. Three tanks of compressed gas were used as a source to produce a white smoke. Low pressure hydrogen chloride and anhydrous ammonia were combined with high pressure nitrogen to provide a highly visible smoke. The smoke tended to interfere with the performance of some of the active instruments located on the test pad and the use of the generator was discontinued after four tests.

Captive Balloons were five-foot meteorological balloons inflated with helium that were lofted prior and during each test to monitor wind direction and obtain low-level wind shear characteristics. Two balloons were generally used tethered at altitudes of 150 to 200 feet. One balloon was located just south of the test pad and the other approximately 100 feet south of the instrumentation vans.

Free Balloons were five-foot meteorological balloons inflated with helium and weighted with approximately 100 grams. These balloons were released at one to five minute intervals prior to test initiation to determine the wind direction and wind shears over the full downwind extent of the test site.

TEST CONDITIONS

To a large extent, the overall test program was directed toward simulating aircraft accident scenarios in which carbon/graphite fibers would be released. To this end, the field test conditions were designed to yield data that when systematically processed and analyzed would support the eventual development of models which would predict the events for different accident incidents. The accident scenario characteristics provided many of the constraints and guidelines for developing the test site configuration, the instrumentation requirements and deployment arrays, the selection of test samples and the specification of test conditions for each test.

For each of the test samples used in the tests, which included both flat plates and in-service components, it was necessary to assure that a compatibility existed between the amount of material predicted to be released (a function of the type and mass of the sample) and the type and location of the instruments selected to collect or monitor the released material. In the case of active instruments, their selection and location depended on matching the sensitivity of each instrument to the expected release phenomenon (released material characteristics) and transport characteristics of each test sample type. (The active instruments sensitivities ranged from the ability to measure only single fibers to the measurement of only heavy mass concentrations.)

In the case of the passive material collectors, the size and location of each collector and the number of collectors were primarily dependent on the scenario characteristics selected for each test. Relatively few, small size collectors located no further than 1000 ft downrange were adequate for those tests which were conducted on samples of low mass and which were burned in a propane flame. However, the tests in which samples were burned in JP-5 pool fires required test samples of relatively higher mass (barrels, spoilers and cockpit) and much more extensive arrays of passive collectors. The ability of the large JP fire plume to transport particles to large distances downrange required collectors as far out as 6000 ft and arrayed crossrange, 1500 ft on either side of the center line. In order to assure that any collected material at these far-out ranges would have statistical significance, it was necessary to use the large (9 ft x 10 ft) passive collectors. Additional arrays of collectors were located at the 1000, 1500, 2000 and 3000 ft downrange distances, also arrayed crossrange, 1500 ft on either side of the center line. These intermediate passive collectors were 6 in x 8 ft in size.

Generally, the test conditions for each of the tests were varied to simulate different scenario characteristics. Besides variations in the test sample material and its mass such scenario factors as the pool fire size and duration, the mode of heating of the sample (radiation or convection) and the explosive characteristics were varied. Each combination of these variables required adjustments or changes in the instrumentation requirements and deployments, test sequencing, personnel requirements, test time and test scheduling and range safety requirements and constraints.

As mentioned above, as the test program progressed it was necessary to field more extensive arrays of instruments and passive collectors since the material released in the later JP-5 fire tests would significantly transport over longer distances downwind. In addition, certain observed phenomenon such as aperiodic transport effects, cloud heights and released material strips suggested the use of additional types of instrumentation and collection techniques. These included the LADAR instrument, the "Jacob's" ladder and the sweep brigade. The requirement to measure the dynamics of the fire plume prompted the more extensive use of the IR scanning camera and the use of a flame velocimeter.

The fielding of these additional instruments and more extensive instrument and collector arrays was judiciously determined for each test based on analytic predictions and "quick look" data analyses of the results of the previous tests. Nevertheless, the later JP-5 fire tests involved the collection of a vast amount of raw data.

Tables A.1 through A.15 given in Appendix A list the detailed test conditions for each of the fifteen tests in the test series. In addition, given below is a description of some of the characteristics unique to each test.

TEST NO. 1 - PLATE TEST

Test No. 1 was the first test of the three conducted at CTS in which sample plates of Thornel 300 were burned and exploded. In this first test, the sample was burned for approximately 40 minutes over a propane burner with air supplied by means of a venturi-suction orifice. The peak flame temperature was recorded at about 1900^{0}F.

Following the burn phase, four 1/2 oz charges of C-4 explosive were detonated 12 inches below the plate burn residue. The explosive charges were contained in four concave holders that effectively generated a planar blast wave. The blast pressure at the plate was estimated to be approximately 0.8 kilobars.

TEST NO. 2 - PLATE TEST

This test was a repeat of Test No. 1 except for the following conditions. The sample was burned for 20 minutes over a propane burner with air supplied from a compressor. This burner configuration yielded a peak flame temperature of about 2300^{0}F. In this test, the four 1/2 oz charges of C-4 explosive were detonated while the explosive holders were in contact with the bottom surface of the burn residue, thus producing a "punch out" effect. The blast pressure at the plate was estimated to have exceeded 120 kilobars.

TEST NO. 3 - PLATE TEST

The differences in test conditions between Test No. 2 and Test No. 3 were 1) the burner propane/air mixture flow rate was increased to produce a hotter flame temperature, about 2600^{0}F and 2) four additional 1/2 oz C-4 explosive charges were placed directly on top of the burn residue (with no backing plate or holders) and detonated together with the four 1/2 oz charges in contact with the bottom of the residue (as in Test No. 2). This blast configuration had the partial effect of squeezing the sample residue horizontally to all sides.

TEST NO. 4 - PLATE TEST

This first test at NWC was a repeat of the first test at CTS (Test No. 1) with three major differences in test conditions. First, the test was conducted in the absence of any enclosure. Second, although the same burner configuration was used as in Test No. 1 (1900°F peak flame temperature), the sample was burned for 20 minutes. And third, a single, 2 oz C-4 explosive charge was detonated 12 inches below the burn residue instead of the four 1/2 oz charges used in Test No. 1. This single explosive charge was contained in a relatively deep steel concave fixture which duplicated the explosive holder used at the NSWC/DL chamber tests. This explosive receptacle results in a semi-shape charge type of explosion and therefore, produced a punch-out effect on the burn residue.

TEST NO. 5 - PLATE TEST

The burn phase for this plate test was identical to the test conditions under which Test No. 2 was conducted, i.e. a "hot" burner with a peak flame temperature of approximately 2300°F. The explosion phase used the same detonation configuration as in Test No. 4, i.e. a single, 2 oz charge, one foot below the burn residue. The LADAR instrument sensor was first used at NWC on this test.

TEST NO. 6 - PLATE TEST

This test was a repeat of Test No. 5 except for minor revisions in some of the passive instrumentation.

TEST NO. 7 - CALIBRATION, EXPLODE ONLY TEST

This test was performed in order to obtain a set of data for calibration purposes for the IR imaging cameras and the motion picture cameras. No passive or active instruments other than the IR imaging and motion picture cameras were fielded in this test. No material sample was used; only a single, 2 oz C-4 explosive charge was detonated identical to the detonation configurations in Test Nos. 4, 5 and 6. The data from this test would reveal the differences in cloud properties between an explosion with and without a fiber cloud.

TEST NO. 8 - BARREL TEST

This test and the two subsequent tests used an experimental barrel fabricated from Hercules AS carbon fiber. However, Test No. 8 was the only test in which the barrel was burned in a propane flame. A JP-5 pool fire was used in Test Nos. 9 and 10.

In the burn phase of this test, an enlarged propane burner was used with air supplied by a compressor, thus producing a "hot" flame as in Test Nos. 2, 5 and 6 with a peak flame temperature of about 2300°F. Prior to the test, the barrel was cut up into twelve segments; two segments were burned at a time, the segments positioned side by side over the burner. The burn duration for each of the "two segment" burns was 20 minutes.

The burn residue from the six 2-segment burns was combined and a single 2 oz C-4 explosive charge detonated 12 inches below the residue using the same explosive holder as in the previous four tests (Test Nos. 4, 5, 6 and 7).

This was the first test in which feather-like clusters ("chicken feathers") of carbon fibers were released after the explode phase. Also in this test, passive collectors were first deployed out to the 1000, 1500, 2000 and 3000-ft downwind stations. The feather-like clusters were noted as far out as the extreme (3000-ft) sticky paper collectors.

TEST NO. 9 - BARREL TEST

Test No. 9 was a burn only, barrel test conducted in two separate burn phases. This test was also the first test in which a JP-5 pool fire was employed. A 20-ft x 20-ft pool, centered at ground zero, was constructed on the concrete pad. A layer of water was flowed into the pool to produce a level surface. Then JP-5 fuel was flowed into the pool on top of the water; a measured quantity of JP-5 fuel was used depending on the fire duration desired. Several tens of gallons of gasoline were poured on the JP-5 fuel and ignited by electrically detonated squibs at the established ignition start time.

In the first burn phase of this test, a half barrel segment (cut longitudinally) was suspended six feet over the pool surface at a location such that the barrel segment was heated only by radiation from the pool fire flame. The total burn time was three minutes. Approximately, three pounds of aluminum and magnesium were added to the fire to elevate the flame temperature.

In the second phase of this test, the partially burned barrel segment was repositioned five feet over the pool at a location such that the segment would be within the pool fire flame and thus heated both by radiation and the intense convection. The total burn time for this test phase was six minutes.

Due to imposed scheduling constraints, no active instrumentation was fielded in this test and Test No. 10. However, approximately fifty percent of the full complement of passive sensors were deployed in both of these tests.

TEST NO. 10 - BARREL TEST

In this test, the burned residue from Test No. 9 was combined with a fresh half-barrel segment and positioned approximately five feet over the 20 ft x 20 ft pool and within the pool fire flame. Approximately four minutes after the JP-5 fuel was ignited, a 2 oz C-4 explosive charge was swung into position underneath the barrel segments and detonated. The pool fire continued to burn after the detonation for approximately four and one-half additional minutes creating a continuous plume downwind.

Unfortunately, just prior to detonation a sudden wind shift to the east caused the fire plume and all fiber fallout to miss the north-south oriented arrays of passive sensors. However, after the detonation, large strips of fibers were observed within and depositing out of the fire plume. These strips could also be seen in the motion picture data. This was the first test in which such fiber

strips were released in a test. (In this test, the strips were up to approximately two inches wide and 12 to 18 inches long). Strips such as these were also released in Test Nos. 11, 12 and 13. Test personnel then swept over the deposition footprint noting very heavy strip deposition on the pad up to 150 feet from the fire, moderate deposition (eight to ten strips in a 20 ft diameter area) out to over 750 feet; and some strips as far out as 1900 feet. In contrast to the strips collected in the subsequent spoiler and cockpit tests which generally had relatively sharply defined edges as if "peeled" off the material sample, the strips from this barrel test were feather-like both on the edges and ends with many fibers peeling off the surfaces of the strips.

TEST NO. 11 - SPOILER TEST

Test Nos. 11 and 12 involved three aircraft spoilers constructed of carbon fiber composite material. In Test No. 11, the three spoilers were burned over a 40 ft x 60 ft JP-5 fire pool. The pool was constructed south of the asphalt pad with the pool long dimension oriented in the north-south direction. The center of the pool was 114 ft south of ground zero and on the north-south site centerline. (All sensor north-south stations are referenced to ground zero, the center of the concrete pad; stations north are designated plus, stations south are designated minus.)

The spoilers were suspended approximately seven feet over the pool fire surface at a location such that the spoilers would be in the center of the flame plume. The total burn duration of the pool fire was approximately four minutes.

A major release characteristic in this test was the release of composite strips during the burn. A sweep brigade was organized and the deposition footprint swept from beyond the 6000-foot station back to the pad. This sweep was repeated three times and it was estimated that 90 to 98 percent of the total strips released were collected. Strips were recovered beyond the 6000-foot station with the heaviest deposition at about 1800 feet from the pool fire. The largest strips were approximately two inches wide and almost four feet long.

TEST NO. 12 - SPOILER TEST

This test was a burn/explode test in which the burned spoiler residue from Test No. 11 was replaced in the same position as for Test No. 11 over the 40 ft x 60 ft pool. The pool was replenished with JP-5 fuel and the fuel ignited. The fire was permitted to burn for approximately 40 seconds until the fire plume stabilized and then a single 2 oz C-4 explosive charge contained in the same type fixture as used in the previous NWC tests was swung underneath the material sample and detonated. The fire continued to burn for an additional six and one-half minutes.

Unfortunately in this test, the cable that moved the explosive under the sample broke before the explosive charge was swung completely into position under the material sample. Consequently, the detonation occurred approximately twelve inches below but approximately two feet to the west side of the sample. The effect of this detonation was to lift the bulk of the material off its suspension fixture and to toss it out of the fire plume to the east side of the site,

ten to fifteen feet outside of the fire pool. Therefore, very little material was lofted into the fire plume and downrange to the instrumentation arrays.

TEST NO. 13 - COCKPIT TEST

This test was the last test that involved an in-service component. An F-16 cockpit, partially fabricated of carbon/graphite fiber composite, was burned over the 40 ft x 60 ft JP-5 pool fire. As in the case of the spoiler tests, the cockpit was suspended seven feet over the pool fire surface within the fire plume. The fuel was ignited and burned for approximately six minutes.

During the last minute of the fire, an interesting phenomenon was observed. At this time, the burned cockpit consisted mainly of its metallic inner structure with some composite material. This structure could be seen within the fire sitting upright on the suspension fixture. The structure still maintained the general cockpit shape as long as the fire burned vigorously. However, as the fire died down, just before the six-minute point, the strength of the fire updraft diminished to a point at which the updraft no longer was strong enough to support the weakened cockpit and the entire cockpit collapsed. Apparently, up to this point, the only forces that held the cockpit remains in the original cockpit configuration were the intense updrafts from the fire.

As in Test No. 11, composite strips released from the cockpit were observed to be trapped and lofted in the fire smoke plume and subsequently falling out of the plume downrange. The entire deposition footprint was again swept by test personnel and these strips collected and their size and deposition location tabulated. The strips were as large as three inches wide, 54 inches long and averaged about one and one-half plies in thickness.

Due to a combination of subsequent adverse meteorological conditions and test schedule constraints, no opportunity was available to follow-up this cockpit test with a burn and explode test similar to Test No. 12.

TEST NO. 14 - PLATE TEST

Test Nos. 14 and 15 were the last two tests of the test series. In these two tests, flat plates of Thornel 300, identical to the plates tested at CTS and in Test Nos. 4, 5 and 6, were burned over a propane burner. The flame temperature for Test No. 14 was approximately 2000^{o}F and the burn time was 20 minutes. The burned plate residue was then placed at ground zero and a single 2 oz C-4 explosive charge was detonated six inches below the residue. The charge holder was identical to the type used in all of the previous NWC explode tests.

Although Test Nos. 14 and 15 were similar in many respects to the earlier NWC plate tests, a major difference was that the Jacob Ladder bridal veil vugraph array was available for these last two tests. However, due to government directives, no active instrumentation nor IR and visual camera coverage was fielded. Also the use of some of the passive sensors was eliminated from these two tests.

Reduction and analysis of the data acquired in Test Nos. 14 and 15 was not included as a part of the subject program and the results of these tests were not available for this report.

TEST NO. 15 - PLATE TEST

The only difference in test conditions between this test and Test No. 14 is the flame temperature for the material sample burn. In this test, the propane burner fuel/air flows were adjusted to yield a flame temperature of approximately 2400^{0}F. The burn time was 20 minutes.

During the explode phase of this test, a sudden wind shift caused the fiber cloud to miss the instrumentation arrays and little, if any, data were acquired.

FIELDED INSTRUMENTATION SUMMARY

Tables 3.4, 3.5 and 3.6 list all of the instruments used for each of the twelve tests conducted at the NWC Test Site. Table 3.4 lists the passive collection techniques; Table 3 5, the active instruments; and the photographic techniques and meteorological instruments are listed on Table 3.6.

These instrument matrices demonstrate the adaptive evolution of the fielded instruments as the tests progressed from relatively small samples burned in propane flames to the larger in-service components burned in large JP-5 pool fires. Except for imposed constraints, the revisions in instrumentation from test-to-test were made for one or more of the following reasons: 1) to improve the quality of the overall data acquisition system based on deficiencies noted in previous tests; 2) to improve the cost and time effectiveness of the field operations; 3) to expand the data acquisition arrays to cover the increased site sampling area for the JP fire tests; and 4) to provide specialized instruments and collection techniques for measuring specific parameters that were peculiar for certain tests, such as the flame velocimeter, the free balloons, the sweep brigade and the large bridal veil frames.

Table 3.4. NWC Test Measurements - Passive Instrumentation

INSTRUMENT \ NWC TEST SAMPLE	NO. 4 PLATE	NO. 5 PLATE	NO. 6 PLATE	NO. 7 NONE	NO. 8 BARREL	NO. 9 BARREL	NO. 10 BARREL	NO. 11 SPOILERS	NO. 12 SPOILERS	NO. 13 COCKPIT	NO. 14 PLATE	NO. 15 PLATE
STICKY PAPER STANDS 8 IN X 10 IN	34	19	19	-	90	90	90	90	90	90	90	90
STICKY PAPER STRIPS 6 IN X 8 FT	44	44	44	-	222	222	222	262	262	262	142	142
STICKY PAPER ROLLS 6 IN X 200 FT	3	11	7	-	-	-	-	-	-	-	-	-
TUNA CANS	77	154	226	-	226	-	-	-	-	-	-	-
BRIDAL VEIL VU GRAPHS 8 IN X 10 IN	-	44	44	-	44	-	-	10	-	-	-	-
BRIDAL VEIL FRAMES 9 FT X 10 FT	-	-	-	-	30	30	30	30	30	30	-	-
BRIDAL VEIL LADDER VU GRAPHS 8 IN X 10 IN	-	-	-	-	-	-	-	342	342	342	342	342
MILLIPORE COLLECTORS	99	99	-	-	-	-	-	-	-	-	-	-
PAD COLLECTION	-	-	-	-	1	1	1	1	1	1	1	1
SWEEP BRIGADES	-	-	-	-	-	-	2	4	-	2	-	-

Table 3.5. NWC Test Measurements - Active Instrumentation

INSTRUMENT \ NWC TEST SAMPLE	NO. 4 PLATE	NO. 5 PLATE	NO. 6 PLATE	NO. 7 NONE	NO. 8 BARREL	NO. 9 BARREL	NO. 10 BARREL	NO. 11 SPOILERS	NO. 12 SPOILERS	NO. 13 COCKPIT	NO. 14 PLATE	NO. 15 PLATE
LED	20	20	20	-	20	-	-	20	20	20	-	-
MICROWAVE	6	6	6	-	5	-	-	4	4	4	-	-
BALL	6	9	9	-	9	-	-	8	8	8	-	-
LADAR	-	1	1	-	1	-	-	1	1	1	-	-
THERMOCOUPLE-SAMPLE	3	3	3	-	-	1	-	3	-	3	3	3
THERMOCOUPLE-FLAME	1	1	1	-	1	1	-	2	-	2	1	1
FLAME VELOCIMETER	-	-	-	-	-	-	-	1	1	1	-	-

Table 3.6. NWC Test Measurements - Photography & Meteorology Instrumentation

INSTRUMENT \ NWC TEST SAMPLE	NO. 4 PLATE	NO. 5 PLATE	NO. 6 PLATE	NO. 7 NONE	NO. 8 BARREL	NO. 9 BARREL	NO. 10 BARREL	NO. 11 SPOILERS	NO. 12 SPOILERS	NO. 13 COCKPIT	NO. 14 PLATE	NO 15 PLATE
PHOTOGRAPHY												
INFRARED IMAGING	2	2	2	2	2	2	2	2	2	2	-	-
MOVIES-VISUAL AND IR	8	8	4	4	4	4	4	4	4	4	-	-
METEOROLOGY												
THERMOCOUPLES	8	8	8	8	8	8	8	5	5	5	5	5
VANES	6	6	6	6	6	6	6	3	3	3	3	3
ANEMOMETERS	6	6	6	6	6	6	6	3	3	3	3	3
SMOKE PUFF GENERATOR	1	1	1	1	-	-	-	-	-	-	-	-
CAPTIVE BALLOONS	2	2	2	2	3	3	3	3	3	3	3	3
FREE BALLOONS	-	-	-	-	-	10-20	10-20	10-20	10-20	10-20	-	-

4. PASSIVE INSTRUMENTATION: DATA REDUCTION AND ANALYSIS

INTRODUCTION

Presented herein are the results of reduction and analyses of field test passive instrumentation data and the performance of laboratory tests toward evaluation of various source generation aspects. A wide spectrum of passive instrumentation techniques were applied as well as variations in the respective instrumentation test layouts. In some cases the test data were relatively limited due to the influence of meteorological conditions toward irregular dispersion of deposition patterns. All available data were analyzed with attention focussed on characterization of the observed particulate in terms of number, mass, length and diameter distributions and evaluation of relative variations associated with the plate, barrel, spoiler and cockpit samples and different test conditions.

DATA REDUCTION METHODOLOGY

Data reduction techniques were applied a appropriate depending on the nature of the record type and particulate domain of interest. In all cases the basic approach consisted of direct measurement of particle dimensions over designated record segments with areas governed by particle densities.

Visual aids and associated magnifications are noted as follows:

- Photographic Enlargement 3X to 9X
- Comparator 7X
- Microfiche Viewer 24X
- Nikon Profile Projector 10X to 50X
- Microscope 10X to 100X
- Metallograph 50X to 1000X

Instrumentation records consisted principally of sticky paper sheets (8"x10") and strips (6"x8') and adhesive-covered bridal veil mounted on tuna can (3.25" diameter) and vugraph (7.5"x9.5") frames. Particle shapes observed to varying degrees for different tests may be categorized as follows:

Designation	Fiber Number
Singles	1
Multiples	2 - 10
Lint	10 - 100
Clumps	10 - 100
Clusters	100 - 1000
Strips	1000 - 100,000

Detailed descriptions and representative photographs are presented in later sections of the report.

Data reduction procedures were developed as most readily applicable to the individual types of instrumentation records. Sequential stages in data reduction of a sticky paper strip record are indicated schematically in Figures 4.1 to 4.3. A similar representation of the data reduction approach for the Jacob's Ladder bridal veil vugraph records is shown in Figures 4.4 and 4.5.

It is noted that particle counting for the sticky paper records was generally performed for all of the 100 1 cm x 1 cm squares corresponding to the transparent grid overlay. However, in a limited number of cases where the particle density was particularly high, the number of squares counted were reduced to the extent that the particle quantity was of the order of several hundred. The selection of specific areas for the counting process was not considered a sensitive statistical factor since in general the particle distributions appeared to be relatively uniform over the extended areas considered in comparison to the total records.

PLATE TESTS

INSTRUMENTATION LAYOUT

Plate tests 1, 2 and 3 were conducted at the TRW Capistrano Test Site and Plate Tests 4, 5 and 6 were performed at the Naval Weapons Center. An exploded view of the passive instrumentation layout for Tests 1 and 2 is shown in Figure 4.6. Sticky paper strips 8" in width and 4' to 6' in length were located on the chamber floor during Test 3. Figure 4.7 indicates the instrumentation layout for Tests 5 and 6. Variations in the geometric array of sticky paper sheets and strips were introduced during Tests 4, 5 and 6 in order to explore optimum patterns for data acquisition. No major advantage for any particular option was apparent.

PARTICLE DISTRIBUTIONS

A representative sticky paper record is shown in Figure 4.9. Records of this nature were observed in Tests 1, 2 and 3 with varying degrees of density and frequency of large particles depending on proximity to ground zero. Similar types of records occurred in Tests 4, 5 and 6 with a progressive decrease in overall density and disappearance of heavy particulate for increasing range.

A comparative plot is represented in Figure 4.9 of the particle number distribution as a function of length and width for Tests 1, 2 and 3. The ordinate values correspond to an integration over the 225 sq. ft. floor area of the test chamber based on the assumption that the particle distribution characteristics established by data reduction of the available records constituted a reasonable approximation of the average over the entire floor area.

In Figure 4.9 it is noted that the several envelopes of occurrence frequency per length interval are quite similar, with significantly higher quantities for Test 3. No striking trend is apparent in the relative occurrence patterns for the

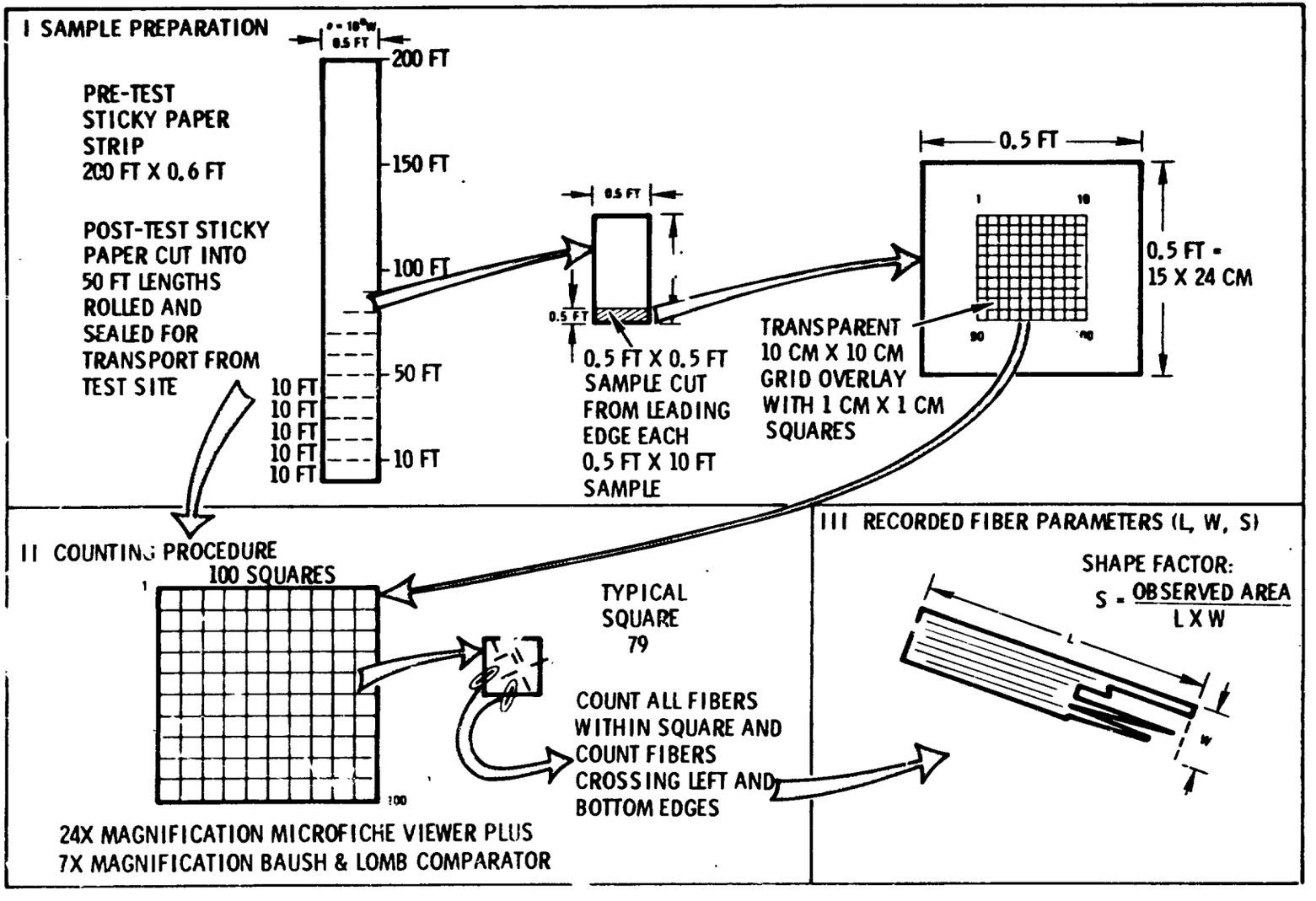

Fugure 4.1. Sticky Paper Data Reduction Methodology - I

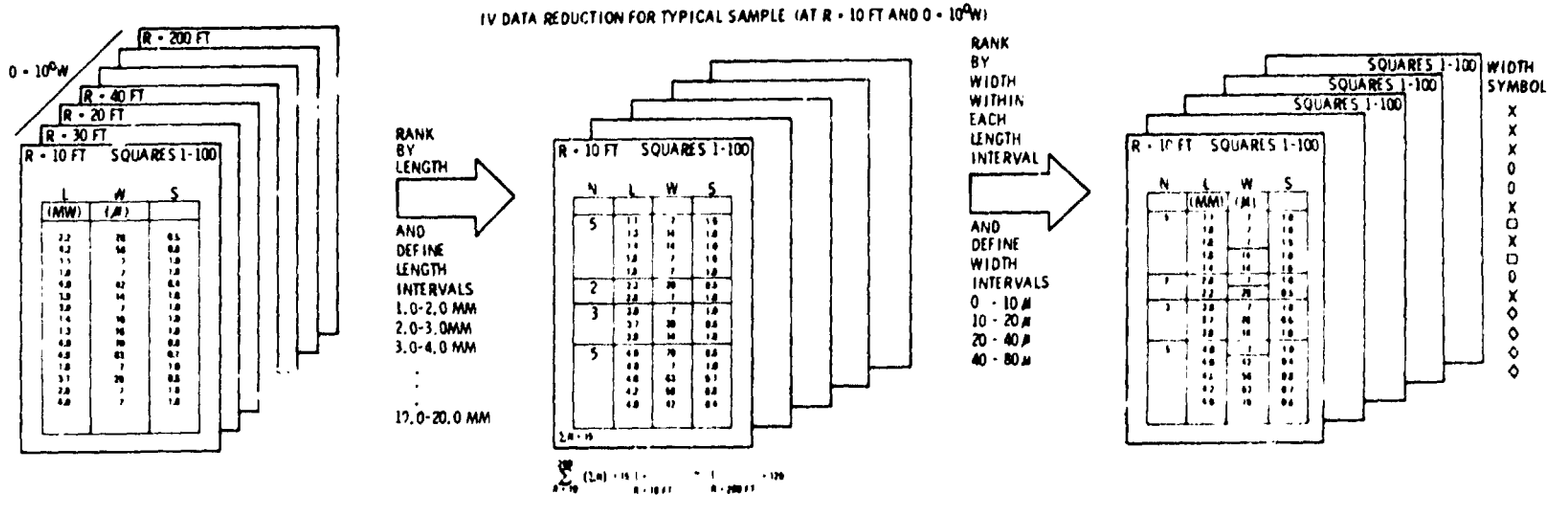

Figure 4.2. Sticky Paper Data Reduction Methodology - II

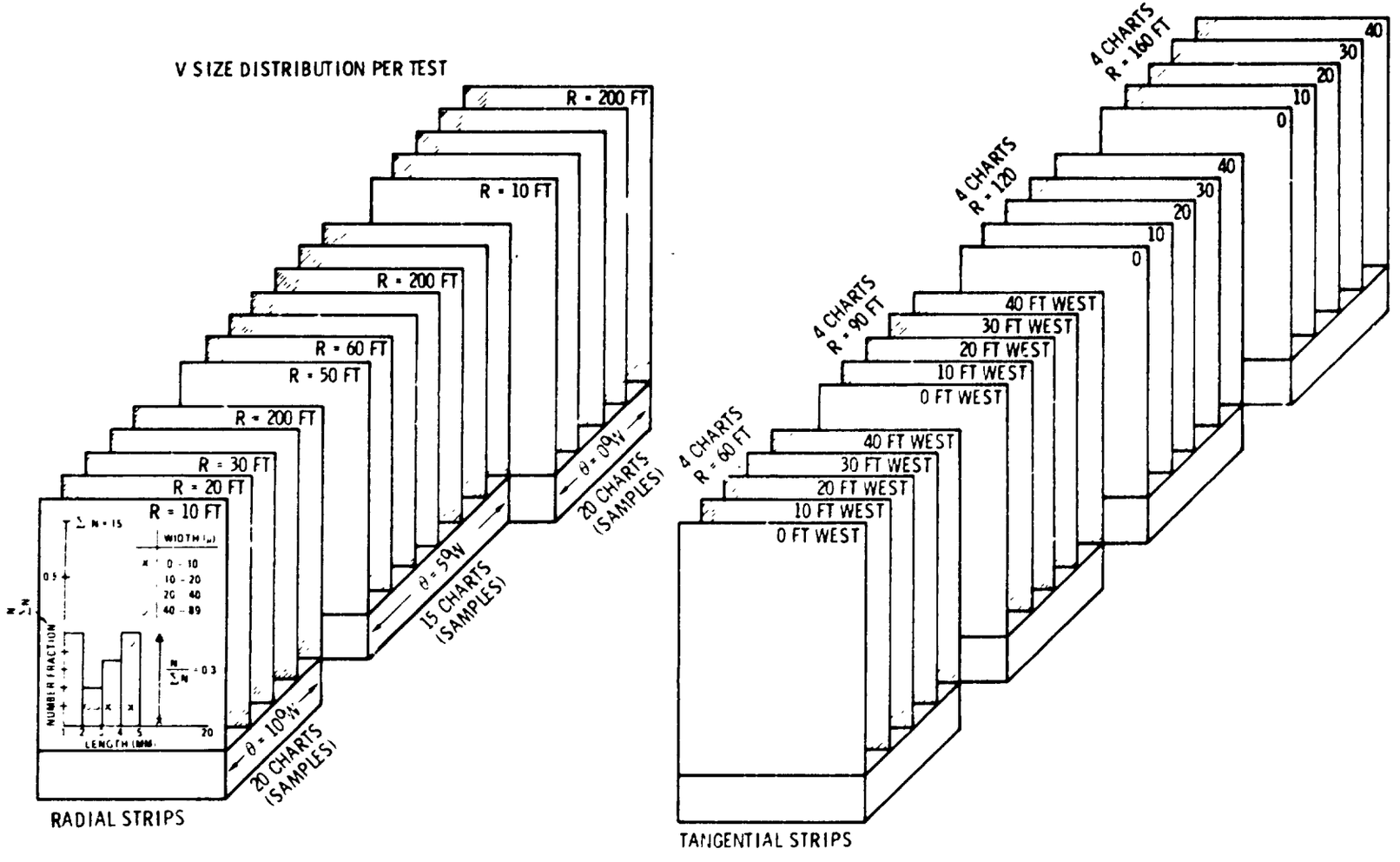

Figure 4.3. Sticky Paper Data Reduction Methodology - III

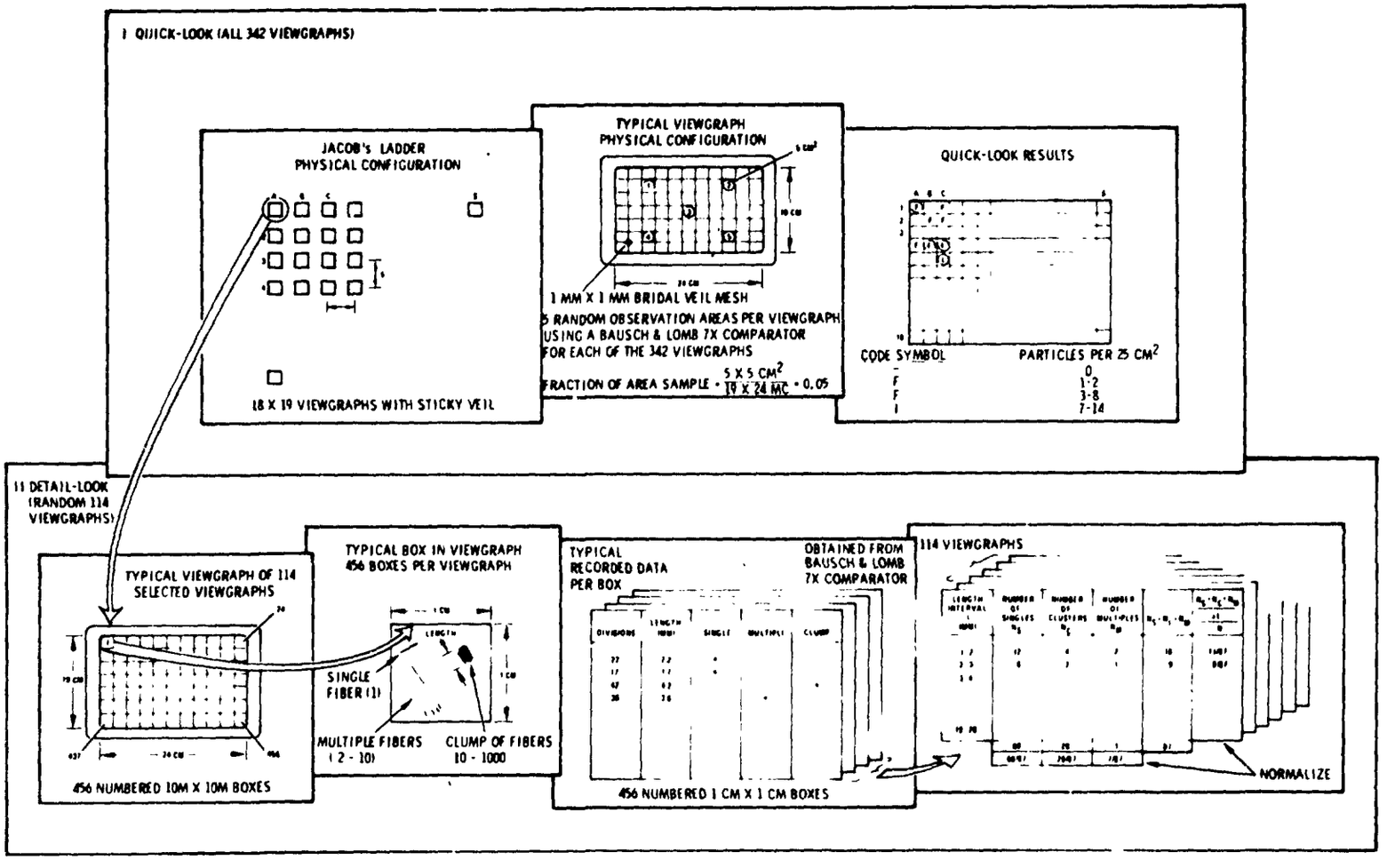

Figure 4.4. Jacob's Ladder Data Reduction Methodology - I

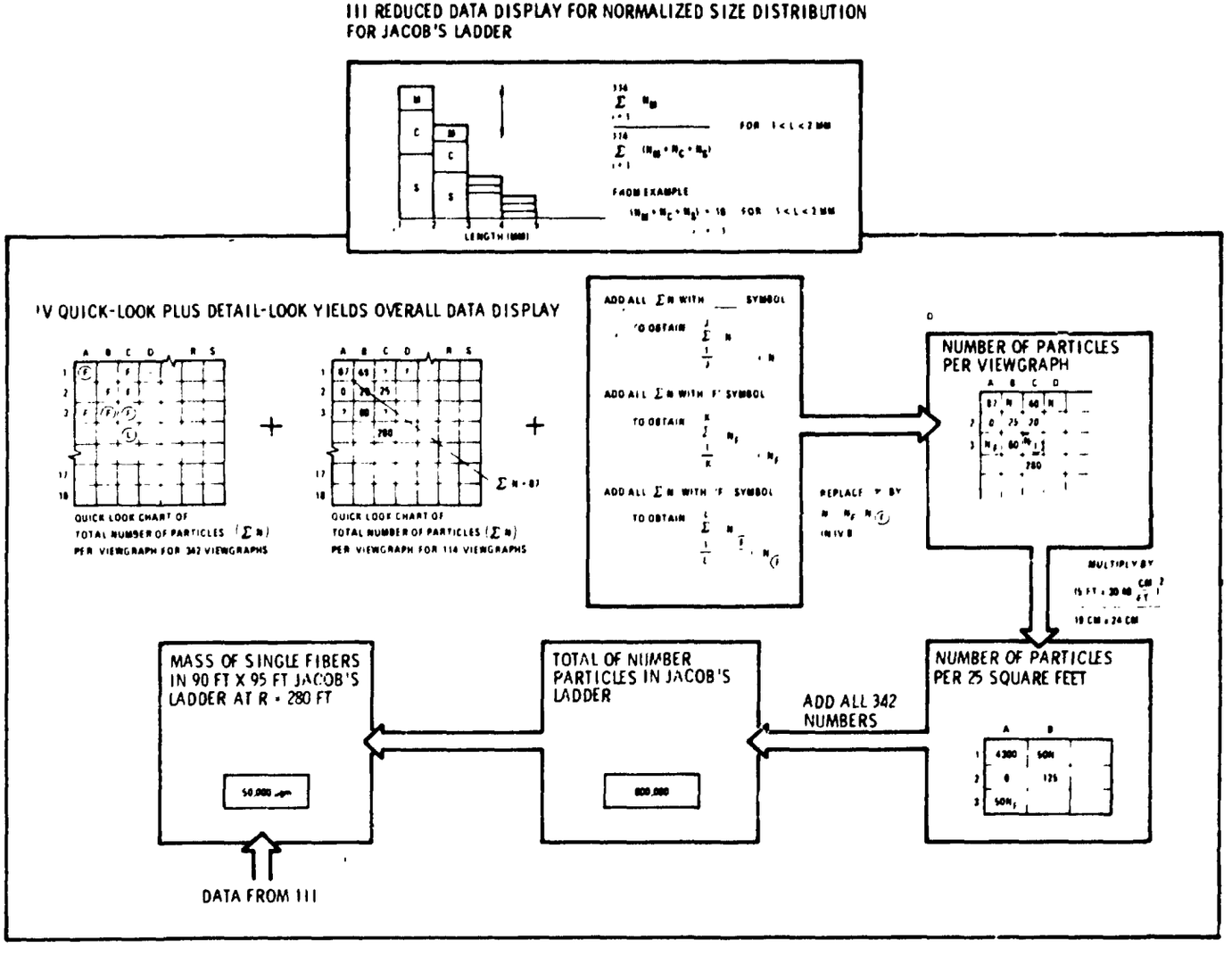

Figure 4.5. Jacob's Ladder Data Reduction Methodology - II

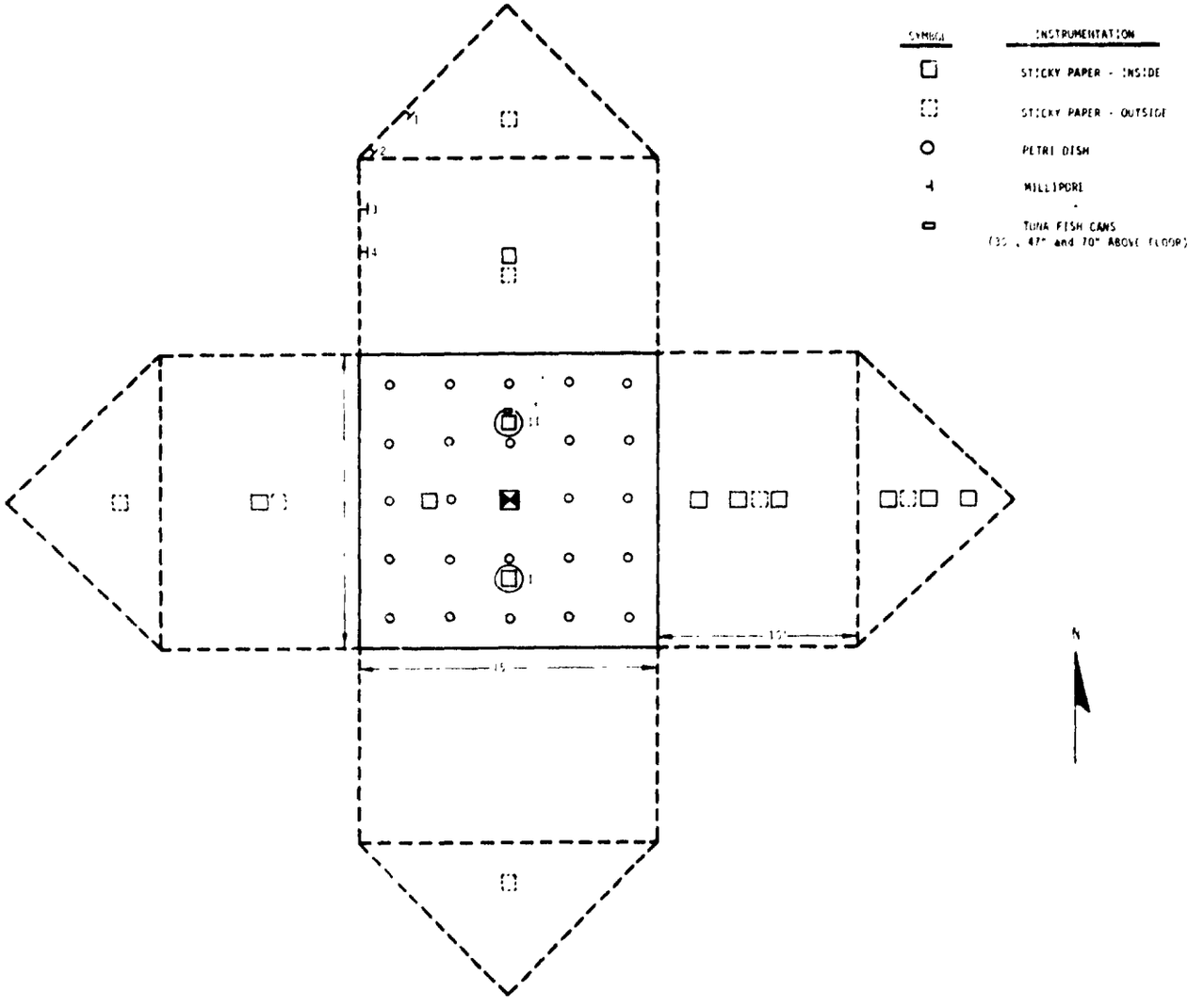

Figure 4.6. Passive Instrumentation Layout for Plate Tests 1 and 2

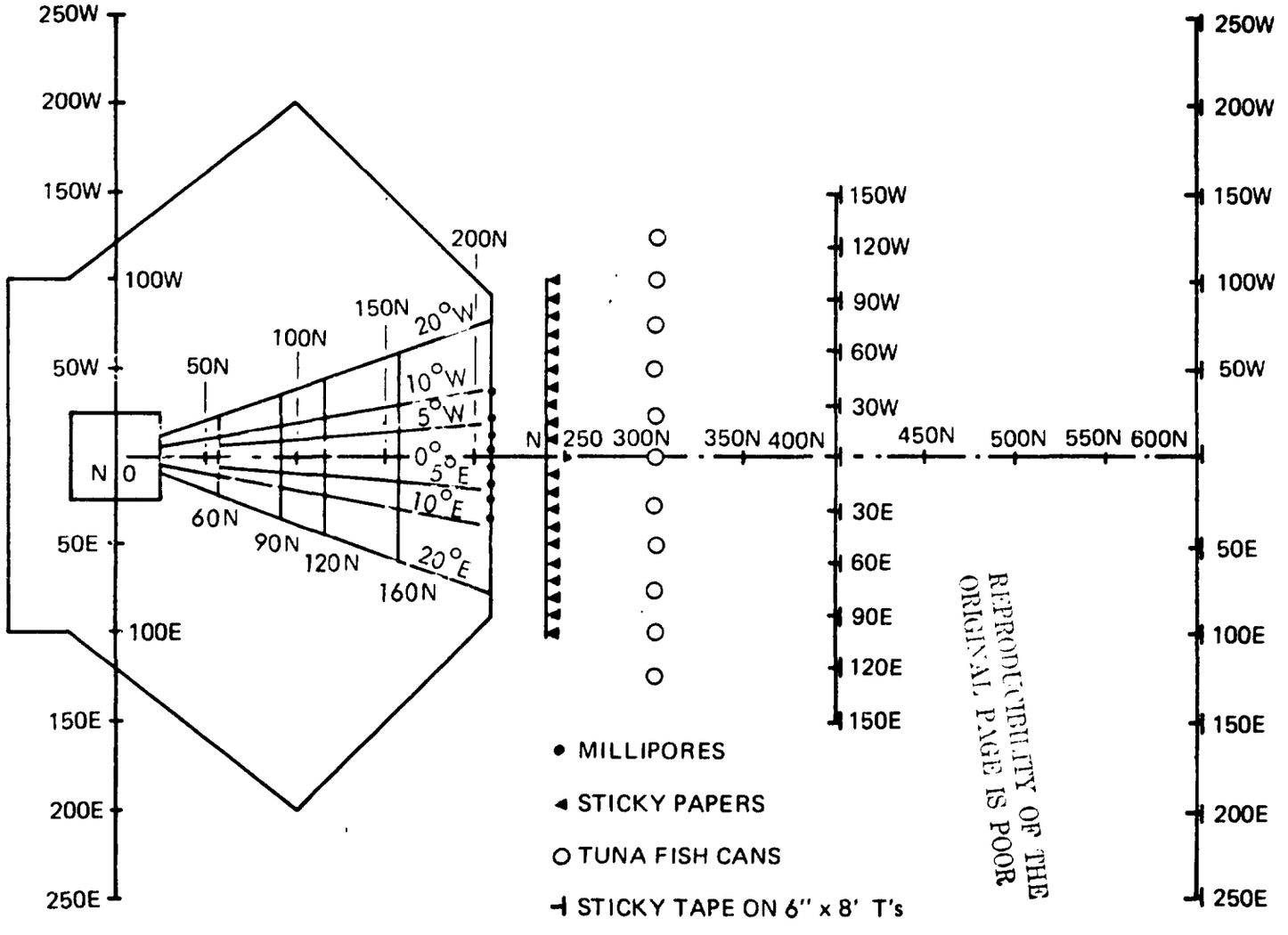

Figure 4.7. Passive Instrumentation Layout for Plate Tests 5 and 6

Figure 4-8. Representative Sticky Paper Record

PLATE TEST 1

PLATE TEST 2

PLATE TEST 3

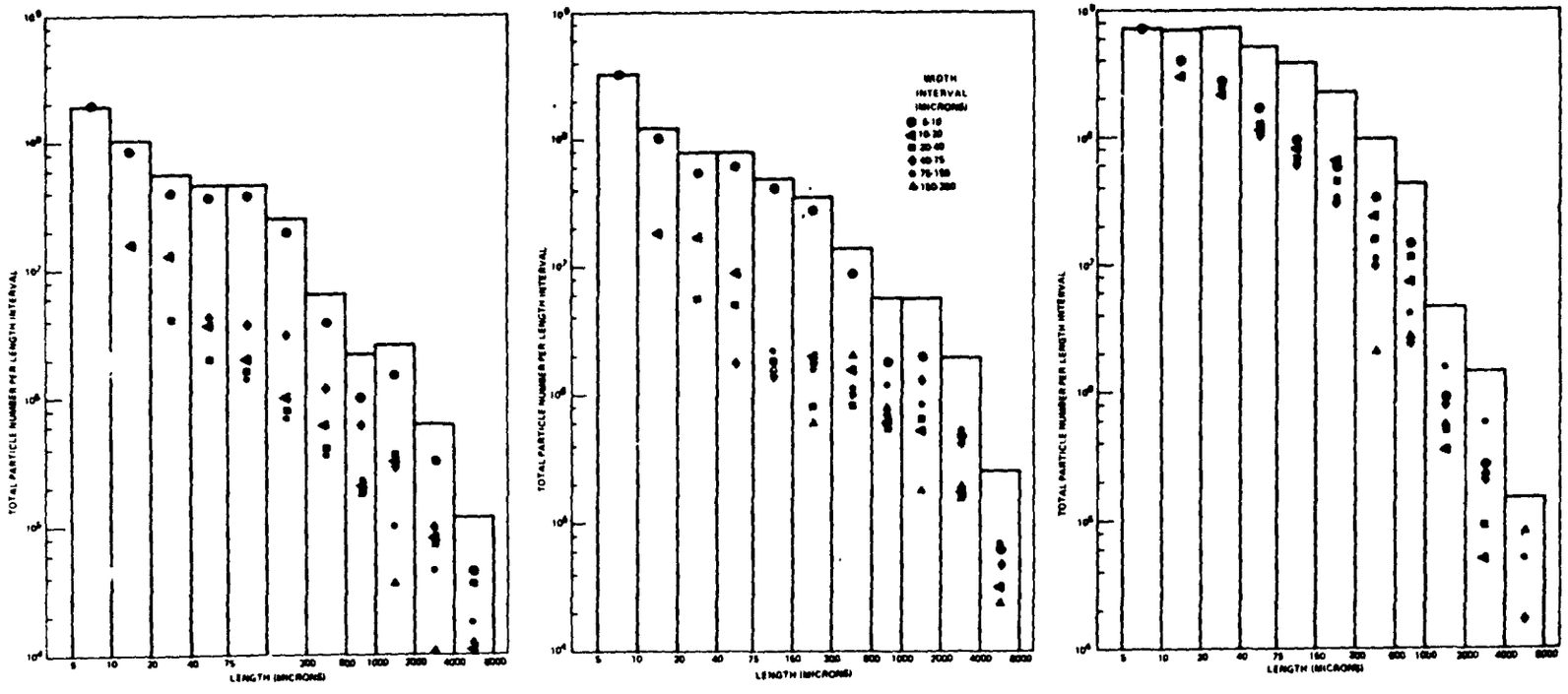

Figure 4.9. Plate Tests 1, 2 and 3 - Comparison of Particle Number Distribution

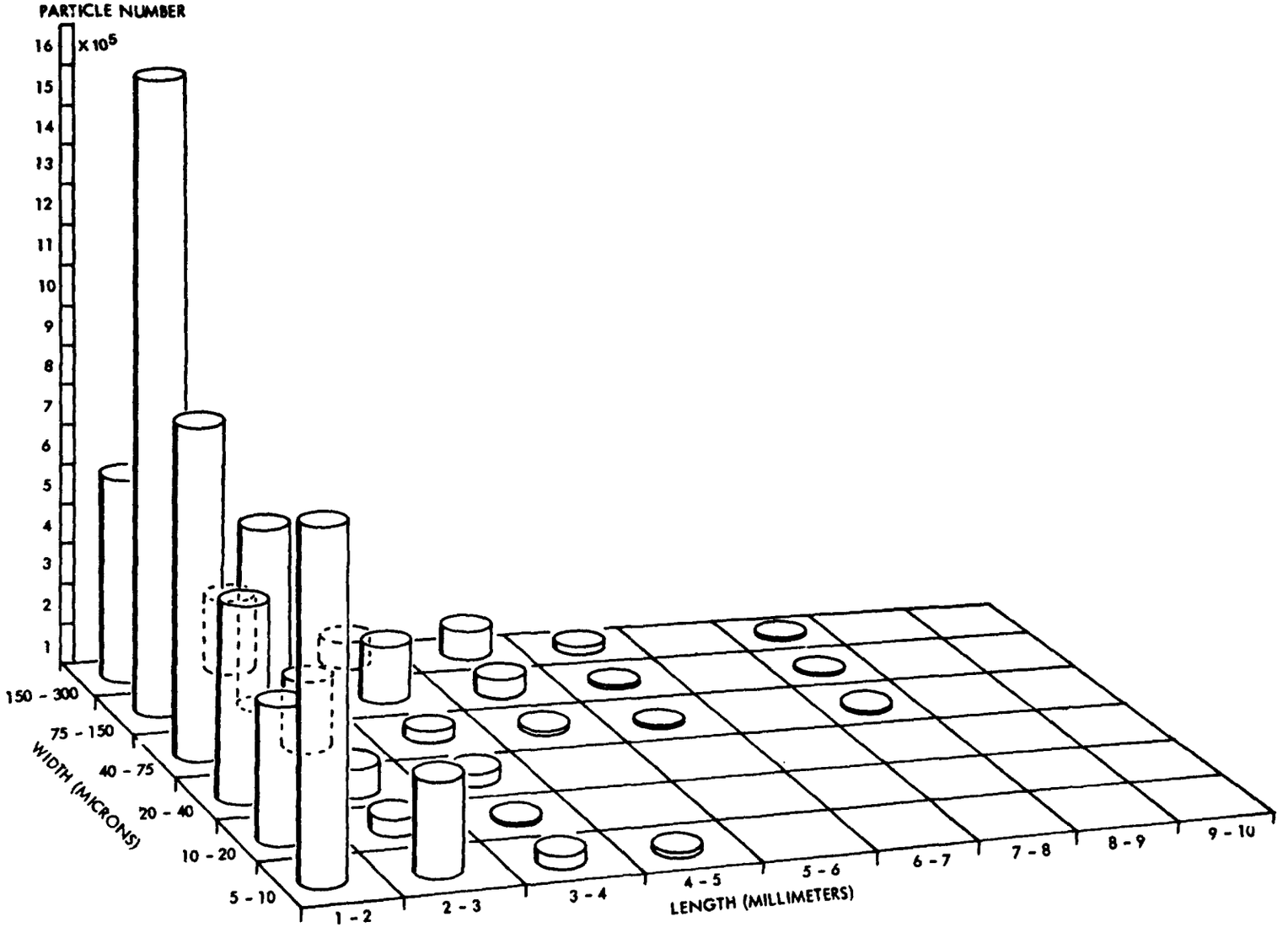

Figure 4.10. Plate Test 3 - Particle Number Distribution

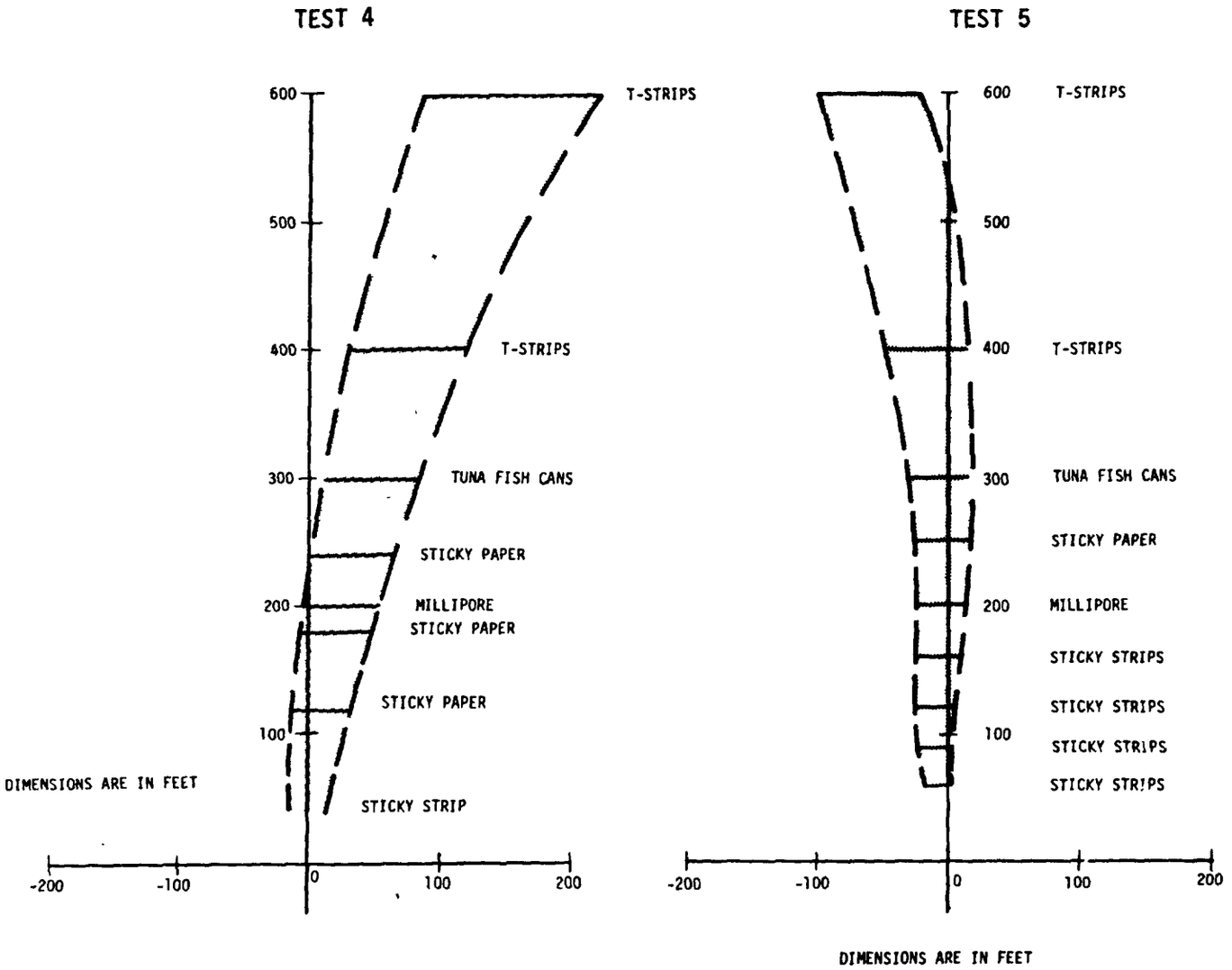

Figure 4.11. Mass Deposition Footprint for NWC Plate Tests 4 and 5

various width domains. A plot of the data for Test 3 corresponding to the length interval of 1 to 10 mm is shown in Figure 4.10.

Particle deposition footprints for Tests 4 and 5 are indicated in Figure 4.11 as determined from the data envelopes reflected by the various types of instrumentation records. Variations in the wind direction during the course of propagation of the particulate cloud are readily apparent. Extensive instrumentation arrays were necessary in order to ensure adequate data acquisition in anticipation of unpredictable vagaries of the wind direction.

Figure 4.12 indicates the particle number distribution obtained with the vertical array of millipore gages (47 mm diameter) covering a region of about 75 ft wide and 30 ft high at a distance of 200 ft from ground zero. The circled values represent particle numbers observed for the gages at the designated location. Multiplication of these values by a factor of 53.5 yields an estimate of the corresponding particle density per square foot. High density values of about 1000 particles/sq ft are noted at 10 to 12 ft west and at a height of 10 ft. Singular high density regions ranging from 1500 to 2000 particles/sq ft occur at elevations of 20 to 30 ft and ranges of 12 to 18 ft west.

Millipore sensor arrays were located at a range of 200 ft during Tests 4 and 5. Although a detailed quantitative evaluation was not performed, it appeared that the particles collected by the millipore filters were generally of lengths smaller than 1 mm, with only a relatively small percentage of greater lengths. The possibility cannot be discounted that data of this nature were an accurate representation of the particle length distribution within the cloud segment that had propagated across the millipore collector network. A careful evaluation of the effectiveness of the millipore gages field test conditions was not possible.

Since some uncertainty developed regarding the efficiency of the millipore instrumentation which could not be resolved within the time frame of interest, and since attention was being focused principally on particles in the 1 to 20 mm length domain, it appeared advisable to replace the millipore sensors (47 mm) by the tuna can gages (8.26 cm) at 200 ft range in Test 8 in order to increase the collector cross-section by a factor of about 1.8 and area by a factor of about 3.1. This arbitrary judgement for the field test considerations of interest was not intended to undermine confidence in the millipore instrumentation for this application. Studies would be required to determine the range of effectiveness of millipore sensors for specific test conditions and data requirements.

Gaussian approximations of azimuth and range variations for the Test 5 sticky paper data yielded the particle density distribution shown in Figure 4.13 over particle length intervals of 1 to 20 mm. For a constant azimuth of 5^{o} west the detailed density variations with range for specific particle length and width intervals are plotted in Figure 4.14. The data appear to indicate that the magnitudes to a first order extent are relatively constant over the range of 60 to 200 ft and that predominant lengths are in the 1 to 3 mm interval and predominant widths in the 5 to 10 micron (singles) and 70-300 micron domains.

The test conditions for Tests 5 and 6 were identical with the exception of the wind direction. The deposition footprint for Test 5 fell within the bounds of the instrumentation array as shown in Figure 4.11. However, due to a sudden change in wind direction at shot time, the Test 6 footprint propagation axis was predominantly 20^{o} west with relatively narrow dispersion in azimuth. Therefore a good set of sticky paper data was obtained principally along the 20^{o} W strip.

Estimates of the particle density variation along the path of maximum densities were determined for Test 5. Comparison of this data with the singular density values along 20^{o}W for Test 6 is shown in Figure 4.15. In general the patterns from 60 to 200 ft are in reasonably good agreement. An interesting manifestation of the Test 6 data is the appearance of two high density regions at 20 and 80 ft with a reduction by a factor of about 20 at 50 ft. It is quite possible that there are two segments of the particulate cloud such that close-by dispersion and subsequent propagation may be attributed to different phenomena.

MASS ESTIMATES

Integration of the sticky paper data for Test 5 over the deposition footprint area from 60 to 600 ft yielded the total particle number spectrum shown in Table 4.1. Corresponding estimates of particle mass are presented in Table 4.2. A comparative plot of the number and mass distribution is given in Figure 4.16. Although a relatively significant number of singles occur, the associated mass estimates are essentially negligible.

It is interesting to note that the particle number distributions for Test 3 in Figure 4.10 and Test 5 in Figure 4.16 are very similar. Comparable agreement occurred for the mass estimates. It appears reasonable to conclude that the chamber test offered a good simulation of the field test conditions in the particulate source generation.

Data reduction techniques for sticky paper records permit observation of only length and width parameters such that some approximations are required in order to establish mass estimates. Figure 4.17 indicates a number of representative profiles. Judgement factors are required even in establishing appropriate width values. With reference to thickness limitations measurements relative to large samples of post-test debris yielded an upper limit generally of the order of 150 microns which corresponded to the thickness of a single ply.

It appears that during the burn phase depolymerization occurs more readily for the interstitial resin than for the resin contained in close proximity to the fiber matrix in a single ply and thereby resulting in single ply pancake layering prior to the explode phase. The plate sample was 0.25" thick and consisted of 40 ply of T-300/5208 graphite composite.

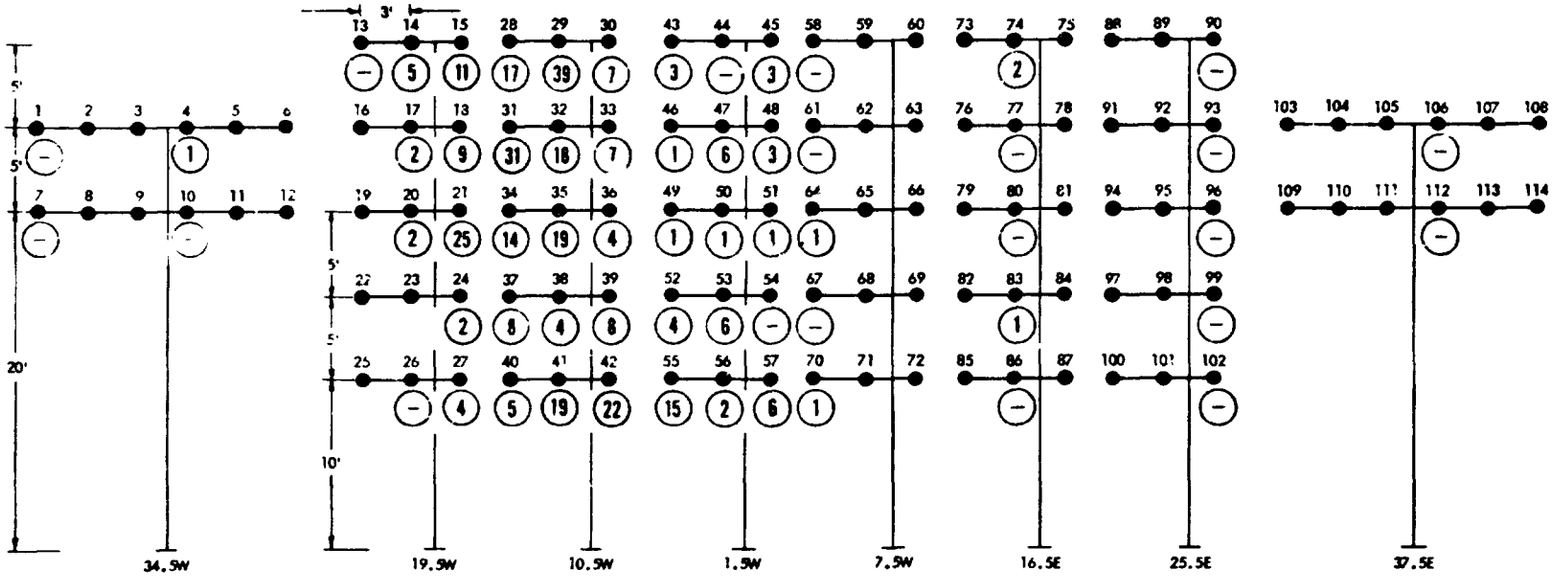

Figure 4.12. Plate Test 5 - Millipore Gage Particle Number

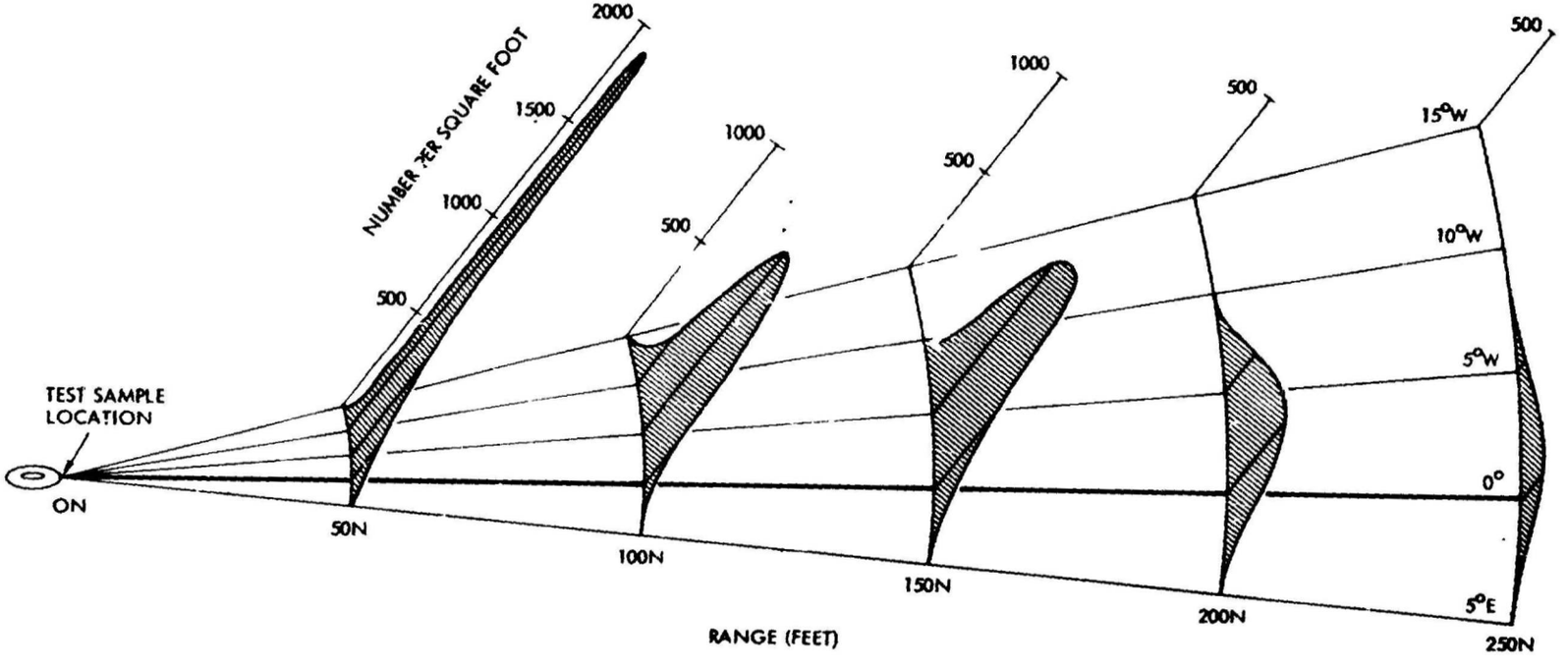

Figure 4.13. Plate Test 5 - Particle Density Distribution

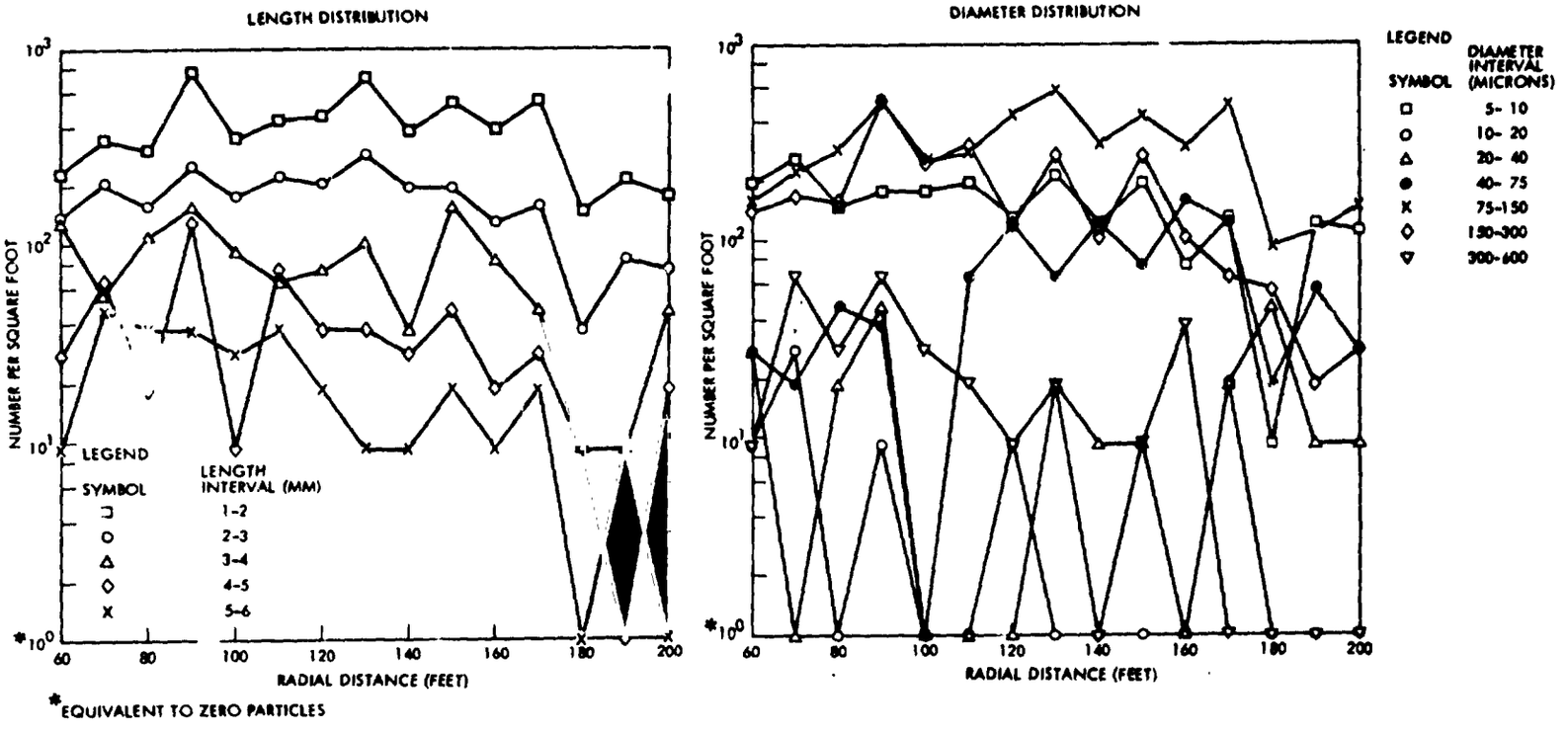

Figure 4.14. Plate Test 5 - Particle Density vs Range for Azimuth of 5 Degrees West

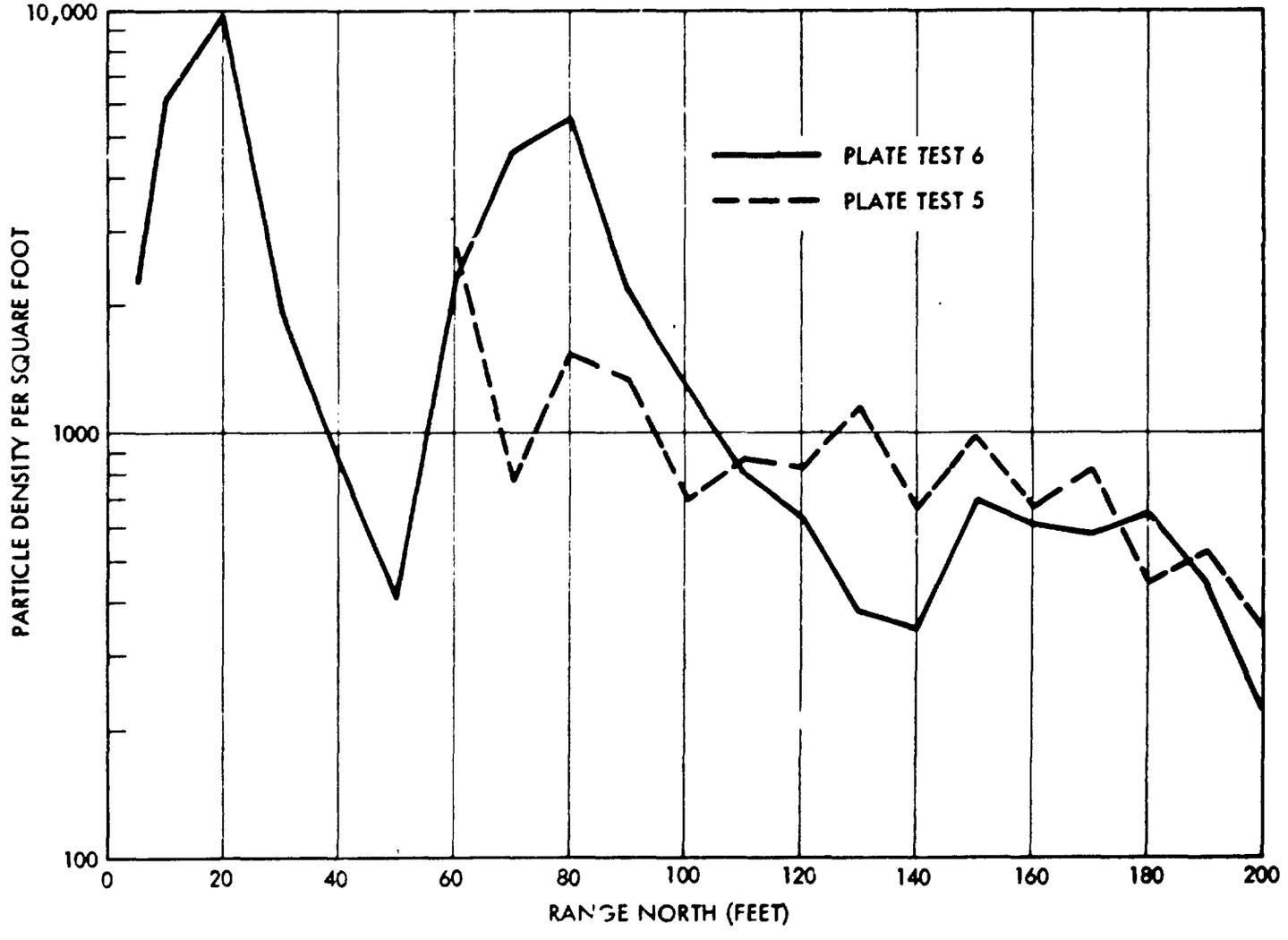

Figure 4.15. Plate Tests 5 and 6 - Comparison of Particle Density vs Range

Table 4.1. Plate Test 5 - Particle Number Spectrum

PLATE TEST 5(NUC2)

PARTICLE WIDTH IN MICRONS FOR EACH LENGTH SIZE(MM)

LENGTH INTERVAL (MM)	SIZE 5-10	SIZE 10-20	SIZE 20-40	SIZE 40-75	SIZE 75-150	SIZE 150-300	SIZE 300-600	SIZE 600-1250	NT
1-2	3.99E+05	1.36E+04	6.88E+04	4.47E+05	8.18E+05	2.02E+05	9.45E+03	0.	1.96E+06
2-3	1.27E+05	1.38E+03	2.12E+04	1.00E+05	3.06E+05	1.26E+05	4.42E+03	0.	6.86E+05
3-4	7.78E+04	1.05E+03	4.46E+03	3.19E+04	1.04E+05	1.03E+05	7.22E+03	0.	3.30E+05
4-5	2.66E+04	3.24E+03	1.48E+03	1.53E+04	6.02E+04	4.17E+04	4.99E+03	0.	1.54E+05
5-6	1.55E+04	1.34E+03	5.92E+03	3.63E+03	1.46E+04	3.27E+04	7.74E+03	0.	8.15E+04
6-7	3.93E+03	5.06E+03	0.	1.42E+03	2.00E+04	8.35E+03	1.78E+03	0.	4.05E+04
7-8	4.30E+03	0.	0.	0.	4.69E+03	1.22E+04	2.27E+03	0.	2.35E+04
8-9	3.61E+03	0.	0.	0.	6.08E+02	7.68E+03	5.67E+03	0.	1.76E+04
9-10	4.80E+03	0.	0.	0.	2.43E+02	6.08E+02	2.23E+03	0.	7.88E+03
10-11	0.	0.	0.	0.	1.66E+03	1.34E+03	8.51E+02	2.43E+02	4.09E+03
11-12	9.32E+02	0.	0.	0.	1.99E+03	1.28E+03	6.08E+02	0.	4.81E+03
12-13	0.	0.	0.	0.	4.82E+03	1.26E+03	1.26E+03	0.	7.33E+03
13-14	1.18E+03	0.	0.	0.	0.	7.70E+02	8.51E+02	0.	2.80E+03
14-15	8.51E+02	0.	0.	0.	0.	0.	1.26E+03	0.	2.11E+03
15-16	1.46E+03	0.	0.	0.	2.43E+02	0.	0.	0.	1.70E+03
16-17	2.43E+02	0.	0.	0.	0.	0.	0.	0.	2.43E+02
17-18	0.	0.	0.	0.	0.	1.91E+03	7.70E+02	0.	2.68E+03
18-19	0.	0.	0.	0.	0.	0.	0.	0.	0.
19-20	0.	0.	0.	0.	0.	0.	0.	0.	0.
NT	6.67E+05	2.57E+04	1.02E+05	6.00E+05	1.34E+06	5.41E+05	5.14E+04	2.43E+02	

TOTAL NUMBER OF PARTICLES IS 3.32E+06

Table 4.2. Plate Test 5 - Particle Mass Spectrum

PLATE TEST 5(NWC2)

PARTICLE WIDTH IN MICRONS FOR EACH LENGTH SIZE(MM)

LENGTH INTERVAL (MM)	SIZE 5-10	SIZE 10-20	SIZE 20-40	SIZE 40-75	SIZE 75-150	SIZE 150-300	SIZE 300-600	SIZE 600-1250	NT
1-2	4.91E-02	4.48E-03	9.20E-02	2.07E+00	1.21E+01	9.34E+00	8.66E-01	0.	2.45E+01
2-3	2.70E-02	9.24E-04	3.16E-02	7.87E-01	7.55E+00	8.79E+00	5.96E-01	0.	1.78E+01
3-4	2.40E-02	5.57E-04	7.46E-03	2.65E-01	3.50E+00	1.17E+01	1.42E+00	0.	1.69E+01
4-5	1.16E-02	1.54E-03	1.55E-03	1.83E-01	3.02E+00	6.80E+00	2.81E+00	0.	1.28E+01
5-6	7.23E-03	6.12E-04	1.22E-02	5.94E-02	8.05E-01	5.49E+00	2.42E+00	0.	8.79E+00
6-7	2.28E-03	3.39E-03	0.	2.69E-02	1.78E+00	1.69E+00	7.53E-01	0.	4.26E+00
7-8	2.90E-03	0.	0.	0.	3.29E-01	2.16E+00	8.75E-01	0.	3.37E+00
8-9	2.60E-03	0.	0.	0.	6.08E-01	2.69E+00	2.73E+00	0.	6.02E+00
9-10	3.98E-03	0.	0.	0.	3.49E-02	2.09E-01	1.33E+00	0.	1.57E+00
10-11	0.	0.	0.	0.	5.34E-02	3.65E-01	6.95E-01	2.68E-01	1.38E+00
11-12	9.17E-04	0.	0.	0.	3.50E-01	3.64E-01	4.93E-01	0.	1.21E+00
12-13	0.	0.	0.	0.	8.49E-01	7.58E-01	1.15E+00	0.	2.76E+00
13-14	1.41E-03	0.	0.	0.	0.	4.32E-01	5.11E-01	0.	9.44E-01
14-15	1.06E-03	0.	0.	0.	0.	0.	1.13E+00	0.	1.13E+00
15-16	1.99E-03	0.	0.	0.	3.75E-02	0.	0.	0.	3.95E-02
16-17	3.49E-04	0.	0.	0.	0.	0.	0.	0.	3.49E-04
17-18	0.	0.	0.	0.	0.	7.70E-01	7.94E-01	0.	1.56E+00
18-19	0.	0.	0.	0.	0.	0.	0.	0.	0.
19-20	0.	0.	0.	0.	0.	0.	0.	0.	0.
NT	1.35E-01	1.15E-02	1.45E-01	3.39E+00	3.10E+01	5.16E+01	1.86E+01	2.68E-01	

TOTAL MASS OF PARTICLES IS 1.05E+02 GRAMS

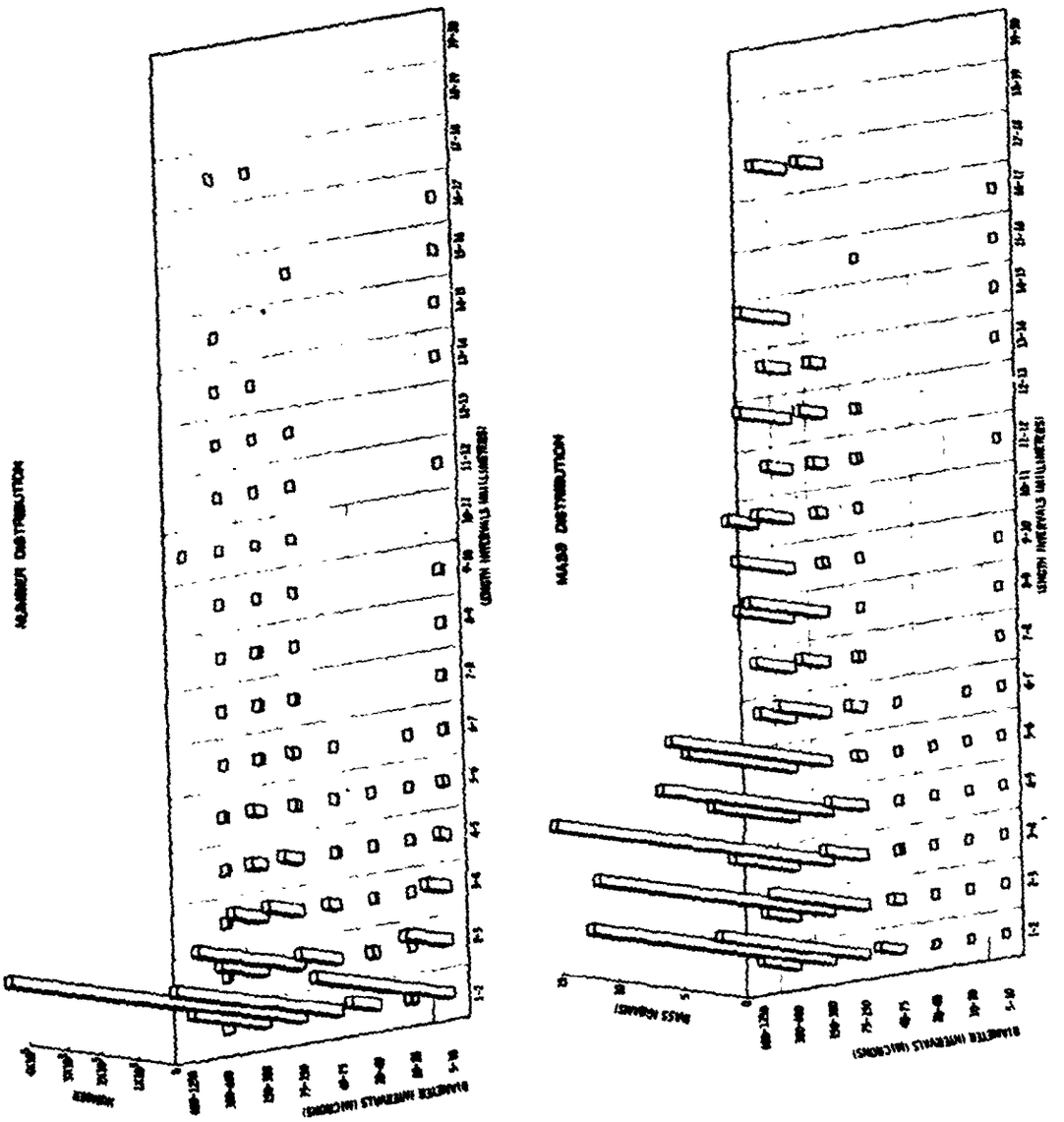

Figure 4.16. Plate Test 5 - Comparison of Number and Mass Distributions

Based on the foregoing considerations, mass estimates were determined by the following approximations:

(a) Assume cylindrical cross-section for widths less than 150 microns, with mass given by:

$$M = \frac{\pi}{4} w^2 L \rho S$$

where M = particle mass
w = maximum particle width
L = maximum particle length
ρ = mass density (1.6 gm/cc)
S = shape factor

The shape factor is defined by:

$$\text{Shape Factor} = \frac{\text{Observed Particle Area}}{\text{Maximum Length x Maximum Width}}$$

with average values over most of the data generally about 0.6.

(b) Assume that when the widths are of a magnitude of 150 microns or greater the thickness has reached a constant upper limit of 150 microns such that the cross-section is rectangular, with mass given by:

$$M = 1.5 \times 10^{-4} \, w \, L \, \rho \, S$$

A comparison of the ratio of particle mass relative to initial sample mass between Tests 3 and 5 is shown in Figure 4.18 for particles in the length interval of 1 to 20 mm. Reasonably good agreement is observed for the total mass particulate as well as for the mass of single fibers only.

The mass of singles for Test 3 corresponding to fiber lengths of less than 1 mm was estimated to be 4.0 gm or about 0.46% of the initial mass of 873 gm.

Figure 4.19 indicates a comparison of single fiber mass estimates as reported by the Naval Surface Weapons Center in relation to the TRW results of Tests 3 and 5. The test sample for the NSWC chamber test and TRW chamber and field tests were in all cases T300/5208 plates, 12" x 12" x 1/4" in dimensions and 40 ply, with similar initial mass and burn times of 20 minutes.

The NSWC test data indicated the single fiber mass as 1.78% of the initial mass, whereas the TRW results were a factor of about 100 times lower with 0.01% for Test 3 and 0.008% for Test 5.

The data reduction technique for the NSWC records was a line intersection counting procedure for single fibers developed by Dr. John Trethewey at the Dugway Proving Ground. The TRW approach was direct counting by means of various optical aids.

Figure 4.17. Plate Test 5 - Representative Particle Profiles

LENGTH INTERVAL (MM)	TOTAL PARTICLE MASS / INITIAL SAMPLE MASS (1)		SINGLE FIBER MASS / INITIAL SAMPLE MASS (1)	
	TEST 3(2)	TEST 5(3)	TEST 3(2)	TEST 5(3)
1 – 2	6.4%	2.8%	0.006%	0.003%
2 – 5	7.8%	5.4%	0.004%	0.004%
5 – 10	1.5%	2.7%	–	0.001%
10 – 20	3.5%	1.1%	–	–
TOTAL	19.2%	12.0%	0.01%	0.008%

(1) INITIAL SAMPLE MASS: TEST 3 – 873 GM; TEST 5 – 873 GM
(2) TRW CTS FACILITY
(3) NWC TEST SITE

Figure 4.18. Plate Test 3 and 5 - Ratio of Particle Mass Relative to Initial Sample Mass

TEST	SITE	AREA	SAMPLE	INITIAL MASS (GM)	DATA REDUCTION TECHNIQUE	TOTAL NUMBER (2)	AVERAGE LENGTH (MM)	TOTAL MASS (2) (GM)	FRACTION OF INITIAL MASS
BT 60/X-37	NSWC	24'X 35'	PLATE (1)	947	NEEDLE INTERSECTION COUNTING (MICROSCOPE)	5.6×10^7	3.19	16.9	1.78%
3	TRW/CTS	15'X 15'	PLATE (1)	873	DIRECT COUNTING (MICROSCOPE)	2.1×10^6	2.32	0.08	0.01%
5	NWC	50 TO 600 FEET RANGE	PLATE (1)	873	DIRECT COUNTING (MICROFICHE VIEWER)	6.6×10^5	2.36	0.07	0.008%

(1) COMPOSITE T300/5208, 40 PLY, 12 X 12 X 1/4 IN., BURN TIME 20 MIN.

(2) SINGLE FIBERS WITH LENGTHS OF 1 TO 20 MM

Figure 4-19. Comparison of Single Fiber Mass Estimates

A relative evaluation between the two techniques was performed recently based on a specified set of NSWC chamber test records being analyzed for single fibers only initially at Dugway and subsequently at TRW. Comparison of results by TRW and Dugway in December 1978 indicated that the Dugway line intersection technique yielded number values consistently greater by a factor of about 2 to 3 than obtained at TRW by the direct counting method, with length values quite similar. A modification suggested by TRW of reducing the line widths of the Dugway reference grids may lead to some reduction of the Dugway values and thus bring the single fiber counting results into even better agreement. It therefore appears reasonable to conclude that the two data reduction techniques are in substantial agreement.

At the present time there is no apparent explanation for the discrepancy by a factor of about 100 in single fiber mass indicated by the NSWC and TRW data presented in Figure 4.19.

BARREL TESTS

INSTRUMENTATION LAYOUT

The sticky paper array on the test pad for Test 8 consisted of 8" x 10" sheets located at 10 ft spacing from 10'N to 200'N over an azimuth range of 25^{o}W to 25^{o}E at 5^{o} intervals. At 240', 400' and 600' North, the sticky paper distribution was similar to earlier tests at NWC. Three series of tuna can poles were were located 200', 285' and 600' North.

For Tests 9 and 10 the sticky paper sheets on the test pad were spaced at 20 ft over azimuths of 20^{o}W to 20^{o}E at 10^{o} intervals. In addition to the unmodified sticky paper distribution at 240', 400' and 600' North, rows of fifty 6" x 8' sticky paper strips spaced 50 ft apart were located at 1000', 1500', 2000' and 3000' North. Tuna can vertical arrays were not included. Bridal veil gages mounted on 9' x 10' frames spaced 100' apart were introduced at 6000' N extending from 1500'W to 1500'E.

TEST RESULTS

Two singular characteristics were observed in the data reduction of the Test 8 records in that (1) a large number of particle clusters had been generated and (2) the frequency of occurrence of single fibers was generally about 80 to 90 percent of the total particulate.

Figure 4.20 portrays the nature of cluster particulate observed in the sticky paper sheets located along the 10^{o}E radial direction. The clusters are wispy in appearance resembling conglomerations of large numbers of single fibers with very little evidence of resin residue. The distribution of cluster width and length dimensions observed on the test pad records is plotted in Figure 4.21. Sizes ranged from about 1 to 9 cm in length and 0.25 to 5 cm in width.

Reduction of the Test 8 sticky paper records indicated the single fiber density distribution shown in Figure 4.22. In general, the total number of particles for the barrel sample of Test 8 was quite comparable to the results of Test 5 for the plate sample.

Figure 4.23 shows a representative tune can record (1 mm mesh) at a range of 200' and elevation of 27' indicating the high percentage of single fibers and the presence of a particle cluster. The single fiber density distribution at 200' range is presented in Figure 4.24. Integration over the entire network yields a cumulative particle total of 6.22×10^6. Based on a mean diameter of 5.2 microns and mean length of 3.2 mm the mass of single fibers integrated over the tuna can array at 200 ft range is estimated as 0.76 gm. It is evident from the particle density distribution shown in Figure 4.24 that some unascertainable portion of the fiber cloud extended above and to the east of the 30 ft tune can network. The total extent of the cloud is uncertain as well as the question whether cloud formation had developed in multiple modes.

Single fiber distributions integrated over the tuna can networks at 200', 285' and 600' range are plotted in Figure 4.25 as a function of fiber length intervals. Integration over the respective contours yields the following results:

Range	Total Particle Number
200 ft	6.22×10^6
285 ft	1.41×10^6
600 ft	0.68×10^6

The attenuation with range of the total particle number may be attributed to normal cloud dispersion and fallout attrition, although some influence may have been exerted by variations in cloud directions due to changes in wind vectors.

Figure 4.26 indicates the relative frequency of occurrence of single fibers as related to length interval. The average length for the distribution is 3.20 mm.

During Test 8 the barrel sample had been subjected to a hot propane burn for 20 minutes followed by initiation of a high explosive charge. The barrel sample of Test 9 was placed at a height of several feet above a JP-5 pool fire and subjected to sequential burns of 3 minutes and 6 minutes. In the case of Test 10, the barrel sample was located in a JP-5 pool fire for 5 minutes and then subjected to an HE explosion.

Sudden unfavorable wind conditions precluded acquisition of any data over the extensive distribution of sticky paper gages for both Tests 9 and 10. Visual post-test inspection on the test pad and outlying areas east of the test pad on Test 10 indicated that a new type of particulate in the form of thin laminar strips had been generated of a nature not observed during the earlier tests. The general strip deposition locations for Test 10 are shown in Figure 4.27 although a comprehensive effort to map the deposition region and accumulate the strips for further study had not been initiated.

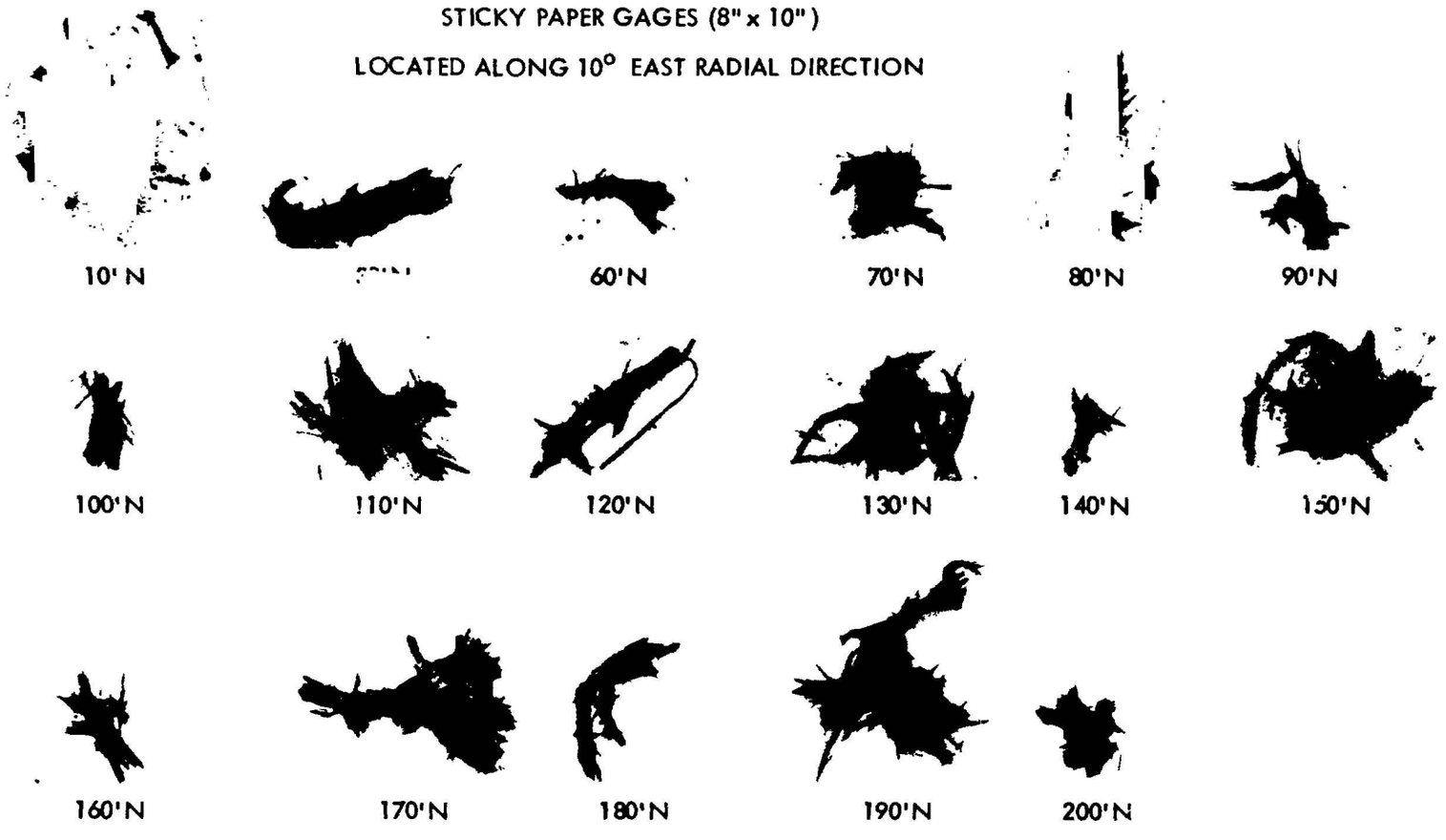

Figure 4.20. Barrel Test 8 - Cluster Particulate

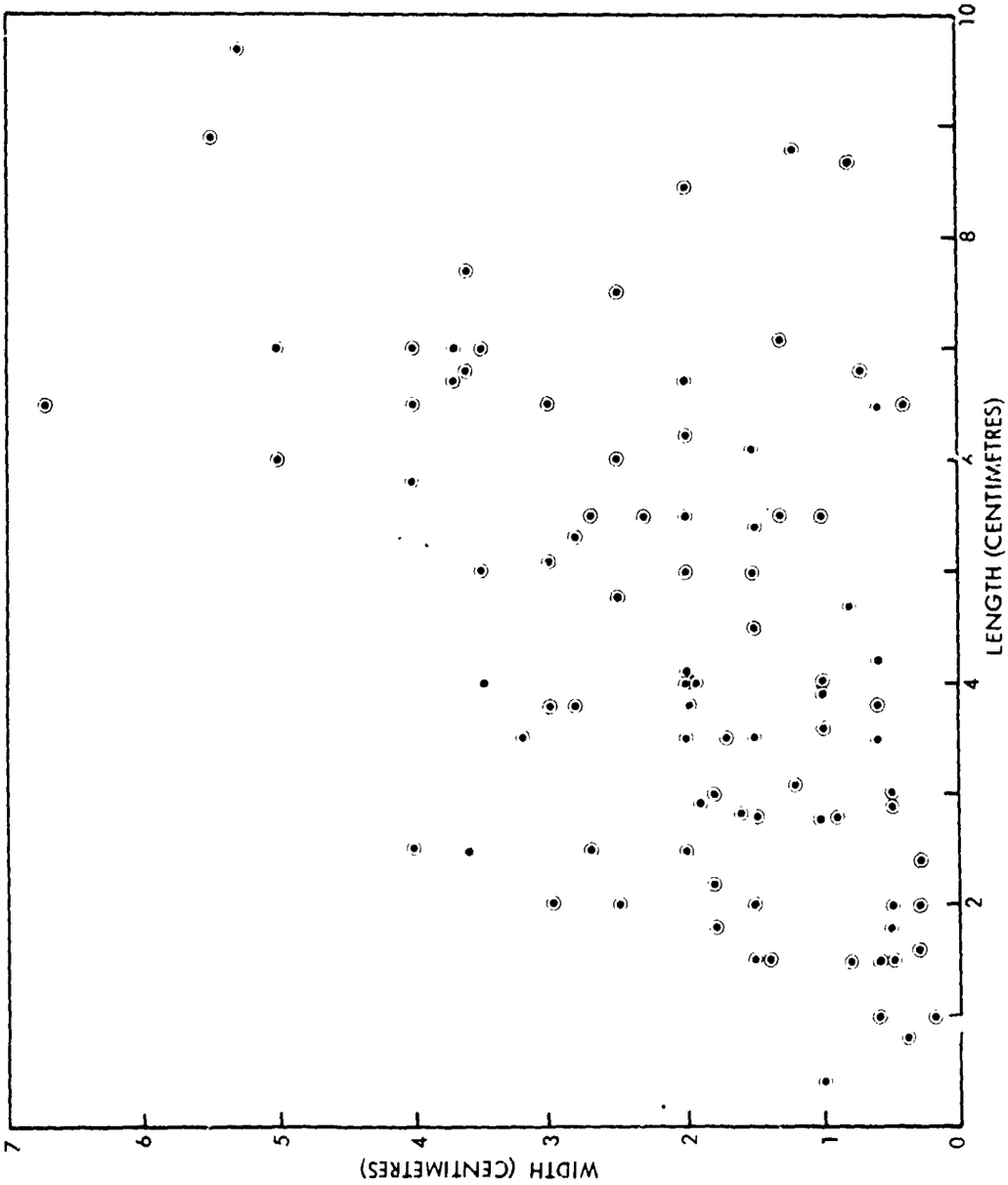

Figure 4.21. Barrel Test 8 - Cluster Dimension Distribution

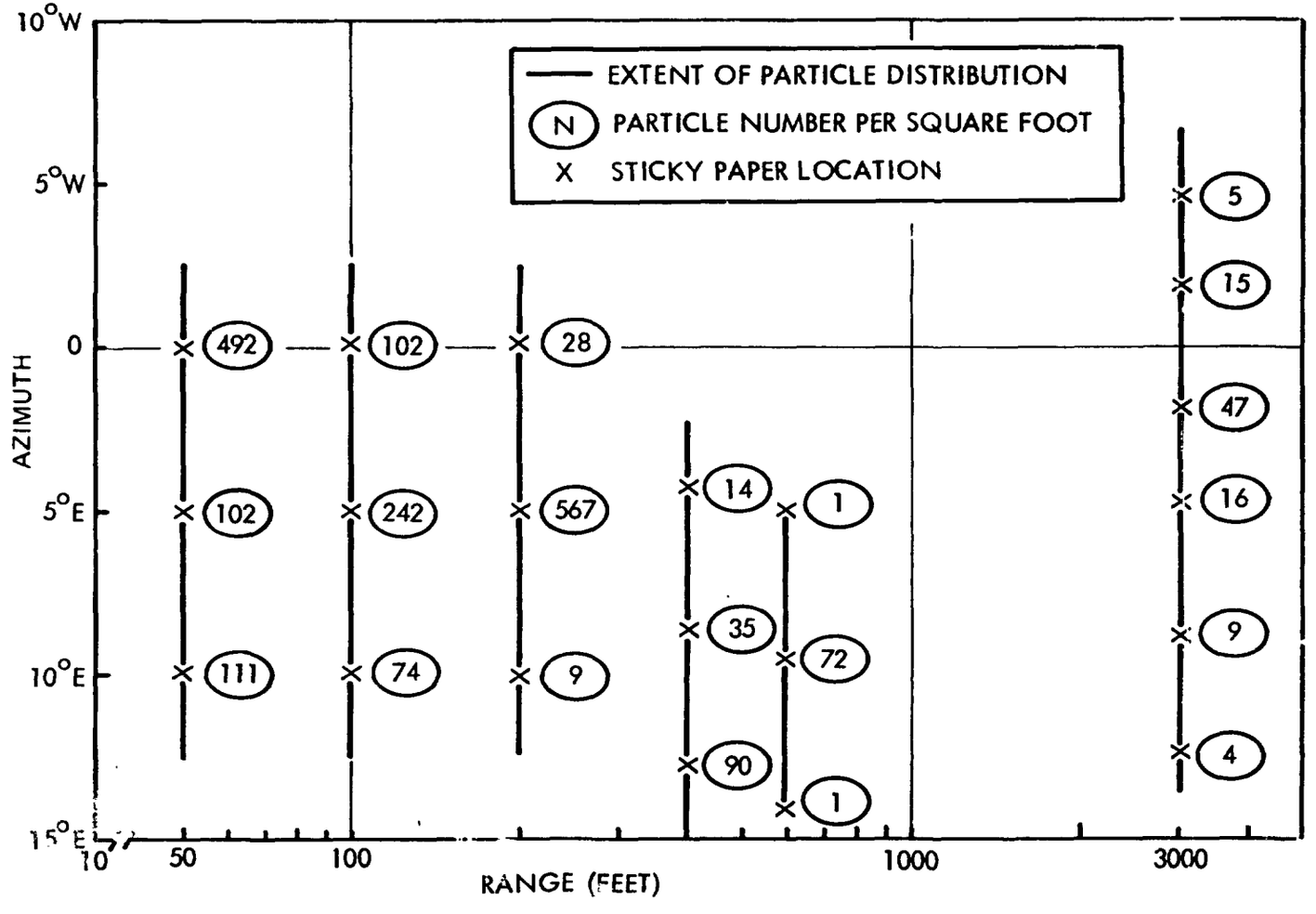

Figure 4 . Barrel Test 8 - Single Fiber Distribution Based on Sticky Paper Data

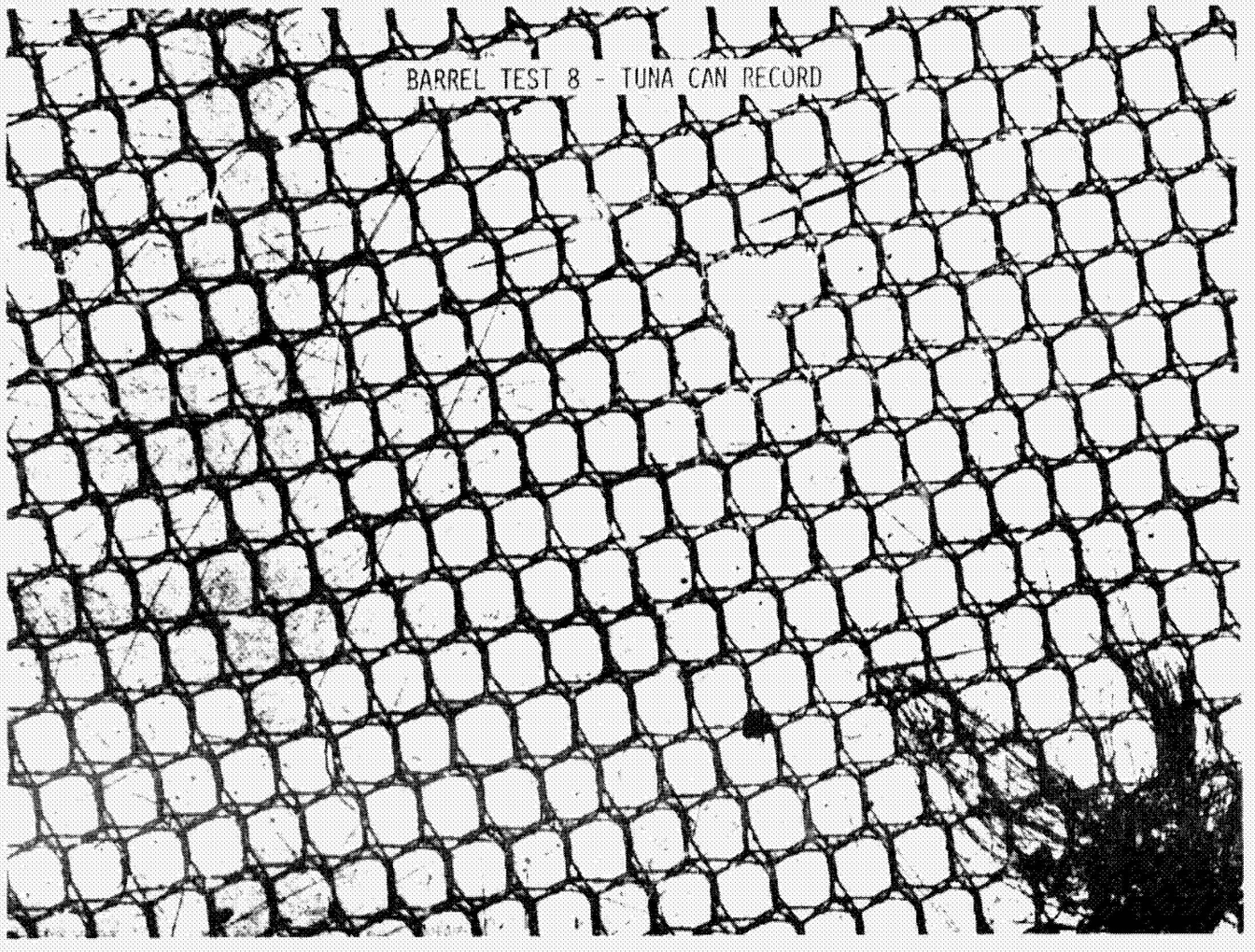

Figure 4-23. Barrel Test 8 - Tuna Can Record

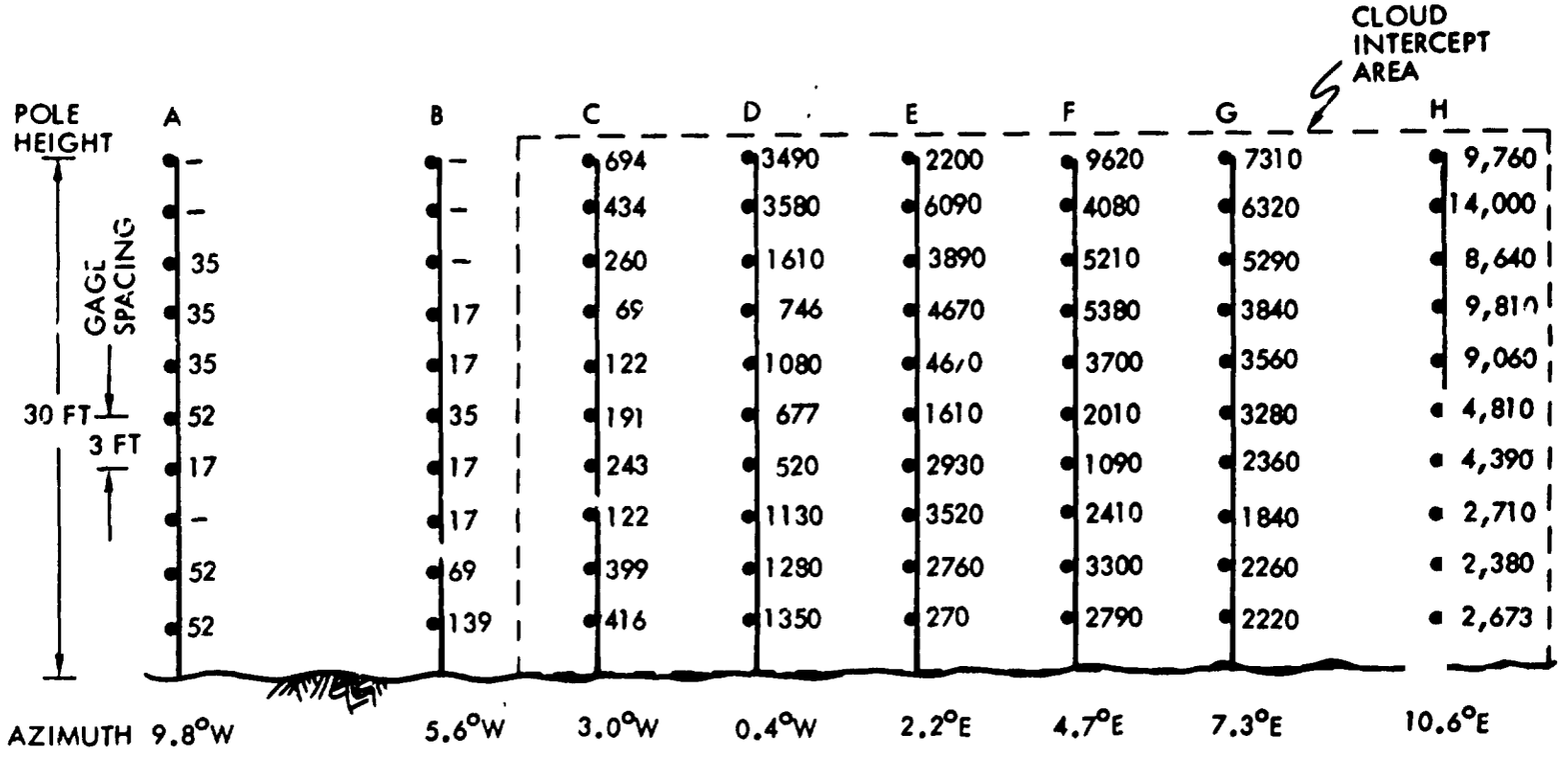

Figure 4.24. Barrel Test 8 - Single Fiber Number per Square Foot at 200 ft Range

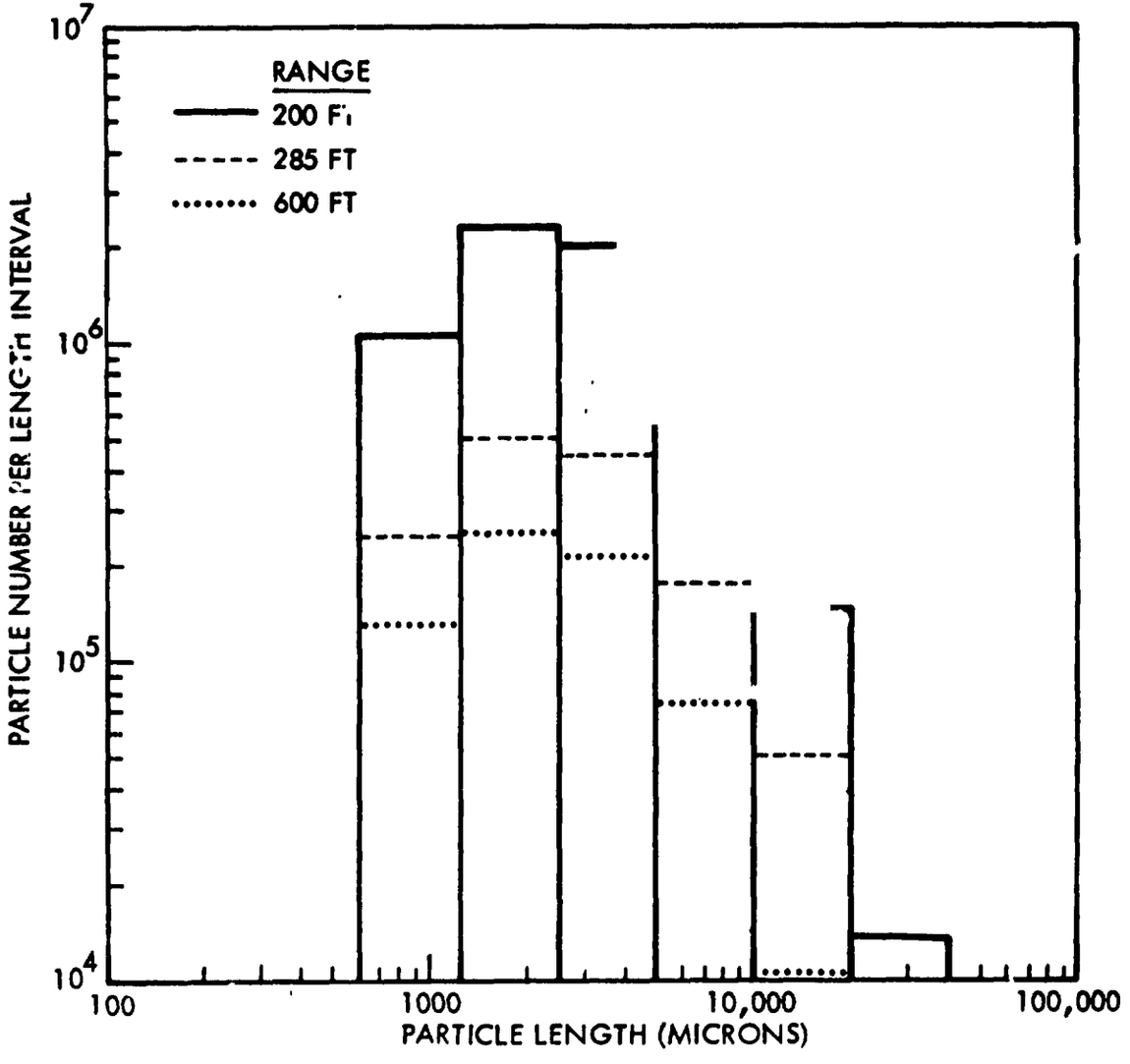

Figure 4.25. Barrel Test 8 - Single Fiber Distribution Over Tuna Can Network

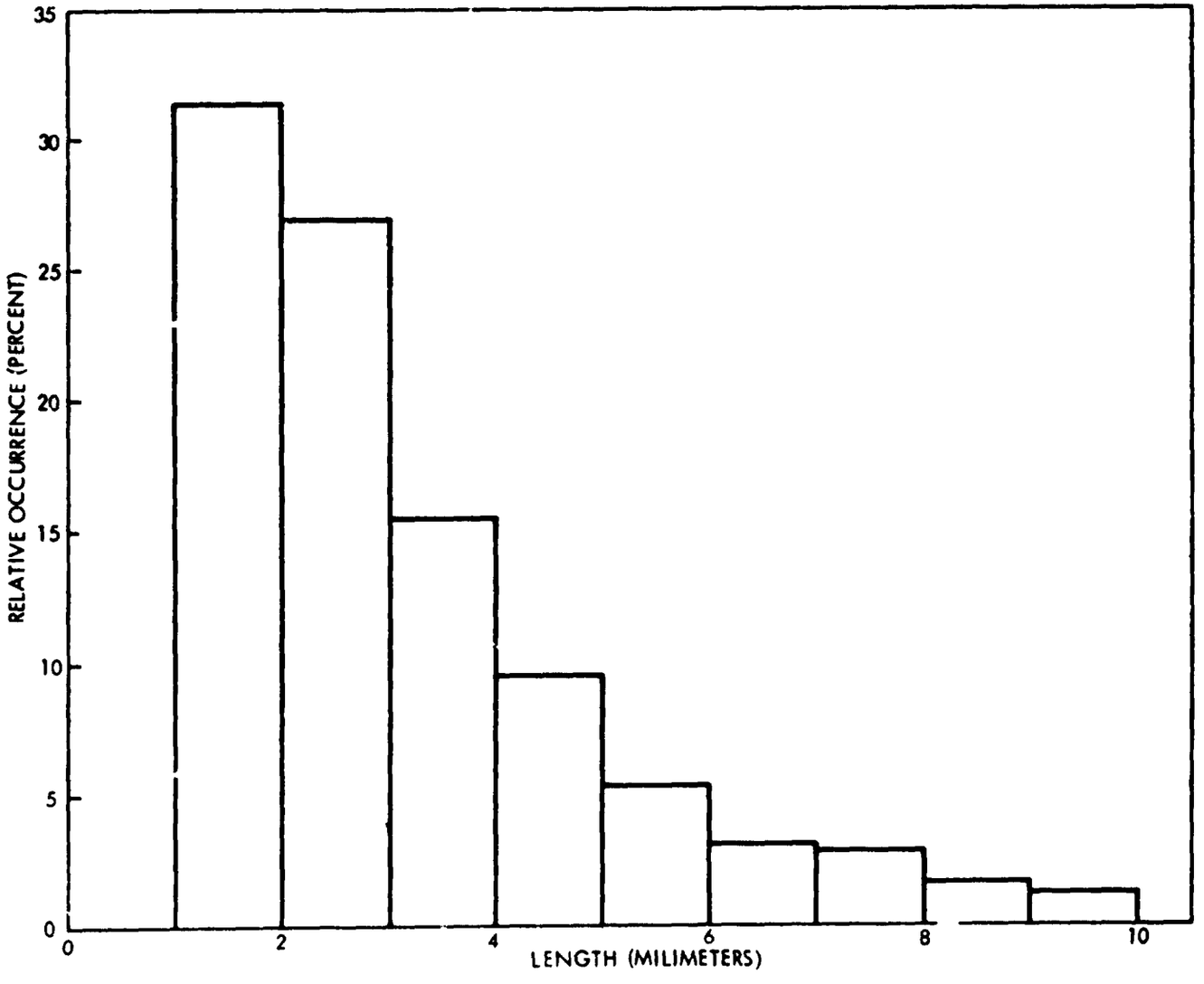

Figure 4.26. Barrel Test 8 - Single Fiber Length Distribution

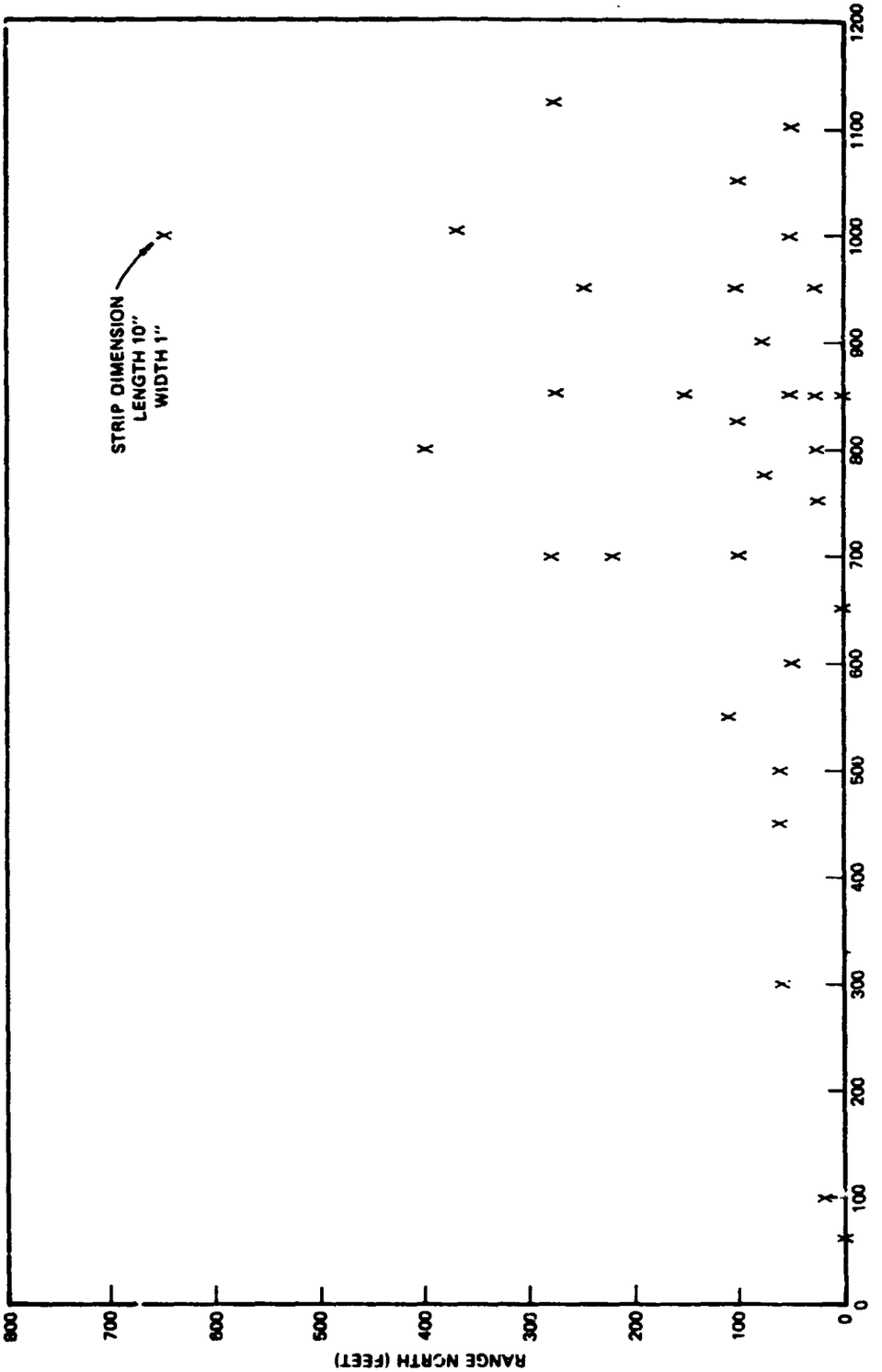

Figure 4.27. Barrel Test 10- Strip Deposition Locations

MASS ESTIMATES

Mass balance considerations for Test 8 are summarized in Figure 4.28. Of an initial sample mass of 9230 gm about 40 percent, or 3690 gm, constituted fiber mass. The post-burn sample mass was 575 gm indicating a loss of about 85 percent relative to the initial fiber mass assuming the residual resin mass was negligible in view of the predominance of single fibers in the test data.

It appears therefore that considerable oxidation of the AS fibers had taken place during the hot propane burn of 20 minutes. In addition, it was anticipated that the post-burn fibers would manifest a graduated reduction in fiber diameter depending on the individual degree of oxidation. By means of a metallograph, measurements were made of the single fiber diameters from pre-test samples and post-test tuna can records. The diameter distributions shown in Figure 4.29 clearly indicate the influence of oxidation effects.

With reference to the mass balance estimates of Figure 4.28 the total post-test mass distribution integrated over the deposition footprint out to 3000 ft range was determined to be about 120 gm. In relation to the post-burn mass of 575 gm it appears therefore that a differential mass of 455 gm need be accounted for.

SPOILER TESTS

INSTRUMENTATION LAYOUT

On the test pad a vertical array of 342 gages were distributed at 5 ft spacing along the nodal points of a 90'x90' Jacob's Ladder at 180'N as shown in Figure 4.30. The gages consisted of adhesive-coated bridal veil mounted on vugraph frames (7.5"x9.5"). A total of 111 sticky paper sheets were located on the test pad in the form of a rectangular array from 80'W to 40'E and from 30'N to 190'N. It is noted that the test sample or ground zero was located at 114'S 20'W with reference to the instrumentation coordinate system. The passive instrumentation layout beyond the test pad was similar to the distribution of Tests 9 and 10.

TEST RESULTS

Surface Deposition

The fallout particulate were only sparsely distributed throughout the entire sticky paper array. Figure 4.31 indicates the particle densities observed for ranges of 30' to 90' North, and the corresponding data for range of 240' to 3000'North are shown in Figure 4.32.

- PRE-TEST SAMPLE MASS — 9230 GM
- PRE-TEST FIBER MASS — 3690 GM
- POST-BURN SAMPLE MASS — 575 GM
- POST-EXPLODE MASS DISTRIBUTION
  - TEST PAD RESIDUE — 70 GM
  - CLUSTERS (10' - 200') — 0.24 GM
  - SINGLES (1 - 20 MM, 50 - 3000 FT) — 0.49 GM
  - CLUMPS (50 - 3000 FT) — < 50 GM

  — 120 GM
- DIFFERENTIAL FIBER MASS — 455 GM

Figure 4-28. Barrel Test 8 - Mass Balance Considerations

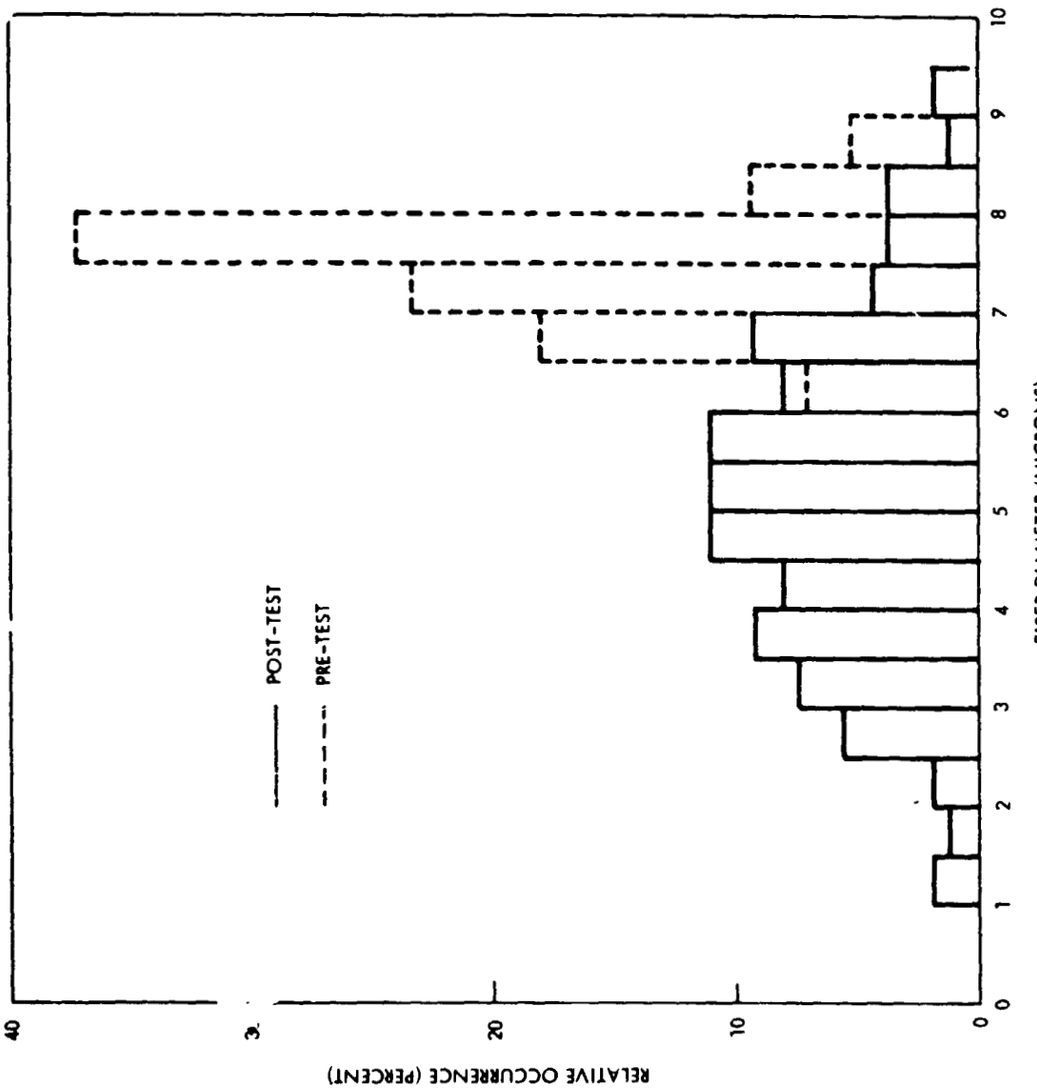

Figure 4.29. Barrel Test 8 - Single Fiber Diameter Spectrum

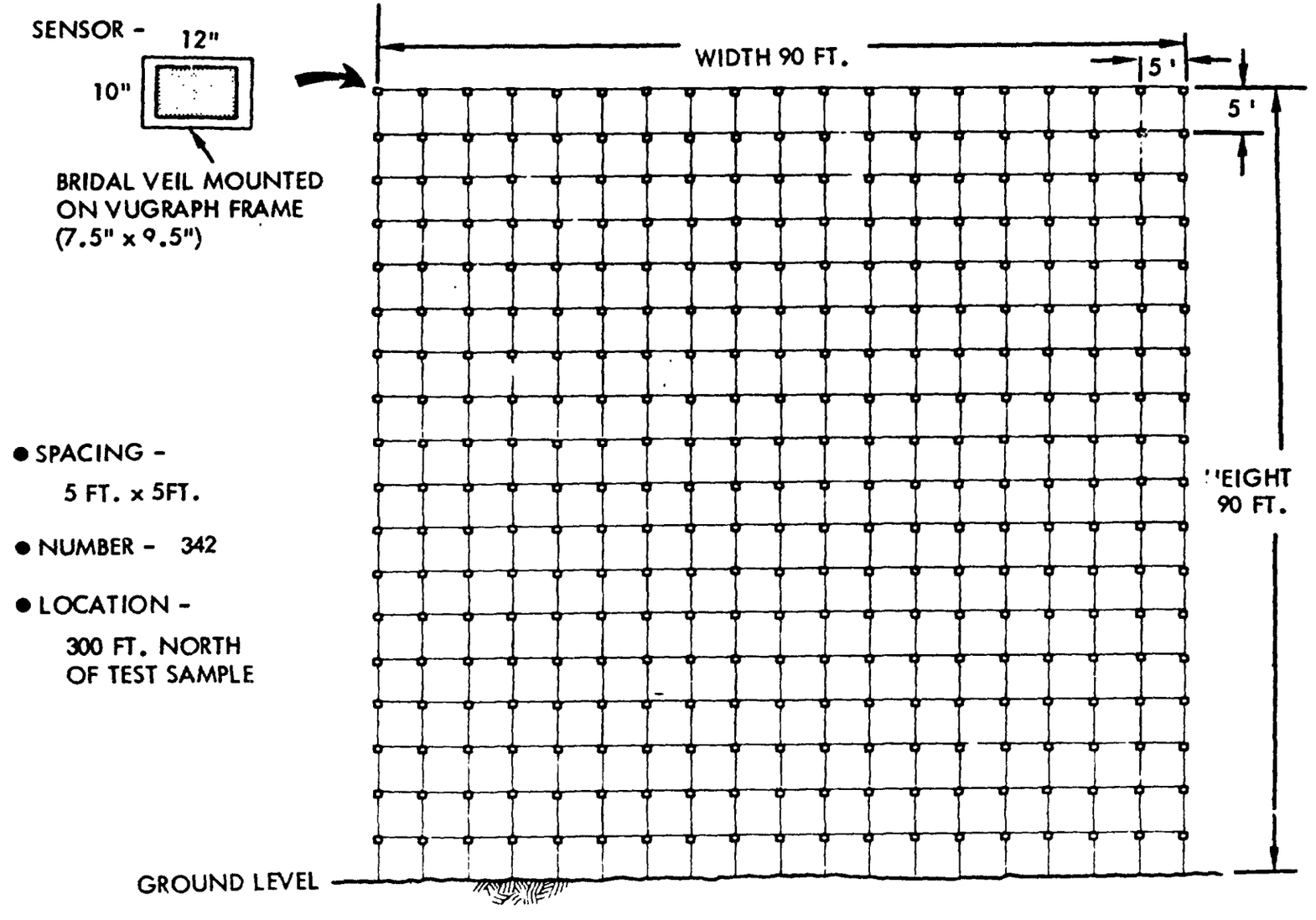

Figure 4-30. Jacob's Ladder Passive Instrumentation Array

RANGE NORTH (FEET)	PARTICLE DENSITY (PER SQUARE FOOT) RANGE EAST/WEST (FEET)												
	80W	70W	60W	50W	40W	30W	20W	10W	0	10E	20E	30E	40E
30	74		–		9		–		9		19		9
40		–		28		9		37		19		28	
50	46		–		19		9		65		19		65
60		–		–		37		–		9		56	
70	56		9		–		19		9		9		37
80		–		19		–		9		9		9	
90	9		9		–		–		–		–		37
100		19		9		9		–		37		37	
110	9		9		9		–		–		19		46
120		–		–		9		9		–		37	
130	–		19		9		–		19		–		19
140		–		19		9		37		19		65	
150	9		–		19		–		–		9		28
160		–		–		–		–		–		28	
170	–		9		–		–		9		28		9
180		–		9		–		–		28		–	
190	–		9		–		–		–		9		19

DISTANCES NOTED ARE GAGE LOCATIONS; UNCORRECTED RELATIVE TO TEST SAMPLE LOCATION AT 114S, 20W

Figure 4-31. Spoiler Test 11 - Test Pad Particle Density

RANGE* NORTH (FEET)

RANGE NORTH (FEET)*						RANGE NORTH (FEET)*				
240		400		600			1000	1500	2000	3000
RANGE E/W * (FEET)	DENSITY (PER SQ FT)	RANGE E/W * (FEET)	DENSITY (PER SQ FT)	RANGE E/W * (FEET)	DENSITY (PER SQ FT)	RANGE* E/W (FEET)	DENSITY (PER SQ FT)	DENSITY (PER SQ FT)	DENSITY (PER SQ FT)	DENSITY (PER SQ FT)
70W	–	150W	–	250W	–	0	2.3	2.3	–	–
60W	–	120W	–	200W	–	100E	–	–	29.0	–
50W	–	90W	N/A	150W	–	200E	–	–	–	–
40W	–	60W	1.2	100W	–	300E	1.2	–	–	–
30W	–	30W	–	50W	N/A	400E	–	–	–	1.2
20W	–	0	4.6	0	N/A	500E	1.2	–	–	–
10W	–	30E	3.5	50E	2.3	600E	–	1.2	–	–
0	9	60E	1.2	100E	2.3	700E	–	–	–	–
10E	–	90E	2.3	150E	1.2	800E	–	–	–	1.2
20E	–	120E	1.2	200E	1.2	900E	–	–	–	–
30E	–	150E	–	250E	–	1000E	–	–	–	–
40E	–					1100E	–	–	–	
50E	28					1200E	–	–	–	
60E	–					1300E	1.2	–	–	
70E	9					1400E	1.2	–	–	
80E	–					1500E	–	N/A	–	

*RANGES CORRESPOND TO GAGE LOCATIONS; UNCORRECTED RELATIVE TO TEST SAMPLE LOCATION AT 114S, 20W

Figure 4 32. Spoiler Test 11 - Sticky Paper Particle Density

Jacob's Ladder Data

An overview of the Jacob's Ladder particle density distribution is presented in Figure 4.33 indicating the relative variations over the entire ladder network. The lowest densities were consistently along the upper third of the ladder array whereas the highest densities were distributed along the bottom third of the ladder. This behavior appears somewhat anomalous since ordinarily it might be anticipated that higher densities would have occurred at higher elevations with progressively decreasing values as the lower elevations were reached. This type of distribution may possibly be attributable to the influence of ground surface effects.

Figure 4.34 indicates the respective density distributions for singles, multiples and clumps and the relative occurrence of each type for the one-third segments of the Jacob's Ladder. It is noted that single fibers consistently predominate the particulate distributions irrespective of ladder location. The relative frequency of occurrence for length intervals in the range of 1 to 10 mm is plotted in Figure 4.35. The average length is 2.79 mm.

Strip Particulate

A post-test survey indicated that a large number of strip-type particulate of the nature shown in Figure 4.36 had been deposited to ranges extending out to 6000 ft principally in the northeast quadrant. A sweep brigade consisting of test personnel was initiated for the purpose of locating and collecting the strips for detailed study. Terrain conditions limited the sweep region to within 6000 ft range. Personnel within the brigade were spaced about 50 ft apart with efforts made to cover intermediate areas. The initial sweep yielded about 90 percent of the total number. Secondary and tertiary sweeps added about 7 percent and 3 percent respectively.

Strip deposition locations are plotted in Figure 4.37, with relative azimuths shown in Figure 4.38. After a range of 2000 ft there appeared to be a convergence in direction toward 10^{o}E.

Figure 4.39 indicates the length distribution as a function of range. Although there were occasional strip lengths of about 50", a major portion were essentially about 20" in length. Principal dimensions of the spoilers were 52" length and 21" width.

A correlation between strip length and strip width is plotted in Figure 4.40. No singular predominance of width is apparent with values ranging almost equally from about 0.25" to 1". The strip thickness distribution with range is shown in Figure 4.41. Single ply thickness for the spoiler composite was 137 microns, with overall thicknesses ranging from 2 to 8 ply.

It appears therefore that the strips originated as delaminations of the composite during the early phases of the pool fire caused by depolymerization of the resin across interstitial planes between plys. Resultant weakening of the composite strength permitted loosening of the respective plys and upward projection caused by the strong updraft of the pool fire.

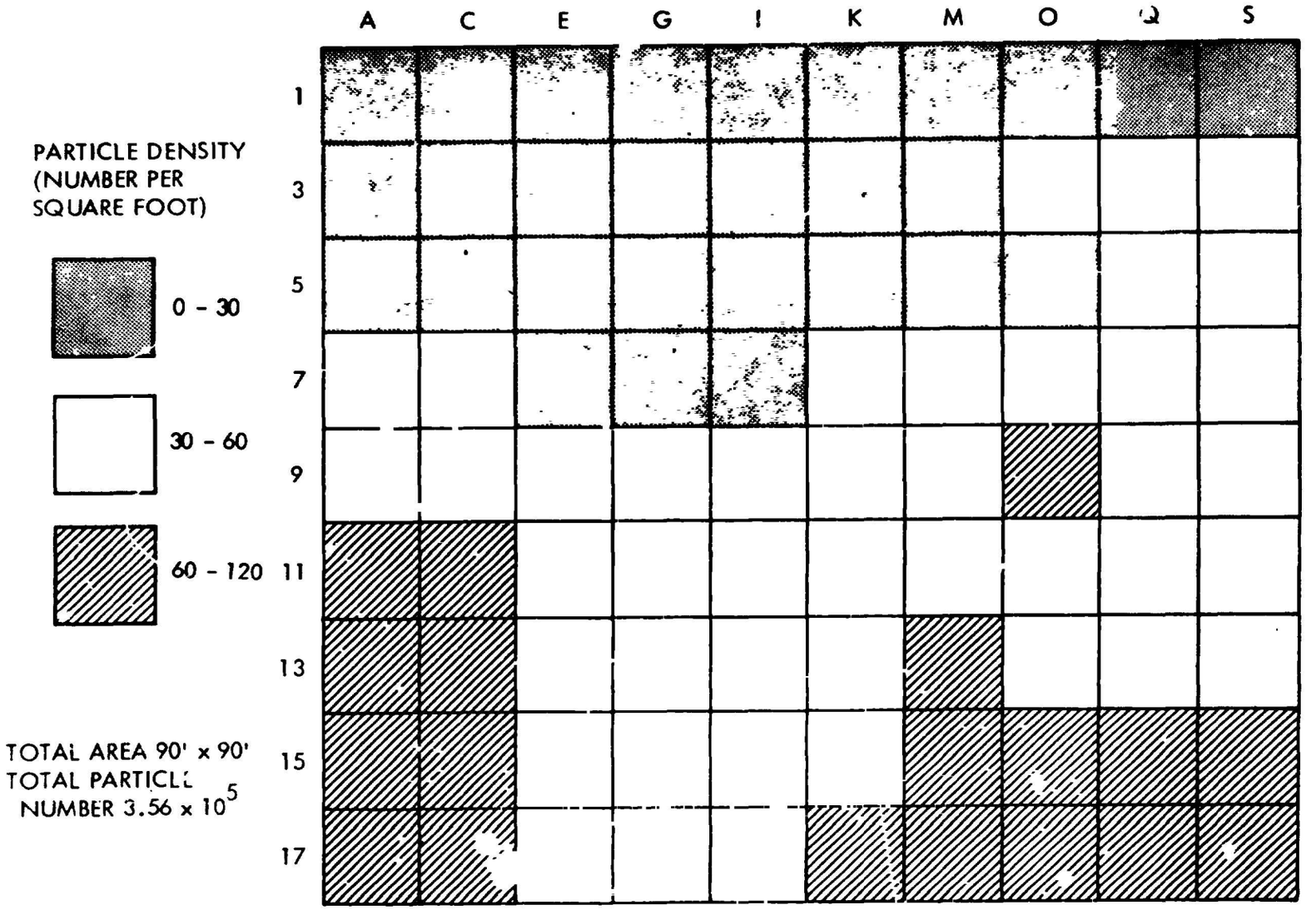

Figure 4.33. Spoiler Test 11 - Jacob's Ladder Particle Density Distribution

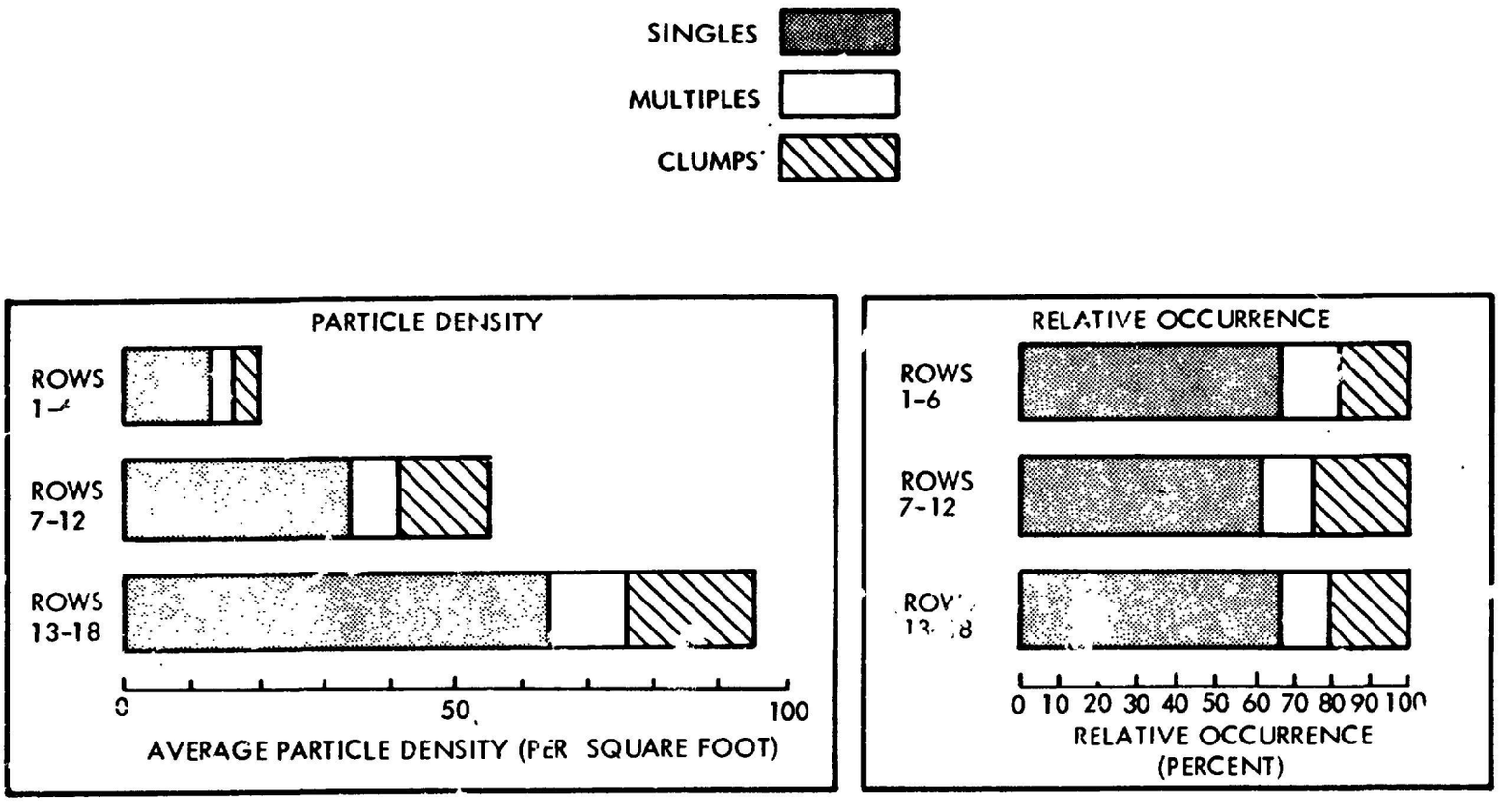

Figure 4.34. Spoil.. Test 11 - Jacob's Ladder Particle Spectrum Distribution

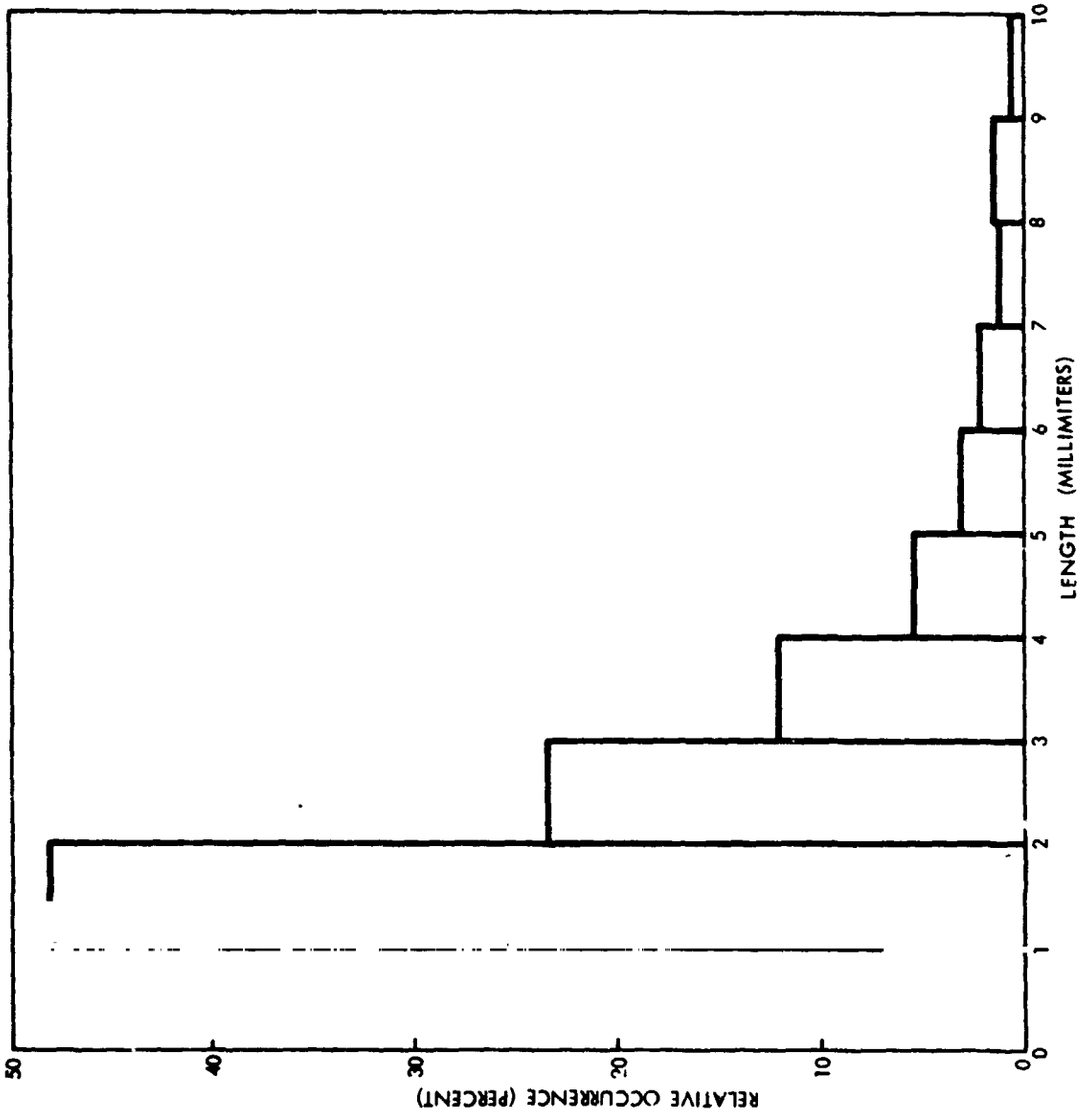

Figure 4-35. Spoiler Test 11 - Jacob's Ladder Length Distribution

C - 2

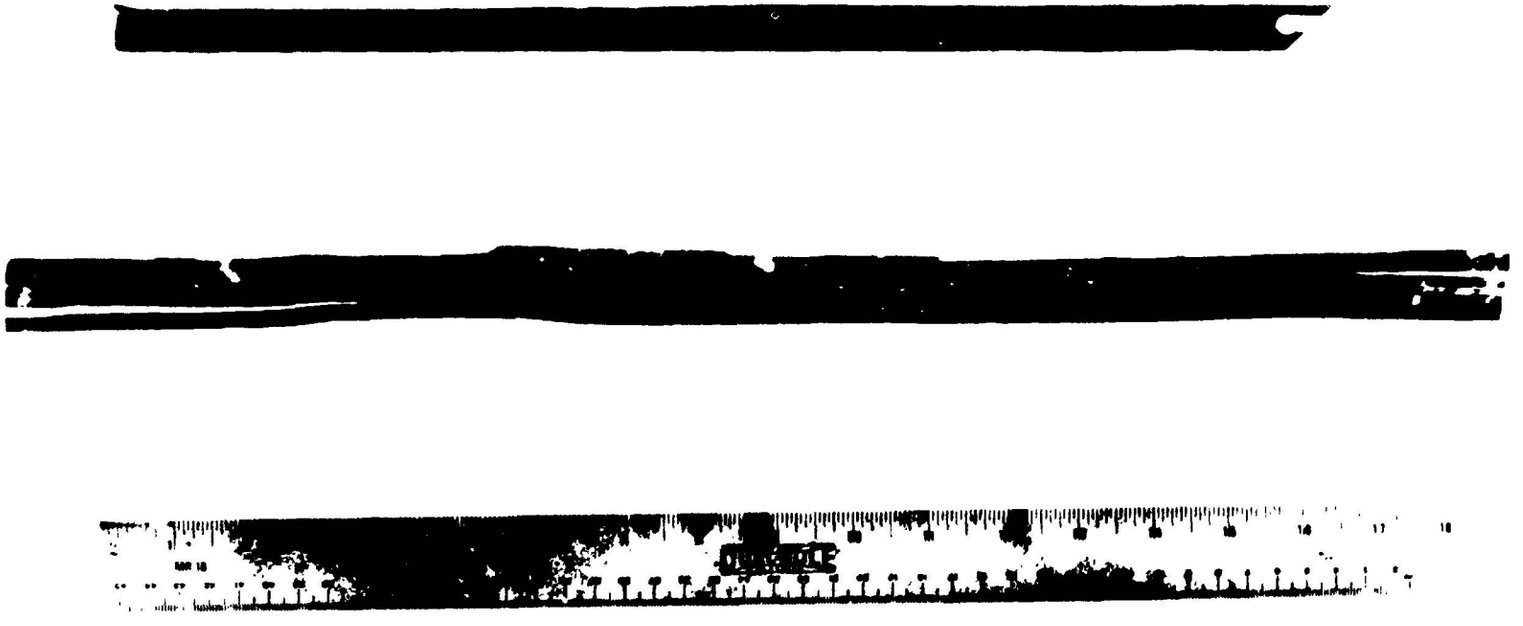

Figure 4.36. Spoiler Test 11 - Representative Strip-Type Particulate

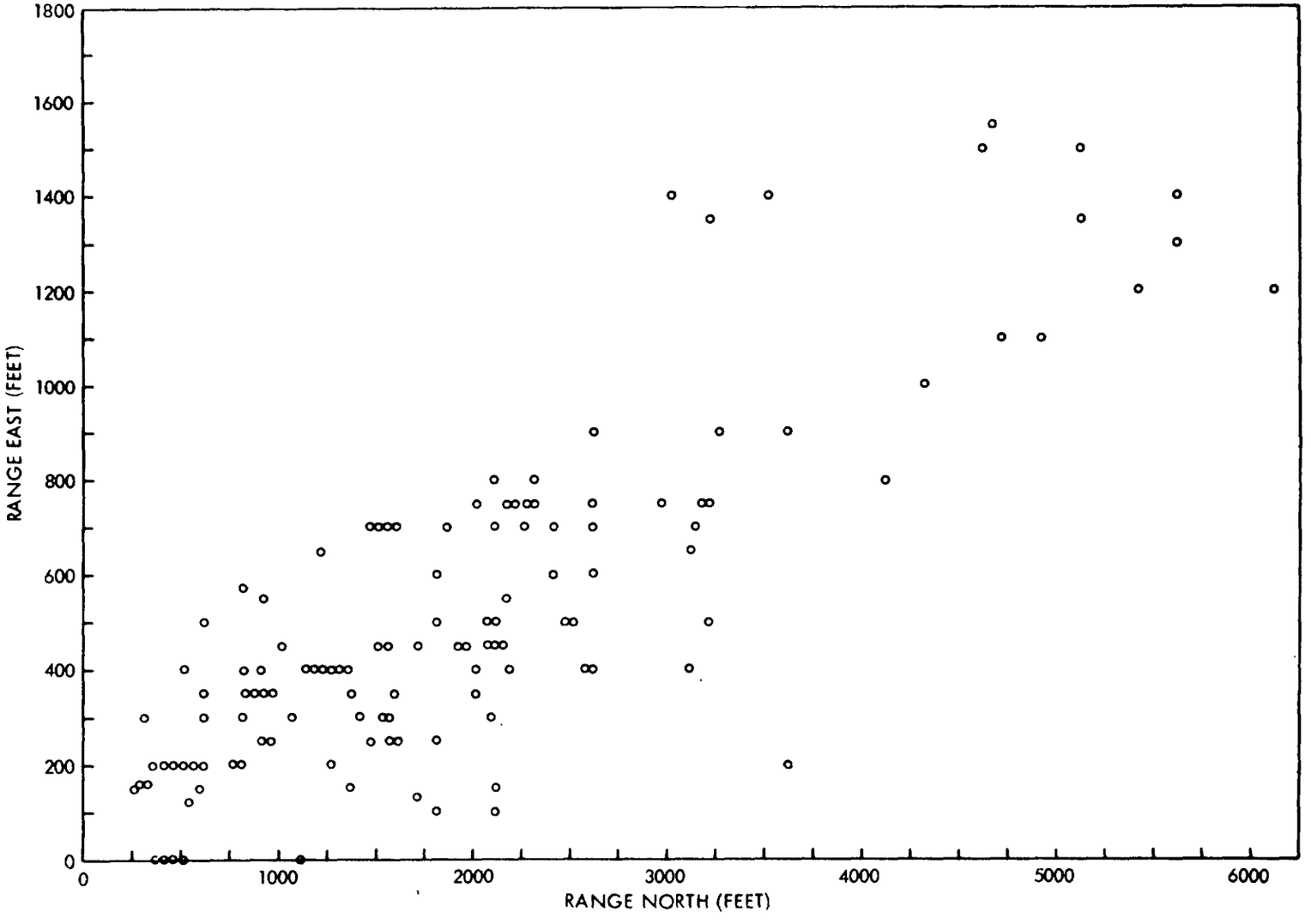

Figure 4.37. Spoiler Test 11 - Strip Deposition Locations

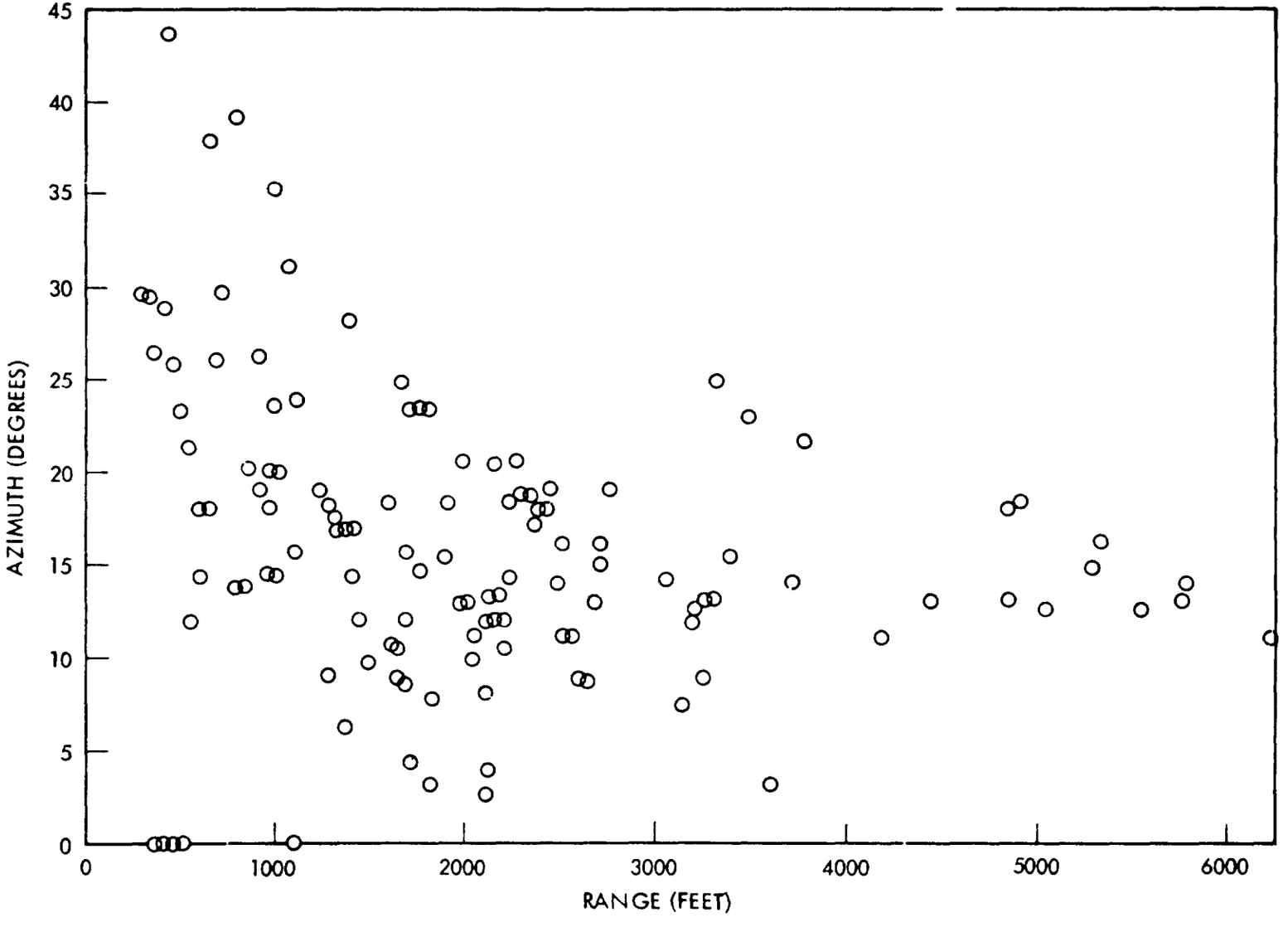

Figure 4.38. Spoiler Test 11 - Strip Deposition Azimuth Vs Range

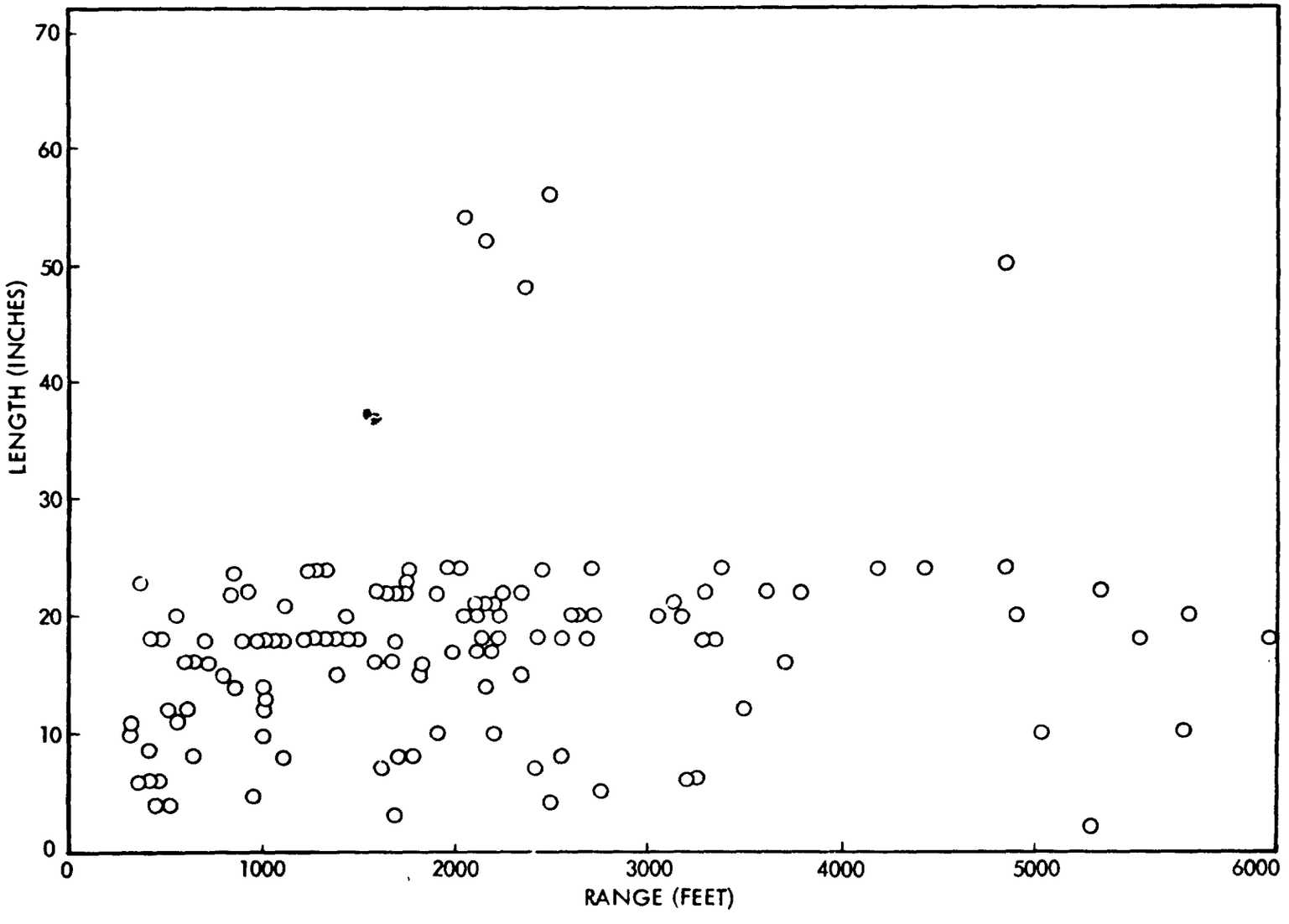

Figure 4.39. Spoiler Test 11 - Strip Length Distribution Vs Range

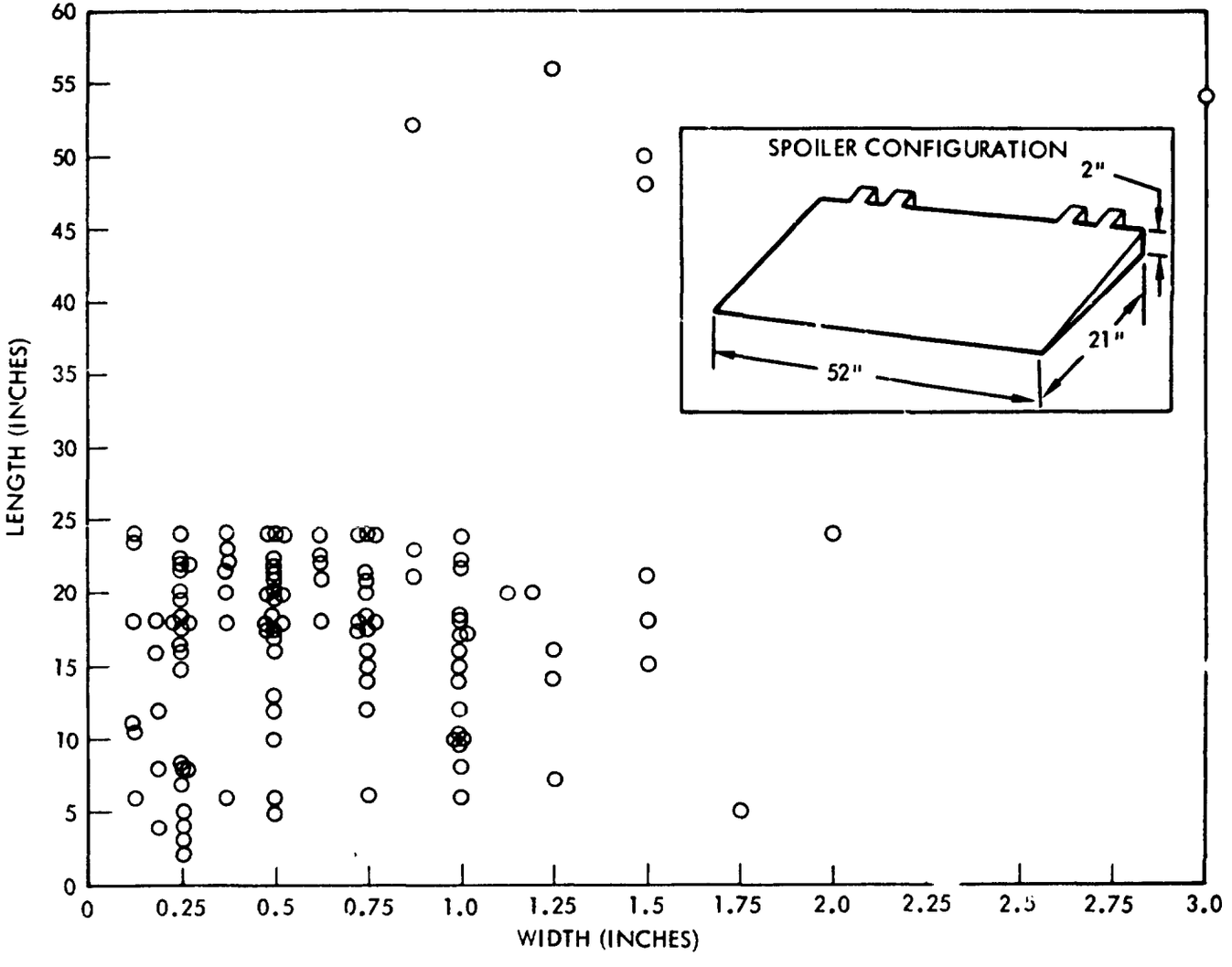

Figure 4·40. Spoiler Test 11 - Correlation of Strip Dimensions

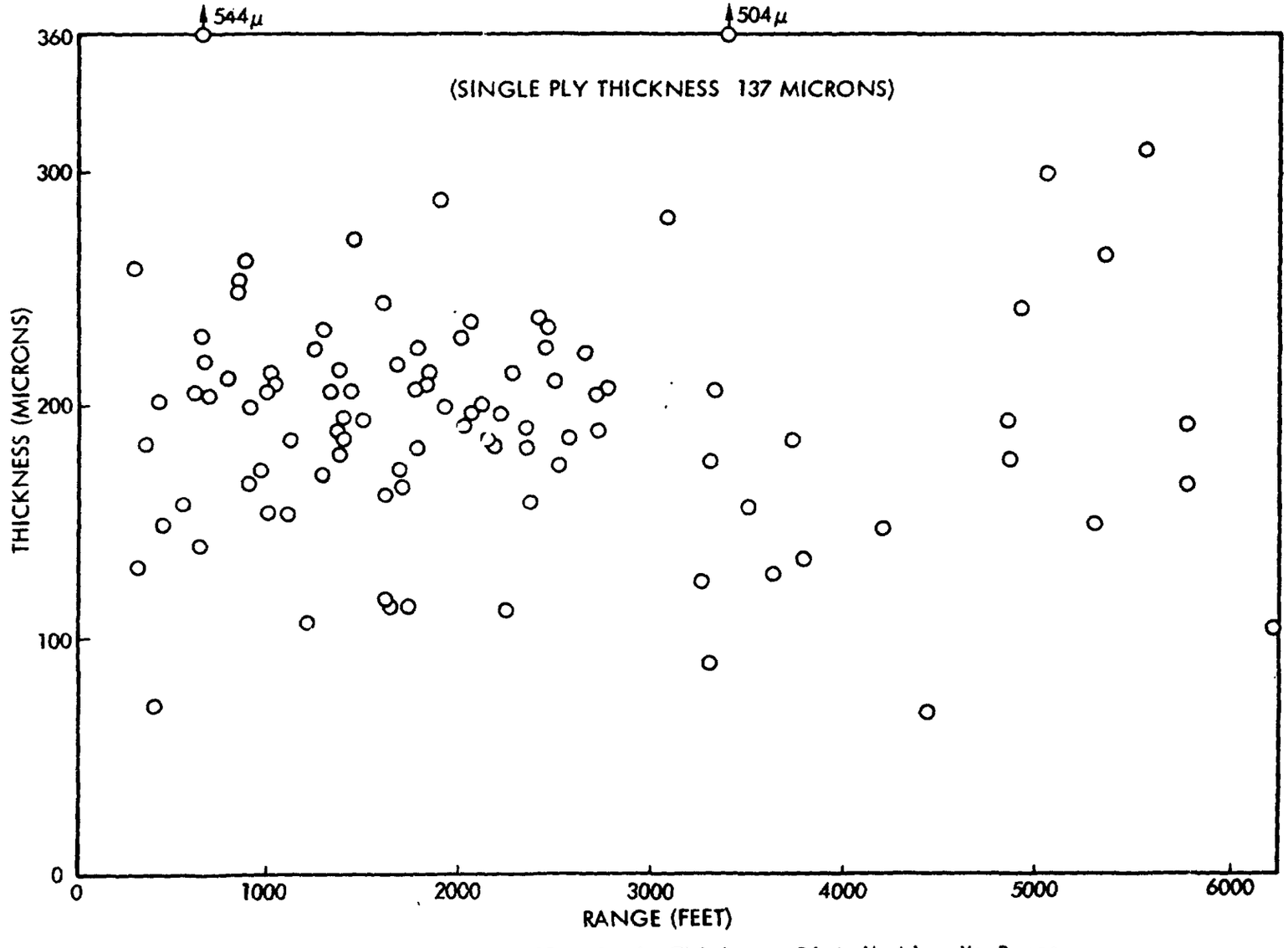

Figure 4.41. Spoiler Test 11 - Strip Thickness Distribution Vs Range

Occurrence frequency as a function of paramter interval is plotted in Figure 4.42 for the length, width and thickness distributions. It was quite surprising to note that the peak in the thickness distribution was in the neighborhood of 190 microns corresponding to 1.5 ply. Some contributions to this domain most probably came from the 2 ply composite layers over about one half of the lower spoiler surface.

Figure 4.43 presents a 3D plot of the strip deposition range dependence in terms of relative contributions by the various length and width intervals.

Mass Estimates

A mass balance analysis is presented in Figure 4.44. The representative mass distribution for a spoiler was recommended by R. A. Pride of NASA Langley. The initial composite mass for the test samples was estimated as 8.3 lb, with fiber mass constituting 70 percent or 5.8 lb.

A total of 4.8 lb represented the post-test cumulative mass of composite debris. Resin content tests of debris samples indicated an average of about 15 percent resin by weight. The net cumulative fiber weight was therefore 4.1 lb resulting in a differential mass of 1.7 lb, or 30 percent of the initial fiber mass.

Spolier Test 12

The instrumentation layout for Test 12 was similar to Test 11. Sticky paper data indicated low particle depositions somewhat similar to Test 11. The particle density distribution over the Jacob's Ladder network is shown in Figure 4.45. There is no apparent density gradient in this case as had been observed for Test 11. It is noted that the total number of particles intercepted by the Jacob's Ladder area was about 1.3×10^6, a factor of 4 greater than estimated for Test 11.

In Figure 4.46 the variation of particle densities for singles, multiples, clumps and lint are compared in relation to rows 1 to 6, 7 to 12 and 13 to 18 of the Jacob's Ladder. In general, the singles constitute about 80 percent of the particles consistently over the network similar to the situation for Test 11.

COCKPIT TEST

INSTRUMENTATION LAYOUT

The total passive instrumentation array for Test 13 was similar to the layouts for Tests 11 and 12.

TEST RESULTS

Surface Deposition

Data reduction of the sticky paper records indicated that a substantial number of lint particulate had been deposited over the test pad area. Figure 4.47

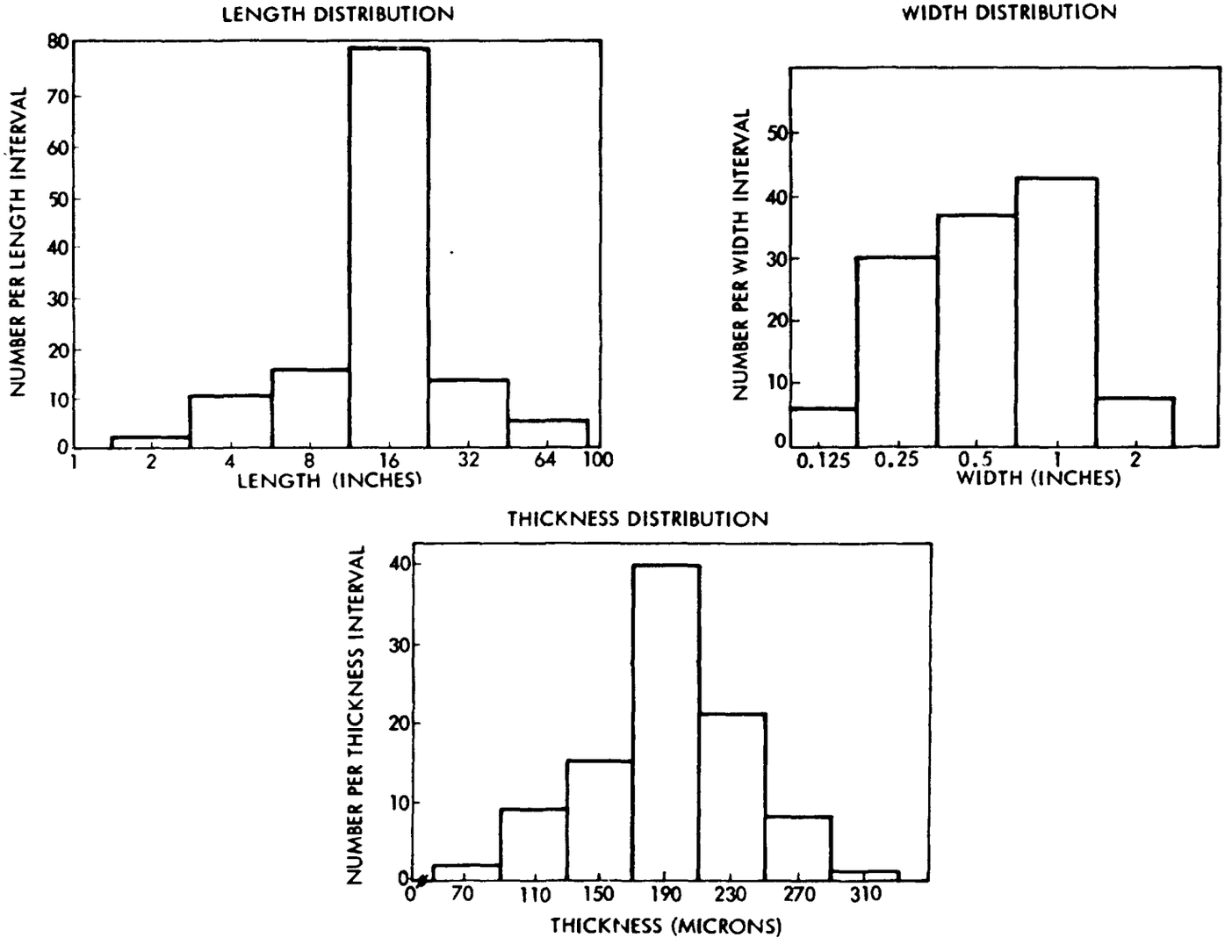

Figure 4-42. Spoiler Test 11 - Strip Length, Width and Thickness Distributions

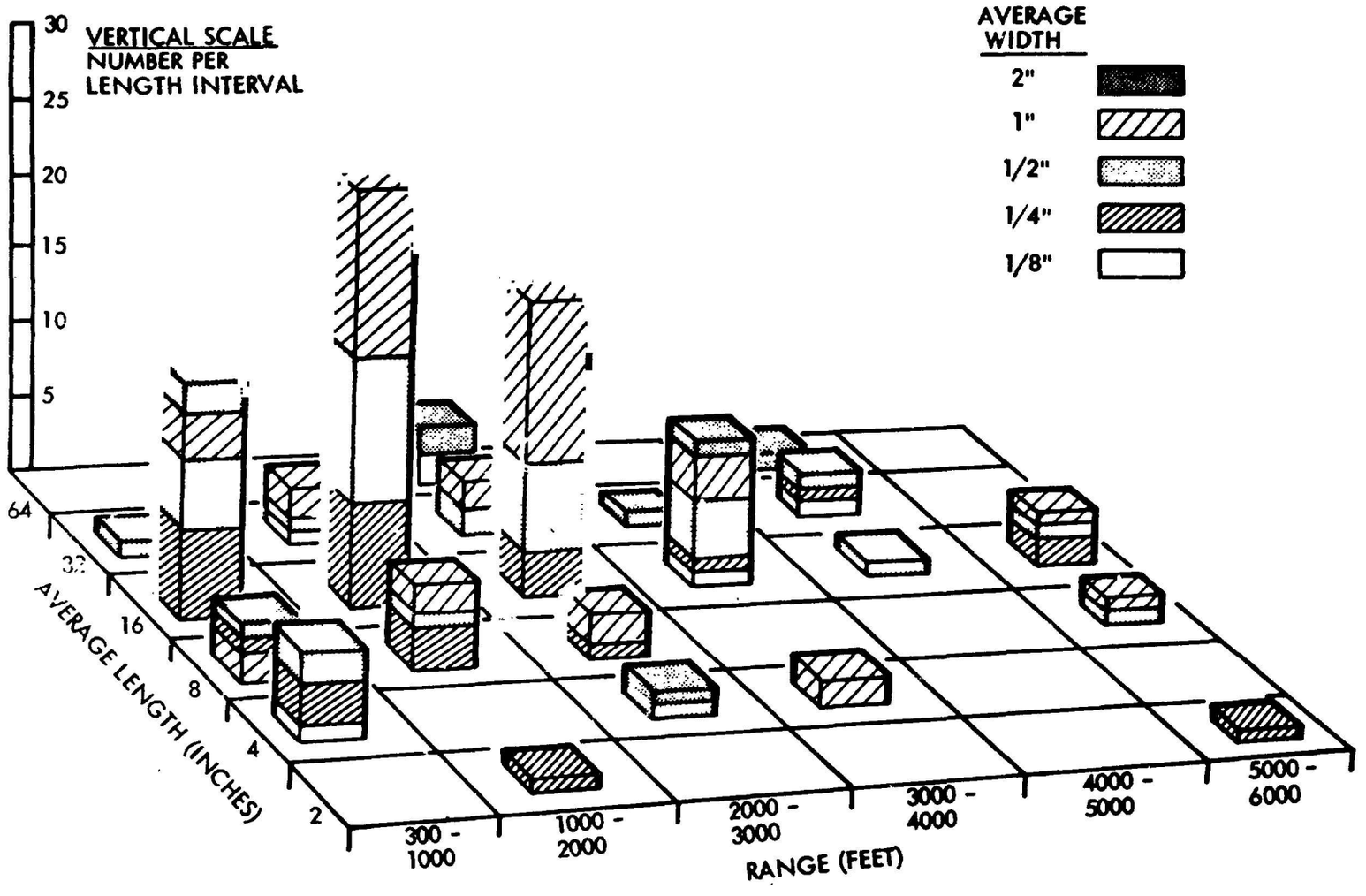

Figure 4.43. Spoiler Test 11 - Strip Deposition Spectrum

REPRESENTATIVE MASS DISTRIBUTION

GRAPHITE–EPOXY SKINS (FIBER 70%, EPOXY 30%)		3.08 LB
CONSUMABLE RESINS		3.04
INERT + METALS		77.69
	TOTAL.	13.81 LB

TEST SAMPLES

NO. 0201		12.8 LB
NO. 0211 (SAMPLE FOR LAB ANALYSIS)		10.9
NO. 0219		13.3
	TOTAL	37.0 LB

INITIAL MASS DISTRIBUTION

GRAPHITE–EPOXY SKINS		8.3 LB
CONSUMABLE RESINS		8.1
INERT + METALS		20.6
	TOTAL	37.0 LB

POST–TEST CUMULATIVE MASS

METAL DEBRIS		13.0 LB
COMPOSITE DEBRIS		
STAND GRID	2.4	
POOL	0.93	
30' TO 80' N OF POOL	0.09	
–40 N TO 0' N (0 TO 50' E)	0.12	
0 TO 50' N (0 TO 150' E)	0.14	
50' TO 100' N (0 TO 150' E)	0.12	
100' TO 150' N (0 TO 150' E)	0.12	
150' TO 200' N (0 TO 150' E)	0.09	
200' TO 900' N (50 TO 300' E)	0.32	
STICKY PAPER (100 – 3000')	0.10	
STRIPS (300' TO 6000' RANGE)	0.38	
		4.8
TOTAL		17.8 LB

MASS BALANCE EVALUATION

INITIAL GRAPHITE FIBER		5.8 LB
MASS LOSS		
COMPOSITE DEBRIS	4.8 LB	
EPOXY CONTENT (15%)	0.7	
NET		4.1
DIFFERENTIAL FIBER MASS		1.7 LB

Figure 4.44. Spoiler Test 11 - Mass Balance Analysis

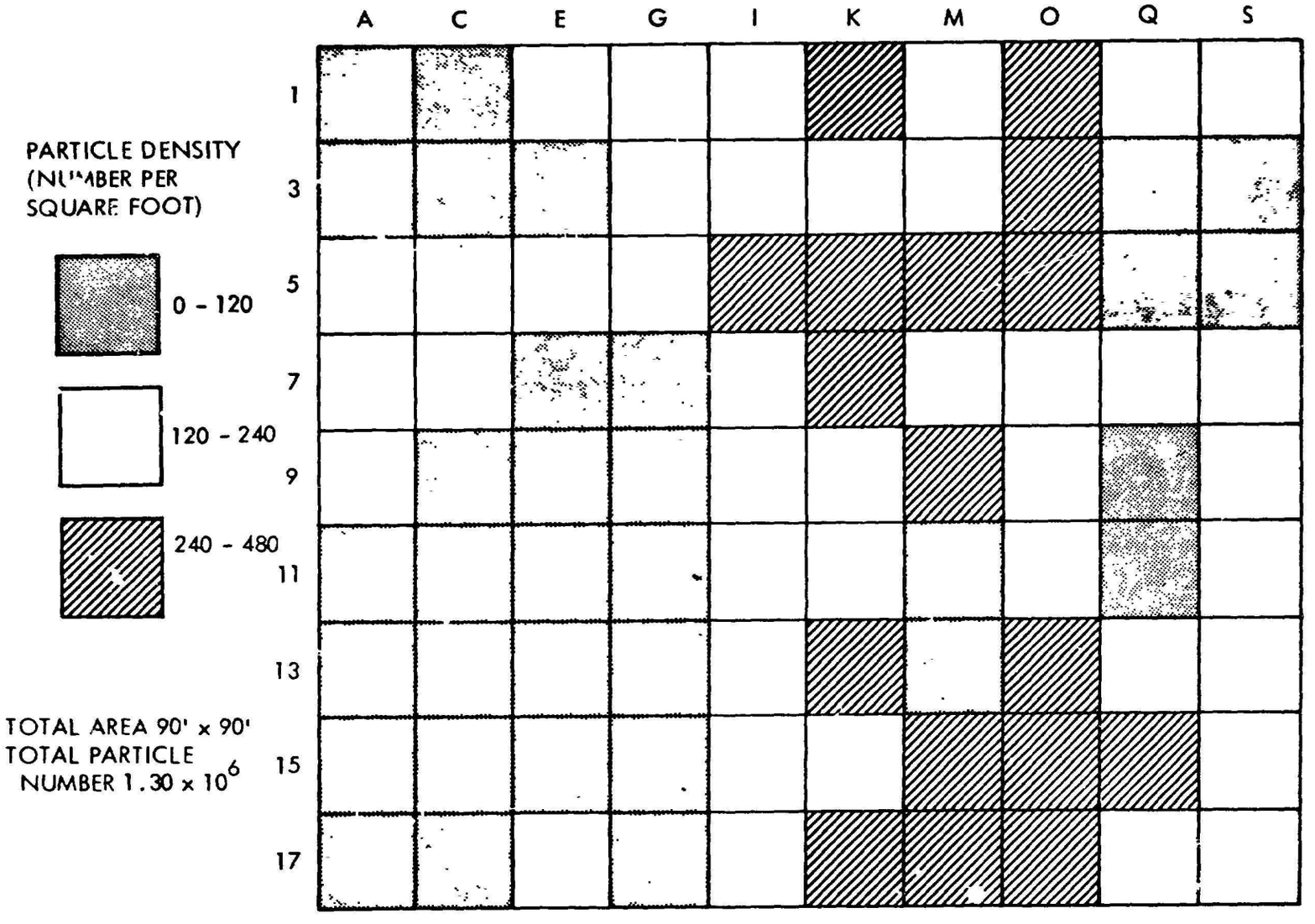

Figure 4.45. Spoiler Test 12 - Jacob's Ladder Particle Density Distribution

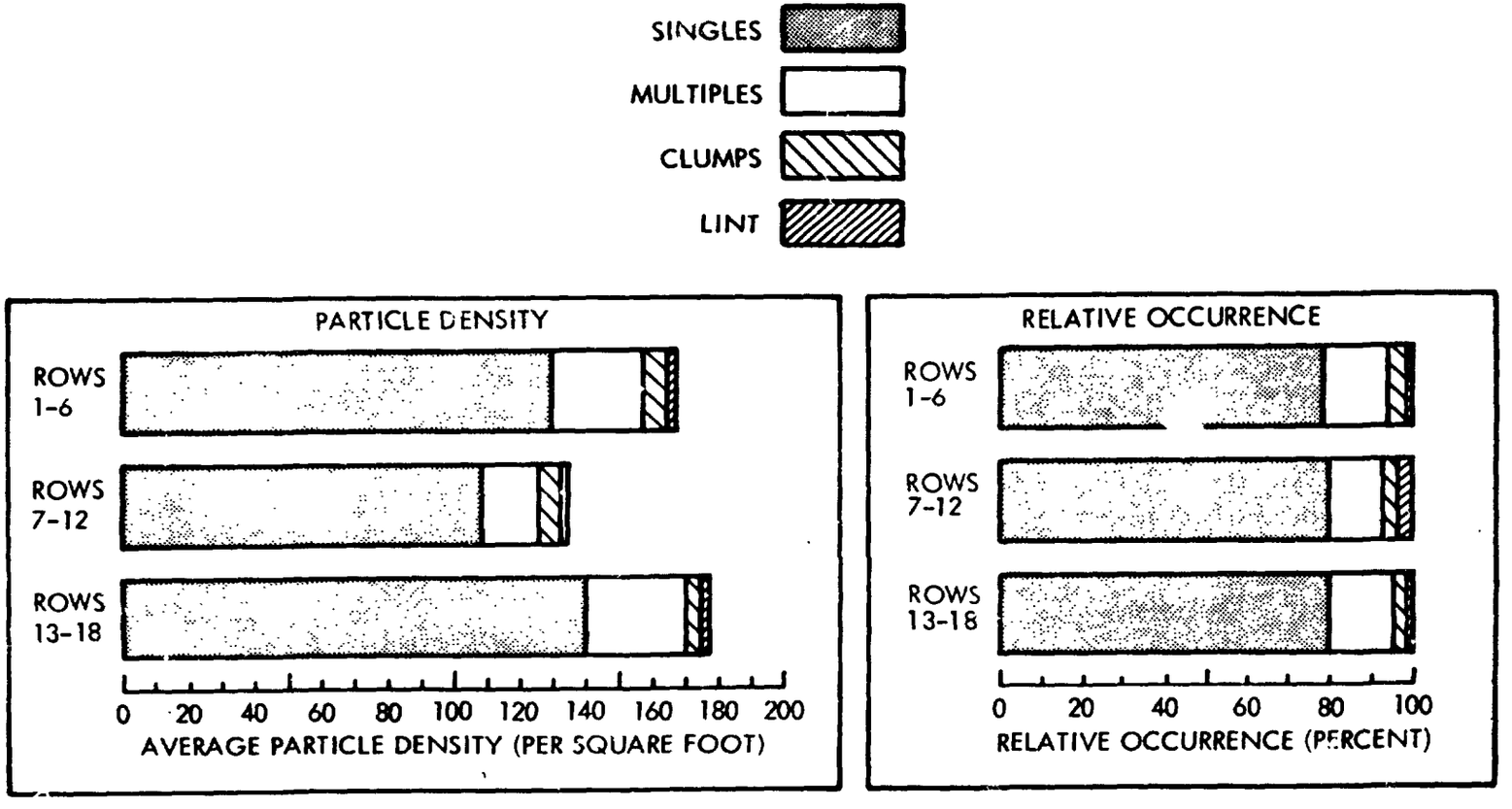

Figure 4.46. Spoiler Test 12 - Jacob's Ladder Particle Spectrum Distributions

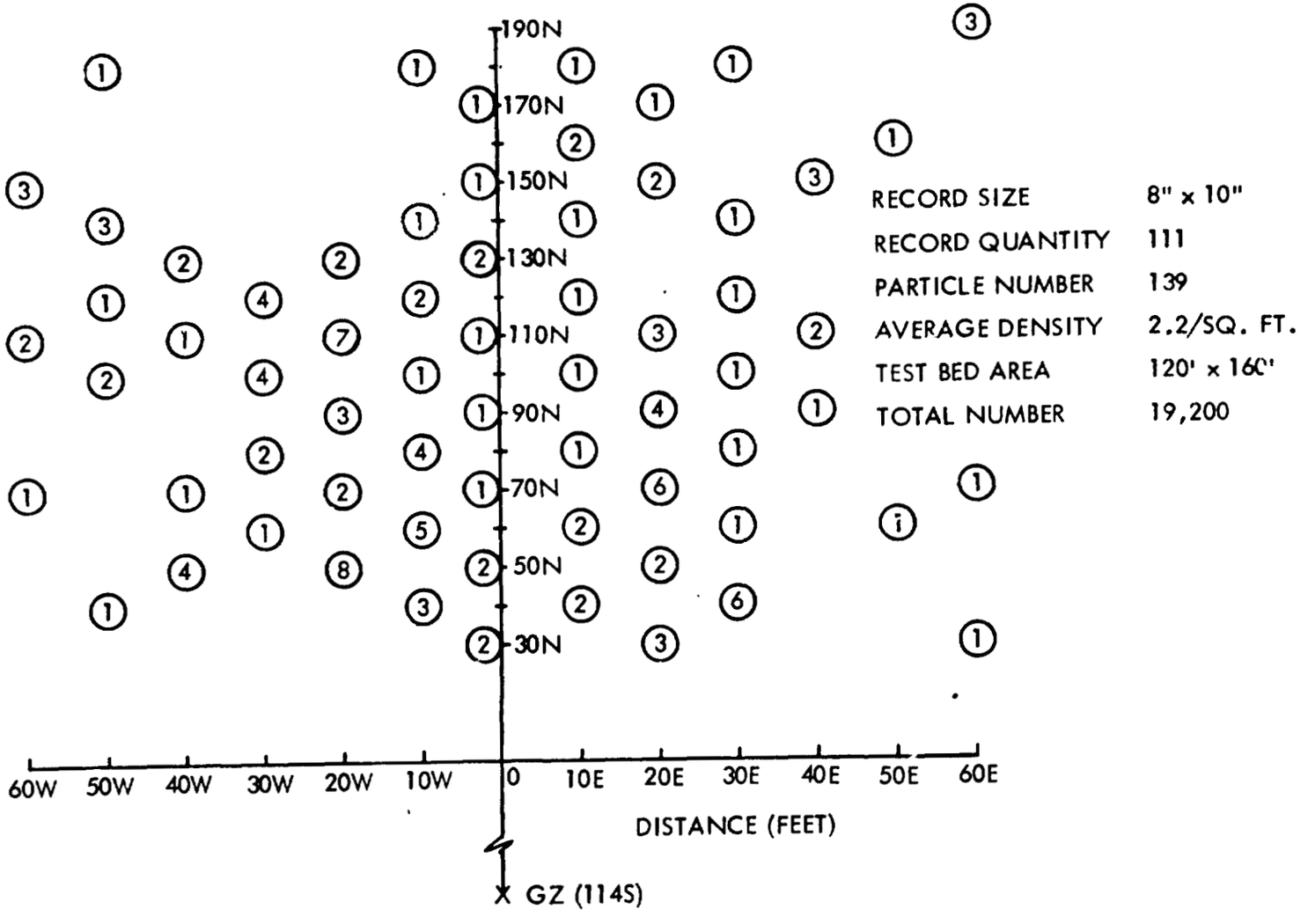

Figure 4.47. Cockpit Test 13 - Lint Particulate Distribution on Sticky Paper Records

indicates the lint distribution as observed on the records. The average density was about 2.2 per square foot welding a total number of 19,200 over the 120'x 160' area of the sensor array.

The distribution of total particle densities from 30'N to 190'N is shown in Figure 4.48. Data corresponding to ranges of 240'N to 3000'N are presented in Figure 4.49.

Jacob's Ladder Data

A large distribution of lint was also observed for the Jacob's Ladder records. A photograph of several representative lint particulate is shown in Figure 4.50. The lint particulate density distribution over the ladder network is presented in Figure 4.51 indicating on the average that greater number were located near the lower elevations. The total number intercepting the entire Jacob's Ladder was estimated as about 33,600. Plotted in Figure 4.52 are contours of the relative occurrence of lint particles in relation to length interval and length/width ratio. The average length was found to be 8.37 mm and average length/width ratio as 35.5.

Figure 4.53 indicates the distribution of total particle densities over the Jacob's Ladder. A striking increase in density for decreasing elevation is again noted similar to the results in the spoiler Test 11. The relative densities for singles, multiples, clumps and lint are shown in Figure 4.54 with a comparison of relative occurrence as distributed over rows 1 to 6, 7 to 12 and 13 to 18 of the Jacob's Ladder. In contrast to the predominance of singles for spoiler Tests 11 and 12, one finds that multiples and clumps govern about 60 to 70 percent of the distributions.

Relative occurrence in relation to length interval is plotted in Figure 4.55. Average particle length is estimated as 2.71 mm. A comparison of pre-test and post-test single fiber diameters is shown in Figure 4.56. The evidence of oxidation effects is again noted.

Strip Particulate

A large dispersion of strip particulate was again observed similar to the occurrence in spoiler Test 11. The principal deposition region was the northwest quadrant. A sweep brigade operation was instituted similar to Test 11 with resulting data on deposition locations and strip dimensions.

A mapping of the strip deposition positions is shown in Figure 4.57 with the corresponding azimuth versus range plotted in Figure 4.58. Beyond 2000 ft range the dispersion pattern was bounded by 15^{0}W to 30^{0}W. Due to terrain limitations at distant northwest ranges the survey was initiated at 4500 ft.

Figure 4.59 indicates the variation of strip length versus range, with correlation of strip lengths and widths shown in Figure 4.60. As noted by the sketch in Figure 4.60 principal dimensions of the cockpit sample were 61" length, 49" width, and 29" height. The strip thickness distribution is plotted in Figure 4.61 as a function of range. The cockpit composite consisted of 8 ply with single ply thickness of 140 microns.

RANGE NORTH (FEET)	PARTICLE DENSITY (PER SQUARE FOOT) RANGE EAST/WEST (FEET)												
	80W	70W	60W	50W	40W	30W	20W	10W	0	10E	20E	30E	40E
30	139		84		84		176		84		37		19
40		93		93		223		130		130		19	
50	65		232		121		130		102		9		65
60		93		130		149		130		139		–	
70	102		195		130		93		195		56		19
80		149		74		102		149		28		–	
90	28		46		65		74		37		28		37
100		46		130		102		65		46		37	
110	93		65		56		121		65		37		37
120		28		102		102		56		74		19	
130	74		28		74		149		28		46		28
140		28		102		56		93		19		56	
150	37		139		19		65		28		28		19
160		56		56		65		65		19		46	
170	46		–		56		65		56		28		28
180		9		46		19		37		19		19	
190	93		56		37		74		46		9		56

RANGES CORRESPOND TO GAGE LOCATIONS; UNCORRECTED RELATIVE TO TEST SAMPLE LOCATION AT 114S, 20W

Figure 4.48. Cockpit Test 13 - Test Pad Particle Density

RANGE NORTH (FEET)*							RANGE NORTH (FEET)*			
240		400		600			1000	1500	2000	3000
RANGE E/W * (FEET)	DENSITY (PER SQ FT)	RANGE E/W * (FEET)	DENSITY (PER SQ FT)	RANGE E/W * (FEET)	DENSITY (PER SQ FT)	RANGE* E/W (FEET)	DENSITY (PER SQ FT)	DENSITY (PER SQ FT)	DENSITY (PER SQ FT)	DENSITY (PER SQ FT)
70W	18	150W	3.5	250W	N/A	1500W	–	N/A	–	–
60W	28	120W	10.4	200W	2.3	1400W	–	–	5.8	–
50W	-	90W	12.8	150W	2.3	1300W	–	1.2	–	–
40W	18	60W	9.3	100W	4.6	1200W	1.2	–	–	–
30W	18	30W	16.2	50W	1.2	1100W	–	1.2	–	–
20W	18	0	12.8	0	2.3	1000W	–	–	–	1.2
10W	28	30E	1.2	50E	4.6	900W	1.2	–	–	–
0	18	60E	2.3	100E	3.5	800W	1.2	2.3	–	–
10E	18	90E	–	150E	–	700W	1.2	–	–	–
20E	18	120E	1.2	200E	–	600W	–	–	-	–
30E	9	150E	4.6	250E	–	500W	2.3	2.3	–	–
40E	9					400W	1.2	–	–	–
50E	9					300W	1.2	1.2	1.2	–
60E	–					200W	–	–	–	1.2
70E	18					100W	3.5	1.2	–	–
80E	37					0	4.6	–	3.5	–

Figure 4-49. Cockpit Test 13 - Sticky Paper Particle Density

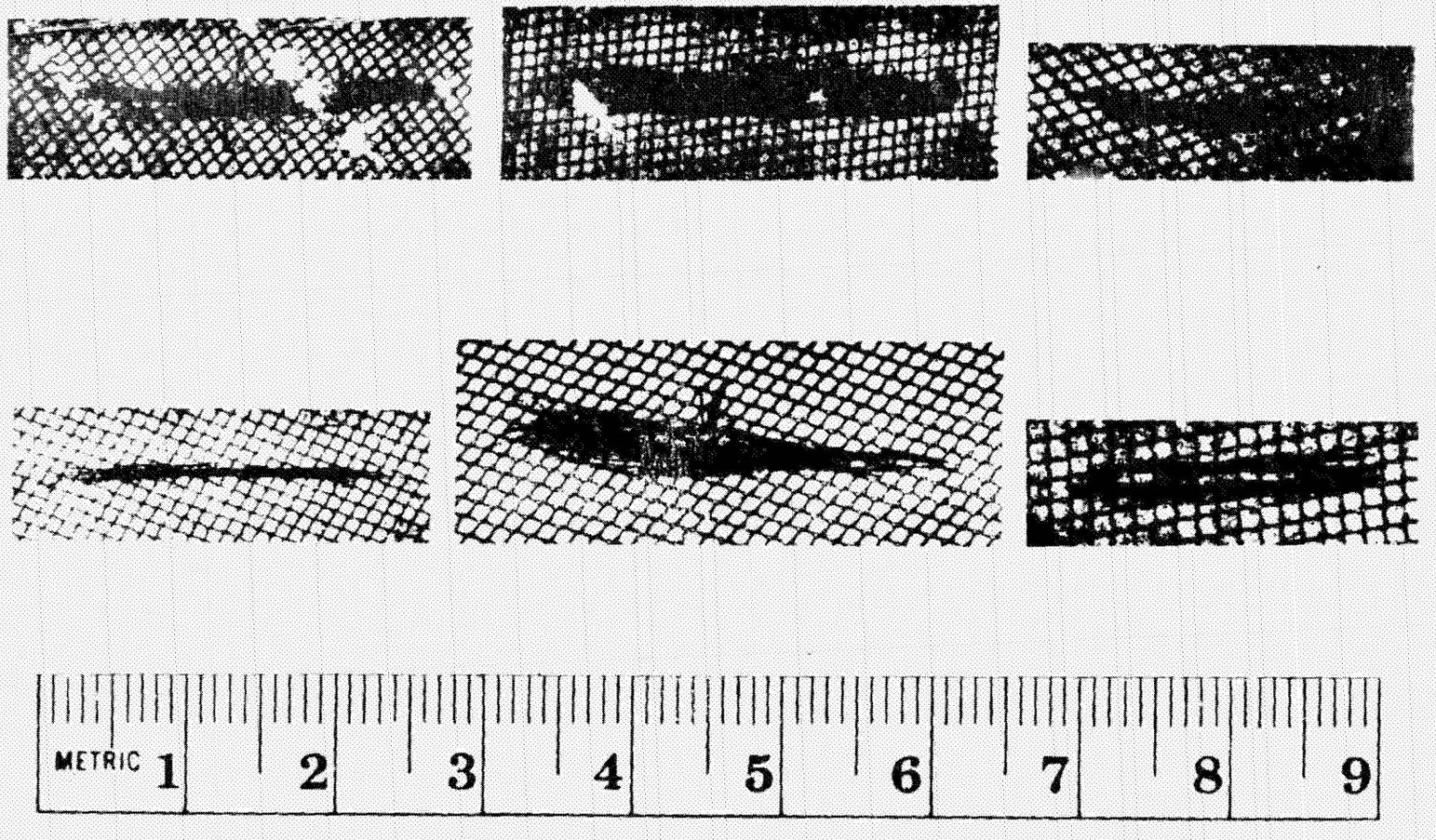

Figure 4-50. Cockpit Test 13 - Lint Particulate

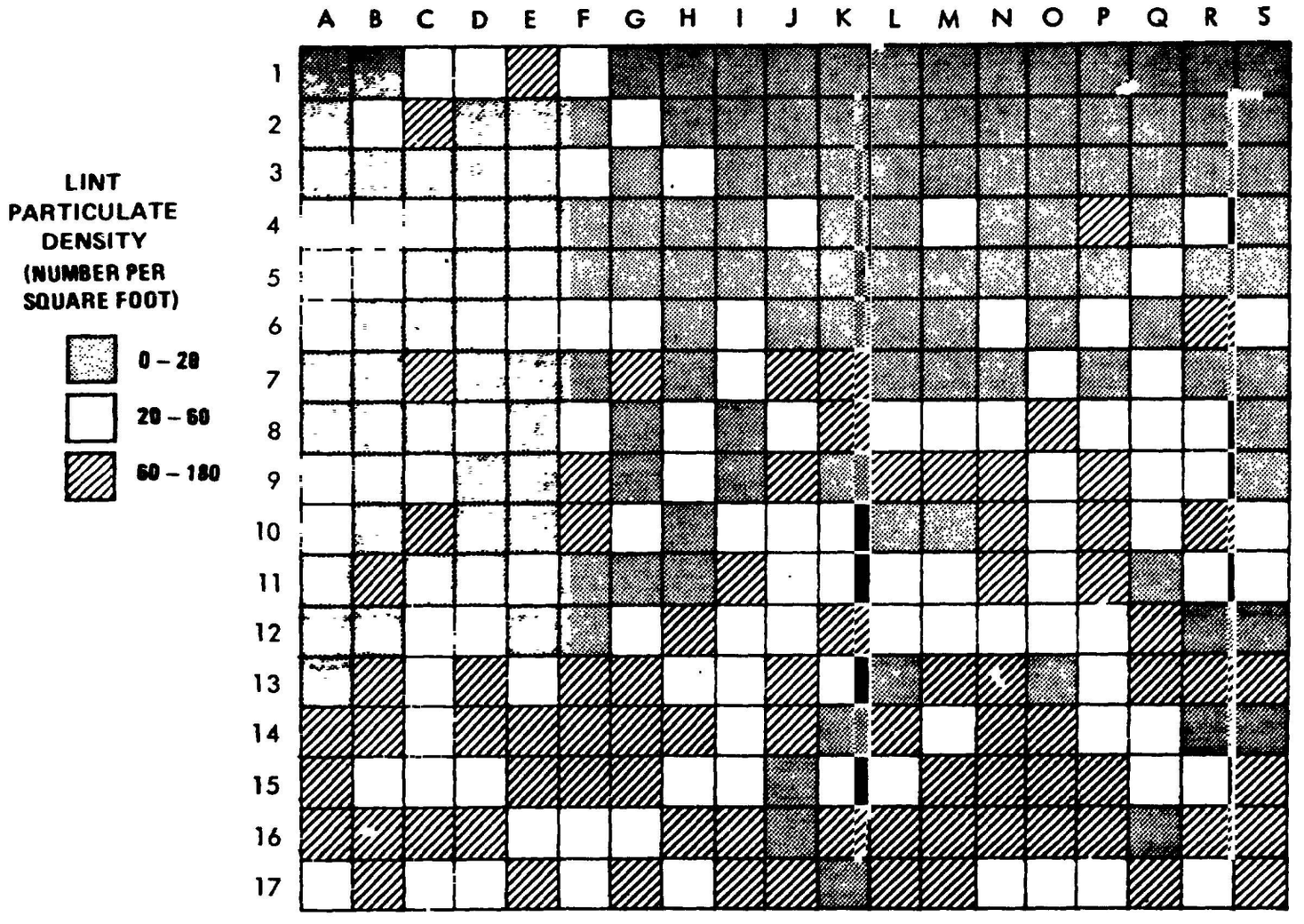

Figure 4.51. Cockpit Test 13 - Jacob's Ladder Lint Particulate Density Distribution

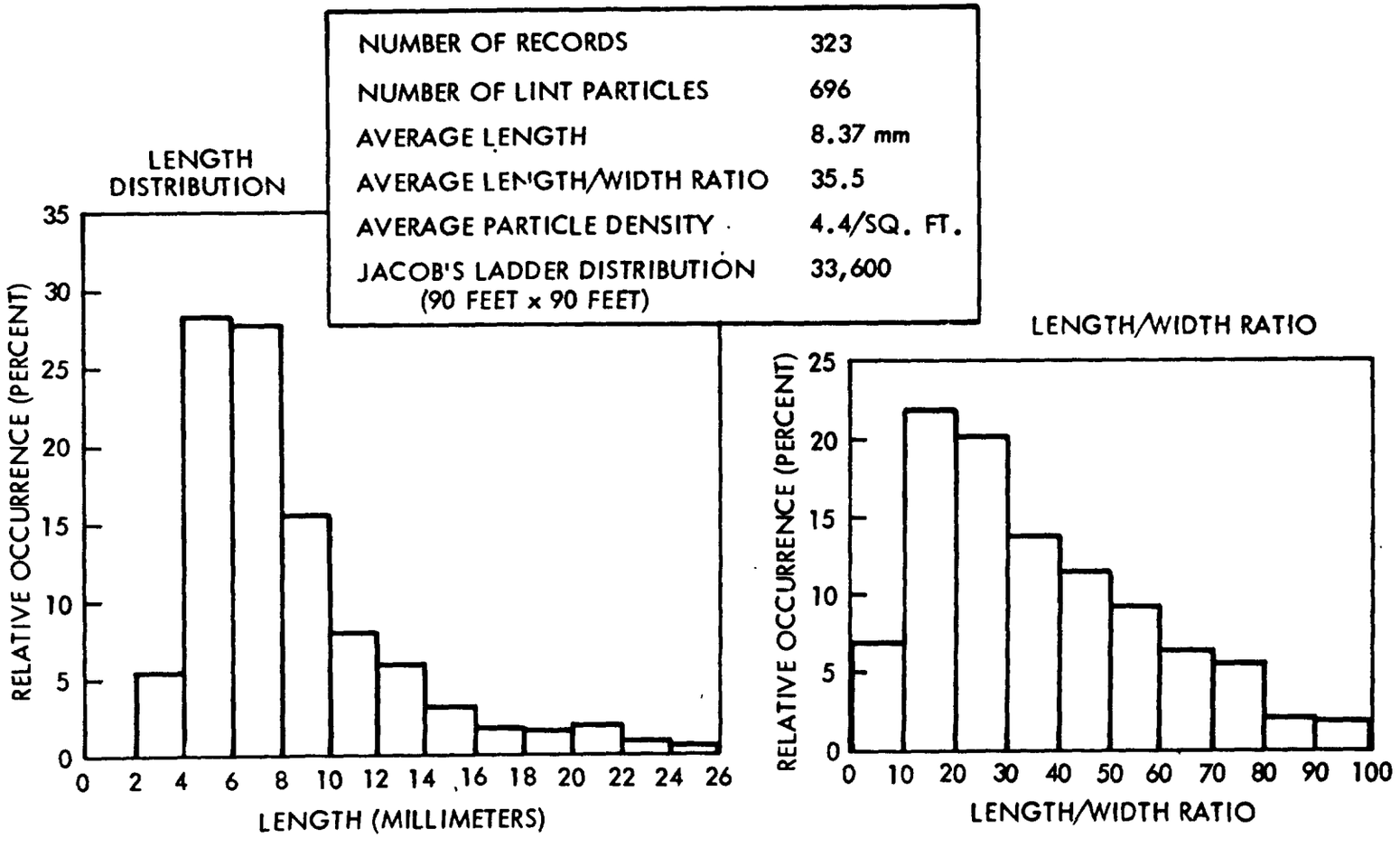

Figure 4.52. Cockpit Test 13 - Jacob's Ladder Lint Particulate Distribution

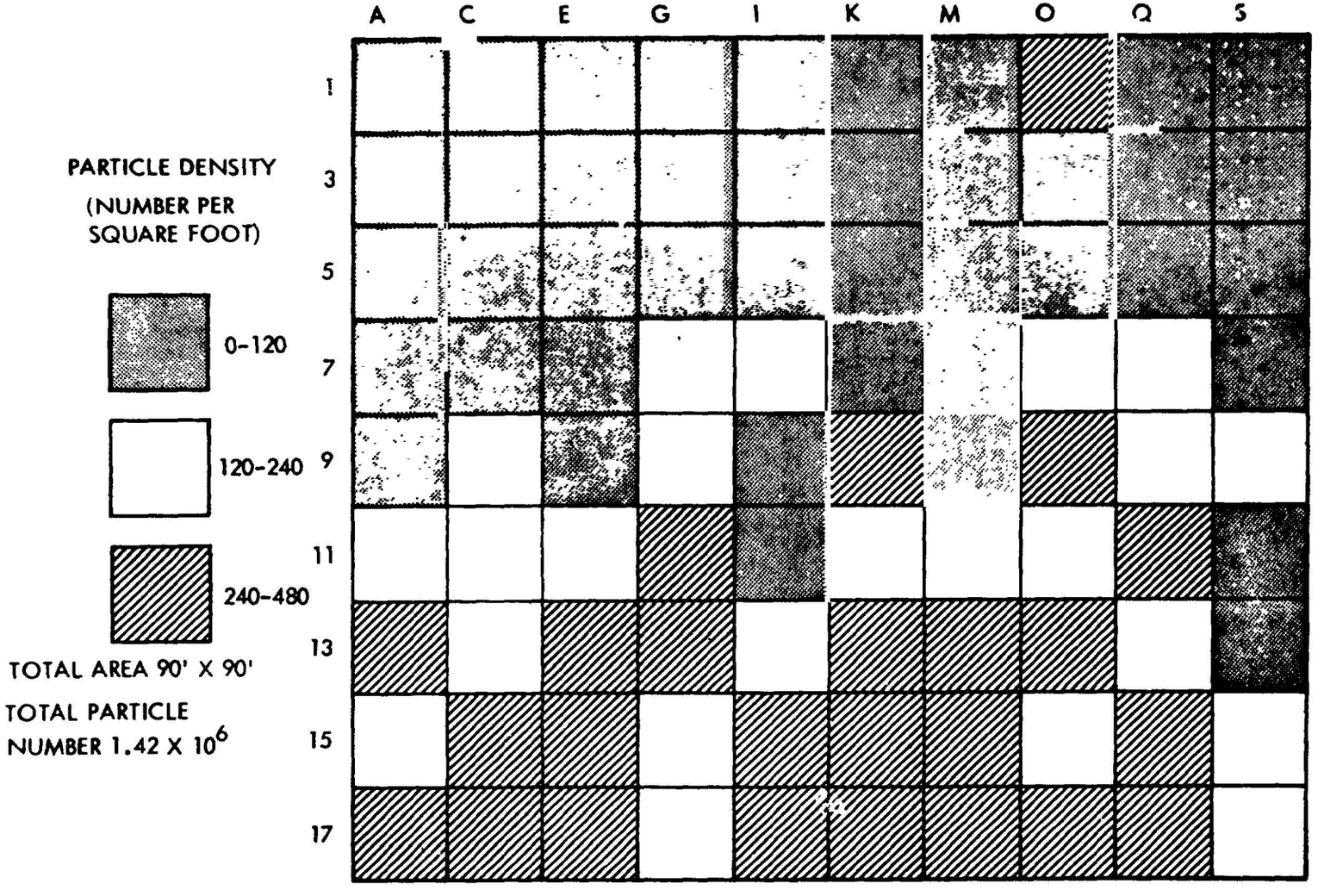

Figure 4.53. Cockpit 13 - Jacob's Ladder Particle Density Distribution

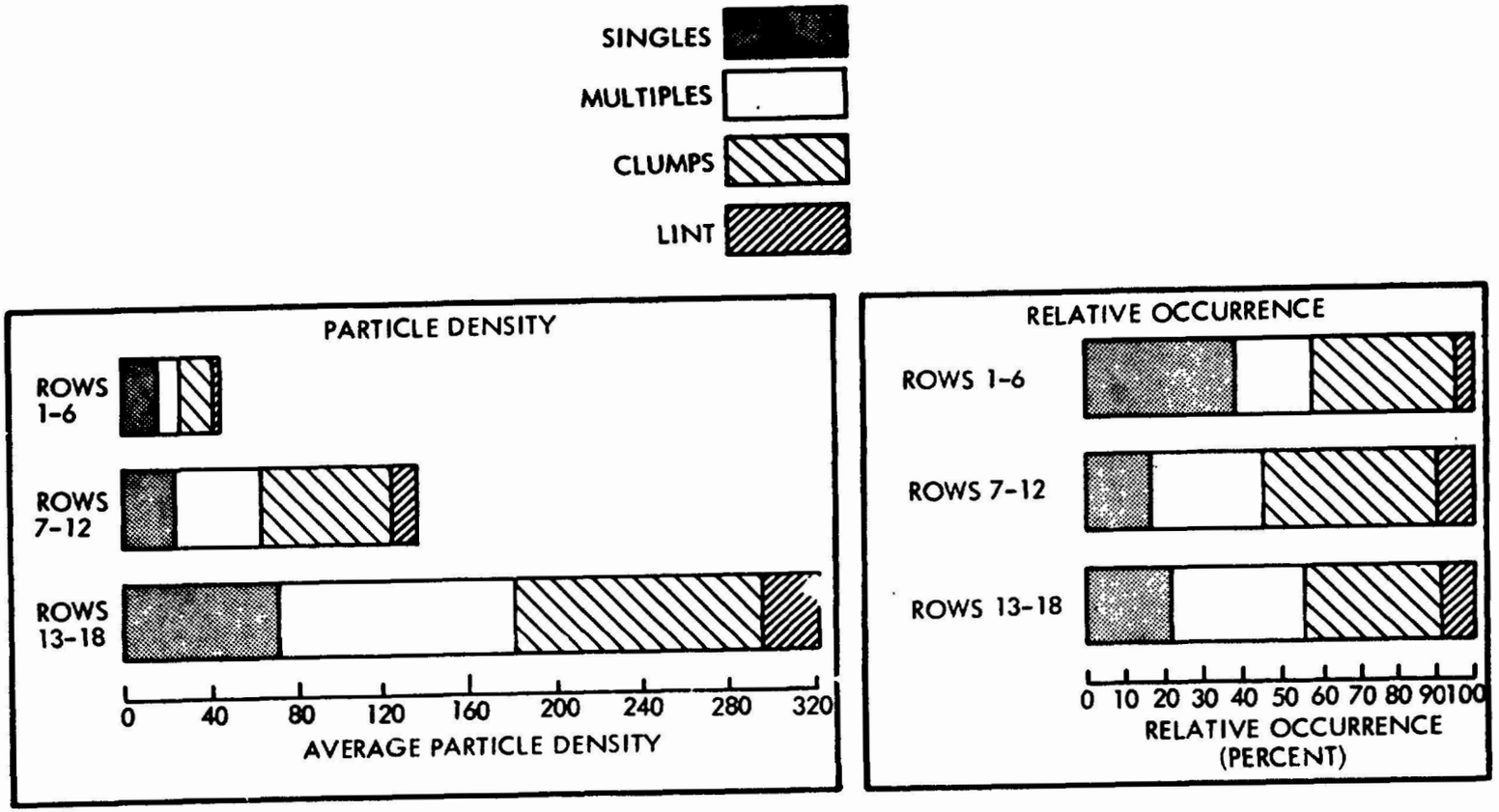

Figure 4-54. Cockpit Test 13 - Jacob's Ladder Particle Spectrum Distribution

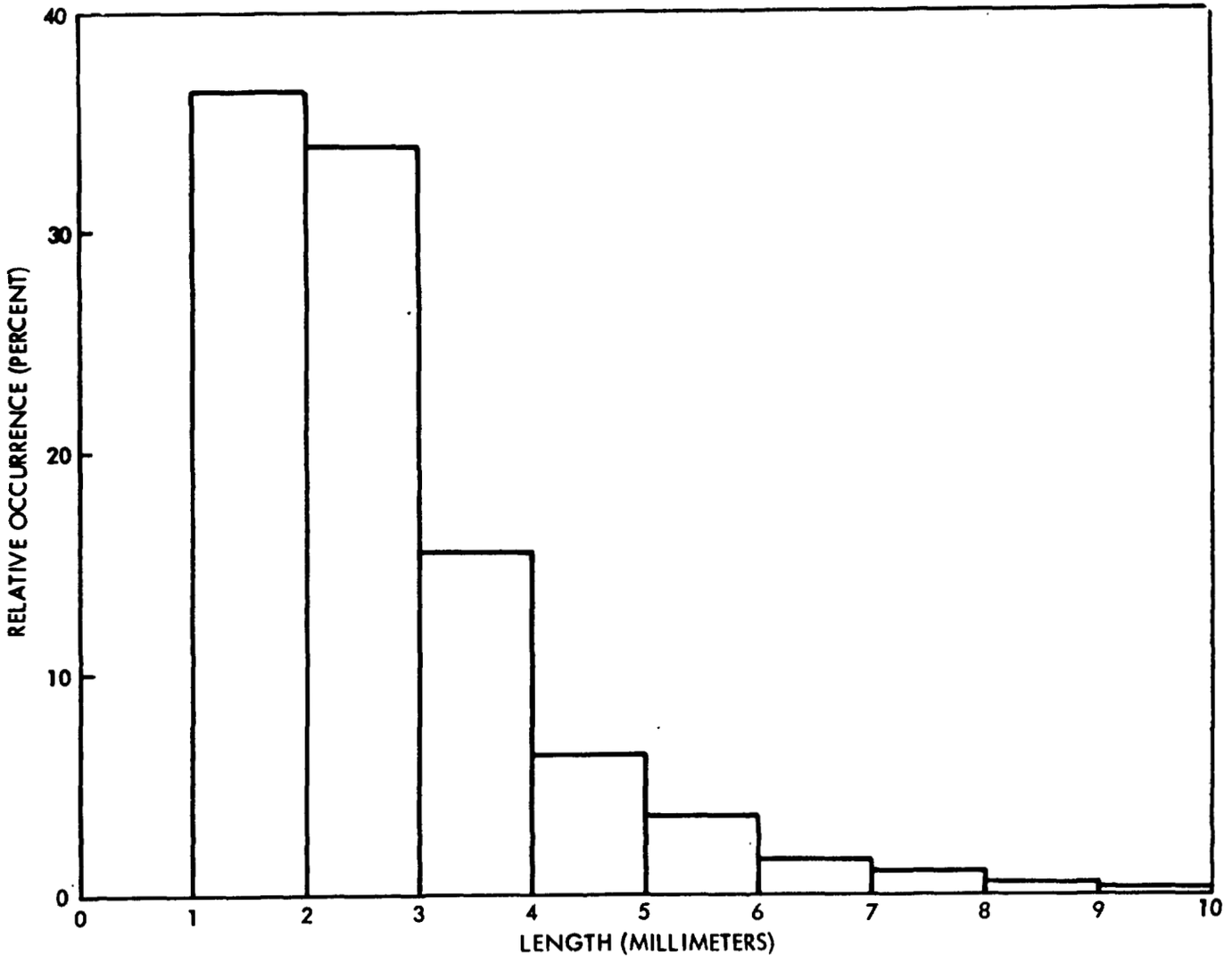

Figure 4.55. Cockpit Test 13 - Jacob's Ladder Length Distribution

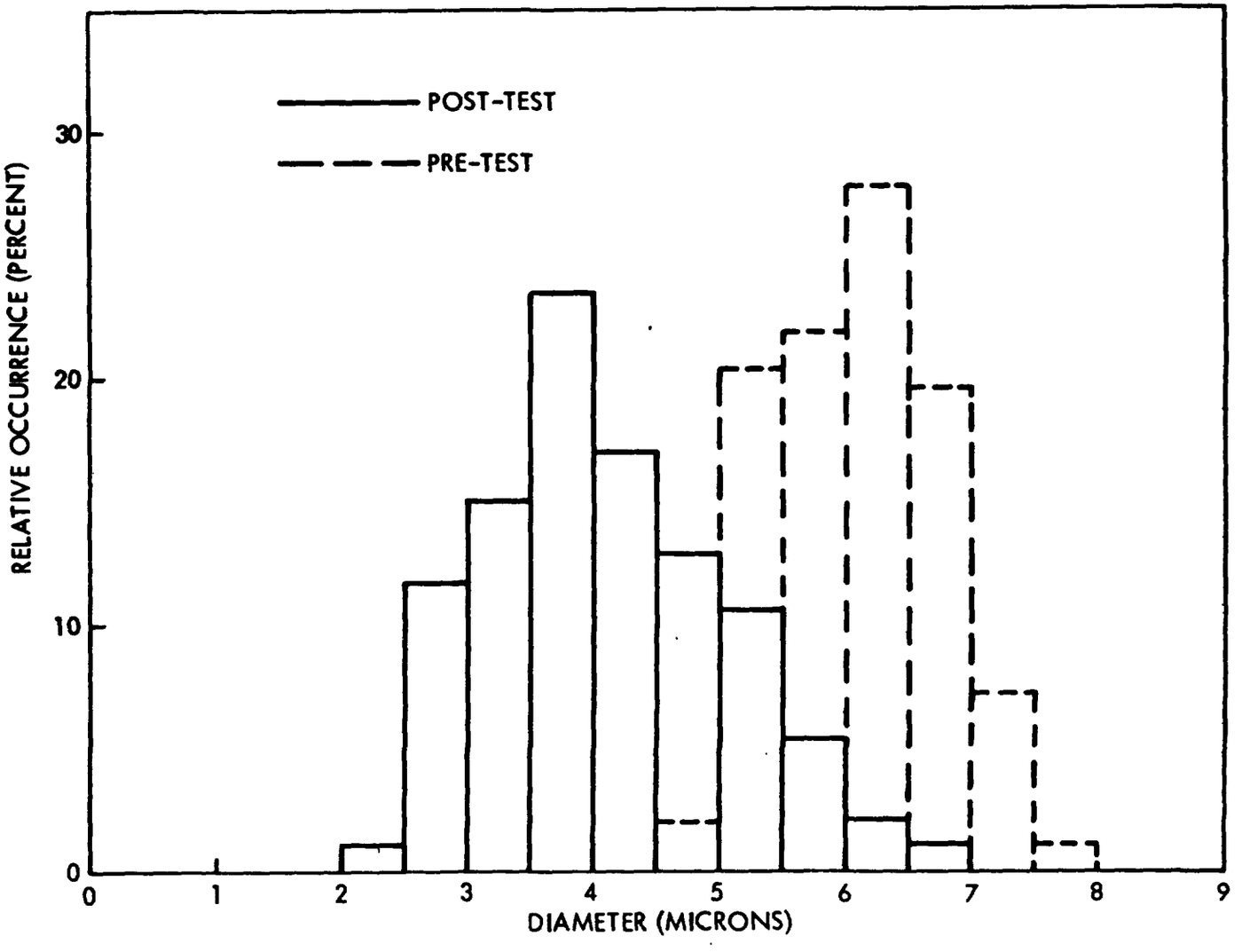

Figure 4-56. Cockpit Test 13 - Single Fiber Diameter Spectrum

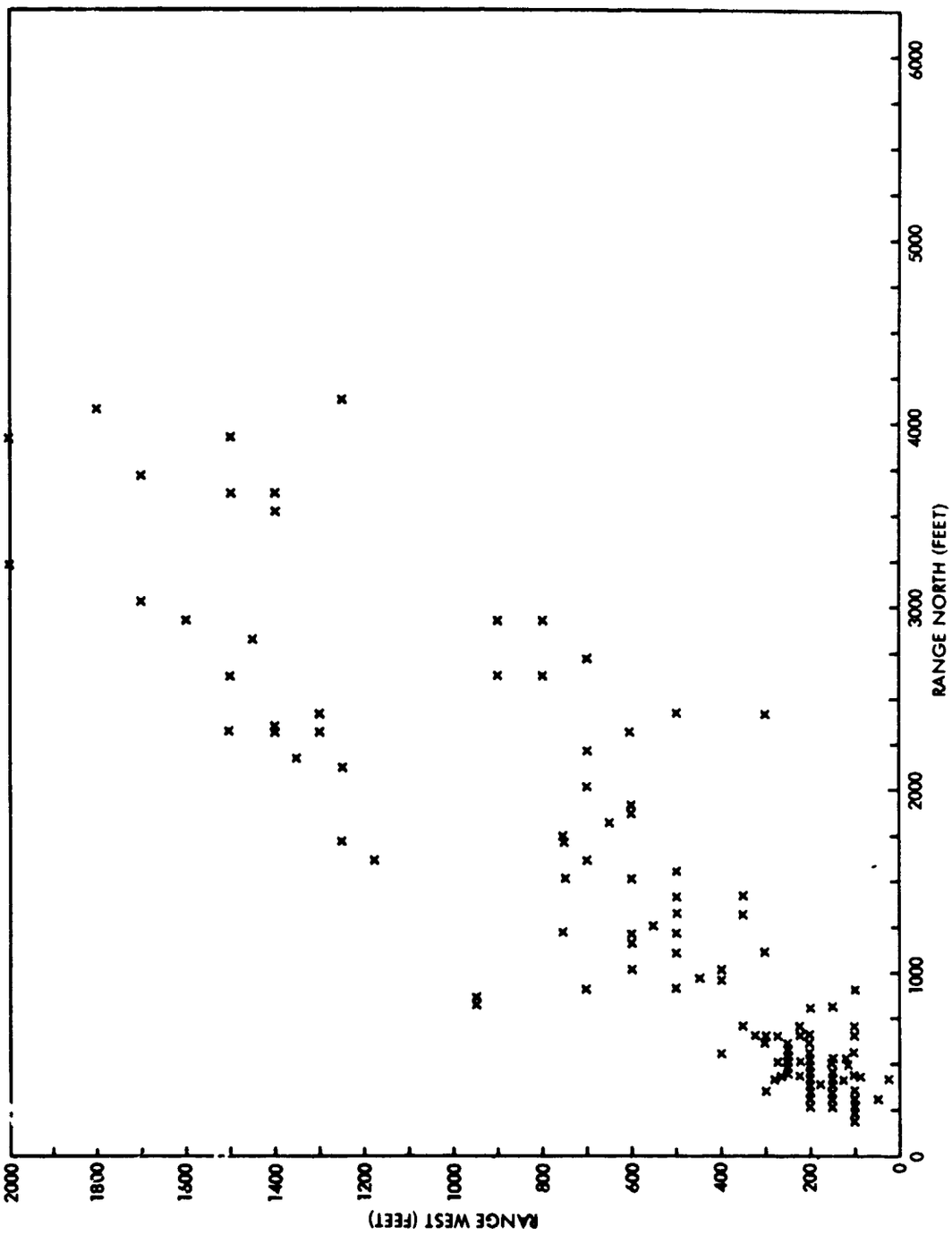

Figure 4.57. Cockpit Test 13 - Strip Deposition Locations

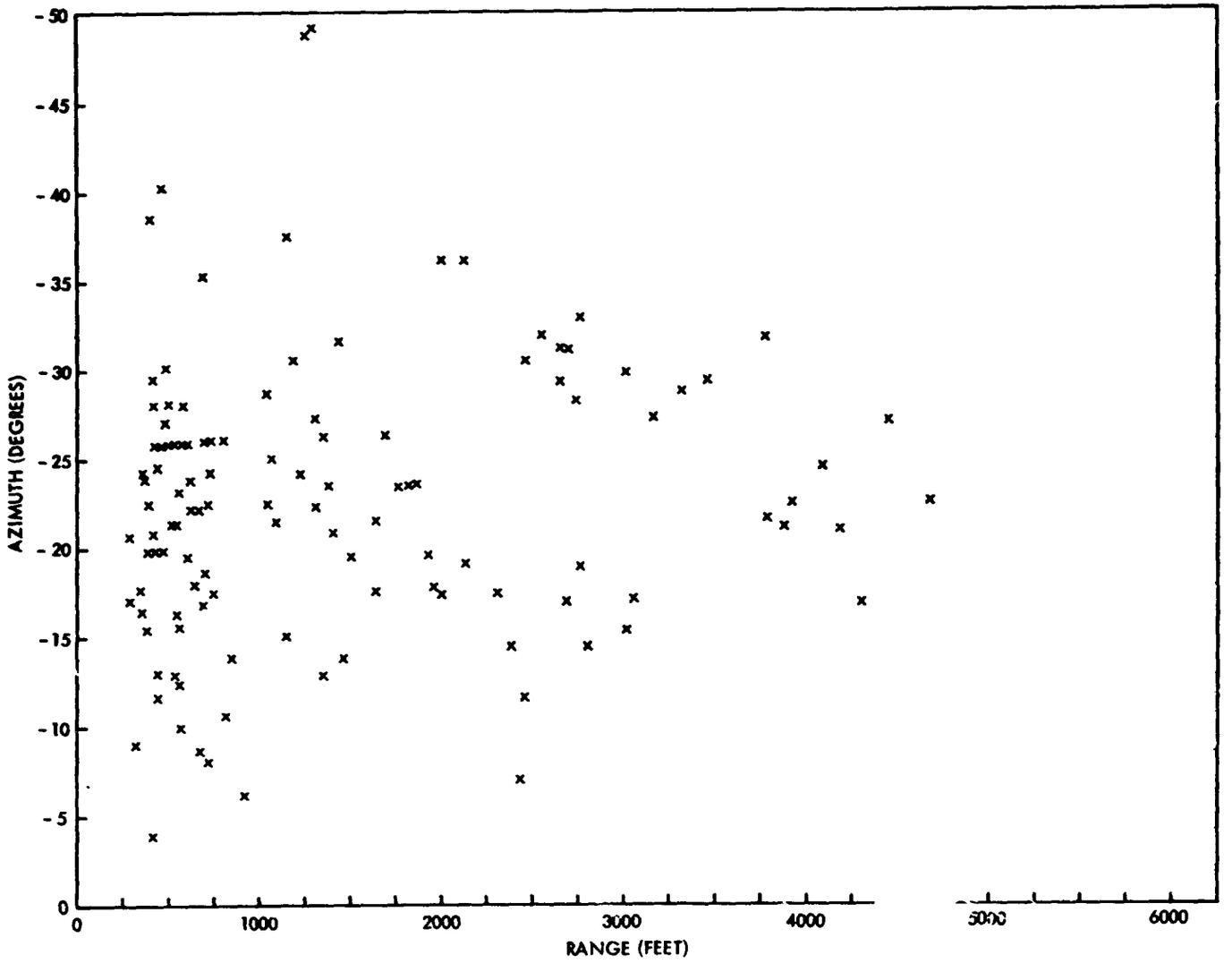

Figure 4-58. Cockpit Test 13 - Strip Deposition Azimuth vs Range

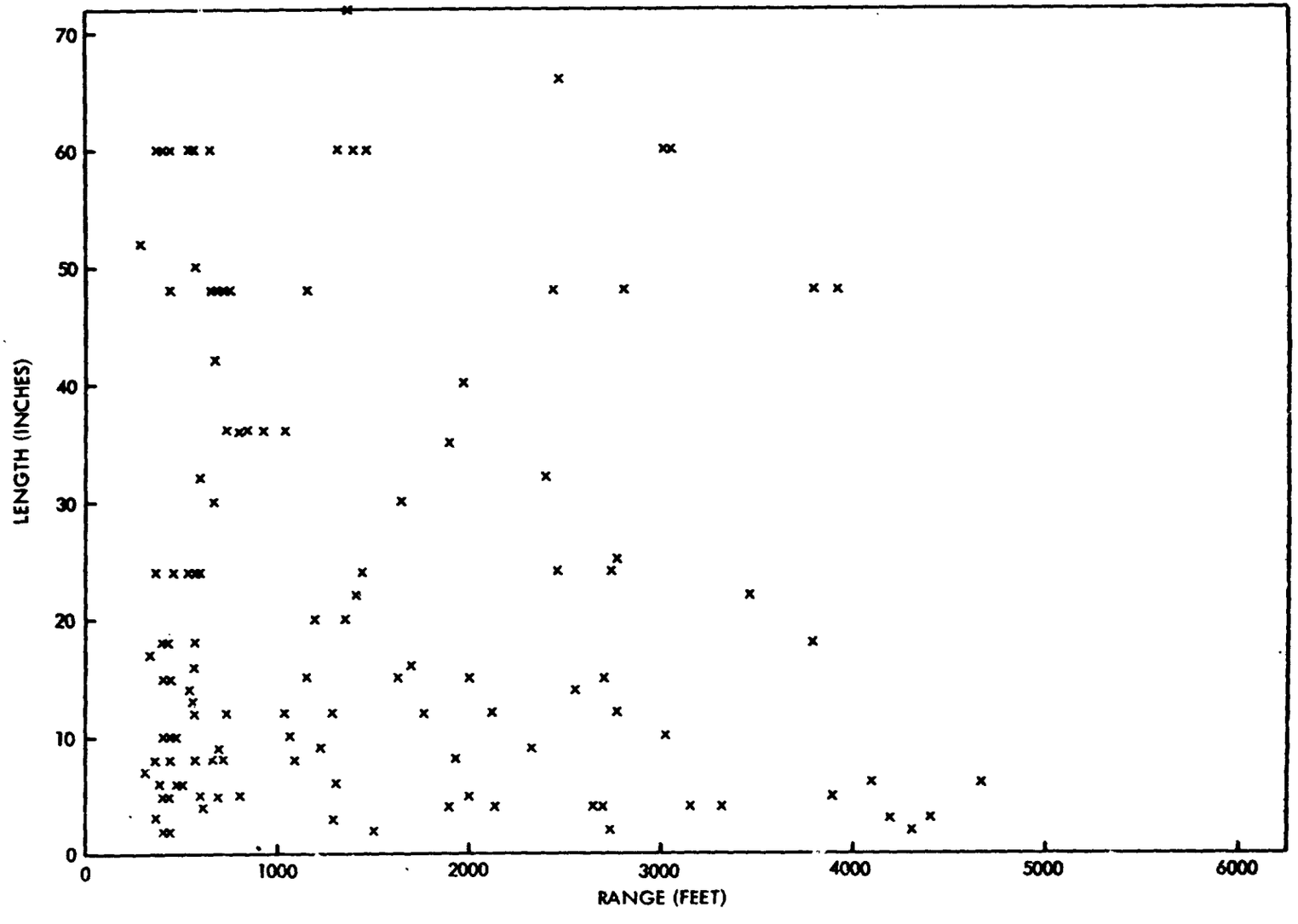

Figure 4.59. Cockpit Test 13 - Strip Length Distribution vs Range

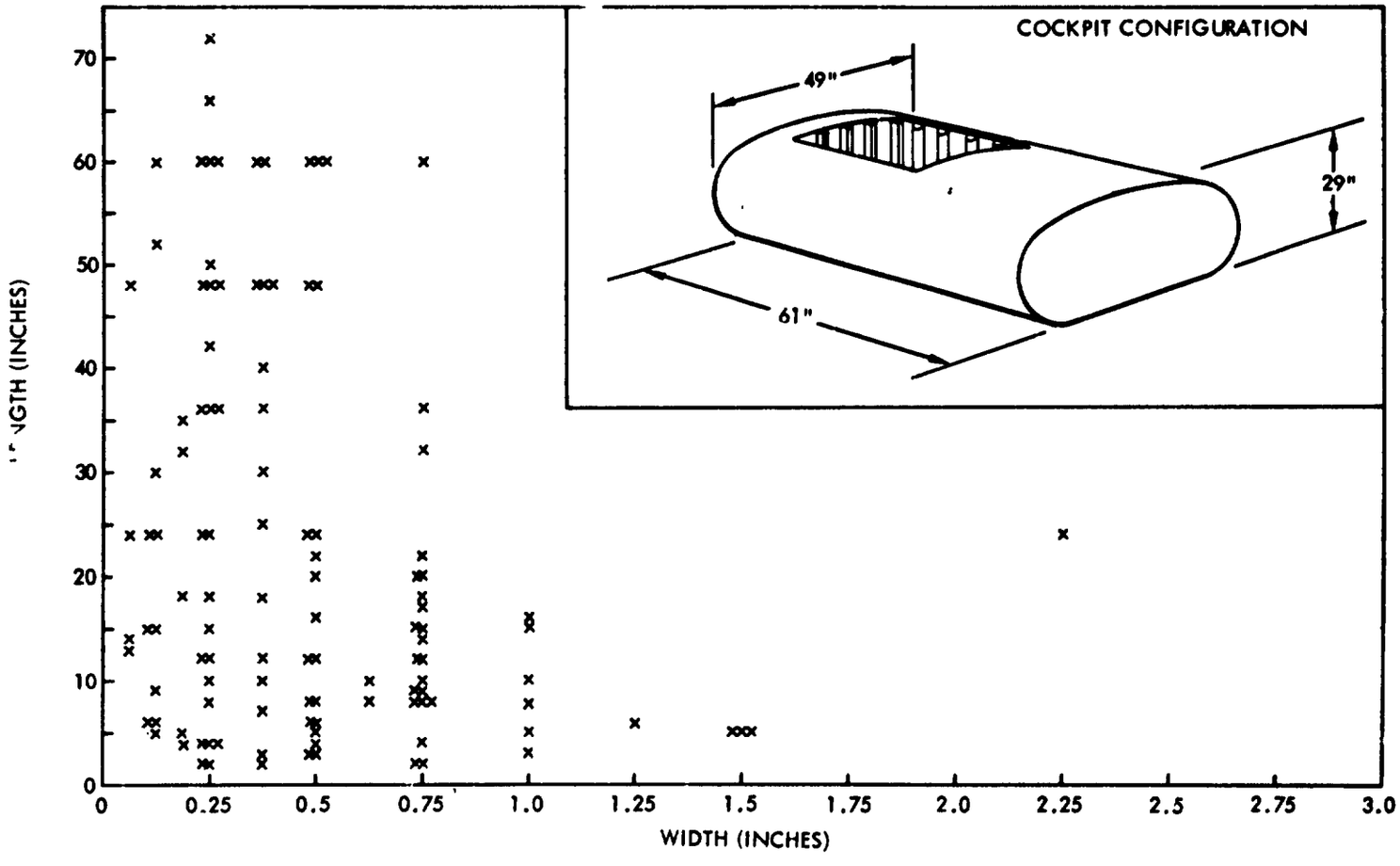

Figure 4.60. Cockpit Test 13 - Correlation of Strip Dimensions

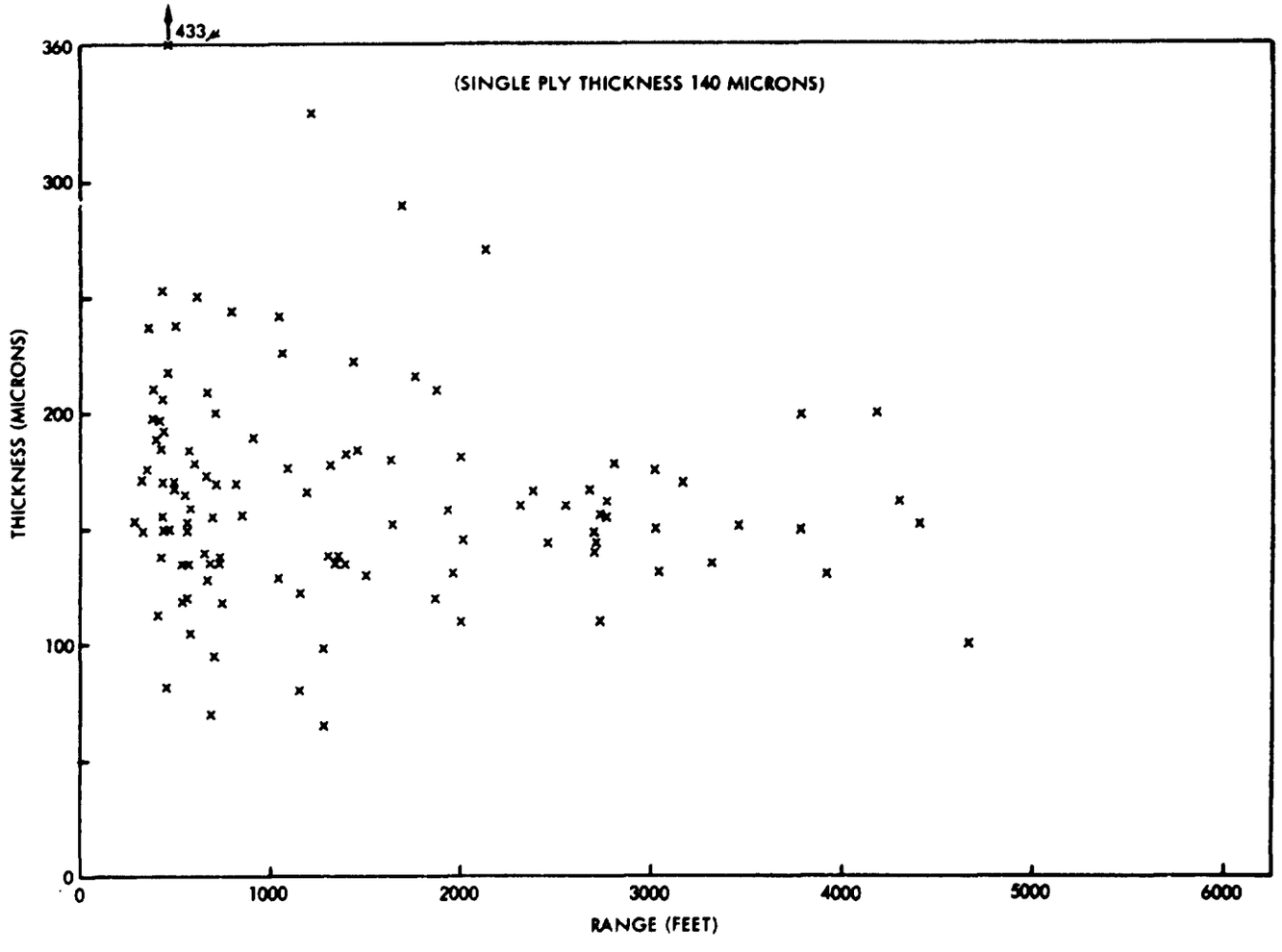

Figure 4.61. Cockpit Test 13 - Strip Thickness Distribution vs Range

A comparison is shown in Figure 4.62 of the variation of strip number with respective intervals of length, width and thickness. Approximately equal densities occurred over the range of 4" to 64" in length and 0.25" to 1" in width. With reference to the thickness distribution, however, about 75 percent of the strips were in the thickness domain of 0.9 to 1.5 ply.

Figure 4.63 presents a 3D plot of the strip deposition number as a function of range in relation to the contributions corresponding to the respective length and width intervals.

Mass Estimates

A mass balance analysis is presented in Figure 4.64. The initial fiber mass was estimated as 35.7 lb. Post-test cumulative mass of the composite debris from various sources was estimated as 10.0 lb. Resin content tests of debris samples indicated an average resin content of about 15 percent by weight. The net fiber mass of the post-test debris was therefore 8.5 lb, leaving a differential fiber mass of 27.2 lb to be accounted for.

COMPARATIVE EVALUATION

Comparisons of particle length distributions as functions of length interval are presented in Figures 4.65 and 4.66. In general the family of contours are quite similar for all of the tests.

A comparison of single fiber pre-test and post-test diameters is shown in Figure 4.67 for plate Test 3, barrel Test 8, spoiler Test 11 and cockpit Test 13. Oxidation effects were not very apparent for the plate sample, whereas significant reduction in average diameter occurred for the barrel, spoiler and cockpit samples. This result may possibly be attributed to the relatively few ply of the latter materials whereby heating effects would cause the resin to disappear early and permit oxidation of the exposed fibers.

A comparative tabulation of average particle lengths and average single fiber diameters is presented in Figure 4.68. The average lengths are quite comparable ranging from about 2 to 3 mm. The post-test diameters for the barrel, spoiler and cockpit samples averaged about 70 percent of the respective initial diameter.

Particle density characteristics and the relative contributions of the various types of particulate corresponding to the Jacob's Ladder data of spoiler Tests 11 and 12 and cockpit Test 13 are compared in Figure 4.69. The spoiler test data manifests a strong predominance of singles whereas multiples and clumps combined contribute the major fraction of particles toward the cockpit test data. With reference to the strong density increase with decreasing elevation shown by the Test 11 and Test 13 plots, the Test 12 data reflects a relatively uniform density distribution over the ladder network as noted in Figures 4.33, 4.45 and 4.53.

Figure 4.70 presents a comparative plot of strip dimensions for the spoiler Test 11 and cockpit Test 13. With reference to the length comparison, about 63 percent of the strip lengths for Test 11 were in the interval of 12" to 24"

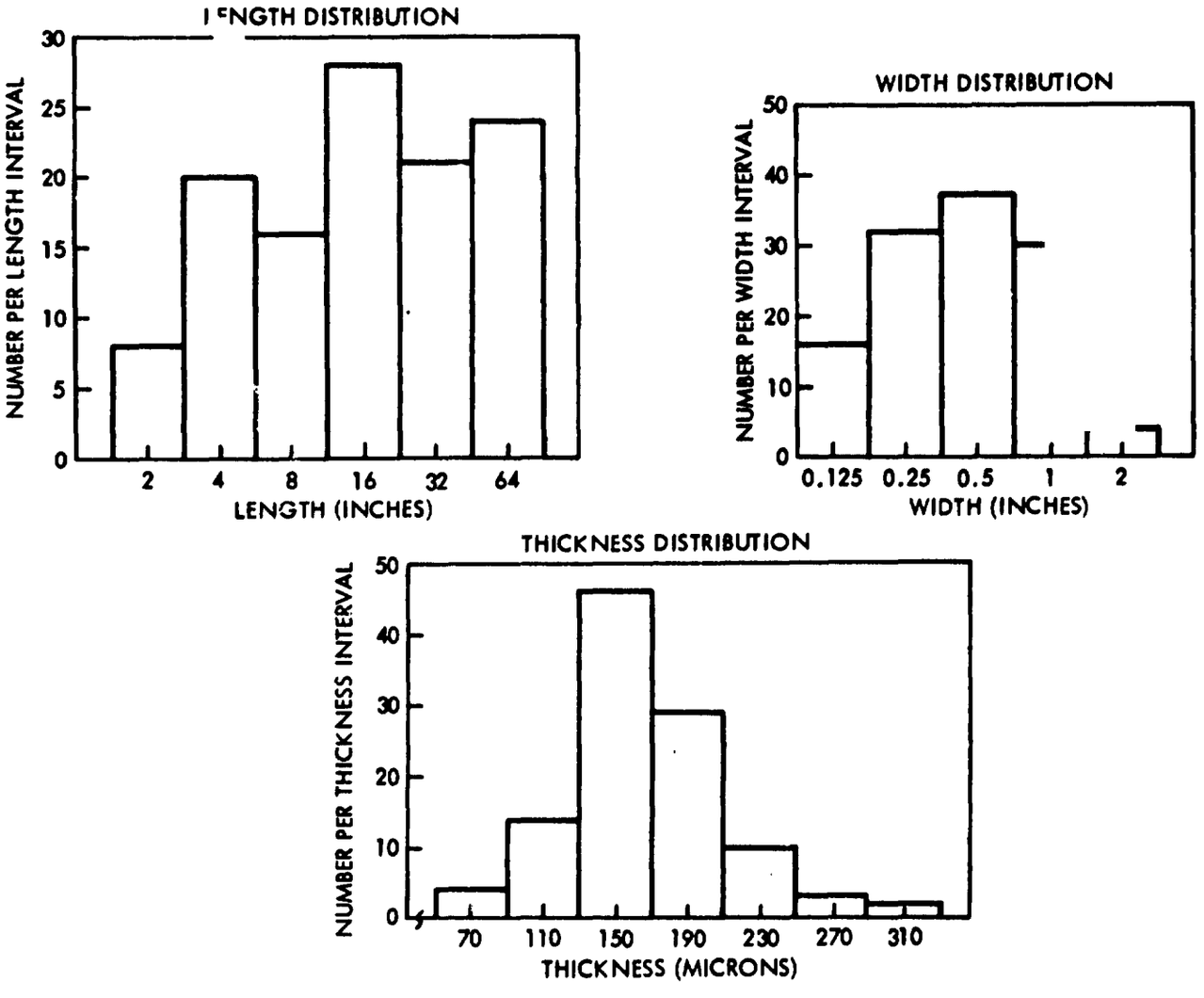

Figure 4-62. Cockpit Test 13 - Strip Length, Width and Thickness Distributions

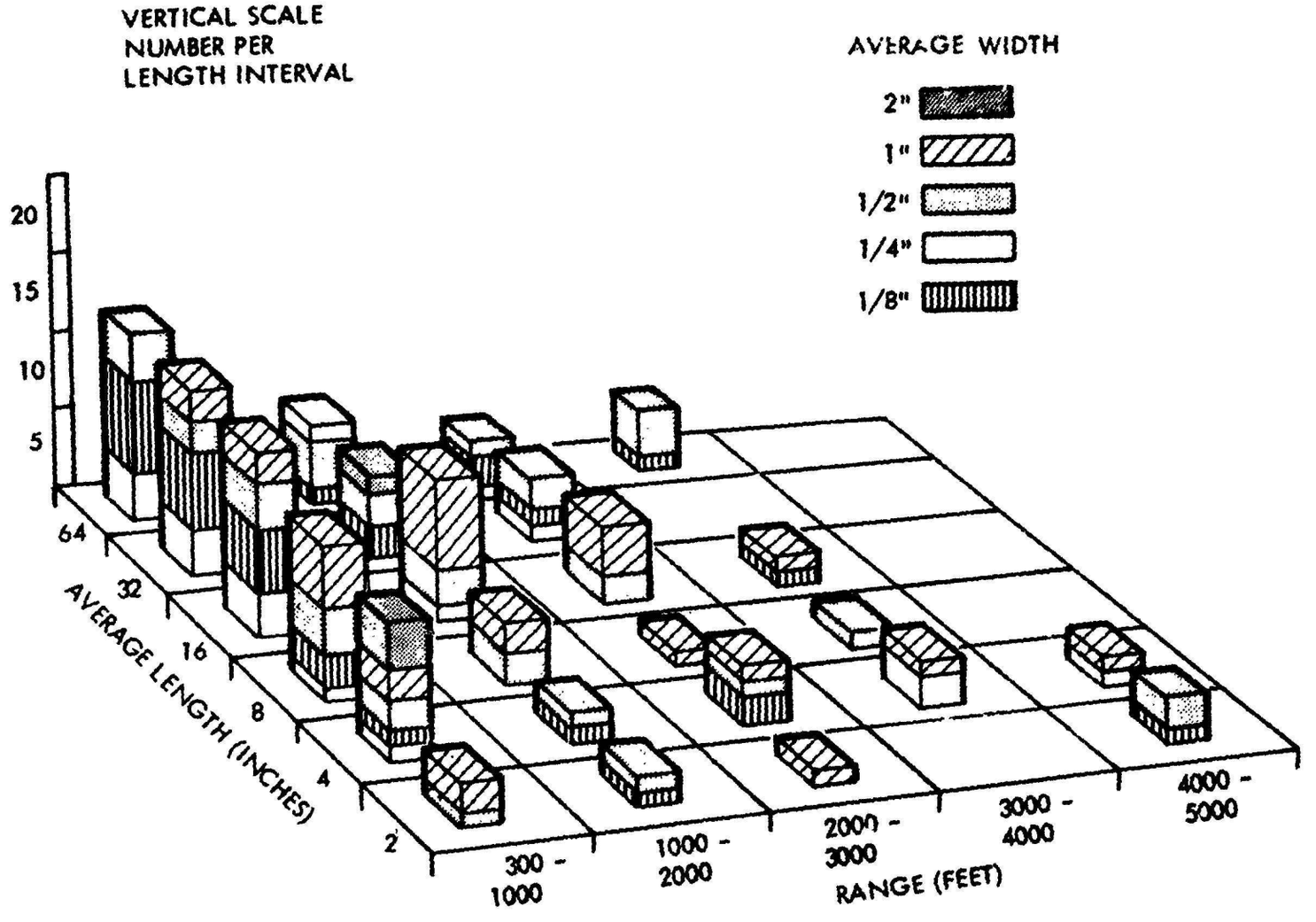

Figure 4.63. Cockpit Test 13 - Strip Deposition Spectrum

REPRESENTATIVE MASS DISTRIBUTION

GRAPHITE/EPOXY (FIBER 72%; EPOXY 28%)	50 LB
GLASS FIBER	25 LB
KEVLAR-49 EPOXY	15 LB
ADHESIVE	6 LB
ALUMINUM/MISCELLANEOUS	20 LB
TOTAL	116 LBS

TEST SAMPLE

PRE-TEST WEIGHT (SAMEPL FOR LAB ANALYSIS)	115 LBS

INITIAL MASS DISTRIBUTION

GRAPHITE FIBER	35.7 LBS
EPOXY	13.9
TOTAL	49.6 LBS

POST-TEST CUMULATIVE MASS

COMPOSITE DEBRIS

POOL	8.8 LB
20' TO 40'W OF POOL	0.14
20' TO 40'N OF POOL	0.33
-40 to 0° N (0 TO 50'W)	0.09
0 TO 50'N (0 TO 100' W)	0.04
50' TO 100' N (0 TO 150' W)	0.03
100' TO 150' N (0 TO 150' W)	0.06
150' TO 200' N (0 TO 150' W)1	0.13
STICKY PAPER (100' TO 3000' N)	0.10
STRIPS (300' TO 5000' N)	0.27
TOTAL	10.0 LBS

MASS BALANCE EVALUATION

INITIAL GRAPHITE FIBER		35.7 LBS
MASS LOSS		
COMPOSITE DEBRIS	10.0 LB	
EPOXY CONTENT (15%)	1.5	
NET		8.5
DIFFERENTIAL FIBER MASS		27.2 LBS

Figure 4-64. Cockpit Test 13 - Mass Balance Analysis

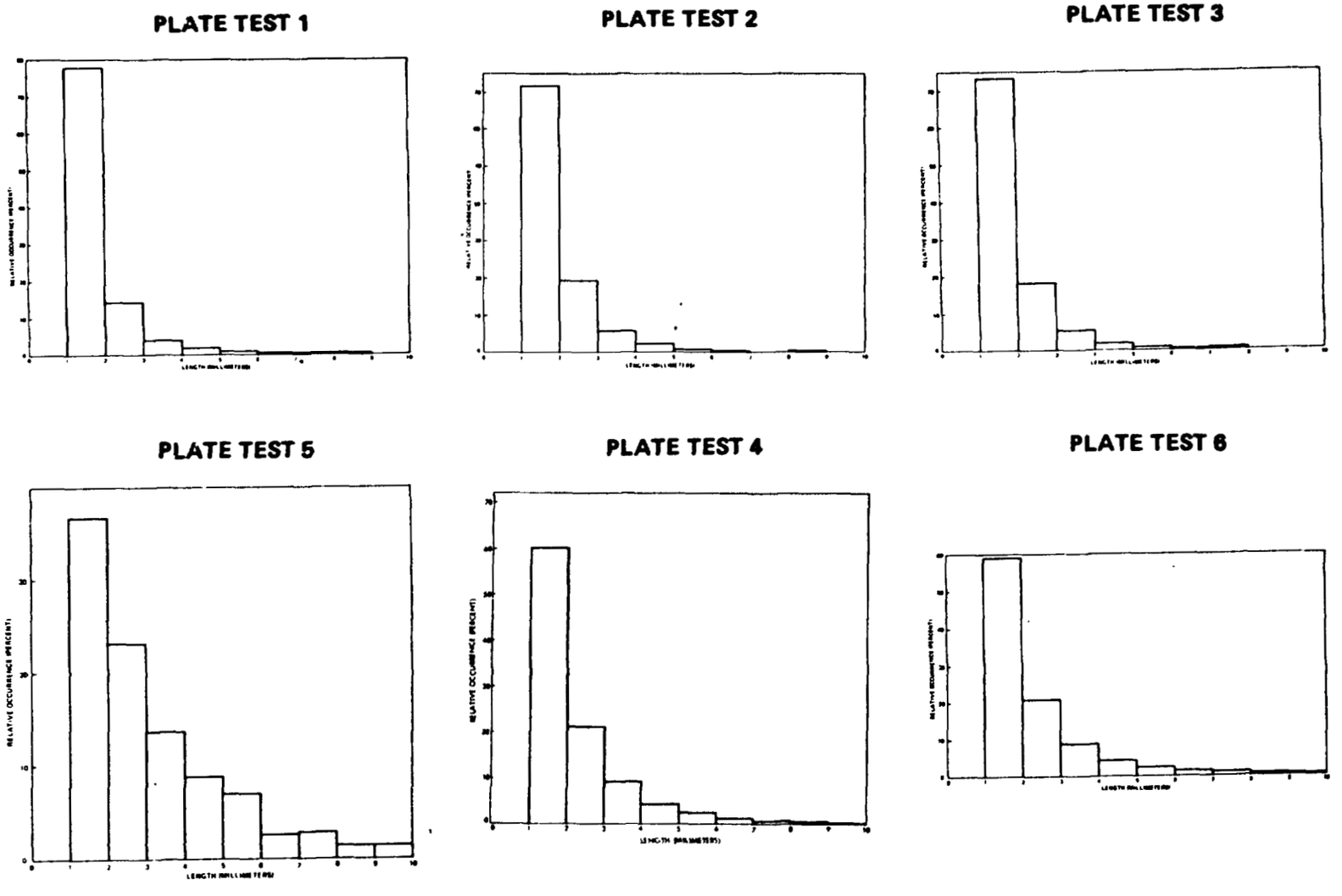

Figure 4.65. Comparison of Particle Length Distributions - I

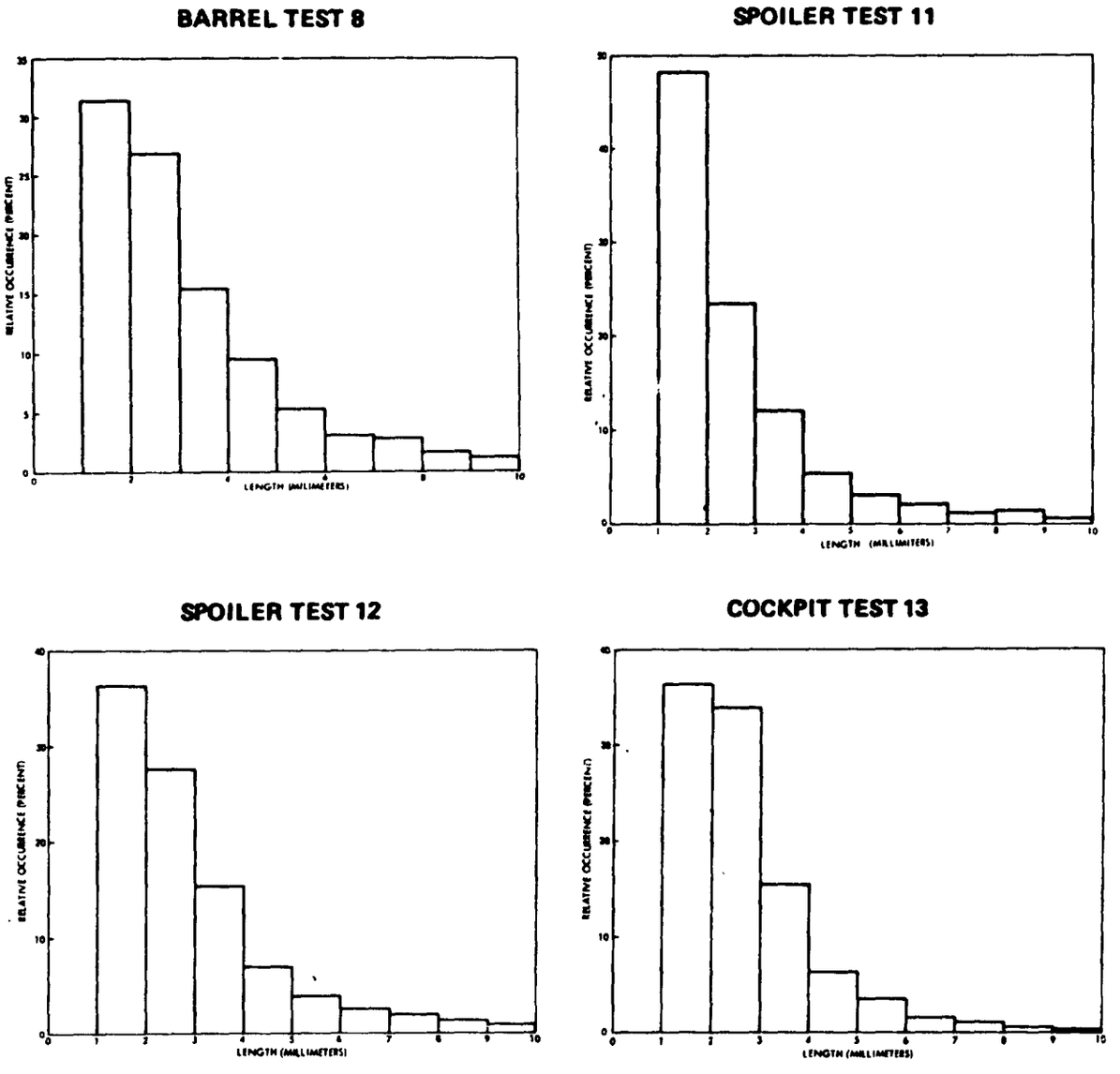

Figure 4.66. Comparison of Particle Length Distributions - II

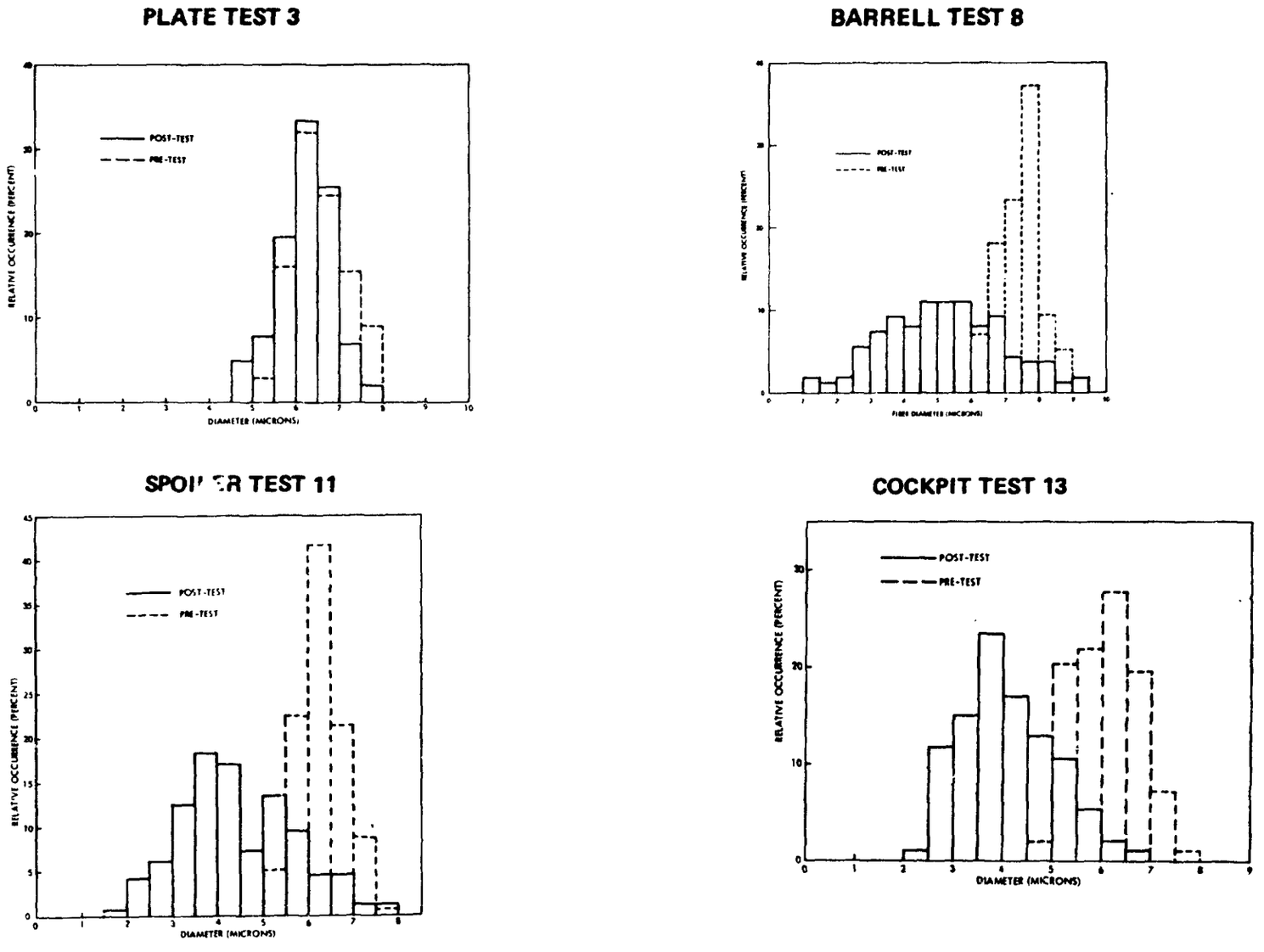

Figure 4.67. Comparison of Single Fiber Pre-Test and Post-Test Diameters

TEST	SAMPLE	AVERAGE PARTICLE LENGTH* (MILLIMETERS)	SINGLE FIBER AVERAGE DIAMETER (MICRONS)	
			PRE–TEST	POST–TEST
1	PLATE	1.76	–	–
2	PLATE	1.83	–	–
3	PLATE	1.82	6.48	6.07
4	PLATE	3.23	–	–
5	PLATE	2.36	–	–
6	PLATE	2.42	–	–
8	BARREL	3.20	7.39	5.19
11	SPOILER	2.79	6.18	4.32
12	SPOILER	3.16	–	–
13	COCKPIT	2.71	6.04	3.99

*LENGTH INTERVAL 1 TO 20 MILLIMETERS

Figure 4-68. Comparison of Particle Dimensions

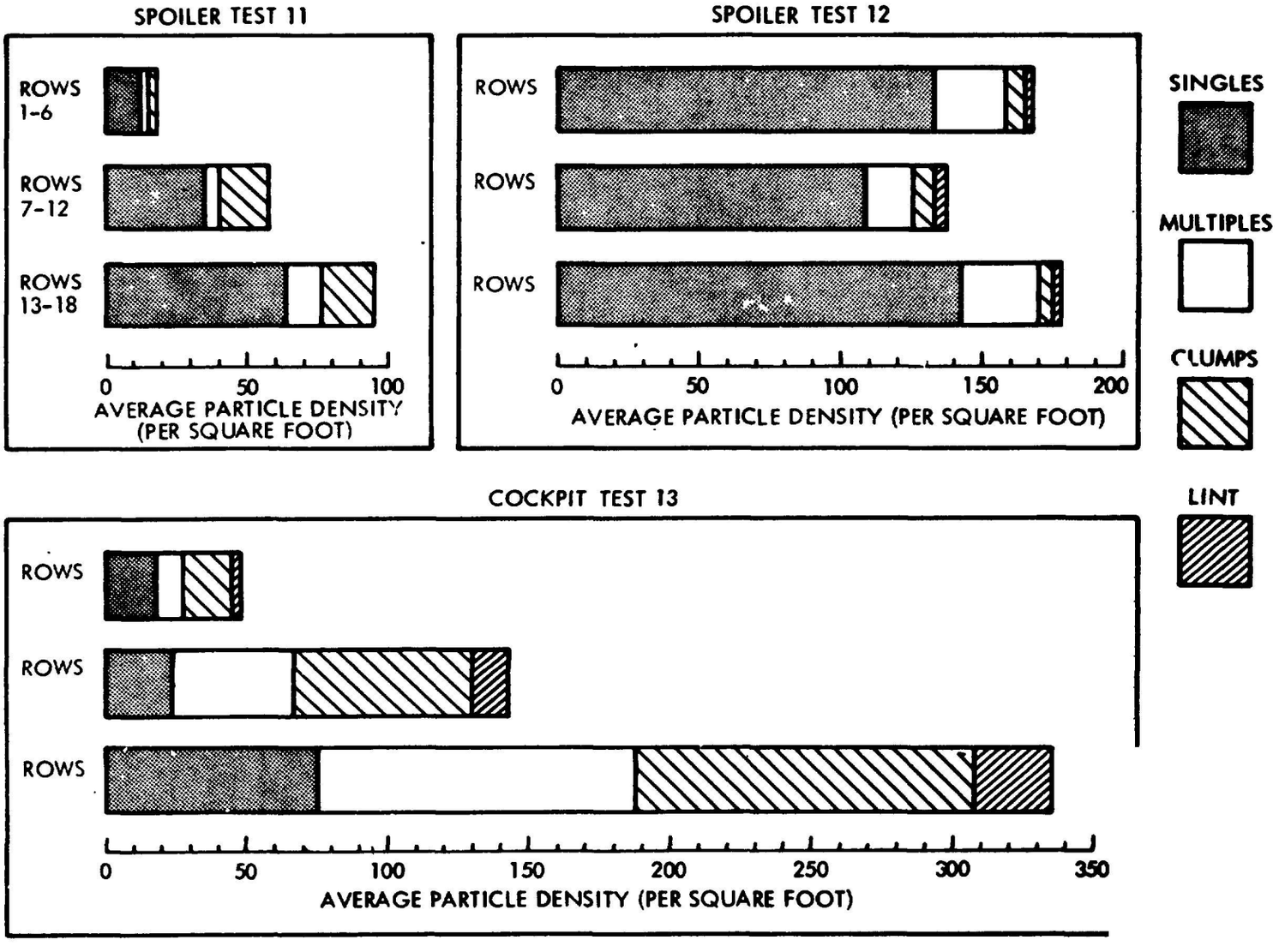

Figure 4.69. Comparison of Jacob's Ladder Particle Spectrum Distributions

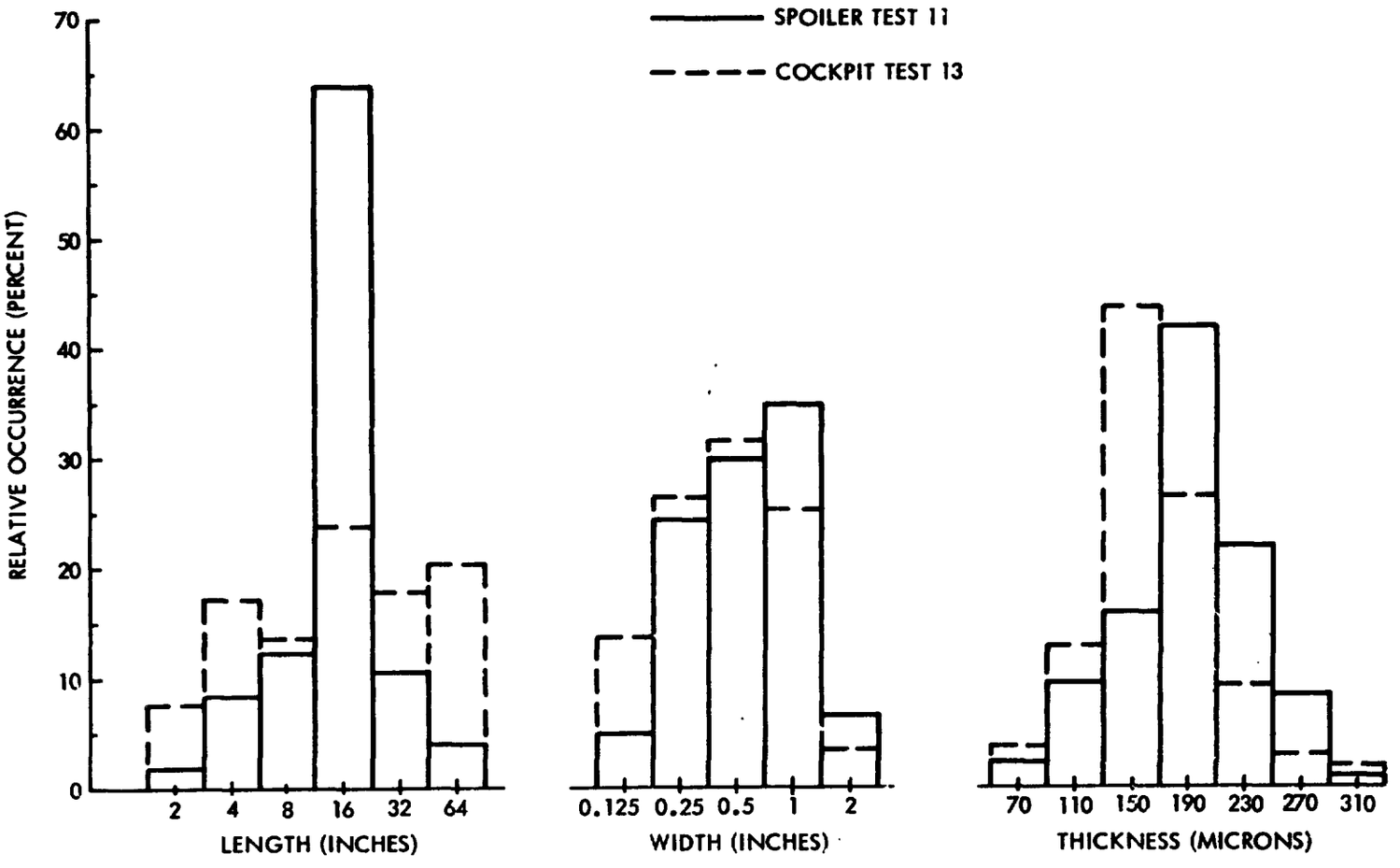

Figure 4.70. Comparison of Strip Dimensions For Spoiler and Cockpit Tests

whereas no singular predominance was observed for Test 13. The width distributions for the two tests are quite comparable with relatively small differences. Examination of the thickness distributions indicates that relative to similar single ply dimensions the Test 11 data reflects a predominance in the interval from 0.9 to 1.2 ply thickness as compared to 1.2 to 1.5 ply thickness for the Test 13 data.

Comparison of particle number and mass corresponding to the sticky paper data for the various tests is shown in Figure 4.71. With reference to the particle number data relatively good agreement is observed within the set of chamber test data from Tests 1, 2 and 3, and within the set of field test data from Tests 4, 5, 6, 11 and 13. The difference between the two sets of data is a higher occurrance for larger particle lengths in the field tests. In conjunction with the mass data good agreement again occurs within the chamber test data of Tests 1, 2 and 3. However, the field test data manifest large variations in specific values for the length interval spectrum between the set for Tests 4, 5 and 6 and that of Tests 11 and 12. Reasonable agreement is observed within plate test data for Tests 4, 5 and 6 with enhanced values for the higher length intervals as compared to the plate test data of Tests 1, 2 and 3.

Figure 4.72 presents a comparison of deposition mass relative to initial mass for the plate, barrel, spoiler and cockpit tests for particle lengths of 1 to 20 mm. For plate test 3 the mass deposition data indicated capture of a total of 19% of the initial composite mass for all particulate. For this high capture efficiency, only 0.01% of the initial composite mass was observed as single fiber mass. Similar results were obtained for plate Test 5 of 12% total mass and 0.008% single fiber mass, respectively.

LABORATORY ANALYSES

Laboratory studies of pre-test and post-test samples were performed in an effort to explore material properties which may have contributed toward generation of the particular particle characteristics observed during the respective burn and explode tests. Determination of resin content was made by means of an acid digestion procedure. Thermal properties were investigated by oven tests and thermal gravimetric analyses (TGA). The TGA equipment consisted of a Dupont No. 990 Termal Analyzer coupled with a Dupont No. 951 Thermogravimetric Analyzer Attachment.

Composite materials consisted fo the following:

Sample	Composite
Plate	T300/NARMCO 5208
Barrel	AS/APCO 2434
Spoiler	T300/NARMCO 5209
Cockpit	T300/NARMCO 5208

PARTICLE NUMBER

LENGTH INTERVAL (MM)	RELATIVE OCCURRENCE (PERCENT)							
	TEST 1	TEST 2	TEST 3	TEST 4	TEST 5	TEST 6	TEST 11	TEST 13
1-2	77.5	71.5	73.0	37.4	58.9	59.0	42.8	47.8
2-5	20.3	27.1	25.5	45.0	35.2	33.8	43.7	43.1
5-10	2.0	1.2	1.3	15.0	5.1	5.8	12.1	8.6
10-20	0.2	0.2	0.2	2.6	0.8	1.4	1.4	0.5

PARTICLE MASS

LENGTH INTERVAL (MM)	RELATIVE OCCURRENCE (PERCENT)							
	TEST 1	TEST 2	TEST 3	TEST 4	TEST 5	TEST 6	TEST 11	TEST 13
1-2	54.2	37.1	40.8	5.3	19.8	15.8	2.9	8.1
2-5	32.4	51.5	49.5	29.8	45.4	33.3	5.7	32.2
5-10	13.4	10.4	9.7	40.6	23.7	27.5	91.4	59.7
10-20	-	1.0	-	24.3	11.1	23.4	-	-

Figure 4.71. Comparison of Particle Number and Mass Distributions

TEST	SAMPLE	INITIAL COMPOSITE MASS (GM)	DEPOSITION REGION	TOTAL DEPOSITION*		SINGLE FIBERS	
				MASS (GM)	FRACTION OF INITIAL MASS (%)	MASS (GM)	FRACTION OF INITIAL MASS (%)
3	PLATE	873	15' x 15' CHAMBER	168	19.2	0.08	0.01
5	PLATE	578	60' - 600' N	105	12.0	0.07	0.008
8	BARREL	7,380	50' - 600' N	50	0.7	0.49	0.007
11	SPOILER	3,770	30' - 200' N	3	0.08	0.01	0.0003
13	COCKPIT	22,500	30' - 200' N	9	0.04	0.04	0.0002

*PARTICLE LENGTH INTERVAL 1 TO 20 mm

Figure 4.72. Comparison of Deposition Mass Relative to Initial Mass

Resin content tests indicated approximately 30% resin by weight for the plate, spoiler and cockpit pre-test samples. However, for the case of the barrel sample of Test 8, the resin content was found to be 50%. In addition, the composite density for the barrel was found to be only 1.09 gm/cm^3 indicating a void ratio of about 30%. Normally void ratios are in the range of 1 to 2%. Discussions with R. Shuford of the Army Material and Mechanics Research Center indicated that two types of barrels had been supplied for the NWC tests, with Type A subjected to the hot propane burn and explode of Test 8 and Type B utilized in the JP-5 pool fire events of Tests 9 and 10. The two barrel types had been manufactured by different processes at different times. For the case of Type A Shuford indicated that a larger void ratio than normally might be anticipated such as perhaps 10 to 15%.

Oven and TGA tests were conducted in the temperature ranges compatible with test conditions. The thermal history of the plate sample of Test 6 is shown by the solid curves in Figure 4.73. Thermocouple measurements were made at depths of 1/16", 1/8" and 3/16" of the 1/4" sample. The contours in Figure 4.73 indicated a sharp rise in temperature within a period of about 1 minute at all levels with a more gradual increasing rate for the subsequent 19 minutes of the burn phase.

The dashed curves of Figure 4.73 were the result of a 1D analytical model assuming a heat source of 2200^{0}F being applied to the front surface of a 1/4" plate with insulated back surface. The thermal conductivity of the T300/5208 plate was assumed to be 10 BTU/HR/FT/^{0}F, specific heat as 38.8 BTU/LB/^{0}F and density as 1.57 gm/cc. The poor agreement between the two sets of contours in Figure 4.73 indicates that the 1D model is ineffective in describing the thermal history adequately.

The edge effects appear to be important from the standpoint of heat being propagated along the fibers and interstitial resin layers in the exposed lateral surfaces. Attention was therefore focussed on oven and TGA tests to gain some insight into mass loss characteristics of the various composite samples, the requirement being that high temperatures be introduced rapidly to simulate the environments of the samples during the field tests.

Figure 4.74 shows the nature of the temperature distribution within a JP-5 jet fuel fire. Thermocouple data during the spoiler Test 11 plotted in Figure 4.75 indicate that the thermal rise times are very short with peak temperatures commensurate with the pool fire temperatures estimated at an elevation of about 6 ft corresponding to the test sample location.

TEST RESULTS

Oven Tests

A thermocouple record obtained during an oven test of a plate sample is shown in Figure 4.76. The sample size was 0.2" cube and oven temperature of 960^{0}F. An effort was made to insert the sample and close the oven door rapidly in order to minimize the drop in temperature and time period to reestablish the original 960^{0}F.

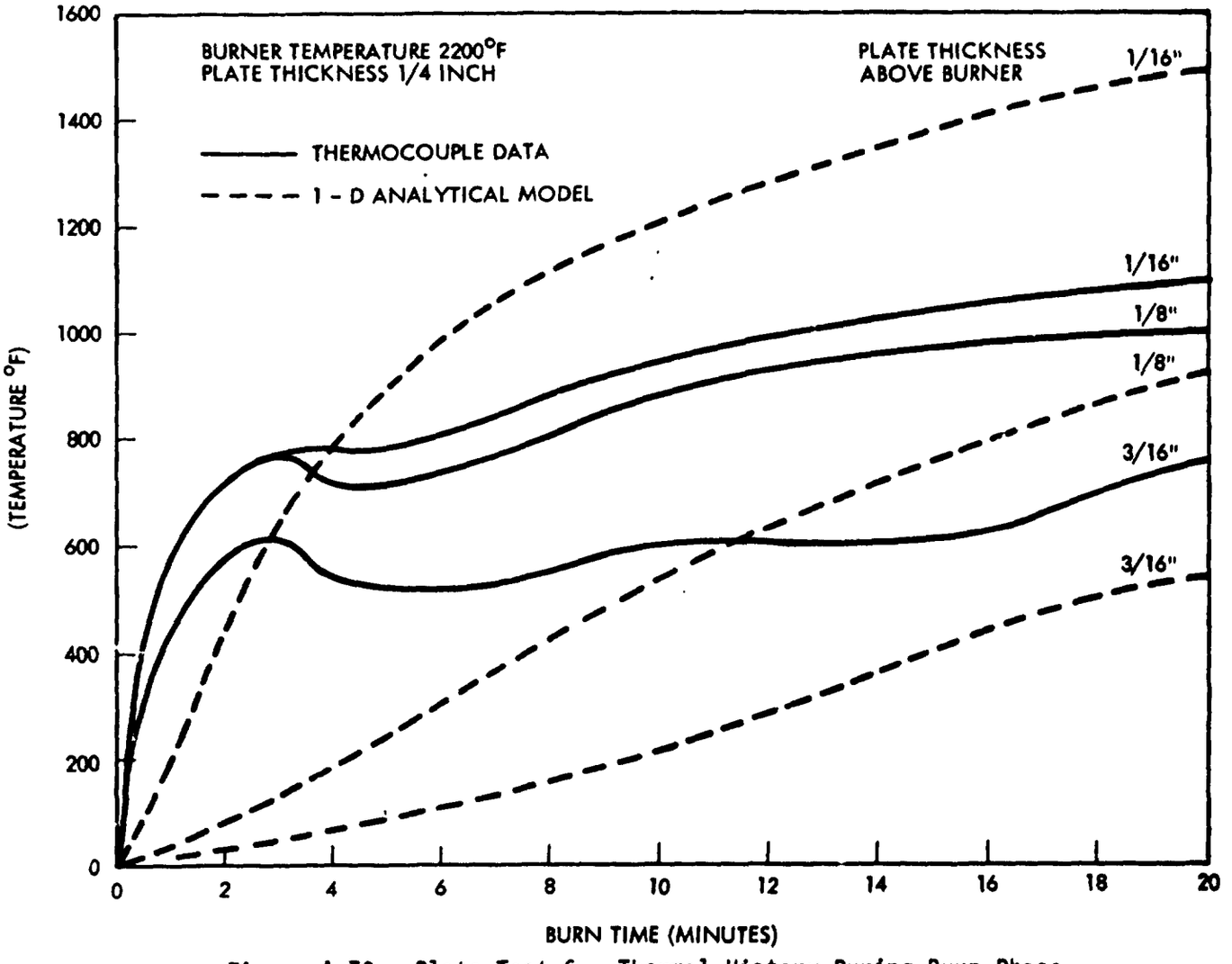

Figure 4.73. Plate Test 6 - Thermal History During Burn Phase

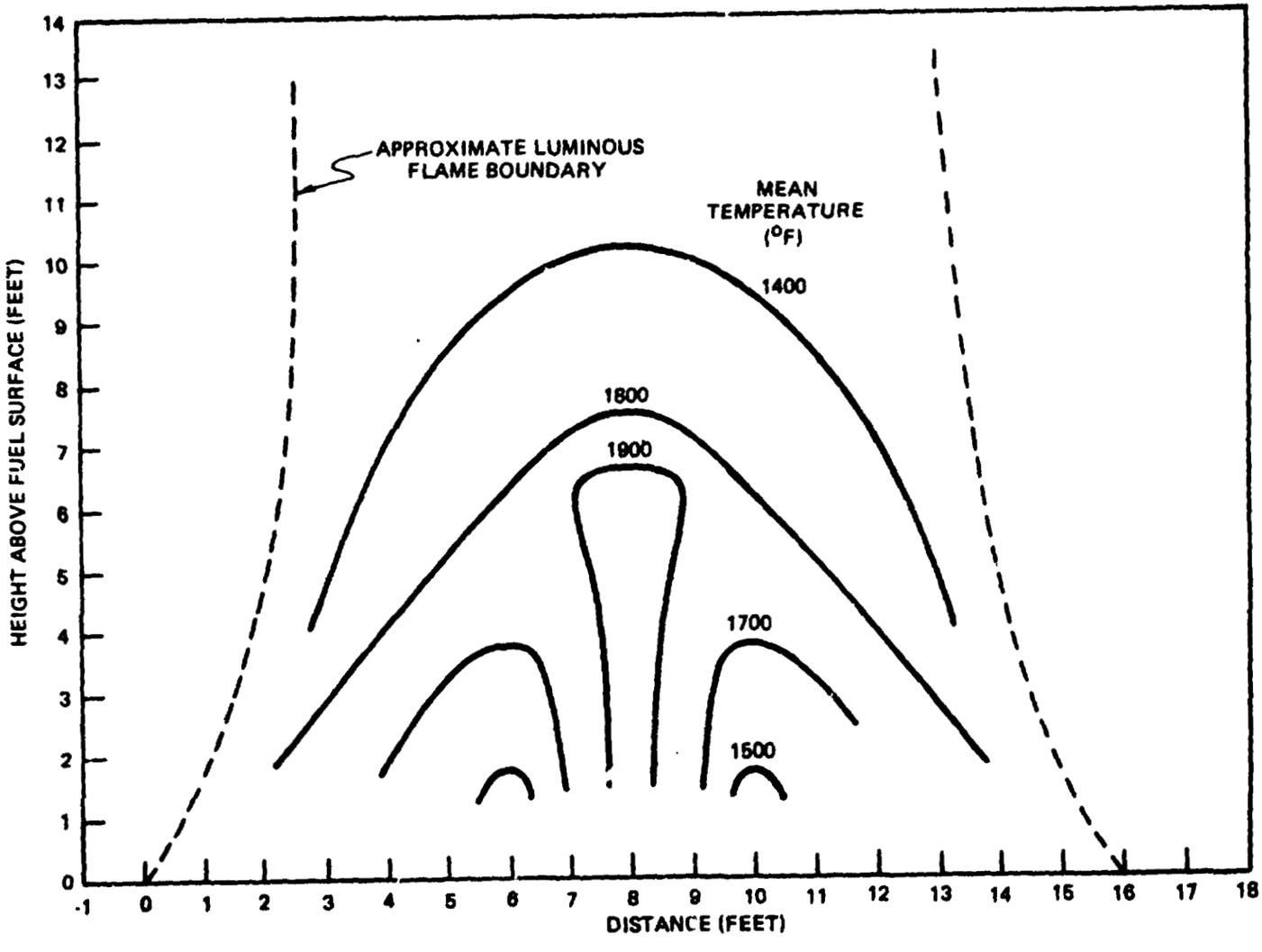

Figure 4.74. Temperature Distribution Within a JP-5 Jet Fuel Fire

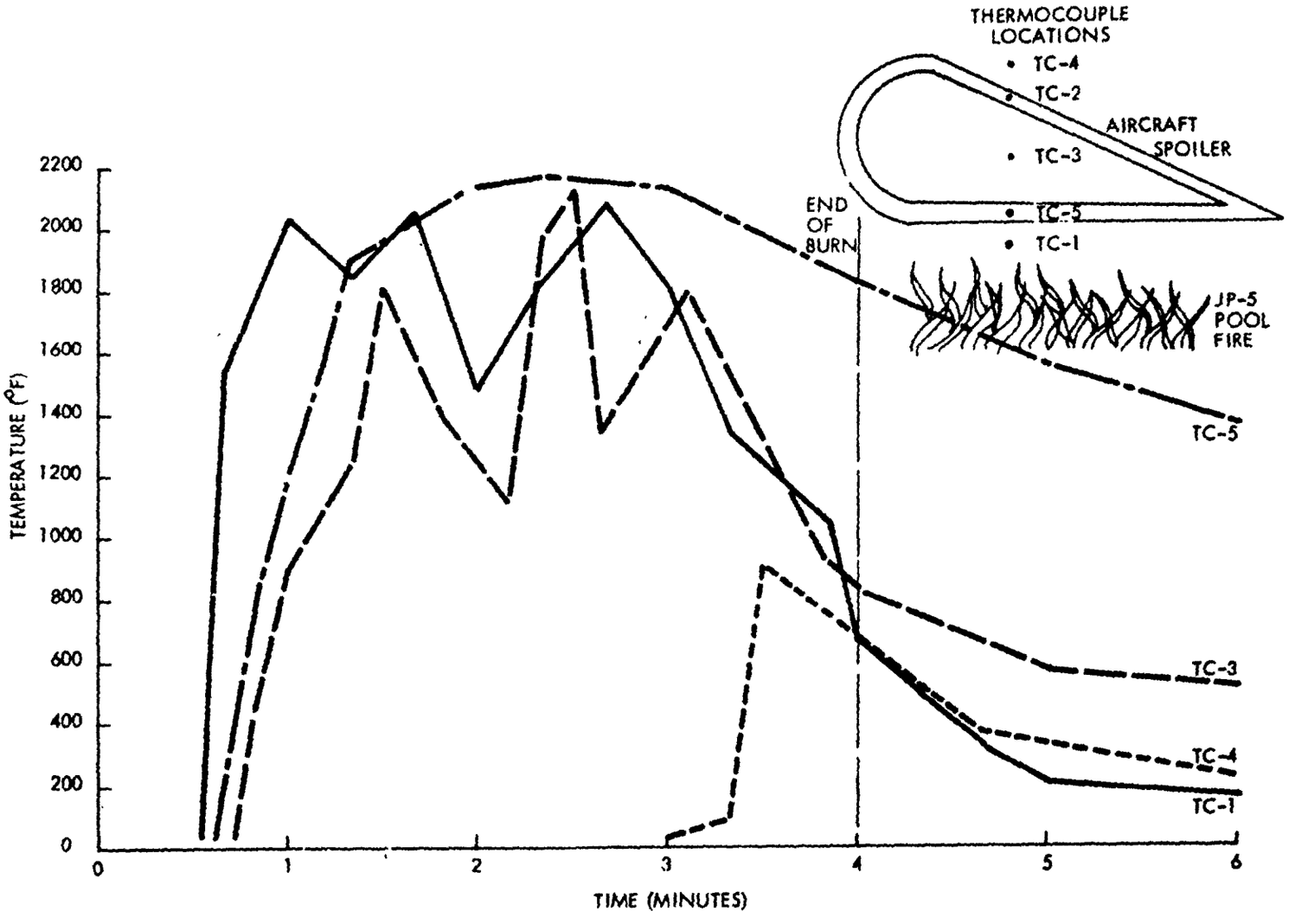

Figure 4.75. Temperature History During Spoiler Burn, Test No. 11

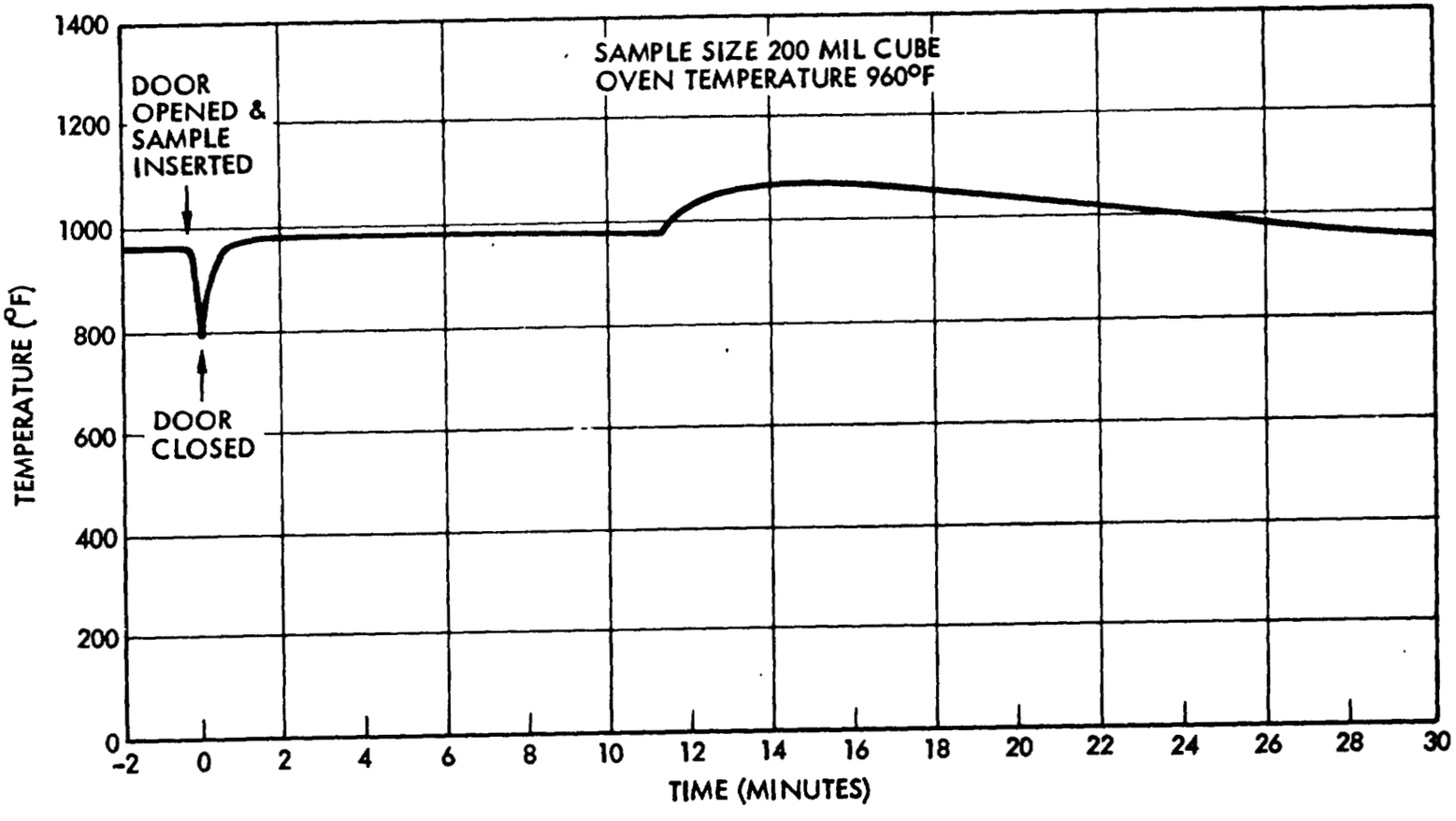

Figure 4-76. Oven Test For Plate Composite Material

A slight increase in termperature occurred at the early stages due to an exothermic reaction during depolymerization of the resin. A level of about 980°F was sustained for a number of minutes until spontaneous ignition of the T300 fiber occurred at about 11 minutes with an associated increase in temperature of 80°F.

Other tests were performed at the same oven temperature but terminated at different time periods both less than and greater than the ignition time t_o. Samples were weighed before and after each test. Corresponding mass loss data indicated an S-shaped pattern with gradual loss rate prior to t_o, a rapid increase for a short period following t_o and then a return to a more gradual rate.

TGA Tests

Figure 4.77 illustrates the thermal history and time history of mass loss from a TGA test of a plate sample of 0.08" cube dimensions. The usual procedure for TGA tests is to increase the temperature at a rate of perhaps 10°F to 20°F per minute up to the required peak value. Time periods of the order of an hour would be involved in reaching temperatures of interest of about 1000°F. This long duration of the heating process would not be a reasonable simulation of the field test burn environment.

The TGA procedure was therefore modified in order to offer a better simulation of the field test conditions. The TGA equipment consists of a hollow cylindrical oven heated by a series of coils and an independent glass bulb within which the sample is placed in a small platinum boat, with a thermocouple being located inside the boat in close proximity to but not in contact with the sample. A thermostatic cut-off control regulates the oven temperature to the designated settings.

Normally the sample is placed in the boat, the mass balance set at 100%, the bulb inserted into the oven and then the heating process initiated. This procedure was modified such that the oven was first heated to the required temperature and then the bulb inserted into the oven chamber. As a result the temperature rose to the required levels in time periods of only about 1 to 1.5 minutes as seen from the thermal history record in Figure 4.77 where the peak temperature setting was 960°F.

In Figure 4.77 a mass loss of 20% occurs quite rapidly due to depolymerization of the resin. At about 12 minutes a sudden increase in temperature occurs coupled with a large increase in mass loss rate. This effect is similar to the oven test data and reflects spontaneous ignition of the T300 fiber.

TGA tests were performed for pre-test samples of the various composite materials, namely plate, barrel, spoiler and cockpit. In addition the test samples also included individual T-300 fibers. Test durations in all cases were 20 minutes with TGA pre-heat values progressively increased for subsequent tests until the mass loss reached 80%. Results of these tests are shown in Figure 4.78.

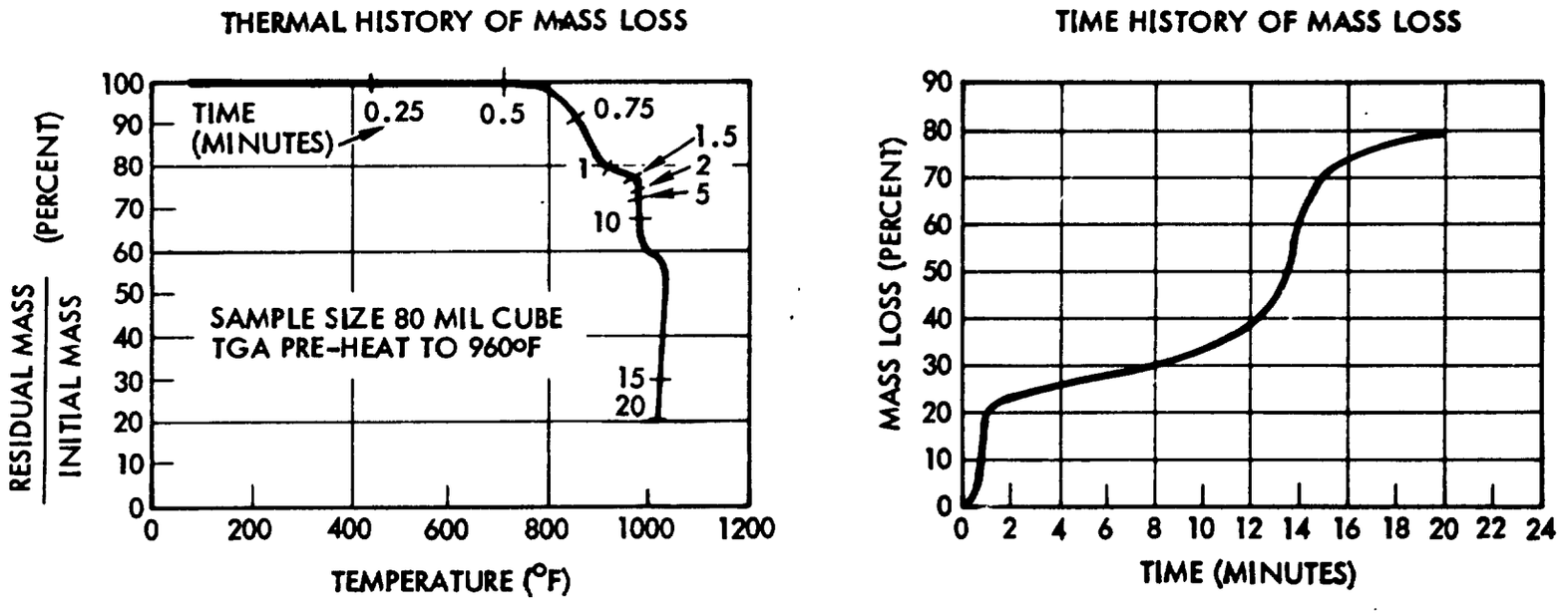

Figure 4-77. Thermal Gravimetric Analysis For Plate Composite Material

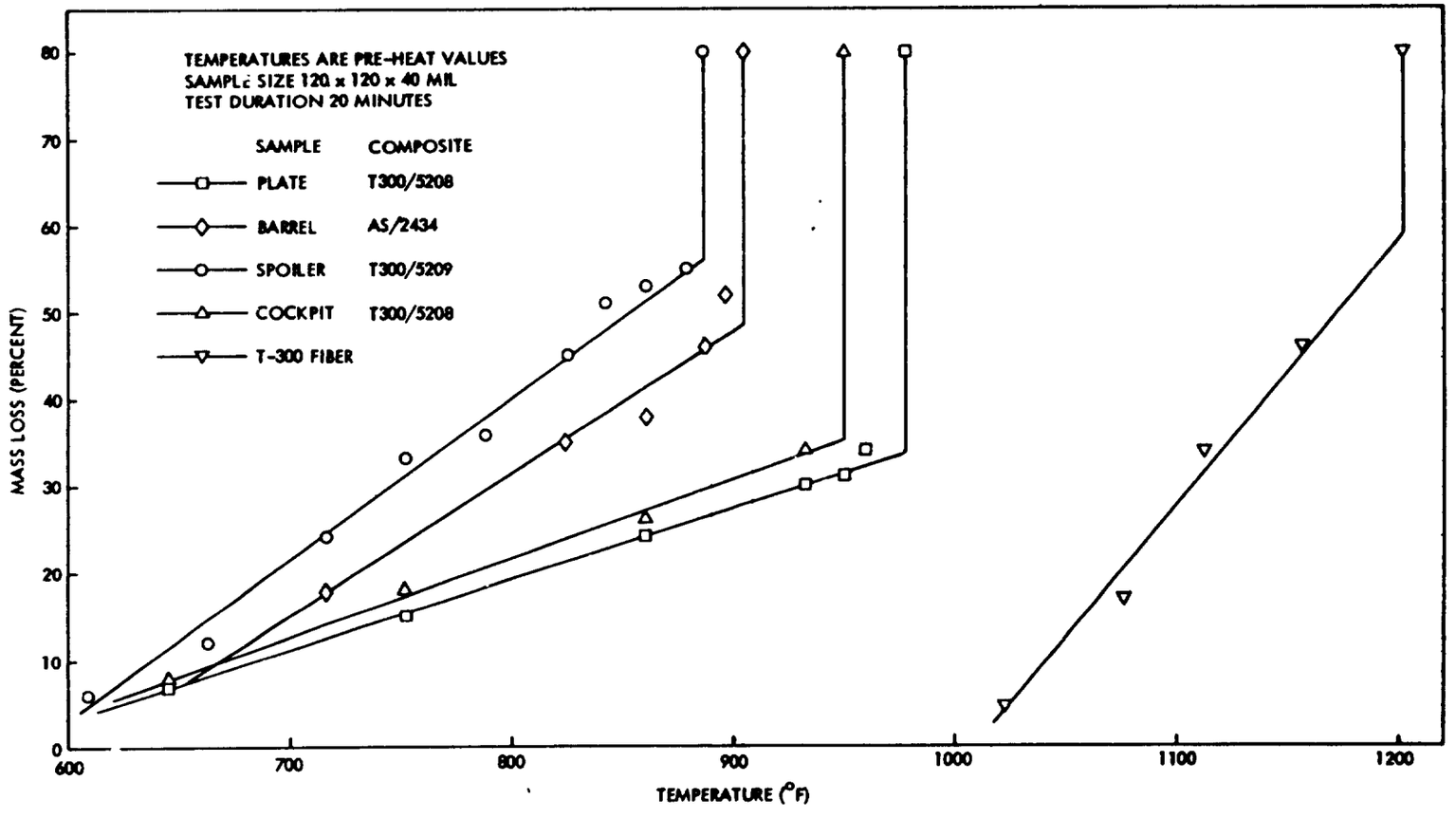

Figure 4.78. TGA Mass Loss Evaluation for Pre-Test Material Samples

Two significant aspects of the data are that the spoiler (T300/5209) curve corresponds to temperatures lower than the barrel (AS/2434) curve rather than in close proximity to the plate (T300/5208) and cockpit (T300/5208) curves. TGA tests of cured 5208 and 5209 resin samples indicated similar mass loss characteristics as a function of pre-heat temperatures.

Based on the data of Figure 4.78 it would appear to a first order extent that the spoiler composite may have been AS/3501 which was one of the fiber/resin systems used in spoiler manufacture. At the suggestion of R. Pride of NASA Langley it appeared advisable to check the spoiler data by TGA tests on another independent spoiler sample supplied by NASA and specified as T300/5209. Comparison of the two sets of spoiler data is shown in Figure 4 79 in addition to sets of similar TGA data for four plate samples from different sources. There is excellent agreement among the respective sets of data for the plate and spoiler samples. One explanation for the anomaly between the spoiler and plate curves of Figure 4.78 is not readily apparent unless the bands of response for various T300 and AS composites would normally overlap. Another possible explanation is that catalytic effects by the depolymerization products of the 5209 resin may lower the oxidation temperatures of T-300 fibers more than achieved by the 5208 resin in the cockpit and plate samples.

The second feature of Figure 4.78 that commands attention is the difference of 200 to 300^{o}F between the curves for T300 fiber and T300 composite. It appears that some type of catalytic effect takes place for the composite and that depolymerization of the resin causes oxidation of the T300 fiber at lower temperatures. Reaction residues on the surface of the fiber may lower the activation energy levels.

A representative TGA thermal history for individual T300 fibers corrresponding to a pre-heat temperature of 1254^{o}F is shown in Figure 4.80, together with a family of time history contours for various pre-heat temperatures. It is of interest to note that for the entire set of TGA records for the T300 fibers there was no evidence of spontaneous ignition at any stage as had occurred with the T300 composite in the oven test (Figure 4.76) and TGA test (Figure 4.77). It appears therefore that the catalytic effects caused by depolymerization of the resin may also influence the probability of spontaneous ignition and therby increase the corresponding mass loss due to a fire environment.

Oxidation Rate

An effort was made to determine the oxidation rate and time history for individual T300 fibers in order to establish a potential frame of reference toward evaluation of the differential mass loss estimates for the various field tests.

The mass loss rate per unit area is given by the Arrhenius equation, namely:

$$\frac{\dot{m}}{A} = \frac{C}{T^{1/2}} e^{\frac{-\Delta H}{RT}}$$

where $\dot{m}$ = mass loss rate

A = surface area

T = temperature (^{o}K)

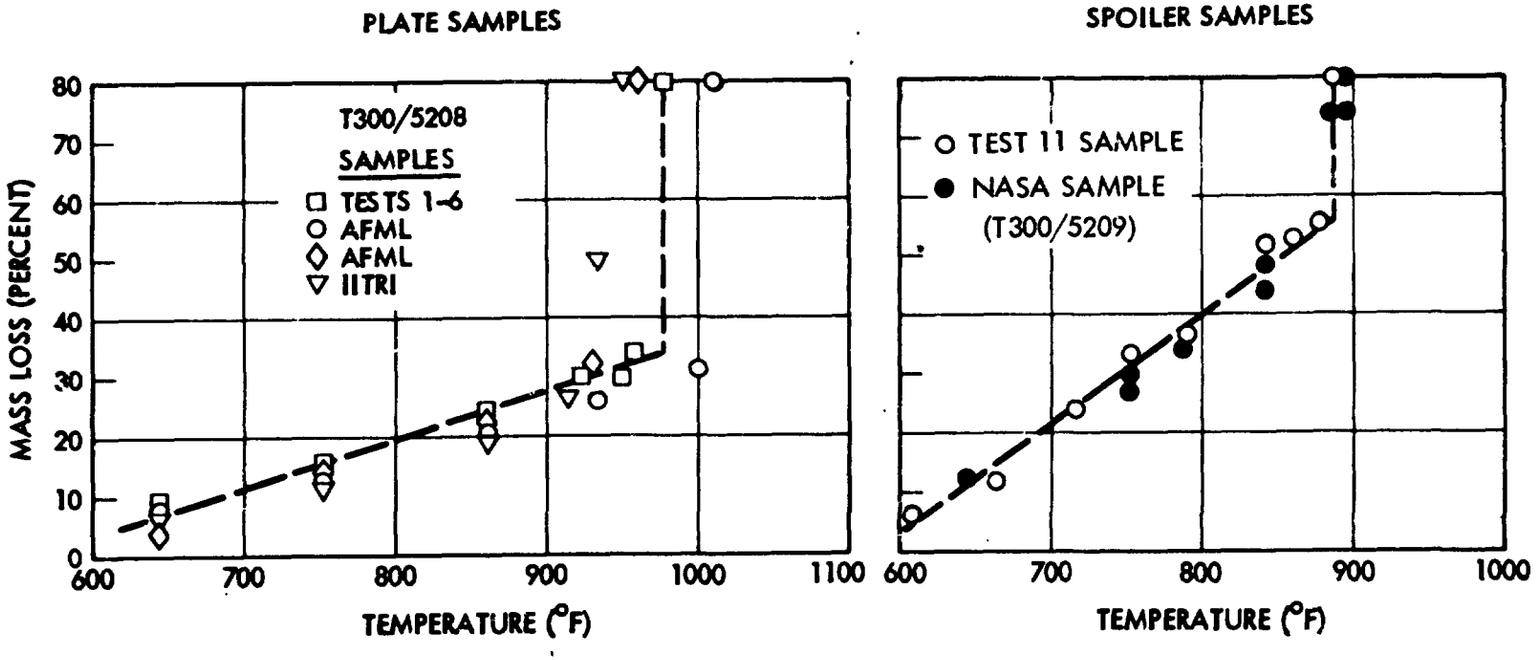

Figure 4-79. TGA Mass Loss Comparison for Plate and Spoiler Samples

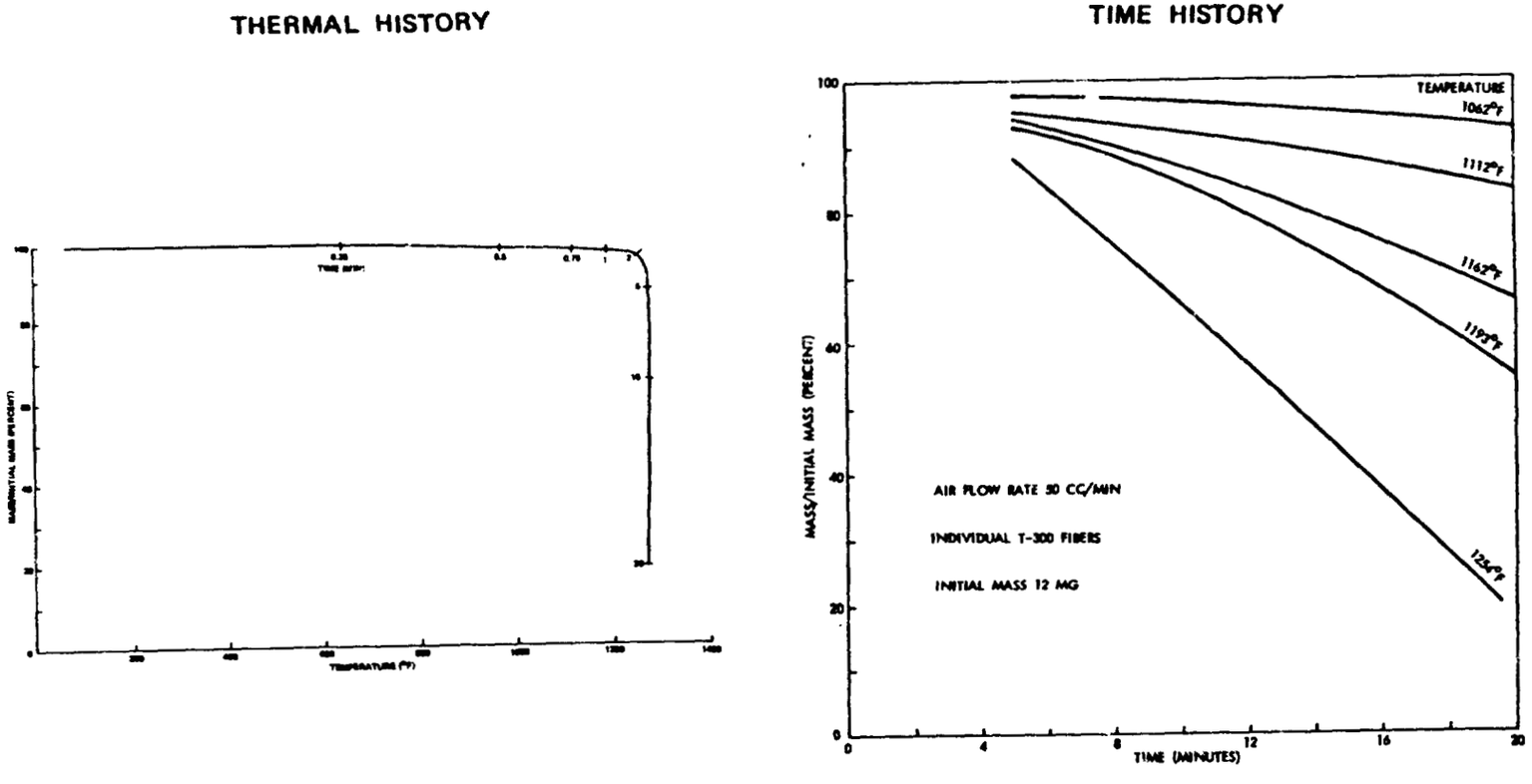

Figure 4.80. Thermal Gravimetric Analysis of T-300 Fibers

ΔH = activation energy

R = universal gas constant

c = constant coefficient

with m_0 as the initial mass and A_0 the initial surface araa.

Based on the data of Figure 4.80, a plot is shown in Figure 4.81 of $\ln \dot{m}/A$ vs $1/T$. The family of straight lines corresponding to m/m_0 values of 0.60, 0.70 and 0.85 indicate uniform slopes. By means of the slope the activation energy ΔH was determined to be 31.0 kcal/mole. The oxidation rate equation is then:

$$\frac{\dot{m}}{A} = \frac{7.10 \times 10^3}{T^{1/2}} \; e = \frac{-\Delta H}{RT}$$

Integration of the Arrhenius equation yielded the curve presented in Figure 4.82 for the total oxidation time for single T-300 fibers. Single fibers exposed to 1400°F would be completely oxidized in about 10 minutes with oxidation time for 1600°F being about 3 minutes.

In view of the field test conditions regarding temperature environments and burn times it appears quite readily that considerable mass loss could have occurred on occasions when single fibers were exposed following depolymerization of the resin. A consideration of this nature would warrant attention in mass balance evaluations associated with the field tests.

FIBER OXIDATION

One of the most important results of this study is the finding that substantial quantities of carbon from burning composites can be oxidized. Attention was focused on two major aspects of fiber oxidation, namely, experimental evidence of reduction in single fiber diameter and theoretical verification of the possibility of significant mass loss over short time periods due to the high fire temperatures and associated fiber oxidation rates.

As noted from the comparison of single fiber pre-test and post-test diameters shown in Figure 4.67, only small diameter reductions were noted for the plate tests whereas relatively large reductions were observed for the barrel, spoiler and cockpit tests. This variation may possibly be attributable principally to the thickness of the plates (0.25 inches) as compared to the thin skins (tens of mils) of the barrel, spoiler and cockpit samples. Other contributing factors most probably were differences in burn phenomena associated with hot propane flames vs large jet fuel fires, as well as response characteristics of different combinations of fibers and resins for the respective composites as noted from Figure 4.78.

In consideration of mass balance between fiber release and deposition data it is recognized that the degree of fiber oxidation would be of major consequence toward resolution of differential magnitudes. A question of interest investigated

during the course of the study was whether a significant mass loss can occur over short periods of time. For the spectrum of temperatures associated with a JP-5 jet fuel fire as shown in Figure 4.74, it appears that T-300 fibers of the thin spoiler and cockpit structural materials with few composite ply could have been completely oxidized during the short duration of several minutes of the corresponding JP-5 fires as indicated by the analytical results of Figure 4.82.

It is of interest to note that escaping single fibers of reduced diameter will have lower settling velocities and therefore may be propagated to greater distances. In addition, the degree of penetrability of ventilation filters will effectively be greater for smaller diameter fibers.

The occurrance of single fiber diameters in the 1 to 2 micron domain as shown by the data of Figure 4.67 indicates that attention need be focused on the question of potential health hazards.

SUMMARY AND CONCLUSIONS

A brief summary of the principal highlights and conclusions associated with the passive instrumentation data reduction and analysis is presented as follows:

- Singular particulate characteristics for the respective test samples were:
  - Plate - Clumps
  - Barrel - Singles and Clusters
  - Spoiler - Singles and Strips
  - Cockpit - Lint and Strips
- Particle length distributions were quite similar for all tests with reference to relative occurrence as a function of length interval, with average lengths generally ranging from 2 to 3 mm.
- Effects of fiber oxidation are manifested by reduction of post-test single fiber diameters as compared to pre-test values.
- Single fiber mass as collected or accounted for by deposition was generally less than 0.1% of initial composite mass for all tests.
- Uncertainties exist regarding the degree to which fiber clouds may have been lofted beyond the areas of passive instrumentation, particularly relative to single fibers which would have been more susceptible due to characteristic low mass and slow fall velocities.

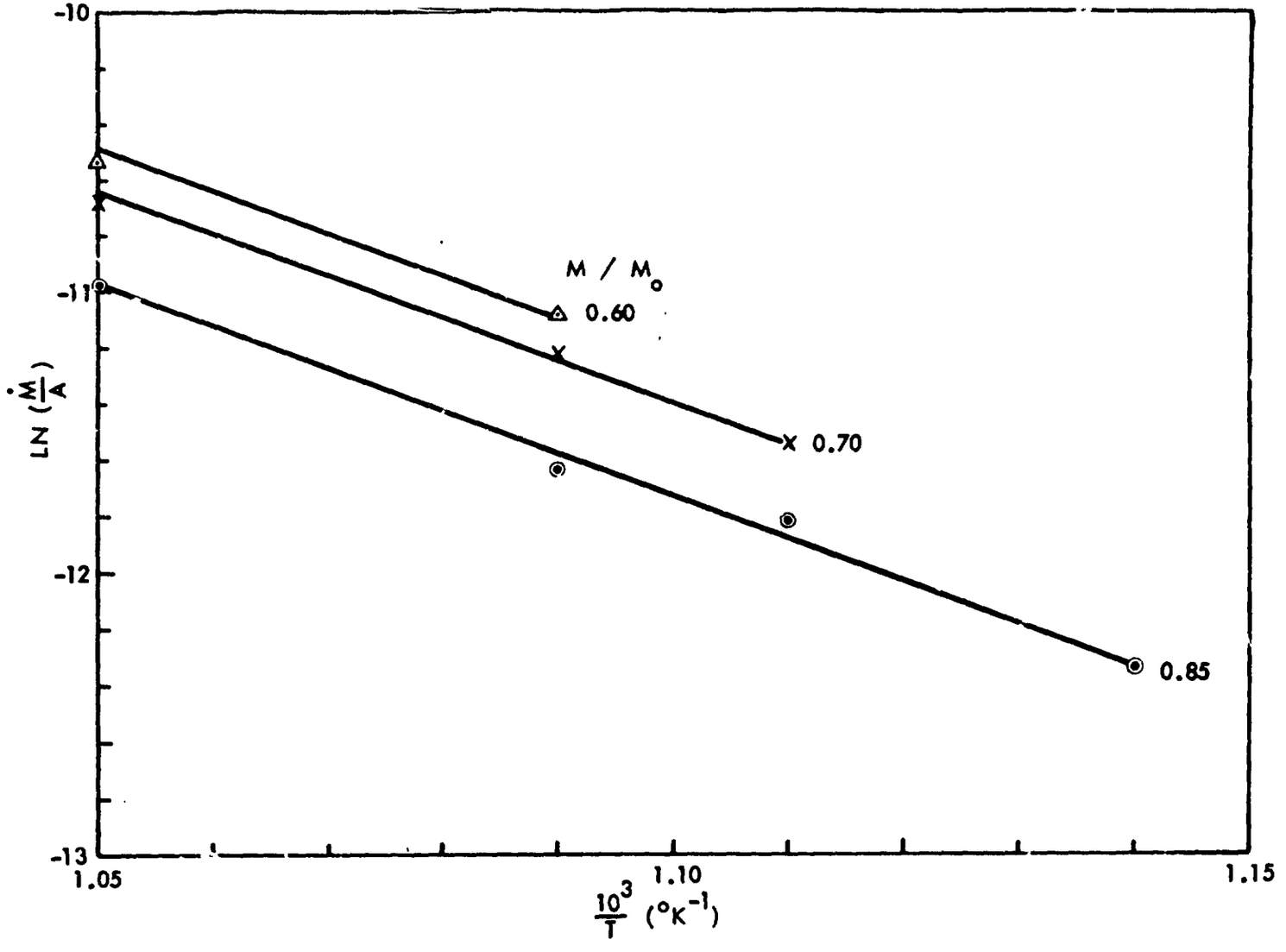

Figure 4.81. Oxidation Rate For T-300 Fibers

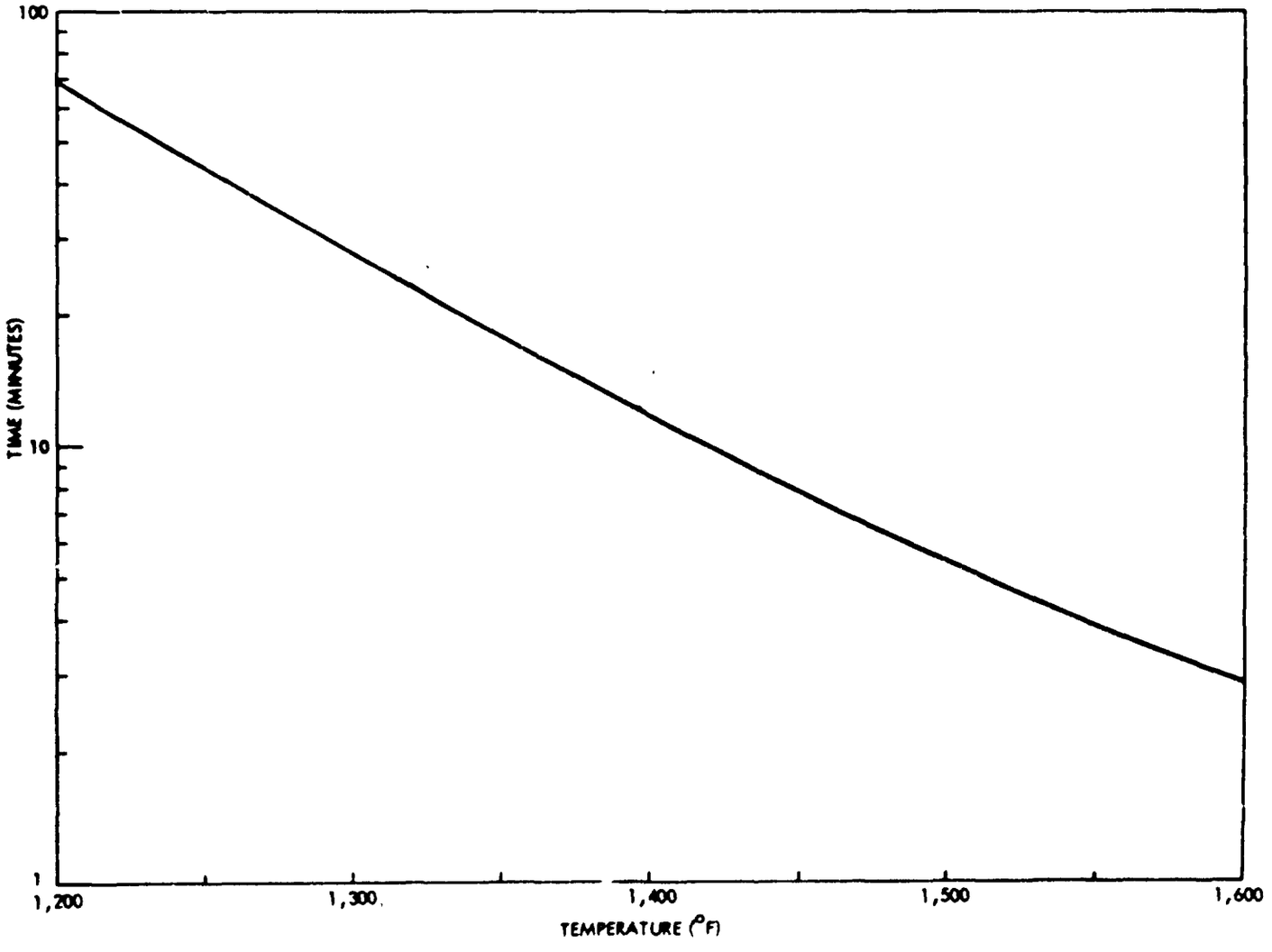

Figure 4.82. Oxidation Time For Single T-300 Fibers

- Close agreement between particle distributions for plate Tests 3 and 5 indicates that CTS chamber test offered a good simulation of the NWC field test and that the particle deposition for Test 5 most probably occurred principally within the bounds of the passive instrumentation array due to favorable meteorological conditions.

- Mass deposition data for plate Tests 3 and 5 indicated a total capture of 10 to 20 percent of the initial composite mass for all particulate in the length interval of 1 to 20 mm, whereas the single fiber mass corresponding to this high capture efficiency was only about 0.008 to 0.01 percent.

- Single fiber mass data from NSWC chamber tests appear to be greater than TRW results from Tests 3 and 5 by a factor of about 100 for similar plate samples and burn times.

- Jacob's Ladder data for Tests 11 and 13 indicating increasing particle densities with decreasing elevations may possibly be attributable to ground surface effects.

- Strip thickness domains for Tests 11 and 13 were predominately in the range of 1 to 2 ply.

- Catalytic effects due to resin depolymerization cause reductions in oxidation initiation temperatures of T-300 fibers.

- Thin structural materials with few composite ply would be susceptible in JP-5 fires to evolution of strip-type particulate and mass loss due to fiber oxidation, with the possibility that significant mass loss can occur over short time periods because of the existence of temperatures considerably in excess of the oxidation initiation temperatures and the associated fiber oxidation rates.

5. ACTIVE INSTRUMENTATION: DATA REDUCTION AND ANALYSIS

The 1978 field testing program at the Naval Weapons Center (NWC) China Lake, California was required to sample the fiber cloud dispersed over a wide area. In conjunction with the passive instrumentation techniques used to determine deposition over a very wide area, a relatively large number of active instruments designed to measure the instantaneous fiber concentration and mass flux were deployed. One group of these instruments, described in Section 6, was designed to detect the overall cloud characteristics from afar by photographic and infrared imaging techniques. The second group of instruments, described in this section, was designed to detect at selected points fibers essentially "in vivo". The second group included LED, high voltage ball and microwave detector systems. These three detector systems were confined to positions near the ground and should be relatable to the deposition as seen by the passive instruments on the ground below. Each of the major three detector systems deployed were mounted on wooden stands approximately 5 ft from the actual ground.

The three detector systems were selected and developed for the program so that the very wide range of fiber concentrations and fiber lengths expected might be covered. The light emitting diode (LED) system, developed by TRW and deployed in quantities of 20-22, was the most sensitive device used and could be utilized to the farthest distances from the generation source. It also, by its nature, could detect down to fiber lengths less than 1 mm long. Since it operates by simple light obscuration, it is incapable of differentiation between carbon fibers and other kinds of non-conducting fibers, and for the complicated fiber distribution expected for field tests does not lend itself easily to measuring the length spectrum. This length distribution has been done for some data records by the use of (1) passive collector adjacent to the LED and (2) statistics relationships.

The ball gage system, originally invented at USABRL, Aberdeen, Md., and developed for field use by TRW is somewhat less sensitive than the LED system and was generally deployed closer in to the sample burns. It, however, has the ability to measure the fiber length through the pulse height of any event impinging on the high voltage ball, at least down to the noise threshold. This threshold was set for measuring greater than 3-4 mm fiber lengths for the tests in the NWC series. The complicated instrumentation employed for this detector did not allow for a large number of systems to be operated. Of the 10 systems employed only six were operable generally in the mode where both fiber concentration and fiber length could be obtained. The four remaining detectors obtained on loan from BRL were attached to a device only capable of measuring the concentration. For reasons discerned later this form of readout proved not to be very useful.

The microwave gage system, developed at TRW, operated on the principle of the absorption of microwave energy by fibers between a transmit horn and receive horn spaced about four in. apart. This system was designed to be sensitive where the other two gage systems would saturate. It naturally measured mass flux and concentration and was deployed the closest to the sample burns.

Because of this insensitivity for many of the tests the data returns were very sparse for this system.

Classified as active instrumentation, as well, are those devices which were utilized to determine the flame and test sample parameters (e.g. flame velocity, flame temperature, sample temperature, during the test. Data from the thermocouples are presented in this section as is the data obtained from a flame velocimeter developed during the program. During the course of the test series several other detector systems were deployed under a development effort. Data from these systems is briefly presented where it appears to provide useful data on the phenomena.

The data reduction is presented in the categories of test samples burned and/or exploded:

- flat plate
- barrel
- spoiler
- cockpit

Within each of these categories, there are discussions of each separate test. Thus, under the flat plate category four tests are described (Test Nos. 4, 5, 6 and 7). Within each test the data is reported according to instrument type. Under each test the sequence of instrument types is:

- thermocouple
- LED detector
- high voltage ball detector
- microwave detector
- other detectors

The data is presented in this section with no description of the detectors and limited reference to the data trends. Section 6 discusses the photographic and meteorological data. It is in Section 7 that the comparison between the active and passive data is made. In Section 8 the data trends are identified and discussed.

FLAT PLATE TESTS AT NWC

Three tests were performed in the regular test series using 1 ft x 1 ft x 1/4 in. (30 cm x 30 cm x 6.3 mm) carbon composite flat plates. For each test the samples were first subjected to a propane burn which extended over the entire sample area. The burn was typically 20 minutes. After burning, explosive squibs were emplaced and exploded.

The active gages detected the concentration histories of the carbon fiber cloud during the passage of the fiber cloud. After passage of the cloud some of the fibers deposited on the ground. Winds then re-lofted some of the grounded fibers to form a new fiber cloud of much lower concentration than the initial cloud. The active gages also detected the re-suspended carbon fibers.

In general there was very little detected during the burning of test samples over the small burner. High fiber densities were the result of large scale fires. Any blast impingement induced even higher fiber cloud densities.

The format of the data display is based upon describing the fiber cloud by

- o number concentration history, $C_n(t)$
- o mass concentration history, $C_m(t)$
- o mass flux history, $\frac{\dot{M}(t)}{A}$.

The LED and ball detectors record number of fibers passing within their respective sampling volume per unit time, $\dot{N}(t)$, while the microwave detector measures C_m for a uniform fiber cloud and measures $\dot{M}/A$ for clumps of fibers. These formulas are valid for a fiber cloud where all fibers are of the same length, l.

It is necessary for the LED and ball detector systems to convert $\dot{N}_i(t)$ for fibers of average length, $\bar{l}_i$ to the three required histories. This is achieved by use of the following relationships:

$$C_n(t) = \frac{\dot{N}(t)}{A \cdot U}$$

$$C_m(t) = \frac{\dot{N}(t) \cdot m}{A \cdot U}$$

$$\frac{\dot{M}(t)}{A} = C_m(t) \cdot U$$

where

A - cross-sectional area of the sampling volume normal to the wind direction

U - wind velocity

m - mass of a single fiber of length, l, equals

$0.54 \left(\frac{\mu gm}{cm}\right) \times l \text{ (cm)}$.

When the fiber cloud is composed of different lengths, it is necessary to obtain data for the size distribution

$$N = \sum_i N_i(\bar{l}_i)$$

which can be obtained from the pulse heights of the active instruments or from passive collectors.

When a detector such as the ball gage is only sensitive to fibers greater than 3-4 mm in length, and the fiber cloud contains mostly fibers less than 2-3 mm in length, special considerations must be given to the original concept of "concentration". When there are very few fibers, existing in a short interval of time, the measured values of $\dot{N}$ are not based on statistically meaningful numbers. More important, it is difficult to specify the time interval between counts which is relevant to a concept of cloud concentration. It is like dealing with a few closely associated fibers moving together in a large room, where the close-in concentration is high and room-wise the concentration is low.

TEST NO. 4

The first test at NWC took place on the morning of January 24, 1978. For this test, the propane was burned for 20 minutes before emplacing explosives and exploding.

Thermocouple Data

The burner was a 1 x 1 ft (30 x 30 cm) venturi-suction and propane/air burner developed and calibrated at TRW. Three chromel-alumel thermocouples were imbedded 1/8 in. (3.2 mm) deep into the carbon fiber composite plate at three locations, as shown in Figure 5.1. An additional thermocouple of tungsten-rhenium was positioned 1/2 in. (1.3 cm) below the composite plate center to measure the center flame temperature. The measurements are presented in Figure 5.1 and show a maximum flame temperature (uncorrected for radiation loss) of about 1950°F (1065°C) and a plate temperature of about 660°F (349°C).

These temperature histories are relevant to setting the criteria for the thermal gravimetric analysis (TGA) tests to be performed in laboratory ovens. It is apparent that the 500-600°F (260°C-316°C) temperatures in the mid-plane of the plate are established within one minute.

Gage Layout

The detector positioning is shown in Figure 5.2. As mentioned before all were mounted on 5 ft (1.5 m) wooden stands. These stands had provisions for covering the detectors against the weather except when a test was in progress. As shown all of the detectors were clustered downwind within 50 ft (15.2 m) of ground zero with the microwave gages closest, ball gages somewhat further out interspersed with LED detectors out to 50 ft (15.2 m). The top of the figure is the north direction with the desired wind direction from the south.

After the burn, the burner was removed and replaced with a single charge explosive positioned 1 ft (30 cm) below the now partially delaminated sample. Detonation occurred at 12:47 pm PST. Ground zero was at the center of the 50 x 50 ft (12.7 x 12.7 m) concrete pad.

The explosive squibs were activated for this test with no warning to the magnetic tape recorder operator so that all the optical tape recordings started a couple of seconds after the explosion. Counting backwards from the twelve minute mark it was determined where zero time would be within an uncertainty

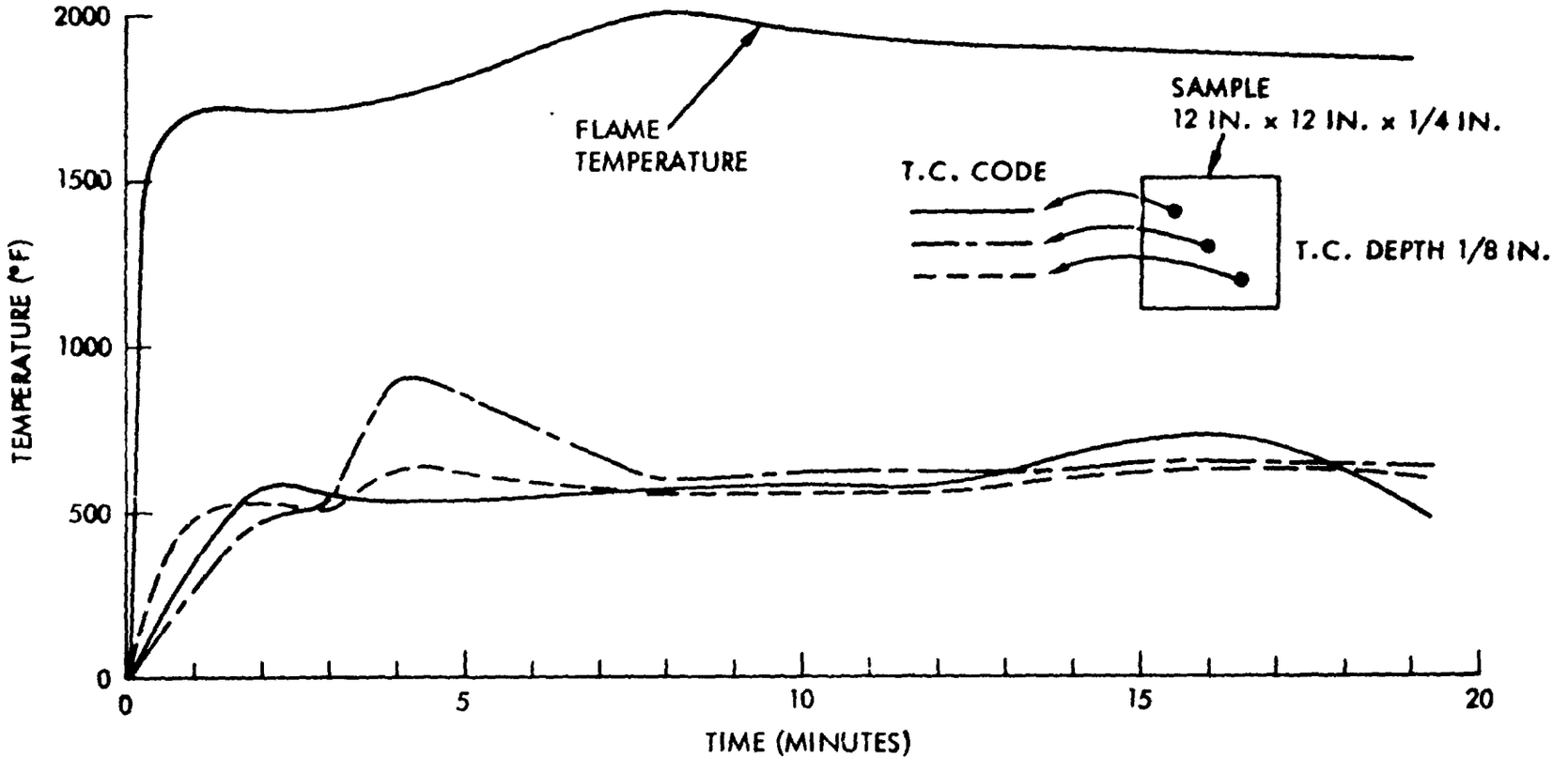

Figure 5.1. Sample Burn Temperature Profiles - Test No. 4

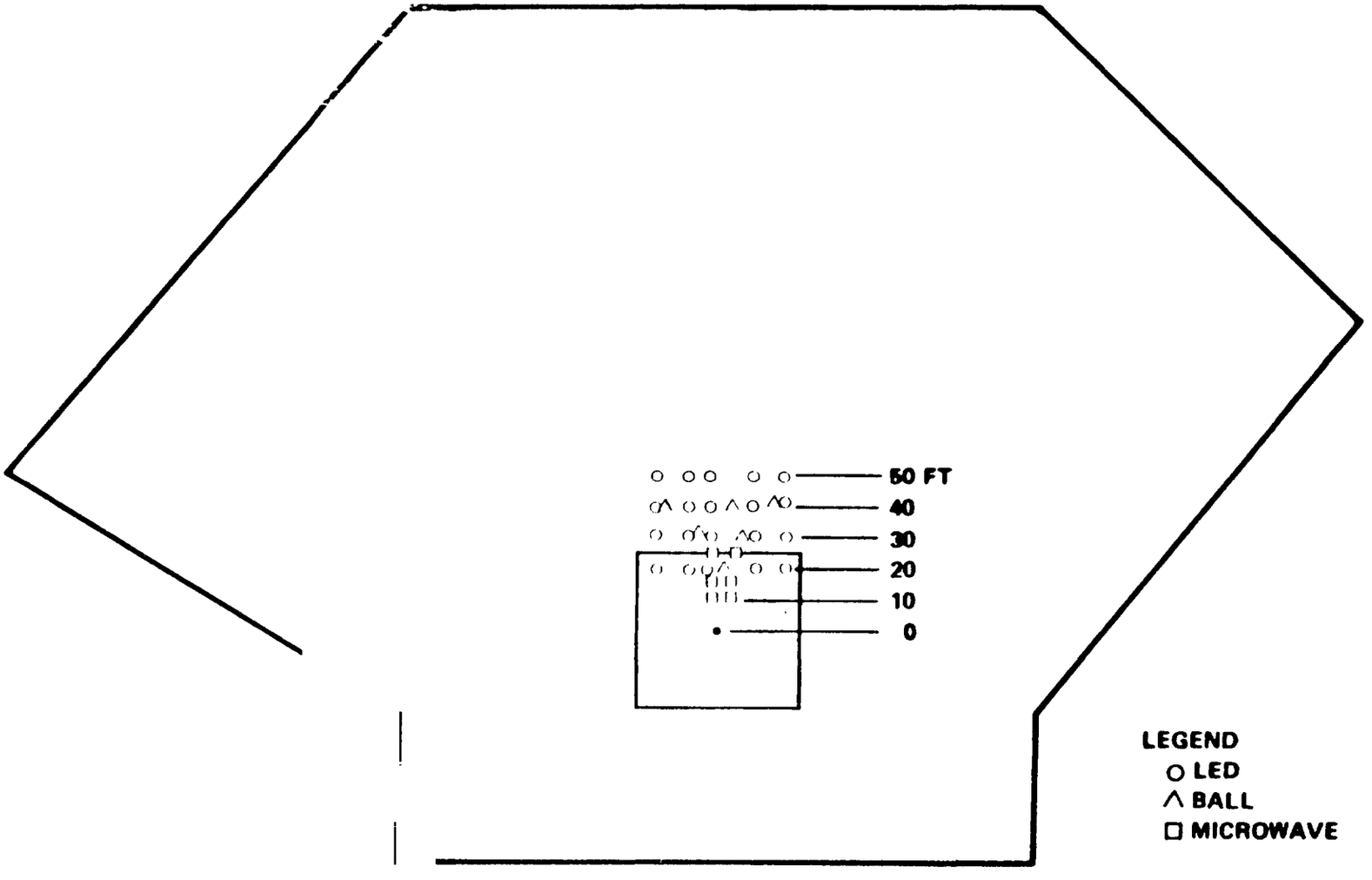

Figure 5.2. Active Gage Configuration - Test No. 4

of about one second.

LED Gages

The proximity of most of the LED gages to the explosion and their mounting on the wooden platforms caused all of the gages to go into violent oscillations and the gage systems saturated immediately after the explosion. These oscillations decayed with time. When the gage systems came out of saturation, the fiber cloud had passed. Hence no useful data was obtained on the LED gages. Subsequent tests were performed at significantly greater gage distances and all stands were weighted down more securely.

Ball Gages

For this test the 6 ball gages built at TRW were situated at distances from 20 to 40 ft (6.1 to 12.2 m) from ground zero.

The ball gage measures number rate of fiber impacts as a function of history. The conversion of number rate to number concentration is through a calibration constant that is dependent upon the length of the carbon fiber and very weakly dependent upon wind velocity.

The mass concentration is obtained by multiplying the number concentration by mass per single fiber. This can be further related to the product of the mass per unit length (0.54 μgm/cm) and the length of a single fiber.

The mass flux is the product of mass concentration and wind velocity normal to the measurement area. This is a measure of mass transport that can be compared to the microwave and LED gages. Figure 5.3 displays the results for the ball gage, presented in terms of mass flux. As shown in the figure, events were recorded on only three of the gages, indicating a narrow plume passing (in agreement with meteorology measurements) somewhat to the east of the centerline. Using the time of receipt of first data a plume velocity at the five-foot (1.5 m) level of 5.9 fps (1.8 mps) is indicated roughly in agreement with the recorded wind velocity.

The fiber length distributions as determined from pulse heights at the three locations are shown in Figure 5.4. The indicated particle distribution for early time 0-10 sec data for all three gages for which events were recorded appears to have a hole in it in the 8-11 mm length region, much as observed at previous CTS tests. The dashed lines indicate the threshold below which lengths are not observable. At the further locations the spectrum suggests that most of the fibers may lie below the 4 mm threshold.

Observation of sticky paper in the vicinity of the gages indicates a preponderance of clumps over long singles, clumps which appear to be rather tightly bound - leading to the conjecture that the particle distribution above 10 mm is primarily due to clumps acting as single counts. Loosely bound clumps are generally separated by the induced fields from the ball and appear as many closely spaced individual pulses on the gage output. These were not observed. Some data shown in Figure 5.5 was returned by the ball gages during the

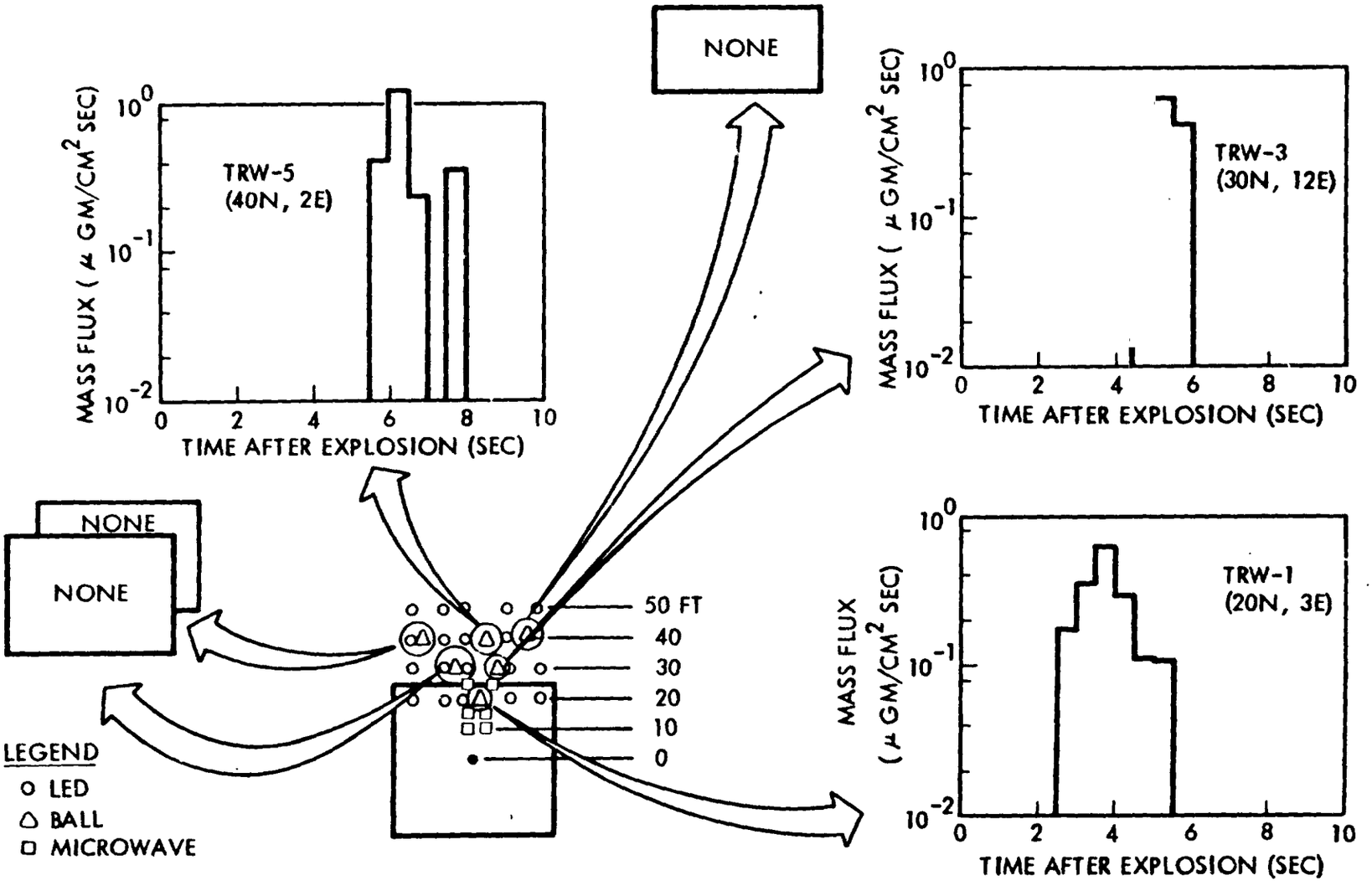

Figure 5.3. Ball Gage Results After Explosion - Test No. 4

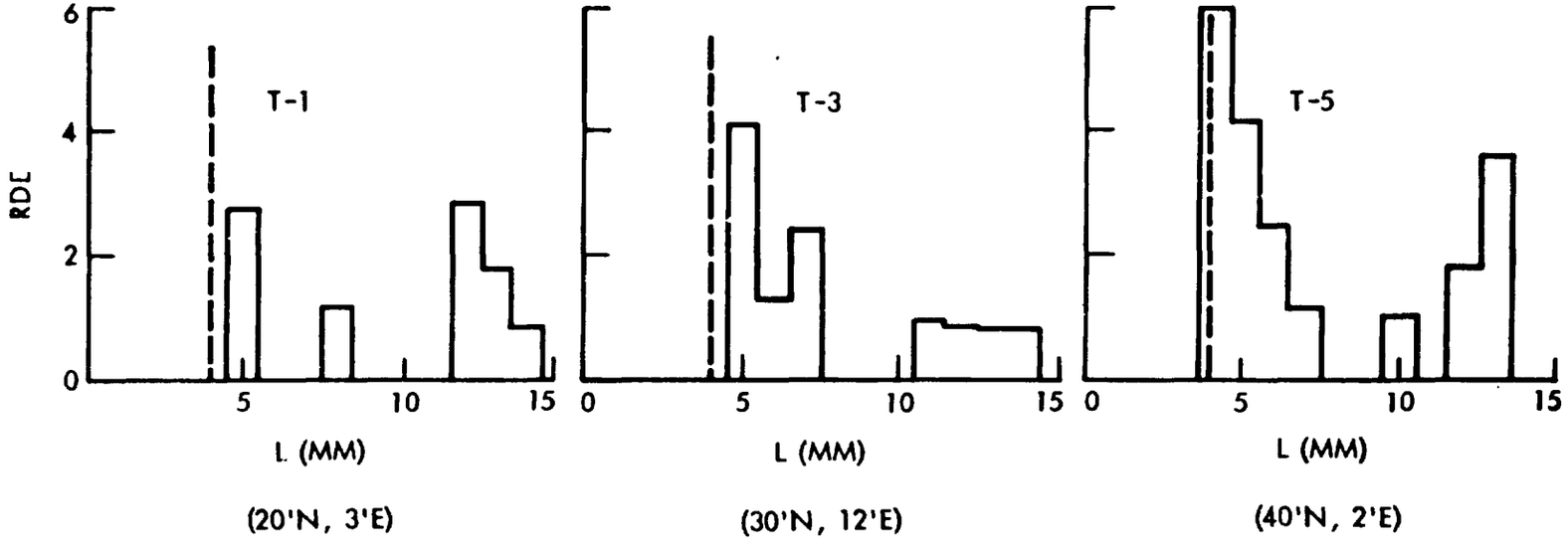

RDE: RELATIVE DIFFERENTIAL EXPOSURE

Figure 5.4. Ball Gage Length Distribution - Test No. 4

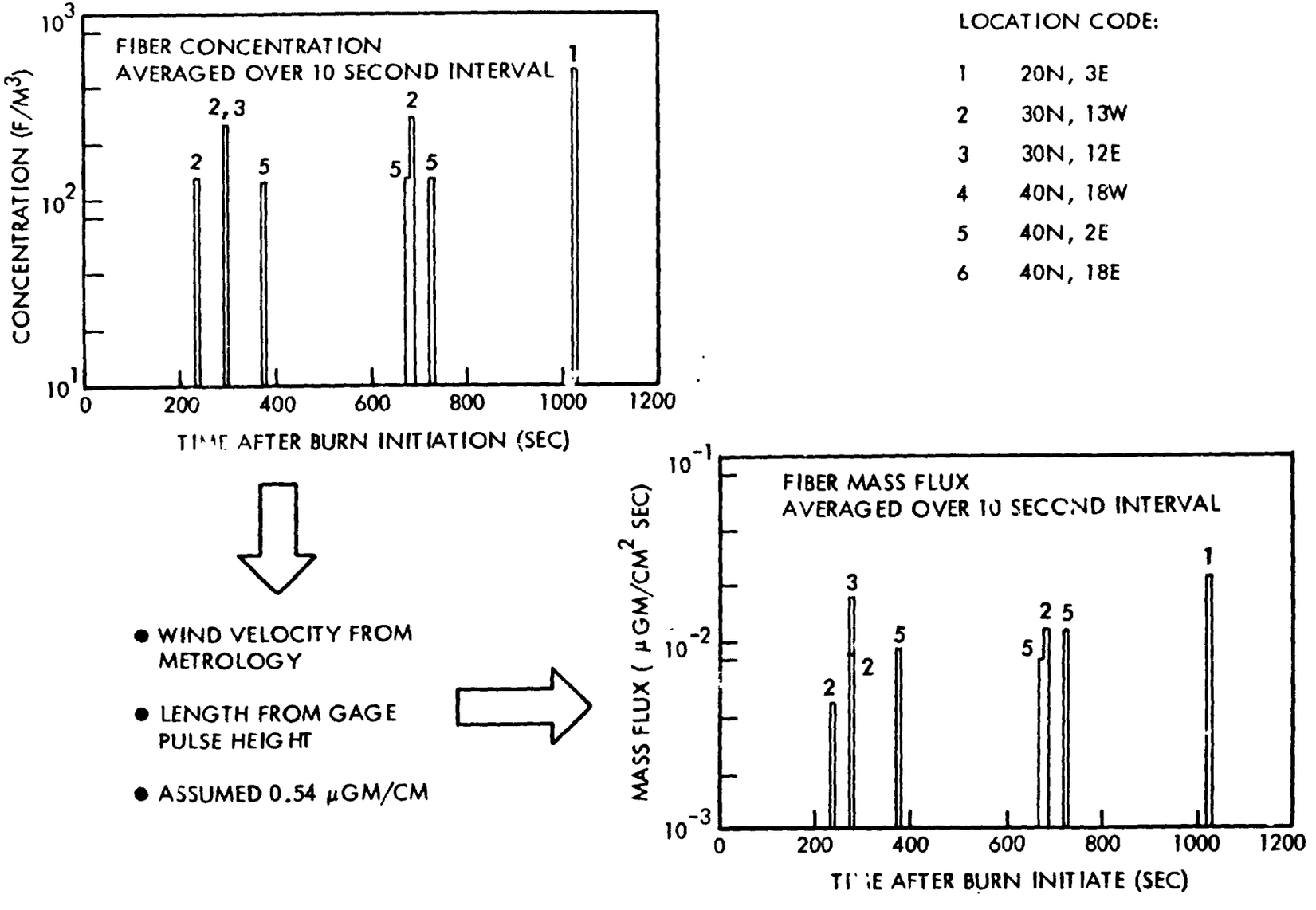

Figure 5.5. Ball Gage Results During Burn Phase - Test No. 4

20 minute burn period. The data is presented both as concentration data averaged over a 10 sec interval and mass flux data using the conversion just discussed. It can be seen that fiber release from the plate has begun as early as 220 sec in the burn.

Microwave Gages

The microwave gages were placed in pairs at 10 ft, 17.5 ft and 25 ft (3 m, 5.3 m and 7.6 m) downwind from ground zero. As shown in Figure 5.6 each of the gages intercepted some of the material in the time interval from 1 sec through 7 sec after the blast. The charts show mass flux in $\mu gm/cm^2$ sec versus time after the explosion. The total mass and deposition recorded by each gage is given in the table. Note that the greatest deposition is recorded by Gage No.6, amounting to 1220 $\mu gm/cm^2$.

TEST NO. 5

The second test at NWC took place February 1, 1978. As before a 1 ft x 1 ft x 1/4 in. (30 cm x 30 cm x 6.3 mm) flat plate was burned in a propane/air fire for 20 minutes at the center of the concrete pad starting at 8:41 am PST and then the plate subjected to an explosion at 9:57 am PST. For this test the burner was adjusted in height and pressure for a much hotter burn.

Thermocouple Data

The thermocouple measurements are displayed in Figure 5.7. As observed during the first 6 minutes, the material was engulfed in flame as the binder was burning. This flame subsided and flared at times as new resin was exposed during layer separation. Material started flaking off after 6 minutes, and this continued until the end of the burn. After 8 minutes most of the layers of composite had separated. As shown in the figure the bulk of the plate reached a much hotter temperature than in the first test. The edges reached over 900°F (482°C) over a prolonged period while the center reached almost to 1100°F (593°C). Flame temperature data was not recorded.

Gage Layout

For this test, in keeping with the indications from the previous test of significant transport to even beyond the 200 ft (61 m) range, all of the gage systems, as shown in Figure 5.8, were dispersed to further ranges. Three additional ball gage systems were added which were connected to a multi-channel analyzer capable of measuring simultaneously the pulse count from each of the three gages. This system however was unable to record at the same time the pulse height data for these gages. As before, the most sensitive system, the LED system was placed down range the furthest with the ball gages somewhat closer and the microwave gages the closest in. As can be seen in the figure the ranges were overlapped to provide a comparison between gaging systems.

LED Gages

The data obtained from the LED systems for times after the explosion is

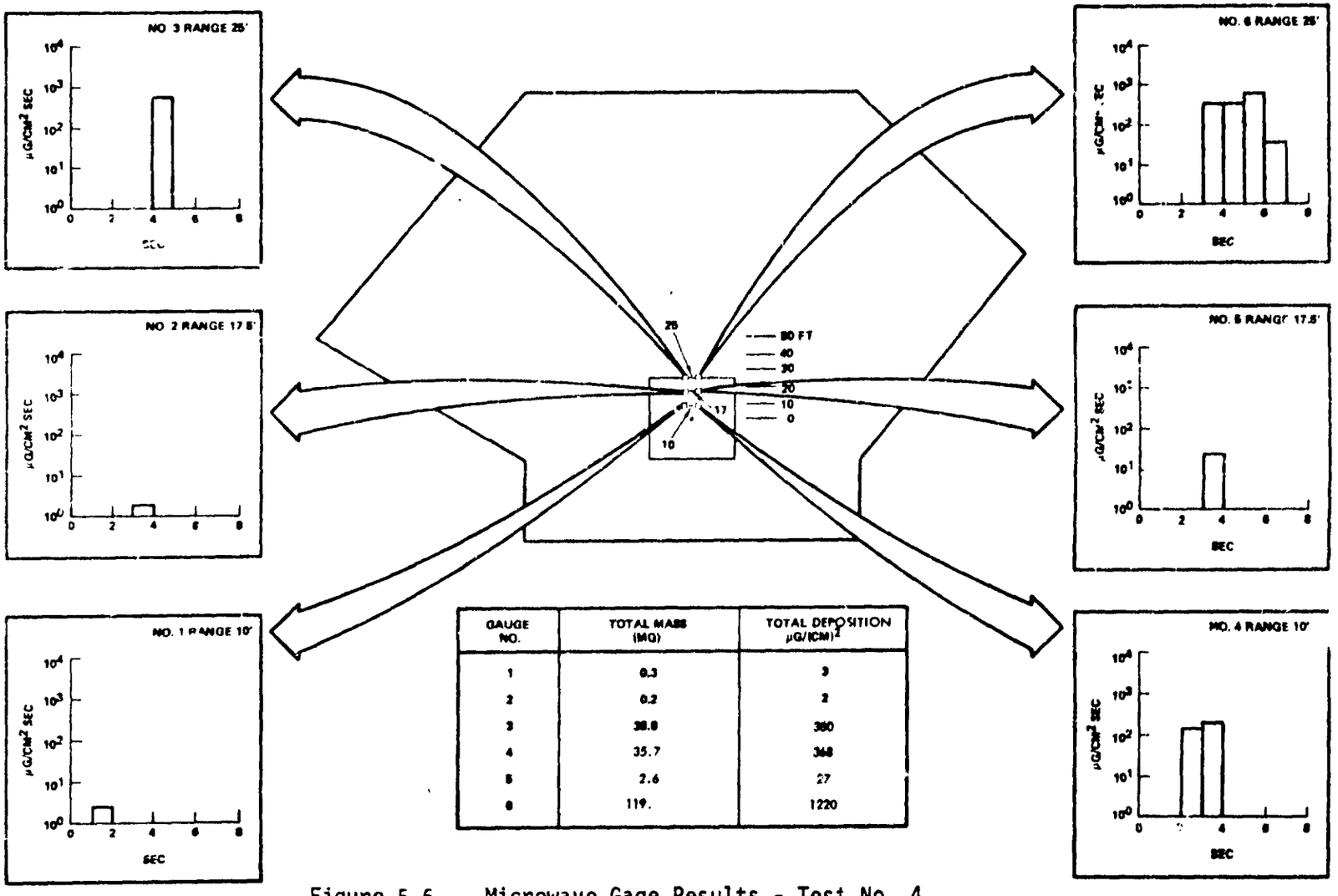

GAUGE NO.	TOTAL MASS (MG)	TOTAL DEPOSITION μG/(CM)²
1	0.3	3
2	0.2	2
3	38.8	380
4	35.7	368
5	2.6	27
6	119.	1220

Figure 5.6. Microwave Gage Results - Test No. 4

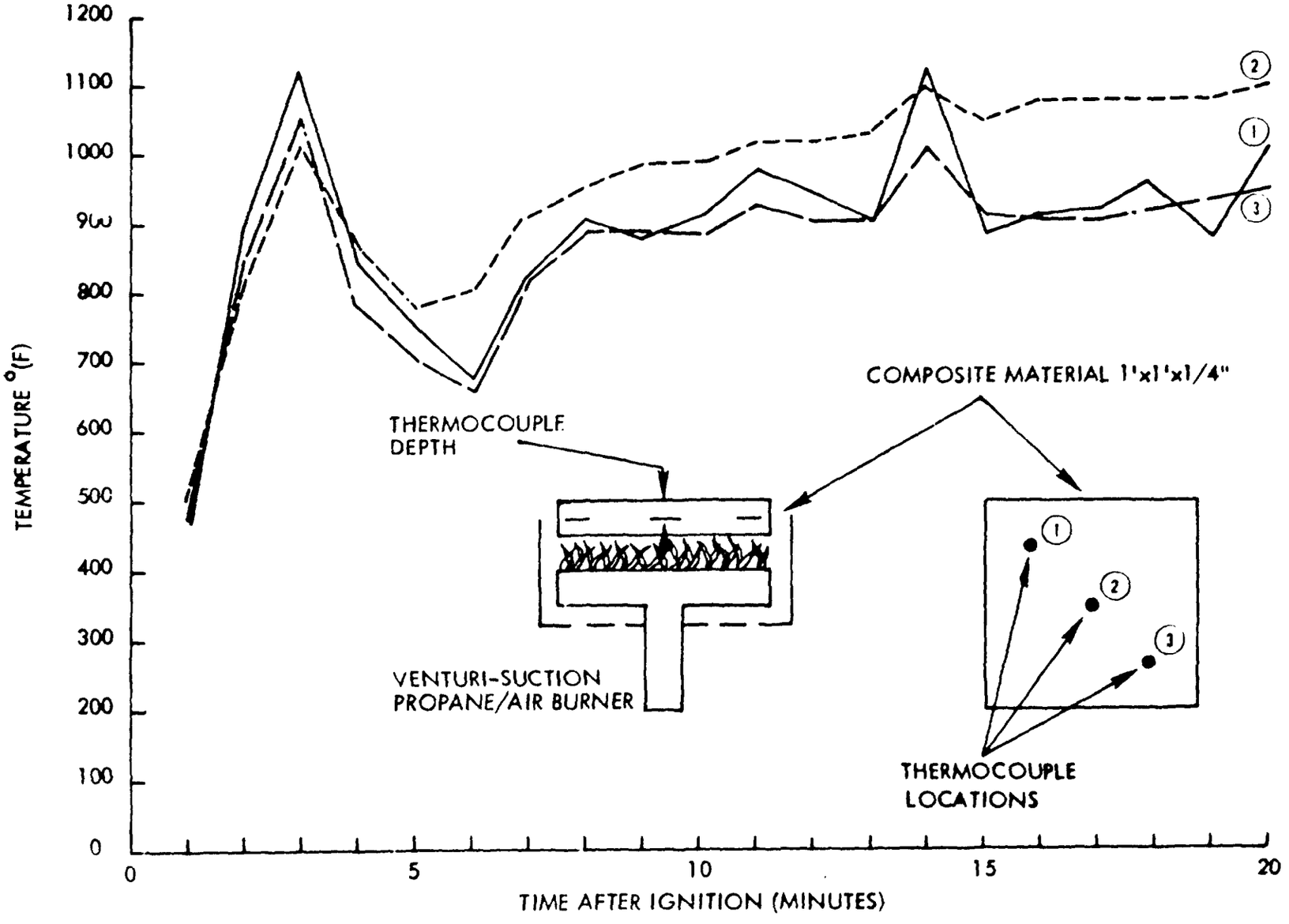

Figure 5.7. Temperature History During Plate Burn - Test No. 5

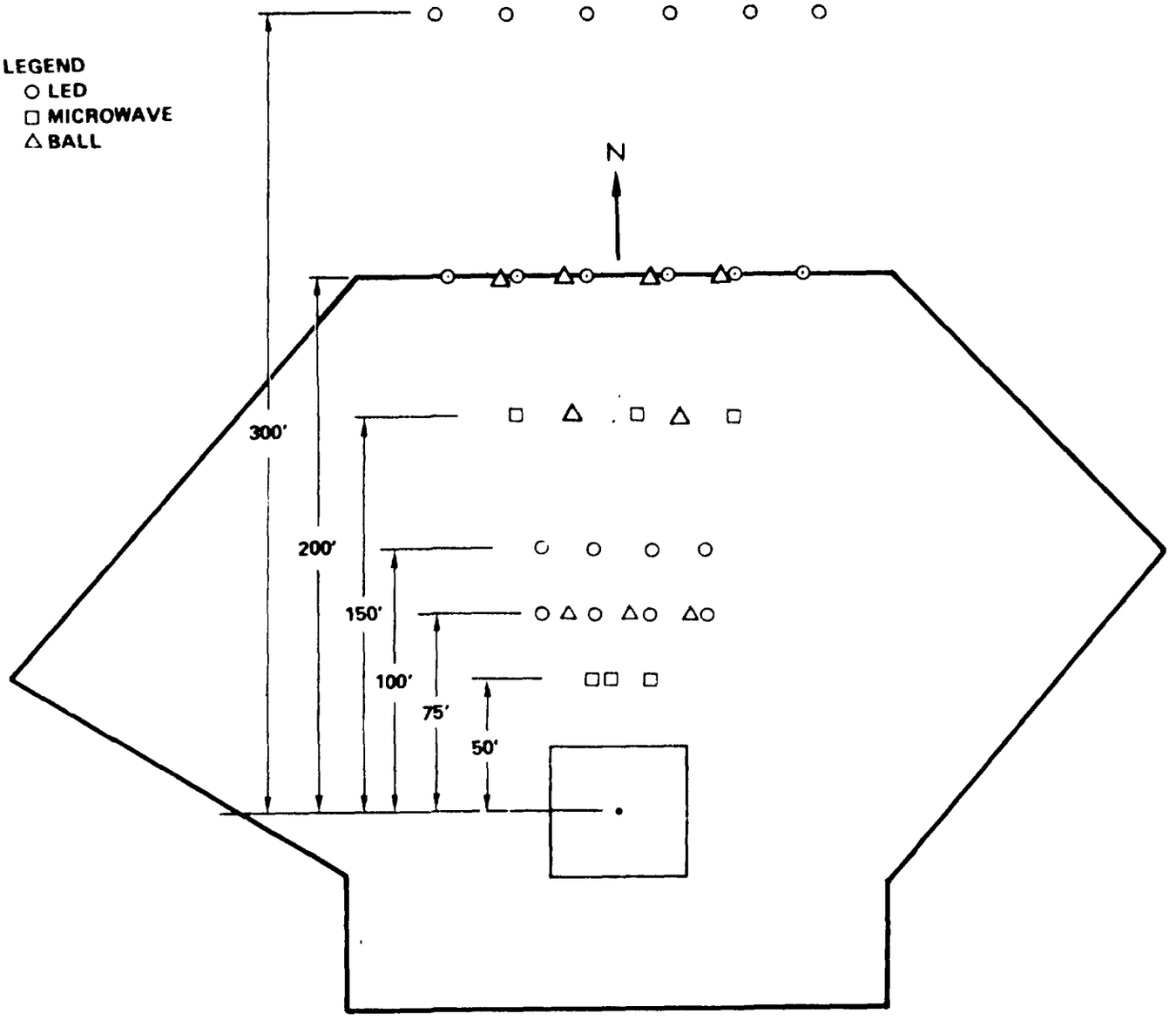

Figure 5.8. Active Gage Configuration - Test No. 5

presented in Figure 5.9. The front of the fiber cloud arrived at the 75, 100, 200 and 300 ft(22.9, 30.5, 61 and 91 m)ranges with a time delay associated with the mean wind velocity. The waveforms of the mass flux history are each aperiodic with small duration spikes and longer duration nulls. This waveform is typical of a meandering plume and/or a discontinuous cloud. This condition of an irregular cloud envelope also explains the different cloud arrival times for active instruments at similar ranges. The mean mass flux amplitude at 75 ft (22.9 m) is about 5 μgms $cm^{-2}sec^{-1}$, while at four times the range the mass flux is attenuated by a factor of sixteen to 0.3μgm cm^{-2} sec^{-1}. This corresponds to the "inverse-distance-squared" concentration attenuation predicted by the Pasquill-Gifford plume formula.

The arrival times of the wavefronts yield about a 5.5 fps (1.7 mps) wind. At 200 ft (61 m) range, the 22 sec duration fiber cloud from the exploded plate indicates 121 ft (36.9 m)length for the cloud extent at the ground level. The LED systems showed higher amplitude mass fluxes for shorter durations on the east side of the test pad at the 75 and 100 ft (22.9 and 30.5 m) ranges, as compared to the west side of the test pad.

Ball Gages

The ball gage results, presented in Figure 5.10, are a good deal more sparse than the LED results. According to the passive sensors which collected fibers deposited in the gage vicinities, the average length was significantly less than the 4 mm threshold of the ball gage, which would explain the difference. Actually only the events from the two westerly gages can probably be considered as seeing plume passage. Those gages east of the plume appear to have first events some time after initial plume passage indicating cross-wind transport at a considerably reduced velocity.

Microwave Gages

The microwave gage results for this test are presented in Figure 5.11. Again the data is quite sparse. The short duration of the fiber cloud and the large empty space between fiber clusters at close-in ranges permit the approximately 3 in. (7.6 cm) diameter by 5 in. (12.7 cm) long gap of the microwave measurement volume to sample only a few fiber clumps in spite of the high mass flux. Gage 1, located at 50 ft (15 m) measures 6.5 times the fiber mass measured by Gage 5, located at 150 ft (45.7 m). This relation appears to almost follow the mass deposition dependence on the inverse of the square of the distance from the source.

Active Gage Summary

The data from the three gage systems have been combined and are summarized in Figure 5.12 which consists of three interrelated subcharts. The composite chart in the upper left hand corner shows the time at which a fiber arrives at a given gage type and gage number (LED gages 1-7, TRW ball gages 1 and 2, BRL ball gages 1A and 2A, and microwave gages 1-5) at the respective stations. The time of the arrival of the first fiber at each range shows a propagation or wind velocity of 6.9 fps (2.1 mps). The LED yielded the most data.

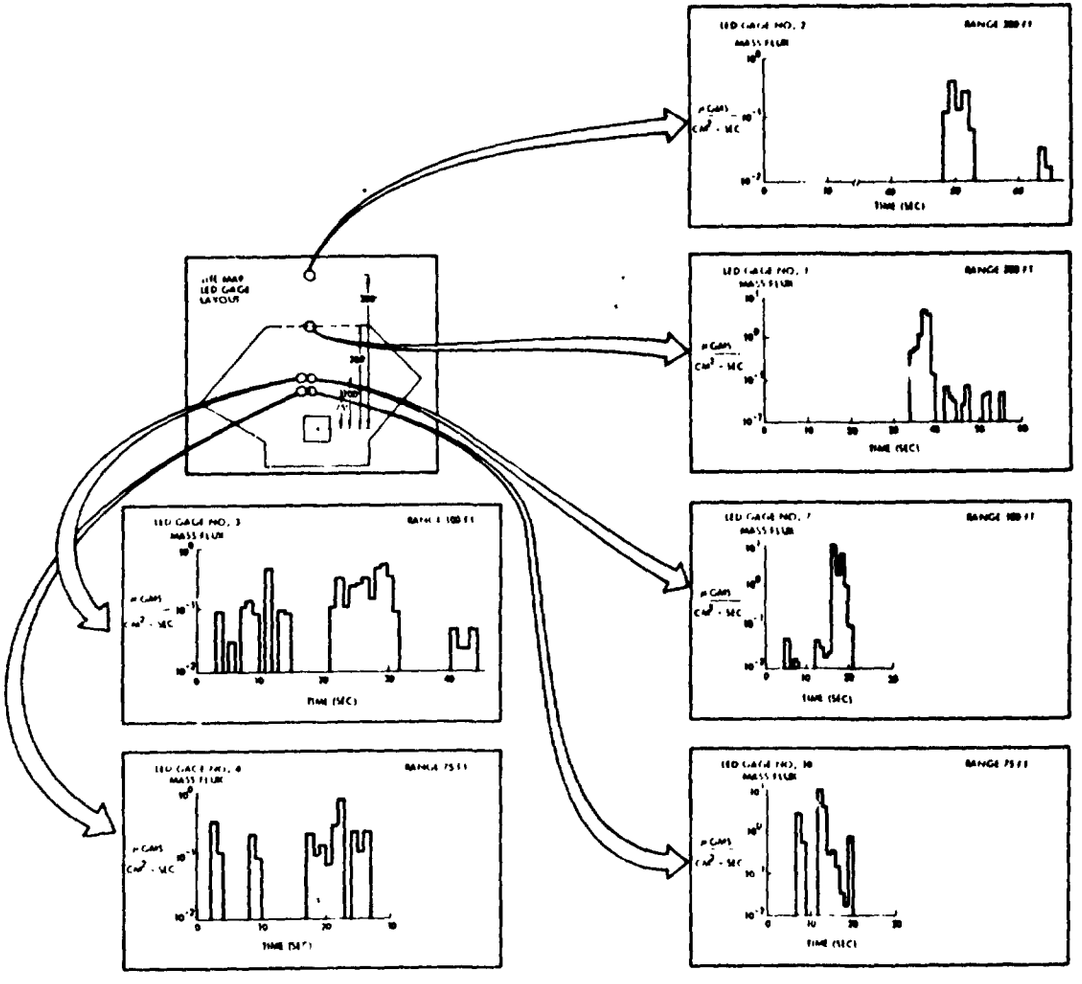

Figure 5.9. Mass Flux Measurements Using LED Systems - Test No. 5

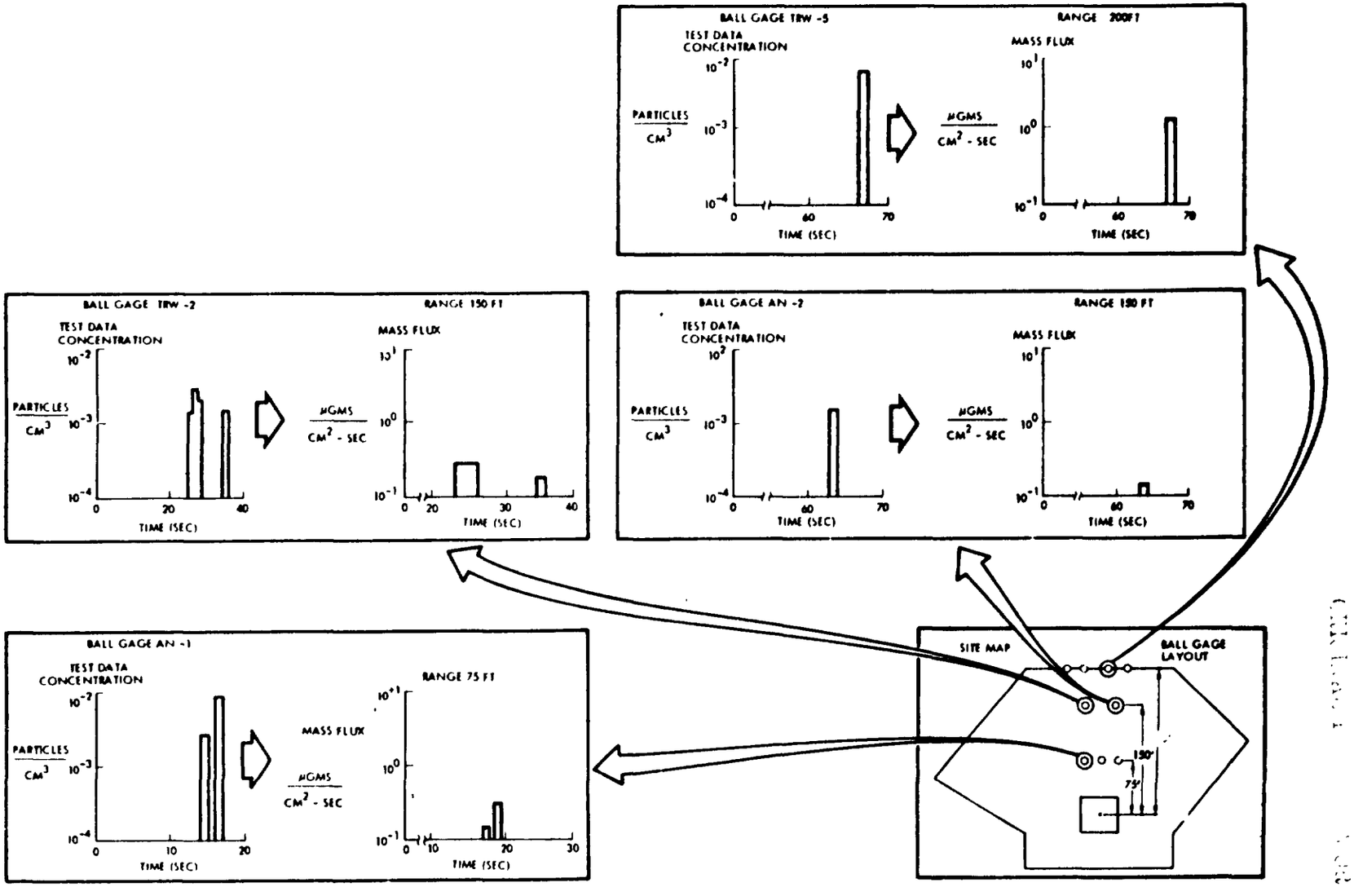

Figure 5.10. Ball Gage Results - Test No. 5

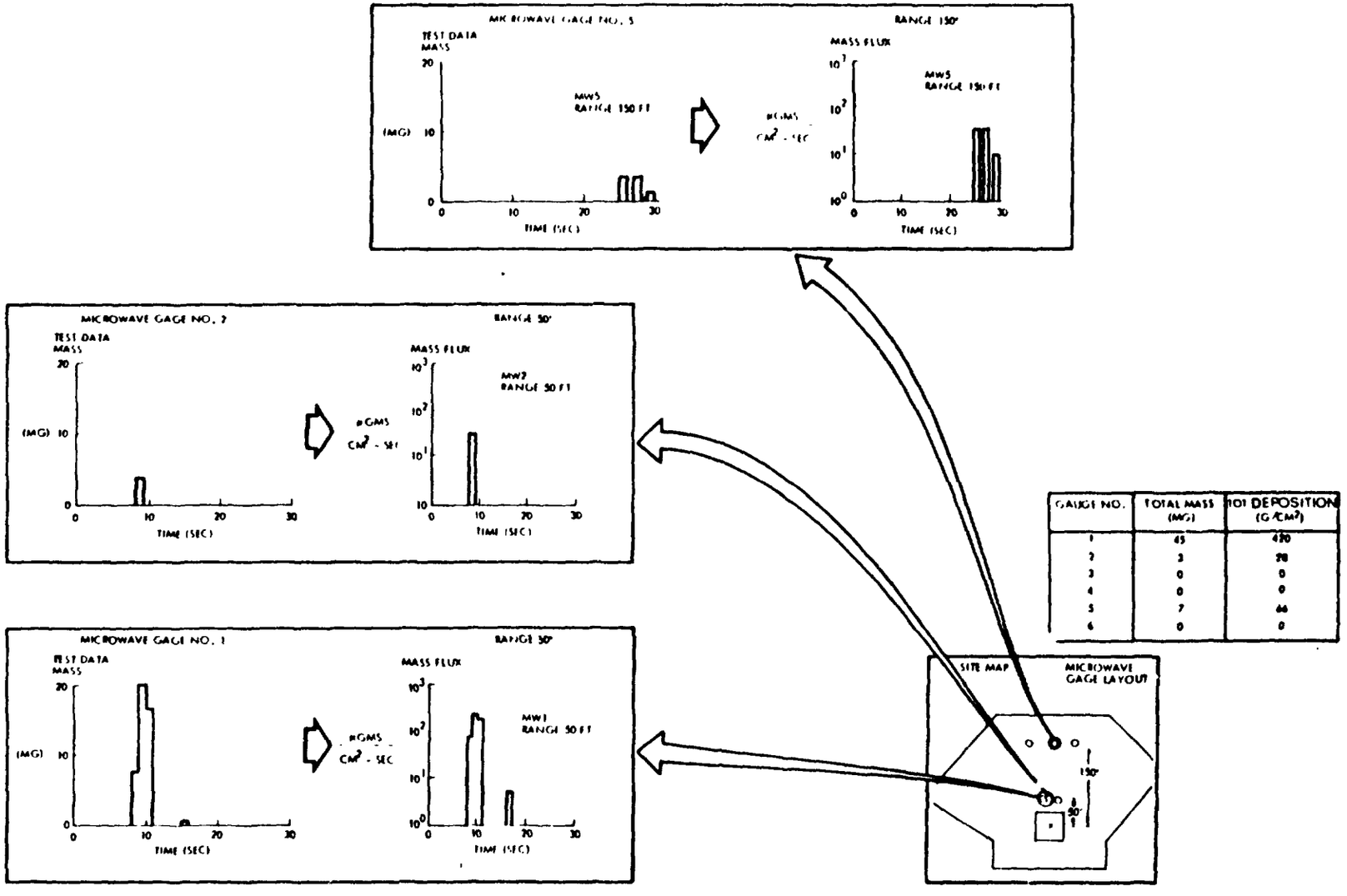

GAUGE NO.	TOTAL MASS (MG)	TOT DEPOSITION (G/CM^2)
1	45	430
2	3	28
3	0	0
4	0	0
5	7	66
6	0	0

Figure 5.11. Microwave Gage Results - Test No. 5

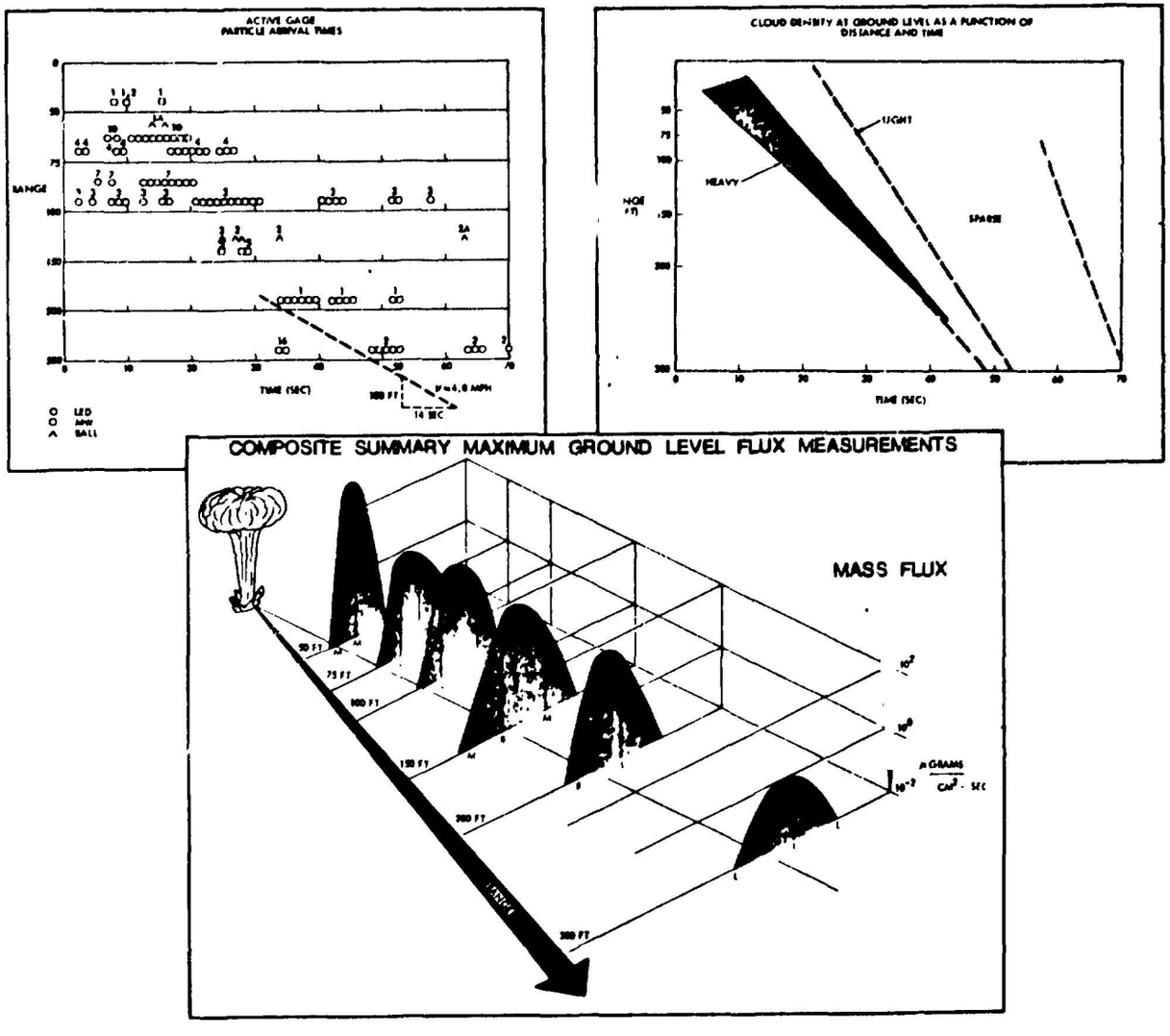

Figure 5.12. Active Gage Summary - Test No. 5

This chart does not indicate the concentration amplitudes.

The display of concentration amplitudes translates the previous chart into the chart in the upper right hand corner. Note that the duration of the cloud decreases with increasing range, which could be attributed to either cloud rise above the ground level measurement systems or to severe deposition that depletes the fibers in the cloud. Also the heavy concentration of fibers disappears at increased range which is to be expected because of areal dispersion and deposition.

The integrated mass flux from each type of gage (M = Microwave, L = LED and B = Ball) and from each station is displayed in a composite summary chart in a three-dimensional plot. Even though each gage type used a different physics principle, they were all smoothly consistent in their measurements.

TEST NO. 6

The third plate test was with the same 1 ft x 1 ft x 1/4 in. (30 cm x 30 cm x 6.3 mm) composite plate. A high temperature propane/air burn for 20 minutes as in the previous test was performed. Date and time of the burn were February 15, 1978 at 3:41 pm PST. The explosion was postponed until February 16, 1978 at 7:59 am PST.

Thermocouple Data

The plate was instrumented for temperature measurement somewhat differently to determine a temperature profile through the plate. The three plate temperature thermocouples were of chromel-alumel construction imbedded at 1/16 in. (0.16 cm) below the upper surface, 1/8 in. (0.32 cm) below the upper surface and 3/16 in. (0.48 cm) below the upper surface. This is shown in Figure 5.13.

Flame temperature was measured with a tungsten-rhenium thermocouple located 1/2 in. (1.27 cm) below the composite plate center. As shown in the figure the flame temperature had reached 2310°F (1265°C) at the time (2.5 minutes) that the thermocouple broke. The lower section of the plate reached a temperature of 1100°F (593°C), while the upper section only reached 700°F (371°C).

Gage Layout

The gages were positioned for the test, as shown in Figure 5.14, much as before except one ball gage at the 75 ft (23 m) range had been removed for tests at Rome Air Develoment Center. An attempt was made at the ball gage locations using vu-graph frames covered with bridal veil and sprayed with glue to directly relate passive deposition to the ball gage data.

LED Gages

The results from the LED gage systems for this test are presented in Figure 5.15. Of the twenty systems in operation only the three most westerly

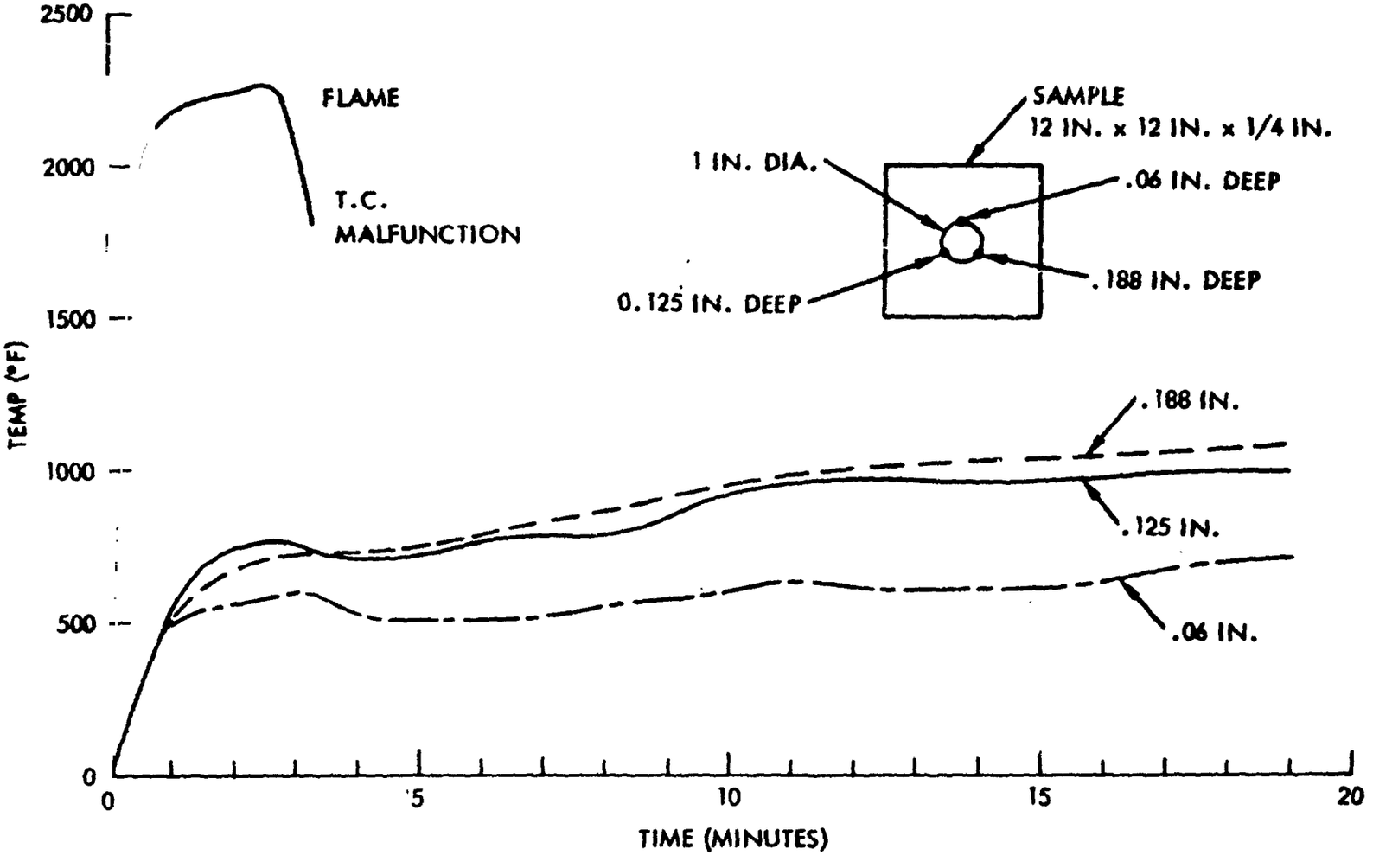

Figure 5.13. Sample Burn Temperature Profiles - Test No. 6

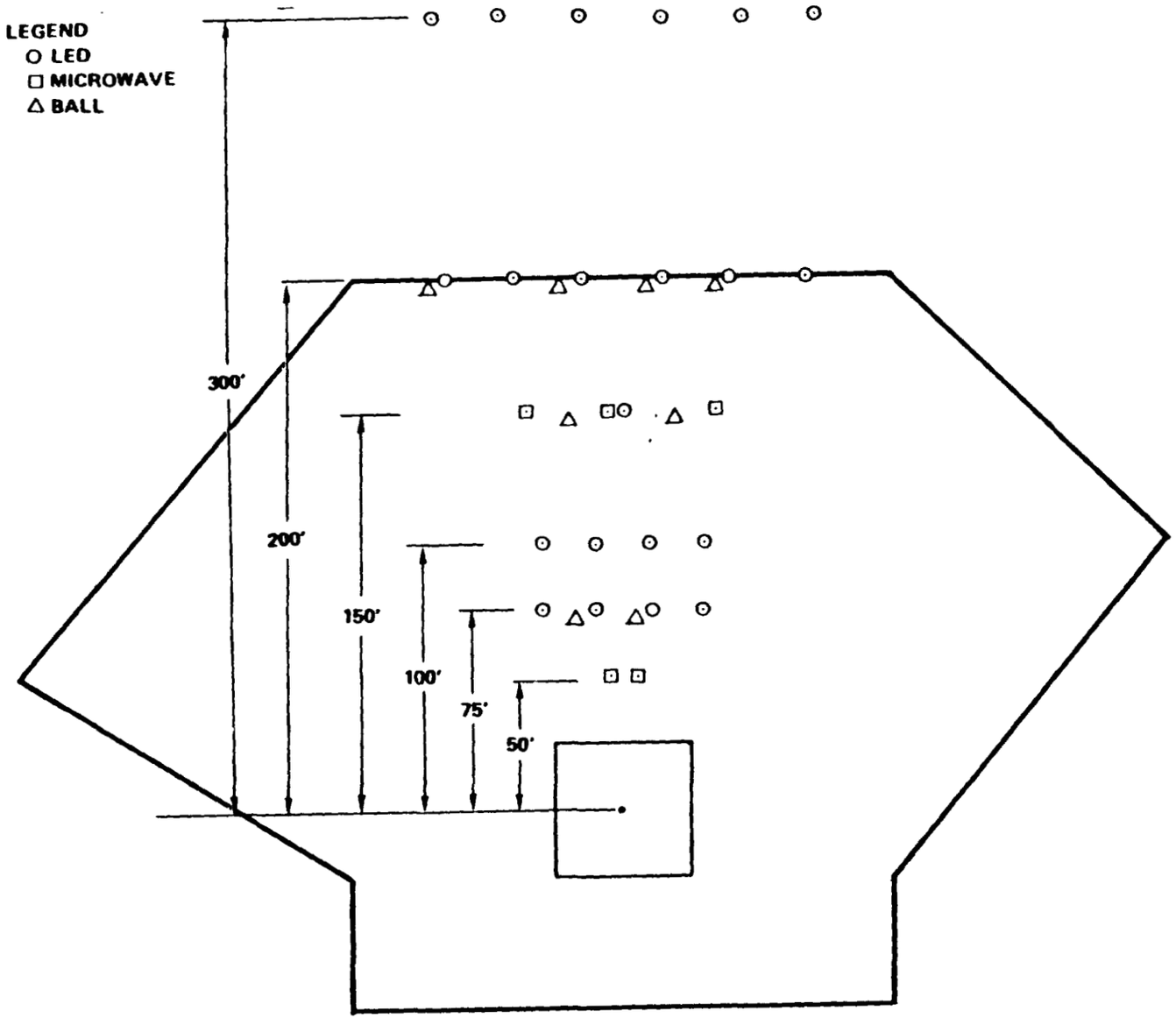

Figure 5.14. Active Gage Configuration - Test No. 6

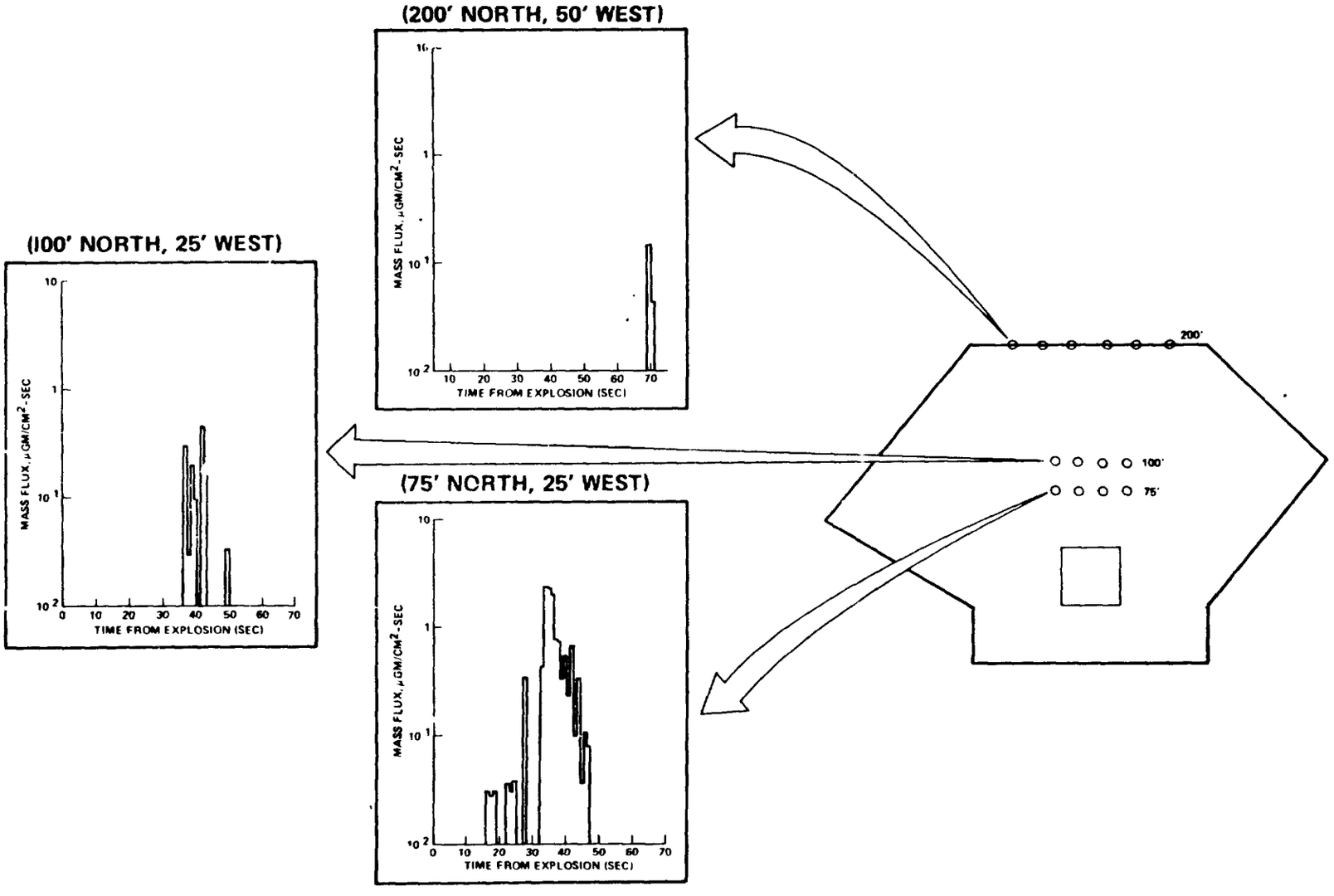

Figure 5.15. Mass Flux Measurements Using LED Systems - Test No. 6

returned a significant amount of data, indicating that the fiber cloud moved in a north westerly direction away from the LED systems.

From the time of arrival of the showers on the three gages, a 3.4 fps (1.5 mps) plume velocity at the 5 ft (1.5 m) height was computed, in good agreement with the meteorological data of 3.2 fps (1.4 mps).

Ball Gages

The ball gage data is presented in Figure 5.16 along with some of the results from co-positioned "bridal veil vu-graphs". As shown only the most westerly station returned any flux data. Data retrieved from the bridal veil plates indicated that the ground part of the plume and fallout passed distinctly west of the centerline. The greater part of the fallout was noted only on the horizontally-oriented plates at (75, -20), (150, -20), and (200, -45). The vertically-oriented plates, even at these locations, collected roughly one-tenth as much as the horizontal plates! For the above three positions, the horizontal collection was respectively 66 clumps/m^2, 570 single fiber/m^2 and 395 single fiber/m^2. For the latter two plates which recorded the single fibers, the effective fall velocity should be somewhere between still air at 1 cm/sec and the recorded wind velocity at 2.9 fps (0.9 mps), say 0.5 fps (0.15 mps), giving exposures of 4 x 10^3 and 3 x 10^3 fiber-sec/m^3, respectively. Since one count is equivalent to 2 x 10^3 fiber-sec/m^3, there should have been between zero and two counts on each ball gage detector before the plume passed (assuming the deposits to be added to the bridal veil during plume passage). The large discrepancy between vertically and horizontally oriented vu-graph data is ascribed to a lack of stickiness on the glue preparation used for this test. A glue of more permanent stickiness was subsequently utilized for Test No. 8 vu-graphs.

Further study of the optical recording indicated a number of pulses at very late times on the gages (18-25 minutes after explode), probably due to personnel in the area (see Figure 5.18). It can be expected that some of the deposited particles on the bridal veils were due to late time activities and not indicative of plume passage and primary fallout. The bridal veil at several gage locations had a large enough count to give a length spectrum. These are shown in the figure.

Assuming a fiber weight of 5.4 x 10^{-7} gm/cm, the particle count including length measurement on each bridal veil were translated to mass deposition. This is shown for both horizontally and vertically oriented plates superimposed on a location plot, Figure 5.17. It can be seen again that by far the preponderance of material was deposited west of center, probably centered beyond the maximum location of the sensors.

The tape records were analyzed out to very late times for this experiment and many events noted. Plume passage, also shown on a previous plot, occurs at about 30 sec on only one detector at 75 ft (22.9 m). The plots showing Figure 5.18 illustrate the ability of fibers, once deposited, to easily re-entrain and cause significantly larger exposures near the ground than would be expected from direct deposition from the plume. The small amount of event

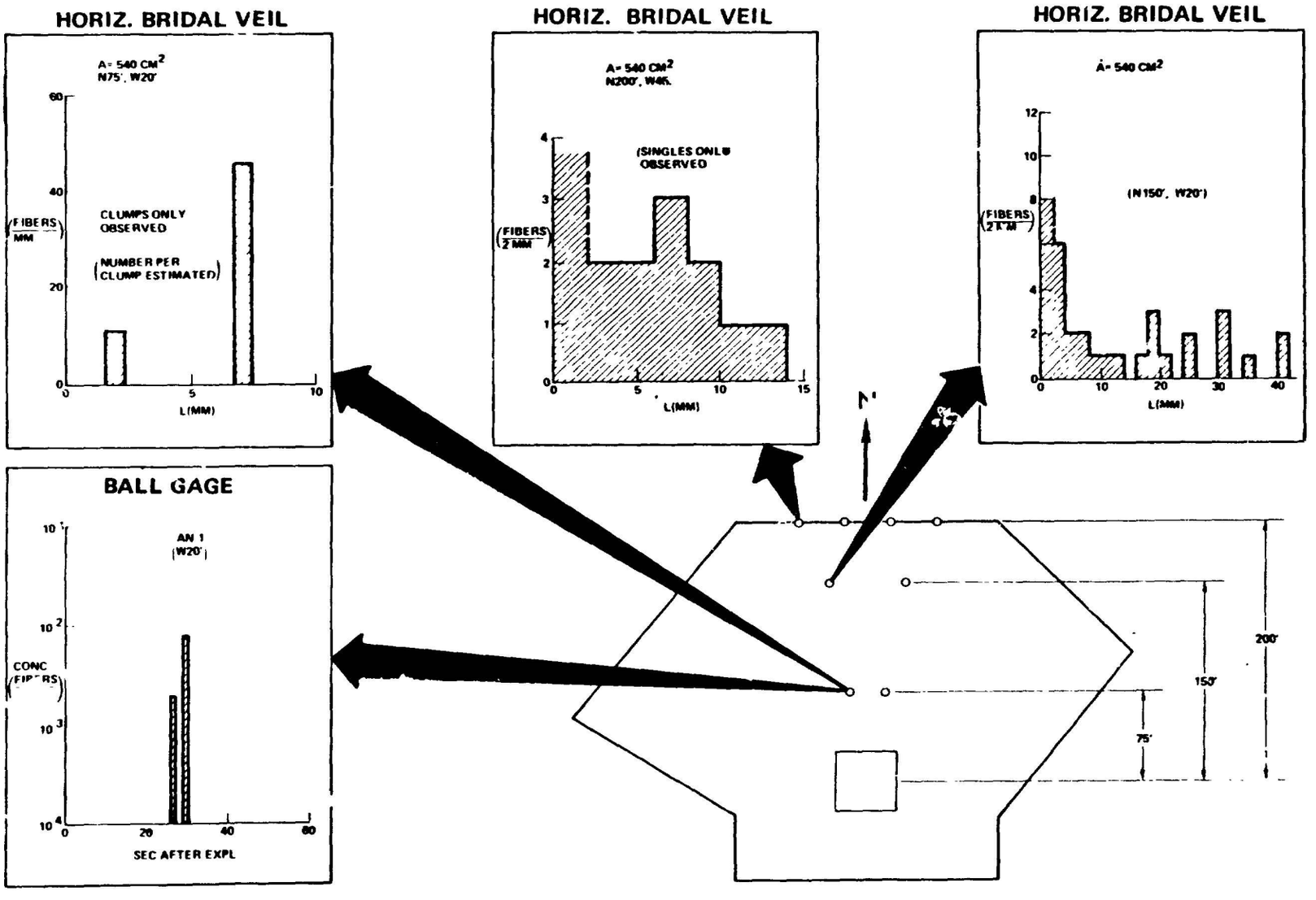

Figure 5.16. Ball Gage and Co-Positional Bridal Veil Results - Test No. 6

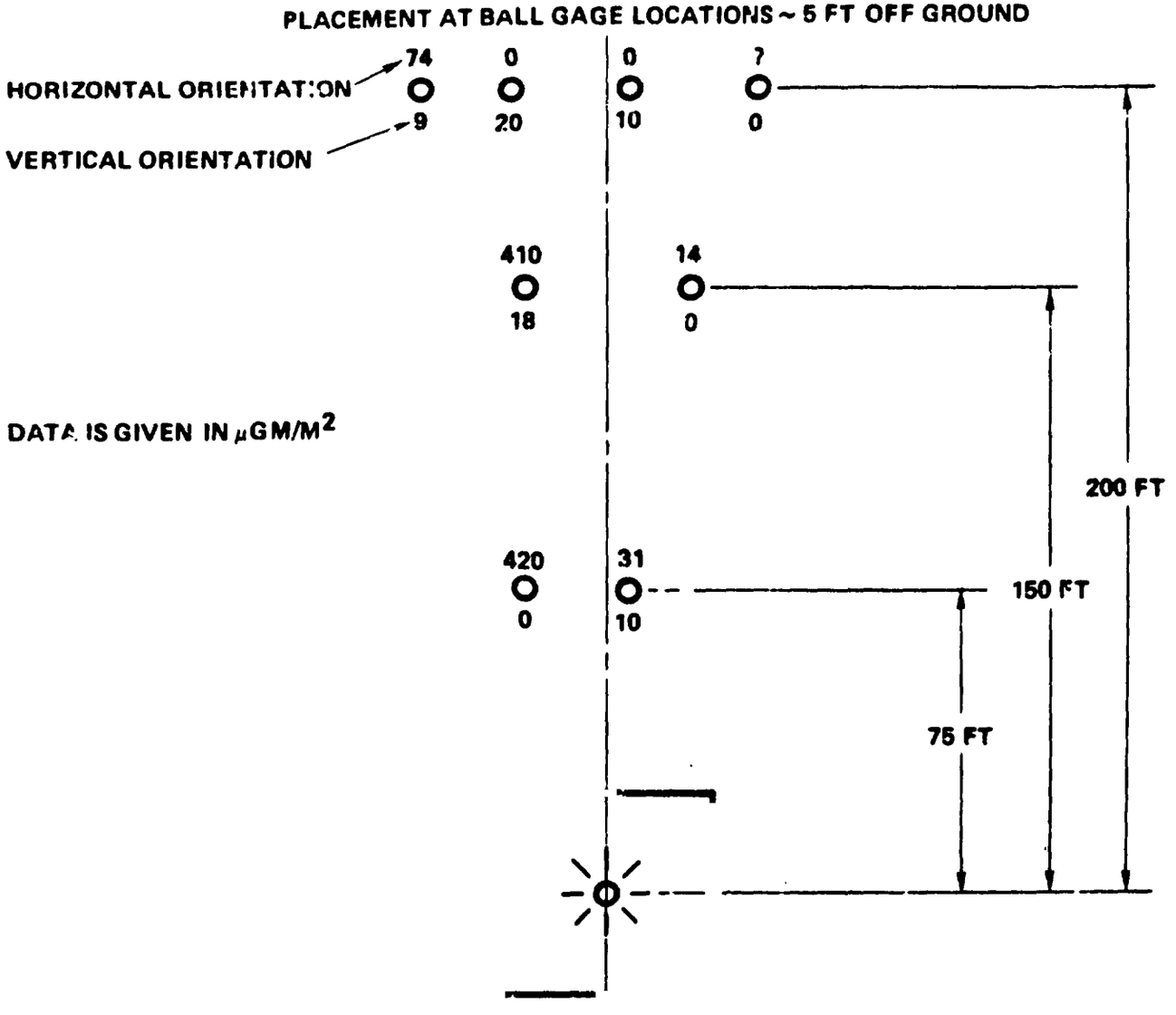

Figure 5.17. Bridal View Gra.. Weight Deposition - Test No. 6

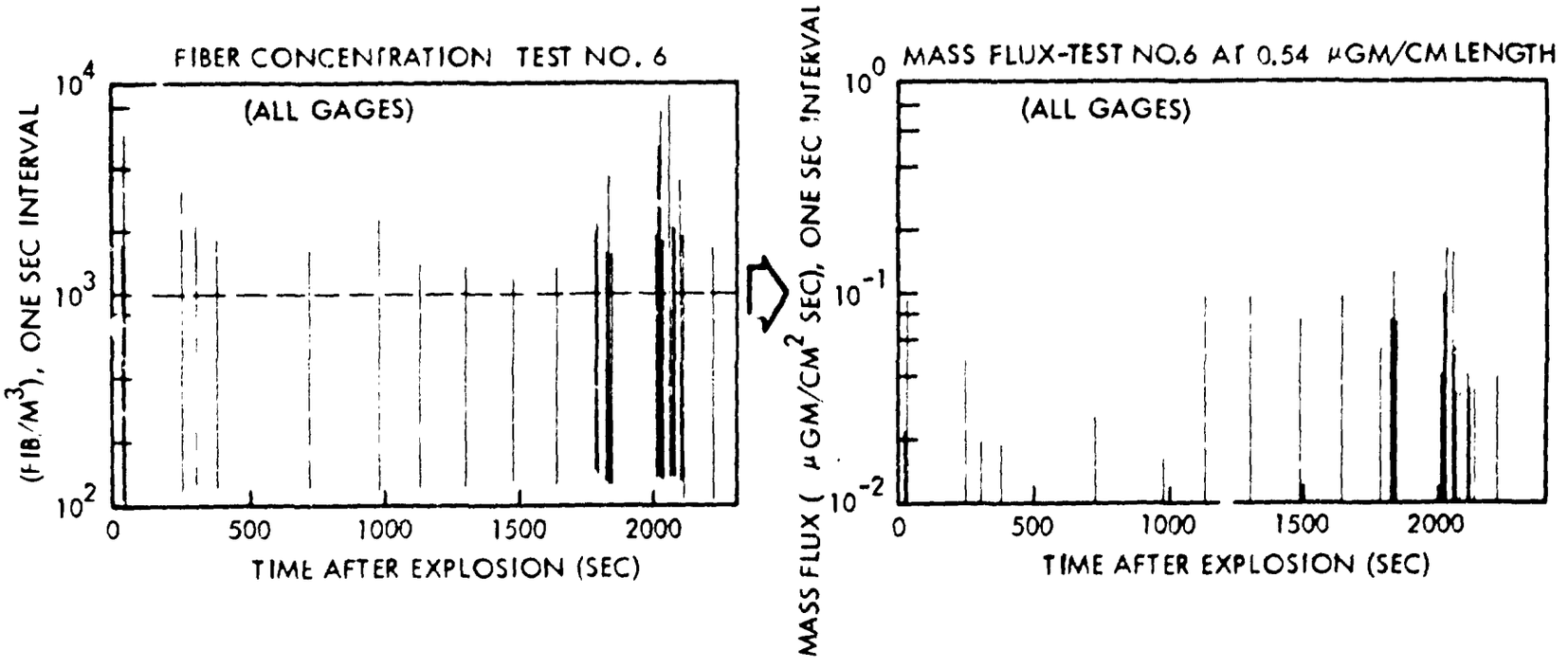

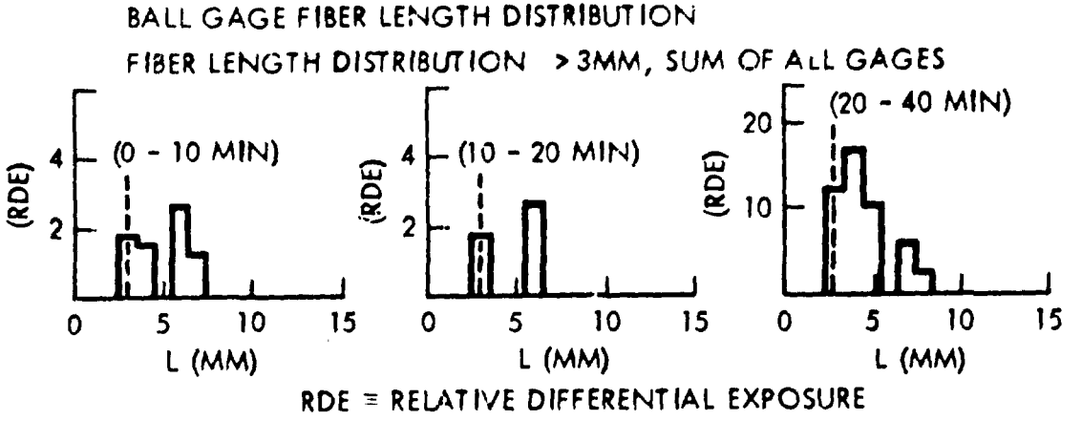

Figure 5.18. Ball Gage Condensed Time Plots - Test No. 6

data precludes strong conclusions from being drawn on the length distribution data; however, it appears that re-entrainment favors shorter lengths.

Microwave Gages

No microwave data were obtained for this test.

NWC BARREL TESTING

Three tests were performed in the series using samples of cut up carbon composite barrels. The first of these tests used a hot propane burn followed by an explosion. The second in the series used a 20 x 20 ft (6.1 x 6.1 m), JP-5 pool burn under the barrel sections. For this test none of the active gage systems were deployed other than the thermocouples. The third test involved another pool burn and an explode phase after burning. Again no active gage systems were deployed.

For the first test in this series, where the active gages were deployed, the transport and fiber distribution results were markedly different from those obtained before with the flat plates.

TEST NO. 8

Test No. 8 utilized a much larger quantity of initial material than in previous tests (9.2 kg versus 0.9 kg). In order to fully subject the barrel to a hot 20 minute propane burn, the barrel was cut up into 12 sections, two of which could be burned at a time. The burns took place on March 6 and 7, 1978. At the completion of each burn the residuals were carefully collected and weighed. It was noted during the burns that a significant amount of material was released to the atmosphere inspite of screens imposed to prevent it from doing so. The major losses however appeared to be complete burning away of the epoxy and apparently burning of the fiber itself. The residuals from the six burns were collected and placed 1 ft (30 cm) above a shaped charge at ground zero on the concrete pad. The explosion was initiated at 7:57 am PST on March 8, 1978.

Thermocouple Data

No thermocouples were emplaced for these burns.

Gage Layout

The placement of gage systems was much as it had been before, as shown in Figure 5.19, except the microwave systems at 150 ft (46 m) were moved to 100 ft (30 m) range and the ball systems at 150 ft (46 m) range were repositioned somewhat. One of the microwave systems was inoperative due to an oscillator failure. For this test, vu-graph bridal veil sensors were again positioned in proximity to each ball gage, vertically and horizontally oriented, using permanently sticky glue on the bridal veil.

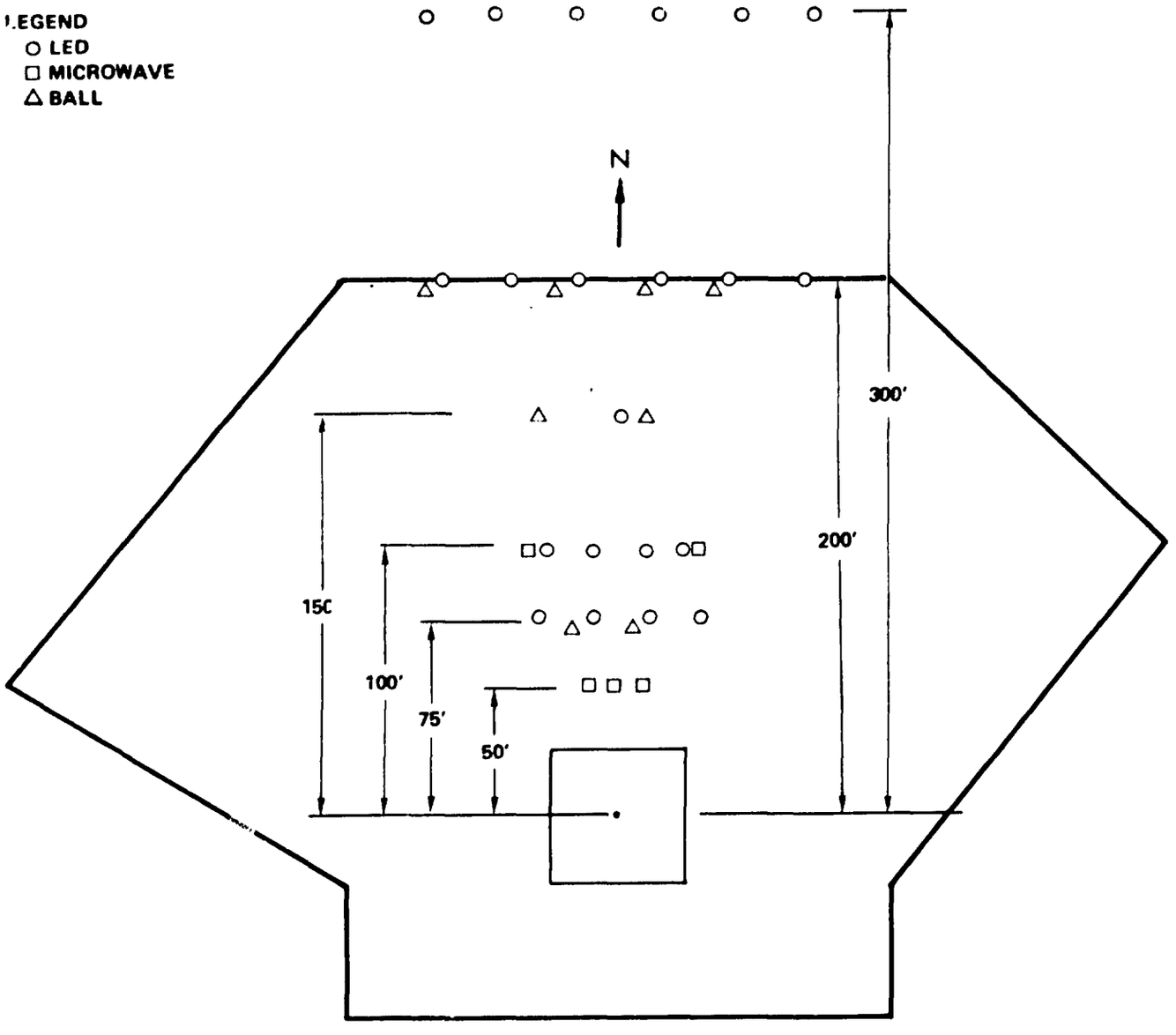

Figure 5.19. Active Gage Configuration - Test No. 8

A LADAR system was set up for this test which sampled on a horizontal line about 5 ft (1.5 m) off the ground at about the 205 ft (62 m) range from the west edge of the pad to the center of the pad. At this point a mirror directed the beam vertically, allowing sampling to occur for vertical ranges at this point.

LED Gages

The LED systems results for this test are presented in Figure 5.20 in terms of mass flux. The aperiodic characteristic of the mass flux history waveforms generated by the flat plate explosions of Test No. 5 repeated itself in the barrel explosion of Test No. 8. The burn and explode of the barrel in Test No. 8 resulted in a lower concentration and shorter duration fiber cloud at ground level as compared to the flat plate Test No. 5.

Ball Gages

The ball gage results are presented in Figure 5.21 in terms of mass flux of singles. Concentration data of single fibers taken by the ball gages was translated to mass flux using a wind velocity of 5.7 fps (1.7 mps), a mass per unit length of 0.54 μg/cm, and the length of each fiber counted, as determined by its pulse height. Data taken using the multichannel analyzer was considered suspect because of noise injection and is consequently not presented. Gage T-6 at 200N, 45W, in operation, did not record any pulses. Threshold for detection of a pulse is about 3×10^{-2} μg/cm^2 sec. As before, the flux values were significantly lower for the ball gages than for the LEDs, indicating a preponderance of fibers with lengths below the ball gage threshold. This is confirmed by the vu-graph data analysis following.

Indicated average velocity for pulse passage at each station is about 7.3 fps (2.2 mps) at 75 ft (22.5 m) and 6.7 fps (2 mps) at 200 ft (61 m). This velocity is significantly greater than the wind velocity of 5.7 fps (1.7 mps), indicating transport by some additional mechanism, most probably by the force of the explosion.

A pulse was received on one detector significantly before pulse passage, indicating the possibility that some fibers deposited during burn had been re-entrained and transported.

Bridal veil vu-graph results indicate that by far the greatest mass transport is by the large clumps which are not included in this presentation and for which no pulse trains were noted by the ball gage records.

The ball gage presents an opportunity to monitor the near ground level downrange transport (gages TRW-3 and TRW-5) and the crossrange transport (gages TRW-5 and TRW-4) of fibers. This is presented in Figure 5.22, where it is shown crudely that the downrange transport, dominated by the mean wind speed, moved the 3-7 mm long fibers faster than the longer 7-15 mm long fibers. The crossrange transport, dominated by the turbulent portion of the wind speed, moved the 3-7 mm long fibers slower than the longer 7-15 mm long fibers. The preferential selection of fiber lengths by laminar and turbulent transport is

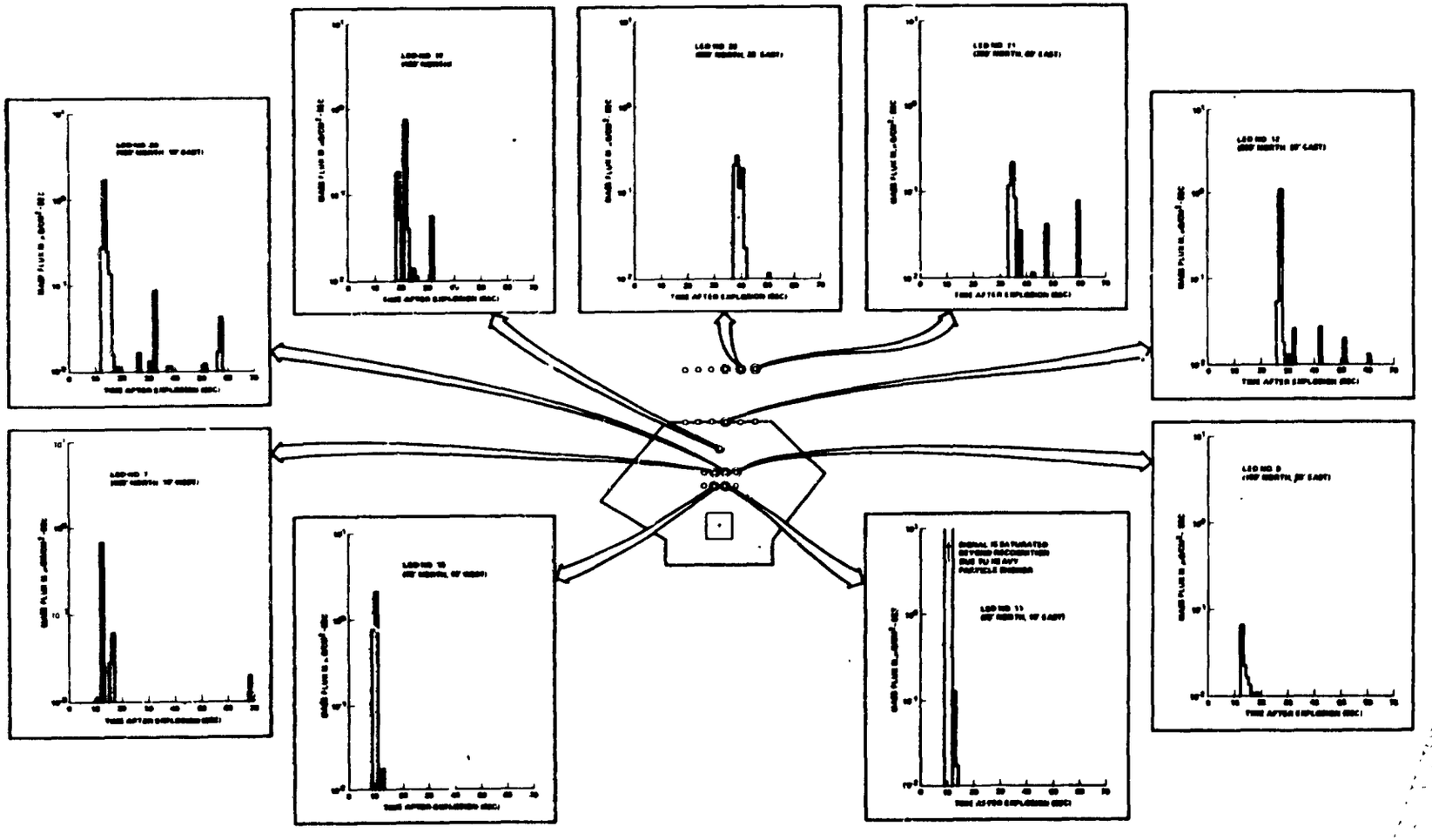

Figure 5.20. Mass Flux Measurements Using LED Systems - Test No. 8

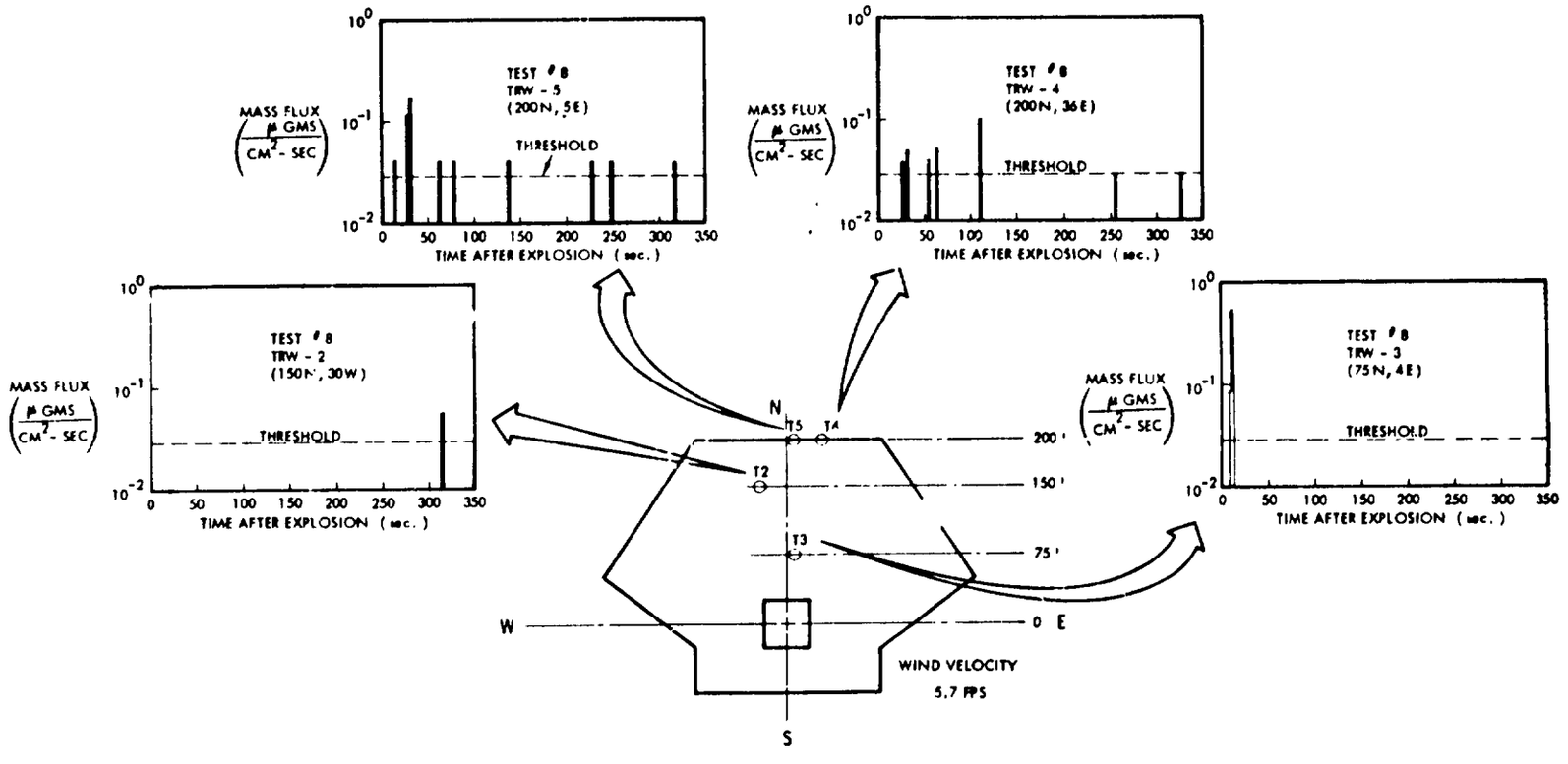

Figure 5.21. Ball Gage Measured Mass Flux of Singles Fibers - Test No. 8

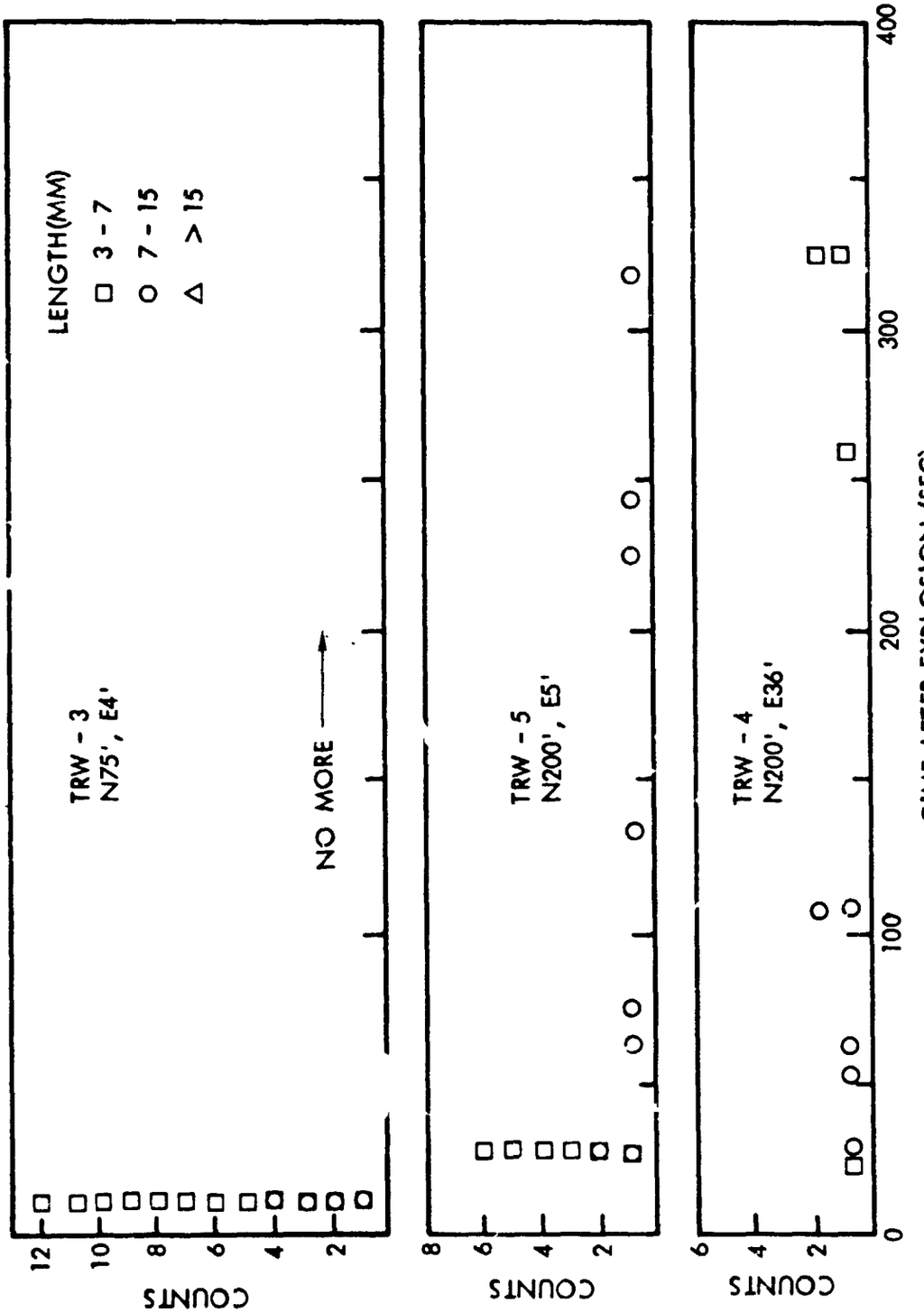

Figure 5.22. Length Discrimination From Ball Gage Data - Test No. 8

an important concept to be considered for modeling.

To provide a field calibration of the ball gage systems, vu-graph shields covered with bridal veil were positioned vertically (V) and horizontally as shown in Figure 5.23 at each ball gage location. Because the ball gage is somewhat capable of modifying the local concentration during the attraction and during the repulsion phase, it is possible that the horizontally placed vu-graph data could be affected. To check this possibility at several locations, "boxes" of vu-graphs were constructed and mounted as shown well away from any potential interaction effects with the ball gage fields. Data obtained from these vu-graphs, both horizontal and vertical agreed with that obtained from the V and H positions. The data show that the spectral composition for horizontally and vertically collected samples is roughly the same, as it should be. However, the ratio of counts in the 1 and 20 mm length range for vertical to horizontal orientation varied significantly with location. If transport is entirely wind driven, than the ratio of vertical to horizontal deposition should be the same as the ratio of wind velocity normal to the vertical vu-graph (5.6 fps[1.7 mps]) is to the fall velocity (1 cm/sec). This ratio is 70, very close to the highest ratio observed at 200N, 5E, and 200N, 36E.

All of the four locations with East coordinates fall within the footprint obtained by ground level passive data acquisition. These are also the ones with significantly higher horizontal as well as vertical deposition.

Ball gage data taken at 750N, 30W (well out of the passive footprint area) shows that the deposition on the vu-graphs must be late time, well after any pulse passage, and because of the low V/H ratio, borne by winds with a substantial vertical component which must be using fibers already deposited within the footprint area as source.

The absolute length distribution obtained from vertically oriented vu-graphs in close proximity to ball gages is compared in Figure 5.24 to the absolute length distribution obtained from ball gages at the same locations. Only those locations with an adequate number of ball gage events are compared. The ball gage data has been transformed to deposition by multiplying concentration data at each length increment by the wind velocity 5.7 fps (1.7 mps). The resolution and noise level of the ball gage precludes observation of fiber lengths under about 3 mm for this test. It can be seen that most of the deposition data lies at lengths shorter than this. The vu-graph data is subject to the filtering action of the approximately 0.9 mm spacing of the mesh. The sparse ball gage data does not disagree with the bridal veil deposition except possibly at the TRW-5 position where, however, both plots indicate a shift in mean length to a longer length.

Table 5.1 presents the final results of the field calibration check of ball gages taken during this test. In preparing this table the vertical orientation vu-graph bridal veil data taken at each ball gage site is transformed to exposure using a wind velocity of 5.7 (1.7 mps) and compared to the exposure results from each gage. For all gage units which used pulse stretching followed by magnetic tape/optical recorder readout, the agreement was well

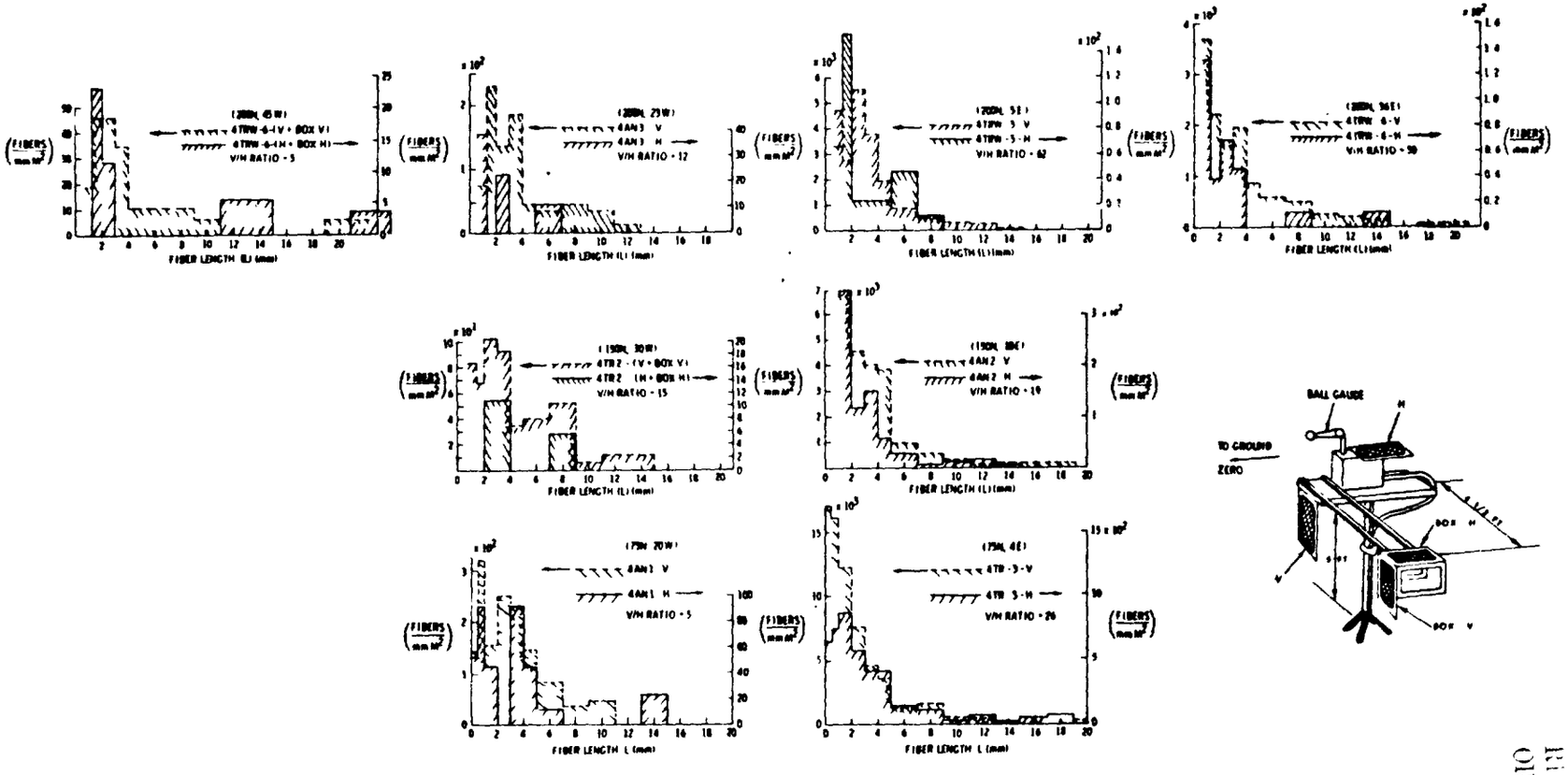

Figure 5.23. Bridal View Graph Study - Test No. 8

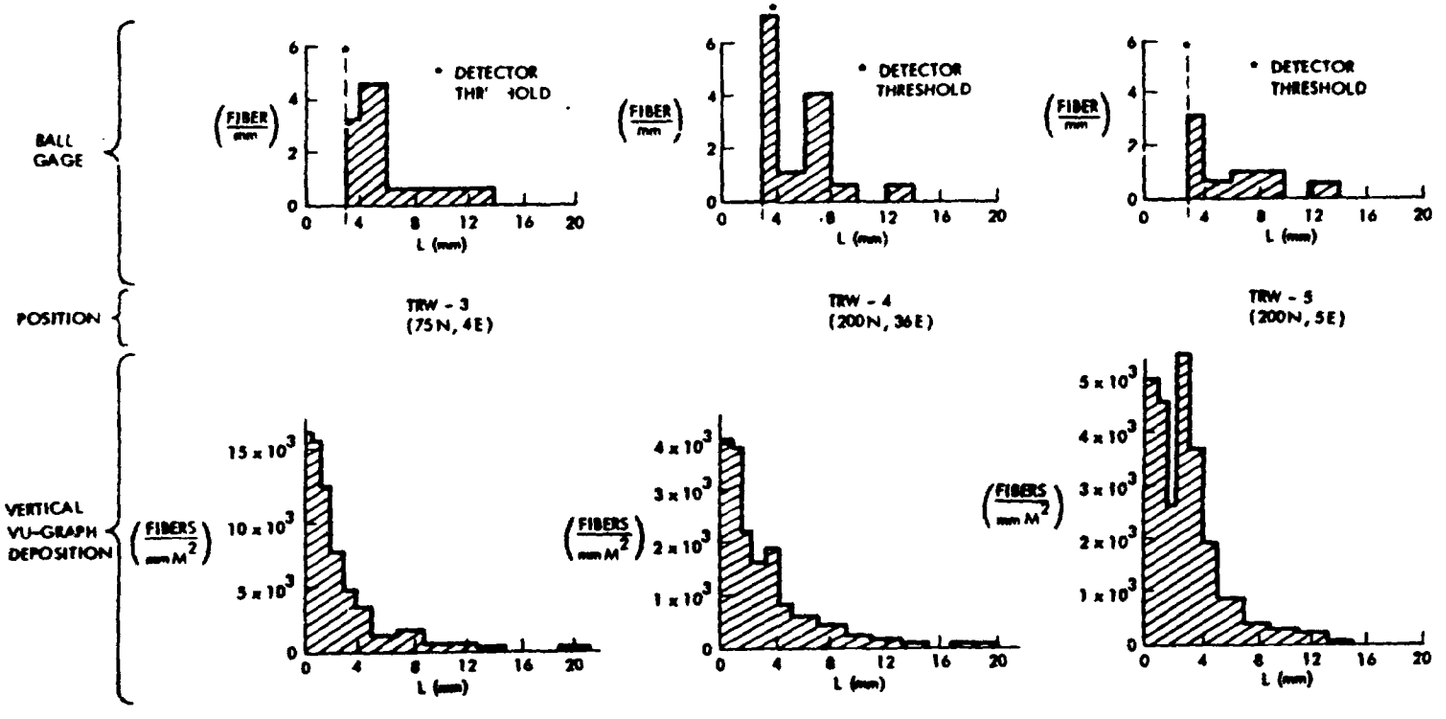

Figure 5.24. Length Distribution, Ball Gage Versus View Graph Deposition - Test No. 8

Table 5.1. Ball Gage Field Calibration Check - Test No. 8

SENSOR	RECORDER†	DISTANCE COORDINATE	MEASURED EXPOSURE L > 3mm FIBER SEC / M^3		NUMBER OF BALL GAGE EVENTS
			VUGRAPH*	BALL GAGE	
TRW - 2	MT	150N,30W	6.1×10^2	1×10^3	1
TRW - 3	MT	75N,4E	2.80×10^4	2.6×10^4	16
TRW - 4	MT	200N,36E	1.12×10^4	1.2×10^4	9
TRW - 5	MT	200N,5E	1.72×10^4	2.1×10^4	15
TRW - 6	MT	200N,45W	2.0×10^2	---	0
AN - 1	MCA	75N,20W	1.21×10^3	3.8×10^{4} **	27?
AN - 2	MCA	150N,10E	1.28×10^4	(NOT OPERATING)	(NOT OPERATING)
AN - 3	MCA	200N,23W	8.5×10^2	5.2×10^{4} **	37?

* USING VERTICALLY ORIENTED VU - GRAPH AND A WIND VELOCITY OF 3.9 mph - BRIDAL VEIL SPACING ≃ 0.9 mm - BRIDAL VEIL MADE STICKY.

** USING A MEAN LENGTH PER COUNT OF 6.5 mm AS DETERMINED FROM TRW 3 FIBER SPECTRUM > 3 mm.

† MT - MAG TAPE THROUGH A PULSE STRETCHER, MCA - MULTICHANNEL ANALYZER;

within the statistics of the number of ball gage events recorded. In contrast, both gages operated into the multichannel analyzer did not agree with the deposition data within the statistics of the counting, almost certainly due to the inability to be able to reject noise pulses.

From other passive data it appears that TRW 3, 4, and AN-2 were almost on the centerline of the passive plume footprint, with TRW 5 well within its boundaries. This is confirmed by the bridal veil vu-graph and ball gage data.

Microwave Gages

The fiber cloud missed all but one microwave station in the barrel burn/explode test. At this 50-ft (15.2 m) station, 370 $\mu gm/cm^2$ was recorded for the time-integrated mass flux for this barrel test. The results are presented in Figure 5.25. The narrowness of the fiber footprint indicated by no data on the remaining 4 gages is verified by the sticky paper data at the two locations and the LED and ball gage results at the 100 ft and 75 ft (30.5 and 22.9 m) locations.

LADAR Results

As mentioned before, the LADAR system was in full operation for Test No. 8, sampling along a horizontal line and a vertical line. The data obtained is presented in Figure 5 26. Only relative intensity information is given, since calibrations of fiber cloud density and/or smoke contamination capability had not been completed.

At 28 sec after detonation of the burned barrel debris, the fiber cloud appears to be composed of three separate clouds. The lowest cloud is about 30 ft (9.1 m) up, the middle level cloud is about 60 ft (18.2 m) up, and the highest cloud is 80 ft (24 m) up; the middle level fiber cloud is the most dense. At 84 sec, there appear to be only two clouds, one at a 10-ft (3 m) and the other at a 30-ft (9.1 m) altitude. This shows that the 21-ft (6.4 m) high tuna can poles and 30-ft (9.1 m) high millipore filter poles are not sampling the complete cloud. However, a 90-ft (27 m) high sampler system would be adequate at the 300-ft (91 m) range for sampling the entire explode plume.

The horizontal portion of the cloud is displayed at 185 sec after detonation. The cloud appears to be separate puffs stacked both in the vertical and horizontal directions.

Active Gage Summary

The active gage data, not including the LADAR, is summarized in Figure 5.27. The composite chart in the upper left corner shows the time at which fibers arrived at the different active gage systems at the respective ranges. The time of arrival of fibers at gages at each range which are in line with each other show a wind velocity of 6.25 fps (1.9 mps). The duration time of the main data acquisition activity was approximately 10 sec.

Mass flux levels as a function of time and distance are summarized in the

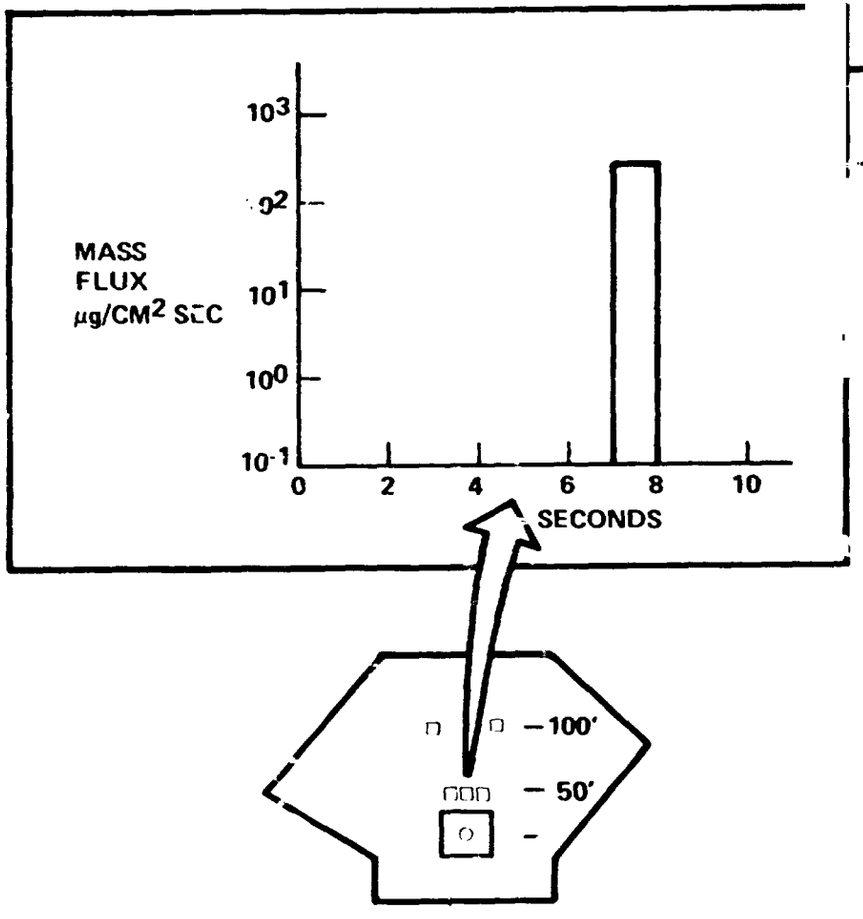

GAGE NO.	TOTAL MASS (MG)	TOTAL DEPOSITION (μg/CM²)
1	0	0
2	37	370
3	0	0
4	0	0
5	0	0

Figure 5.25. Microwave Gage Results - Test No. 8

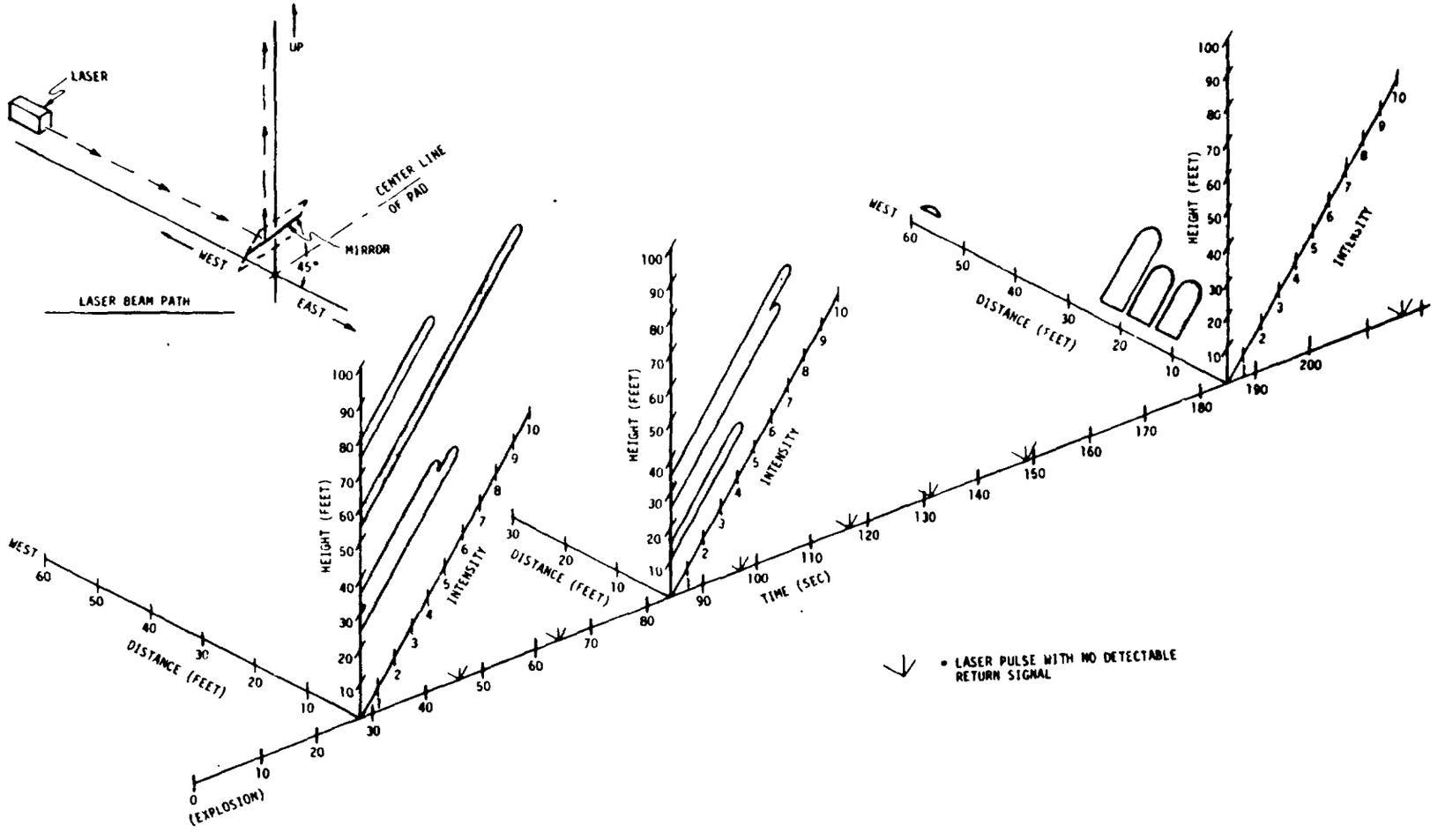

Figure 5.26. Relative Density Distribution Along Laser Beam Path - Test No. 8

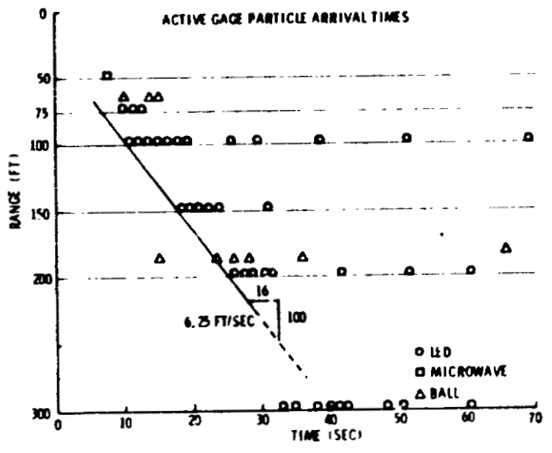

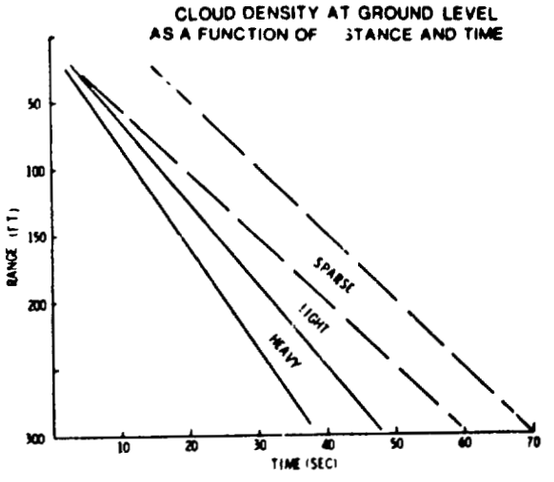

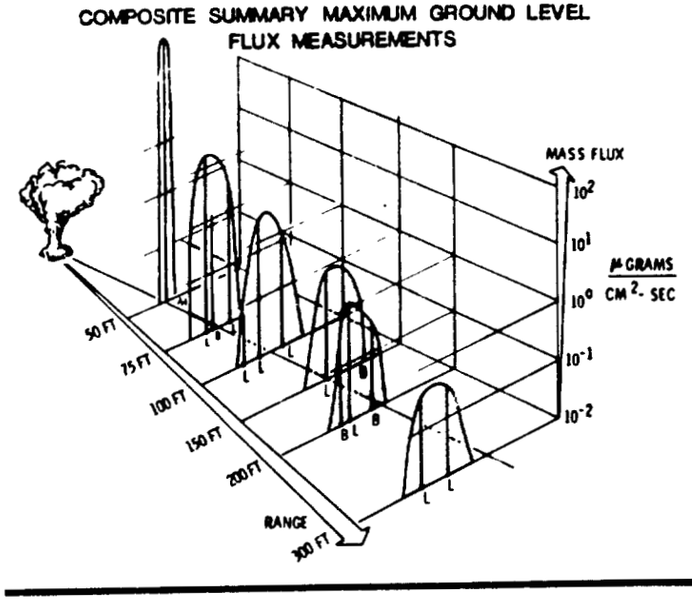

Figure 5.27. Active Gage Summary - Test No. 8

upper right hand corner. Note that the cloud density out to 200 ft (61 m) is almost constant, after which it rapidly decreases.

The integrated peak mass flux is displayed in the lower chart of each gage system (LED, Ball and Microwave) as a function of range and cross range. Again, consistency of results is shown between gage systems. There is a discrepancy at the 75 ft (22.9 m) ball gage location, however, which can be accounted for. Since most of the fibers at that location were less than 4 mm long, the ball gage did not record them. Hence, a lower mass flux resulted. Note that the peak levels drop off as a function of range from 350 $\mu gms/cm^2/sec$ at 50 ft (15.2 m) to 3 $\mu gms/cm^2/sec$ at 300 ft (91 m).

With regard to the LADAR data, the LADAR system sees the cloud in agreement with the other data, for its location at 205 ft (62.5 m) range; however, no data is returned at the 5-ft (1.5 m) elevation along the horizontal path, only at 20 ft (6.1 m) above the ground. This can perhaps be explained by the position of the LADAR beam which was behind a 4-1/2 ft (1.4 m) bridal veil fence at the 200 ft (61 m) range. This might also have caused the wind to sweep upward at this distance insuring no data return below about 10 ft (3 m) vertical height.

TEST NO. 9

For Test No. 9 a half barrel was positioned 6 ft (1.8 m) above a 20 x 20 ft (6.1 x 6.1 m) JP-5 pool fire centered at ground zero on the concrete pad. The test, in two phases, took place over a period from 11:26 am PST March 23, 1978 to 1:42 pm PST that day. In the first burn for 3 minutes burn time the wind velocity was high, causing the pool fire to be tilted toward the downstream; consequently the half-barrel missed the main fire plume. The burn was repeated for a 6-minute burn later in the day. The barrel was repositioned 5 ft (1.5 m) north of the pool center and only 4.5 ft (1.4 m) above the fire.

Thermocouple Data

Chromel-alumel thermocouples were mounted as follows for both tests:

#1 Thermocouple: Located at the center of the half barrel.

#2 Thermocouple: Located on the upper side of the barrel.

Results of the measurements are presented in Figures 5.28 and 5.29. As expected, the second burn produced a much hotter temperature in the barrel for a much longer period of time.

Active Gage Summary

For this test (as noted before) no active gages were utilized.

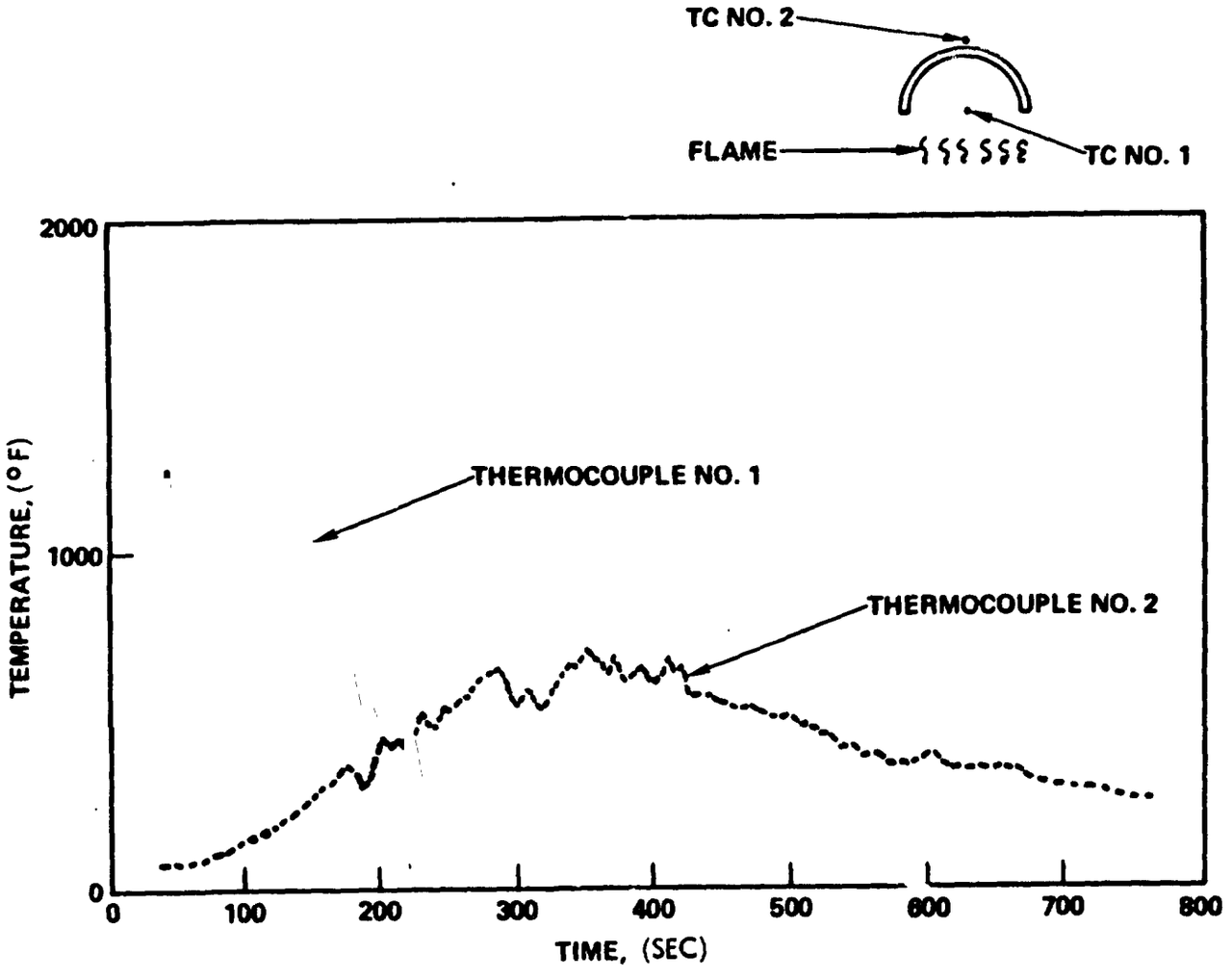

Figure 5.28. Flame Temperature Measurements, First Burn - Test No. 9

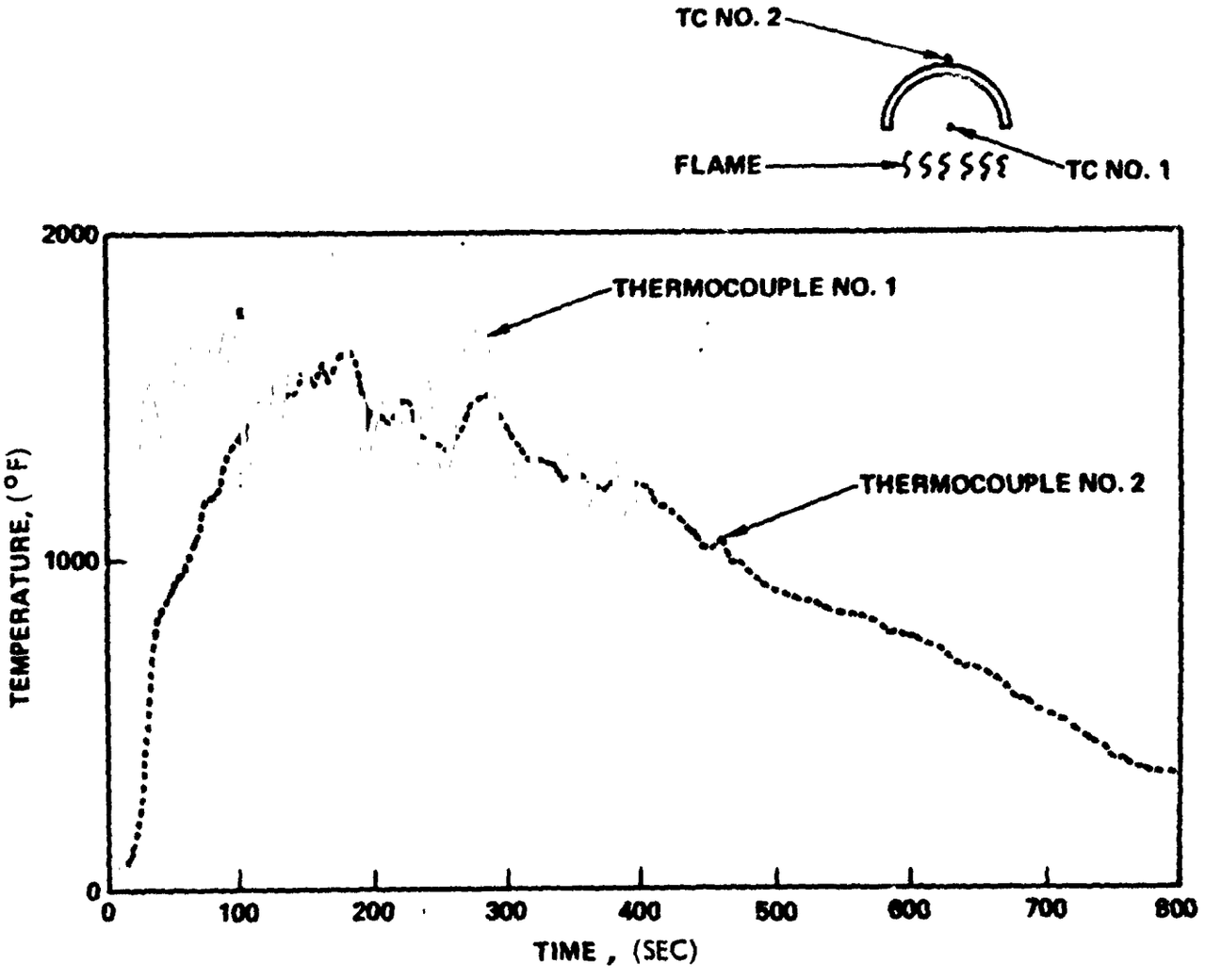

Figure 5.29. Flame Temperature Measurements, Second Burn - Test No. 9

TEST NO. 10

Test No. 10 consisted of a 5 minute pool burn of another half barrel and the residues from the first burn, followed by an explosion of the lot. For this test no temperature data was taken and no active gages utilized.

AIRCRAFT SPOILER TESTING AT NWC

Two tests were performed with aircraft spoilers using a nominal 40 x 60 ft (12.2 x 18.3 m) JP-5 pool fire with three spoilers located 7 ft (2.1 m) above the fire bed to simulate their probable location during an actual aircraft fire. The first was a 4 minute burn, the second a 7 minute slow burn the debris from the first burn plus an explosion roughly 2 minutes into the burn. All active gage systems were in operation for both tests. In addition, several new instruments were fielded.

TEST NO. 11 - SPOILER BURN

For the initial burn test of the three spoilers thermocouples were installed to measure flame temperature. The three spoilers, burned in the JP-5 fire, were located 7 ft (2.1 m) above the fire bed to simulate their probable location during an actual aircraft fire. The fire bed was a 40 x 60 ft (12.2 x 18.3 m) rectangular pool in which enough JP-5 fuel to burn four minutes was floated on a water base. The burn was started at 10:45 am PDT on May 3, 1978 and completed about 10:49 am.

Thermocouple Data

Thermocouples were installed to measure flame temperature just below the sample (TC-1), in the bottom skin of the spoiler (TC-5), in the air space between the upper and lower spoiler surfaces (TC-3), in the upper surface skin (TC-2) and above the spoilers (TC-4). TC-2 and TC-4 malfunctioned during the test. However, some data was obtained from TC-4.

Temperature returns are shown in Figure 5.30. For this large a pool the JP-5 fuel was ignited by adding a small amount of gasoline to its top which spread the fire faster. Even so it can be seen that temperatures start to rise in the vicinity of the spoilers only after a half a minute into the burn. The maximum temperature of about 2180°F (1193°C) is reached only by the lower side of the spoiler and is above 2000°F (1093°C) for a little less than two minutes.

Gage Layout

The active gage layout for Test No. 11 is shown in Figure 5.31. Spoiler samples were located on a steel framework somewhat north of the pool center to account for the wind direction. This location was 114 ft (34.7 m) south and 20 ft (6.1 m) west of the original ground zero on the concrete pad. The gages were shifted so that there would be equal coverage on either side of the new north-south centerline. To better measure the expected fiber fallout the microwave gages were shifted from the 100 ft (30.5 m) to the 75 ft (22.9 m)

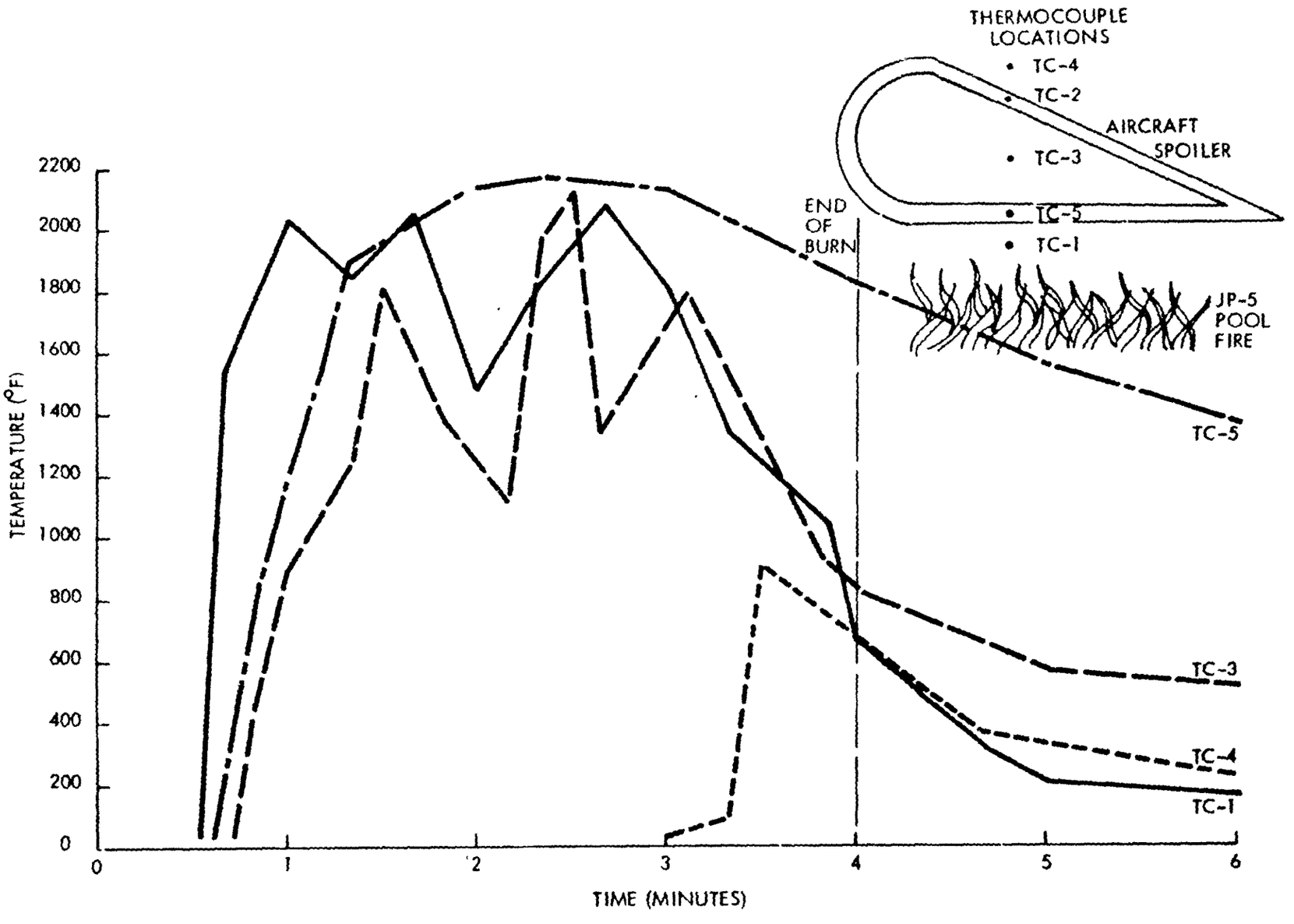

Figure 5.30. Temperature History During Spoiler Burn - Test No. 11

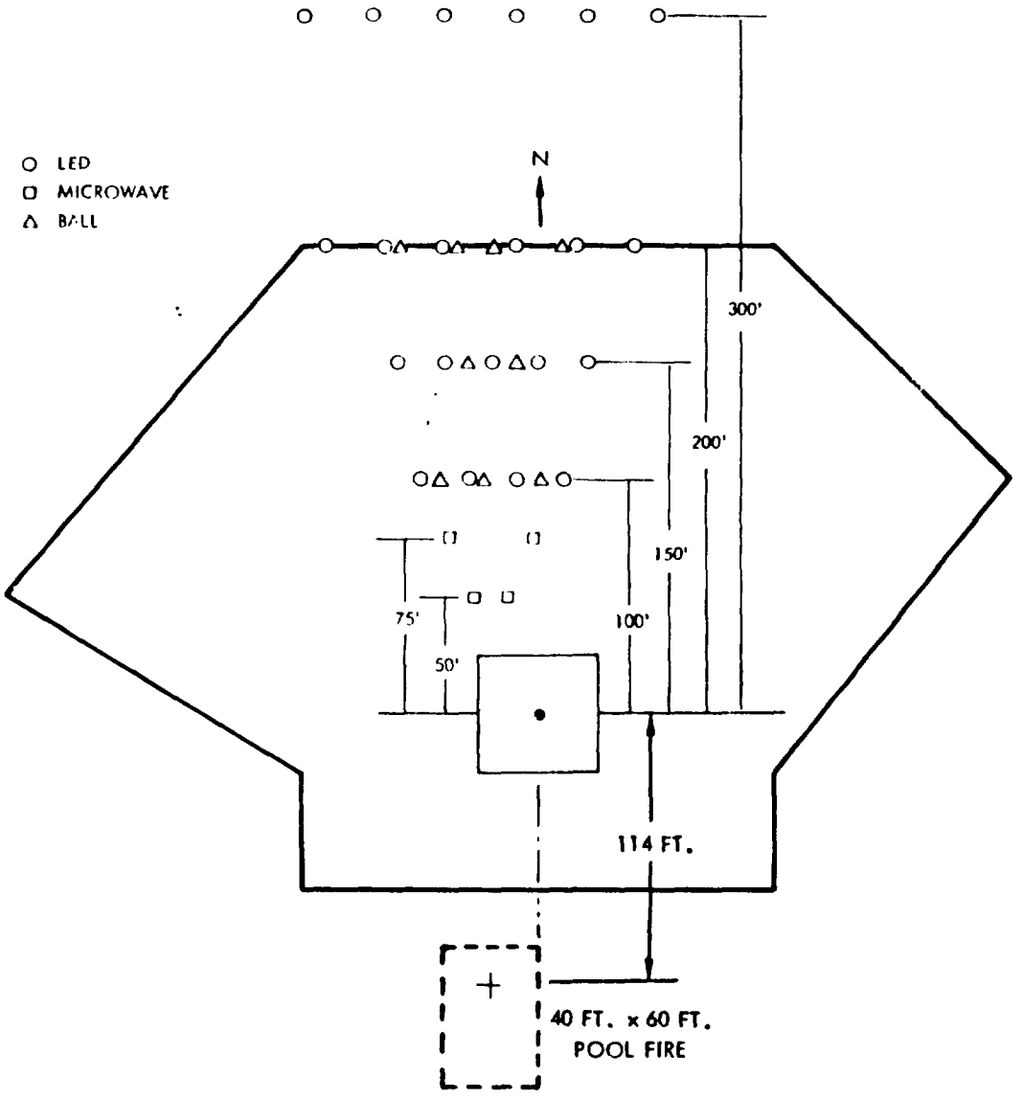

Figure 5.31. Active Gage Layout for Test Nos. 11, 12, and 13

position (range 189 ft [57.6]), the LED gages at 75 ft (22.9 m) were shifted to the 150 ft (45.7) position (range 264 ft [80.5m]) and ball gages were moved from the 75 ft (22.9 m) to the 100 ft (30.5 m) position (214 ft range [65.2 m]).

As described in Section 4, a large "Jacob's ladder" filled partially with vu-graph bridal veil sensors was positioned for these tests just south of the 200 ft (61 m)(range 314 ft [95.7 m]) line. It can be expected that the wind velocities and particle flux north of this location were somewhat compromised by this sensor so that active data flux/concentration obtained at 314 ft (95.7 m) range might be expected to be low by perhaps 20%.

The layout for Test No. 12 was the same as for Test No. 11.

LED Gages

The LED sensor layout for this test is presented in Figure 5.32, which gives a summary of the data display presented in the following figures. In terms of counts most of the release appears to occur at about 100 seconds into the burn - regardless of position. From temperature data, the spoiler material does not reach high temperatures until about one minute into the burn. Lofting velocities in this fire are very high (up to 38 fps [11.6 mps]) as indicated by the flame velocimeter (data following); hence material can be dispersed into the plume over the entire active sensor field in a few seconds, from where it can rain out upon a large area.

Figure 5.33 presents the LED data reduced to mass exposure as a function of range. Peak exposure at each of the stations is shown for times of 80, 100, 140 and 350 sec. The cross range position scale is given in terms of the original ground zero reference and, in parenthesis, the centerline of the JP-5 pool fire.

As shown the exposure levels at the end of the burn are approximately the same over the area covered by the measurements, even though there was a wide variation during the early burn times. This peak is below 10^4 fiber sec/m^3.

Note, at early times, (80 sec), only 414 ft (126 m) and 314 ft (95.7 m) stations had any exposure. Further data reduction of some of the detector positions along the footprint gave length distributions versus time and mass flux versus time. These data are plotted in Figure 5.34. The position coordinates for the individual plots are given in terms of the original pad ground zero which is 20 ft (6 m) east of the actual fire north-south line.

As indicated by these plots, fiber data was obtained in spurts with initial data arriving at the far stations (N 200 and N 300) before arriving at the close-in stations. The time of arrival of data correlates with the wind direction data which is shown later. The simultaneous arrival of data at all ranges in the time period of 100 to 120 sec suggests a rain out of fibers from the fire plume at ranges up to 400 ft (121.9 m).

The particle distribution plots show that for the close-in station (N 100),

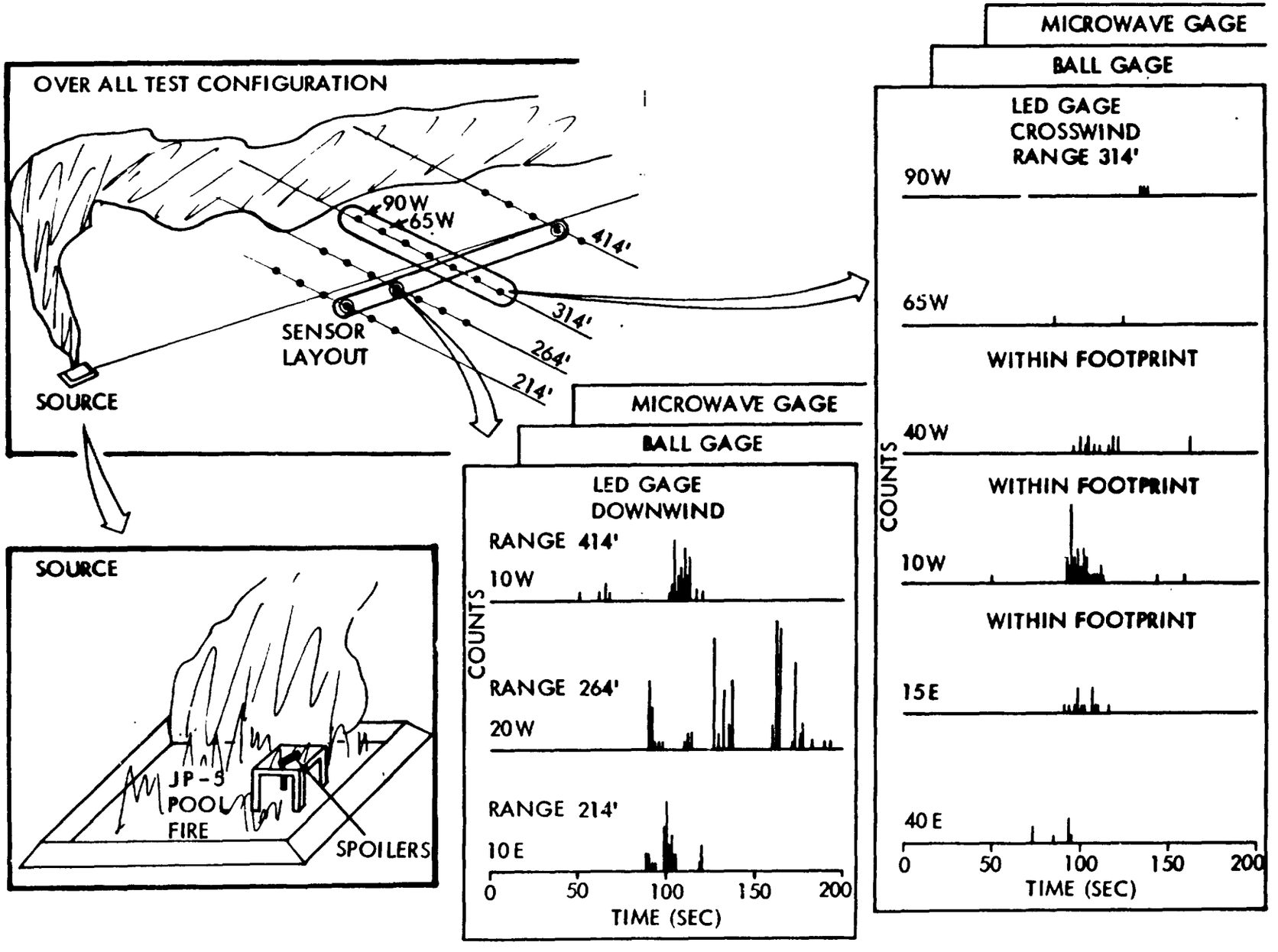

Figure 5.32. Sensor Layout and Data Display - Test No. 11

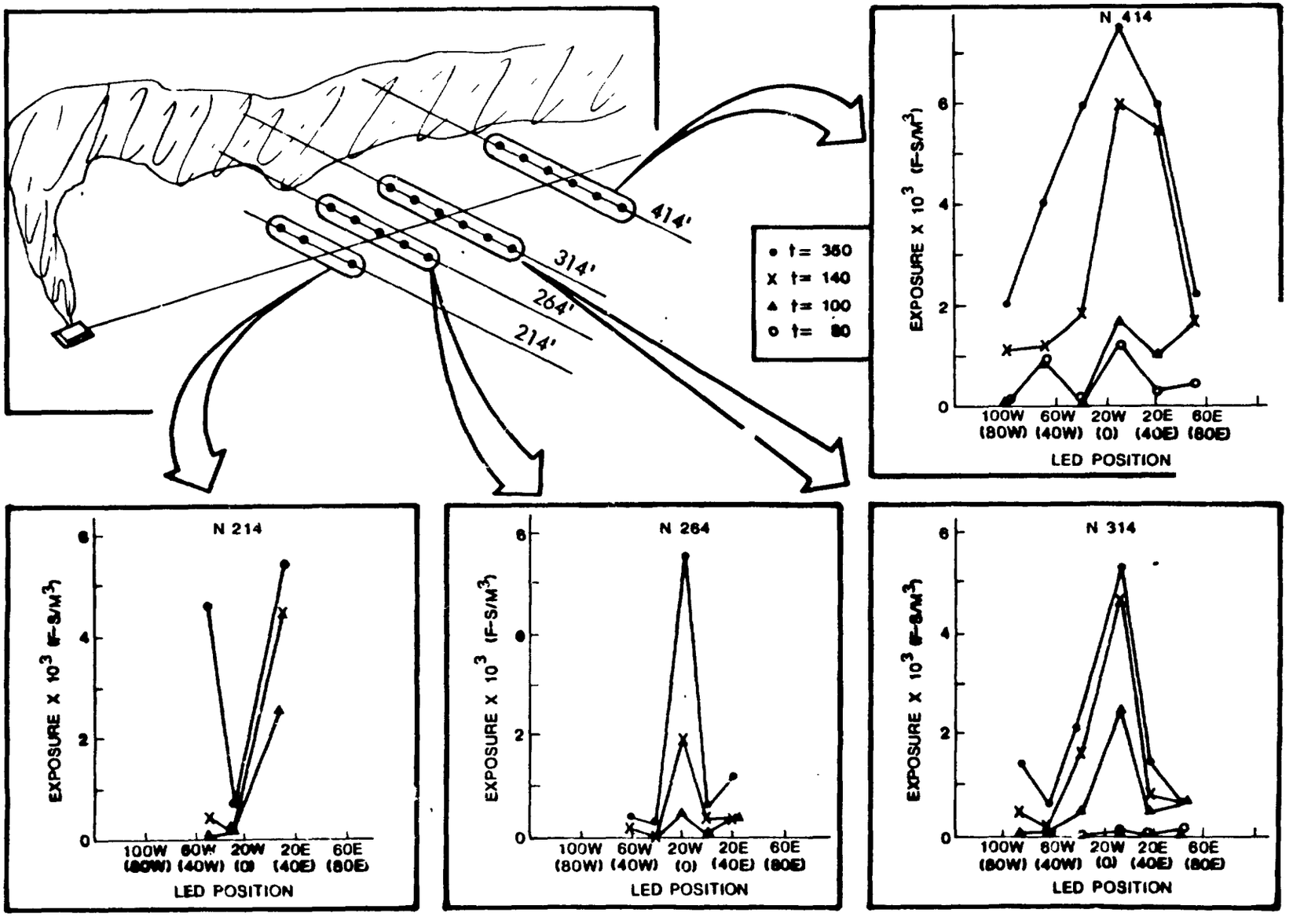

Figure 5.33. LED Measured Exposure Versus Range - Test No. 11

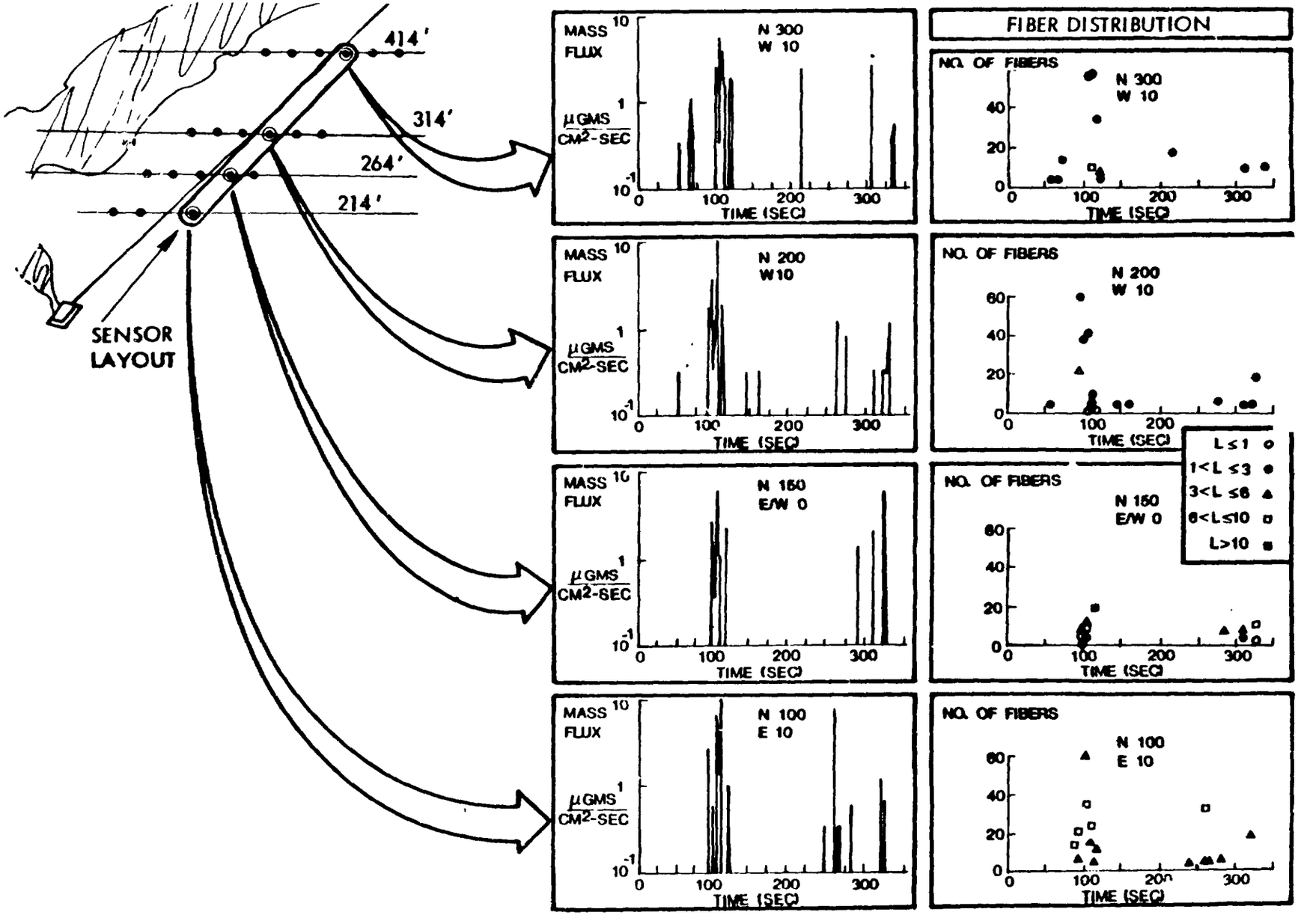

Figure 5.34. LED Measured Mass Flux and Fiber Distribution - Test No. 11

the fibers are greater than 3 mm long over the entire recording time. At the second station (N 150) a full range of particles were observed. At the N 200 and N 300 stations the fiber lengths become primarily 1 to 3 mm long.

Ball Gages

Ball gage results are presented in Figure 5.35 for all gages operating into the pulse-stretcher recorder chain. As before, concentration measurements have been translated into mass flux using a wind velocity of 10 fps (3 mps), a mass per unit length of 0.54 μgm/cm, and the length of each fiber counted, as determined by its pulse height. The threshold below which pulses could not be detected is about 3 mm length corresponding to about 9 x 10^{-2} $\mu g/cm^2$ sec. The data returned by the ball gages were extremely sparse, indicating small mass fallout of fibers above 3 mm in length in the near field region out to 200 ft (61 m). The first recorded event occurred 122 sec after burn began, somewhat later than indicated by the LED detectors.

Microwave Gages

No data was returned by the microwave systems because of the low mass concentrations occurring.

Active Gage Summary

Figure 5.36 summarizes the active gage results for this first large pool JP-5 burn. The particle arrival time chart in the upper left hand corner is considerably different from that obtained in Tests 4 and 8. As seen the far out gages (414 ft and 314 ft [126 m and 95.7 m]) recorded data earlier than the close-in gages. Also shown is that there are two time periods when data was recorded. Both of these phenomena are caused by the wind shifting in direction during the burn.

The mass flux levels as a function of time and range summarized in the chart in the upper right hand corner is also different than those obtained in Tests 4 and 8. Two periods of high mass flux density corresponding to the data acquisition activity shown in the chart to the left were recorded instead of one. Also the duration times for high density cloud remains almost constant over the measurement range.

The peak mass flux at each range taken for the time period 75-125 sec after start of the burn as shown in the lower chart is again different from those obtained in Tests 4 and 8. The peak levels are almost constant over the entire range and do not drop off. The mass flux envelope shape does not fall off either side of the maximum at each range like it did for the previous tests. The wind variance and burn duration are the probable reasons for these differences.

Flame Velocimeter

A flame velocimeter developed at TRW during the NWC test series was used for the first time to scan the Test No. 11 fire. The results are shown in Figure 5.37. The velocity of 38 fps (11.6 mps) observed near the center of the fire,

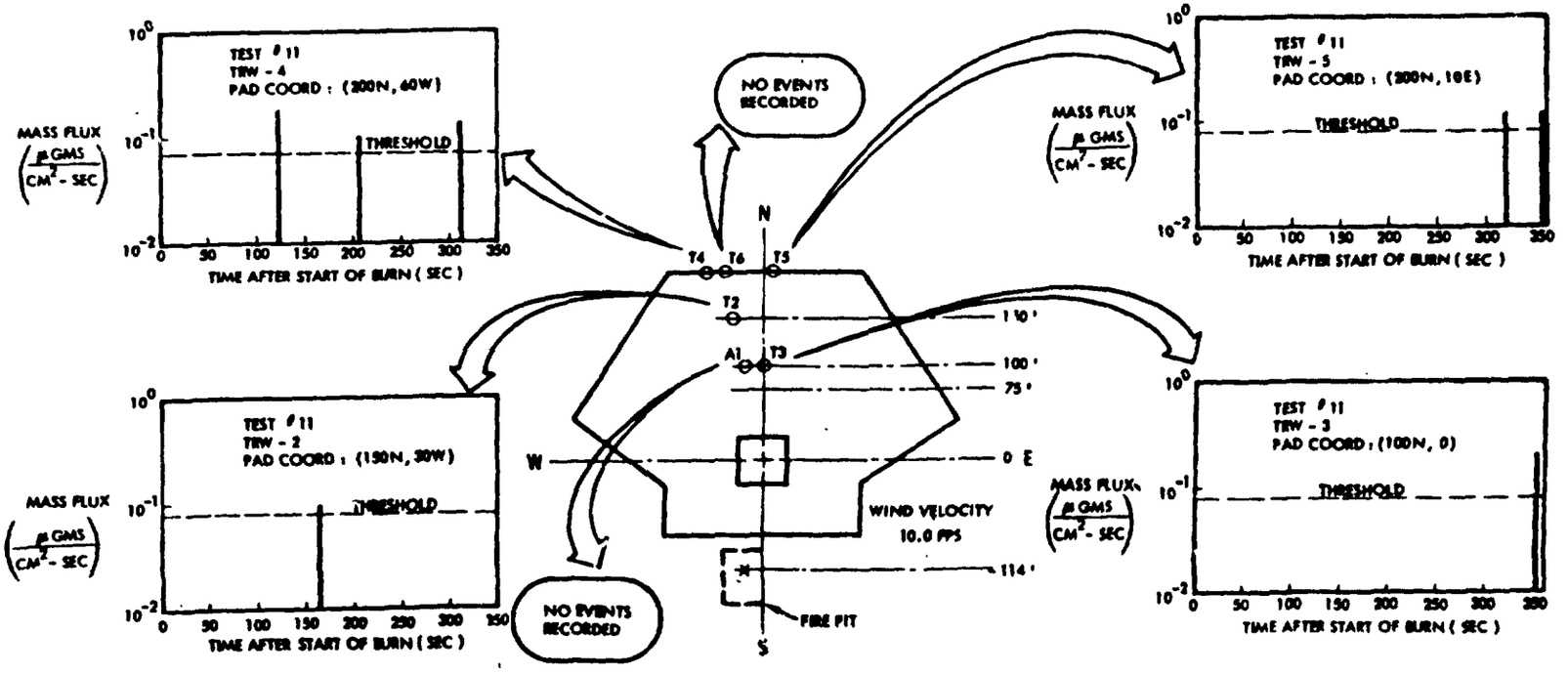

Figure 5.35. Ball Gage Measured Mass Flux of Single Fibers - Test No. 11

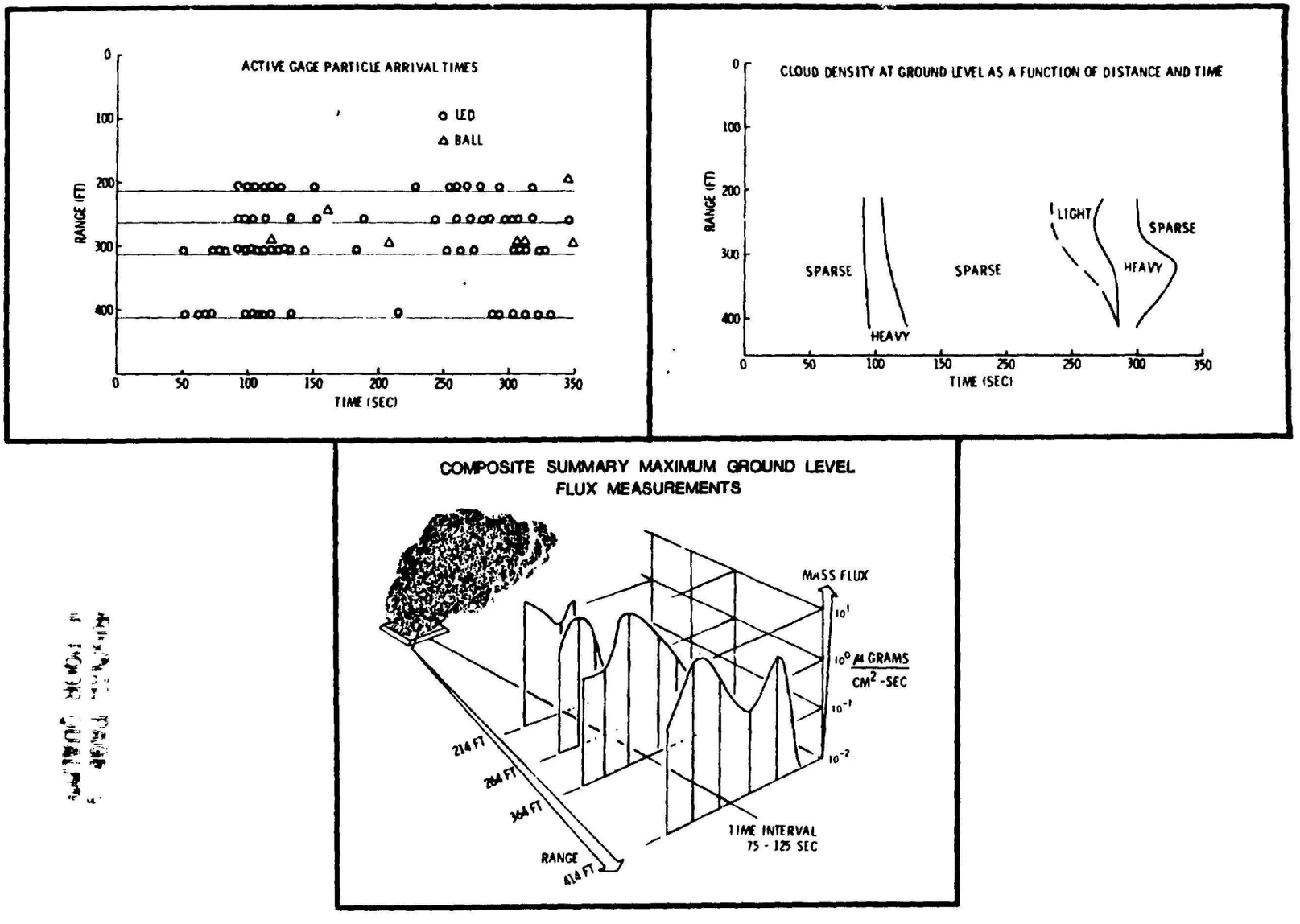

Figure 5.36. Active Gage Summary - Test No. 11

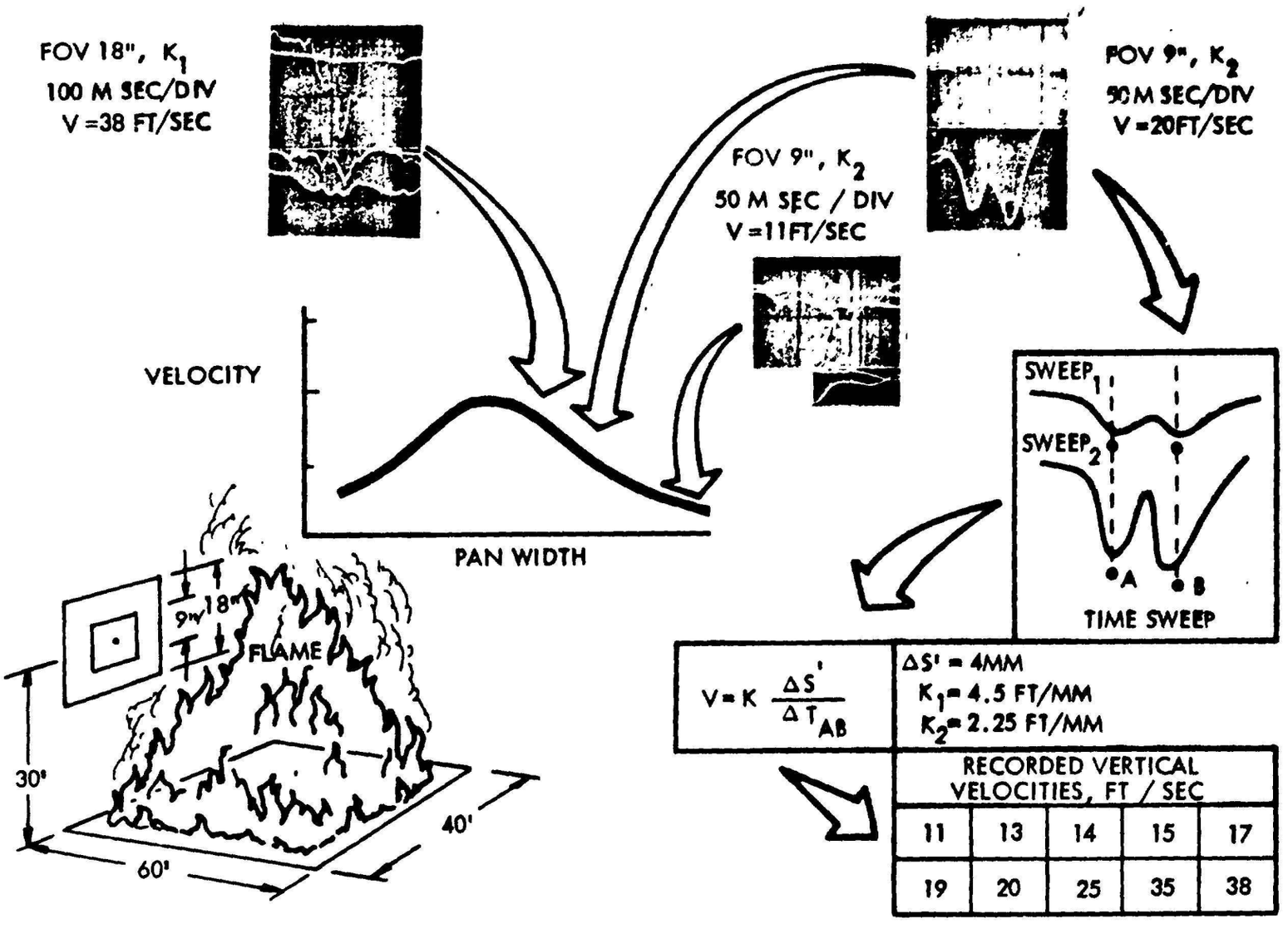

Figure 5.37. Vertical Flame Velocity Distribution - Test No. 11

can be compared to the 35 fps (10.7 mps) predicted by computer calculations for a 30 ft (9.1 m) diameter pool. If adjustment is made for the difference in pool fire size by Froude number scaling, the measured and predicted vertical velocities still remain in agreement.

It can be seen that as expected the vertical gas velocity reduces in value from center to edge. The 11 fps (3.4 mps) vertical value noted at the edge of the pool can be compared with the 10 fps (3.05 mps) horizontal wind velocity outside the fire plume region during most of the burn.

TEST NO. 12 - SPOILER BURN AND EXPLODE

The debris from the previous spoiler burn was collected and positioned on a grid over the 40 x 60 ft (12.2 x 18.3 m) pool. As before, JP-5 was used and some gasoline added to hasten ignition of the JP-5. After two false starts, ignition was finally achieved at 12:34 pm PDT on May 4, 1978. However, most of the gasoline had evaporated by this time so that it took a long time for the JP-5 to completely ignite. The scheduled 4 minute burn was actually completed at 12:41 pm PDT. A shaped charge one foot below the debris was exploded 2-1/2 minutes into the burn at 12:36 pm PDT.

Thermocouple Data

Because of the nature of the debris it was impracticable to attach thermocouples. Flame temperature was not measured either, although it is expected that much the same temperatures would be reached as in the previous test.

Gage Layout

The active gage configuration was the same as in Test No. 11 (see Figure 5.31).

LED Gages

Figure 5.38 presents the total particle count histories of all LED systems at the 100, 200 and 300 ft (30.5, 61 and 91 m) down range pad positions (Add 114 ft [34.7 m] for range). As indicated, there was a continuous shower over the active gage locations. The difference in arrival times of data activity at each range indicates a wind speed of 7.7 fps (2.3 mps), which is in good agreement with wind speed data obtained directly. This is in marked contrast to Test No. 11 where there appeared to be a rain out of fibers concurrently at all ranges. The relationship between count rate and concentration is also shown in Figure 5.38. Particle count data for selected downrange and cross range LED systems are displayed in Figure 5.39. Each location is given in terms of the original pad coordinates. The time scale is begun at start of the burn, and the time of the explosion is indicated with a dashed line. An envelope of the data is presented, in contrast to the individual particle counts shown in Figure 5.38. Only a small amount of material appears to be detected after the explosion, most particularly at the closest position of 100 ft (30.5 m), (214 ft range [65.2m]). This is most certainly due to an unfortunate shift in the wind direction from southerly to 80° west of south about the time of the explosion, continuing in this direction for about two minutes before

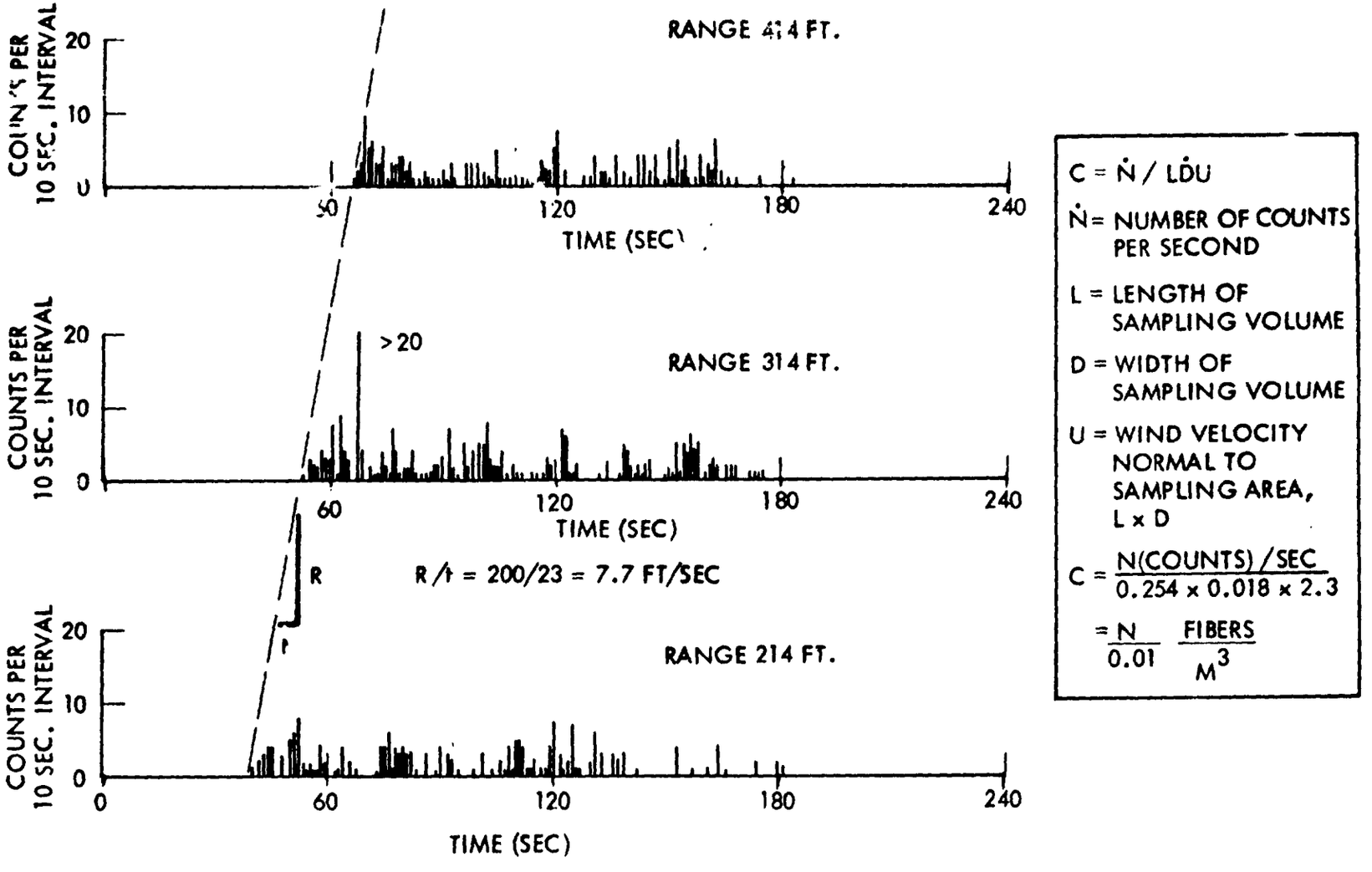

Figure 5.38. LED Particle Count History at Each Range - Test No. 12

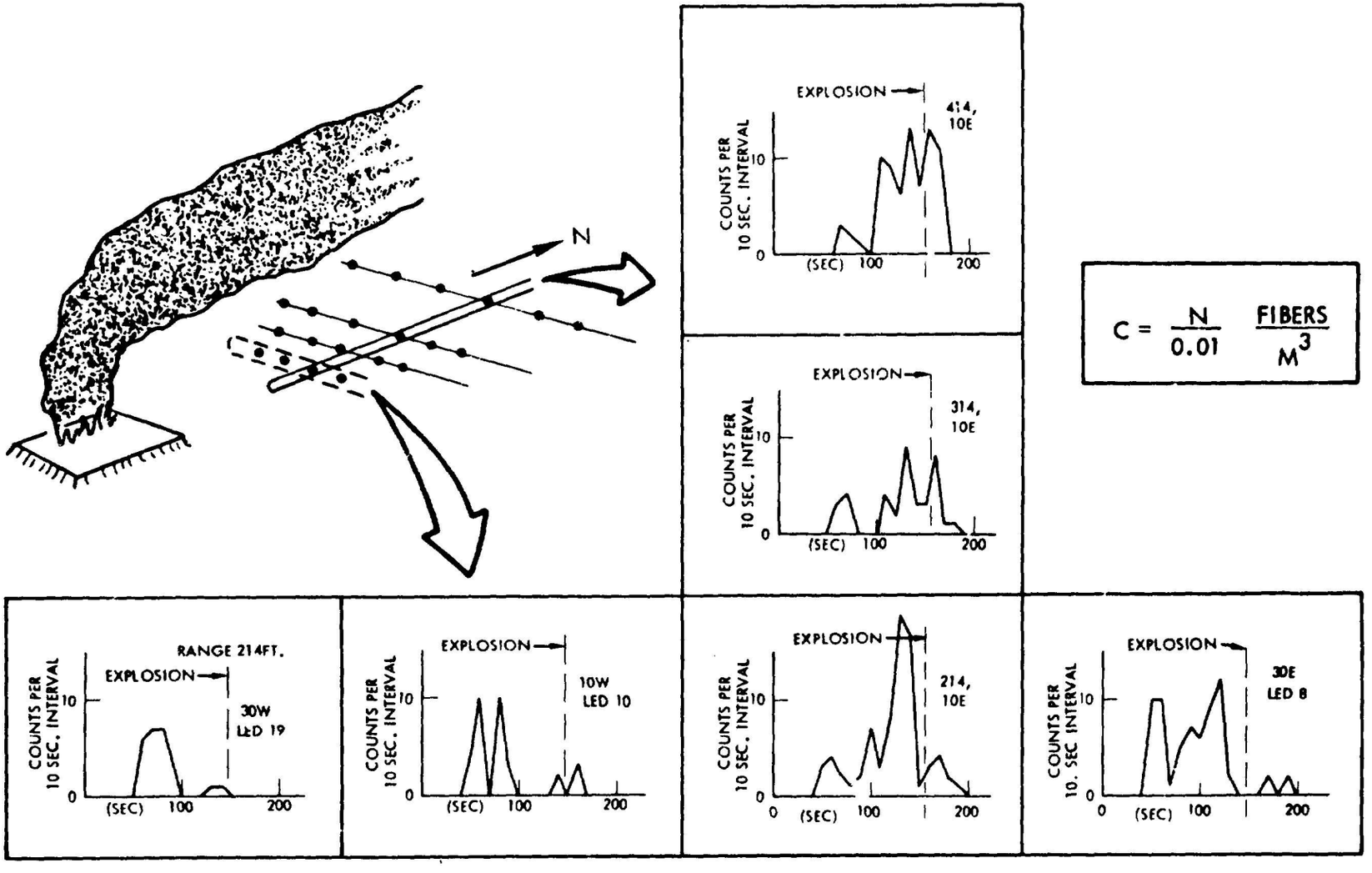

Figure 5.39. LED Particle Count History, Down Range and Cross Range - Test No. 12

returning for another 2.7 minutes to a southerly direction.

Ball Gages

Extremely sparse data was returned by the ball gages for this test, indicating low concentrations and mass flux in the gaging area above 3 mm lengths. No events were recorded on any of the ball gages during the 146 sec of burn preceding the explosion. This is in sharp contrast to the LED data returns, strongly indicating that the great preponderance of release, transport and deposition, at least prior to the explosion, was fibers with lengths shorter than 3 mm.

Even after the explosion, the data returned by the ball gages was sparse as indicated in Figure 5.40 and, as noted in the length distribution obtained, strongly indicated the most probable lengths to be less than the 3 mm threshold of the ball gage systems.

Microwave Gages

Again, probably because of the low concentrations as observed on ball gages, no data were returned on the microwave gage systems.

LC Deposition Gage

A new gaging system under development at TRW during the test series was fielded for this test. The gage was positioned 70 ft (21 m) north of the explosion point about one foot off of the ground. It was provided with a piece of sticky paper, as used in the passive detectors for each test. The results for this "LC deposition gage" are presented in Figure 5.41. Receipt of the first fiber is indicated about 6-1/2 sec after the explosion, followed at 10 sec by several larger sized pulses. No pulses were noted at later times. Only three fiber clusters are noted on the sticky paper. The horizontally oriented deposition plate is 230 cm^2 in area.

The record shows four clusters were received and only three remain on the surface. It is probable that one bit of carbon fiber material landed and then re-entrained into the air because of an inability to stick to the sticky paper.

AIRCRAFT COCKPIT TEST AT NWC

One test was performed at the NWC test site using an aircraft cockpit manufactured partially out of carbon composite material. As in the previous two tests the cockpit was positioned above the 40 ft x 60 ft (12 m x 18 m) nominal pool filled with JP-5 over water with a bit of gasoline added to hasten ignition.

All active gage systems were in operation and were located as in the previous two tests, see Figure 5.31. The "Jacob's ladder", containing many passive vu-graph bridal veil sensors, was positioned as in the previous two tests,

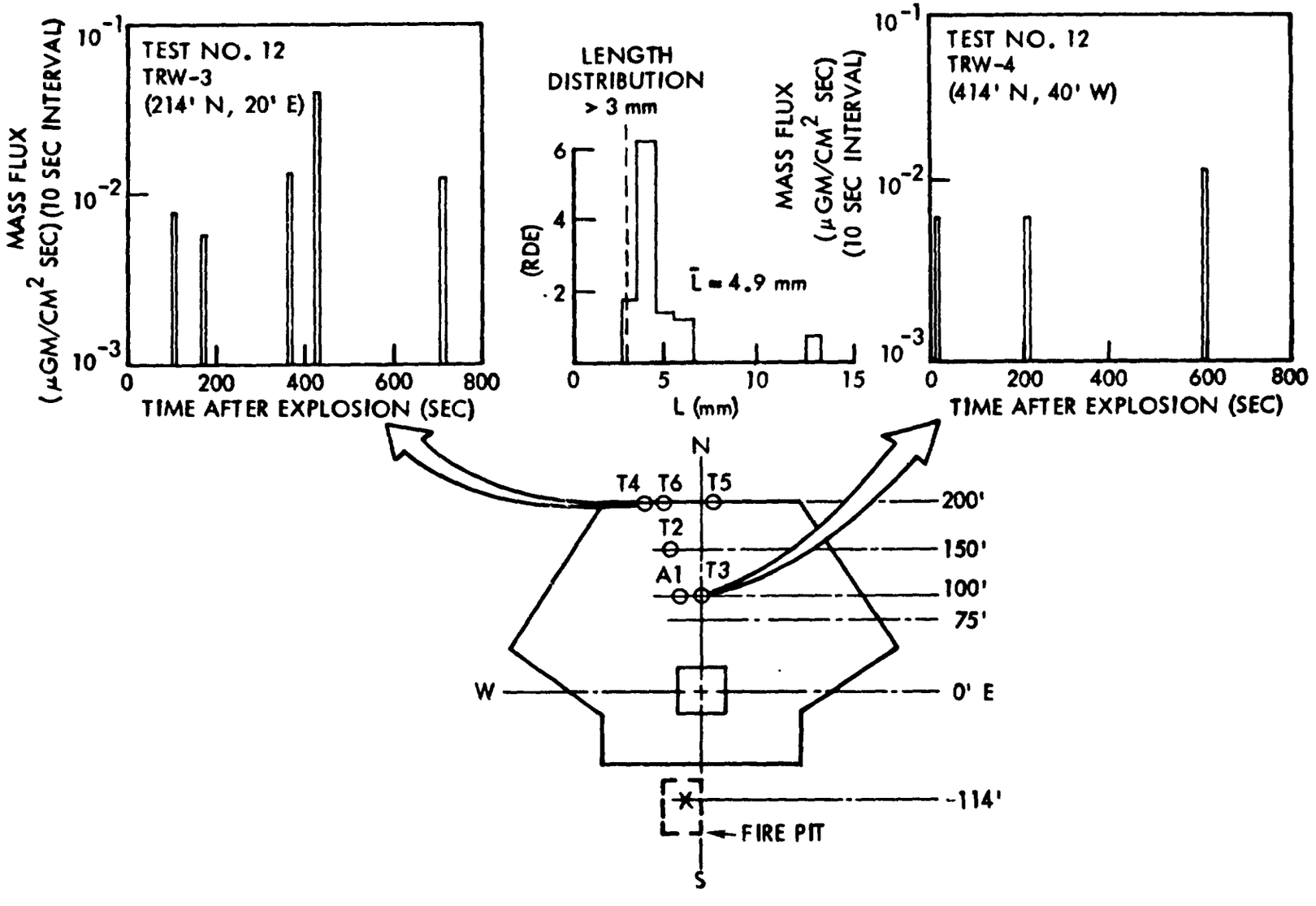

Figure 5.40. Ball Gage Measured Mass Flux - Test No. 12

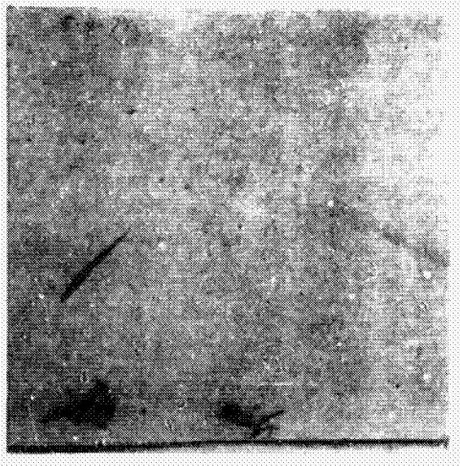

MATERIAL DEPOSITED ON THE
SURFACE OF DEPOSITION PLATE

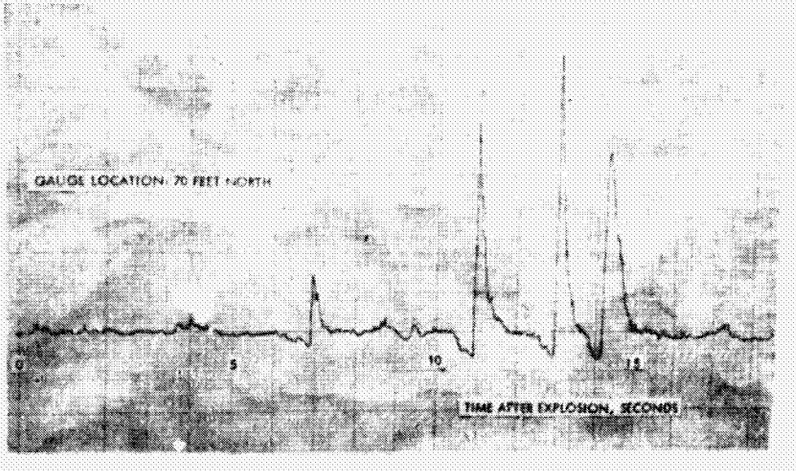

CHART RECORD

Figure 5 41. Carbon Sensitive LC Deposition Gage Results - Test No. 12

probably compromising the data at the nominal 200 ft (60 m), (414 ft [126 m] range), positions by perhaps 20%.

TEST NO. 13 - COCKPIT BURN

The burn, programmed to be for 6 minutes, was begun at 11:45 am PDT on May 5, 1978 and ended at approximately 11:51 am PDT.

Thermocouple Data

Thermocouples were installed at four locations on the cockpit with a fifth thermocouple directly under the cockpit to measure flame temperature. All were of chromel-alumel construction. Table 5.2 gives the legend for the Thermocouple positioning.

Table 5.2. Cockpit Test
Thermocouple Positions

No.	Position
1	Thin End Bulkhead, Outside
2	Cockpit Internal Seat
3	Thick End Bulkhead, Inside
4	Flame Temperature, Below
5	Thick End Bulkhead, Outside

The temperature returns are presented in Figure 5.42. TC-3 amplifier appeared to be zeroed initially and was changed to the sensing mode about 1.6 minutes into the burn. As noted by observers during the middle portion of the burn, the wind and plume were directed to the west and seemed to partially miss the cockpit. This is borne out by the abrupt drop and recovery in all temperatures except on the high heat capacity bulkhead. During this portion, the flame thermocouple exhibited high amplitude, high frequency, noise so that the averaged data from it during this period is somewhat questionable. (Also the flame temperature readings have not been corrected for radiation losses). As noted by observers, the major portion of the cockpit fell into the fire at about 5-1/2 minutes into the burn. At this point the TC-3 abruptly returned to the negative stop of the recorder channel and stayed there. All other TCs except No. 5 returned rapidly to baseline indicating they were still attached and that the cockpit in that area was probably in or very near the water. TC-5 continued at high temperature, slowly drifting down in temperature over the next 15 minutes. Presumably it remained attached and significantly above the water. During the active portions of the burn the fire was extremely hot. The composite reached a maximum temperature of over 2250°F (1232°C) and was typically above 2000°F (1093°C) for 2-3 minutes. All parts of the composite were above 1350°F (732°C) for almost 5 minutes.

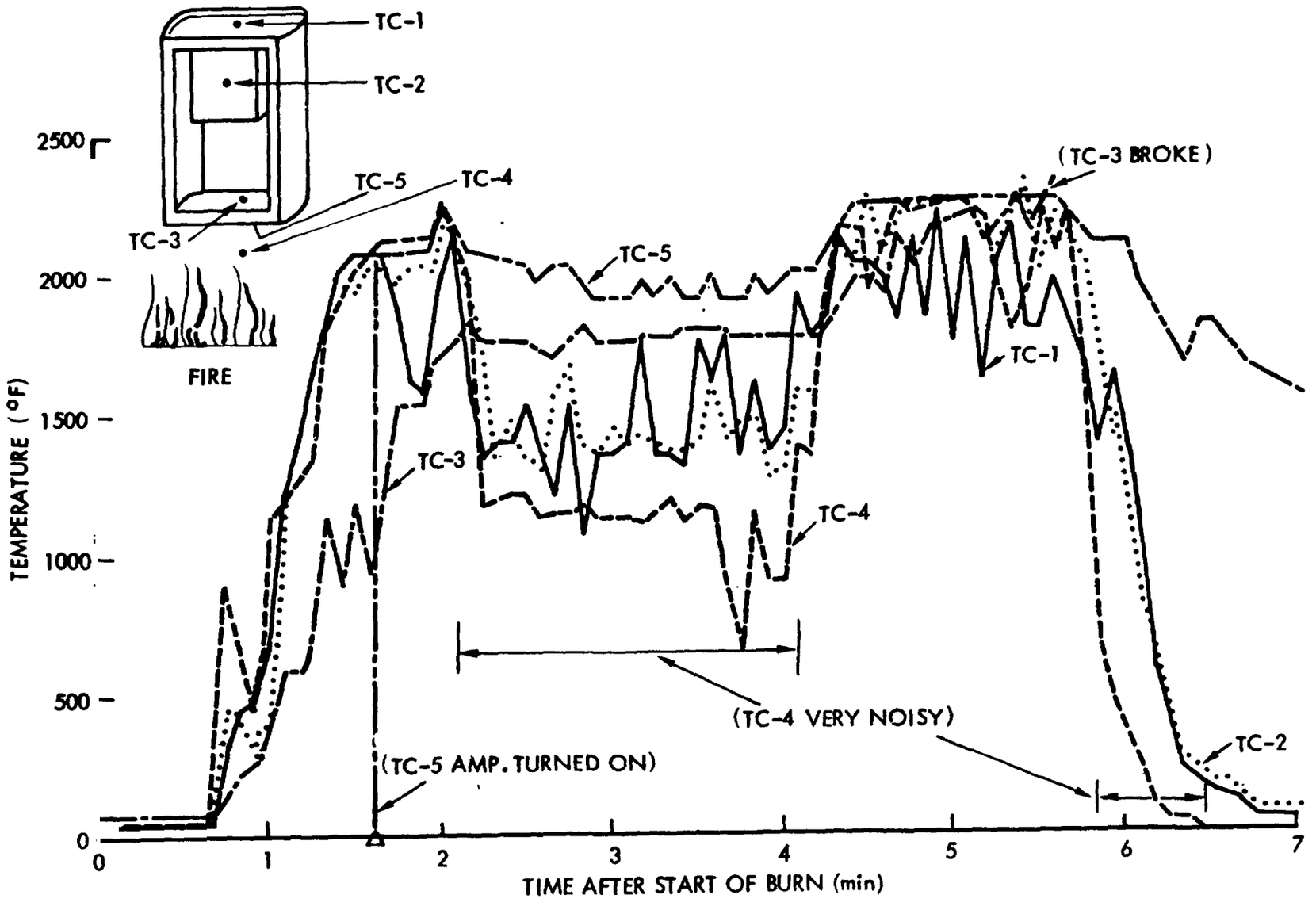

Figure 5.42. Temperature History During Cockpit Burn - Test No. 13

Gage Layout

The active gage layout was the same as in Test No. 11(see Figure 5.31).

LED Gages

Of the twenty-one LED systems deployed as shown on the site map, data was recorded on nineteen gages. The other two gages were not operating during this event (Figure 5.43 displays the results). Shown is the mass flux of three gages at downrange pad coordinates of 100, 200, and 300 ft (30.5, 61 and 91 m) at the cross range position of 10 west. These data are representative of the other LED returns. As indicated by these plots, the mass flux is mostly in the 10^{-1} to 10^{0} $\mu gms/cm^2$ sec regime. As before the source center is 114 ft (34.7 m) south of ground zero and 20 ft (6.1 m) west.

Fiber bundle size, the number of fibers detected, are shown for the same three systems as indicated here. The larger bundles (greater than 80 fibers) are mostly detected at the close in range location.

Particle count envelope data from three downrange LED systems is displayed in Figure 5.44. The counts appear to be more evenly distributed in time at the farther out stations. Data returns after the end of the burn (6 minutes) indicate a random rainout of particles from the plume. The relationship between count rate and concentration is also shown in this figure.

Cross range particle count envelope data from the LED systems at locations of 100 ft (31 m) (214 ft range [65.2 m]) are presented in Figure 5.45. As plotted it appears that the particle count is higher at the early times. The lack of data from 200-350 sec time is due almost certainly to the wind shift mentioned before. This shift, as seen at the cockpit, occurs from 2 to 4 minutes after the burn is initiated.

Ball Gages

The mass flux as seen by the ball gages is plotted in Figure 5.46. Events occur only on the gages located at the 314 ft (95.7 m) range on the time scale of most interest. As with the LED detectors, no events are noted from 150 to 300 sec due to the wind shift.

For this test the tape records were followed out to rather late times. The results are interesting and are presented in Figure 5.47, both as fiber concentration and as mass flux.

After 12-14 minutes many events are noted. This is probably due for the most part to the presence of personnel in the area covering all of the sticky paper passive sensors, and indicates that a significant amount of material which has deposited on the ground initially is capable of re-entrainment - causing a significant added exposure. In fact the total exposure noted at late times is about 3-4 times that noted during or directly from plume passages.

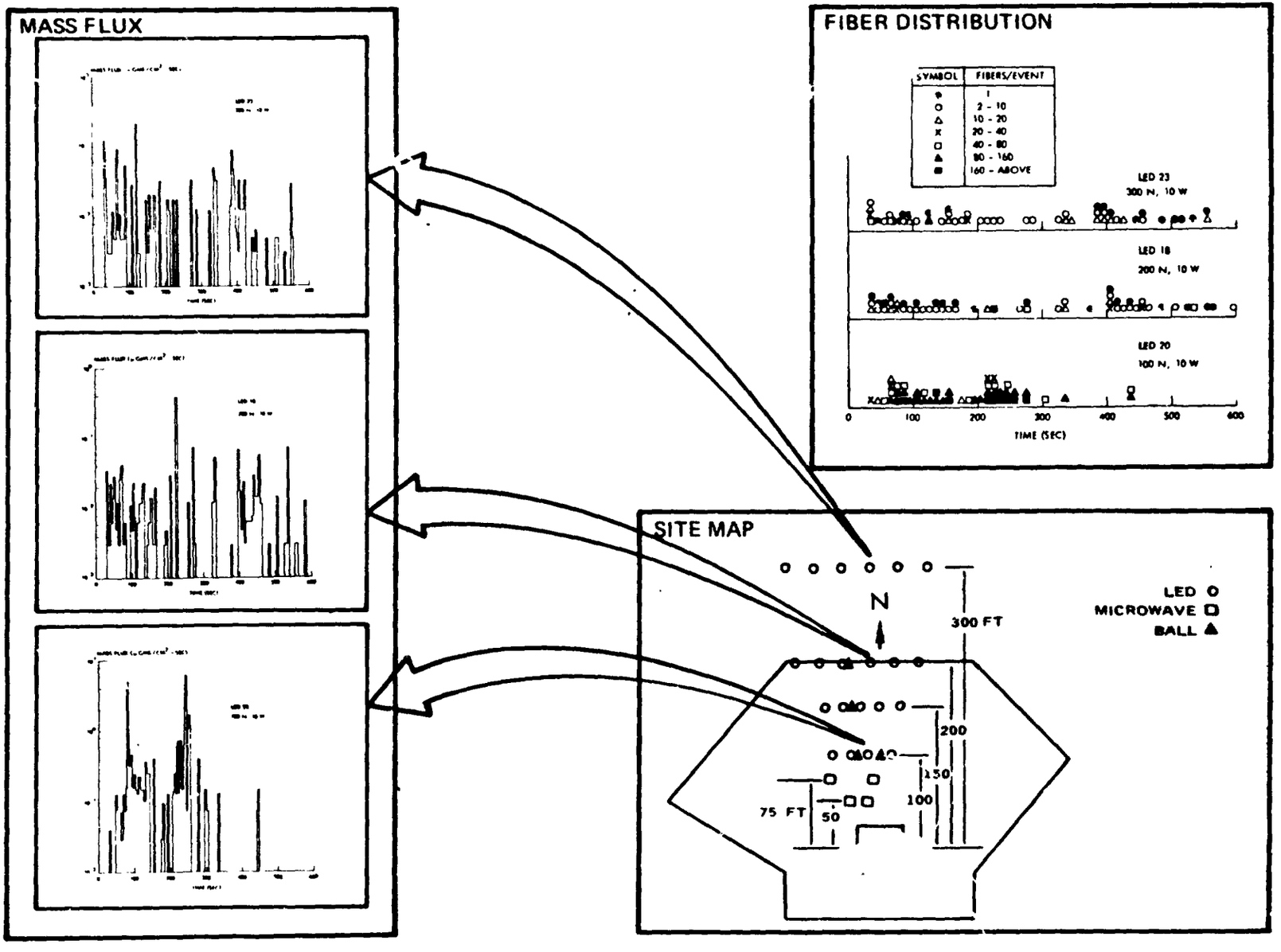

Figure 5.43. LED Measured Mass Flux Distribution - Test No. 13

$$C = \dot{N}/LDU$$

$$= \frac{N\ (\text{COUNTS})/10\ \text{sec}}{0.254 \times 0.018 \times 3.5}$$

$$= \frac{N}{0.016}\ \frac{\text{FIBERS}}{M^3}$$

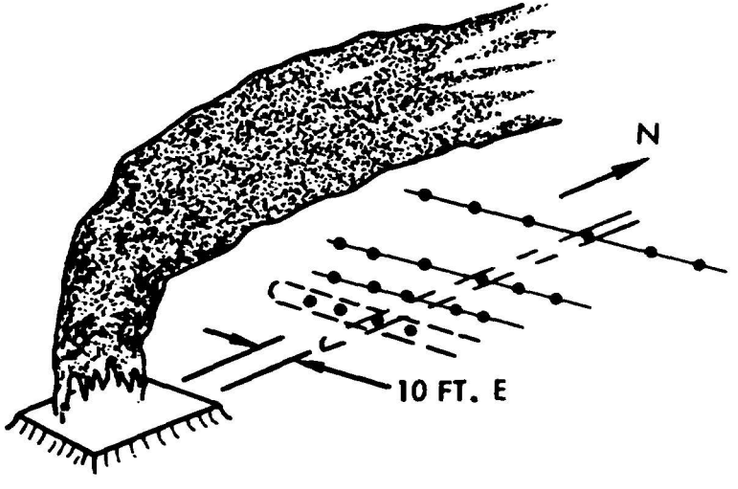

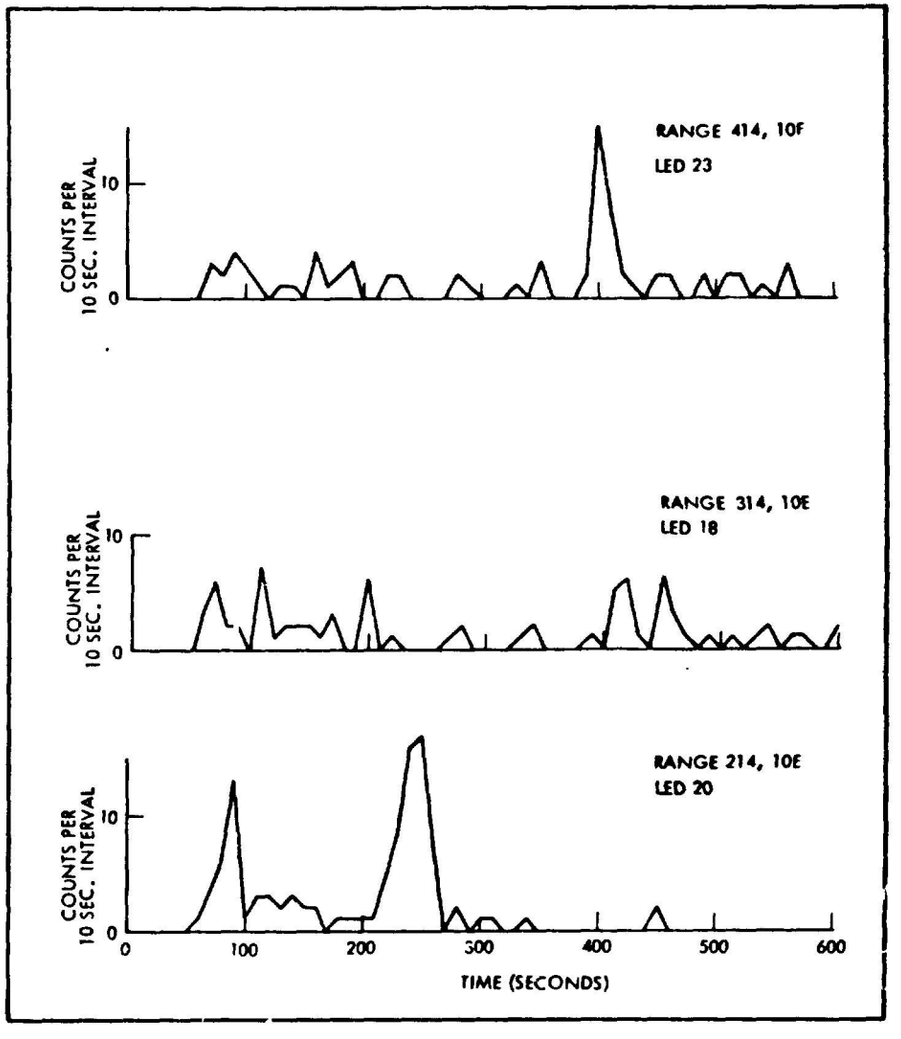

Figure 5.44. LED Down Range Particle Count History - Test No. 13

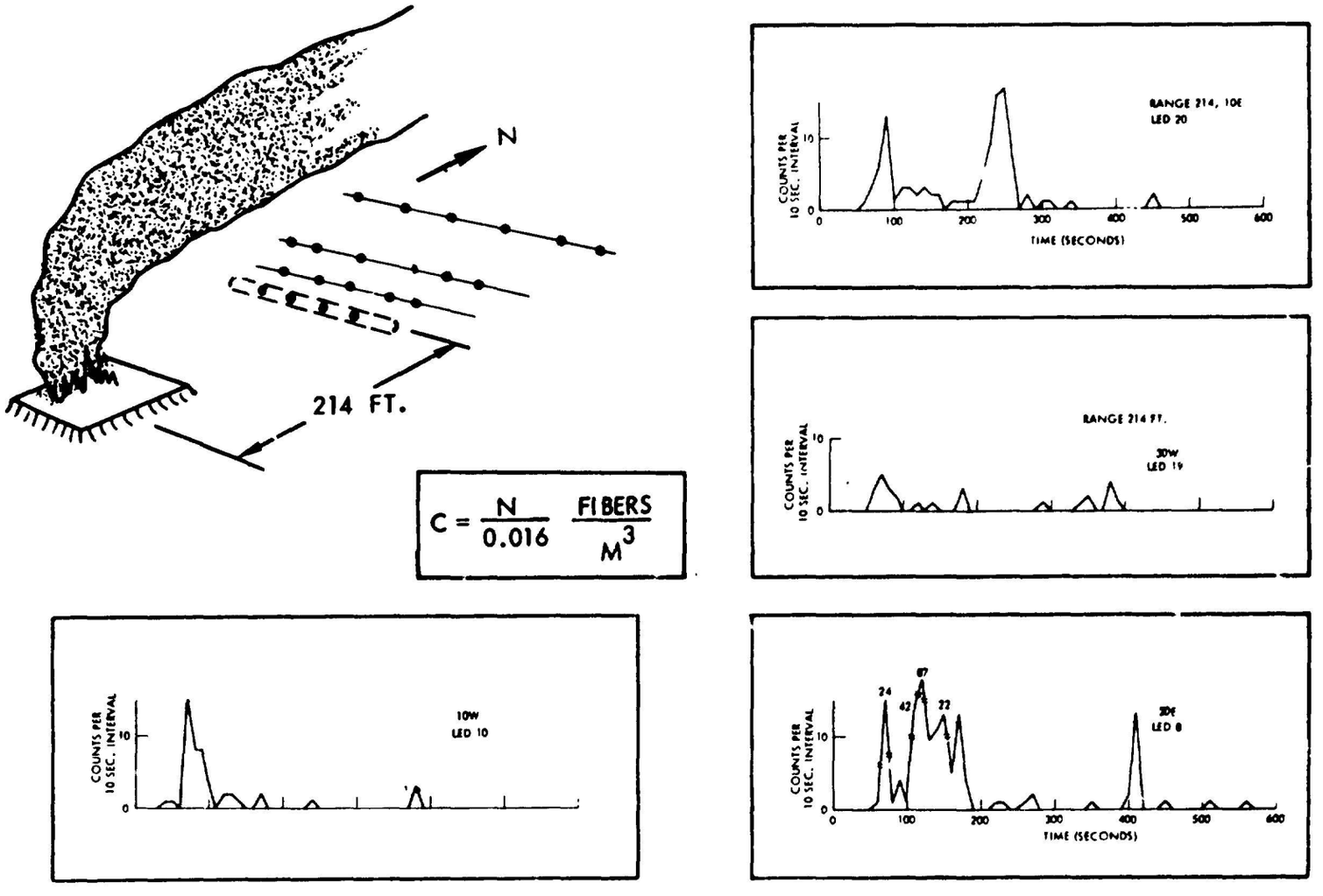

Figure 5.45. LED Cross Range Particle Count History - Test No. 13

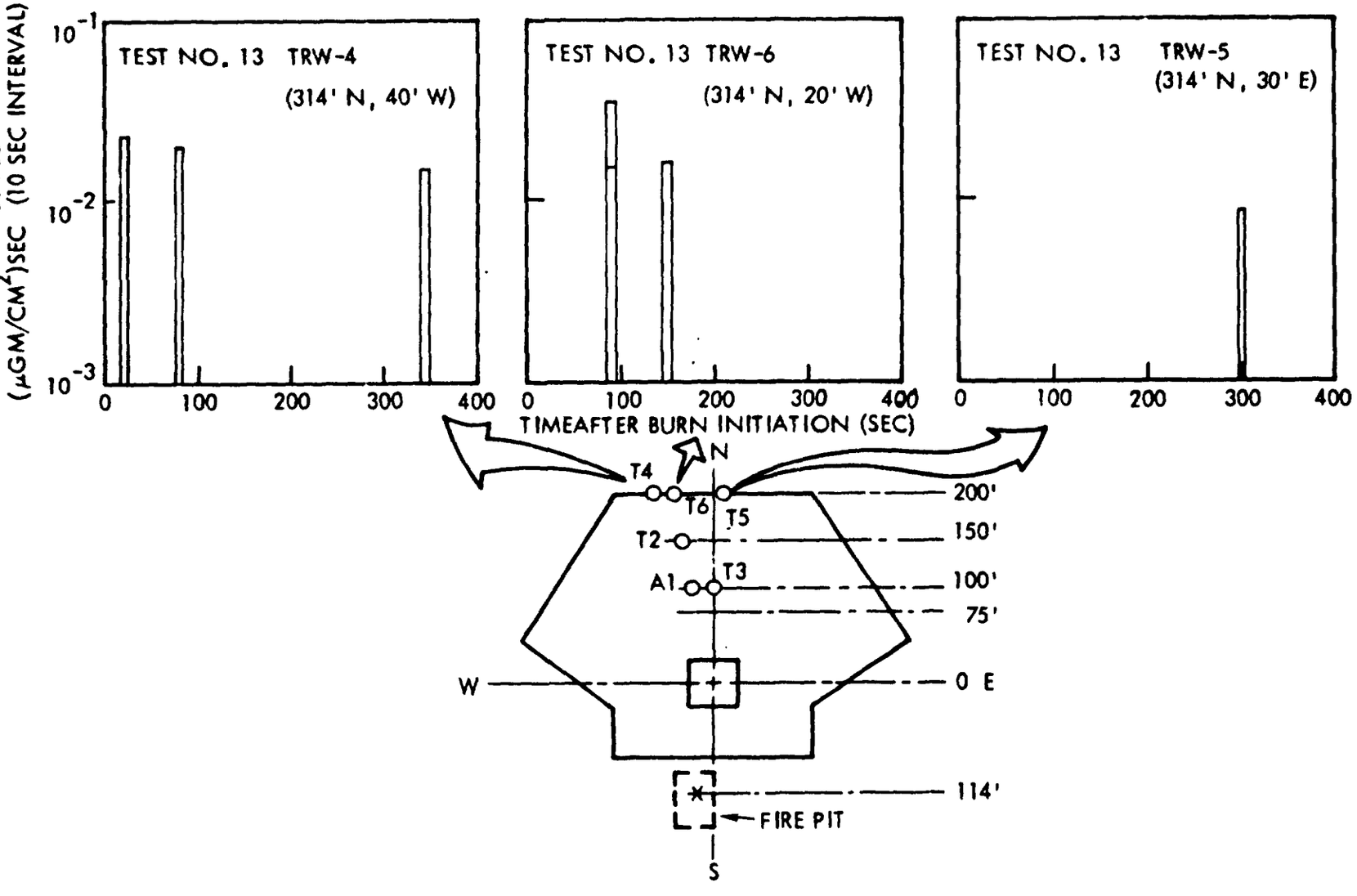

Figure 5.46. Ball Gage Measured Mass Flux Data - Test No. 13

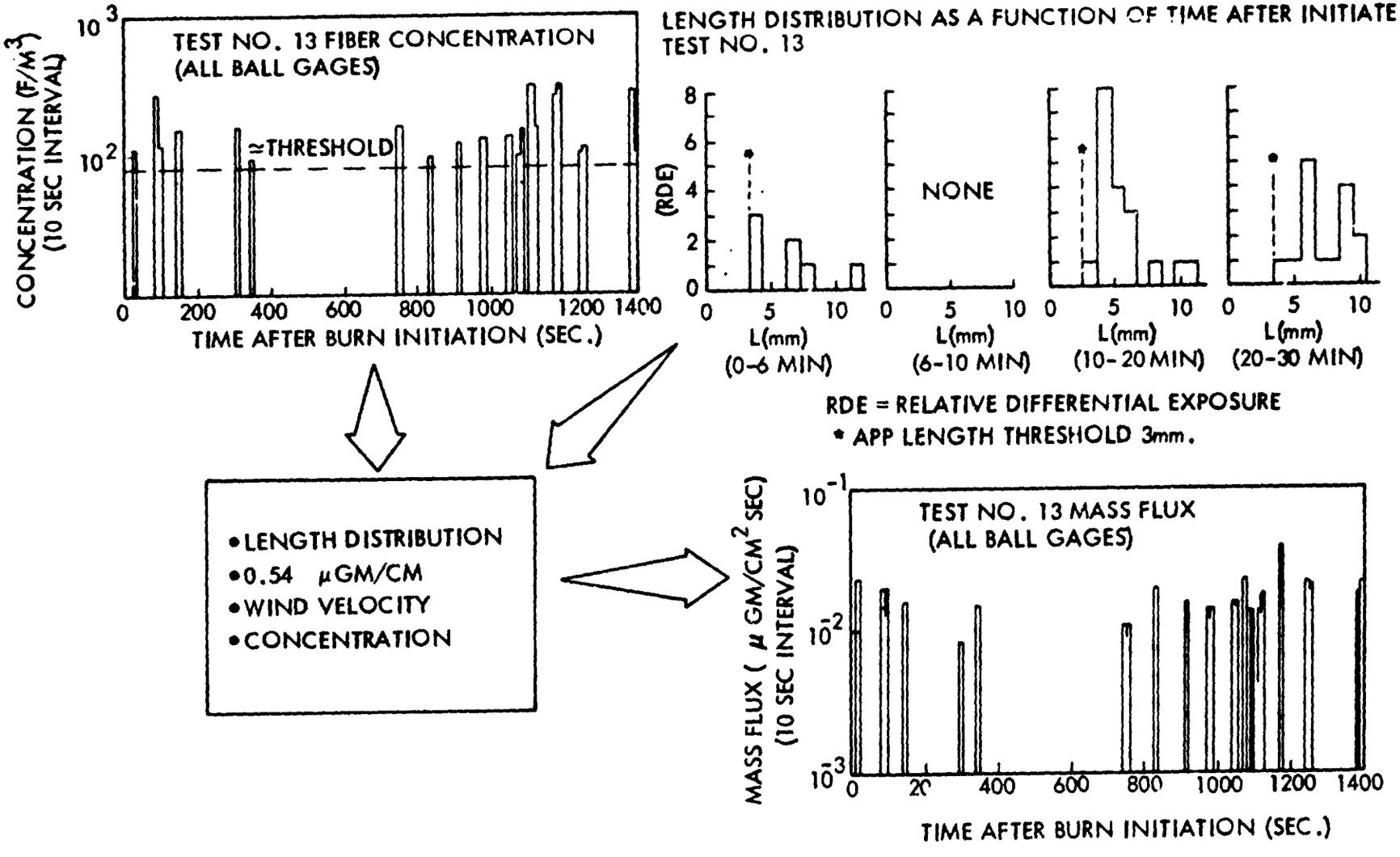

Figure 5.47. Ball Gage Condensed Time Plots - Test No. 13

Also displayed in the figure is the length distribution down to the 3 mm threshold as a function of the time after initiation of the burn. Those particles re-entrained from 20-30 minutes appear not to peak below the threshold but well into the 3 to 20 mm region.

Microwave Gages

No returns of significance were obtained from the microwave gage systems for this test as in several previous tests.

6. PHOTOGRAPHIC AND METEOROLOGICAL INSTRUMENTATION: DATA REDUCTION AND ANALYSIS

Several types of photography were employed at NWC field tests to record the plumes generated by the C-4 explosions and JP-5 fires. Visual movie cameras were positioned upwind and crosswind from the test pad to permit several views of the tests. Infrared (IR) thermovision was used to record IR images. The visual data was used to develop the following information presented herein: 1) C-4 explosion puff growth profiles and puff growth histories, 2) typical JP-5 fire plume profiles with grid overlays for smoke plume dimensions, fire plume dimensions, fire plume heights and vertical speeds, smoke plume vertical speeds, and JP-5 generated smoke puff rotational motion parameters. The IR display was used to obtain the rise and fall of fragments of exploded material and of flying debris generated by the JP-5 fire. IR thermography images and visual photographs are displayed together for comparison of the different puff growth histories as seen at long and short wavelengths.

Near surface wind velocity measurements were taken at three different heights on the meteorological (met) towers and summarized in this section. Ambient temperature values at the three different heights are also quoted.

The data reduction and analysis results presented herein have been grouped into several categories corresponding to the energy source. These fall naturally into the chronological order in which the tests were performed; in each category the results are grouped according to a particular test. The data is preceded by a brief summary of the visual movie analysis methodology. The photography data for each test is preceded by a summary of the near surface meteorological conditions which apply to the plume generation and propagation.

VISUAL MOVIE ANALYSIS METHODOLOGY

Using known reference heights such as the met towers, telephone poles, and local hill tops, photographic image to actual object sizes in the photographs were established by geometric transformation techniques. This approach was used to establish actual dimensions of C-4 explosion puffs and JP-5 fire plumes. Explosion puff dimensions could readily be obtained from photographs, because the image to object transformation factor does not vary appreciably across the puff photograph. Overlay grids for photo images of the JP-5 fire plumes were prepared to permit quick determination of the dimensions, since the image to object transformation factor varies considerably across the plume photograph. Typical photographs with grid overlays are deployed for Test No. 11 in its respective subsection (Figures 6.30 to 6.35).

A typical sequence of steps leading to flame or smoke heights and vertical speeds is shown in Figure 6.1, which applies directly to Test No. 11. The west view establishes the leading edge angle, Θ, for the plume as viewed from the south. A plot of Θ, as measured from the near west view (camera located 680 ft [207 m] west of pool center), is shown as a function of time. This plot can be divided into two regions with the following average values

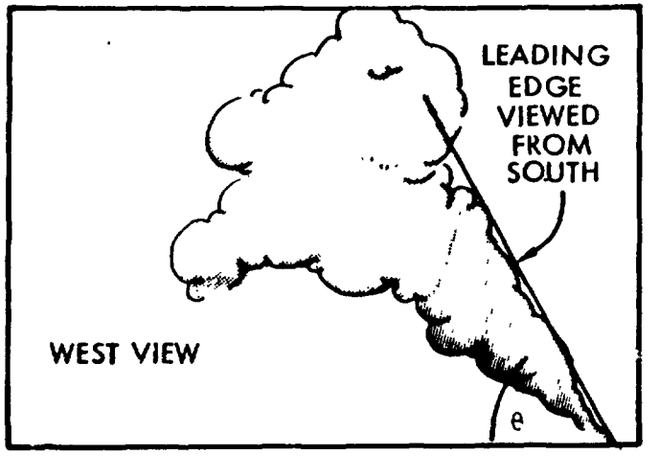

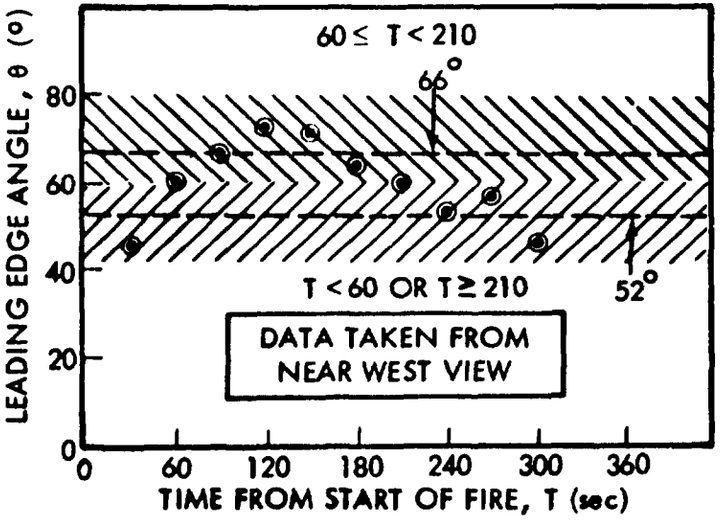

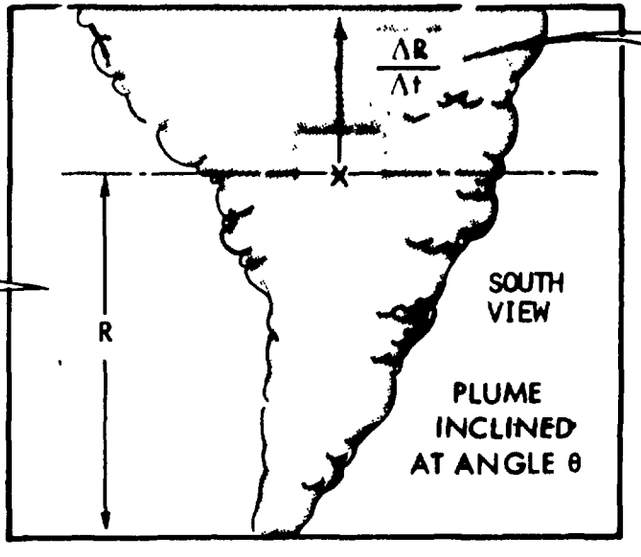

FOR FLAME HEIGHT, H

$H = R \sin \theta$

FOR FLAME OR SMOKE VERTICAL SPEED

$\frac{\Delta H}{\Delta t} = \frac{\Delta R}{\Delta t} \sin \theta$

$$\theta = \begin{cases} 52° \text{ for } T < 60 \text{ sec or } T \geq 210 \text{ sec} \\ 66° \text{ for } 60 \leq T < 210 \text{ sec} \end{cases}$$

These two values were used in preparing the grid overlays for the south views presented in Figures 6.32 to 6.35.

PROPANE BURN/EXPLODE TESTS

The data in this subsection covers propane burns of carbon fiber composite flat plates and barrels followed by a C-4 explosion of each burned sample. Since the propane burn essentially melted away the epoxy binder of the carbon/graphite composite material with little or no fiber release, the time period of interest for carbon fiber release and propagation is after the start of the C-4 explosion. Met and photography data is presented for this period.

TEST NO. 4

The near surface (20.5, 37.5 and 55.5 ft [6.2, 11.3 and 16.9 m] above the ground) wind data is shown in Figure 6.2 for Test No. 4. Digitized wind speed and direction data is presented for the three measurement heights as a function of time after explosion. Northeast meteorological tower results are displayed because this tower is closest to the downstream region where material was recovered. Average values for the entire ten minute period are also presented. Average wind speeds varied from 5 to 6 fps (1.5 to 1.8 mps), while average wind direction varied from 175° to 210° as measured from true north. Thus the winds were predominantly southerly (blowing from south to north).

Ambient temperature was also measured and found to be 48°F (8.9°C). Specific values as a function of height are as follows:

Table 6.1. Ambient Temperature For Test No. 4

Height Above Ground (ft)	Temperature (°F)
3	48.0
18	47.5
28	---
38	47.2

Figure 6.3 exhibits a sequence of superimposed time lapse tracings of projections of selected frames imaged by the near south positioned Fastax camera that utilized a telephoto lens. The Fastax cameras were operated at a nominal "freeze-action" rate of 4000 frames per sec, and thus provided an excellent impression of the dynamics of the developing explosion, the initial "jet pulse", which was unique to Test No. 4, and also of the more familiar smoke puff initiation. Since the telephoto lens restricts the field of view to less than 24 ft (7.3 m) vertically, the rapidly decaying top of the "jet pulse" exits from the field of view before ~0.08 sec after the explosion, and the smoke puff

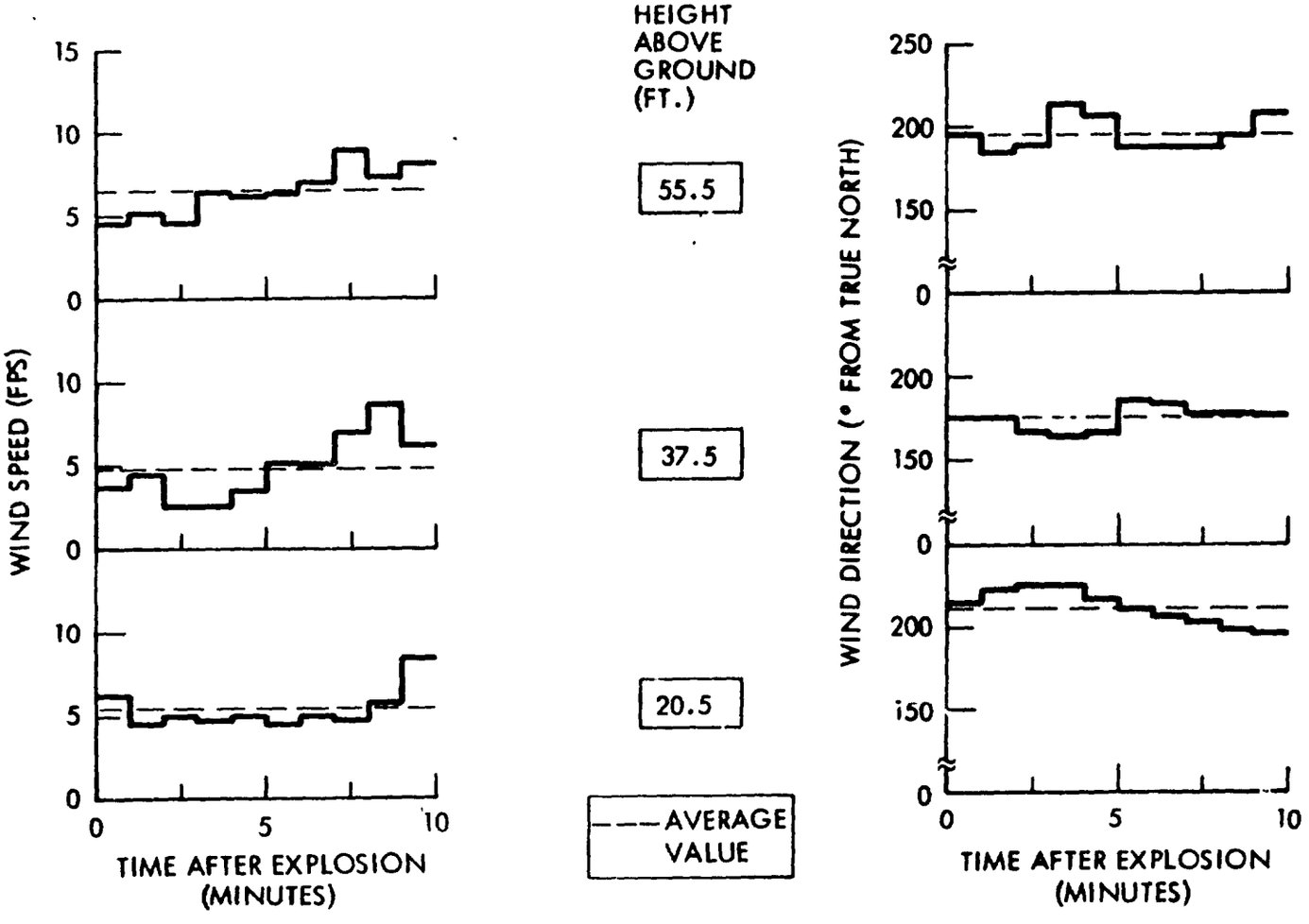

Figure 6.2. Near Surface Meteorology Data - Test No. 4

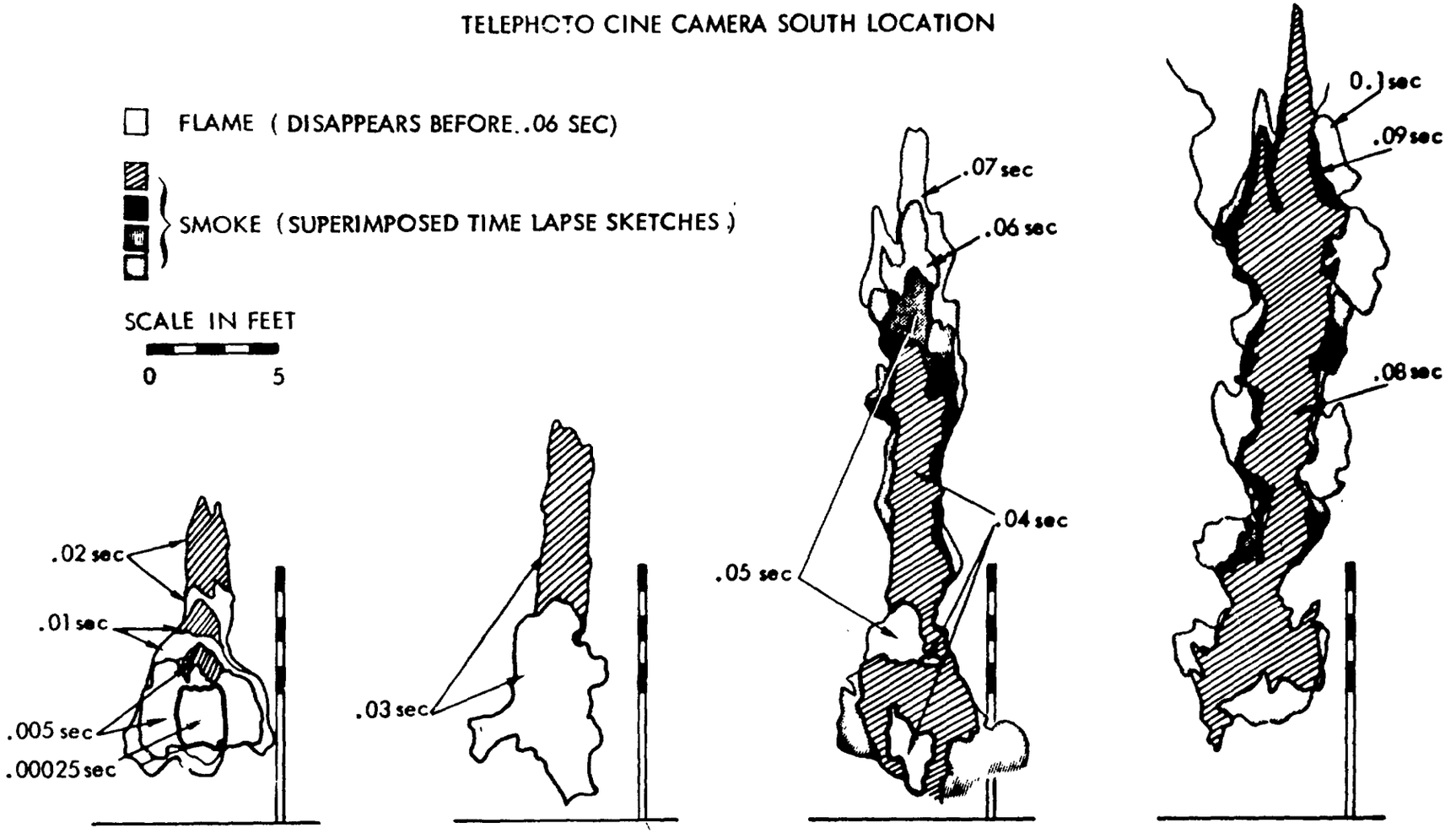

Figure 6.3. Early Time "Jet Pulse" - Test No. 4

begins to exit shortly after ~ 0.1 sec. An image-to-object distance conversion bar is shown. The "jet pulse" height and rise velocity histories plotted in Figure 6.4 were computed from this camera film data.

The Test No. 4 cameras, particularly the telephoto Fastax camera, imaged a narrow, extremely rapidly rising transient "jet pulse" rising through and above the normal longer lasting explosion puff. This "jet pulse", possibly owing to multiple reflections of the explosion shock front, exhibited detectable contrast for less than 0.1 sec. Figure 6.4 exhibits the rise height and rise velocity histories of this transient "jet pulse".

The data displayed in Figure 6.5 were obtained from camera images using conventional color film with a "wide angle lens" and situated approximately 550 ft (168 m) west and 100 ft (30.5 m) north of ground zero. Camera images were of relatively poor quality, with appreciably less than desirable puff to background contrast. In particular, the lower portion of the puff became very difficult to discern against the terrain hill background after approximately 5 sec of wind propagation. Thus the positions of the puff maxima, seen against sky background, are more accurate than those of puff center.

TEST NO. 5

The near surface wind data is shown in Figure 6.6 for Test No. 5. Only the northeast met tower results are displayed, because southwest tower data did not differ significantly from these values. Average wind speeds varied from 5 to 6 fps (1.5 to 1.8 mps), while average wind direction varied from 160° to 180° as measured from true north. Thus the winds were predominantly southerly (blowing from south to north).

Ambient temperature was also measured and found to be 49°F (9.4°C). Specific values measured at several heights are:

Table 6.2. Ambient Temperature For Test No. 5

Height Above Ground (ft)	Temperature (°F)
3	49.8
18	49.4
28	49.2
38	49.2

Figure 6.7 exhibits superimposed time lapse tracings of selected frames imaged by one of the near south positioned Fastax Cine cameras, the one with the relatively wider field of view. The other Fastax camera utilized a telephoto lens to restrict its field of view to only a small fraction of that shown herein, and would be of interest primarily for a study of the dynamics of the explosion pulse flames. Both Fastax cameras operated at a nominal rate of 4000 frames per sec. In both, the puff contrast decays rapidly after approximately 0.5 sec (2000 frames) after the explosion. When played back at normal 24 or 16 frame per sec speeds, the telephoto camera film (not shown) exhibits interesting details, in very exaggerated slow motion, of exploded fragments flying about and changing aspect.

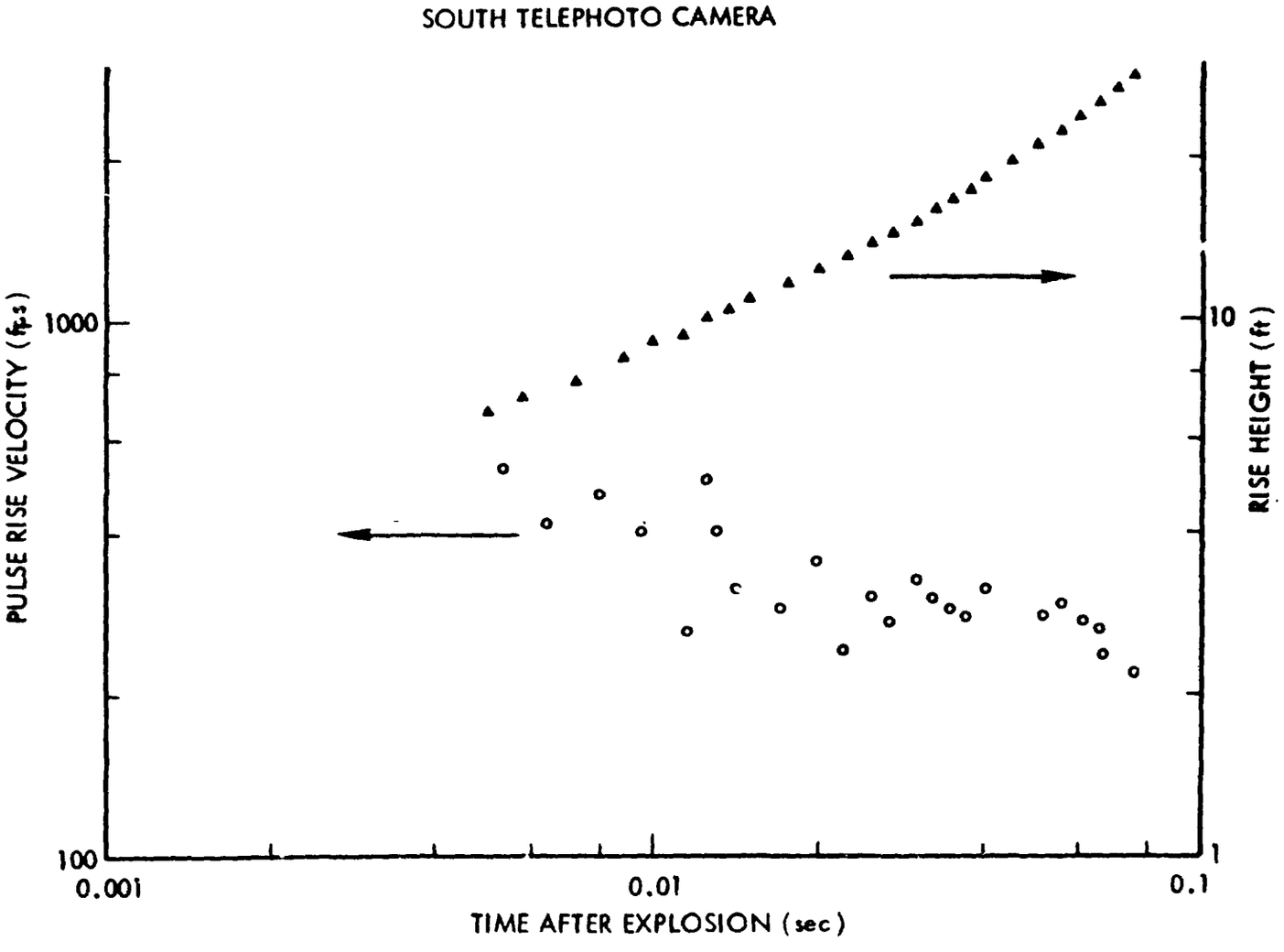

Figure 6.4. Early Time "Jet Pulse" Histories - Test No. 4

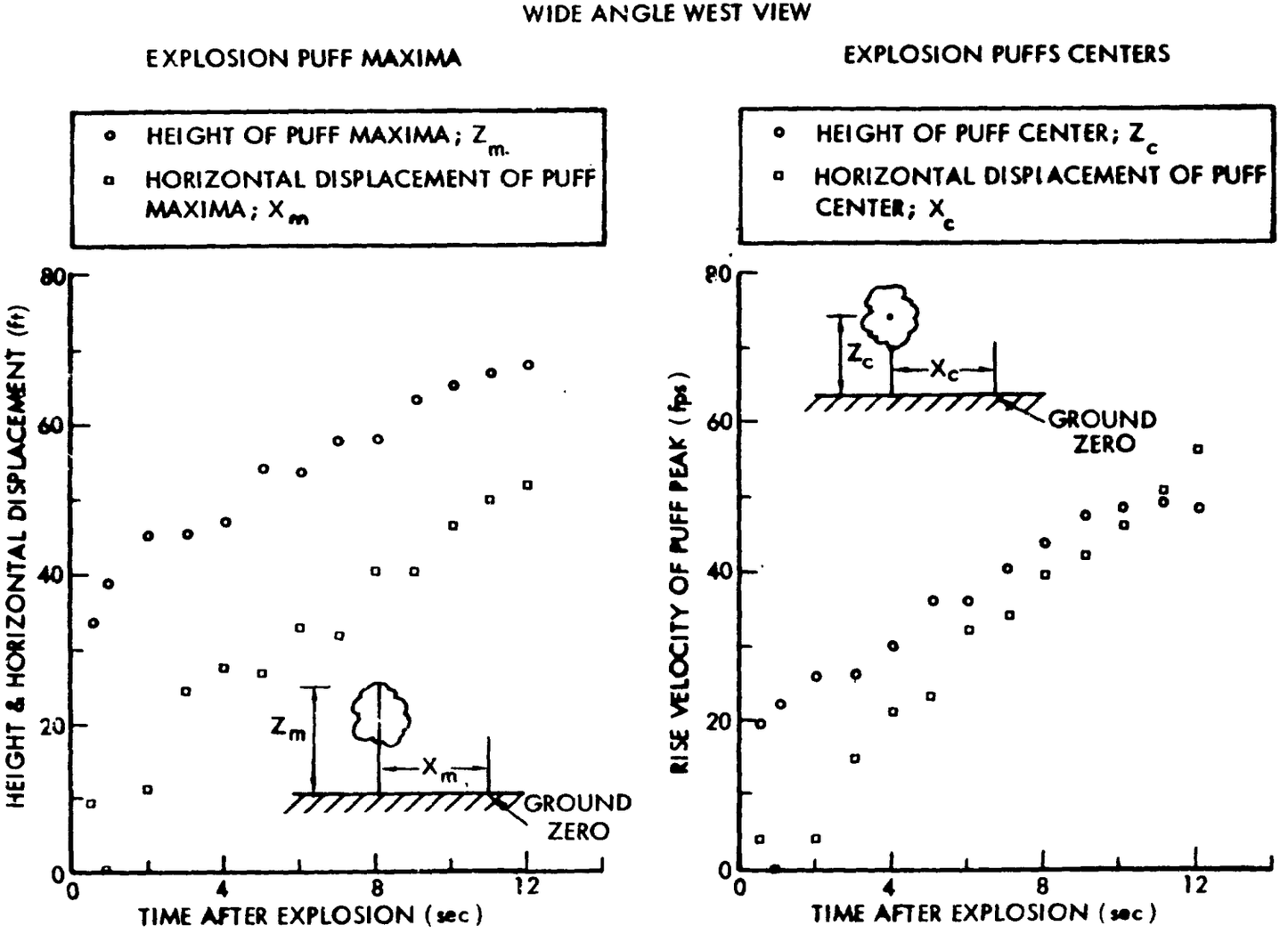

Figure 6.5 Puff Height and Displacement [illegible]

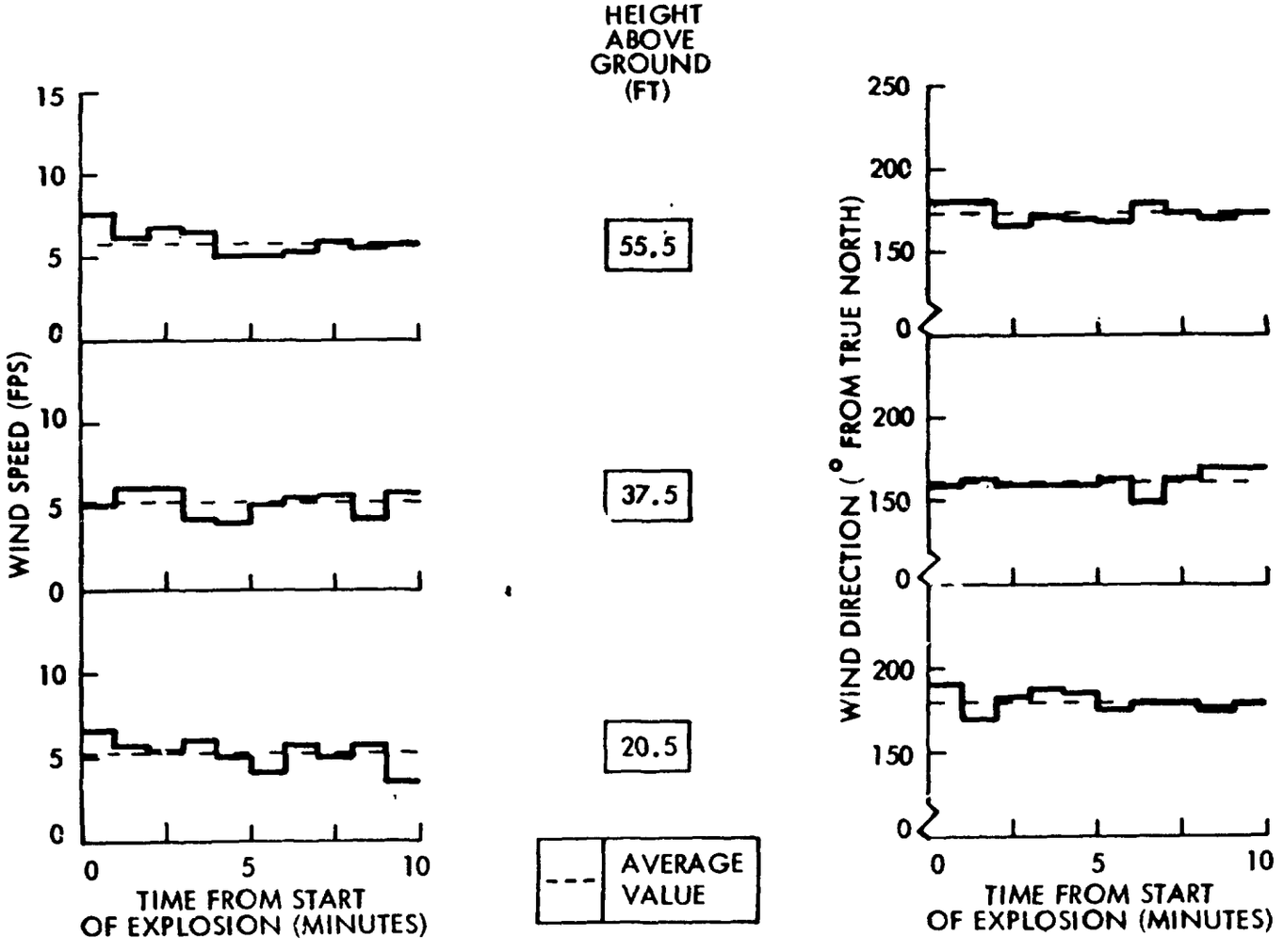

Figure 6.6. Near Surface Meteorology Data - Test No. 5

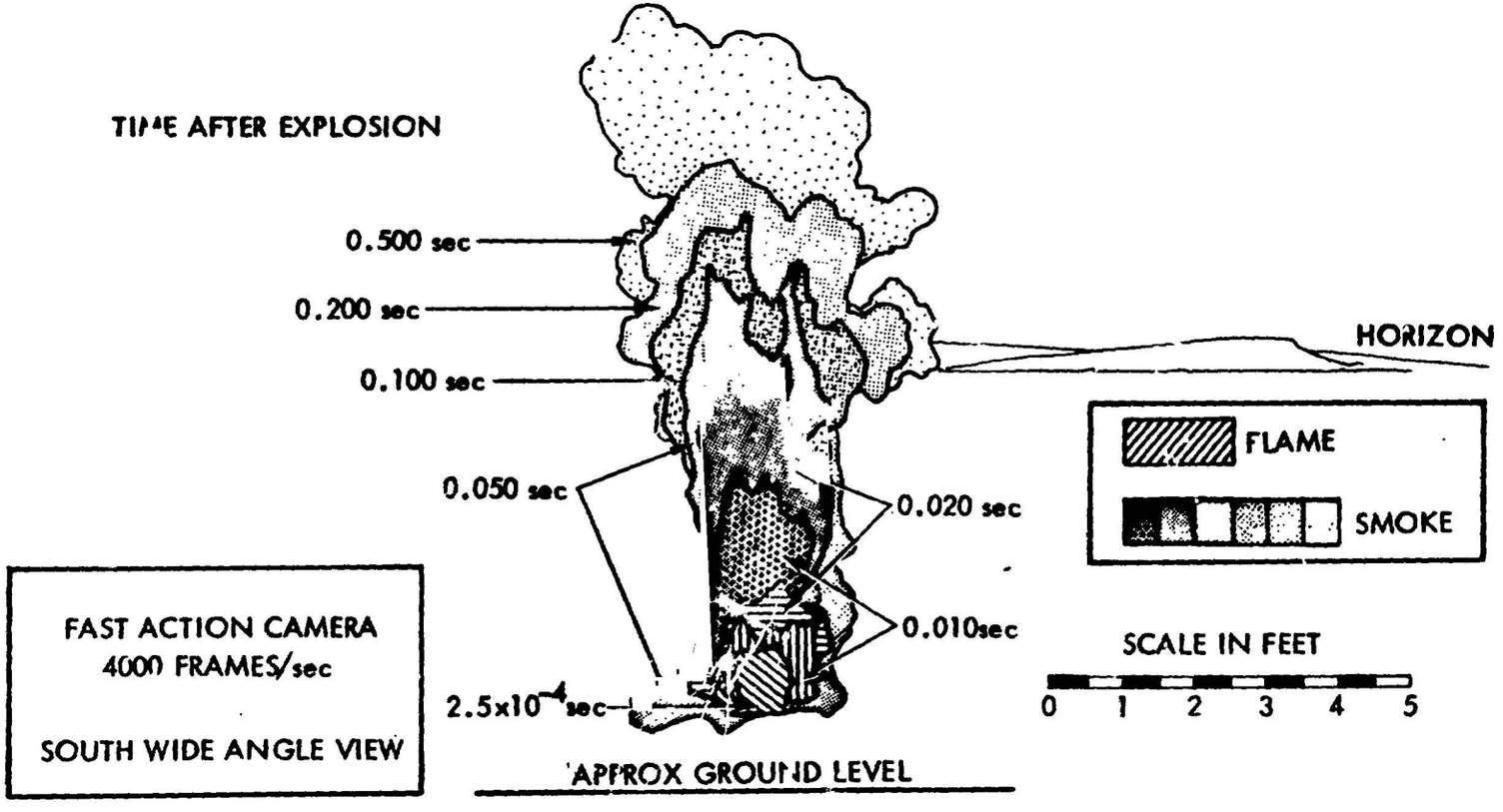

Figure 6.7. Early Time Puff Growth - Test No. 5

Tracings of selected frames from the near south wide angle camera that used standard color film are displayed in Figure 6.8. Computed puff widths and puff vertical dimensions are shown on the tracings. These plume dimensions are subject to a systematic error within approximately ± 10%, plus comparable random errors arising from plume image contrast fluctuations, etc. The random errors tend to increase sharply as the smoke plume becomes dimmer with passing time.

Figure 6.9 shows tracings of selected time-lapse frames from the near west wide angle camera, located in a vicinity approximately 550 ft (168 m) west and 100 ft (30.5 m) north of ground zero. The image to object space scale bar shown represents an approximate average for the imaged smoke plume view area. The true smoke cloud scale factor varies by approximately ± 5%. This factor depends upon both image space distance from the point P_0 shown, and upon the direction cosines between displacements of interest and the corresponding radius vector from P_0.

The data plotted in Figure 6.10 were obtained by applying calculated image-to-object space dimensional transfer factors to the selected frames of the "infrared extended color film" image profiles shown in Figure 6.9 (obtained from the near west wide angle camera). The Cine images were of poor quality, with relatively poor contrast between object space features and between the wind propagated explosion plume and the background. The detectable plume center position, and more particularly the plume dimensions, are dependent upon visibility contrast as well as upon the space-time distribution of plume particles and gases. Within approximately 10 to 12 seconds after the explosion, the outer boundaries of the plume are detectable more from frame-to-frame changes in contrast than by static viewing. Beyond 15 sec, the entire plume is quite diffuse and difficult to observe.

The thermovision 2-5 micron wavelength scanning camera shows the detonation puff of the flat plate test to be higher and wider, and to be in greater contrast than indicated by the visible light movie camera. These comparisons are presented in Figure 6.11. Both types of cameras are looking at the same fiber cloud over the same field of view. Beyond 10 sec after detonation, the infrared system clearly shows more of the cloud than the visible light movie camera; after 50 sec the infrared system still shows the fiber cloud which can no longer be seen in the visible light movies.

The cloud height and radius growth histories for the explosive puff generated by two ounces of explosives shattering a burned carbon fiber composite plate are shown in Figure 6.12. Note how the IR sees twice the cloud width at later times, as compared to visible light movies, and sees the cloud for periods six times longer.

TEST NO. 6

The near surface wind data is presented in Figure 6.13 for Test No. 6 for the northeast met tower. Average wind speeds were quite low, varying from 1 to 2 fps (0.3 to 0.6 mps), while avarage wind direction varied from 110° to 140° as measured from true north. Thus the winds blew predominantly from the southeast.

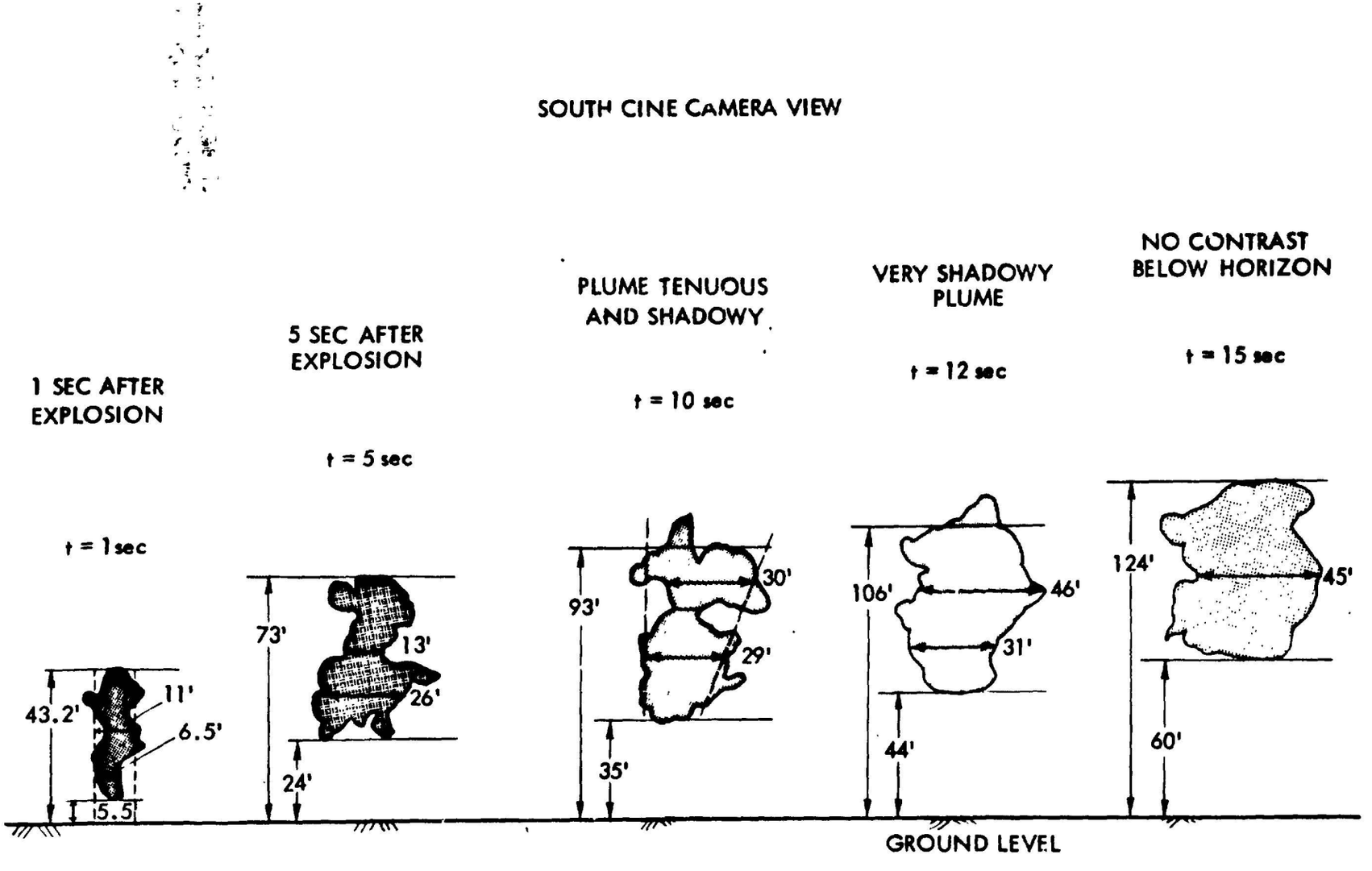

Figure 6.8. Puff Growth Profiles, Downwind View - Test No. 5

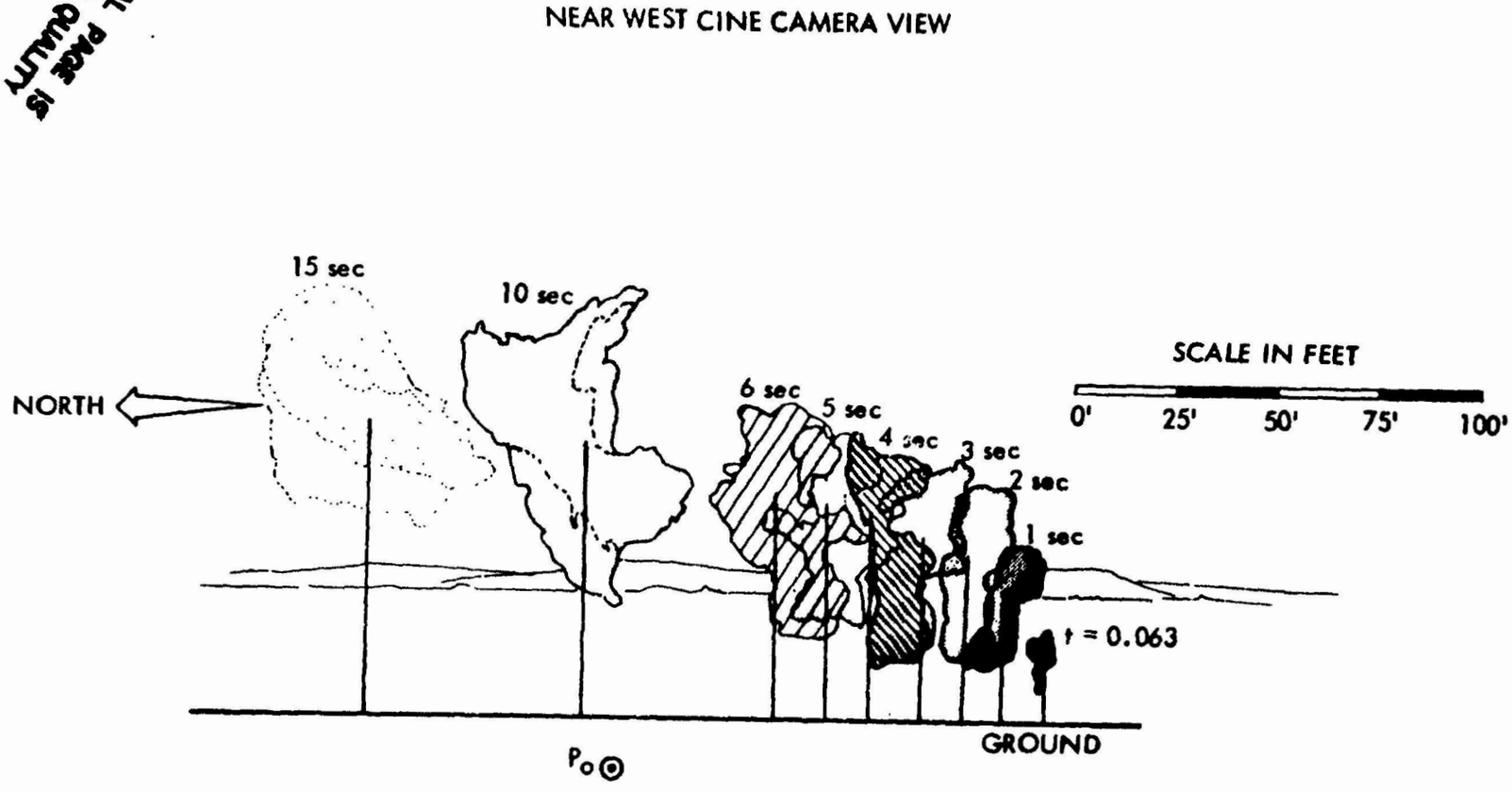

Figure 6.9. Puff Growth Profiles, Crosswind View - Test No. 5

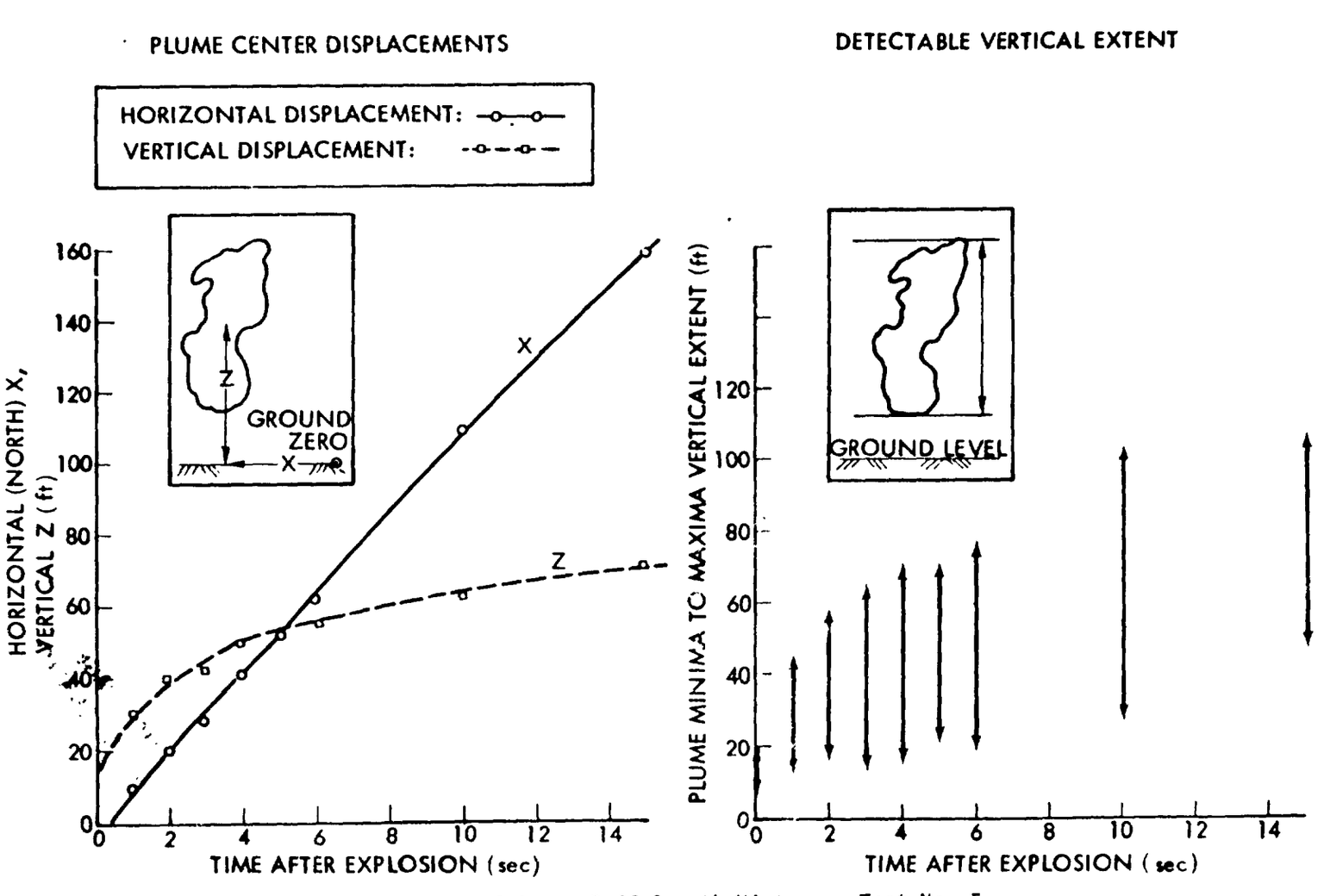

Figure 6.10 Puff Growth History Test No. F

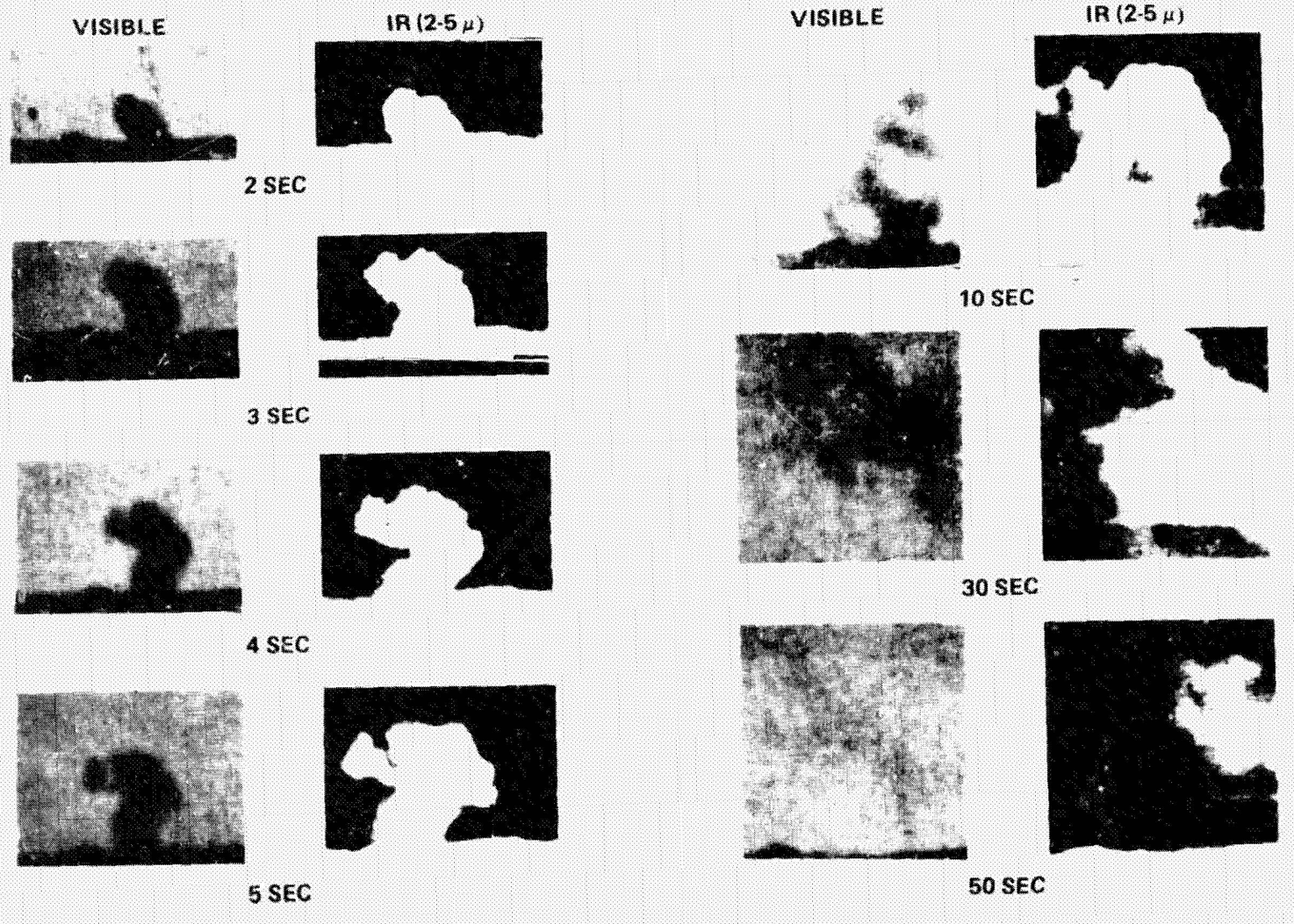

Figure 6.11. Comparison of IR Thermography and Visible Photography - Test No. 5

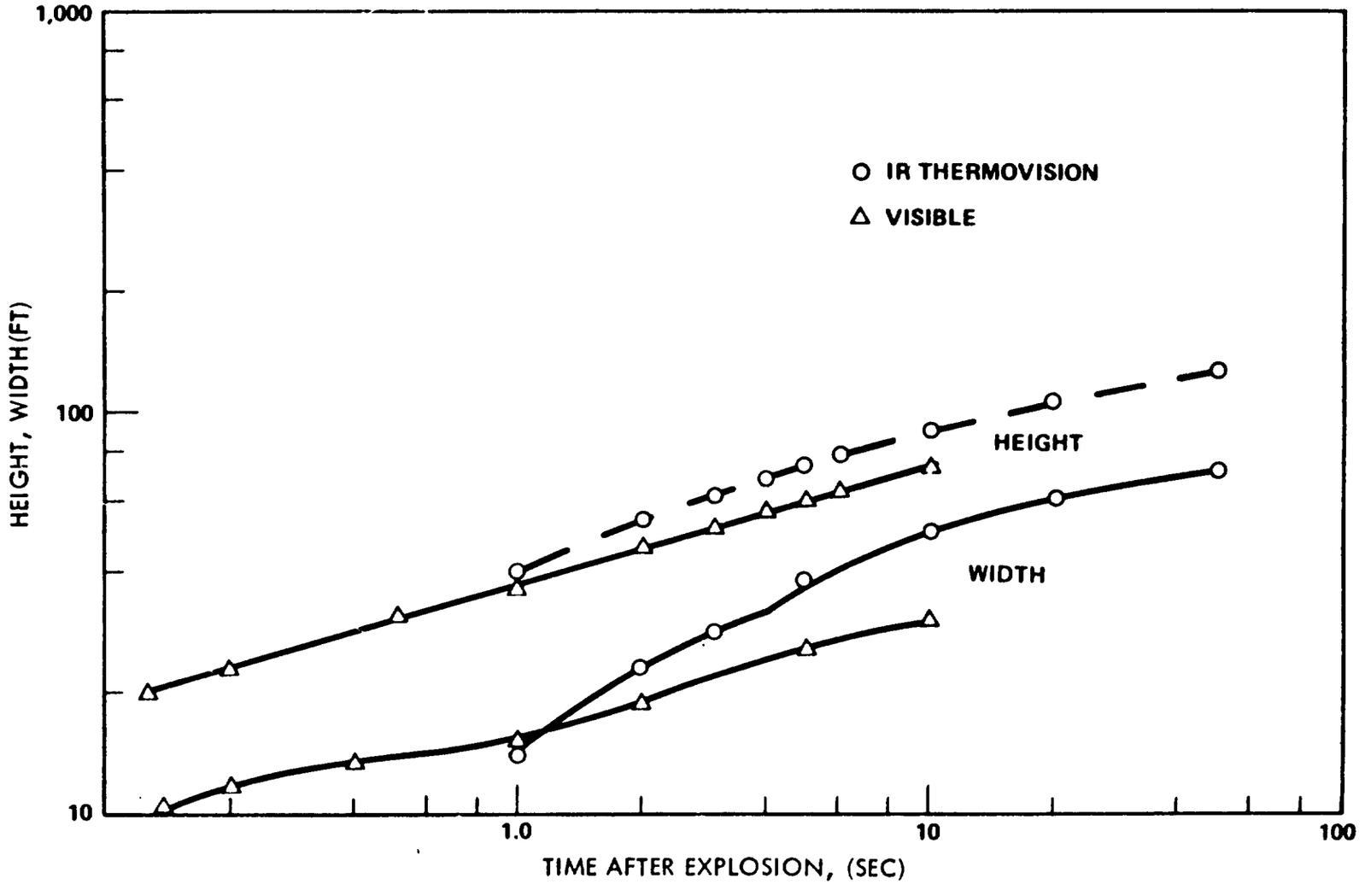

Figure 6.12. Puff Growth History, IR and Visible Comparison - Test No. 5

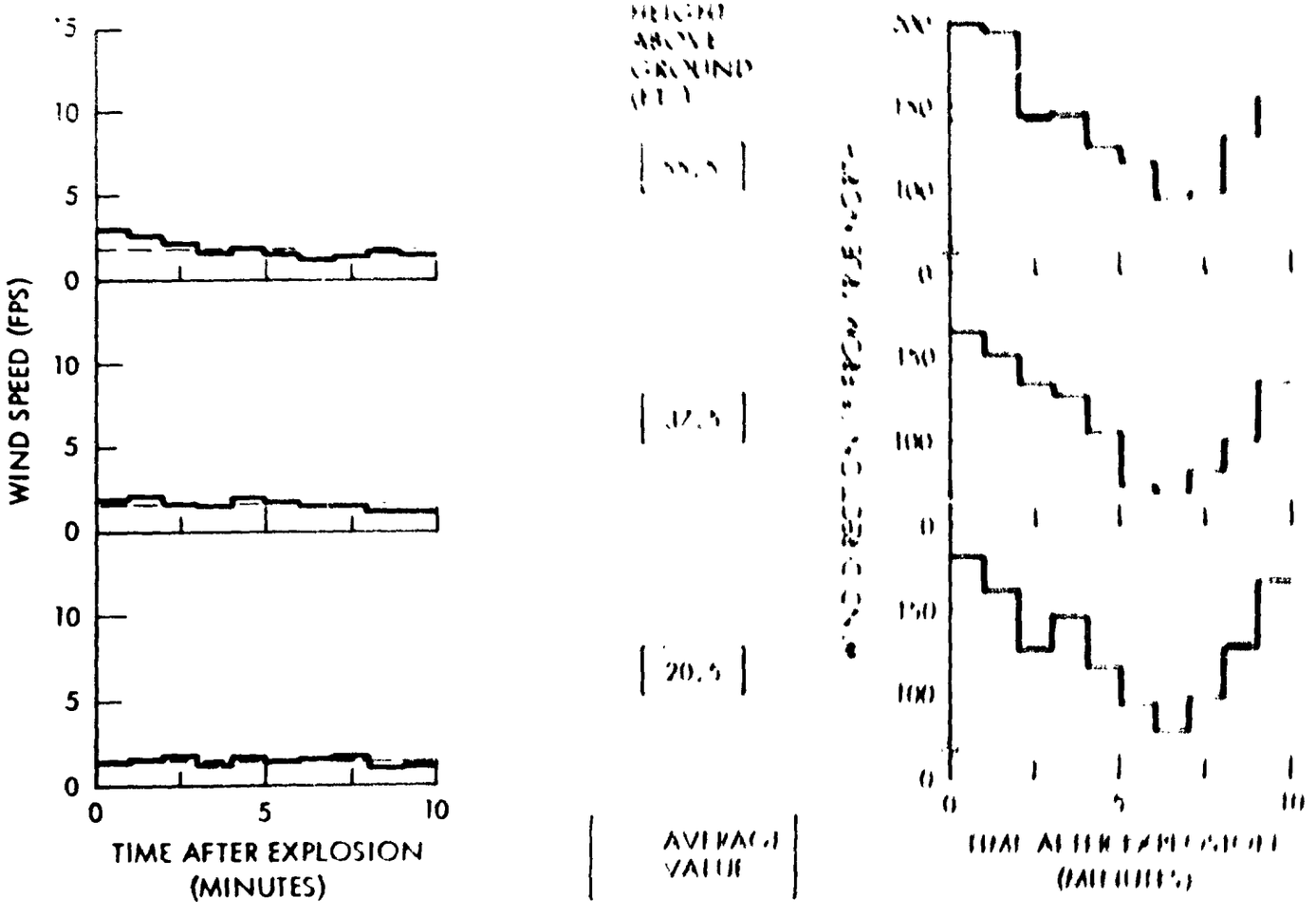

Figure 6.13. Near Surface Meteorology Data Test No. 4

Ambient temperature was also measured and found to be 40°F (4.4°C). The following table provides specific values as a function of height:

Table 6.3. Ambient Temperature For Test No. 6

Height Above Ground (ft)	Temperature (°F)
3	40.2
18	40.0
28	---
38	39.9

Figure 6.14 exhibits a sequence of tracings of Polaroid camera stills of selected images recorded by the video camera boresighted with the infrared thermovision/thermograph equipment, which for Test No. 6 was situated 700 ft (213 m) due west of ground zero. Sixty image fields per sec were recorded on a video tape recorder for later evaluation. An image-distance to object-distance scale bar is included. The sequence of tracings illustrate the smoke puff growth and northward drift with the prevailing wind. It is seen that as time progresses, the smoke puff tends to become more spherical.

The explosion puff history is presented in Figure 6.15 as reduced from pictorial data depicted in Figure 6.14 for the boresighted near west camera. This video data is superior to Cine camera data obtained from the camera that was situated approximately 550 ft (168 m) west and 100 ft (30.5 m) north of ground zero, in that detectable contrast persists for a longer time and extends to larger detectable puff image dimensions. The extent of both temporal and spatial detectable puff contrast, however, still is inferior to that obtained from the IR thermovision thermographs with which the video camera was boresighted. Figure 6.16 displays variation with time of the maximum height (Z_m) and corresponding horizontal displacements of the puff profile for Test No. 6, as observed by the video camera boresighted with the IR thermovision thermograph instruments. The rise velocity of the explosion puff vertical maxima, ($\Delta Z_m/\Delta t$), is exhibited in Figure 6.17 as a function of time after explode. The puff maximum height data was reduced from polaroid stills of the taped boresight video camera data, as for preceding figures. The taped video images were recorded at the rate of 60 interlaced "fields" (30 frames) per sec, thus allowing the rapidly decelerating early time rise velocities to be determined at short time intervals.

A comparison of visible photography and IR thermograph images for several contrast levels is presented in Figure 6.18. The photograph in the visible light regime shows the combined clouds from the smoke generator and from the fiber plume generated by the explosion of the flat plate. The two clouds cannot be individually identified or outlined. The infrared image at the right of the figure is set at even greater contrast to eliminate the lower emissivity gases and to maintain the higher emissivity fragments. This effect can be used to track fragments when they are hidden by a plume background.

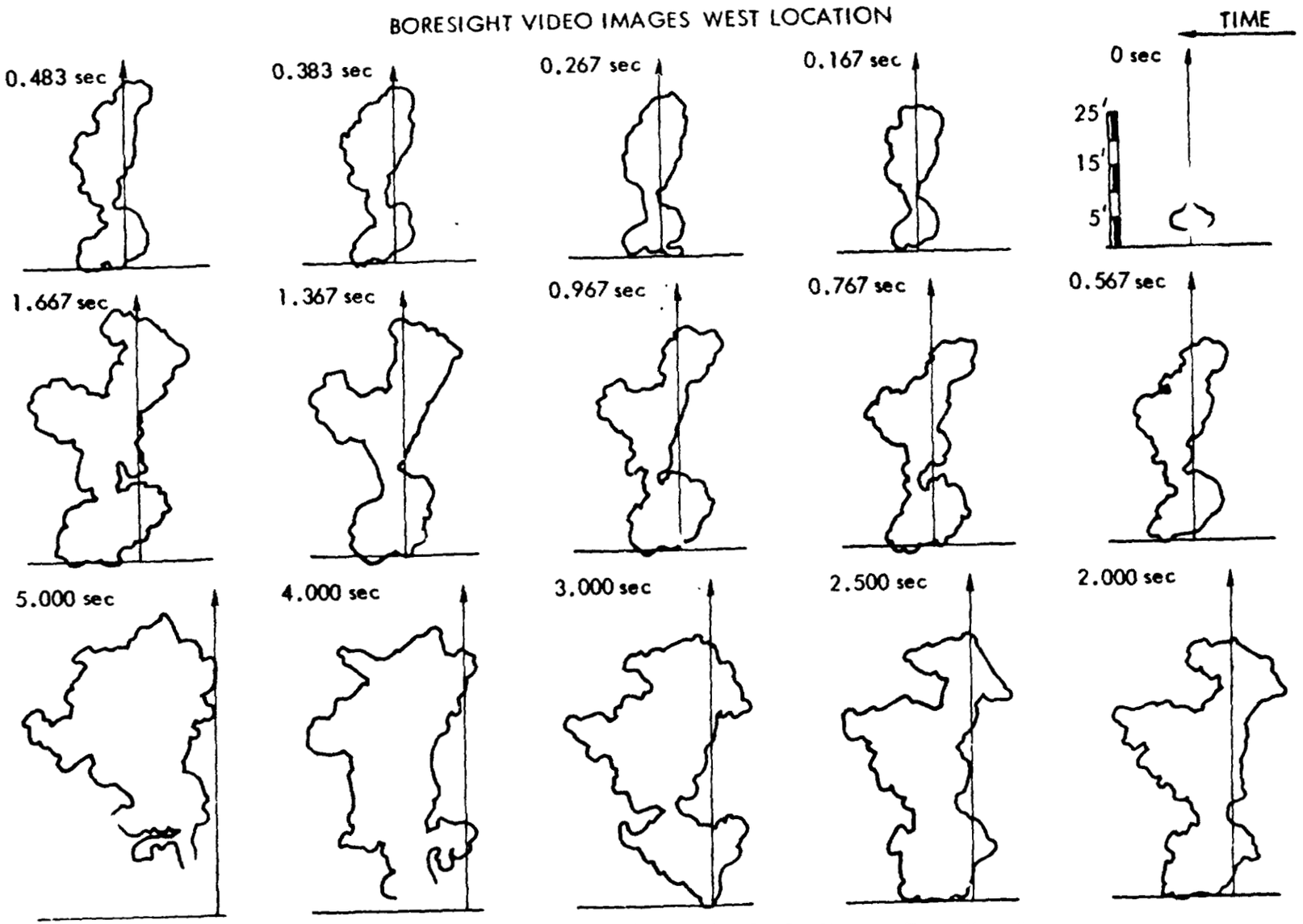

Figure 6.14a. Explosion Puff Growth, Early Time - Test No. 6

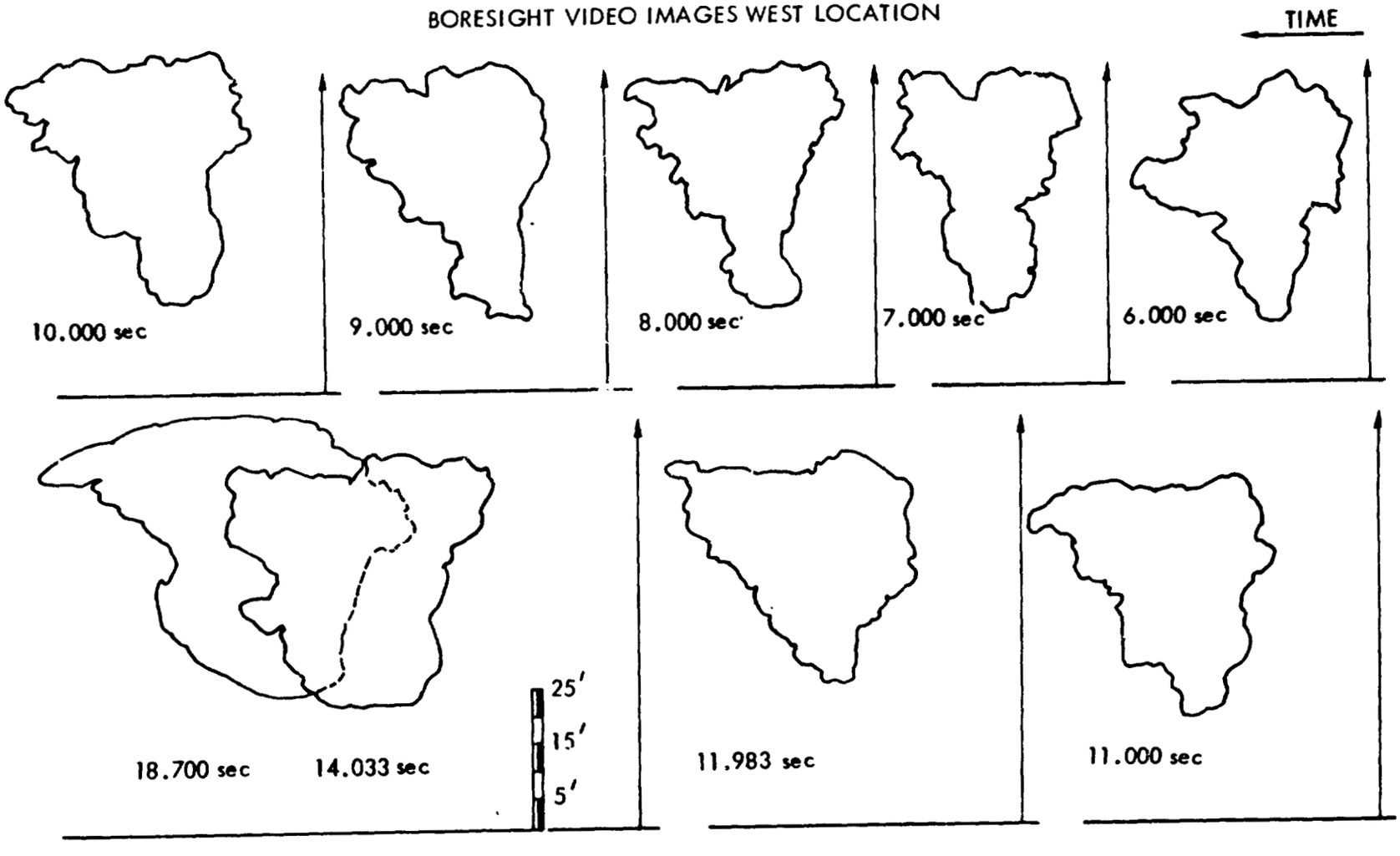

Figure 6.14b. Explosion Puff Growth, Late Time - Test No. 6

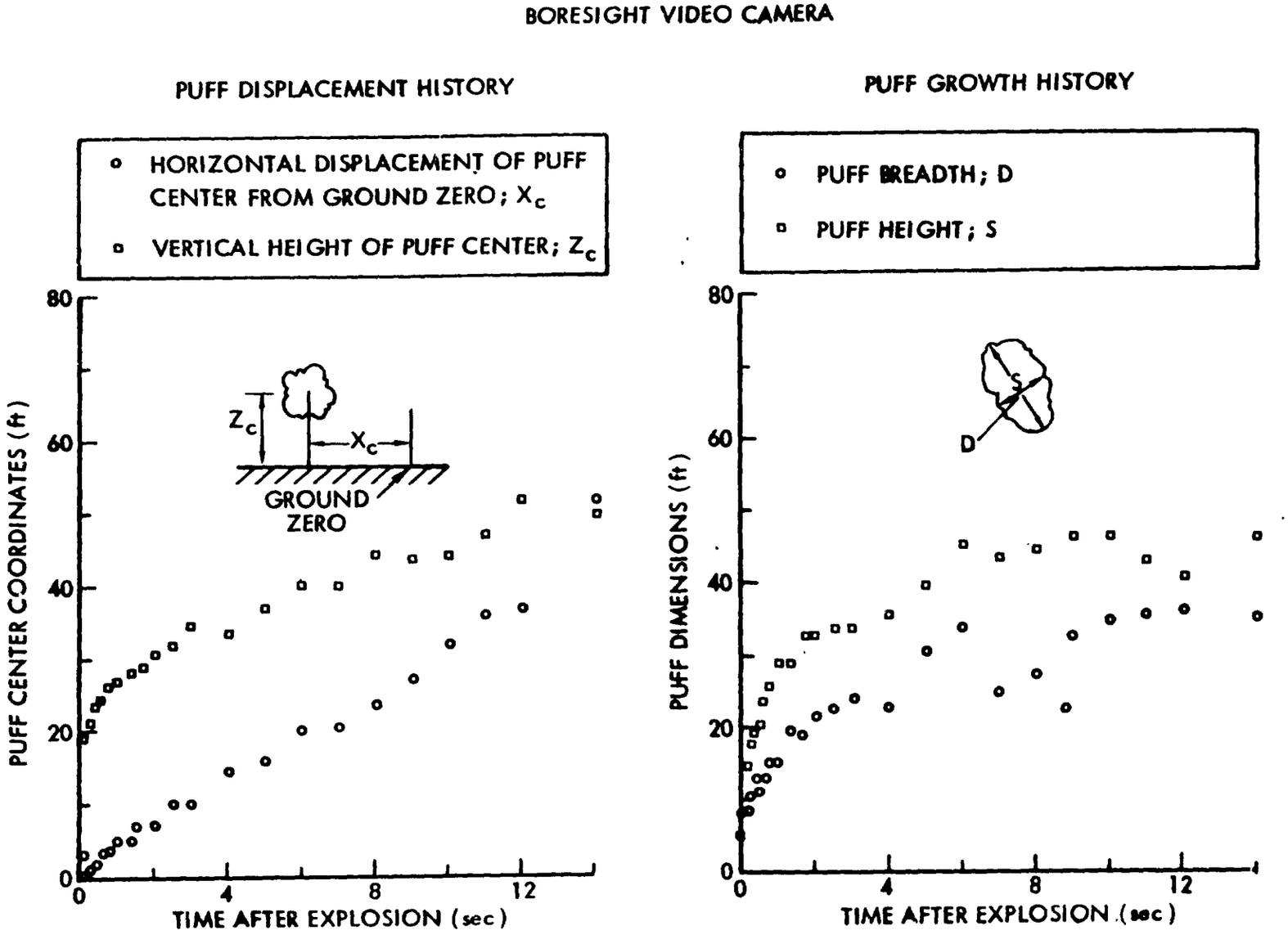

Figure 6.15. Explosion Puff History - Test No. 6

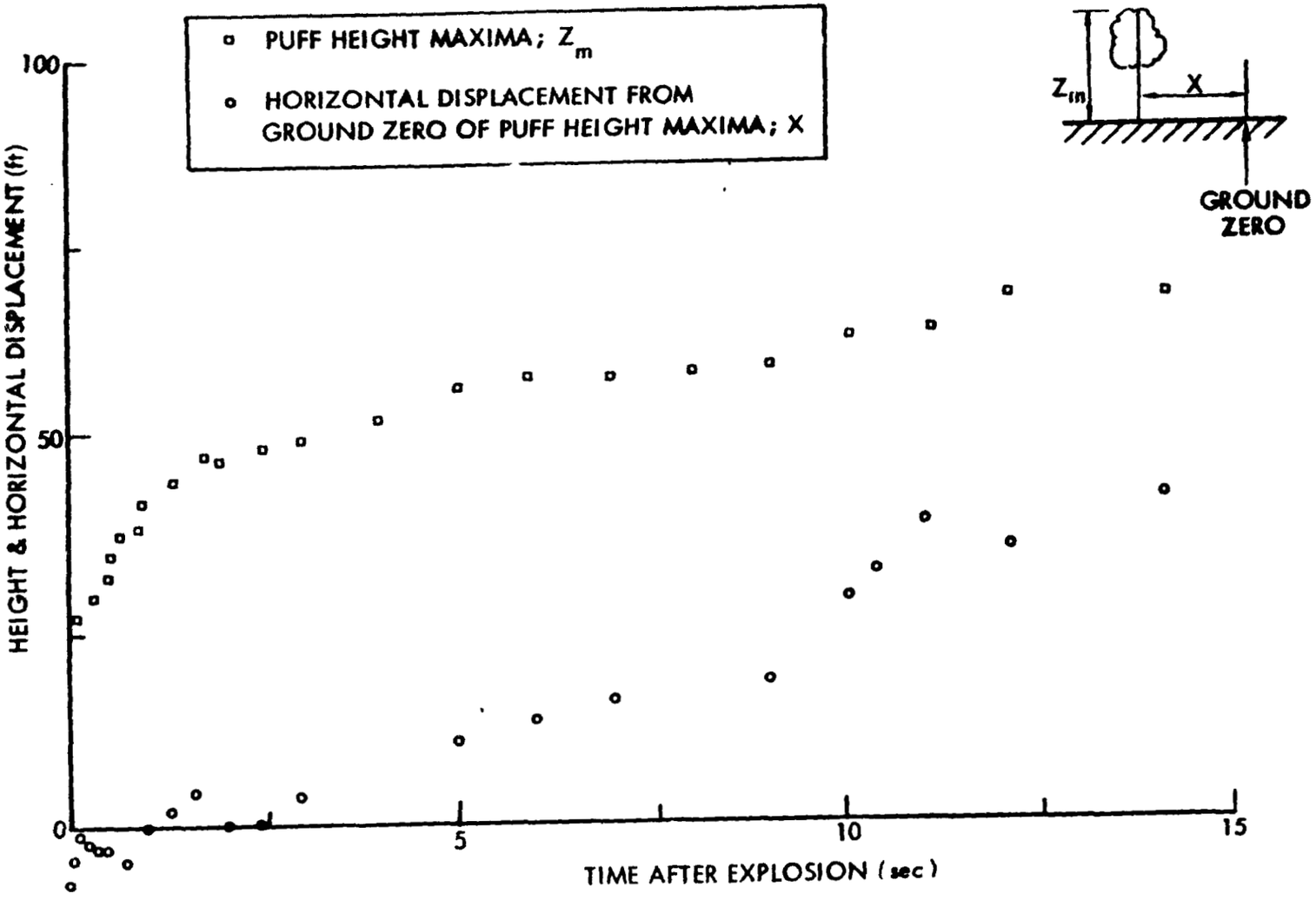
PUFF HEIGHT MAXIMA; Z_m
HORIZONTAL DISPLACEMENT FROM GROUND ZERO OF PUFF HEIGHT MAXIMA; X
Z_m
X
GROUND ZERO
HEIGHT & HORIZONTAL DISPLACEMENT (ft)
100
50
0
5
10
15
TIME AFTER EXPLOSION (sec)

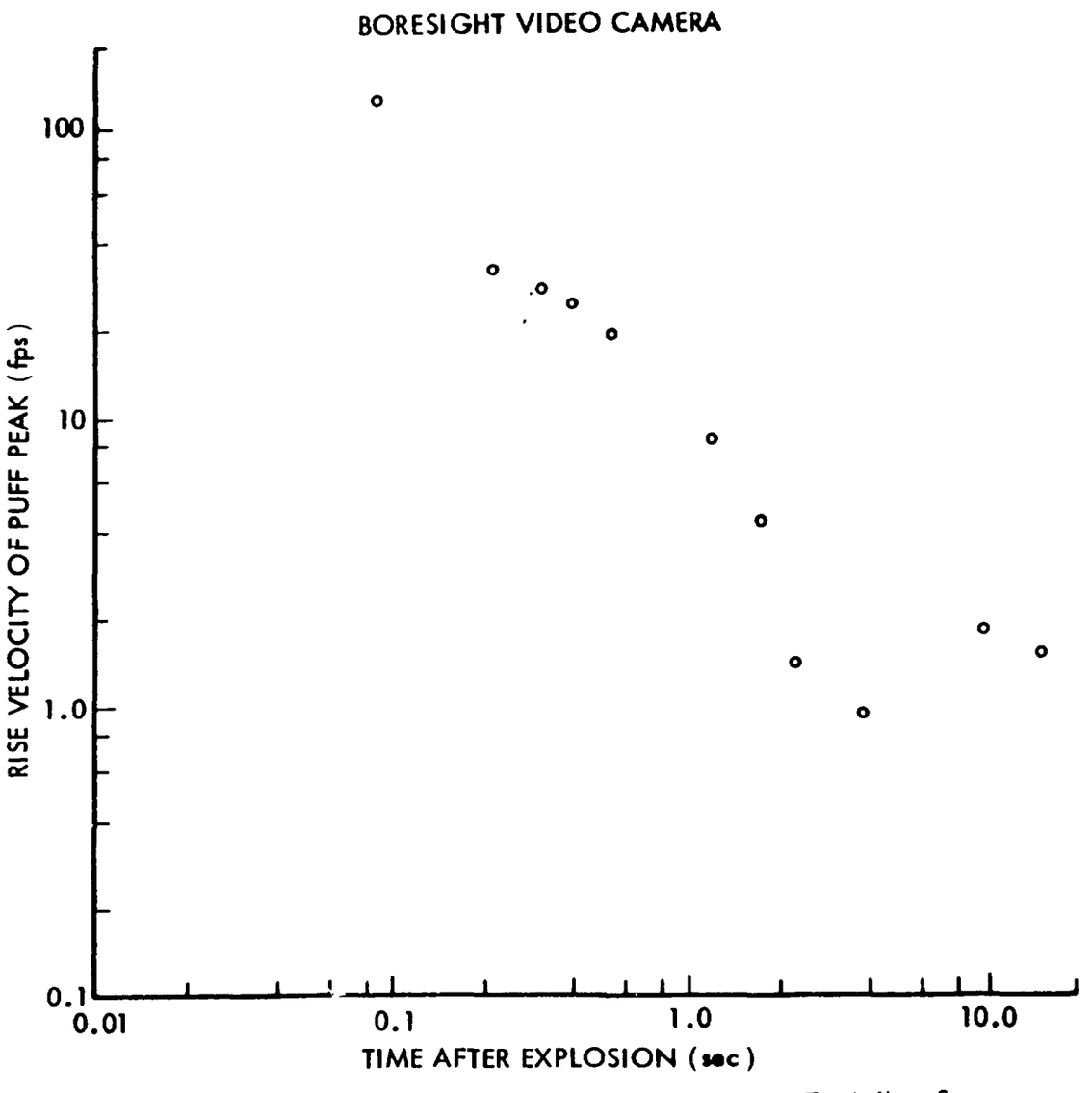

Figure 6.17. Puff Rise Velocity History - Test No. 6

Figure 6.18. Adjustable Contrast Display of IR Thermograph Data - Test No. 6

Typical IR image results for Test No. 6 are depicted in Figure 6.19. At 1.06 sec after the explosion, the five fragments circled on this figure were tracked with the IR thermovision. Note the entire frame was 8 ft (2.4 m) above ground level and viewed in a field 56 ft (17 m) high by 51 ft (15.5 m) across. This data could not be obtained from visible light movie cameras.

Height from ground level to the top of the puff and puff width histories are plotted in Figure 6.20 from IR thermovision and visible images. The IR data persisted out to 30 sec, while the visible data lasted only out to 10 sec after explosion. Both height and width are greater for the IR data because of better contrast than with the visible images.

TEST NO. 7

This test was conducted without a carbon composite sample to obtain photographic data just on the C-4 explosion. The resulting puff did not contain carbon fibers. Data from Test No. 7 was not reduced as part of this data reduction and analysis program; hence no data is presented here.

TEST NO. 8

The near surface wind data is shown in Figure 6.21 for Test No. 8. Average values for the entire ten minute period are also presented. Average wind speeds varied from 5 to 6 fps (1.5 to 1.8 mps), while average wind direction varied from 175° to 190° as measured from true north. Thus the winds were predominantly southerly.

Ambient temperature was found to be 51°F (10.6°C). Specific values for several heights are as follows:

Table 6.4. Ambient Temperature For Test No. 8

Height Above Ground (ft)	Temperature (°F)
3	51.7
18	51.2
28	---
38	51.0

The plotted data in Figure 6.22 were obtained by applying calculated image to object dimension transfer factors to selected frames of camera color film obtained from a camera located approximately 490 ft (149 m) due south of ground zero for Test No. 8. The usable background features were fewer than for Test No. 5, but gave a better correlation for the transfer factors. The plotted data scatter, however, still indicates appreciable random error, part of which may result from the variations in background brightness which effect plume to background contrast. The apparent relative maxima in plume vertical and lateral dimension occurring around 20 sec after the explosion may be real, but also may result, at least partially, from the difficulty in determining visibility contours in very low contrast images.

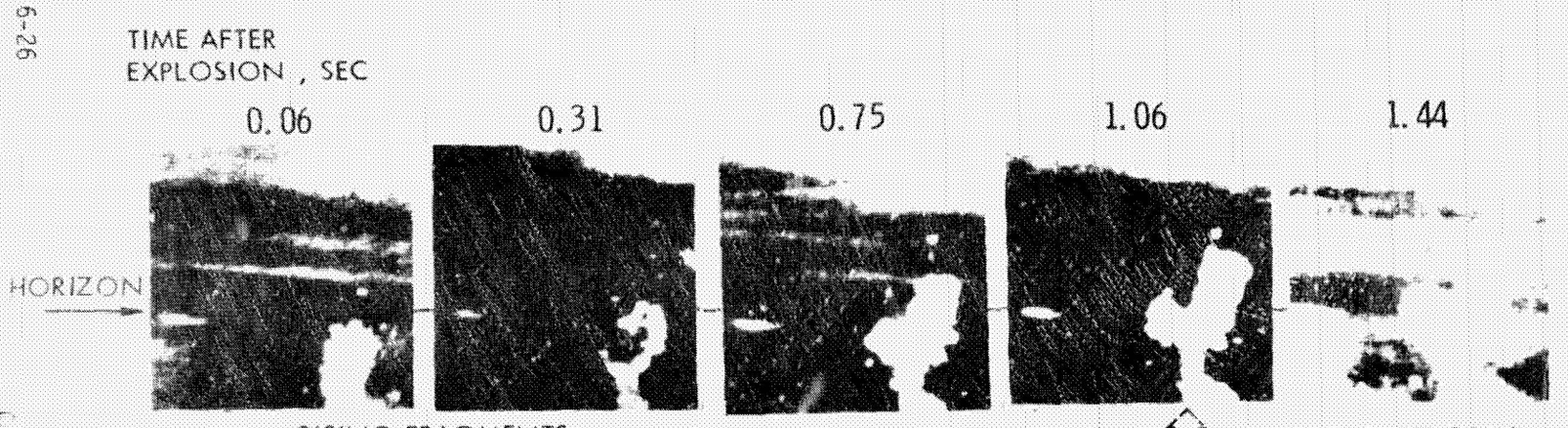

FRAGMENT NO. / TIME (SEC)	VELOCITY, FT / SEC			
	1	2	3	4
0.31 - 0.75	6	12	24	12
0.06 - 0.31			12	8

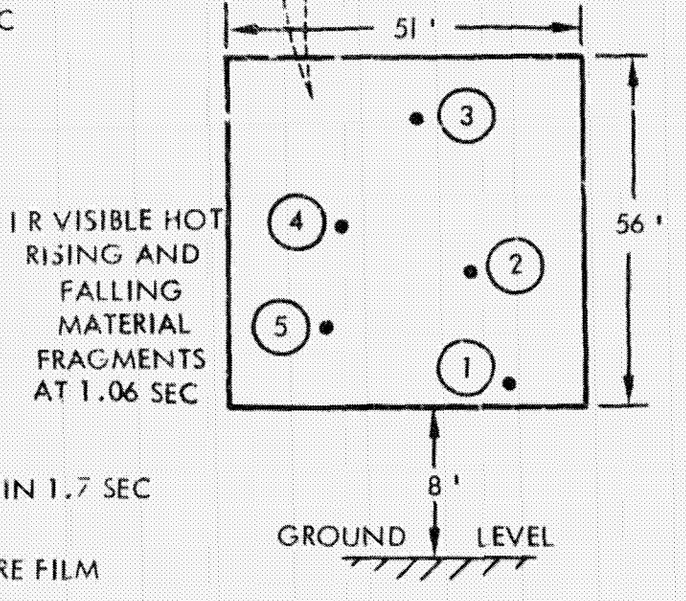

- AVERAGE VERTICAL VELOCITIES OF FRAGMENTS
- ALL IR DETECTED FRAGMENTS FELL BACK TO GROUND WITHIN 1.7 SEC FOR THIS EVENT
- FRAGMENTS ARE INVISIBLE ON THE VISIBLE MOTION PICTURE FILM

Figure 6 19. IR Display of Rising and Falling Fragments of Exploded Material - Test No. 6

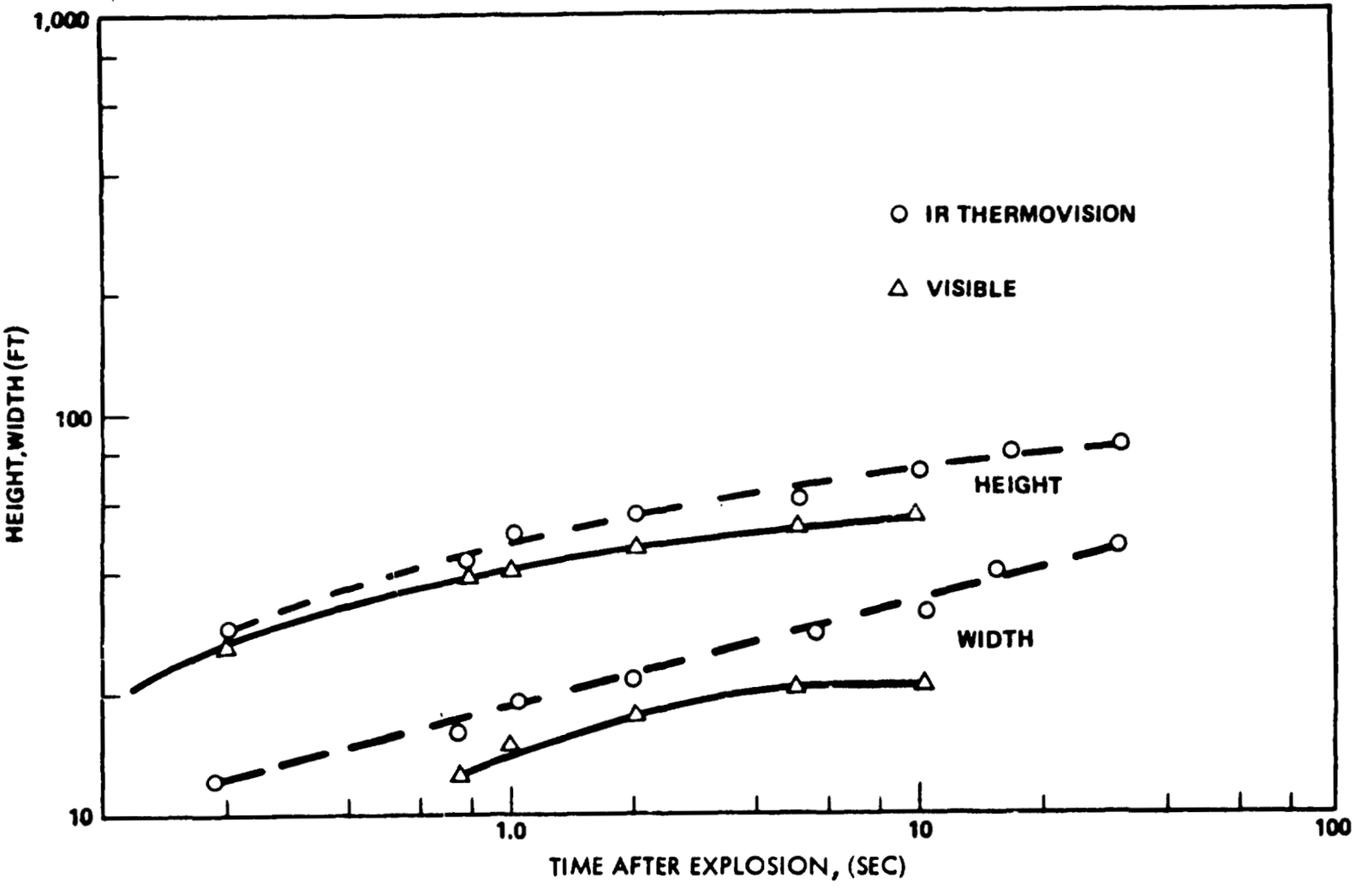

Figure 6.20. Puff Growth History, IR and Visible Comparison - Test No. 6

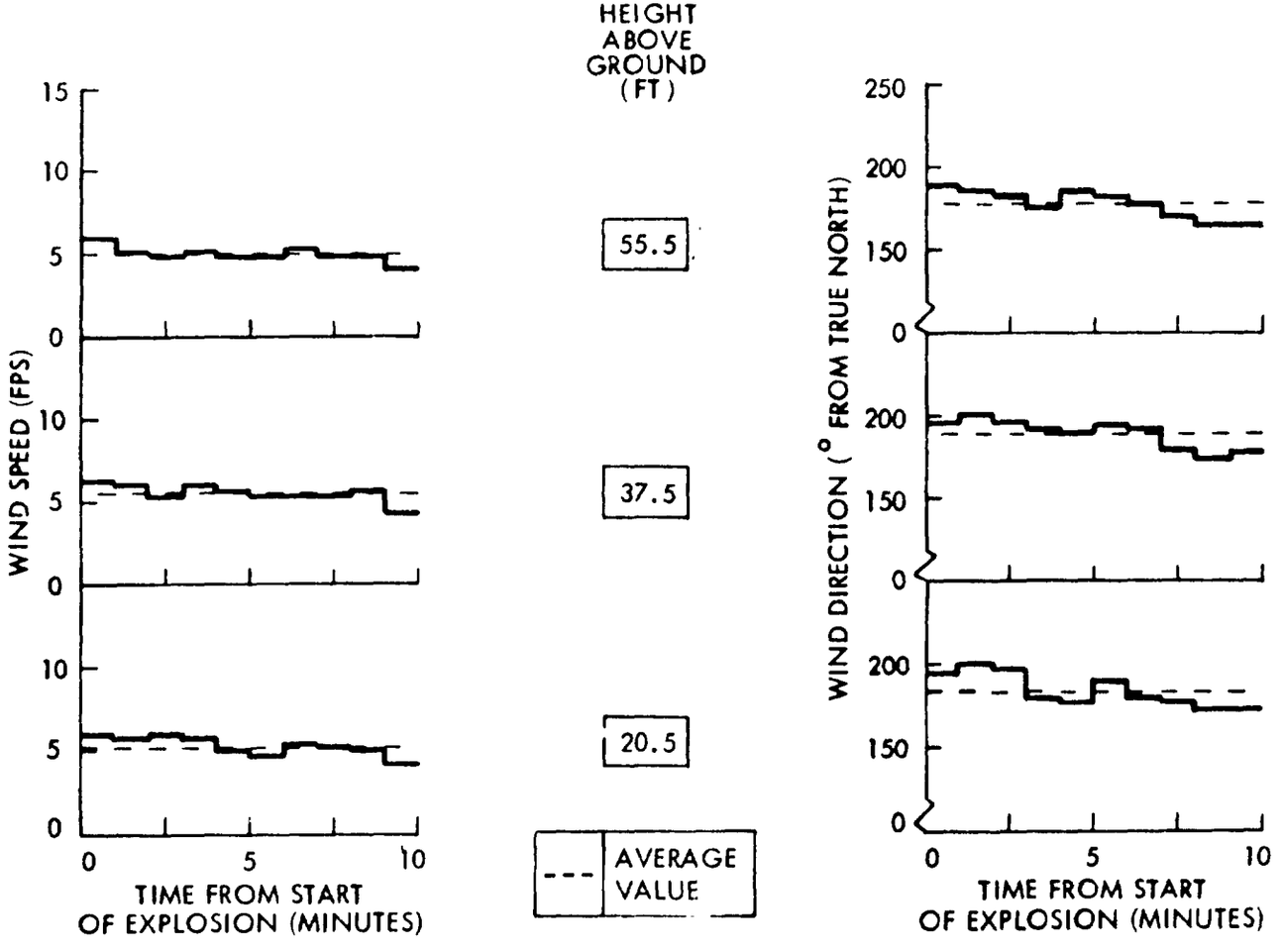

Figure 6.21. Near Surface Meteorology Data - Test No. 8

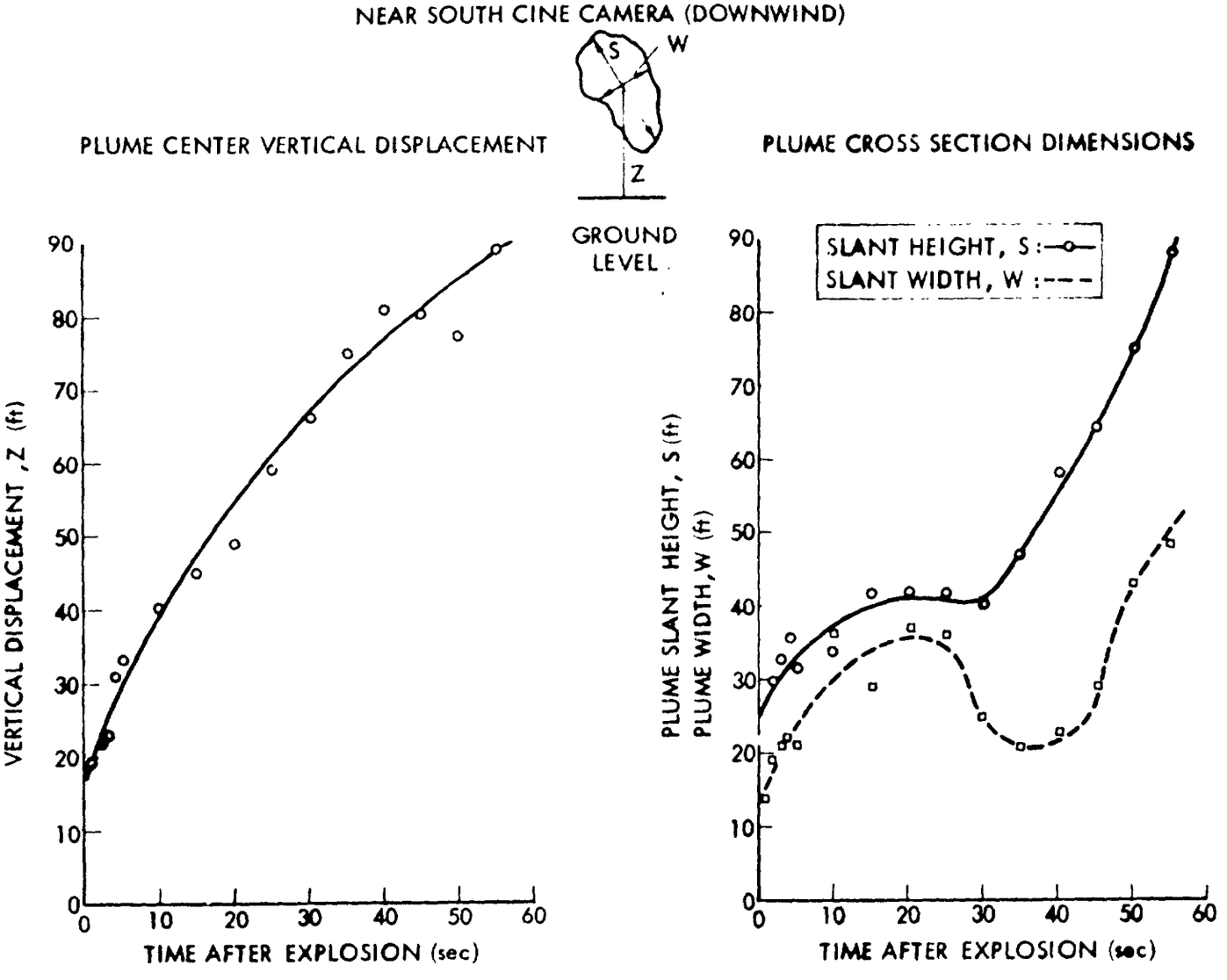

Figure 6.22. Puff Growth History, Downwind View - Test No. 8

The data displayed in Figure 6.23 were obtained from selected frames of camera color film obtained from the camera boresighted with the IR imaging system. The cameras were located approximately 1930 ft (588 m) west and 210 ft (64 m) north of ground zero. The images obtained from this boresight camera were of much superior quality, showing more detail for appreciably longer duration, than the corresponding poor contrast images obtained from the near west camera located approximately 550 ft (168 m) west and 100 ft (30.5 m) north of ground zero. Puff growth data from this near west camera are not shown since, where reliable, they merely serve to confirm the superior boresight film data. As would be expected the puff image dimensions, again where reliable for $t \leq 15$ sec after the explosion, generally are a few percent larger for the nearer camera which should be able to detect a more diffuse concentration of smoke particles.

Comparison of the infrared puff pictograms with corresponding visible images obtained from motion picture film, shown in Figure 6.24, lead to the conclusion that both the spatial extent (height and width) and detectable contrast persistance of the imaged smoke puff appear to be larger for the IR pictograms than for the camera film images. The limited frame size and problems with contrast against the terrain background hinder IR plume detection for a short interval immediately after explosion.

The thermovision 2-5 micron IR scanning camera photographs in Figure 6.25 show that the early detonation puff is composed of two components. It is conjectured that the top consists of combustion gases. It moves upward faster, separates from the rest of the puff and gets dissipated earlier than the lower particle cloud. It is conjectured that the lower cloud consists of carbon fibers. The fiber cloud, being heavier, moves slower and persists longer i.e. is trackable for a longer period of time. The vertical velocities of both components are determined and are plotted as a function of time for 1-2 seconds after the explosion.

MODERATE SIZE JP-5 FIRE TESTS

The data in this subsection covers Test Nos. 9 and 10, each used a 20 ft by 20 ft (6.1 m by 6.1 m) JP-5 pool fire located at ground zero on the test pad. Infrared and visible image comparisons, and IR tracking of barrel debris and hot fragments are presented for Test No. 10 here, because time did not permit visible film data reduction for these early JP-5 tests. The following subsection entitled "Large Size JP-5 Fire Tests" provides extensive film data for the 40 ft by 60 ft (12 m by 18 m) JP-5 fire tests.

Comparison between the smoke images of the JP-5 fire for Test No. 10 obtained using the IR scanning thermovision and visible light motion picture cameras is shown in Figure 6.26. IR images of the hot flying fragments obscured by smoke in the visible light pictures are produced by suppressing electronically the colder smoke background. Due to a high setting of the IR camera sensitivity control, the lower halves of the smoke images are saturated. The distortion caused by saturation is accompanied by ringing which produced multiple images.

The hot flying debris of the burned half barrel in the Test No. 10 JP-5 fire

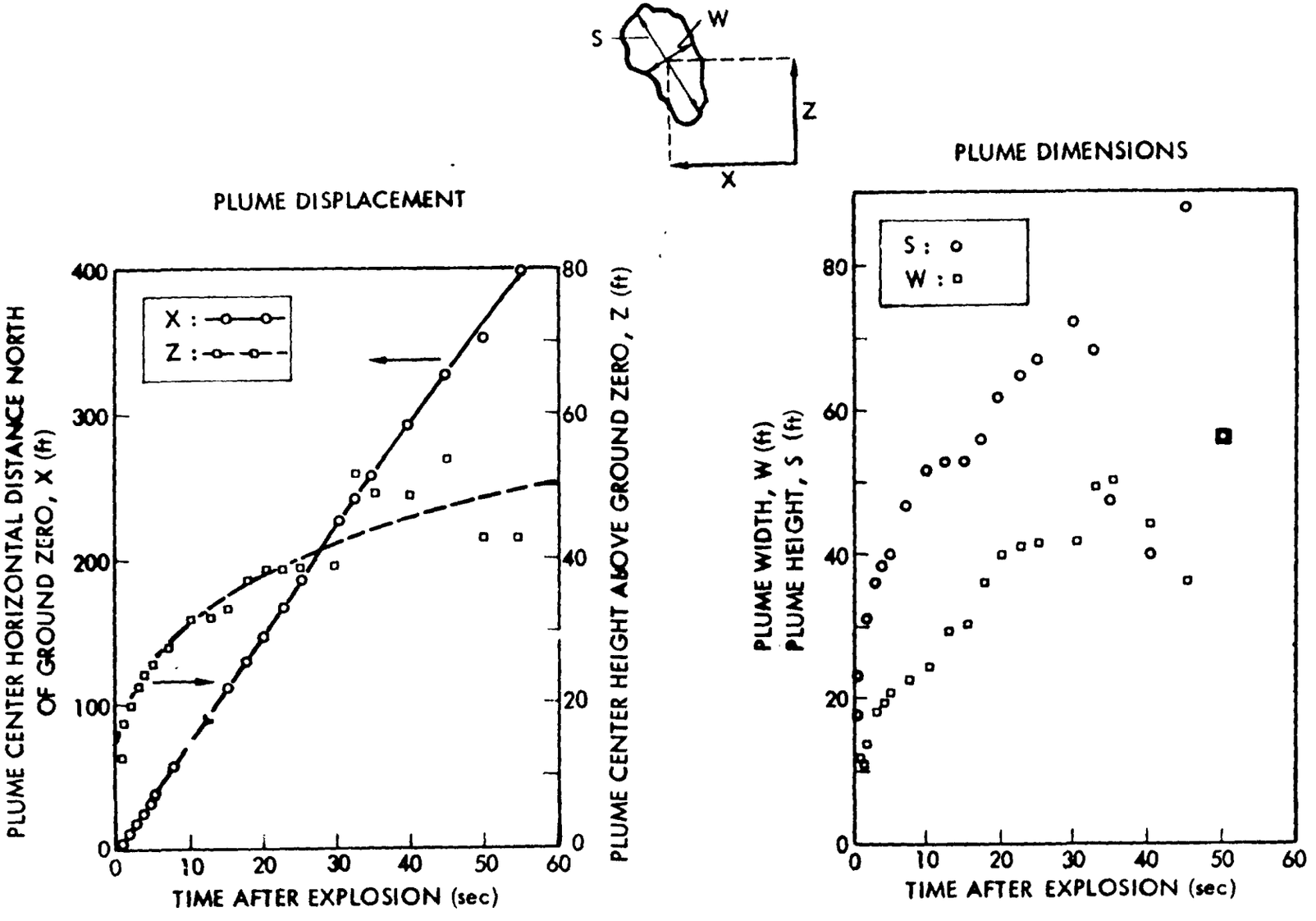

Figure 6.23. Puff Position and Configuration, Crosswind View - Test No. 8

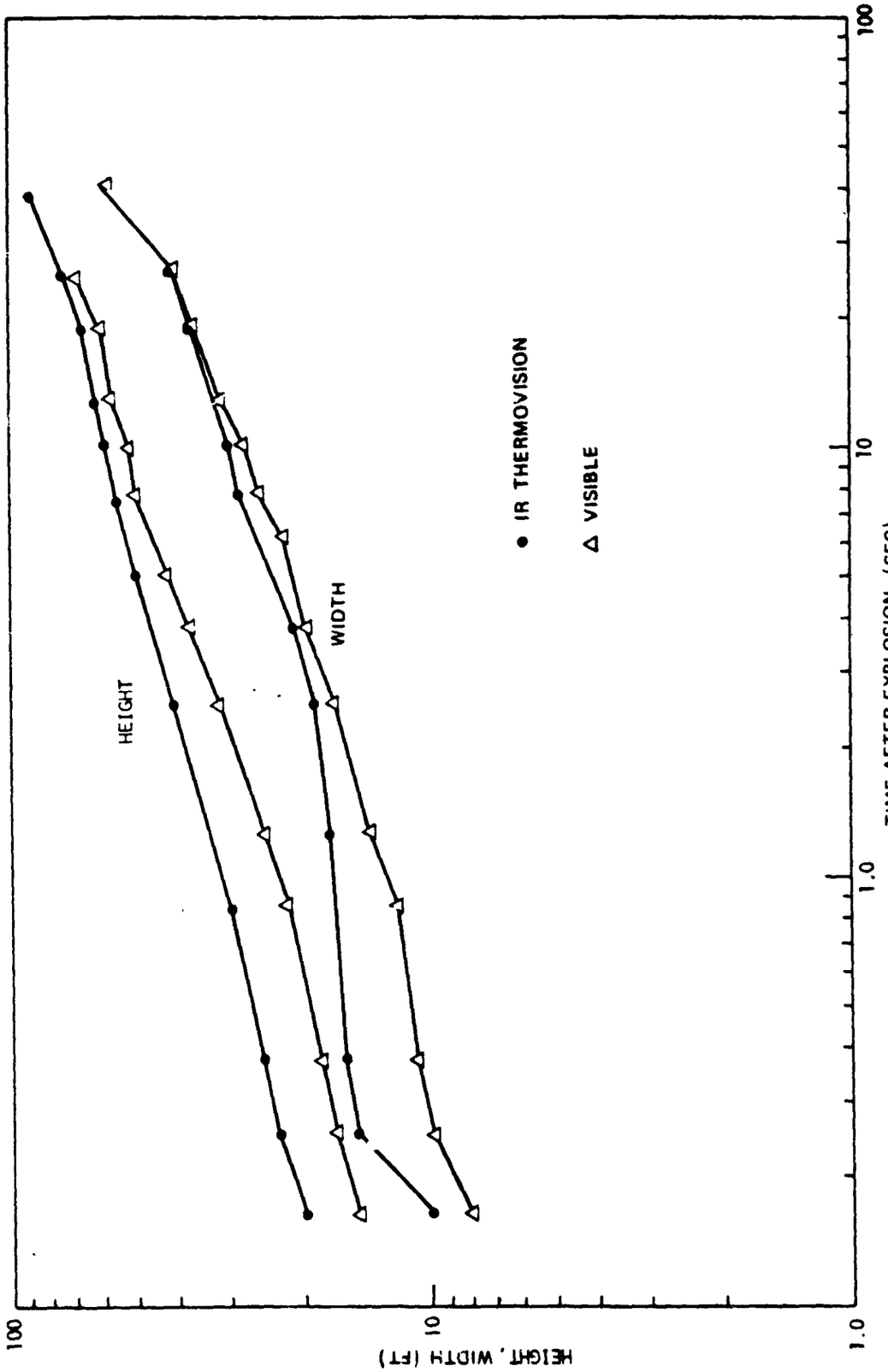

Figure 6.24. Puff Growth History, IR and Visible Comparison - Test No. 8

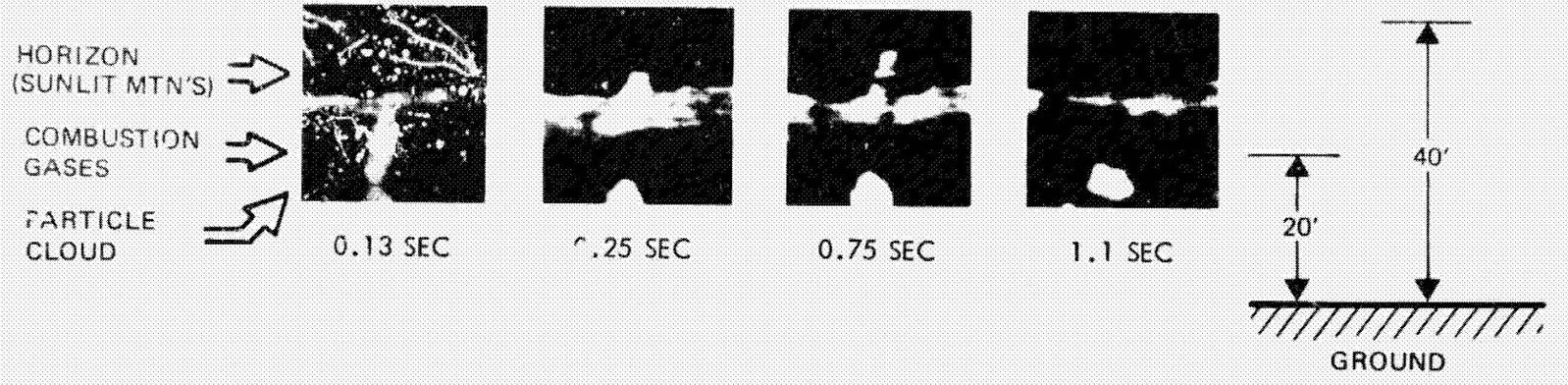

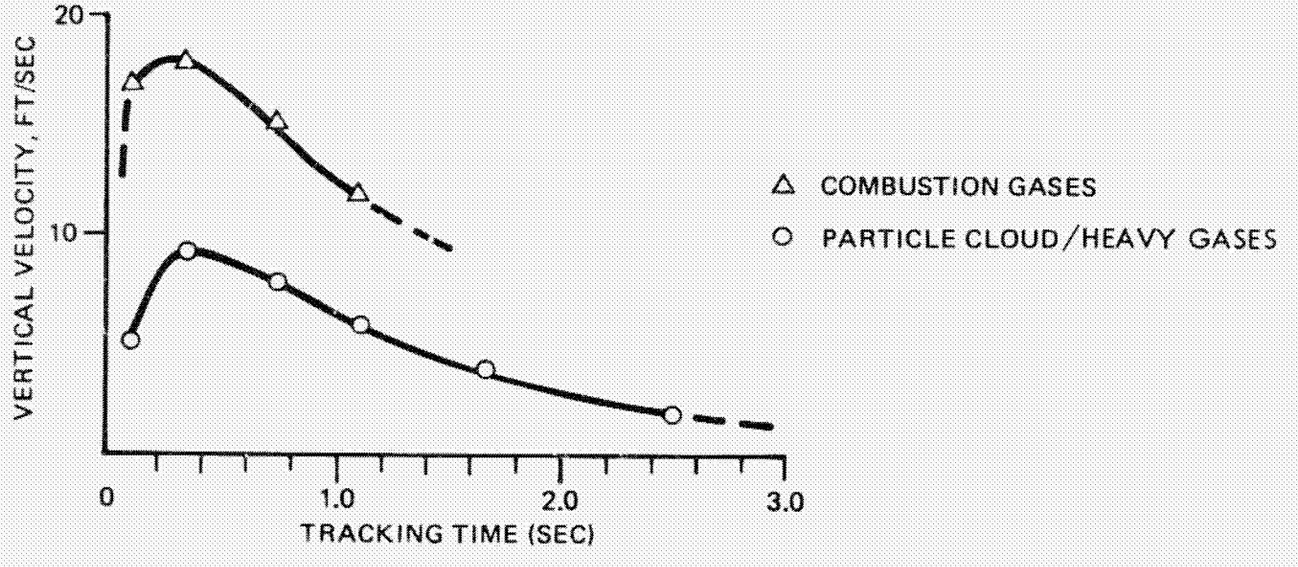

Figure 6.25. IR Imagery of Combustion Gas and Particle Cloud Rise - Test No. 8

IR

VISIBLE

Figure 6 26. Comparison Between IR and Visible Images - Test No. 10

and falling fragments are displayed in Figure 6.27 using the IR thermovision 2-5 micron wavelength scanning camera with a field of view 166 ft (50.6 m) high and 153 ft (46.6 m) across. A single vertically falling fragment, indicated by an arrow, was tracked for several seconds, and its average fall velocity and fall velocity history within the observation time interval were determined. This sequence of pictures was obtained approximately one minute after the start of the fire. The hot fragments are visible only in the infrared and are completely obscured by smoke in the corresponding visible light motion picture frames.

A hot fragment was tracked by the IR scanning thermovision camera, and its average vertical and horizontal velocities were determined. This fragment was located approximately 250 ft (76 m) above the ground and 320 ft (98 m) from the fire pool 115 sec after the start of the fire. The corresponding frames of the boresight visible light motion picture in Figure 6.28 show no trace of this fragment. Fragment position, as seen on the corresponding IR picture, is marked by a circle on the visible photograph.

LARGE SIZE JP-5 FIRE TESTS

The large JP-5 fire test data are presented for Test Nos. 11, 12, and 13 in this subsection. The 40 ft by 60 ft (12 m by 18 m) fire pool was located south of ground zero just off the test pad. Met and photography data is displayed for the time period after the start of the fire.

TEST NO. 11

The near surface wind data is shown in Figure 6.29 for Test No. 11 for the northeast met tower, the only met tower in operation for the large JP-5 fire tests. Average values for the entire ten minute period are also presented. Average wind speeds vary from 9.5 to 11.5 fps (2.9 to 3.5 mps), while average wind direction varied from 175° to 195° as measured from true north. Thus the winds were predominantly southerly.

Ambient temperature was found to 75°F (24°C). The following table provides specific values as a function of height:

Table 6.5. Ambient Temperature For Test No. 11

Height Above Ground (ft)	Temperature (°F)
3	75.3
18	74.4
28	74.3
38	74.2

Figure 6.30 shows continuous growth of the plume from Test No. 11 taken with the far west camera. Cloud dimensions will be displayed in Figure 6.36. The plume angle to the horizon varies with time. The leading edge angle, whic' is

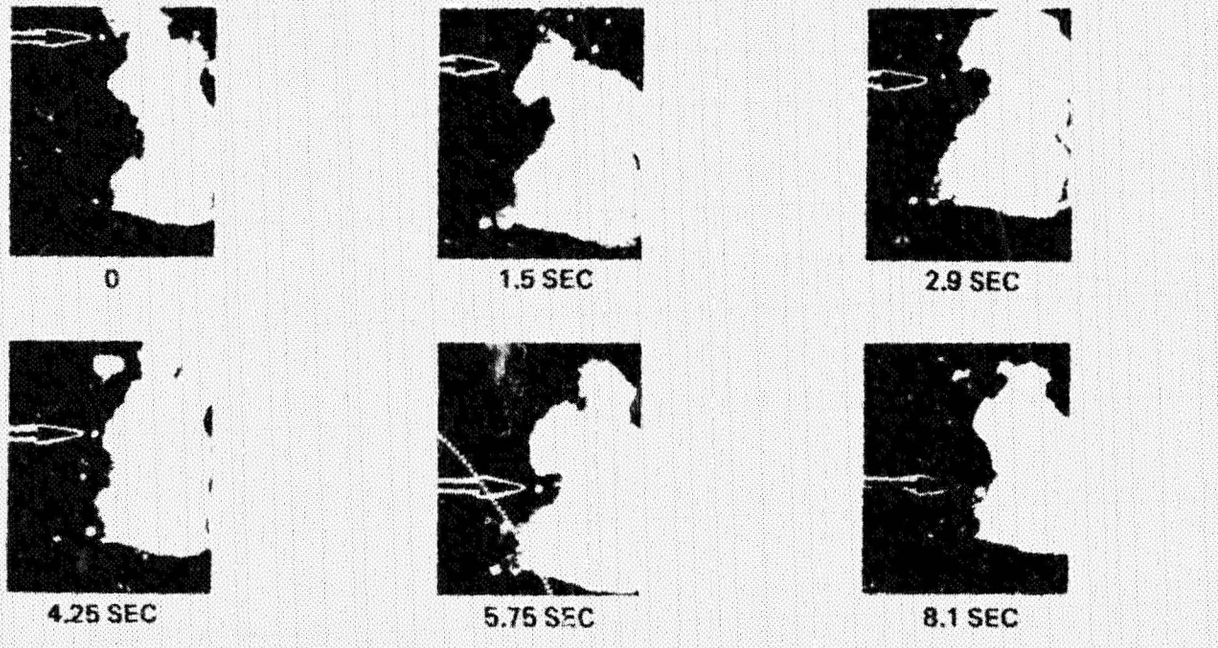

$V_{AVERAGE}$ = 8.2 FT/SEC

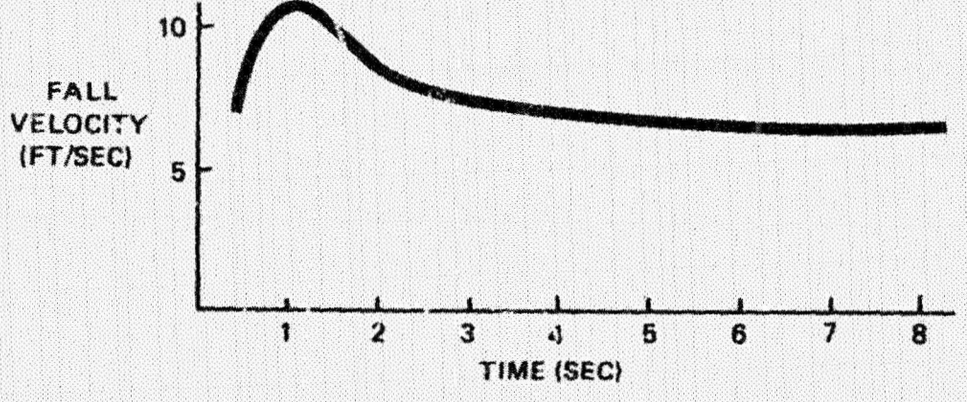

Figure 6.27. IR Imagery of Flying Barrel Debris Fallout - Test No. 10

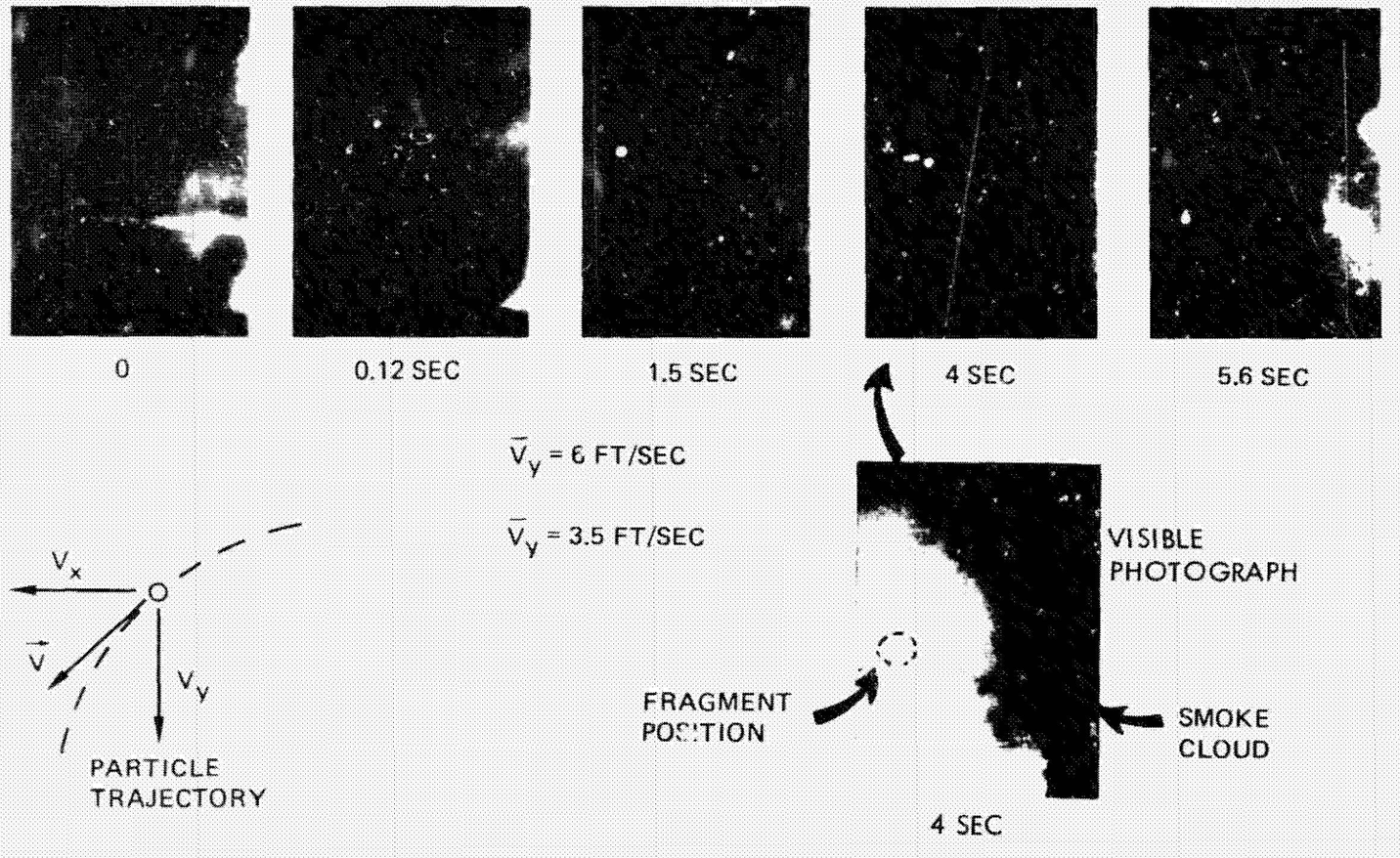

Figure 6 28. IR Measured Trajectory of Hot Fallout Fragment - Test No. 10

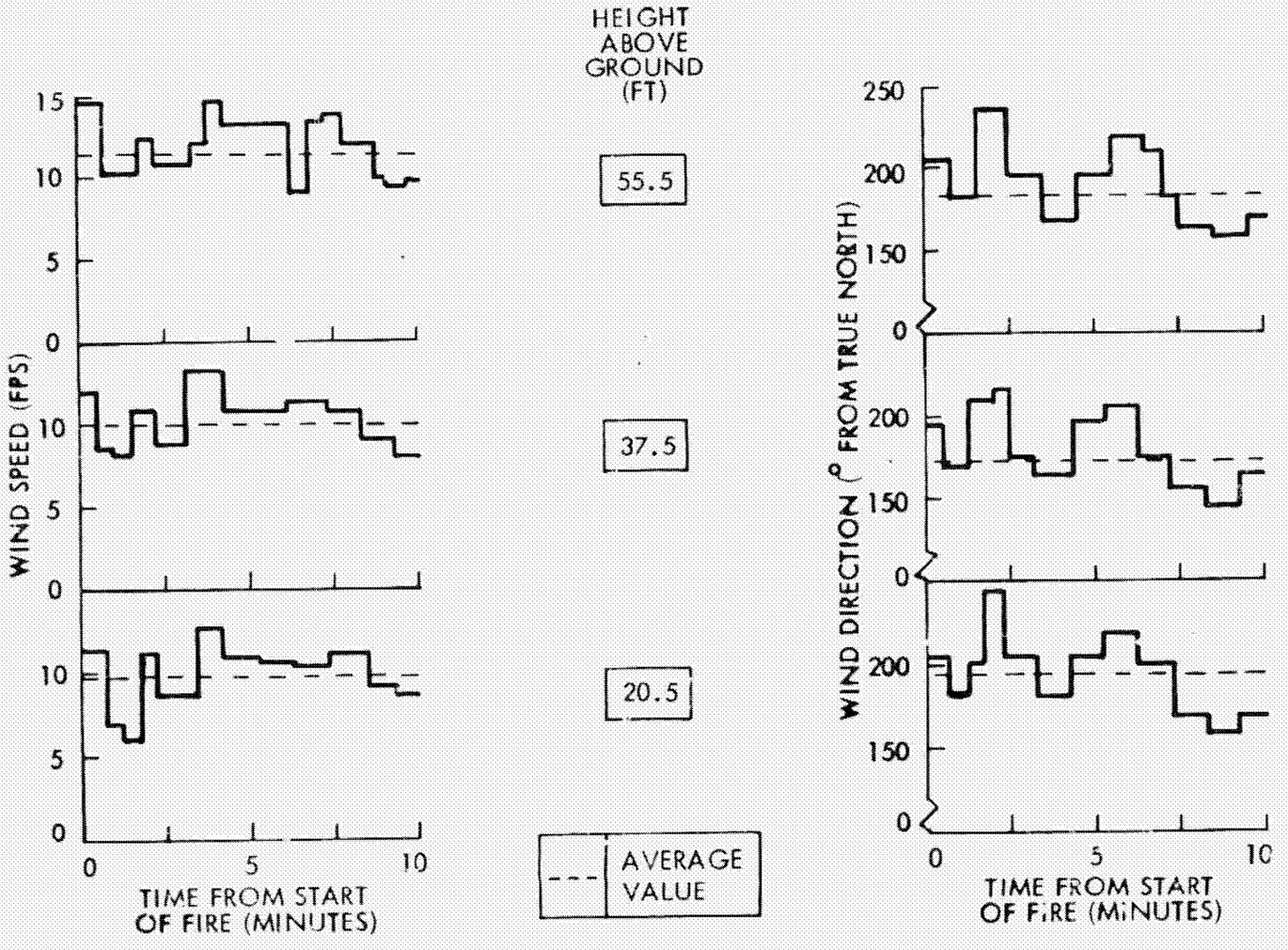

Figure 6.29. Near Surface Meteorology Data - Test No. 11

Figure 6.30. Far West Photography - Test No. 11

needed for south view analysis, was presented in Figure 6.1. The plume can be divided into 3 regions which are used when comparisons are made with LED measurements:

- an opaque white cloud at the top
- a dense black smoke region
- an optically thin smoke region below the main plume

No flame can be seen at this far west distance (3550 ft [1080 m]) from the pool center.

A grid has been overlayed on the photographs to permit easy reading of dimensions directly from the photograph, since the image to object transformation factor varies appreciably across the plume photograph. Radial lines are separated by 100 ft (30.5 m), with 200 ft (61 m) spacing beyond 3200 ft (976 m) from pool center. Later time far west photographs are displayed in Figure 6.31. The largest cloud which is attached to the pool is shown at 240 sec. Fire burnout is evident at 270 sec and later in time. The plume shows characteristics of a puff at 300 and 360 sec.

Plume growth is exhibited in Figure 6.32 from the far south camera 730 ft (222 m) south of the pool center. The plume oscillates about a vertical line in each picture. Flame can be seen in the lower portion of the picture. Maximum flame heights will be presented in Figure 6.38.

Grid overlays are shown for two leading edge angles, 52° and 66°. Selection of these angles are justified in Figure 6.1. For 52° radial lines are separated by 100 ft (30.5 m) starting with 50 ft (15.2 m), while 500 ft (152 m) spacing is used beyond 2050 ft (625 m) from pool center. For 52° transverse tic marks are spaced 100 ft (30.5 m) apart, with 1000 ft (305 m) spacing beyond 2050 ft (625 m) from pool center. For 66° radial lines are separated by 100 ft (30.5 m) starting at the pool center, while transverse tic marks are also spaced 100 ft (30.5 m) apart.

Later time far south photographs are presented in Figure 6.33. Plumes are very similar for 240 and 270 sec. Evidence of flame burnout is seen at 300 sec and beyond. The puff character is depicted at 300 sec.

The near south camera was located 360 ft (110 m) south of the pool center. The flame is readily seen in Figure 6.34. Grid overlays are shown for the same two leading edge angles as in the far south figures, 52° and 66°. Radial lines and transverse tic marks are separated by 10 ft (3 m).

Figure 6.35 shows later time photographs from the near south camera. Pool fire burnout appears to be just beginning at 270 sec. The plume is optically thinning out at 300 sec and is very thin at 360 sec. The Jacob's ladder with numerous vu-gr phs containing bridal veil for catching particulate matter is readily seen in these photographs.

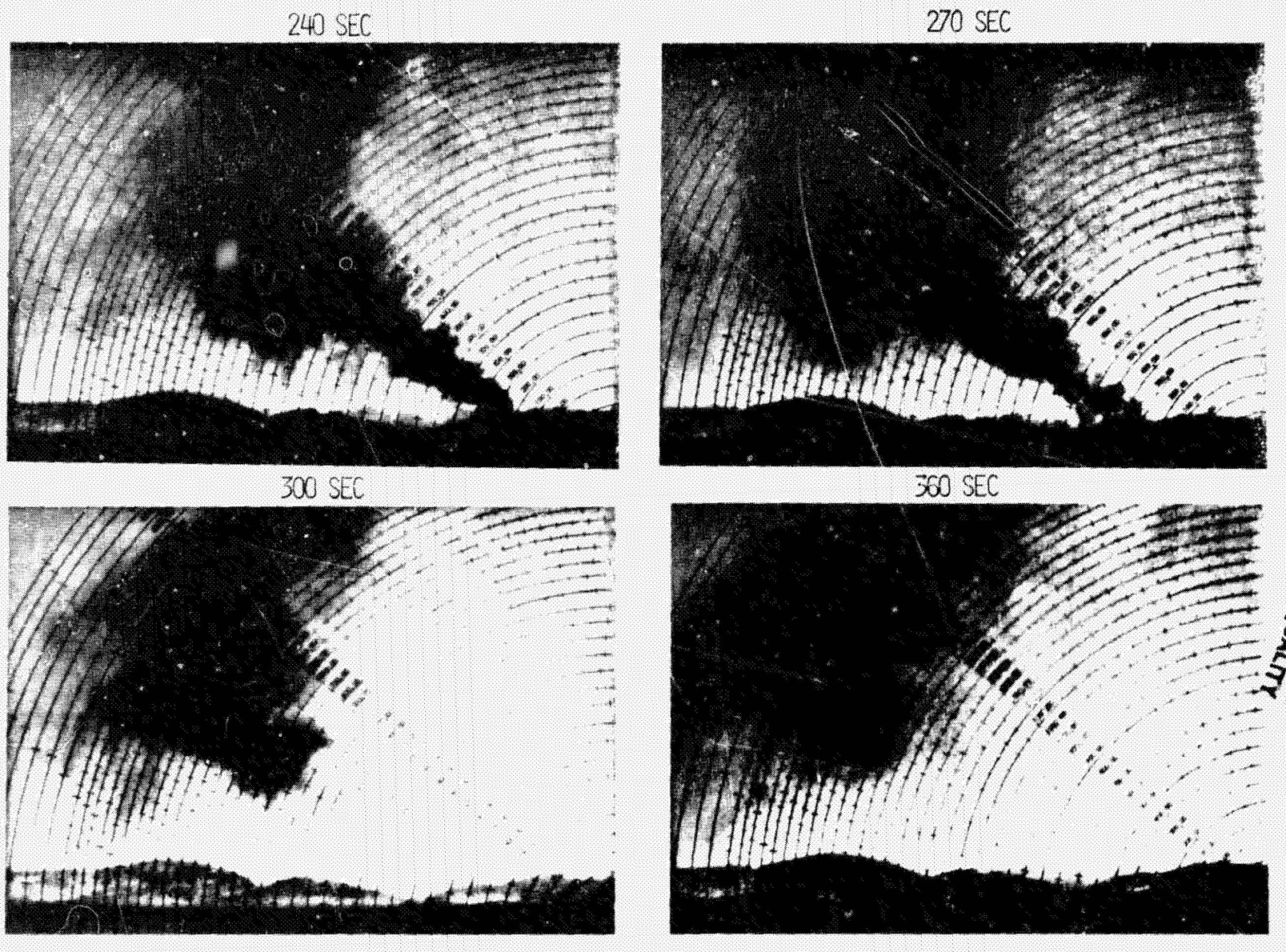

Figure 6 31. Far West Photography at Late Time - Test No. 11

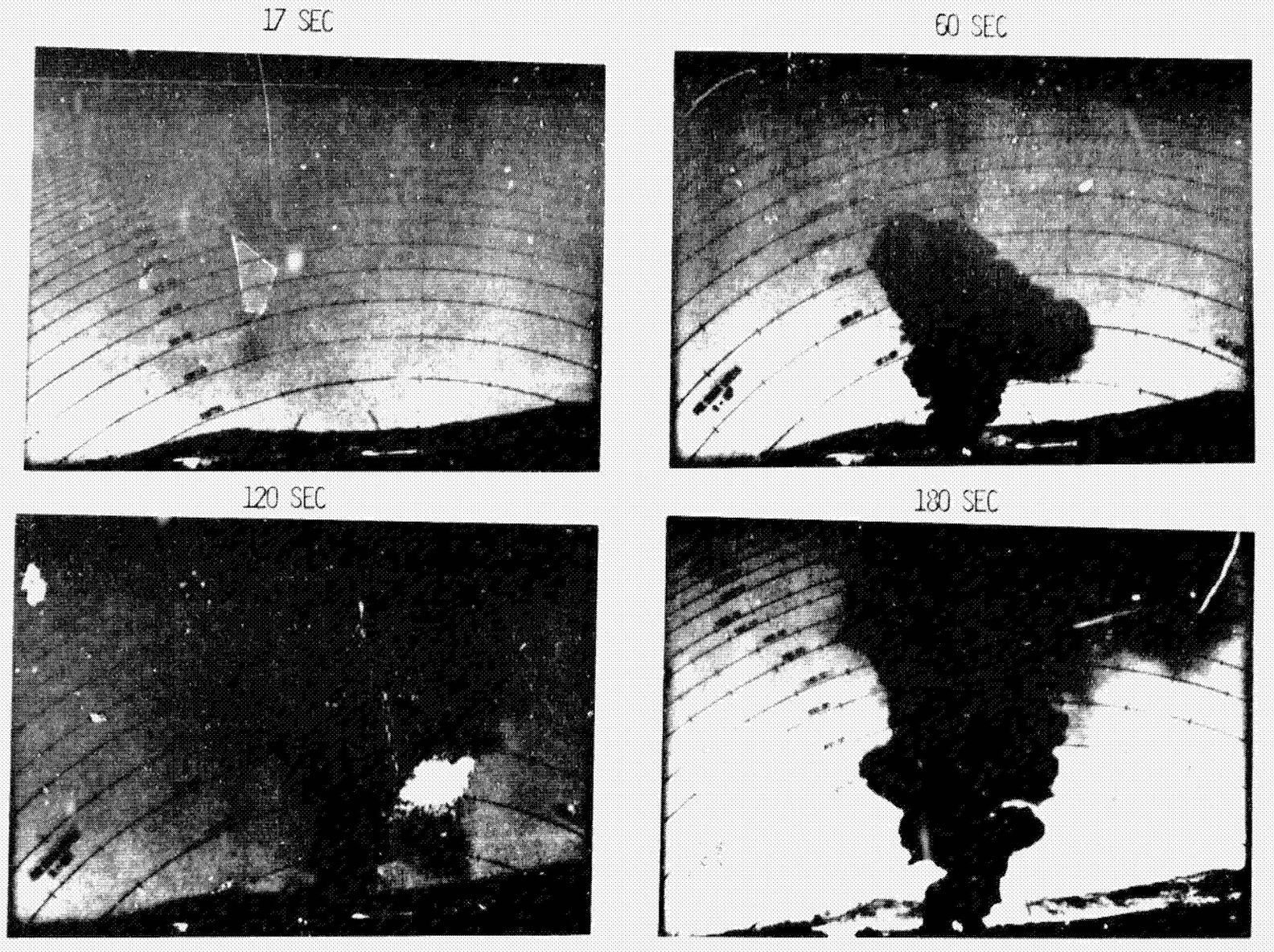

Figure 6.32. Far South Photography - Test No. 11

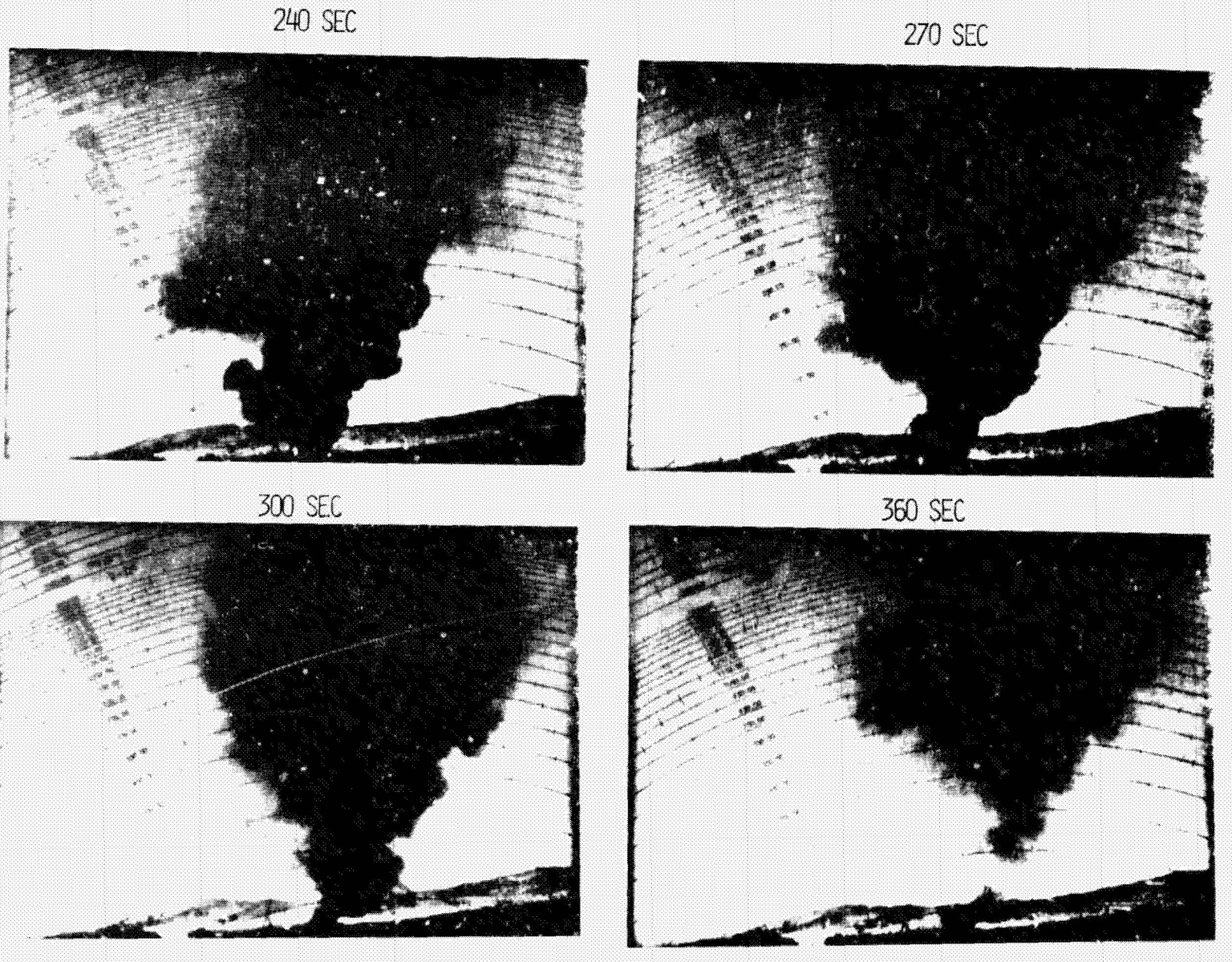

Figure 6 33. Far South Photography at Late Time - Test No. 11

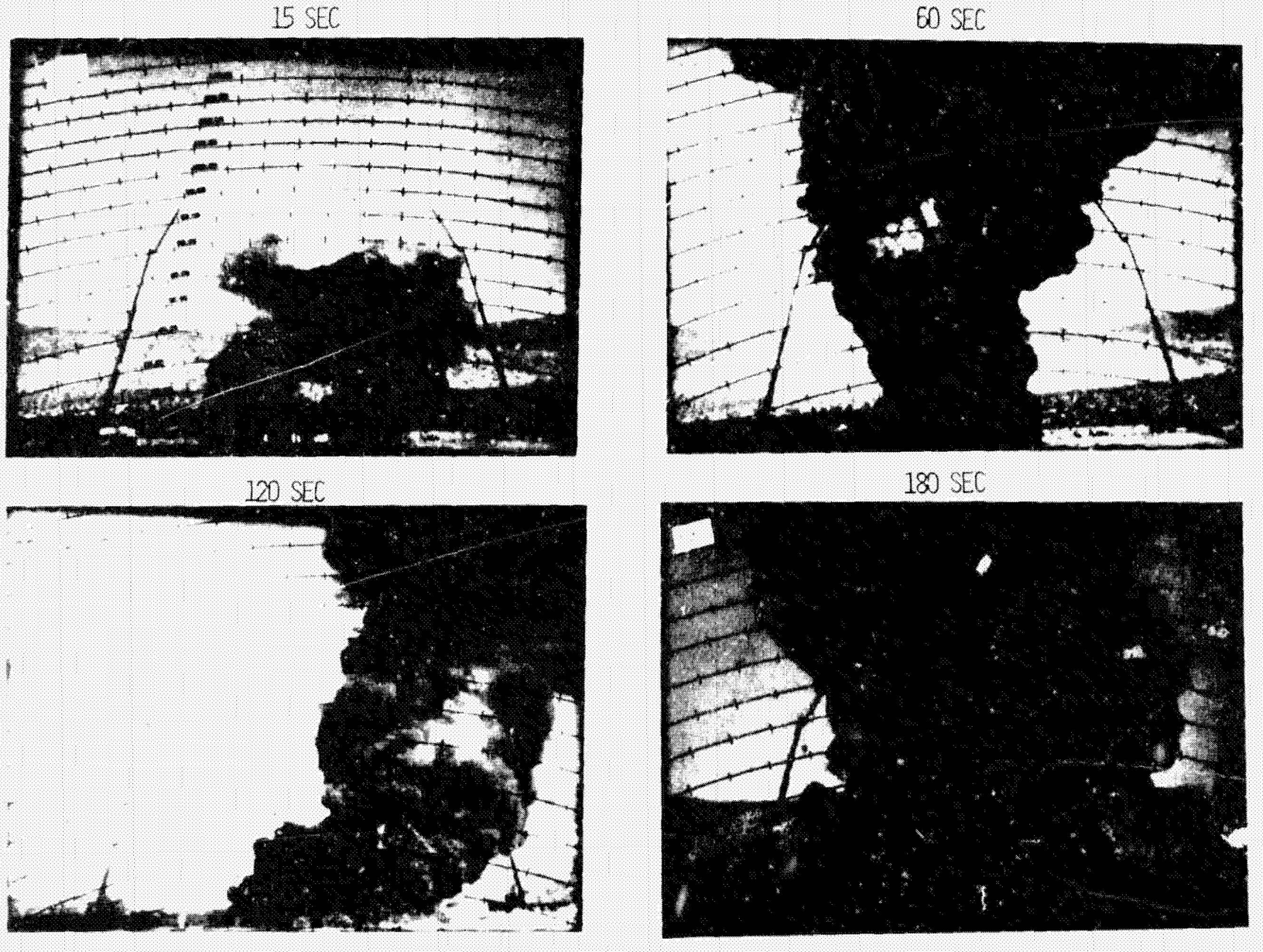

Figure 6.34. Near South Photography - Test No. 11

240 SEC

270 SEC

300 SEC

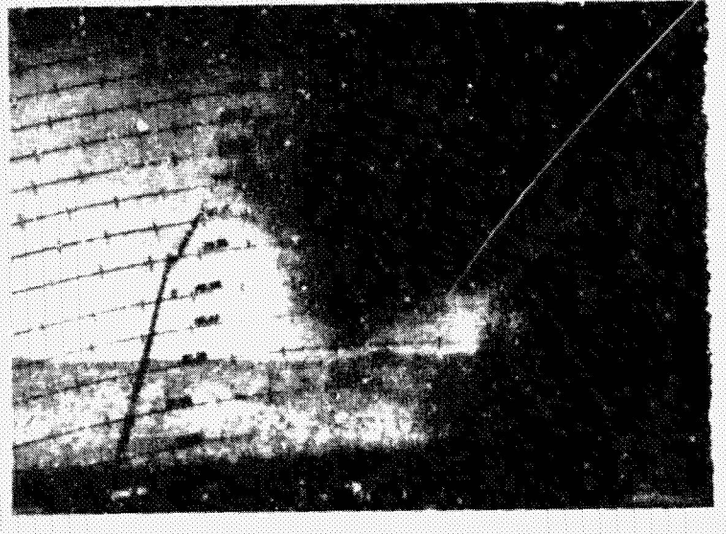

360 SEC

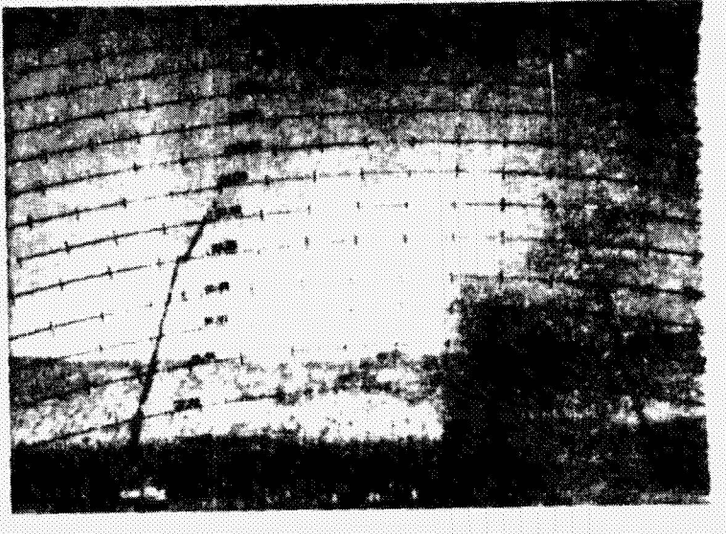

Figure 6.35. Near South Photography at Late Time - Test No. 11

Plume heights and horizontal distances are displayed as a function of time after start of fire in Figure 6.36. For plume heights the maximum height and maximum height along dense smoke centerline are presented. The last 2 centerline points represent an uncertainty in defining the centerline. The maximum height levels off at about 3000 ft (1000 m).

For horizontal distance the maximum distance, neglecting the optically thin smoke region, and distance corresponding to the maximum height along the dense smoke centerline are shown. The largest horizontal distance goes out to approximately 3300 ft (1100 m) from the pool center.

Flame speeds for Test No. 11 are depicted in Figure 6.37. Only a few flame speed data points were taken from the near west view. The vertical component of velocity averages 25 fps (7.6 mps). Considerably more data was taken from the near south view, with an average vertical component of 31 fps (9.5 mps). These two values compare quite well.

Maximum flame heights were observed at the south periphery of the plume when not obliterated by smoke and are plotted in Figure 6.38. Flame height increases with time from start of fire, with the central band varying from 70 to 115 ft (21 to 35 m) above the pool center. After burnout begins, maximum heights drop to about 20 ft (6.1 m) approximately 300 sec after start of fire.

Figure 6.39 compares the vertical component of velocity for smoke puffs as seen from three views. The near west view yields an average value of 15 fps (4.6 mps). Only a few data points were taken from the near south view, which resulted in an average value of 32 fps (9.8 mps). Numerous data points from the far south view produced an average vertical velocity component of 43 fps (13 mps). Thus considerable variation in smoke speed can be observed, depending on camera view. The far south smoke speed is also displayed in Figure 6.40, together with a plot of smoke speed versus height at which the speed was measured. Any analytical fit to this height profile would be quite arbitrary.

When viewed from the south, smoke puffs are observed to rotate about an axis to the east, as sketched in Figure 6.41. In some instances the axis is either inclined downward 20 to 30 degrees or directed to the south. The period for rotation is shown to average about 1.25 sec with variations of a factor of 2.

A plot of vortex center height versus vortex outer speed on the periphery of the smoke puff shows a definite trend. Outer speed increases with height, with values calculated to be as high as 600 fps (183 mps).

IR imagery was used to track four horizontally moving fragments as summarized in Figure 6.42. The average horizontal velocities vary from 6 to 15 fps (2 to 4.5 mps).

TEST NO. 12

Near surface wind data for Test No. 12 is displayed in Figure 6.43 for the northeast met tower. Average wind speeds over the 10 minute period after start

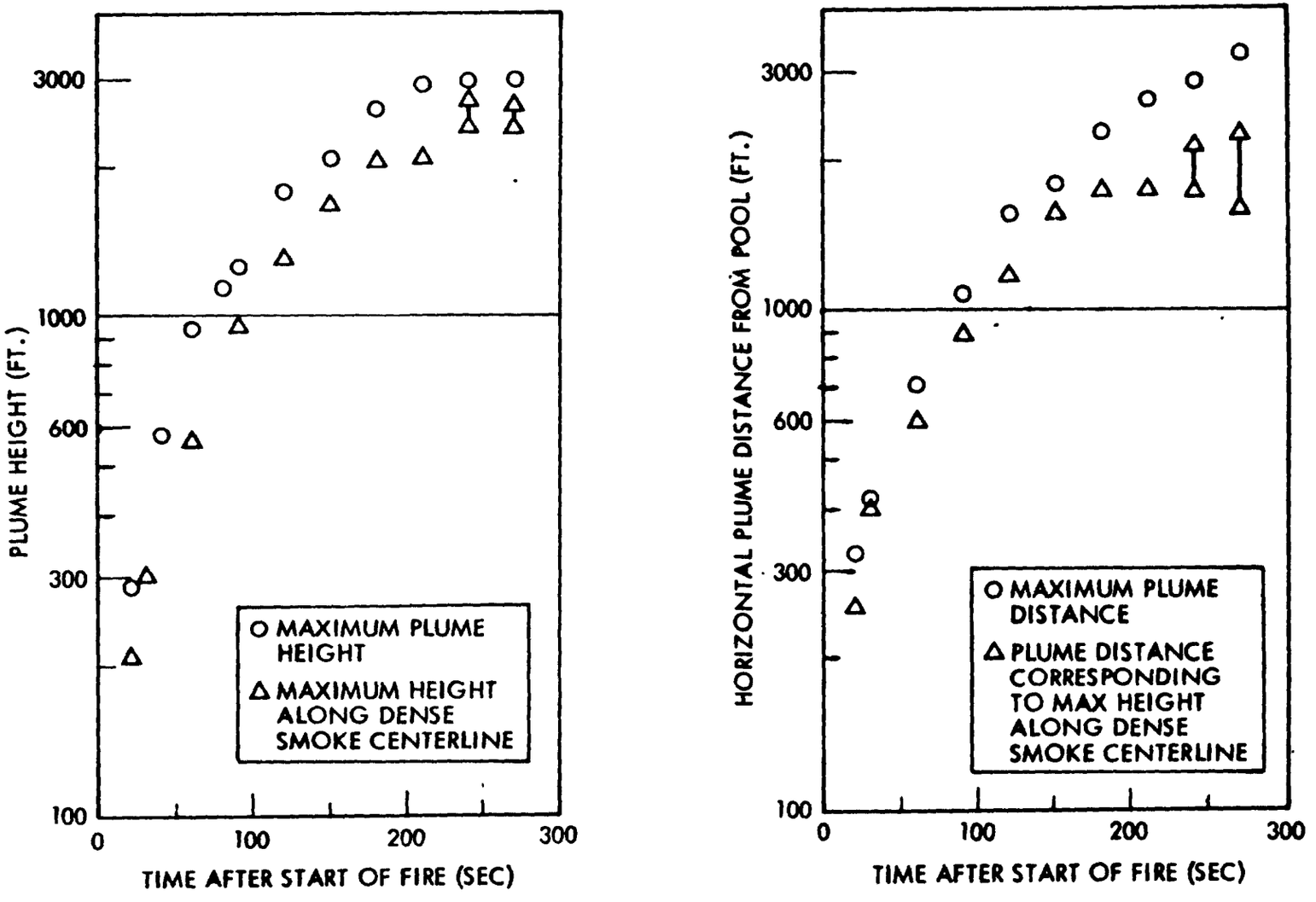

Figure 6.36. Plume Height And Displacement History - Test No. 11

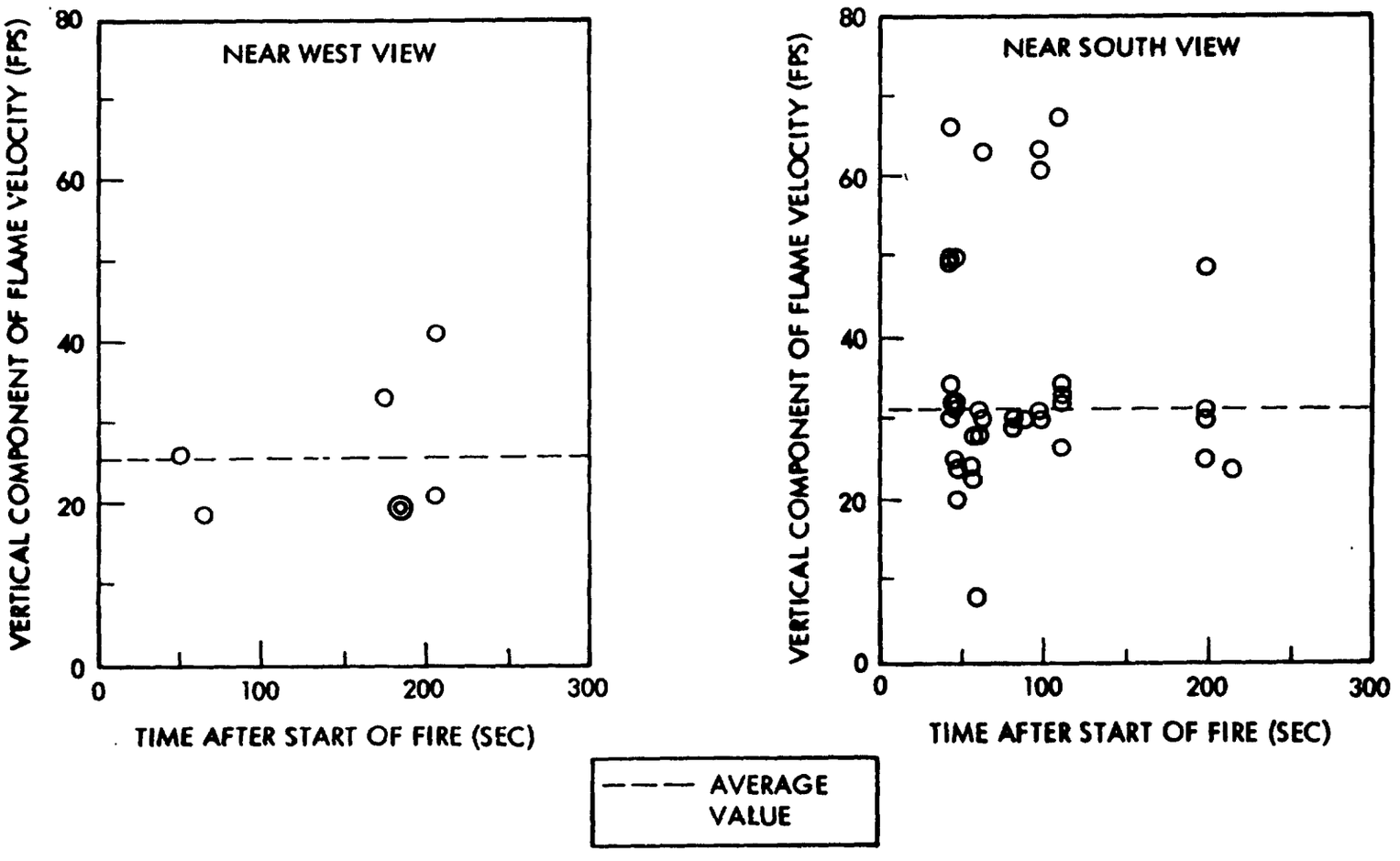

Figure 6.37. Flame Rise Speeds - Test No. 11

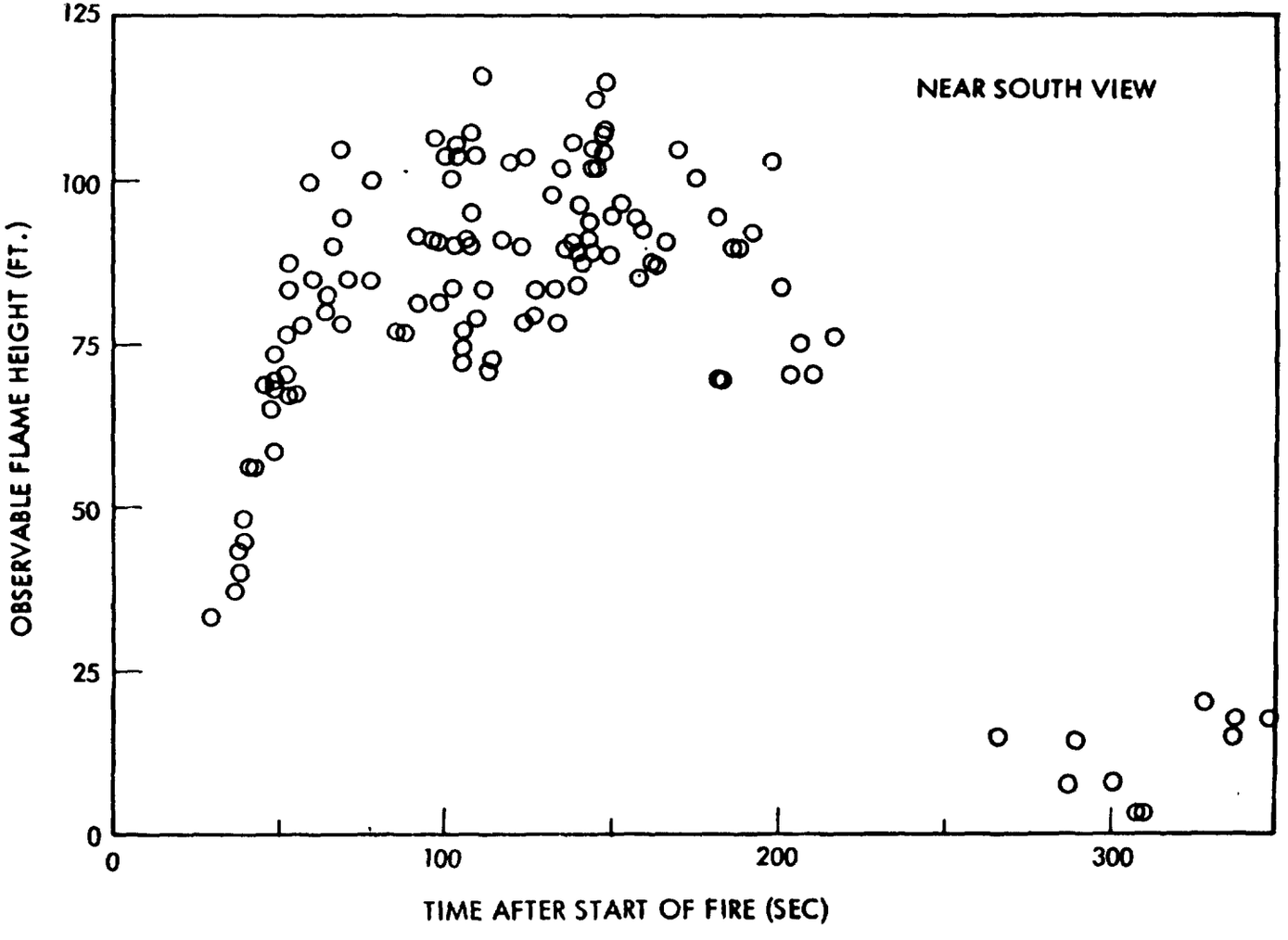

Figure 6.38. Flame Heights - Test No. 11

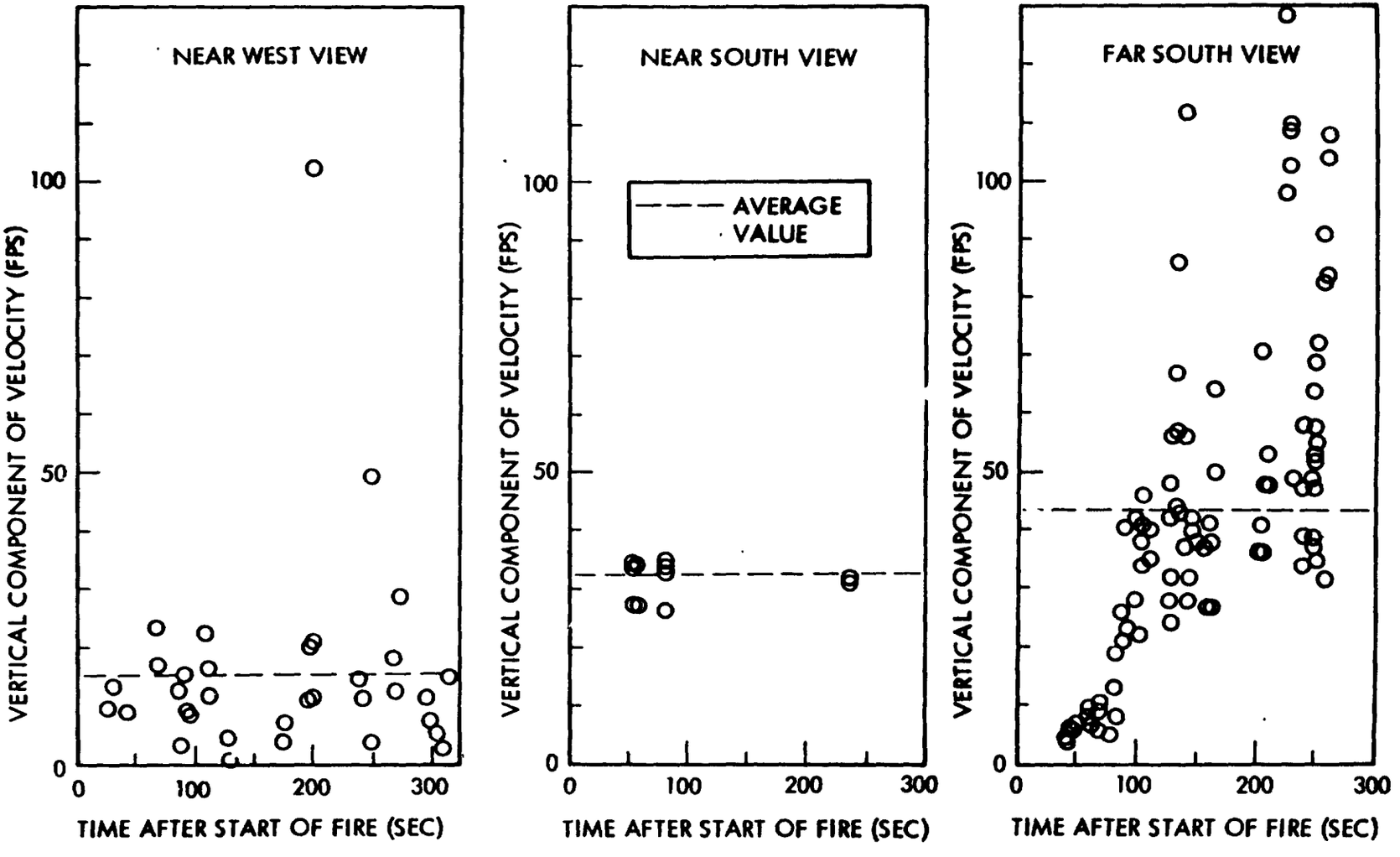

Figure 6.39. Smoke Rise Speeds - Test No. 11

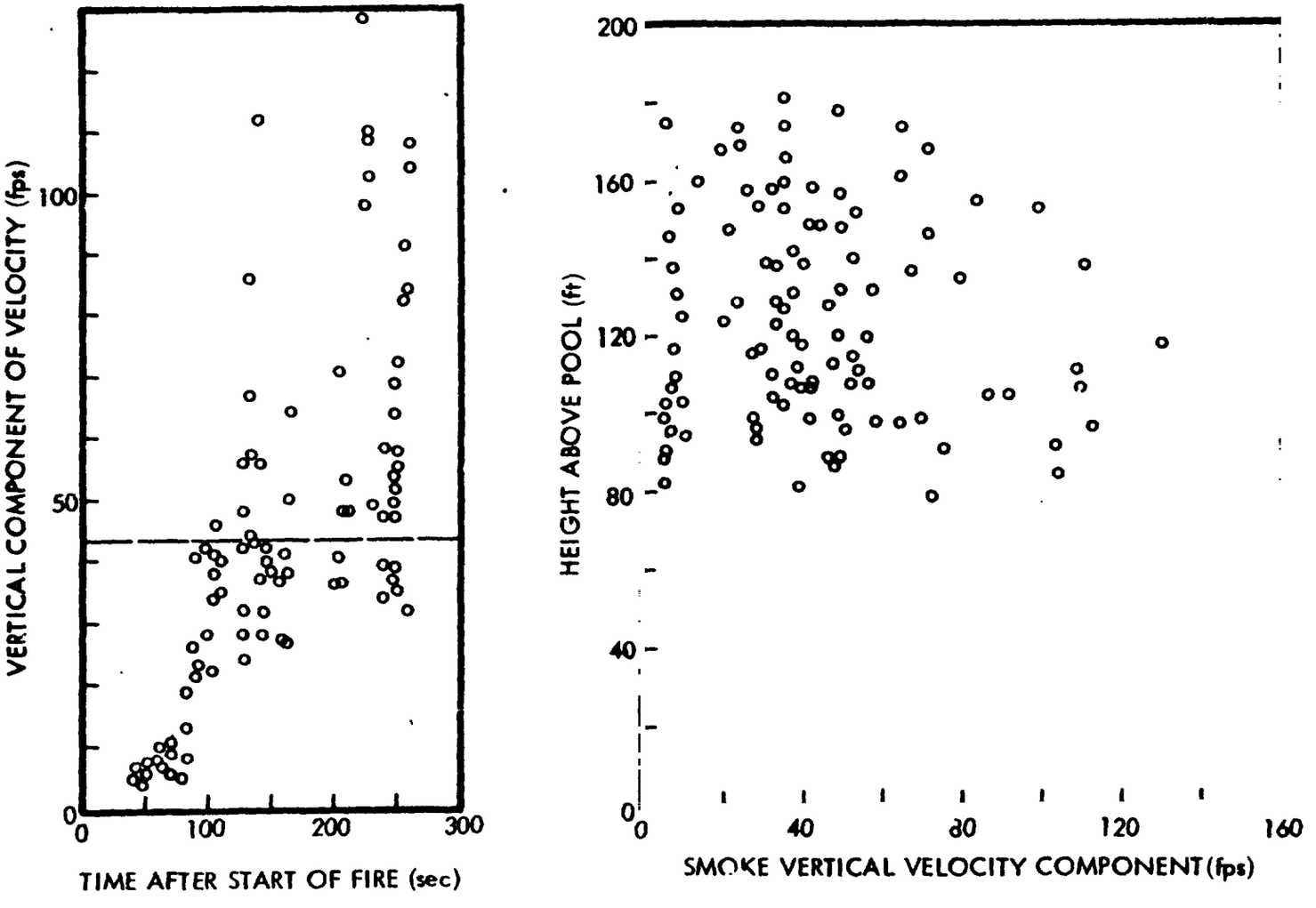

Figure 6.40. Smoke Rise Speeds, Downwind View - Test No. 11

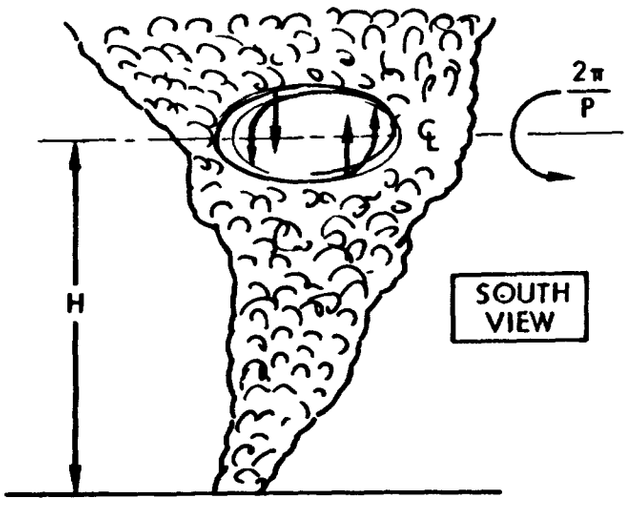

H - HEIGHT OF VORTEX CENTER ABOVE GROUND (FT.)

P - ROTATIONAL PERIOD (SEC)

S - LATERAL SIZE OF VORTEX (FT.)

T - TIME AFTER START OF FIRE (SEC)

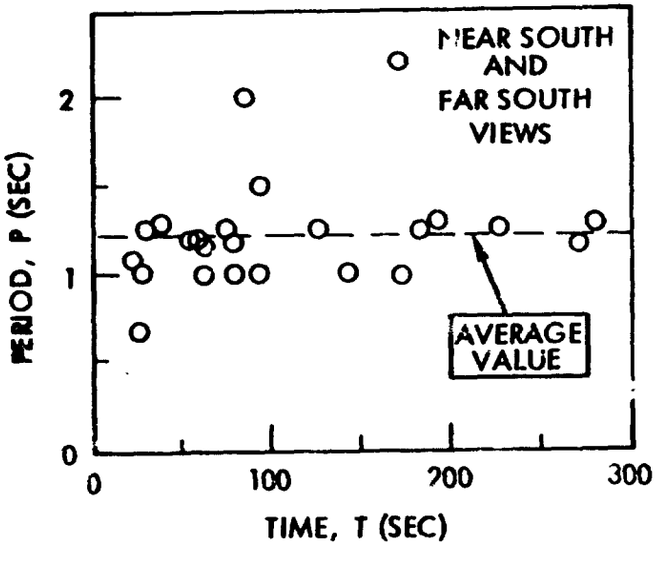

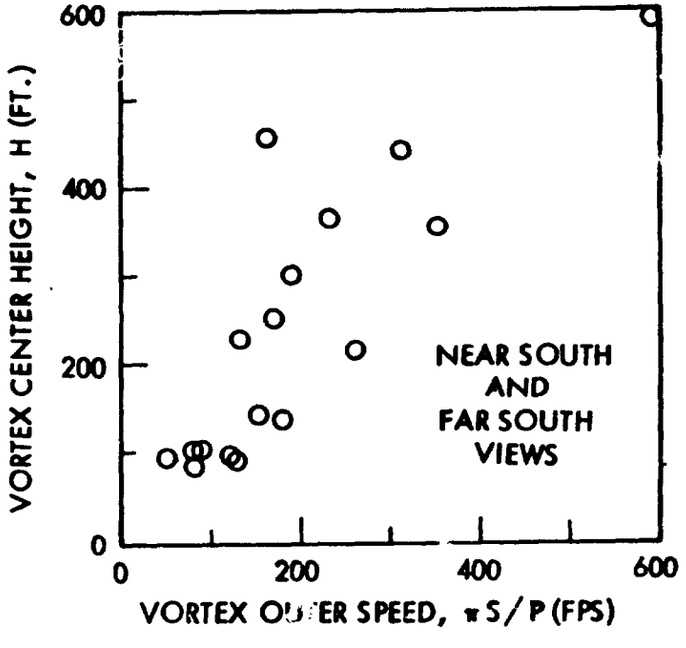

Figure 6.41. Smoke Rotational Motion - Test No. 11

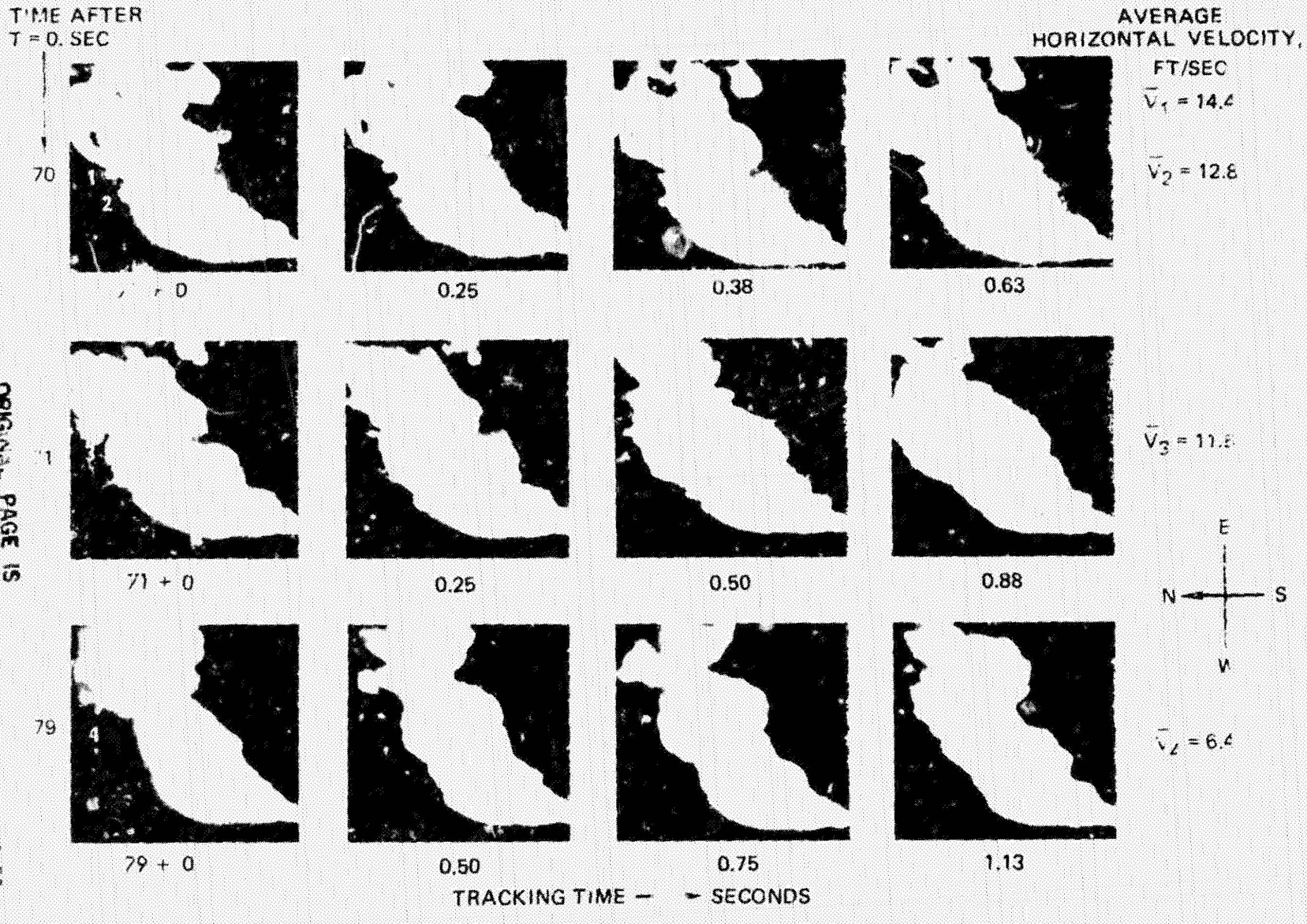

Figure 6.42. IR Display of Horizontally Moving Fragments - Test No. 11

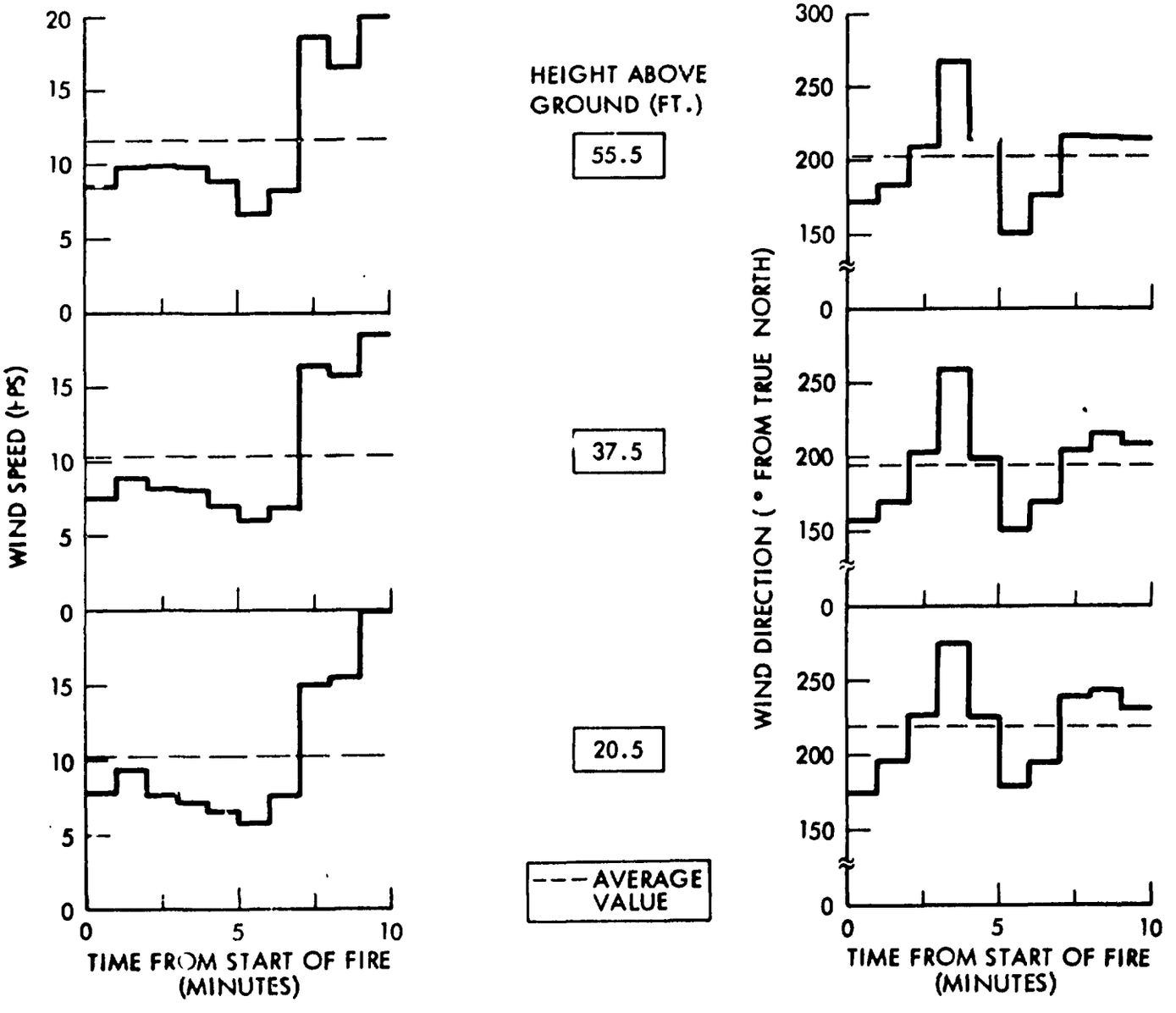

Figure 6.43. Near South Meteorology Data - Test No. 12

of fire vary from 10 to 12 fps (3 to 3.7 mps). Note that the speed is below 10 fps (3 mps) until 7 minutes after fire start, where it jumps to over 15 fps (4.6 mps) for the remainder of the 10 minute period. Average wind direction varied from 195° to 220° as measured from true north, with direction changing by about 120° over the 10 minute period.

Ambient temperature was measured at 81°F(27°C). Specific values for several heights are as follows:

Table 6.6. Ambient Temperature For Test No. 12

Height Above Ground (ft)	Temperature (°F)
3	81.9
18	80.7
28	80.4
38	80.2

Maximum plume heights are displayed in Figure 6.44 as a function of time after start of fire; both observable absolute maximum heights and maximum heights along the dense smoke centerline are presented. Results are shown for the initially observed smoke plume and for a portion of the plume which "breaks through" the initial plume and rises above it. After 100 sec only the "breakthrough" plume is observed. For the last three times shown, the plume peaked above the camera view frame, and coinciding estimates of these two types of plume maxima are presented. These estimates should be reasonably valid within the error bars shown. It is seen that the estimated maximum plume heights for $t \approx 340$ sec is of the order of 4400 ft (1340 m).

The essentially northward horizontal displacements from ground zero of the maximum plume heights are plotted in Figure 6.45 as a function of time. The horizontal displacements of both the absolute plume maxima and of the (highest) end point along the dense plume centerline are shown for both the early plume and "breakthrough" plume described above. The plotted data were reduced from pictorial information obtained from the far west camera by the same procedure as that used to obtain the corresponding maximum vertical heights. The last three time points shown again are extrapolations with wide error bars, since the actual plume maxima were imaged above the view camera frame. For the later times the growing plume also was propagated horizontally appreciably outside of the view frame.

Figure 6.45 plots some observed flame heights and corresponding calculated vertical flame velocities for Test No. 12. The flame puffs selected for observation were restricted to those which were most clearly distinguishable from smoke obscuration and represented characteristic height maxima for their time intervals.

IR data for Test No. 12 is not presented here because of poor quality images for this particular test.

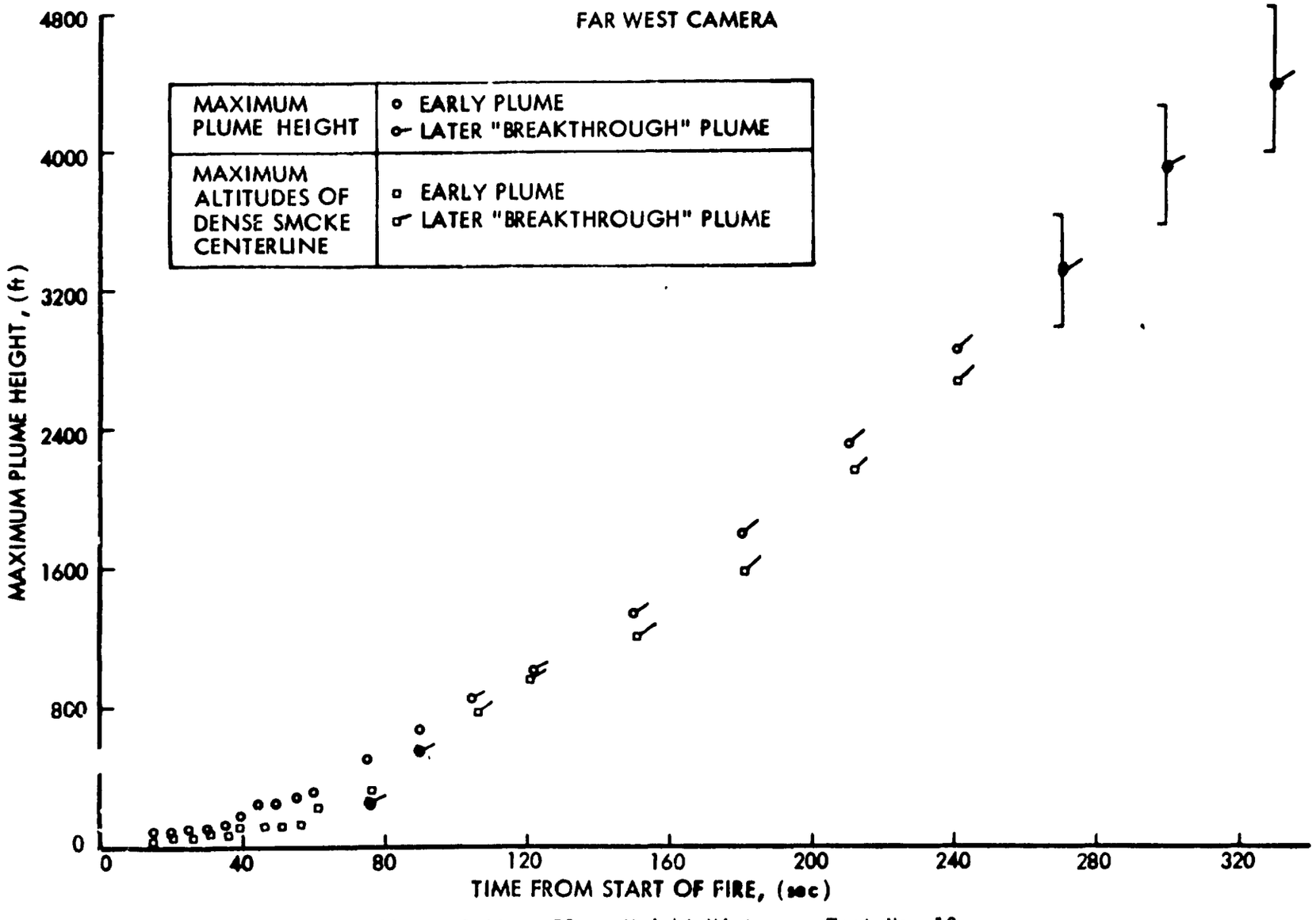

Figure 6.44 Plume Height History - Test No. 12

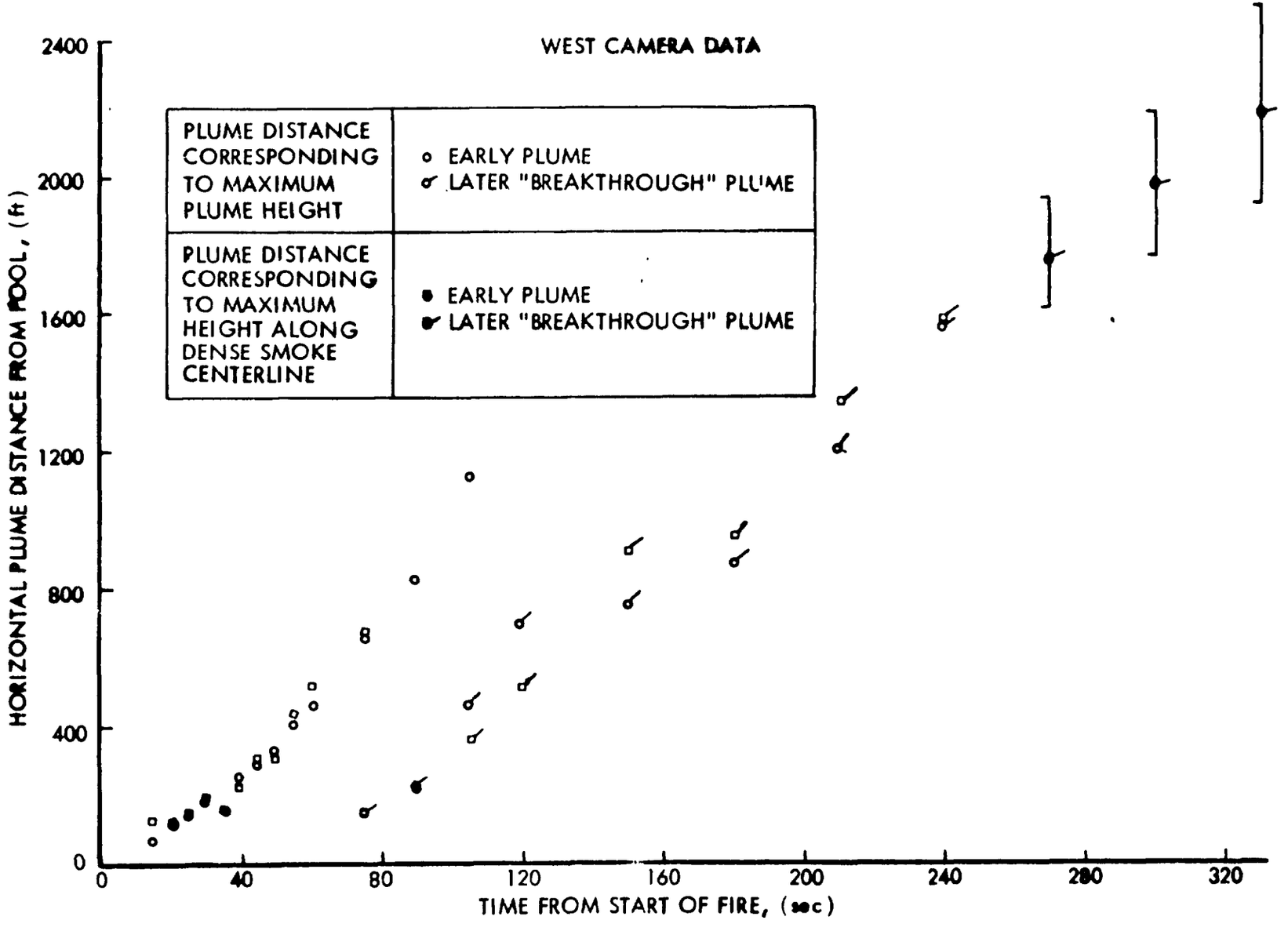

Figure 6.45. Plume Horizontal Displacement History - Test No. 12

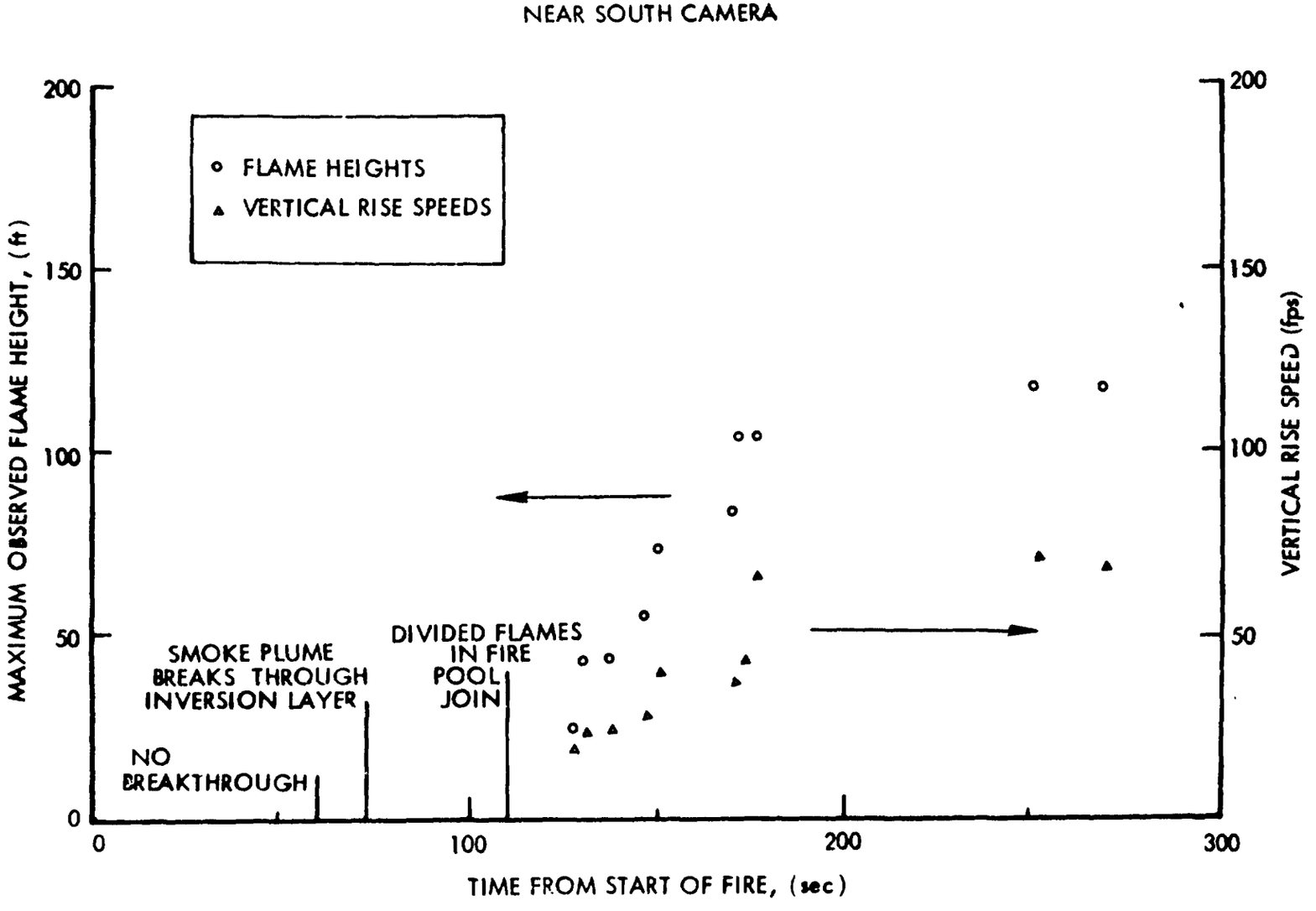

Figure 6.46. Flame Speeds and Rise Speeds - Test No. 12

TEST NO. 13

Near surface wind data for Test No. 13 is shown in Figure 6.47 for the northeast met tower. Average wind speeds vary from 11.5 to 13 fps (3.5 to 4 mps). The speed generally decreased with time after start of fire, except for a gusting period from 5 to 7 minutes after fire start. Average wind direction varied from 155° to 175° as measured from true north, indicating the winds were predominantly southerly (blowing from south to north).

Ambient temperatures were found to be 70°F (21°C). The following table presents specific values as a function of height:

Table 6.7. Ambient Temperature For Test No. 13

Height Above Ground (ft)	Temperature (°F)
3	71.5
18	70.2
28	70
38	69.8

Reduced data for plume heights and horizontal distances from the center of the fire pool are displayed in Figure 6.48 as a function of time after start of fire. For plume heights the overall maximum height and also the maximum height along the dense smoke centerline are presented. Both the top of the plume and the far end of the centerline project out of the camera image frame after approximately 200 sec. By 210 sec both the plume height maxima and its horizontal displacement from the fire pool center are greater than approximately 2500 ft (760 m), and still rising and receding. The horizontal displacements plotted in the figure correspond to the positions of the overall plume maxima, neglecting some tenuous optically thin smoke regions, and to the positions of maximum height along the dense smoke centerline.

The peak flame heights recorded in Figure 6.48 were determined from near south camera images. The top of the camera view frame is interpreted to lie between 109 and 114 ft (33 to 35 m) high. Several of the flame pulses observed in the time interval between 100 and 320 sec after fire pool ignition were observed to rise through the top of the view frame. Most of the observed flames are only transiently visible, since they tend to be obscured by opaque black smoke during most of their rise and decay. The figure plots height maxima for selected flame pulses which were judged both to be fairly characteristic of upper bounds for their occurrence time interval and to be non-obscured by smoke during the peak of their rise.

Figure 6.50 plots vertical flame rise velocities for the observed flame pulses presented in Figure 6.49. The points on (or very nearly on) the same vertical generally correspond to the velocity decay of the same rising flame pulse. With finer time scale, the velocities of such a flame pulse would be seen to

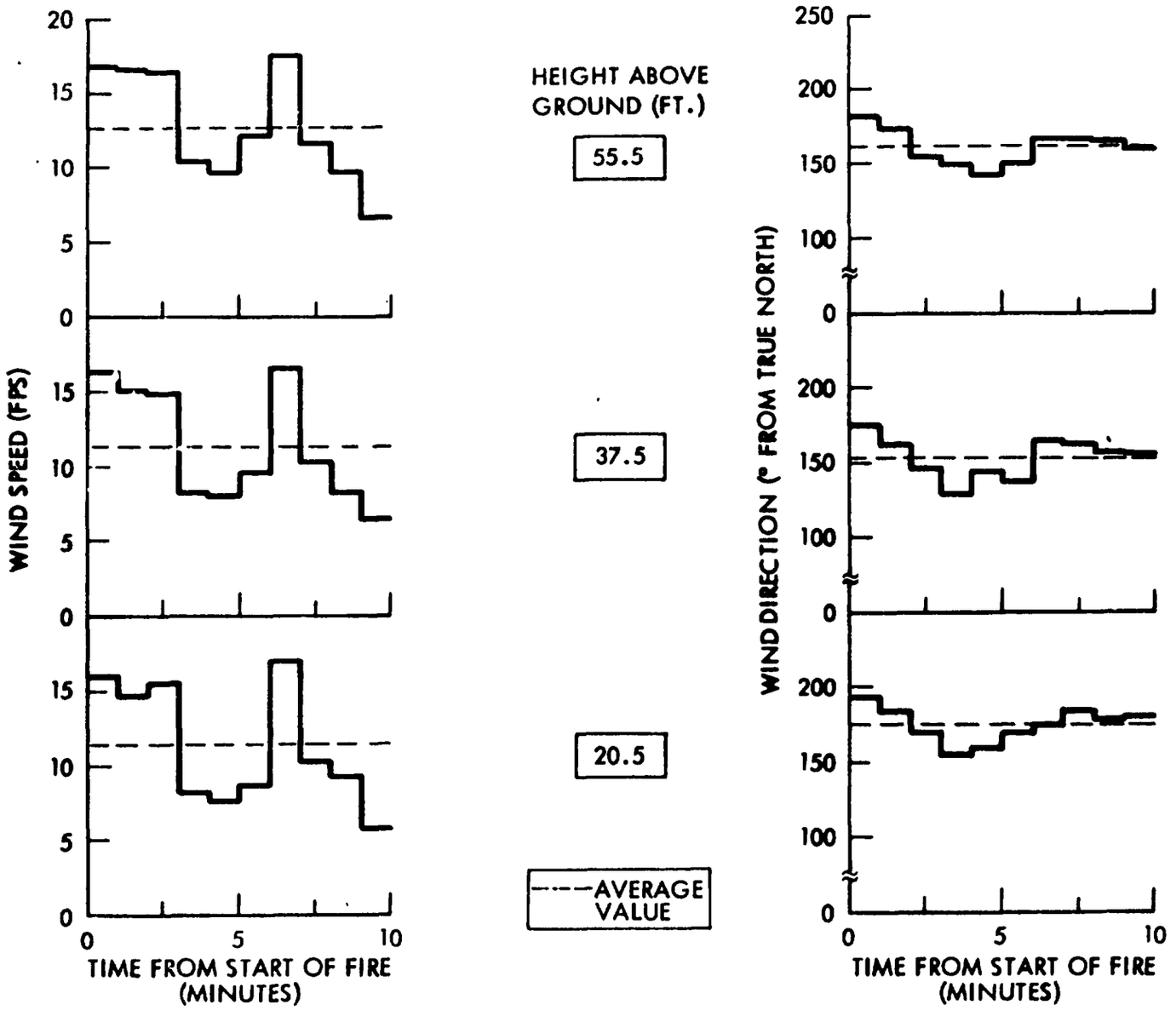

Figure 6.47. Near Surface Meteorology Data - Test No. 13

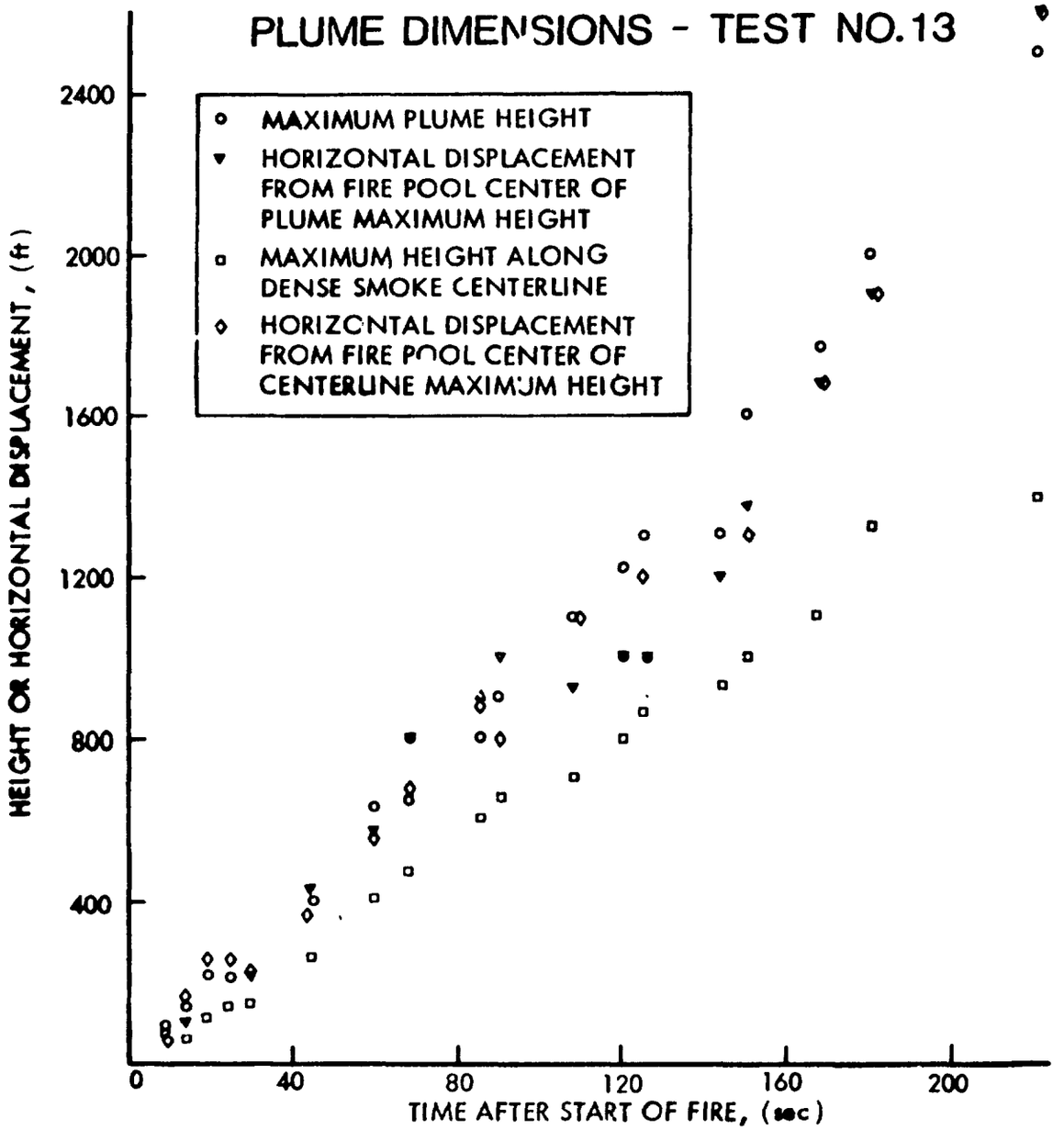

Figure 6.48. Plume Height and Displacement History - Test No. 13

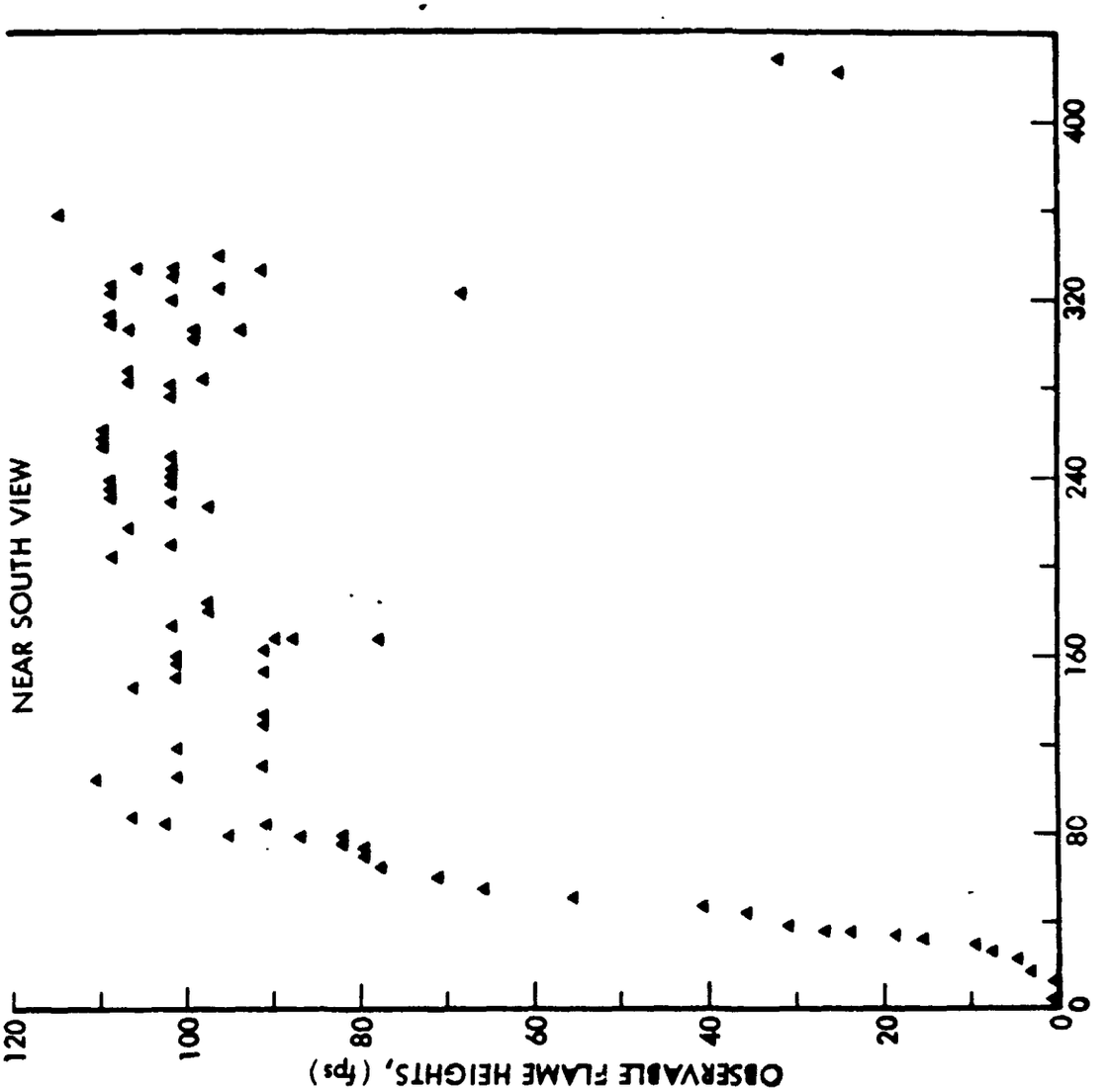

Figure 6.49. Flame Heights - Test No. 13

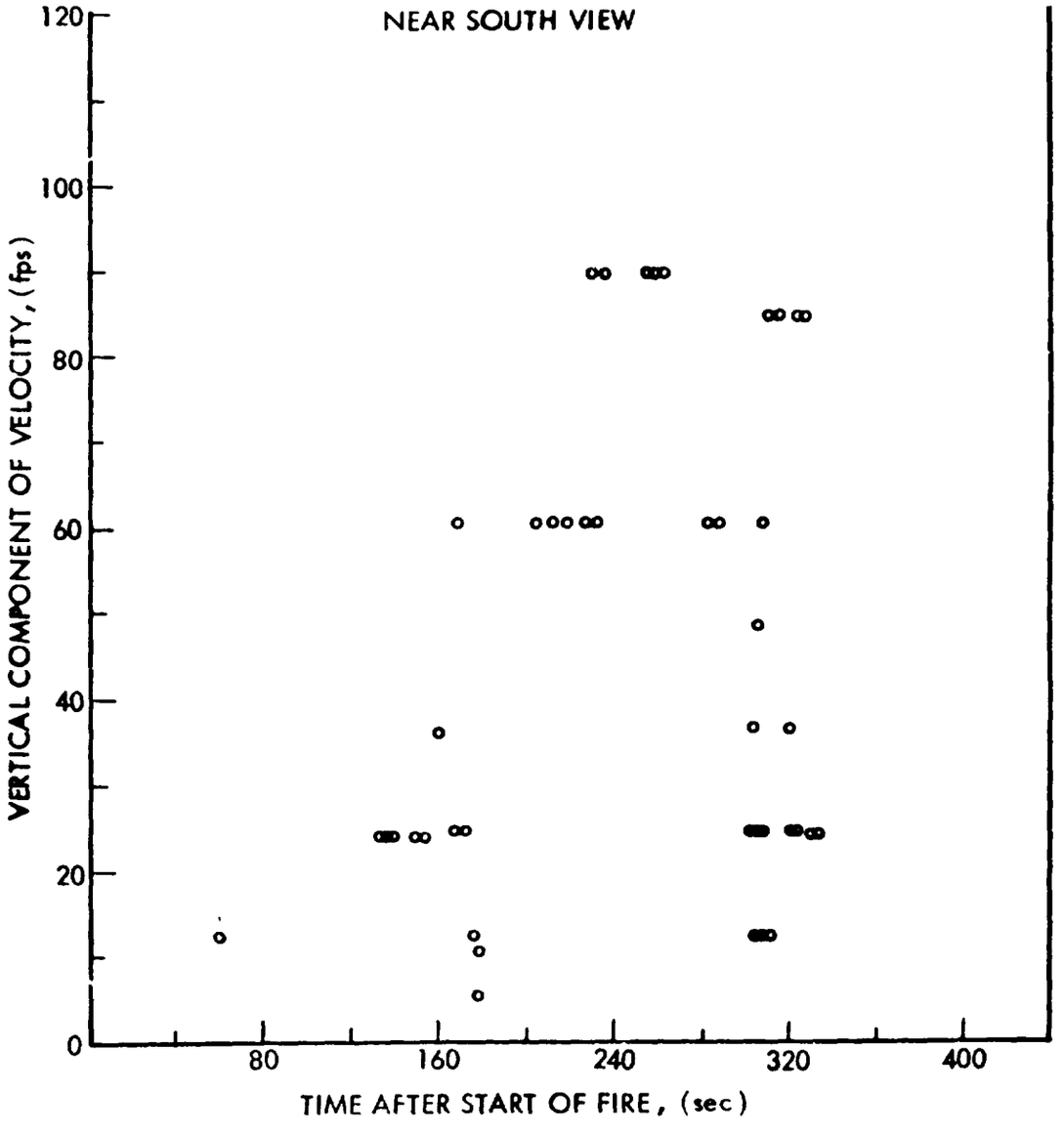

Figure 6.50. Flame Rise Speeds - Test No. 13

decrease, with increasing time, as the pulse rises. It can be seen that peak flame velocities exceeding 160 fps (49 mps) were observed between 220 and 330 sec after fire pool ignition.

Composite material fragments lofted by hot combustion gases and air during Test No. 13 were imaged by the IR scanning camera in the 2-5 micron wavelength band as shown in Figure 6.51. The time of occurrence is given in seconds after the start of the fire. The first particle image appears on the screen approximately 100 sec after the start. The total burn duration was approximately 360 sec.

IR thermograph particle tracking in the JP-5 pool fire plume for Test No. 13 is shown in Figure 6.52. The particle being tracked, which presumably is trapped in an entrained air volume, is identified by an arrow in each of the successive frames. The table inset in Figure 6.53 shows the times and velocities measured in the smoke plume for a particle moving from A to A'. The particle presumably was trapped in an entrained air volume. The drawing inset shows the distance of the IR scanning camera from the particle being tracked, and the optics of the camera which determines the field of view. The time between pairs of selected frames and the distances between A and A' in these frames yield the particle velocity.

The fragment of a cockpit lofted by hot gases is tracked for 3.5 sec by the IR scanning camera with results summarized in Figure 6.54. The fragment's velocity has two components, the vertical due to free fall and the horizontal due to wind drag. Average values are shown in the figure.

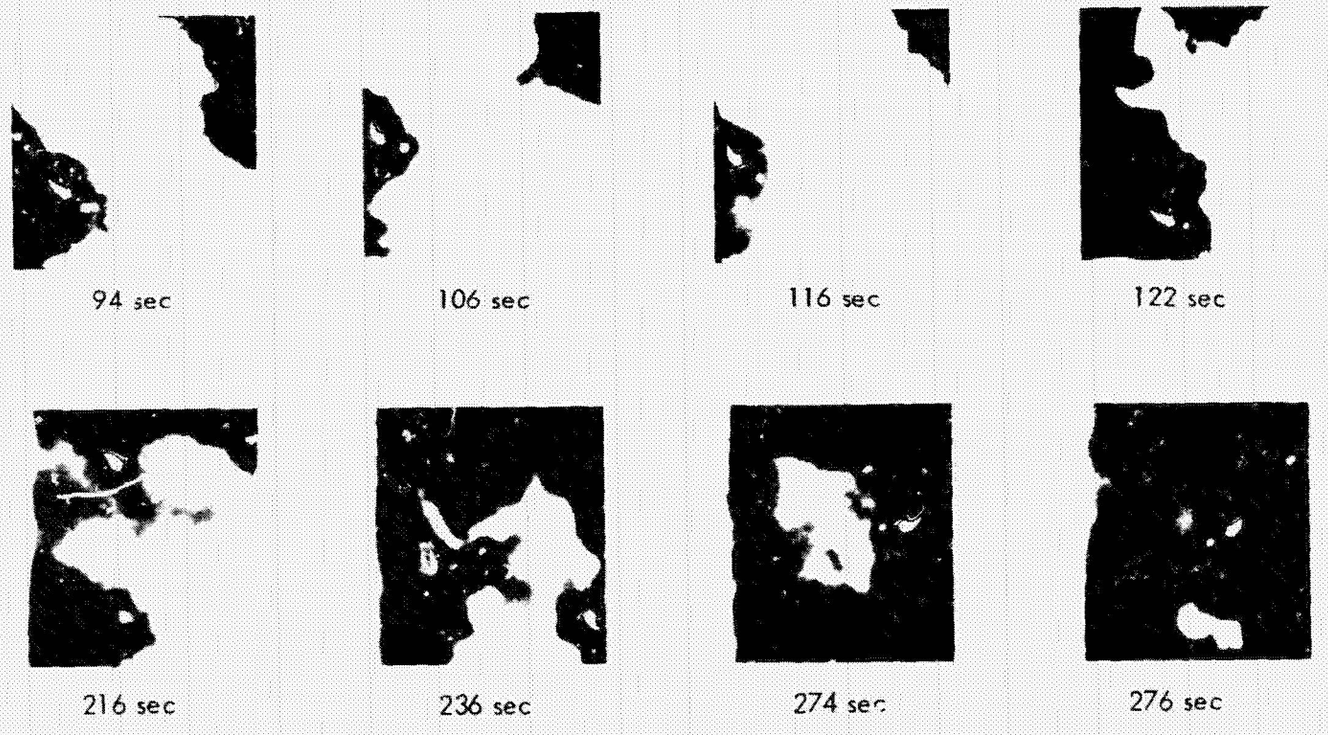

Figure 6 31. IR Thermovision Images of Falling Cockpit Debris - Test No. 13

Figure 6 52. IR Thermograph Particle Tracking - Test No. 13

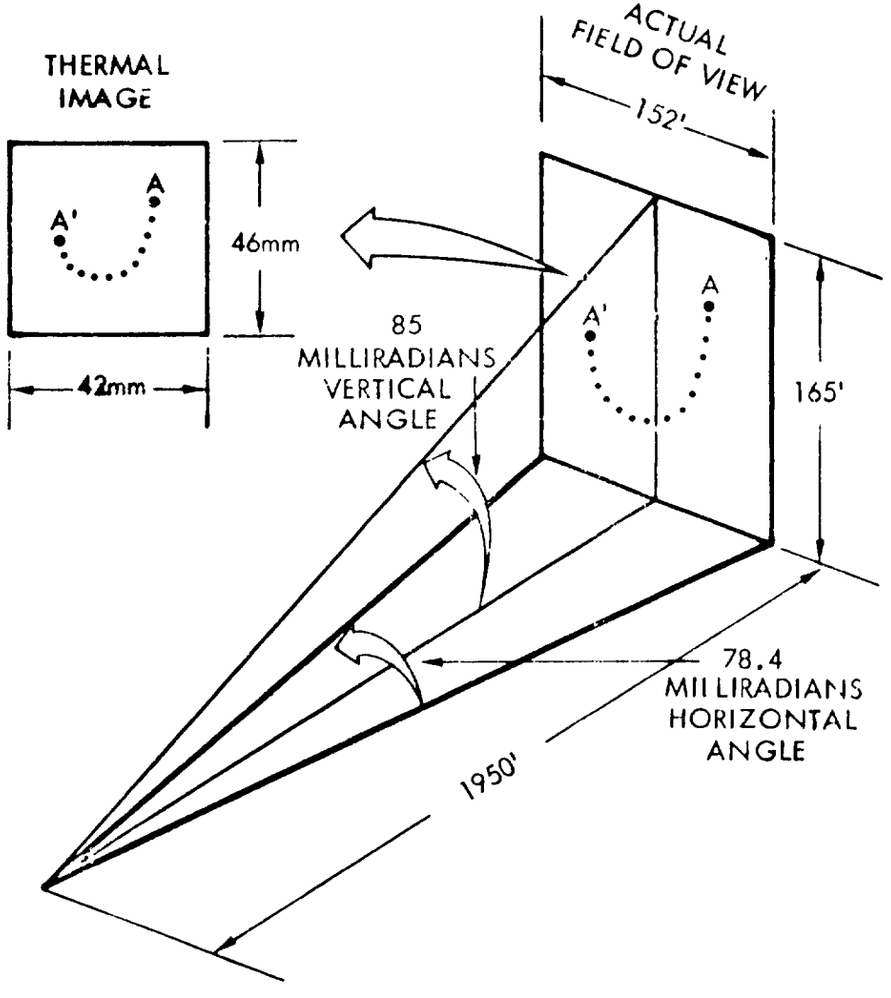

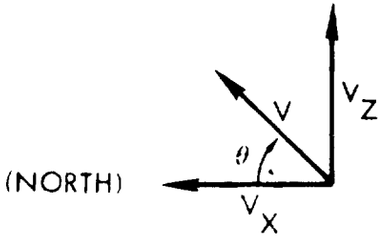

TIME AFTER START OF BURN (sec)	PROJECTED MEAN PARTICLE VELOCITY	
	V (ft/sec)	θ (degrees)
252	24	-15
252.6	24	3
254	26	20
254.5	28	30
256	22	41
257		

Figure 6.53. Velocity of Hot Fragment in IR Field of View - Test No. 13

SEQUENCE STARTS ≈200 SEC AFTER START OF FIRE

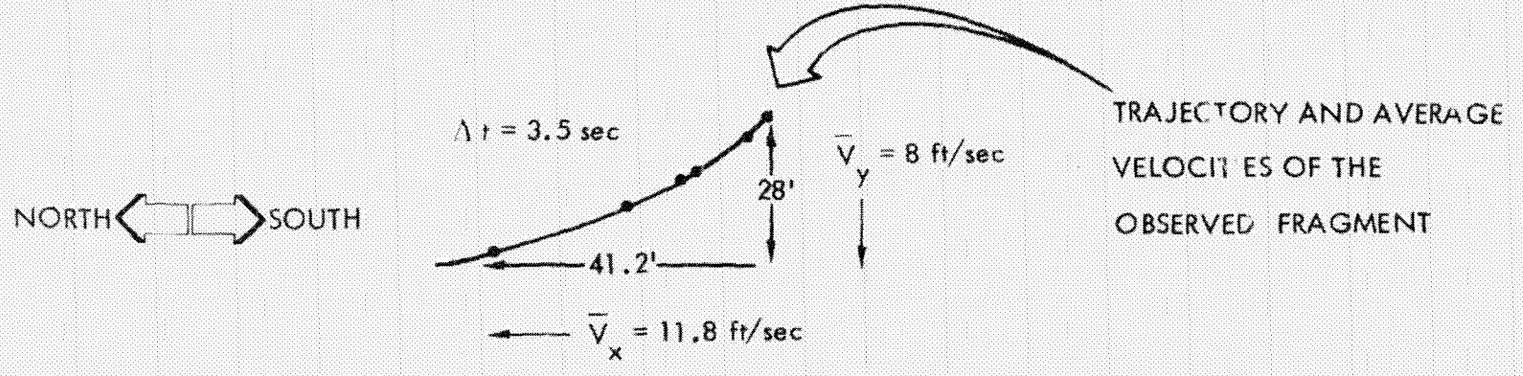

Figure 6 54. IR Thermovision Segmential Display of Falling Fragment - Test No. 13

7. RESULTS AND ANALYSES

The results and analyses are described in this section as follows:

- passive gages
- laboratory tests
- meteorological gages
- cameras
- active gages
- cross-comparison of data from different measurement systems

There have been several innovations introduced in the conduct of these experiments.

- passive gage analysis has been extended from considering just the counts of single carbon fibers, to the counts of multiple and clusters of carbon fibers as well as lint and strip particulate.
- passive gage analysis has been extended to considering changes in fiber diameter.
- active gages have been introduced to supplement the passive gages to gain an additional "time" dimension to the acquired data.
- passive and active gages were arranged to sample the fiber cloud passing above the ground based gages.

PASSIVE GAGES

The passive gages data displayed in Section 4 describe the carbon fiber release characteristics. This sub-section discusses the six key characteristics.

- Number Deposition
- Size Distribution
- Mass Deposition
- Ratio of Single Fibers Mass to Initial Mass
- Footprint
- Fiber Diameter Reduction

NUMBER DEPOSITION

The number of single carbon fibers and multiple carbon fibers deposited per unit area on horizontal sticky paper and on vertical sticky bridal veil, is given as a function of range, azimuth and height in the figures of the following table:

Figure Numbers in Section 4

	Plate	Barrel	Spoiler	Cockpit
• range	13,14,15	22,27	31,32	47,48,49
• azimuth	13	22,27	31,32	47,48,49
• height	12	24	33,45	51,53,54

Most of the fibers for the plate tests 5 and 6 were 1-2 mm in length and deposited about 7000 particles per square foot (7.7 part/cm^2) in the first 30 ft from the source. The deposition decreased to 350 particles per square foot (0.38 part/cm^2) in the next 60 to 200 ft from the source (Figure 7.1).

The barrel prior to explode weighed as much as the plate just prior to explode. And about 360 particles per square foot were deposited from the barrel test in the range of 60 to 200 ft, about the same that was deposited in the plate test.

The spoiler test used 5.8 pounds of carbon fibers initially, compared to the 1.29 pounds of carbon fiber of the plate or of the 1.28 pounds of carbon fiber of the burned barrel. Yet only 14 particles per square foot were collected in the range of 144 to 200 ft for the burn-only test. On the basis of per unit weight of carbon fiber, this spoiler deposition compared to the plate or barrel deposition represents two orders of magnitude reduction and is primarily attribiuted to the fire plume lofting of the fibers to greater ranges, reducing the deposition. For example: plate deposition per unit weight is $351/1.29 = 272\ ft^{-2}lb^{-1}$. Spoiler deposition per unit weight is $14/5.8 = 2.4\ ft^{-2}lb^{-1}$. Hence ratio of deposition spoiler to plate is 0.0088.

The cockpit test used 35.7 pounds of carbon fibers and deposited 40 particles per square foot in the range of 144 to 200 ft for the burn-only test. The cockpit burn-only represents about the same deposition as the spoiler burn-only deposition on a per initial pound basis of carbon fibers.

PREDICTIONS OF CRITICAL EXPOSURE LEVELS BASED ON DEPOSITION DATA

The significance of these numerical results can be related to two separate concepts of critical failure environments (1) exposure and (2) deposition. The exposure obtained by burn/explode of plates and/or barrels in the range to 200 ft is calculated from

$$E = \frac{D/A}{V}$$

where the deposition of single fibers per unit area (D/A) in Test 8 (Figure 7.1) is

$$D/A = 0.987 \frac{\text{single fibers}}{\text{particles}} \times \frac{0.38}{1.28} \frac{\text{particles/cm}^2}{\text{lb initial carbon fiber}} = 0.293 \frac{\text{fibers}}{\text{cm}^2/\text{lb}}$$

TEST	WIND VELOCITY (FT/SEC)	SAMPLE	DATA SOURCE	RANGE (FT)	(1) PERCENT OF SINGLE FIBERS TO ALL PARTICLES	PERCENT OF SINGLE FIBERS		ALL PARTICLES		SINGLE FIBERS 3-20 MM LONG	
						(2) LENGTH 1-3 MM	(3) LENGTH 3-20 MM	(4) MEASURED DEPOSITION PER UNIT AREA (PER SQ FT)	(5) CALCULATED EXPOSURE ($F\text{-}SEC/M^3$)	MEASURED DEPOSITION PER UNIT AREA (PER SQ FT)	CALCULATED EXPOSURE (1)x(3)x(5) ($F\text{-}SEC/M^3$)
5	5.5	PLATE	STICKY PAPER	200	9.0	82.4	17.6	351	12.6×10^4	5.6	0.2×10^4
8	5.5	BARREL	STICKY PAPER	200	98.7	80.8	19.2	362	13×10^4	68.6	2.5×10^4
			TUNA CANS		95.0	54.0	46.0	3530	2.27×10^4	1538	1.0×10^4
11	10.1	SPOILER	STICKY PAPER	300	50.0	66.7	33.3	14	0.5×10^4	2.3	0.08×10^4
			LADDER		65.3	83.0	17.0	44	0.01×10^4	4.8	0.0001×10^4
13	12	COCKPIT	STICKY PAPER	300	32.1	50.0	50.0	40	1.4×10^4	6.4	0.2×10^4
			LADDER		22.3	68.1	31.9	175	0.05×10^4	12.4	$.0035 \times 10^4$

Figure 7.1. Single Fiber Deposition and Exposure Characteristics

and the deposition velocity of single fibers (V) is assumed equal to or less than the settling velocity of single fibers

$$V \leq 3 \text{ cm/sec}$$

Hence the exposure within 200 ft range of the burn/explode of a pound of barrel is

$$E \geq 0.1 \frac{\text{f-sec}}{\text{cm}^3} = 10^5 \frac{\text{f-sec}}{\text{m}^3}$$

Eighty percent of the single fibers are in the 1-3 mm lengths (Figure 7.1) so that exposures of the order of $10^8 \frac{\text{f-Sec}}{\text{m}^3}$ would be needed to fail equipment susceptible to carbon fibers. But twenty percent of the fibers are in the range of 3-20 mm in length which would result in an available 2×10^4 fiber/sec/m^3 exposure, where 10^4 fiber/sec/m^3 is the critical threshold for the onset of equipment failure for 6 mm long fibers. An increase in the source weight of 1 pound to 100 pounds would raise the available 3-20 mm long fibers to 2×10^6 fiber-sec/m^3 where it is likely that susceptible equipment will fail.

The critical exposure for the burned and exploded plates is reduced by an order of magnitude from the burned and exploded barrel because only nine percent of the total number of particles detected (or counted) were single fibers rather than 98.7 percent detected in the case of the barrel (see Figure 7.1).* Thus ten pounds of burned and exploded plate would be required to produce 2×10^4 fiber-seconds per cubic meter at up to 200 ft range, to induce incipient failure in susceptible equipment; and 1000 pounds for 2×10^6 fiber-seconds per cubic meter for likely failure of susceptible equipment.

The calculation for critical exposure for the spoiler and cockpit burns will use two orders of magnitude less deposition of particles per unit area per pound of initial carbon fiber mass, as compared to the barrel. The produce of (1) percent of single fibers compared to total mass and of (2) percent of 3-20 mm long fibers compared to all particles is about the same for all three cases (Figure 7.1).

---

* An element of caution should accompany any interpretation of the data from the barrel test, since the barrel used in test No. 8 was very poorly constructed. With 30% void (p.4-87) in the barrel, there were undoubtedly many strands of single fibers which were unwetted and thus unbound by the resin. These sections of virgin fiber were thus just waiting to be released as single fibers, rather than as clusters, clumps, or fragments.

Thus, 100 pounds of a burning spoiler and a burning cockpit will result in incipient failure of susceptible equipment placed within 200 ft of the fire plume; and 10,000 pounds for more likely failure. Thus the lofting of the fibers by the JP-5 fire plume made the single fiber environment benign at the close-in range. The rather high updraft leads to fallout at the far range. However, some fallout from the rising plume due to large turbulence results in deposition within the short range. Although this fallout is only a fraction of the total mass of fibers released, it is deposited over a relatively small area because of its proximity to the source. Therefore, the depositon density can be significantly higher.

Structure	Burn		Explode	Required Weight (pounds)
	Small Plume	Large Plume		
Plate	•		•	1,000
Barrel	•		•	100
Spoiler		•		10,000
Cockpit		•		10,000

Figure 7.2. Initial Weights Required to Achieve 10^6 $\frac{\text{fiber-seconds}}{\text{Cubic-meter}}$ at 200 ft. range, with single fibers 3-20 mm long.

Figure 7.2. shows that the small plume from the burn and explode tests resulted in a requirement for small weight of carbon fiber composite material to achieve critical exposures at close-in ranges. The large buoyant fire plume results in excessive requirements for initial weight of carbon fiber to achieve and electrical hazard potential at close-in ranges (200 feet). It is difficult or nearly impossible to predict the amount of carbon composite which would have to be burned to reach critical exposure levels at longer distances, based on the results of the tests in this report.

Note that the vertically oriented tuna cans and bridal veil collectors caught between 3- to 10-times the fibers caught by the horizontal collectors. The vertically oriented collectors are more related to the local wind velocity to obtain exposure, while the horizontally oriented collectors are more related to the fiber deposition velocity. Thus a given fiber cloud exposure will deposit, at 150 cm/sec wind velocity, 50 times more fibers on the vertical than on the horizontal collector when the settling velocity of the fiber is 3 cm/sec.

At this time, criteria for critical depositions have not been established for generic classes of equipment. Thus the significance of the measured depositions will not be discussed. Although it has been conjectured that four fibers, 6-cm long, would be required in a one square centimeter area of susceptible equipment for the onset of failure, more tests are required to verify this threshold.

SIZE DISTRIBUTION

The number of single fibers and the number of multiple fibers on a given sticky paper, is given as a function of length interval and diameter interval as follows:

Figure Numbers in Section 4

	Plate	Barrel	Spoiler	Cockpit
• length interval	9,10,16,65, 71	21,25,66, 71	35,42,66, 71	52,55,62, 66,71
• diameter interval	9,10,14,16, 67	29,67	42,67	52,56,62, 67

The greatest number of fibers released were in the 1-2 mm length interval, and were either single fibers or a ply thick. But these do not represent a threat because of the extremely high exposures (> 10^8 fiber/seconds per cubic meter) required before any susceptible equipment would fail.

However, it is important to note that the single fibers represent between 10 and 95 percent of all particles deposited (although they represent extremely low fraction of the fiber mass) between 17 and 50 percent of these fibers are in the electrically significant range of 3 to 20 mm in length. These fibers can induce equipment failures at exposures of 10^4 to 10^6 fiber seconds per cubic meter over such large lethal radii as 200 ft from burn/explode sources using 100 pounds of carbon fiber initial weight. There is a restriction that the source be a plume no higher than 100 ft. It is likely that these equipment failures do not take into consideration contributions of other fiber species (lint, clumps, strips, etc.) to the failure of electrical equipment such as outdoor power systems.

Figure 7.3 shows that the burn and explode tests of plates resulted primarily in clumps. It should be pointed out that passive instrumentation only went out to 600 ft underground for the burn and explode plate tests. Therefore, it is possible that single fibers which were released could have been lofted and transported beyond the passive instrumentation.

The hot propane burner did generate singles and clusters in the burn/explode of barrel A while the JP-5 pool fire of barrel B did not permit deposition of significant numbers of single fibers but did deposit large strips in the burn/explode tests. This appears to be more a function of the size of plume and its fast rise velocity, as well as the short duration of heating after delamination.

The burn-only of the aircraft spoiler resulted in singles and strips; while the burn/explode of the spoiler resulted mostly in singles as a result of the shattering effects of the explosion.

The burn-only of the cockpit resulted in lint and strips.

There is no doubt that the formation and dispersion of large numbers of clusters of fibers (as in the barrel burn) and the generation and transport of long strips of fibrous residue (from the spoiler test) as shown in Figure 7.3 created a new awareness of types of carbon fiber materials other than single fibers which could, under entirely imaginable siutations, represent threats to outdoor electrical equipment.

MASS DEPOSITION

The mass of single carbon fibers and multiple carbon fibers deposited per unit area on horizontal sticky paper and on vertical sticky bridal veil was not displayed as a function of range azimuth and height in Section 4.

However, Figure 7.4 shows the mass per unit area of deposited particles as a function of range for all tests along the direction of peak deposition. The extreme scatter and precipitous decay with range describe this figure. The portion of the fiber cloud that will deposit on the ground achieves this deposition within 200 ft, and thereafter, the cloud becomes airborne. The plate tests, with their low altitude plumes, resulted in a deposition inversely proportional to range raised to the 1.5 power.

The spoiler and cockpit depositions from their 3000 ft high plume, at ranges closer than 300 ft, were random and spread over five orders of magnitude.

The mass per unit area deposited is a vital parameter in that it tends to reflect the contribution of the longer and more electrically hazardous fibers. Thus a fiber which has a mass of 0.5 μgm per centimeter length, and has an average length of 0.4 centimeters, will have an average mass of 0.2 μgm per fiber. At 10 ft range, the 800 $\mu gm/cm^2$ deposition represents 800 x 0.2 fibers/cm^2; and at 200 ft range, the 10 $\mu gm/cm^2$ deposition represents 10 x 0.2 fibers/cm^2.

Figure 7.5 shows the deposition on vertical collectors. The tuna cans were on holders up to 30 ft high, while the Jacobs Ladder was up to 90 ft high. These show that the vertical and horizontal collector data are consistent. In theory, the vertical collection to horizontal collection factor is given by the ratio horizontal wind velocity to settling velocity, i.e. 150 cm/sec to 3 cm/sec or a factor of 50. But the four orders of magnitude spread of deposition hides the factor of 50.

PARTICLE TYPE	TEST SAMPLE					
	PLATE	BARREL A	BARREL B	SPOILER		COCKPIT
SINGLES		▶		▶	▶	
MULTIPLES						
LINT						▶
CLUMPS	▶					
CLUSTERS		▶				
STRIPS			▶	▶		▶
		●Hot Propane Burn ●Explode	●Pool Fire Burn ●Explode	●Pool Fire Burn	●Pool Fire Burn ●Explode	● Pool Fire Burn

Figure 7.3. Singular Particulate Characteristics

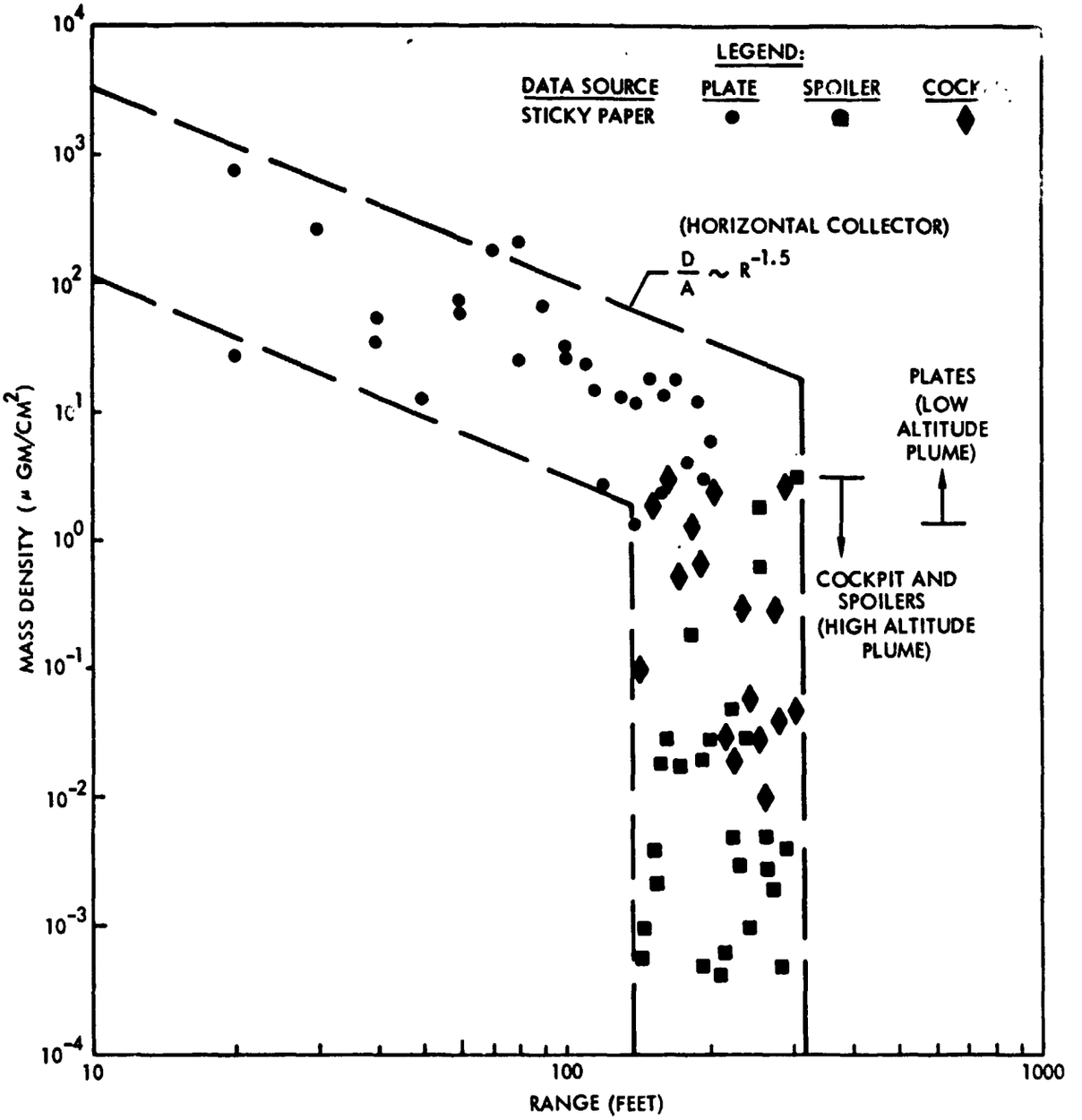

Figure 7.4. Deposition of Particles on Sticky Paper as a Function of Range

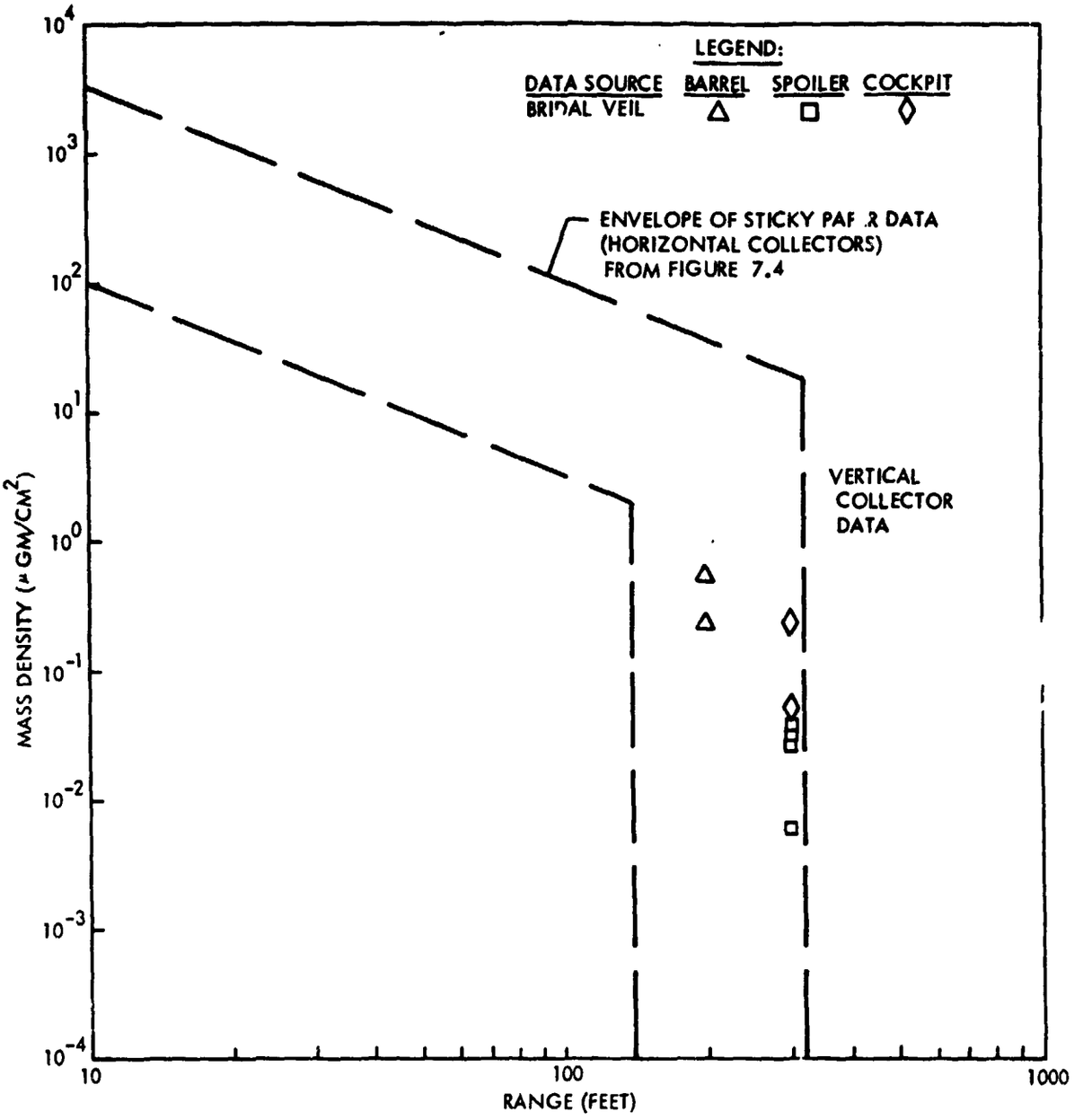

Figure 7.5. Deposition of Particles on Sticky Bridal Veil as a Function of Range

RATIO OF SINGLE FIBERS MASS TO INITIAL MASS

The ratio of the mass of carbon fibers released as single fibers to the mass of the initial resin and carbon fiber is given as a function of each burn/explode test as follows:

Figure Numbers in Section 4

Plate	Barrel	Spoiler	Cockpit
18,19,72	28,72	44,72	64,72

Figure 4-72 shows the mass ratios to be of the order of 0.02%, no matter which test is considered. However, there is more confidence in this ratio for the flat plates where much of the released mass was sampled.

This small ratio is particularly significant for risk analyses, in that the only real threat to electrical equipment may occur only in the close-in areas adjacent to the source and all far-out regions will receive only small quantities of fibers diluted over great volumes. For extremely large diameter pool fires (more than 50 feet in diameter) the close-in areas are more dilute because of the strong updraft.

FOOTPRINT

The footprint of the fiber deposition is given as a function of range and azimuth as follows:

Figure Numbers in Section 4

Plate	Barrel	Spoiler	Cockpit
11,13	22,27	37	57

FIBER DIAMETER REDUCTION

The comparison of the pre-test and post-test carbon fiber diameter is as follows:

Figure Numbers in Section 4

Plate	Barrel	Spoiler	Cockpit
68	29,68	68	56,68

The fibers imbedded in a 40-ply structure of the plate did not experience the oxidation that those incorporated in the thin ply structures of the barrel, spoilers and cockpit. The latter three structures had their fibers experience a 30 percent decrease in diameter on the average.

It is important to note that there were considerable numbers of fibers in the 1 and 2 micron diameter range from the barrel burn which approach the size of fiber that should be investigated for possible health risks.

LABORATORY TESTS

The laboratory tests indicate two important trends. First, carbon fibers react with sufficient rapidity at 2000° F temperatures that even a few minutes exposure will cause measurable mass loss due to oxidation. Second, the presence of the resin acts as a catalyst, so that even lower temperatures lead to the same mass loss in a few minutes.

For carbon fiber composite structures having just a few ply, in the midst of a burn environment where there is sufficient local oxygen available, the possibility of mass loss to carbon fiber oxidation must be considered as a mechanism for accounting for mass loss. This is a factor not presently being considered in aircraft crash risk analysis scenarios. It certainly is a factor that must be considered in the design of efficient incinerators for disposal of future carbon fiber waste material.

It is worthwhile considering the introduction of those elements in the resin that catalyze the carbon fiber reaction to facilitate mass loss. This will reduce the carbon fiber release from accidental aircraft crash fires and from incinerator smoke stacks.

Archibald of AFML (1978)[2] performed isothermal weight loss tests of carbon fibers aged at 450°F, 500°F, 550°F, 600°F and 700°F for intervals of 1000 hours in an air circulating over. He determined the following activation energies:

Manufacturer	Fiber Grade	Activation Energy (kilocalories/mole)
Hercules	HM-S	57
Hercules	HTS(0)	53.6
Modmor	MM II	48
Hercules	A-S	29.9
Union Carbide	T-300	29.0
Hercules	HTS(N)	22.9
Hercules	HTS(66-7)	30.6

The activation energy of the TRW thermal gravimetric analysis tests for T-300 resulted in 31.0 kilocalories per mole as compared to the above value of 29.0 kilocalories per mole. This is interesting in that the TRW TGA tests were operated at 1000°F and used only one minute to 20 minute time intervals.

Radcliffe and Appleton of MIT (1971)[3] studied carbon soot oxidation rates at 1300 to 1700°K, and with various levels of partial pressure of oxygen ranging from 0.04 to 0.1 atmospheres. The activation energy for oxidation suggested in their report indicates E = 39.3 kilocalories/mole.

Lee, Thring and Beer (1962) determined the carbon soot oxidation rate to be directly proportional to the partial pressure of oxygen.

$$\omega = 1.085 \times 10^4 \frac{P_{O_2}}{T^{1/2}} \exp\left(\frac{-39,300}{RT}\right)$$

where

ω oxidation rate (gms carbon - cm^{-2}-sec^{-1})

P_{O_2} partial pressure of oxygen (atm)

T absolute temperature (^oK)

R universal gms constant (cal -$^oK^{-1}$-$mole^{-1}$)

This linear dependence on P_{O_2} was also found to be true for pyrographite. These results are of interest in design of incinerators. Since the proper addition of secondary air, the proper temperature, and proper residence time can completely consume the carbon fibers. The addition of sodium as a catalyst can further reduce the activation energy and enhance the rate of carbon fiber consumption.

METEOROLOGICAL GAGES

The meteorology data obtained from the towers were used to yield

- average wind direction
- average wind velocity
- wind direction and velocity as a function of time
- average temperature
- standard deviation of wind direction

The average wind direction during the two to twenty minutes after the test initiation indicated whether the peak concentrations of carbon fibers passed through the instrumentation network. The first two minutes were vital with regard to the instrumentation within 600 ft from the source point, while the later time was applicable to the instrumentation at 6000 ft from the source. A steady south wind was required for the maximum data yeild.

The average wind velocity, and the distance from the carbon fiber source, determined the arrival time of the carbon fiber cloud from the low altitude plume (Figures 5.12 and 5.17). However, during the pool fire tests the fiber cloud from the high altitude cloud arrived simultaneously at several ranges indicating that the fiber cloud was descending from above (Figure 7.6).

The long distance of flat uninterupted terrain at the test site suggests that the wind system is large scale. Thus average wind speed and average wind direction readings from a meteorological tower should be valid over a large distance at each time interval. Thus the meteorological tower wind speed history and wind direction history can be combined to sketch the meandering of the fiber cloud after it has been released from its source. This has been demonstrated by comparing the meteorological data to the measured sticky paper footprint and active gage footprint (Figures 7.7, 7.8, 7.9 and 7.10).

The average temperature can be obtained from the meteorological tower. The 300-ft cross-dimension of the black-top test pad, and only 54-ft height of meteorological tower, results in the thermal effects of the black-top strongly influencing the lowermost thermocouple.

The atmospheric stability of the air according to the Pasquill stability classes A through G is given by the Nuclear Regulatory Committee Safety Guide 23. (See Figure 7.11. Either σ_{wD} or $\Delta T/\Delta Z$ determines the stability class necessary to establish which plume equations apply. Another approach is to use the extreme range of the wind direction in a 15-minute period and divide it by six to obtain the effective standard deviation of horizontal wind direction (σ_{wD} = R/6). No matter which of the three calculational schemes is used, the same stability class will be identified.

As an example of the methodology, application of the methodology, and display of results compared to analysis, Test 11 will be discussed in detail.

The wind variation data will first be considered to determine the Pasquill atmospheric stability category. Figure 6.29 shows the wind velocity history for ten minutes, whereas it is better to use 15 to 60 minutes. Using the ten-minute wind direction history, the extreme limits are 220^{o} and 145^{o}. The standard deviation is obtained by dividing this range by six, $\sigma_{wD} = (220^{o}-145^{o})/6=12.5^{o}$. According to Figure 7.11, this lies between slightly unstable category C and neutral category D.

The temperature gradient data will next be considered to determine the Pasquill atmospheric stability category. Figure 7.12 shows the meteorological tower temperature data with Test 11 highlighted. Figure 7.13 shows the range of temperatures at a given elevation near test time. The temperature gradient of -0.05^{o}F/10 ft equals -0.9^{o}C/100 M. Figure 7.11 shows that this temperature gradient falls between -1.5^{o}C/100 M and -0.5^{o}C/100 M, Pasquill atmospheric stability category D, neutral.

In Test Number 11, spoilers burn, the wind direction variation resulted in the slightly unstable Pasquill category C to neutral stability Pasquill category D; and the temperature gradient result in category D. It is of interest that in

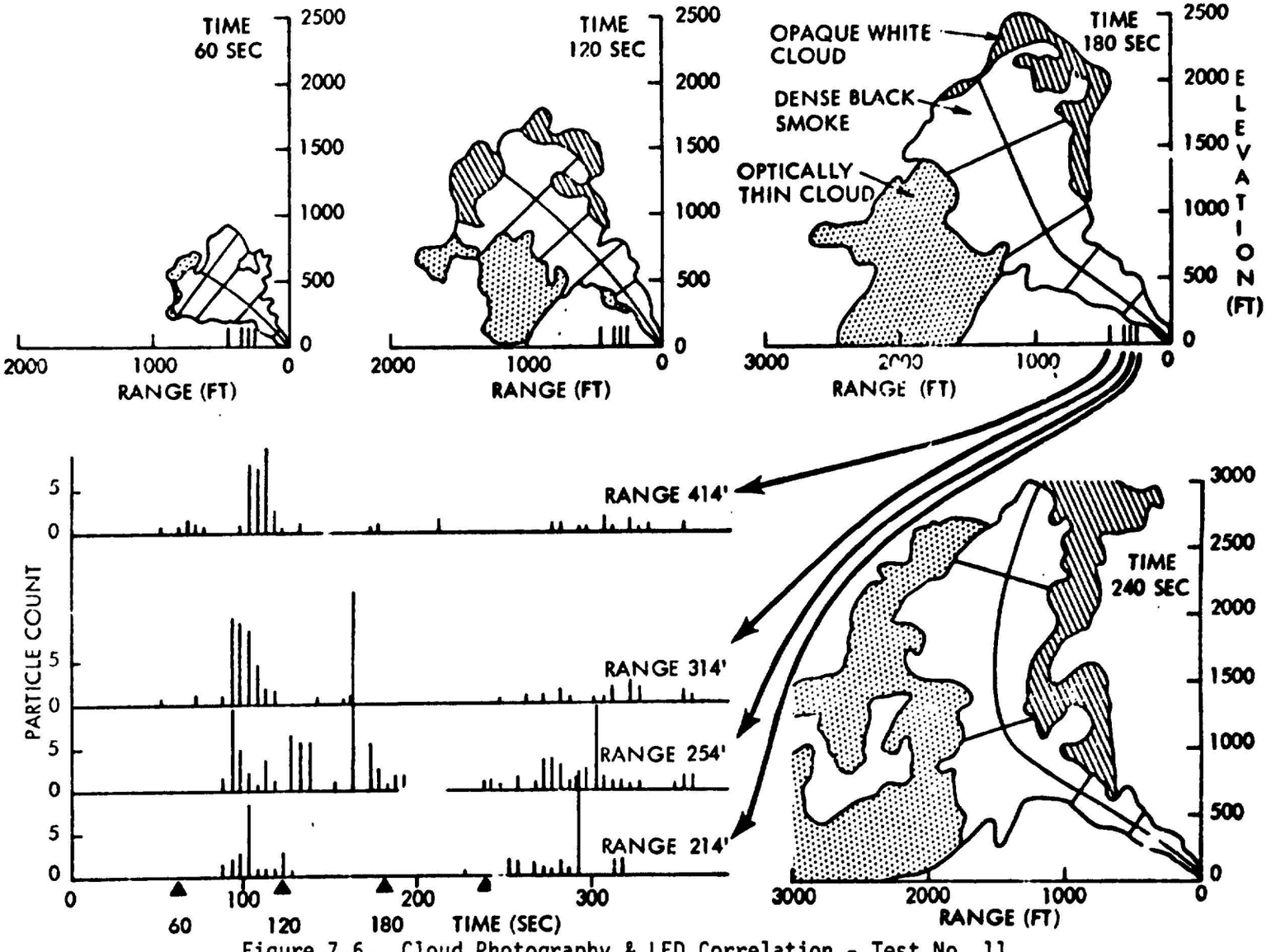

Figure 7.6. Cloud Photography & LED Correlation - Test No. 11

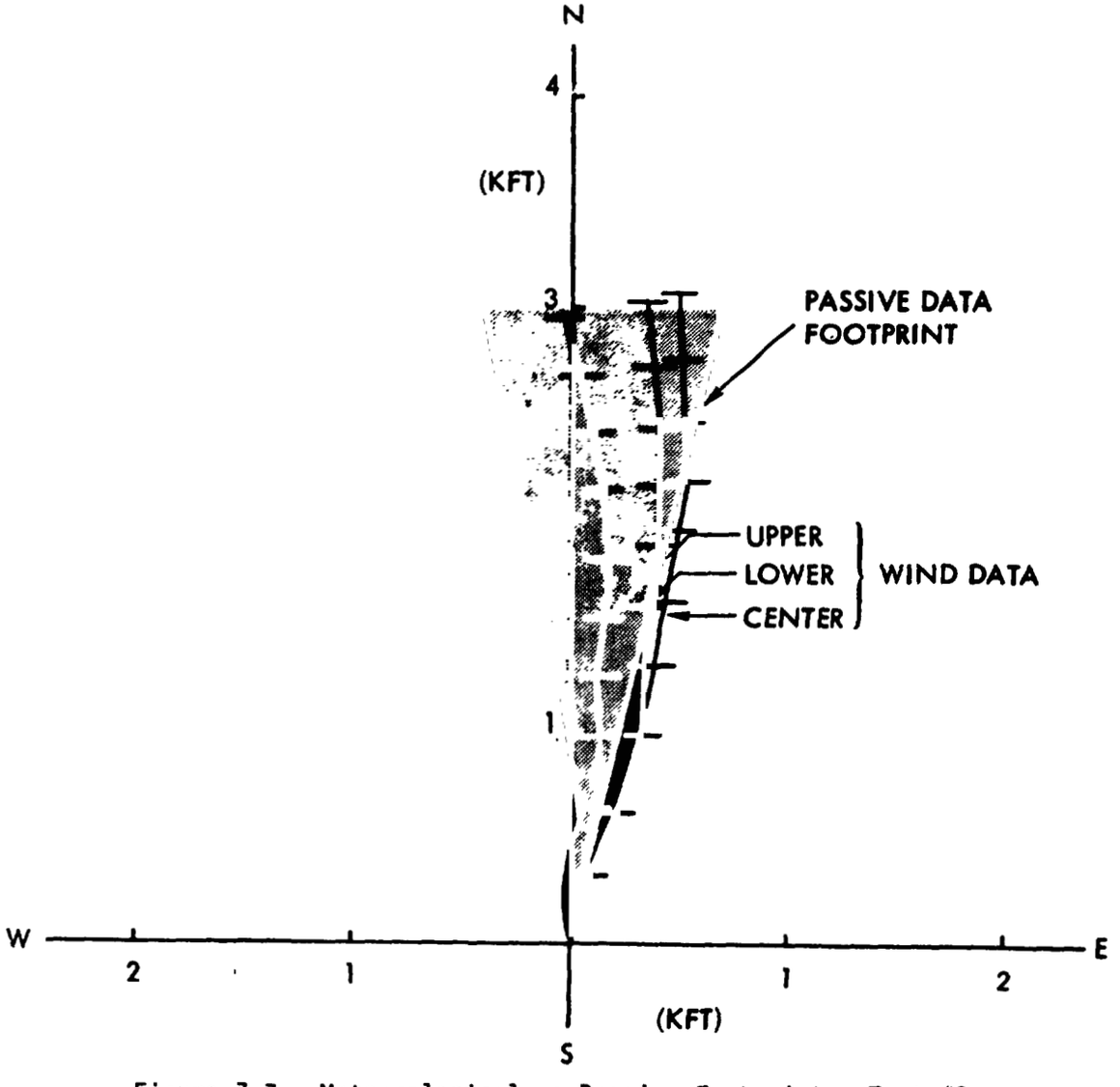

Figure 7.7. Meteorological vs Passive Footprint - Test #8

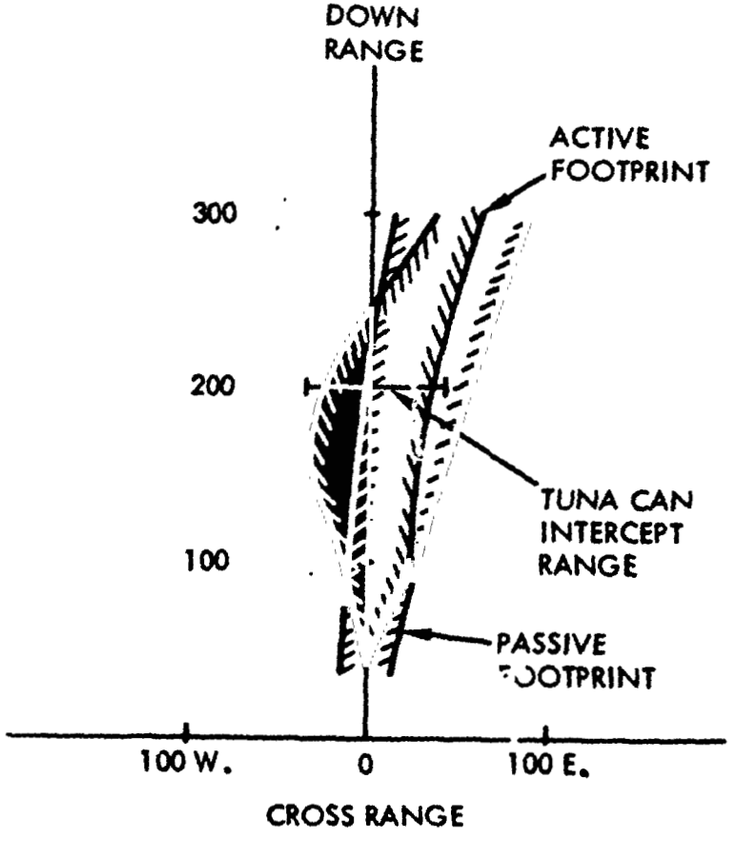

Figure 7.8. Active/Passive Footprint Comparison - Test #8

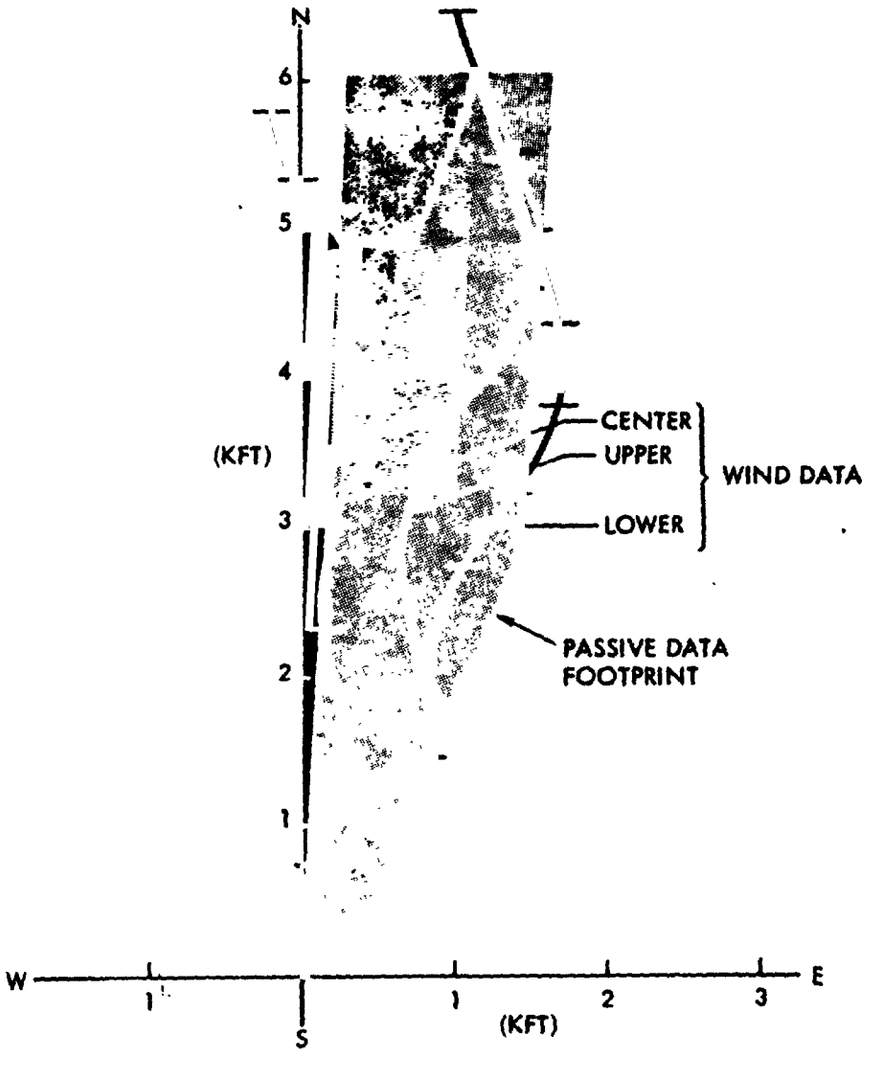

Figure 7.9. Meteorological vs Passive Footprint - Test No. 11

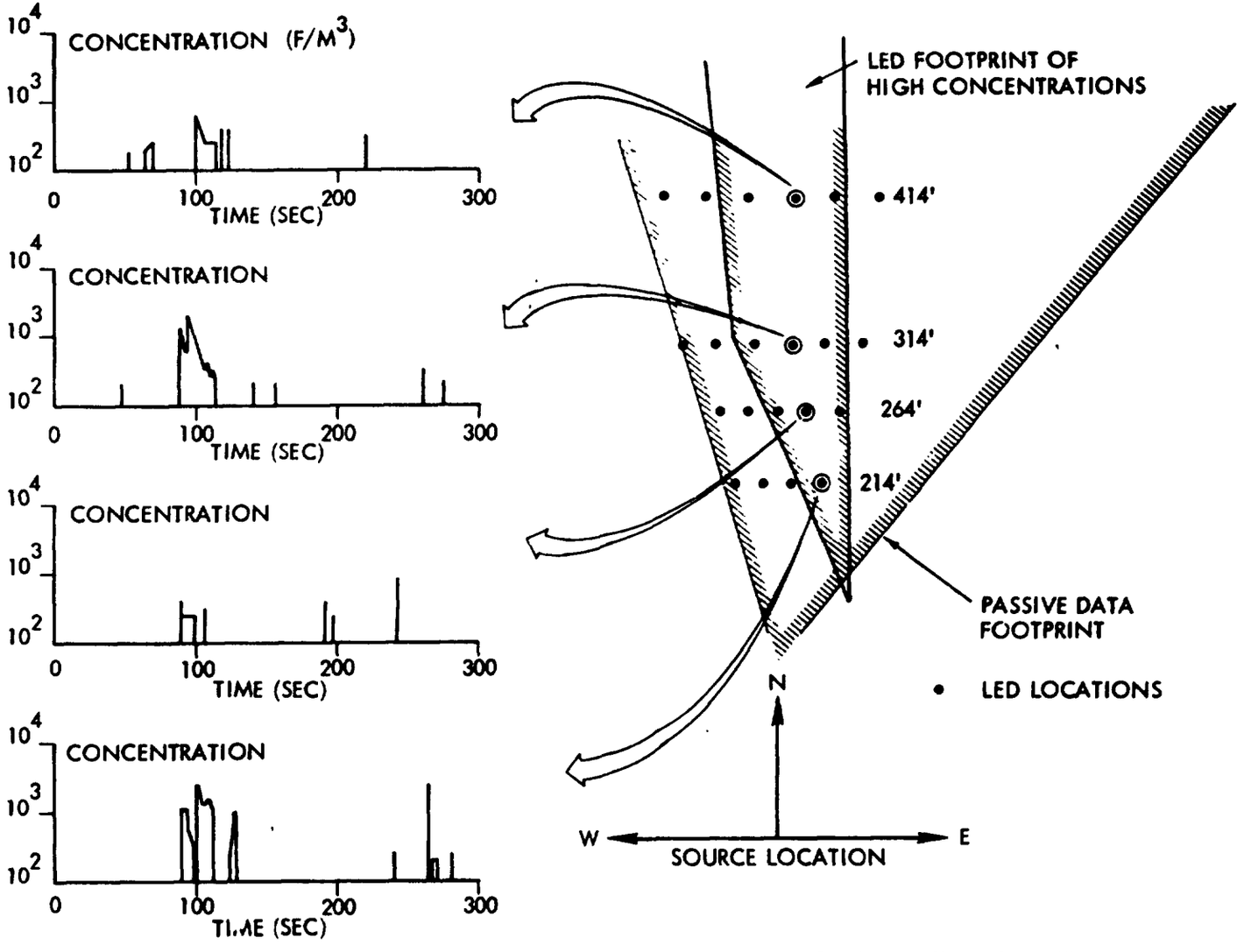

Figure 7.10. Deposition Footprint & Active Data Correlation - Test No. 11

Stability Classification	Pasquill Categories	σ_{WD}^{**} Degrees	$\frac{\Delta T}{\text{Temperature Change With Height}}$ $^{o}C\ 100\ m^{-1}$
Extremely unstable	A	25.0	< - 1.9
Moderately unstable	B	20.0	- 1.9 to - 1.7
Slightly unstable	C	15.0	- 1.7 to - 1.5
Neutral	D	10.0	- 1.5 to - 0.5
Slightly stable	E	5.0	- 0.5 to 1.5
Moderately stable	F	2.5	1.5 to 4.0
Extremely stable	G	1.7	> 4.0

** Standard deviation of horizontal wind direction fluctuation over a period of 15 min - 1 h. The values shown are averages for each stability classification.

Figure 7.11. Classification of Atmospheric Stability, According to NRC Safety Guide 23 (4)

NEAR SURFACE TEMPERATURE DATA

TEMPERATURE (°F)

TEST NO. \ HEIGHT (ft)	3	18	28	38
4	48.0	47.5		47.2
5	49.8	49.4	49.2	49.2
6	40.2	40.0		35.9
7				
8	51.7	51.2		51.0
9				
10				
11	75.3	74.4	74.3	74.25
12	81.9	80.7	80.4	80.2
13	71.5	70.2	70.0	69.8

Figure 7.12. Near Surface Temperature Data

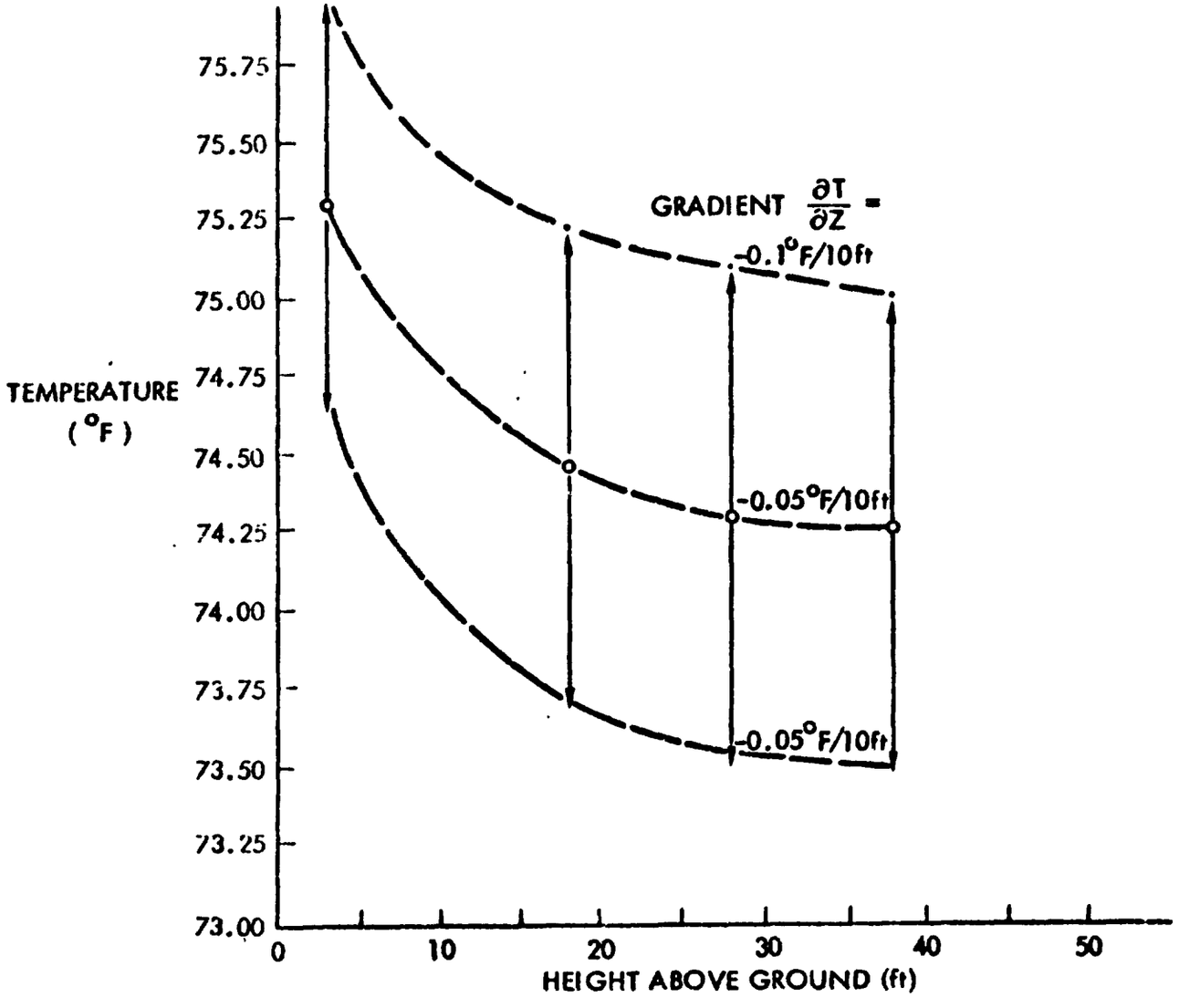

Figure 7.13. Temperature vs Height - Test No. 11

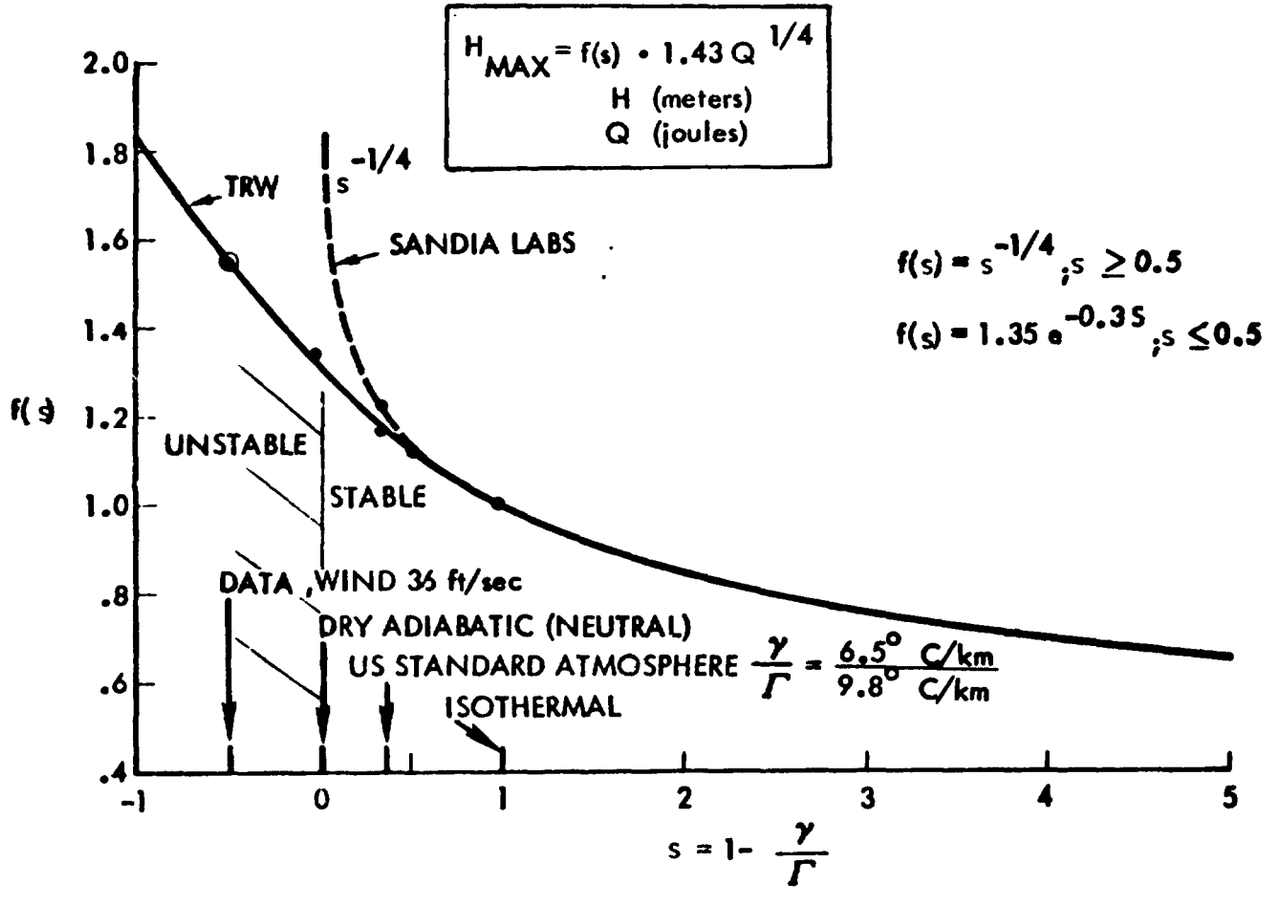

Figure 7.14. Maximum Height for Range of Stabilities

spite of the presence of the black top test pad, the meteorological tower proved useful in specifying the stability condition. This stability condition is validated by the plume stabilization height achieved in Test 11, as described in the following section.

The stability is vital in specifying the plume height. The stability parameter is defined as either

$$s = 1 - \frac{dT/dZ}{(-9.8^{o}C/100\ M)}$$

or

$$S = \frac{g}{T} s$$

where

g = gravitational constant

T = absolute temperature

Z = altitude

$\frac{d}{dZ}$ = vertical gradient

The maximum height (H_{max}) achieved by a puff generated by a pool fire is given by

$$H_{max} = 1.43 \cdot f(s) \cdot Q^{1/4} \quad \text{(meters)}$$

where

f(s) = see Figure 7.14

Q = heat released by JP-5 fuel (test 11, Q = 1.2×10^{11} joules)

The coefficient 1.43 converts to 4.7 for H_{max} in feet.

Figure 7.15 shows that the neutral to slightly unstable stability condition is predicted to yield maximum plume heights of 3780 to 4480 ft for Test 11. Figure 7.6 indicates the cloud is stabilized at above 3000 ft altitude.

CAMERAS

The first portion of this section selects Test 11 to show the derivation, data and analysis of plume variables obtained by means of visible light cameras. The second portion discusses the results obtained from the infrared cameras.

CINE CAMERAS

The methodology of the simplified data reduction, the data, the simplified analysis of the plume trajectories and plume histories, and use of the meteorological

Stability Classification	Pasquill Categories	Average Temp. Change with Height °C/100 M	Stability Parameter s	f(s)	Max. Height (FT)
Extremely unstable	A	- 1.9	- 0.9	1.8	5040
Moderately unstable	B	- 1.8	- 0.8	1.7	4760
Slightly unstable	C	- 1.6	- 0.6	1.6	4480
Neutral	D	- 1.0	0	1.35	3780
Slightly stable	E	0.5	1.5	0.90	2520
Moderately stable	F	1.7	2.7	0.78	2180
Extremely stable	G	4.0	5.0	0.67	1880

$$\text{MAX HEIGHT} = H_{max} = 4.7 \cdot f(s) \cdot Q^{1/4} \quad \text{(FT)} \qquad \text{PUFF}$$

Figure 7.15. Maximum Height as Function of Pasquill Stability Classifications - Test No. 11

data are shown in this section in Figures 7.16 to 7.20.

It is important to note that there are more complex techniques available to analyze the plume data. For instance the fundamental classical momentum and energy diffusivity coefficients, entrainment factors, apparent masses, conservation equations, and the introduction of radiation transport to correct the plume properties, can all be used to specify plume parameters in an elaborate state-of-the-art computer calculation. Simplifications of Gaussian model vertical velocity distributions have been used in the past. However, the presented simple approach is consistent with the requirements of a risk analysis.

The camera photographs contain qualitative and quantitative data. The qualitative data includes the general shape of the plume and puff formation at several times, the general direction of the motion, swirling of large scale eddies of smoke comprising the plume, the fall-out of large strips of burned material, and the orange flame height compared to the pool dimension. This qualitative information is best seen in the color photographs of Figures 6.30 to 6.35.

The quantitative data reduction requires the development of a three dimensional analysis to convert photo data from two separate cameras viewing the same scene at right angles. Figure 7.16 shows the two-dimensional data reduction scheme for the camera located south of the fire plume and for a south wind. Calibration was performed by taking photographs of vertical poles of height H_1 and H_2, and measuring the distances from the camera to each pole and between poles. The angles θ_1 and θ_2 were then calculated based on the horizontal and vertical distances. For vertical objects the values of θ_1/h_1 and θ_2/h_2 were averaged to yield the parameter $\alpha_{vertical}$. Similarly the angle between the base of the poles θ_3, compared to the distance between the poles h_3, yielded $\alpha_{horizontal}$. The α_1, α_2 and α_3 values proved to be close so that a single value of α was selected. Figure 7.16a and 7.16b explain the development of true dimensions by using the calibration photographs, plume photographs and mapping equations.

A grid on a transparent sheet was overlayed on each photograph to obtain true dimensions. Note how errors in measurement of the plume top are more severe than the same error at the closer-in plume bottom. Figure 7.17 shows the grid constructed for the far west camera for Test 11, and the derivations for the construction of the grid is shown in Figure 7.17a. Specific values for parameters are given in Figure 7.17b.

In the next series of figures the plume data shown in Section 6 will be shown along with the correlation equation, and the next figure will show the TRW computer mode correlation equation parameters. Figure 7-18a and 7-18b (data from Figures 6.38 and 6.39) shows the correlations of flame height history and vertical velocity history until the stabilization height Z* is obtained, while Figure 7.18c shows the derived correlation equations. These correlation equations are based upon empirical constants developed for fire plumes and puffs.

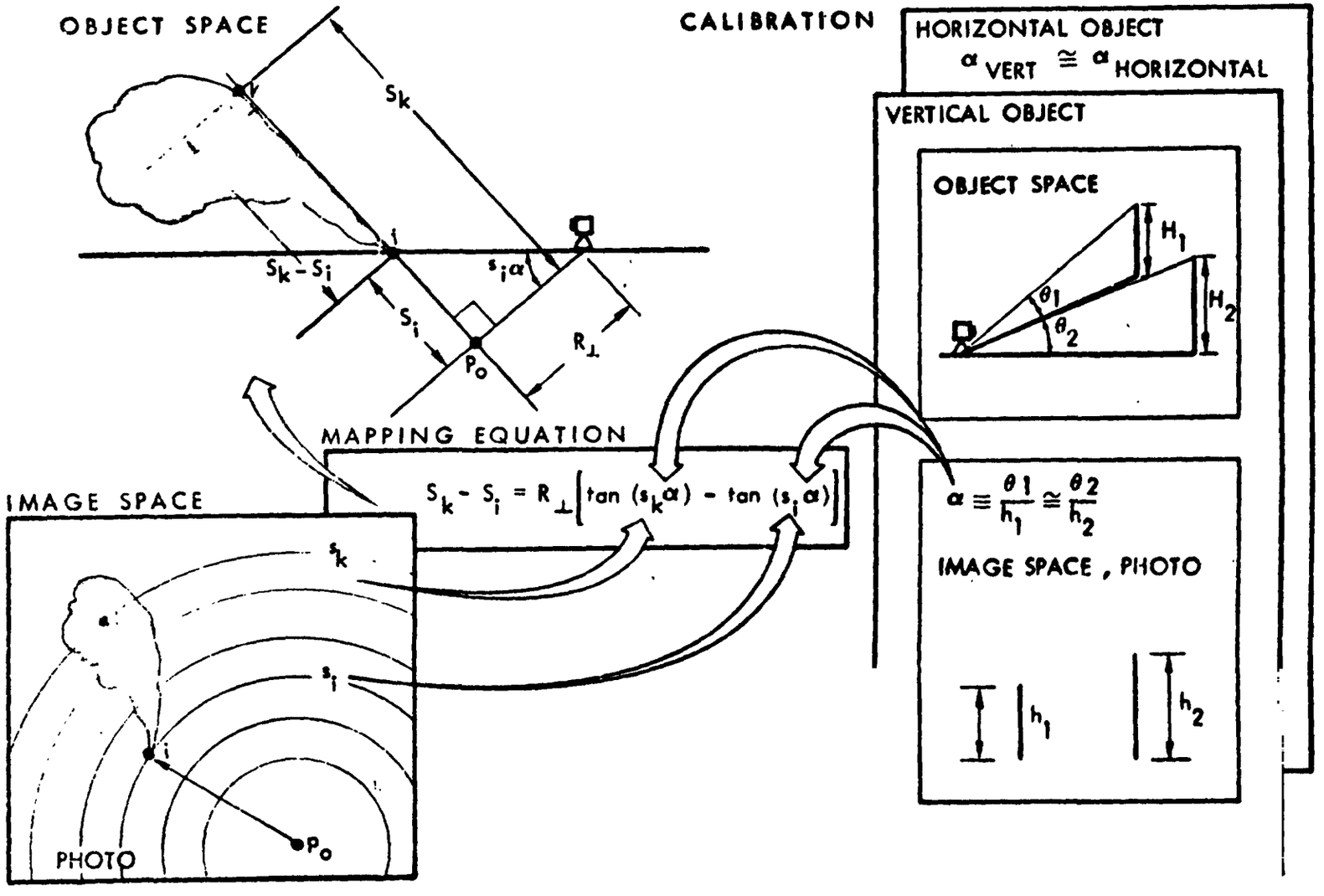

Figure 7.16. Data Reduction

- CAMERA MAPS EQUAL ANGULAR SEPARATIONS AS MEASURED FROM THE IMAGING CAMERA IN OBJECT SPACE INTO EQUAL LINEAR SEPARATIONS IN IMAGE SPACE
- AN OBJECT TO IMAGE SPACE TRANSFER PARAMETER, α IN UNITS OF RADIAN PER INCH, MUST BE OBTAINED. THE VALUE OF α VARIES SLIGHTLY, BUT IS TAKEN AS CONSTANT.
  - FIRST, SELECT READILY RECOGNIZABLE OBJECT SPACE FEATURES AND COMPUTE THE ANGULAR DISTANCE IN RADIANS SUBTENDED AT THE CAMERA BY EITHER THE HEIGHT OF INDIVIDUAL FEATURES OR THE TRANSVERSE SEPARATION OF PAIRS OF SUCH FEATURES
  - NEXT, MEASURE THE CORRESPONDING IMAGE HEIGHTS OR IMAGE SEPARATION DISTANCES IN INCHES
  - FINALLY, COMPUTE THE TRANSFER PARAMETER, α. THE RATIO OF THE OBJECT SPACE ANGULAR SEPARATION DIVIDED BY THE CORRESPONDING LINEAR IMAGE SPACE SEPARATIONS.
  - FOR TEST NO. 11, FAR WEST VIEW, α = 0.07 RADIAN/IMAGE INCH.
- ASSUME THE VIEWED PORTION OF IMAGE PLUME (I.E. FOREGROUND) LIES IN A PLANE, A NECESSARY SIMPLIFICATION. THIS PLANE CONTAINS THE FIRE POOL CENTER AND ITS ORIENTATION IS DETERMINED FROM MUTUALLY PERPENDICULAR CAMERA VIEWS AND/OR FROM THE TEST FALLOUT FOOTPRINTS.
  - FOR THE WEST VIEWS OF TEST NO. 11 THIS PLANE WAS TAKEN AS VERTICAL AND 9^{o} EAST OF DUE NORTH.
  - FOR THE SOUTH VIEWS OF TEST NO. 11 THE BASE OF THE PLANE WAS ON AN EAST-WEST LINE WITH THE PLANE INCLINED AT AVERAGE ANGLES OF $\theta = 52^{o}$ AND $\theta = 66^{o}$ FOR DIFFERENT TIME PERIODS.

Figure 7.16a. Basis for Photo Analysis

- GIVEN THE PLUME PLANE LOCATION AND ORIENTATION AND ALSO THE CAMERA LOCATION, COMPUTE THE SHORTEST DISTANCE OF THE CAMERA TO THE PLANE AND LOCATE THE INTERSECTION OF THIS LINE WITH THE PLANE. THE LENGTH IS SYMBOLIZED BY $R_{\perp}$, AND THE INTERSECTION POINT IS CALLED THE FIDUCIAL POINT, P_o. THE CORRESPONDING POINT IN IMAGE SPACE IS p_o.
- FROM SOLID ANALYTICAL GEOMETRY, THE EQUATION OF THE OBJECT SPACE DISTANCE, S_i OF ANY POINT P_i IN THE ASSUMED PLANE FROM THE OBJECT SPACE FIDUCIAL, P_o IS GIVEN BY THE RELATION

$$S_i = R_{\perp} \tan(s_i \alpha) \tag{1}$$

WHERE $R_{\perp}$ AND α WERE PREVIOUSLY DEFINED AND s_i IS THE LINEAR DISTANCE BETWEEN THE IMAGE POINT p_i CORRESPONDING TO OBJECT SPACE P_i AND THE IMAGE SPACE FIDUCIAL, p_o. THE DISTANCE FROM THE CAMERA TO ANY POINT ON THE PLANE, R_i IS GIVEN BY

$$R_i = R_{\perp} \sec(s_i \alpha) \tag{2}$$

- THE RATE OF CHANGE IN THE RADIAL AND TANGENTIAL DIRECTION ARE OBTAINED FROM SUITABLE DIRECTIONAL DERIVATIVES AS

$$dS = \left[\alpha R_{\perp} \sec^2(s\alpha)\right] \cdot ds \tag{3}$$

AND

$$dL = \left[\alpha R_{\perp} \sec(s\alpha)\right] \cdot dl \tag{4}$$

WHERE dS AND dL REFER TO RADIAL AND TANGENTIAL CHANGE IN OBJECT SPACE AND ds AND dl TO THE CORRESPONDING CHANGES IN IMAGE SPACE.

Figure 7.16b. Analysis Procedures

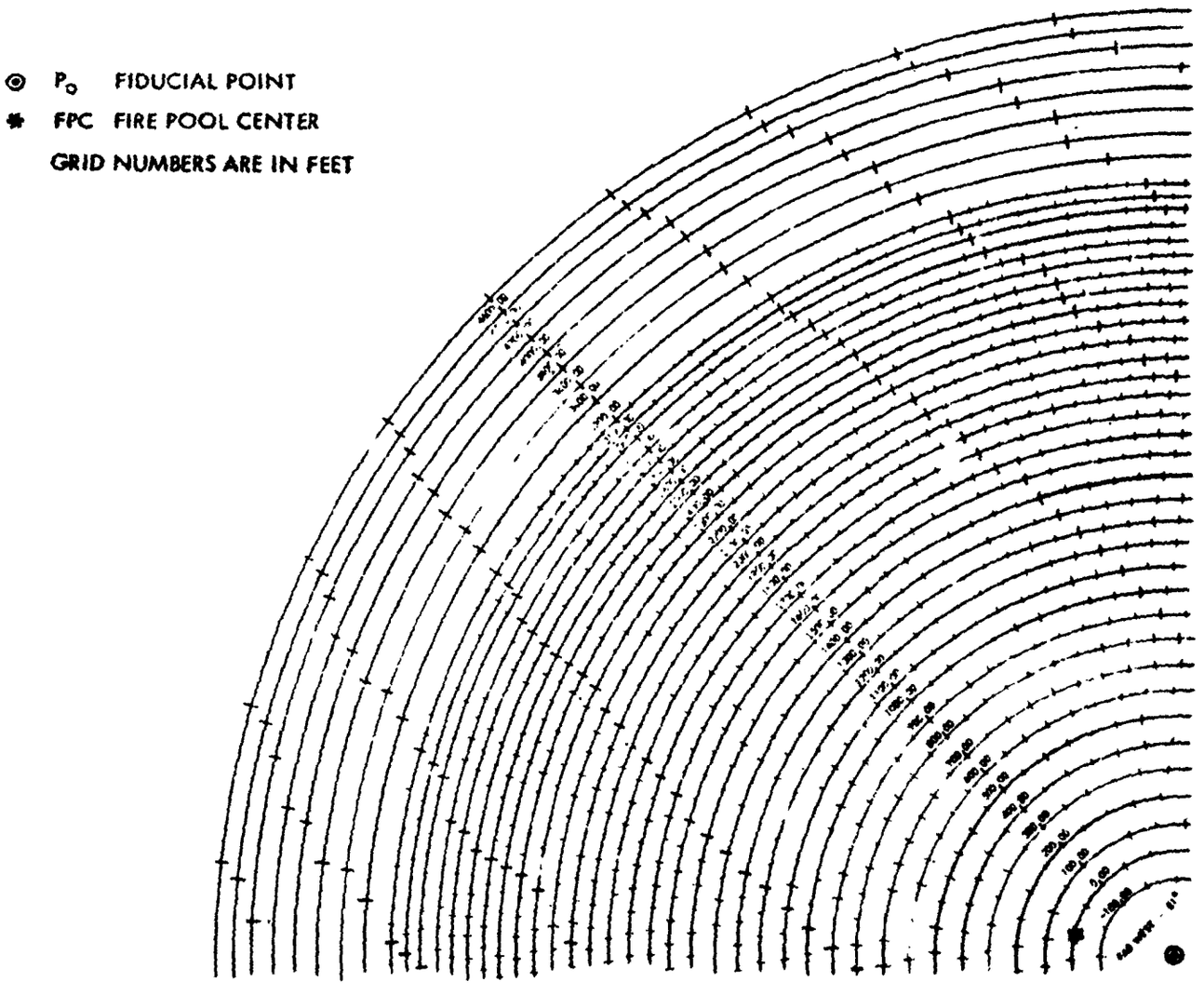

Figure 7.17. Far West View - Test No. 11

- TO PLOT A GRID IT IS CONVENIENT TO INVERT EQUATIONS (1), (3) AND (4) AND OBTAIN

$$s_i = \alpha^{-1} \tan^{-1} (S_i / R_\perp) \qquad (1a)$$

$$ds = \left[\alpha^{-1} R_\perp^{-1} \cos^2(\alpha S)\right] \cdot dS \qquad (3a)$$

$$dl = \left[\alpha^{-1} R_\perp^{-1} \cos(\alpha S)\right] \cdot dL \qquad (4a)$$

WHERE s_i REPRESENT THE RADII OF THE CIRCLES IN THE CIRCULAR GRID WITH THE CENTER AT p_o. FOR SELECTED INTERVALS OF S_i, EQUATION (1a) PROVIDES THE UNEQUALLY SPACED RADII OF THE GRID CIRCLES. FOR CONVENIENCE SAKE MOST GRIDS HAVE THE CIRCLES LABELLED WITH $S_i - S_o$, WHERE S_o REFERS TO THE GRID RADIUS PASSING THROUGH THE FIRE POOL CENTER, THUS LABELLING THE LATTER CIRCLE AS ZERO FEET.

- IN ADDITION TO EQUAL RADIAL SPACING THE EQUAL SPACED DISTANCES IN THE TANGENTIAL DIRECTION CAN BE OBTAINED FROM EQUATION (1a). TANGENTIAL SPACING INTERVALS EQUAL TO CORRESPONDING RADIAL SPACING INTERVALS

$$dL = dS \qquad (5)$$

OBTAINED FROM EQUATION (3a) AND (4a) ARE INDICATED BY THE LIGHT TICK MARKS ON THE GRID CIRCLES OF THE FOLLOWING VUGRAPHS.

Figure 7.17a. Derivation of Circular Grid

- DISTANCE CAMERA TO FIRE POOL CENTER, R_o 3536 FT
  DISTANCE CAMERA TO FIDUCIAL POINT, $R_\perp$ 3515 FT
  OBJECT TO IMAGE SPACE TRANSFER PARAMETER 0.07 RAD/IMAGE IN.
  LEAN ANGLE OF PLUME PLANE, θ 81^o

- FROM EQUATION (1a)

$$s_i = 14.3 \tan^{-1}(S_i/3515) \qquad (1b)$$

  WHERE S_i (FT) CHOSEN IN INTERVALS OF 100 FT

$$\tan^{-1}\left(\frac{S_i}{3515}\right) \quad \text{(RADIAN)}$$

$$s_i \quad \text{(INCHES)}$$

- THE CIRCULAR GRIDS, EQUATION (1b) ARE SHOWN ON THE FOLLOWING VUGRAPH WITHOUT A PLUME AND ON THE NEXT TWO VUGRAPHS WITH THE PLUME AT EIGHT DIFFERENT TIMES. THE FIDUCIAL POINT AND THE FIRE POOL CENTER ARE CLEARLY VISIBLE.

- NOTE THAT THE GRIDS ARE DECIDEDLY NON-LINEAR WITH LINEAR SCALE FACTORS NEAR THE FIDUCIAL AND AT 3000 FT DIFFERING BY A FACTOR OF 2 IN THE RADIAL DIRECTION AND BY A FACTOR OF $\sqrt{2}$ IN THE TANGENTIAL DIRECTION.

Figure 7.17b. Sample Calculation - Test No. 11
Far West View

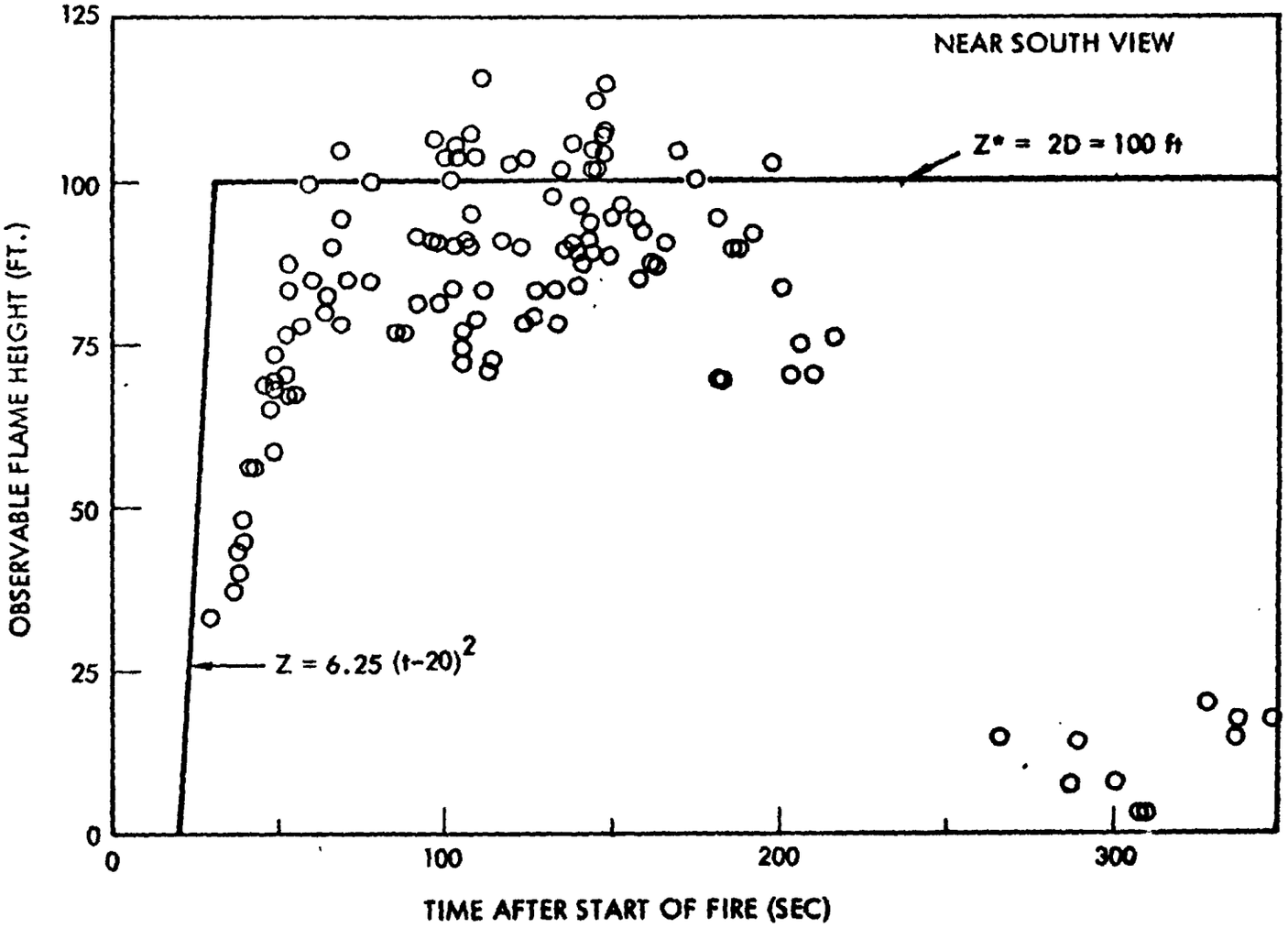

Figure 7.18a. Flame Heights - Test No. 11

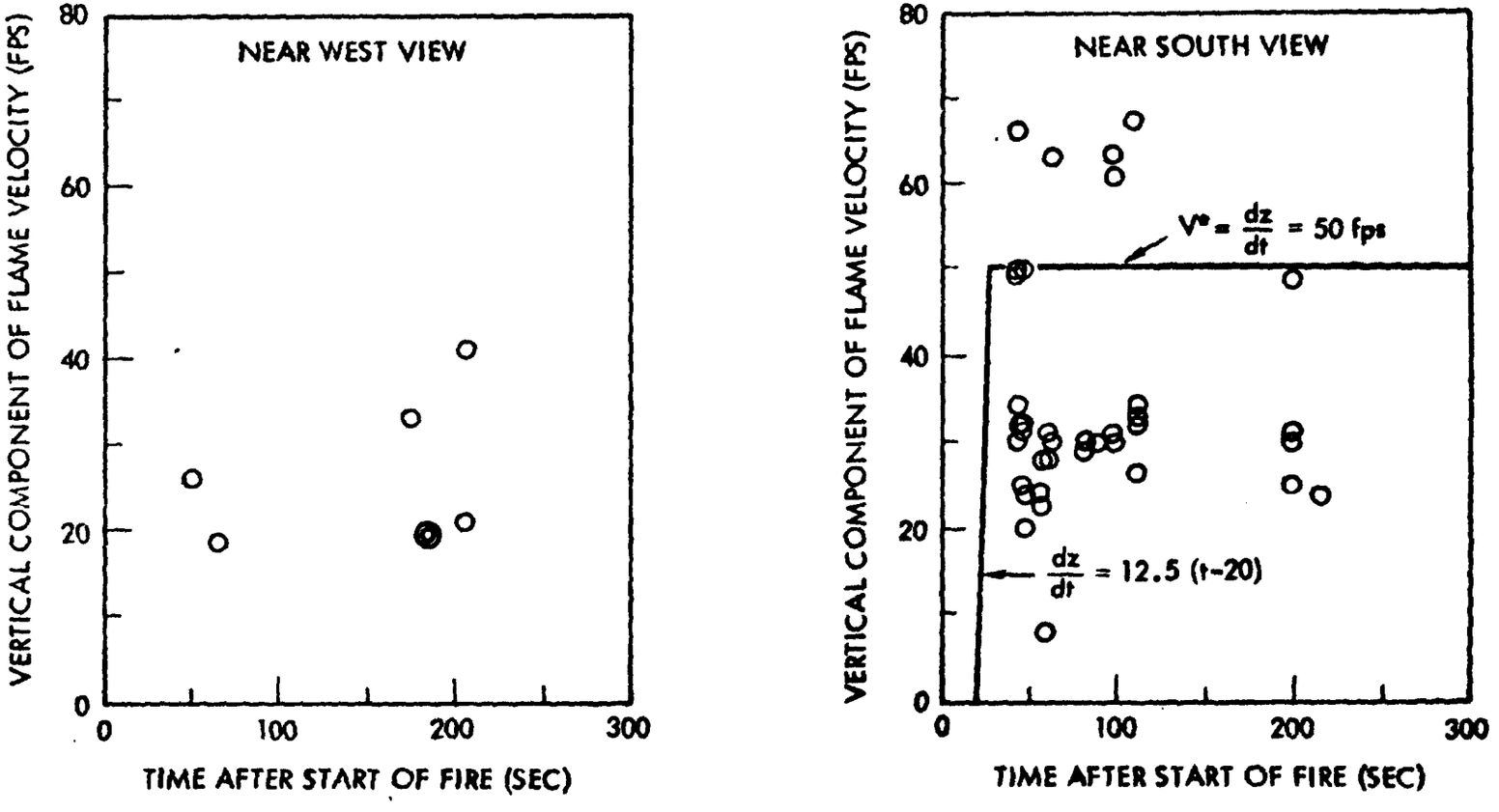

Figure 7.18b. Flame Speeds - Test No. 11

900 GAL JP5 : Q_H = 18,500 BTU/LB_m

FLAME HEIGHT AND FLAME RISE VELOCITY HISTORY

TEST CONDITIONS

$Q = 1.2 \times 10^{11}$ J

$Q = 1.2 \times 10^{8}$ CAL/SEC

$t_{BURN} = 240$ S

THEORY

- $\frac{dz}{dt} = \frac{V^*}{z^{*1/2}} z^{1/2} = 5z^{1/2}, \quad z < z^*$

$V^* \approx 0.1\, Q^{1/3} = 50$ FT/S

$z^* \approx 2D = 100$ FT

- $t^* = \frac{2z^*}{V^*} = 4S$

$t = \frac{2z}{dz/dt}$

- $z = 6.25t^2$

- $\frac{dz}{dt} = 12.5\, t$

Figure 7.18c. Test #11, Spoilers

Figure 7.19a shows the plume height histories for both the dense smoke as well as the more rarefied smoke; and the horizontal distance traversed by these plumes as a function of time. The correlations are based on the empirical relations shown in Figure 7.19b. The plume trajectory is shown in Figure 7.20a, and derivation is shown in Figure 7.20b.

INFRARED CAMERAS

The infrared cameras show the extent of the plume to be greater than indicated by the cine cameras, and for longer times (Figures 6.12, 6.20 and 6.24). Since carbon fiber clouds are particularly rarefied, this is an important attribute of the infrared system.

The infrared cameras are able to suppress the soot and fiber clouds to highlight hot spots in the plume. These hot spots were tracked and represented the trajectories of large pieces of carbon fiber laminate inside the cloud. It is apparent that repeated viewing of these same scenes, and using more subtle contrast settings, could reveal smaller laminates and their trajectories, which more closely track the local aerodynamics (Figures 6.27, 6.28 and 6.42). This is useful for plume modelling.

The infrared cameras appear to show a low hanging fiber cloud below the combustion product gases (Figure 6.25). This, too, requires further study.

ACTIVE GAGES

The active gages showed the concentration history, fiber length distribution as a function of time, intermittent character of the fiber cloud, the duration of the fiber cloud, and the effect of resuspension caused by personnel walking in the test area. These are properties not measurable by any of the passive gages, and never before measured.

The high voltage ball gage was particularly interesting in that it was sensitive to only those fibers greater than 3-4 mm long. It is exactly these longer fibers that are capable of damaging electrical equipment with exposures in the range of 10^4 to 10^7 fiber-seconds per cubic meter. Thus the ball gage gave a direct measure of the history of the fiber cloud which is of most interest for specifying the potential electrical hazards. The ball gage showed exposures of the order of 10^4 fiber-seconds per cubic meter for the plate, barrel and cockpit to ranges of 300 ft from the source, and the spoiler at an exposure of 10^3 fiber-seconds per cubic meter. (Figure 7.21). The plate and barrel achieved these exposures with peak concentrations of the order of 0.5 to 1.3 x 10^4 fibers per cubic meter, whereas the spoiler and cockpit showed almost no detectable concentration of fibers ($<10^3$ fibers per cubic meter). The spoilers and cockpit had such a rarefied cloud that the concept of a continuum is questionable with regard to the definition of concentration, but over 200 to 1500 seconds there was a measurable exposure that for the cockpit proved to attain the critical threshold value of exposure for the onset of susceptible electrical equipment failure. It is important to note that the fiber cloud was at least 2500 seconds in duration for the plate test.

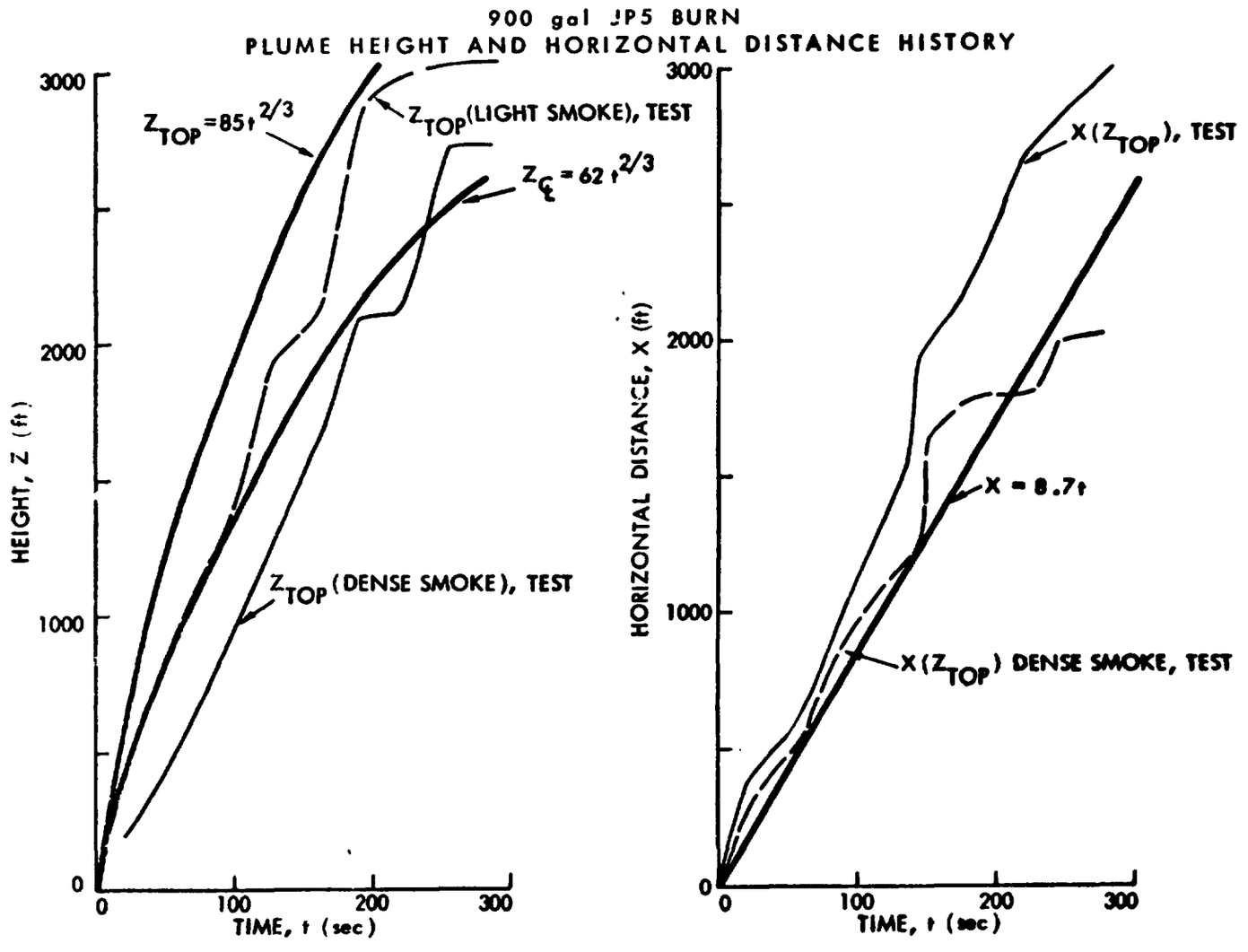

Figure 7.19a. Test No. 11, Spoilers

900 GAL JP5 : Q_H = 18,500 BTU/LB_m

PLUME HEIGHT AND HORIZONTAL DISTANCE HISTORY

TEST CONDITIONS:

$Q = 1.2 \times 10^{11}$ J

$\dot{Q} = 1.2 \times 10^{8}$ CAL/S

$F = 4.3 \times 10^{-3} \dot{Q}$ FT^4/S^3

U = 8.7 FT/S

$S = 1.1 \times 10^{-4} S^{-2}$ (U.S.S.A.)*

t_{BURN} = 240 S

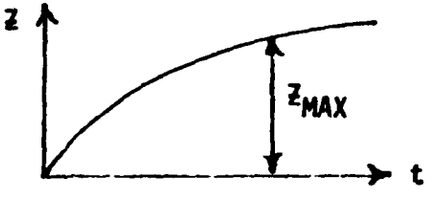

THEORY:

- $z_{\ell} = 1.6F^{1/3}U^{-1/3}t^{2/3} = 62\ t^{2/3}$
- $z_{TOP} = 1.38z_{\ell} = 85\ t^{2/3}$
- $x(z_{TOP}) = x(z_{\ell}) = Ut = 8.7\ t$ (BRIGGS '75)
- z_{MAX} $U \to 0$ $= 5.0F^{1/4}S^{-3/8} = 4000$ ft (MORTON-TAYLOR-TURNER '56)
- z_{MAX} $U \neq 0$ $= 2.9\ (F/US)^{1/3} = 2400$ ft (BRIGGS '75)

* UNITED STATES STANDARD ATMOSPHERE

CONCLUSION

- PLUME HEIGHT HISTORY FORMULA OVER-PREDICTS UP TO 40%
- HORIZONTAL DISTANCE HISTORY FORMULA UNDER-PREDICTS UP TO 50% WITH THE GAP NARROWING FOR LATER TIMES

Figure 7.19b. Test #11, Spoilers

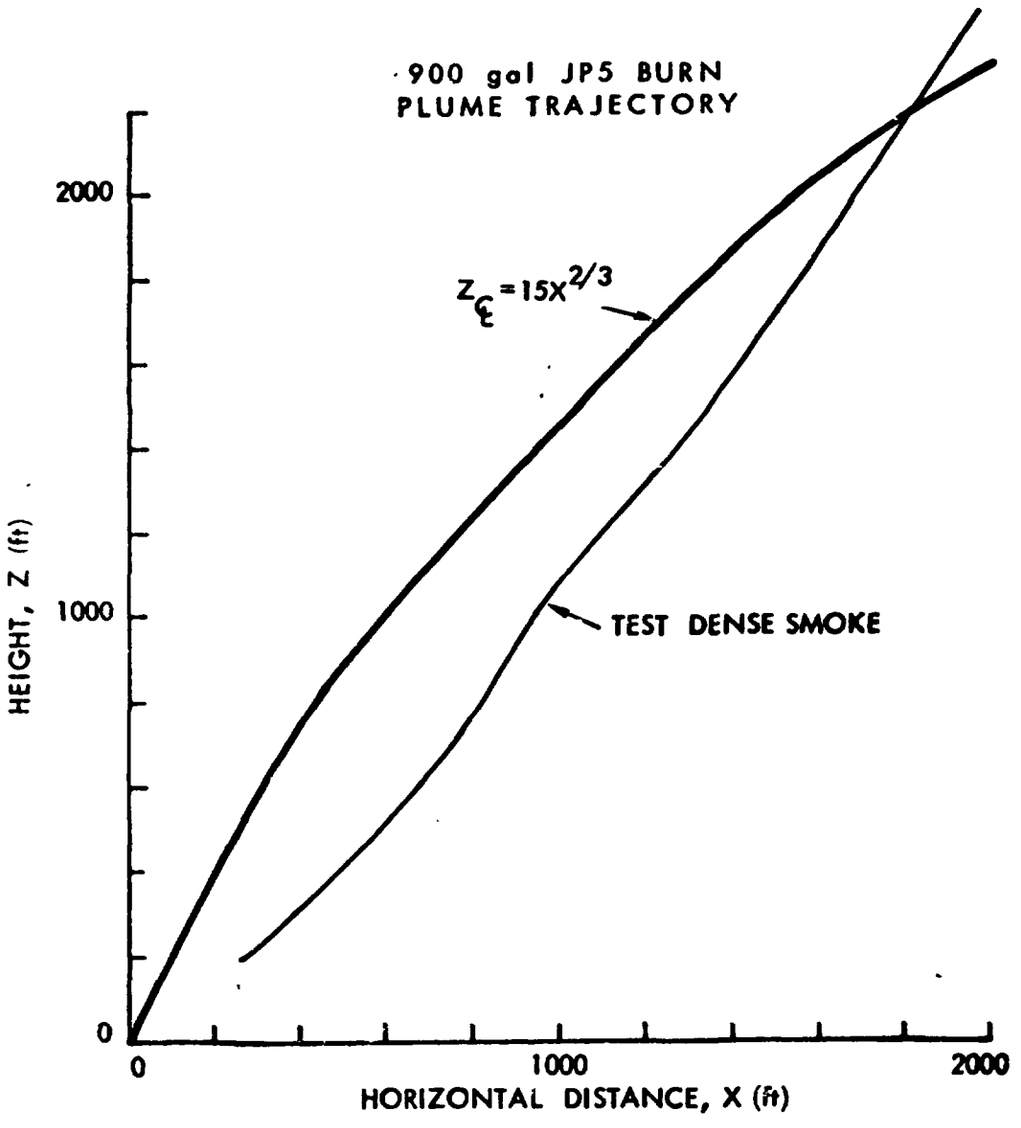

Figure 7.20a. Test No. 11, Spoilers

900 GAL JP5 : Q_H = 18,500 BTU/LB_m
PLUME TRAJECTORY

TEST CONDITIONS:

$Q = 1.2 \times 10^{11}$ J

$\dot{Q} = 1.2 \times 10^{8}$ CAL/S

$F = 4.3 \times 10^{-3}\dot{Q}$ FT^4/S^3

U = 8.7 FT/S

$S = 1.1 \times 10^{-4} S^{-2}$ (U.S.S.A.)*

t_{BURN} = 240 S

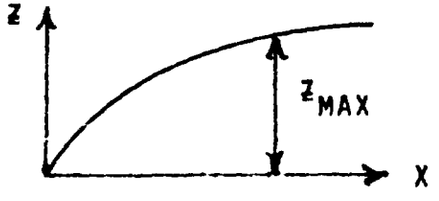

THEORY:

- $z_c = 1.6F^{1/3}U^{-1}x^{2/3} = 15\ x^{2/3}$
- $x(z_{TOP}) = x(z_c) = Ut = 8.7\ t$ (BRIGGS '75)
- z_{MAX} $U \to 0$ $= 5.0\ F^{1/4}S^{-3/8} = 4000$ ft (MORTON-TAYLOR-TURNER '56)
- z_{MAX} $U \neq 0$ $= 2.9\ (F/US)^{1/3} = 2400$ ft (BRIGGS '75)

* UNITED STATES STANDARD ATMOSPHERE

CONCLUSION

- PLUME HEIGHT AS A FUNCTION OF HORIZONTAL DISTANCE OVER-PREDICTS THE TEST DATA UP TO 60%, BUT AGREES AT Z_{MAX}

Figure 7.20b. Test #11, Spoilers

STRUCTURE	CARBON FIBER WEIGHT AFTER BURN (pounds)	RANGE (ft)	PEAK CONCENTRATION (10^3 fiber/M^3)		PEAK EXPOSURE (10^4 fiber-sec/M^3) & DURATION (sec)			
					E	t*	E	t
			LED	BALL	LED	LED	BALL	BALL
Plate	1.29	75	2.1	5	.53	25	1.4	700
		100	4	-	1.81	41	-	
		150	-	4.2	-	-	2.9	700
		200	2.6	<1	.94	19	2.9	700
		300	2.35	-	.43	22	-	-
Barrel A Test #8	1.28	75	>100	13.4	>100	5	2.3	364
		100	18.4	-	3.9	46	-	-
		150	5,9	<1	1.5	14	0.1	364
		200	12.5	8.7	1.5	35	2.1	364
		300	4.3	-	1.3	6	-	-
Spoiler A Test #11	5.8	214	11	<1	1.8	179	.1	235
		264	12.8	<1	6.2	264	.2	235
		314	2.7	<1	2.1	295	.4	235
		414	1.2	-	.7	290	-	-
Cockpit	35.7	214	339	<1	220	431	1.2	1510
		264	-	<1	-	-	0.5	1510
		314	17.7	<1	5.8	589	1.4	1510
		414	89.7	-	13.4	481	-	-

* Data reduced to this time

Figure 7.21. Peak Concentrations, Peak Exposures and Fiber Cloud Duration

On the other hand, the LED gage measured all the fibers that the ball gage detected, and also the smaller fibers in the 1-3 mm length that the ball gage did not detect. Since there was a dominant number of fibers in the 1-3 mm lengths, the LED yielded higher concentrations than the ball gage. For the spoiler tests, the data was reduced for comparable times and the LED gave exposures 30 times higher than the ball gage. The peak concentrations of single fibers was of the order of 10^3 fibers per cubic meter for the flat plate at up to 300 ft range. The barrel and spoiler concentrations achieved 10^4 fibers per cubic meter, and the cockpit achieved 10^5-10^6 fibers per cubic meter.

The microwave system was placed in just a few locations to spot check for the mass flux of large clumps. These clumps would have saturated the ball LED systems. In the 25-50 ft range locations the microwave yielded 300 to 500 μgm/cm^2-sec mass flux for the plate and barrel tests. There were just a few of these systems available and they were not always in the center of the fiber cloud. However, it is interesting to compare the data from this system which measure large clumps, to the data from the LED and ball systems which measured single and multiple fibers as is done in the next section.

The ladar showed the fiber cloud to be composed of three separate clouds as a function of height, the 28-second instant after the explosion of the barrel. The clouds appear 5-10 ft high with 20 ft vertical separations. The uppermost fiber cloud is at 80 ft. At 85-seconds, only two fiber clouds pass and the uppermost cloud is only 30 ft off the ground. At 185-seconds, there is only the low lying fiber cloud about 10 ft off the ground (Figure 5.26).

The flame velocimeter measured the 11-38 ft per second vertical rise of the smoke/flame from the JP-5 pool fires. This is a device newly developed at TRW, and has the capability of validating computer models of the fire plume (Figures 5.37).

The L-C deposition history gage is another device newly developed at TRW to measure the mass per unit area history of clumps depositing on the ground. The device was shown feasible, but not used to develop data for this project (Figure 5.41).

COMPARISON OF MEASUREMENT SYSTEMS

The consistency of the different measurement systems is vital. Prior to the field test program, the instrumentation that was available was designed to measure single fibers. That instrumentation plus a microwave and LED instrumentation was thereafter applied to multiple fibers, clusters and clumps. Thus it is necessary to compare the data from each measurement system to assure consistency.

Figure 7.22 shows the integrated mass flux of the active instrumentation against the deposition per unit area measured on the sticky paper. The circles represent the plate tests; triangles the barrel test; squares the spoilers; and diamonds the cockpit. Note that the microwave gages measured high, the LED gages measured within the envelope of sticky paper data, and the ball gages measured low in the plate tests; whereas the decay of deposition for each gage system was at the 1.5-power of range. Considering the different physics principles

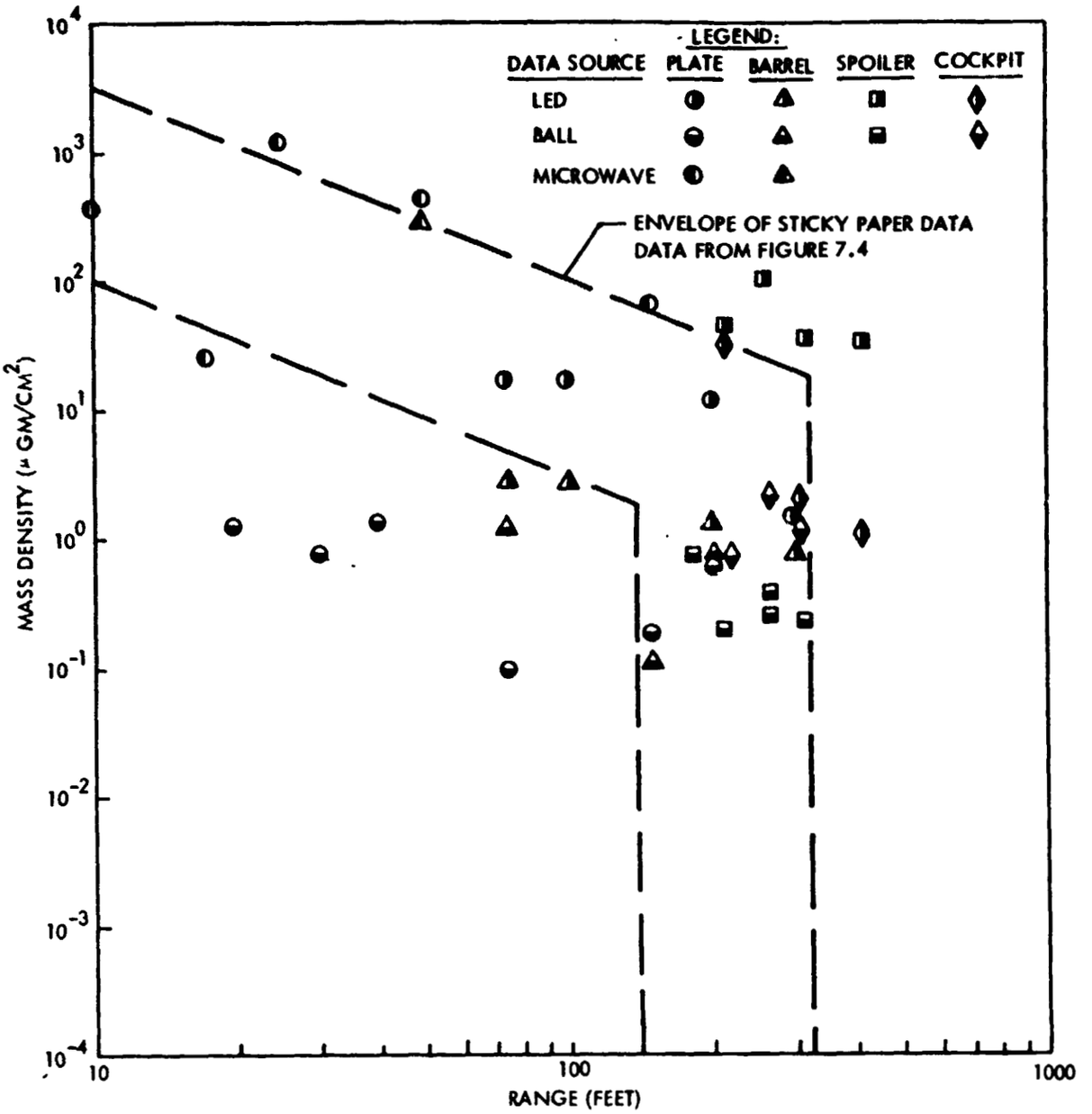

Figure 7.22. Integration Mass Flux through Active Gages as a Function of Range

involved in each of the gage systems, this represents good agreement. Also by considering that the ball gage is insensitive to fibers below 4 mm in length, and that the microwave gage is insensitive to single fibers when in low concentration and is designed to detect clumps; the order of ball gage (below envelope),LED gage (within envelope) and microwave gage (above envelope) is reasonable. And the wide swing of the flux measurements at a given range is consistent with the phenomenology being measured.

The barrel test was on the average lower in mass flux than the sticky paper envelope. The microwave gage read at the upper limit of the sticky paper envelope, while the LED and ball gages read at the lower limit of the sticky paper limit; but the slope was consistent with the 1.5-power decay with range as shown in Figure 7.22.

The spoiler test mass flux data was just above and below the envelope determined by the plate test data; again the LED gages read higher and the ball gages read lower. It should be recalled that the spoiler test involved about a factor of five increase in weight, which should result in an increase in integrated mass flux, but on the other hand, the introduction of the pool fire plume with its updraft results in a decrease in integrated mass flux at the ranges less than 300 ft. Thus these competing effects appear to cancel each other.

The LED gage and ball gage data from the cockpit test fell between the respective data from the spoiler test, and within the passive data envelope. This agreement was obtained in spite of the highest initial carbon fiber mass. Again, the effect of the buoyant plume compensated for the high initial weight to cause the cockpit data to fall with the other test structures.

Figure 7.22 is particularly interesting in that different initial carbon fiber weights, different burn temperatures and burn times, explode and non-explode, and different plume sizes were involved. There is widespread scatter of the data as may be expected from the differences in the tests, but there is an overall trend that shows the active data following the pattern of the passive data.

The cloud photography for Test No. 11 showed the overhead carbon fiber cloud development. Figure 7.6 showed the carbon fibers arriving at the furthermost LED gage at the earliest time with this trend continuing until the closest to the source LED gage shows the carbon fiber cloud arriving at the latest time. This effect can only be explained by a fall-out of carbon fibers from the overhead plume along a front such that the furthermost carbon fibers in horizontal range fall earliest.

Note that in Figure 7.6, the fiber cloud touches the ground at 1000 ft at the start and sweeps along the ground to 3000 ft. Figure 7.23 shows the deposition matching this pattern, with the peak deposition at 2000 ft.

The meteorological data compares well with the passive gage footprint (Figures 7.7, 7.8, 7.9 and 7.10).

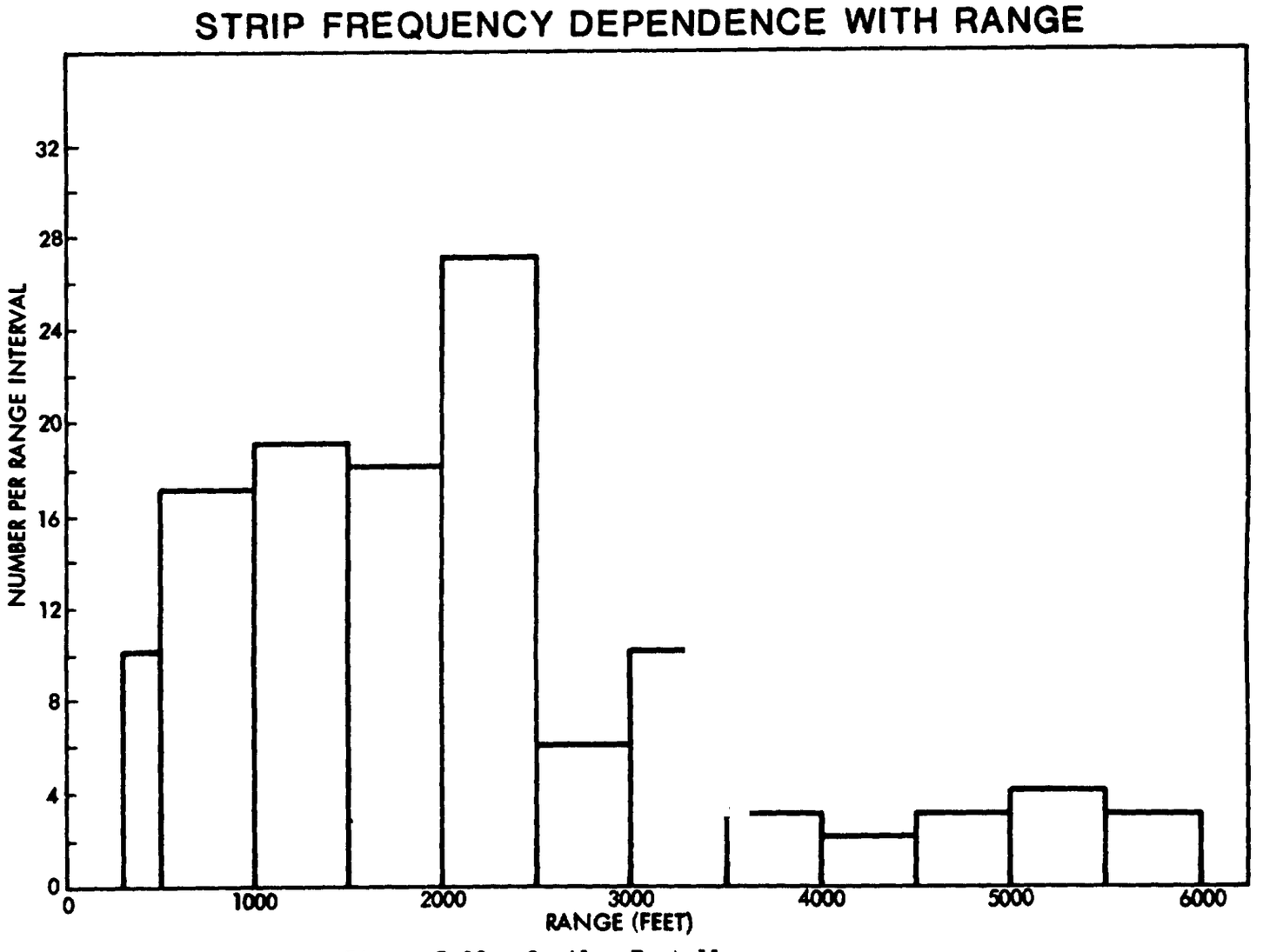

Figure 7.23. Spoiler Test 11

Comparison of the ladar data showing the descending carbon fiber cloud (Figure 5.26) with the infrared pictures (Figure 6.25) showing the descending carbon fiber cloud, indicates that the hot rising cloud of detonation gases is higher than the falling heavy carbon fiber cloud in the barrel Test No. 8.

8. CONCLUDING REMARKS

The concluding remarks will be presented in terms of target type (plate, barrel, spoiler and cockpit) in field tests and laboratory tests, as well as in terms of passive and active instrumentation.

- Thick Plate/Propane Burner/Explode

  The mass of single fibers released from burn and explode tests are less than 0.02% of the initial composite mass. This percent was obtained from the outdoor field tests at the Naval Weapons Center Test Site and from the outdoor screen enclosure chamber tests at the TRW Capistrano Test Site. This is 100 times smaller than the percent measured at the indoor chamber at the Naval Surface Weapons Center, Dahlgren Laboratory. This small percent is based on the deposition capture of 12 - 19 percent of the initial mass.

  The outdoor screen enclosure chamber tests yield fiber length and fiber diameter distributions comparable to those obtained in outdoor field tests.

  Passive data indicated that of the single fibers in the 1 to 20 mm range, about 50 to 80 percent were in the length range of 1 to 3 mm, with the balance principally in the range of 3 to 6 mm. It is fibers in the length range of 3 to 20 mm that represent a potential hazard to electrical equipment.

  The burn and explode tests of plates resulted in mostly blast fragments (clumps) by comparison to the single fibers. The 40-ply structure of the plates appears to influence this result.

  Burn and explode of plates in the range of 1000 pounds can induce the critical exposure of 10^6 fiber seconds per cubic meter within 200 ft of the source, with fibers 3 - 6 mm long.

- Thin Barrel/Propane Burner/Explode

  The hot propane burn of the barrel followed by explode, resulted predominantly in single fibers and clusters. The single fibers were mostly in the 1 - 6 mm length interval.

  Distribution of the clusters extended from near ground zero out to the limits of the passive instrumentation array at 3000 ft downrange.

- Thin Barrel/Pool Fire/Explode

  A JP-5 pool fire burn of another barrel and then explode, caused a strong reduction in single fiber deposition close-in because of the ability of the post fire plumes to loft fibers to several thousand feet altitude and for the wind to transport the lofted fibers to great horizontal distances.

The rapid heating of the thin structure with few ply resulted in delamination of each ply, and the plume updraft did not permit the separated and rising ply to remain very long in the hottest portions of the pool fire. Thus, these plys eventually deposited as strips.

Several strips reached 1200 ft downwind. One was 10" long and 1" wide. No strips were generated in the propane burner and explode tests.

- Thin Spoilers/Pool Fire

The burn of the spoilers in the JP-5 pool fire resulted in the emission of principally single fibers by virtue of the turbulent action of the fire, and the short residence time in the fire/updraft again resulted in strip formation.

The strips were mostly 12" to 24" long, 0.25" to 1.0" wide, and 1 to 1.2 ply thick. They deposited mostly in the 1000 to 2000 ft downwind range, with almost as many reaching 2000 to 3000 ft downwind range. These sizes and ranges are of special interest to composite materials in fires near power substations.

- Thin Spoilers/Pool Fire/Explode

After explode, there was a greater deposition of single fibers and with no strips.

Of all the particles caught in the Jacob's ladder bridal veil, about 80% were single fibers.

- Thin Cockpit/Pool Fire

The cockpit burn over a JP-5 pool fire resulted in rapid delamination and generation of lint and strips, with relatively few single fibers.

Most of the strips generated by a large size pool fire are 1 - 2 ply thick, 1/4 to 1 inch wide and have a length comparable to the initial lay-up length.

The plume from the large size pool fire controlled the fiber deposition. Most all of the deposition is in strips because of rapid delamination, and they fall out directly below the plume. Single fibers were detected in the vertical plane of the Jacob's ladder, but these particles were carried to beyond 3000 to 6000 ft. Thus, the meteorological conditions and JP-5 pool size, which control the plume size and tilt, also control the fiber deposition.

- Laboratory Tests

Prolonged burning of carbon fiber structures composed of a few ply, for several minutes at greater than 1000^{o}F, will result in the oxidation of carbon fiber. Present test data showed that this oxidation created

fibers that were in the range of 1 - 3 microns diameter, where health may be a factor to be considered.

There are catalytic effects of the resin that cause more rapid oxidation of the carbon fibers. There were differences in oxidation temperatures noted due to such subtle variations as tests involving Narmco 5208 versus Narmco 5209 resins.

- Passive Instrumentation

Passive instrumentation data comprises the majority of the data reduction effort, and results in the deposition footprint and the fiber size distribution at many stations in the footprint. The initial placement of inexpensive and large number of passive sensors did not require a great effort. However, in order to evaluate the data sufficiently, it was necessary to expend several personnel for several months as compared to the active instruments which are expensive to deploy but simpler and more rapidly evaluated for data reduction.

There are several broad conclusions with regard to the effectiveness of each type of passive sensor:

- millipore filter/vacuum - This system was not effective in capturing sufficient number of fibers by comparison to the other nearby sensor types. The low capture efficiency may be related to its small diameter and the millimeter fiber lengths of interest.

- tuna can/bridal veil - This system was effective in capturing fibers greater than 1 millimeter in length. The tuna can arrays extended to only 30 ft in height, and therefore did not sample the entire cross-section of the fiber cloud.

- sticky paper - Good representations of fiber characteristics and size distributions were obtained by means of the sticky paper gages. The adhesiveness retained its strength sufficiently to afford good data records even though the sensors on some occasions were exposed to the dustiness, dew, wind and sunshine for extended periods due to test initiation delays because of meteorological conditions. It is recognized that there is a difference between the "deposition" capture efficiency of sticky paper versus the "exposure" capture efficiency of the bridal veil.

- Jacob's ladder - The Jacob's ladder was an innovation in that it was designed to intercept all of the plume generated by a propane burn and explode test, and was used effectively to intercept a portion of the fire plume generated by a jet fuel pool burn test. This permitted gaining information regarding vertical distributions of the carbon fibers in the overhead cloud.

- Active Instrumentation

The active data yielded an additional dimension to the data analysis that gives more insight into the passive data and gives support to the dynamics of the phenomenology so important to model development. It should be noted that this was the first field effort wherein many of the laboratory instruments were used. However, considering the importance of these field tests, the effort proved worthwhile.

The meteorological data from a 54-ft high tower was adequate for predicting the carbon fiber cloud footprint based on the wind speed history and wind direction history over short time intervals. Also the meteorological data defined the atmospheric stability category based on either (1) standard deviation of wind direction history over a 1/4 to 1 hour period or (2) thermal gradient in the vertical direction.

The plume from an explosion that creates a near vertical cylinder of detonation gases and carbon fibers, deposits a downwind footprint that is dictated by the local wind speed and local wind direction. Thus it is possible to use meteorological tower data to predict a carbon fiber footprint as a result of a burn and explode accident.

The cine cameras recorded the characteristics of the puff of smoke/fibers after the propane burn and explode of the flat plate and barrel A. These characteristics included the overall size of the cloud at each instant, and the trajectory of the centerline at each instant. These measured characteristics correlated with the trajectories predicted by explosive fireball empirical formula for puffs based on non-dimensional groups. Similarly, the cine cameras recorded the characteristics of the plume of smoke/fibers after the JP-5 pool fire burn and burn/explode of barrel B, spoilers and cockpit. As in the case of the puff, the measured trajectories correlated with the predictions by the empirical formula for plumes based on non-dimensional groups.

Comparison of the cine camera results to the active instrument data showed the cloud to rise and move downwind, and then fall and move further downwind. The cloud arched over the active instrumentation array. The simultaneous arrival of the carbon fiber cloud at all active instruments at the different radial stations therefore showed that the fiber cloud was dropping from the overhead cloud down to ground level.

Comparison of the cine camera profiles to the deposition footprint in the pool fire tests showed that the plume footprint at ground level and deposition footprint coincide. Comparison of the cine cameras vertical velocity for rising smoke swirls was consistent with the vertical velocities of hot spots measured with the infrared cameras and with the newly developed TRW flame velocimeter.

The infrared imaging cameras continued to track the puffs and plumes for longer times and over greater distances, as compared to the cine camera observation limits. Adjustment of the signal level and contrast level

for a specific scene suppressed the soot cloud and revealed trajectories of hot objects within the cloud, which permitted data acquisition with regard to the aerodynamics inside the plume (updraft and also horizontal entrainment velocities). There appears to be the potential of further separating the fiber cloud image from that of the gas products in downwind ranges, but further data reduction is required.

The high voltage ball gages were sensitive to fibers having lengths greater than 4 mm long, the size of importance to the electrical equipment hazards. The ball gages showed for these longer lengths that exposures of the order of 10^4 fiber-seconds per cubic meter, in the 200 ft range, were achieved per pound of carbon fiber source for the 100 ft high puff; whereas this critical exposure would be achieved in the same range by a 35 pound carbon fiber source even when there is the benefit of a 3000 ft high plume spreading fibers over a greater area. Fiber cloud durations ranged from 235 seconds to 1500 seconds. Peak concentrations of 10^4 fibers per cubic meter of fibers, at least 4 mm long, were measured within 200 ft range for the plate and barrel tests where the 100 ft high puff was the source.

The LED gages were sensitive to fibers having lengths greater than 1 mm in length. Most of the fibers were measured to be in the 1 to 3 mm length, which require more than 10^8 fiber-second per cubic meter exposures to induce circuit failures. The LED will measure concentrations and exposures of the 1 - 3 mm and also the 3 to 20 mm length fibers. The total of these two sources of concentrations is too high for purposes of resolving the electrical hazard potential.

The gages recorded concentrations 1.5 to 5 times the ball gage concentrations for the plate and barrel and 10 to 400 times the ball gage concentrations for the spoiler and cockpit. These ratios represent the ratio of LED data for fibers 1 - 20 mm in length compared to ball gage data for fibers 4 - 20 mm in length. These peak concentrations were of the order of 10^3 fibers per cubic meter for the plates, 10^4 fibers per cubic meter for the barrel and spoilers, and 10^5 fibers per cubic meter for the cockpit. Analysis of the LED and ball gage recordings show the importance of the late-time fiber cloud.

It was observed as expected that the integrated mass flux from the microwave gage fell at the upper envelope of all the data for integrated mass flux versus range due to the fact that this gage records massive pieces falling through its sampling volume.

The broad conclusions for the active instrumentation are as follows:

- ball/LED/microwave - These systems showed the fiber cloud relative arrival times at different ranges, the comparative deposition rates at different time intervals, the overall deposition period, the late-time reentrainment of fibers induced by wind gusts and personnel entering the area. In addition there were the concentration and mass flux histories

that were measured which supplemented the deposition data measured by the passive sensors. The data obtained by means of the active instrumentation uniquely specifies the observed deposition and is therefore of value toward validation of computer models.

- visible/infrared cameras - These systems yielded plume trajectories and propagation phenomena that were useful in explaining the fiber cloud transport and observed deposition footprint.

- meteorological - The meteorological sensors (wind speed, wind direction and vertical temperature gradient) were vital in both the execution of each test, as well as in establishing the data interpretation. The wind speed and direction were used to assure that the fiber cloud would pass over the instrumentation array. The wind velocity history from the towers were effective in predicting the deposition footprint to 3000 ft.

APPENDIX

TEST CONDITIONS

Given in this appendix in Tables A.1 through A.15 are the detailed test conditions for each of the fifteen tests conducted in the test series. A description of some of the characteristics unique to each test is given in Section 3, pp 3-27 through 3-32.

Table A.1. Test Conditions for Test No. 1

TRW TEST NO. 1 NWC TEST NO. _____ CTS TEST NO. 1

TEST SITE CTS, within a 15 ft x 15 ft screened enclosure

TEST TITLE Flat Plate, Thornel 300/Narmco 5208 Plate
1 ft x 1 ft x 1/4 in

TYPE OF BURN Propane
BURN DURATION 40 minutes
BURN LOCATION Center of Pad
BURN DATE 11-9-77
TIME OF BURN _____

EXPLODE MODE Delayed
CONFIGURATION 4 ea 1/2 oz C-4
_____
EXPLODE LOCATION Center of Pad
EXPLODE DATE 11-9-77
TIME OF EXPLODE _____

PASSIVE INSTRUMENTATION		ACTIVE INSTRUMENTATION	
SP SHEETS	23	LED	2
SP STRIPS		MICROWAVE	1
SP ROLLS		BALL	2
TUNA CANS		LADAR	
BV VUGRAPHS		TC IN SAMPLE	4
BV FRAMES		TC IN FLAME	1
BV LADDER		VELOCIMETER	
MILLIPORES	4		
PAD COLLECTION		METEOROLOGY	
SWEEP BRIGADES		THERMOCOUPLES	
PHOTOGRAPHY		VANES	
INFRARED IMAGING		ANEMOMETERS	1
MOVIES	1	SMOKE GENERATORS	
		CAPTIVE BALLOONS	
		FREE BALLOONS	

Table A.2. Test Conditions for Test No. 2

TRW TEST NO. 2 NWC TEST NO. _____ CTS TEST NO. 2

TEST SITE CTS, within a 15 ft x 15 ft screened enclosure

TEST SAMPLE Flat Plate, Thornel 300/Narmco 5208 Plate
1 ft x 1 ft x 1/4 in

TYPE OF BURN	Hot Propane	EXPLODE MODE	Delayed
BURN DURATION	20 minutes	CONFIGURATION	4 ea 1/2 oz C-4
BURN LOCATION	Center of Pad		
BURN DATE	11-10-77	EXPLODE LOCATION	Center of Pad
TIME OF BURN		EXPLODE DATE	11-10-77
		TIME OF EXPLODE	

PASSIVE INSTRUMENTATION		ACTIVE INSTRUMENTATION	
SP SHEETS	6	LED	4
SP STRIPS		MICROWAVE	1
SP ROLLS		BALL	2
TUNA CANS	2	LADAR	
BV VUGRAPHS		TC IN SAMPLE	4
BV FRAMES		TC IN FLAME	1
BV LADDER		VELOCIMETER	
MILLIPORES	4		
PAD COLLECTION		METEOROLOGY	
SWEEP BRIGADES		THERMOCOUPLES	
PHOTOGRAPHY		VANES	
INFRARED IMAGING		ANEMOMETERS	1
MOVIES	1	SMOKE GENERATORS	
		CAPTIVE BALLOONS	
		FREE BALLOONS	

Table A.3. Test Conditions for Test No. 3

TRW TEST NO. 3 NWC TEST NO. _____ CTS TEST NO. 3

TEST SITE CTS, within a 15 ft x 15 ft screened enclosure

TEST SAMPLE Flat Plate, Thornel 300/Narmco 5208
1 ft x 1 ft x 1/4 in

TYPE OF BURN	Hot Propane	EXPLODE MODE	Delayed
BURN DURATION	20 minutes	CONFIGURATION	8 ea 1/2 oz C-4
BURN LOCATION	Center of Pad		
BURN DATE	12-13-77	EXPLODE LOCATION	Center of Pad
TIME OF BURN		EXPLODE DATE	12-13-77
		TIME OF EXPLODE	

PASSIVE INSTRUMENTATION		ACTIVE INSTRUMENTATION	
SP SHEETS	7	LED	
SP STRIPS	2	MICROWAVE	
SP ROLLS		BALL	
TUNA CANS		LADAR	1
BV VUGRAPHS		TC IN SAMPLE	2
BV FRAMES		TC IN FLAME	1
BV LADDER		VELOCIMETER	
MILLIPORES			
PAD COLLECTION		METEOROLOGY	
SWEEP BRIGADES		THERMOCOUPLES	
PHOTOGRAPHY		VANES	
INFRARED IMAGING		ANEMOMETERS	1
MOVIES	1	SMOKE GENERATORS	
		CAPTIVE BALLOONS	
		FREE BALLOONS	

Table A.4. Test Conditions for Test No. 4

TRW TEST NO. 4 NWC TEST NO. 1 CTS TEST NO. _____

TEST SITE NWC

TEST SAMPLE Flat Plate, Thornel 300/Narmco 5208
1 ft x 1 ft x 1/4 in

TYPE OF BURN	Propane	EXPLODE MODE	Delayed
BURN DURATION	20 minutes	CONFIGURATION	1 ea 2-oz C-4
BURN LOCATION	Ground Zero		
BURN DATE	1-24-78	EXPLODE LOCATION	Ground Zero
TIME OF BURN	1102	EXPLODE DATE	1-24-78
		TIME OF EXPLODE	1247

PASSIVE INSTRUMENTATION		ACTIVE INSTRUMENTATION	
SP STANDS	34	LED	20
SP STRIPS	44	MICROWAVE	6
SP ROLLS	3	BALL	6
TUNA CANS	77	LADAR	
BV VUGRAPHS		TC IN SAMPLE	3
BV FRAMES		TC IN FLAME	1
BV LADDER		VELOCIMETER	
MILLIPORES	99		
PAD COLLECTION		METEOROLOGY	
SWEEP BRIGADES		THERMOCOUPLES	8
PHOTOGRAPHY		VANES	6
INFRARED IMAGING	2	ANEMOMETERS	6
MOVIES	4	SMOKE GENERATORS	1
		CAPTIVE BALLOONS	2
		FREE BALLOONS	

Table A.5. Test Conditions for Test No. 5

TRW TEST NO. 5 NWC TEST NO. 2 CTS TEST NO. _____

TEST SITE NWC

TEST SAMPLE Flat Plate, Thornel 300/Narmco 5208
1 ft x 1 ft x 1/4 in

TYPE OF BURN	Hot Propane	EXPLODE MODE	Delayed
BURN DURATION	20 minutes	CONFIGURATION	1 ea 2-oz C-4
BURN LOCATION	Ground Zero		
BURN DATE	2-1-78	EXPLODE LOCATION	Ground Zero
TIME OF BURN	0841	EXPLODE DATE	2-1-78
		TIME OF EXPLODE	0957

PASSIVE INSTRUMENTATION		ACTIVE INSTRUMENTATION	
SP STANDS	19	LED	20
SP STRIPS	44	MICROWAVE	6
SP ROLLS	11	BALL	9
TUNA CANS	154	LADAR	1
BV VUGRAPHS	44	TC IN SAMPLE	3
BV FRAMES		TC IN FLAME	1
BV LADDER		VELOCIMETER	
MILLIPORES	99		
PAD COLLECTION		METEOROLOGY	
SWEEP BRIGADES		THERMOCOUPLES	8
PHOTOGRAPHY		VANES	6
INFRARED IMAGING	2	ANEMOMETERS	6
MOVIES	4	SMOKE GENERATORS	1
		CAPTIVE BALLOONS	2
		FREE BALLOONS	

Table A.6. Test Conditions for Test No. 6

TRW TEST NO. 6 NWC TEST NO. 3 CTS TEST NO. _____

TEST SITE NWC

TEST SAMPLE Flat Plate, Thornel 300/Narmco 5208
1 ft x 1 ft x 1/4 in

TYPE OF BURN	Hot Propane	EXPLODE MODE	Delayed
BURN DURATION	20 minutes	CONFIGURATION	1 ea 2-oz C-4
BURN LOCATION	Ground Zero		
BURN DATE	2-15-78	EXPLODE LOCATION	Ground Zero
TIME OF BURN	1537	EXPLODE DATE	2-16-78
		TIME OF EXPLODE	0755

PASSIVE INSTRUMENTATION		ACTIVE INSTRUMENTATION	
SP STANDS	19	LED	20
SP STRIPS	44	MICROWAVE	6
SP ROLLS	7	BALL	9
TUNA CANS	226	LADAR	1
BV VUGRAPHS	44	TC IN SAMPLE	3
BV FRAMES		TC IN FLAME	1
BV LADDER		VELOCIMETER	
MILLIPORES			
PAD COLLECTION		METEOROLOGY	
SWEEP BRIGADES		THERMOCOUPLES	8
PHOTOGRAPHY		VANES	6
INFRARED IMAGING	2	ANEMOMETERS	6
MOVIES	2	SMOKE GENERATORS	1
		CAPTIVE BALLOONS	2
		FREE BALLOONS	

Table A.7. Test Conditions for Test No. 7

TRW TEST NO. 7 NWC TEST NO. 3+ CTS TEST NO. _____

TEST SITE NWC

TEST SAMPLE (Calibration Shot - No Sample)

TYPE OF BURN	None	EXPLODE MODE	No Delay
BURN DURATION		CONFIGURATION	1 ea 2-oz C-4
BURN LOCATION			
BURN DATE		EXPLODE LOCATION	Ground Zero
TIME OF BURN		EXPLODE DATE	2-17-78
		TIME OF EXPLODE	0823

PASSIVE INSTRUMENTATION		ACTIVE INSTRUMENTATION	
SP STANDS		LED	
SP STRIPS		MICROWAVE	
SP ROLLS		BALL	
TUNA CANS		LADAR	
BV VUGRAPHS		TC IN SAMPLE	
BV FRAMES		TC IN FLAME	
BV LADDER		VELOCIMETER	
MILLIPORES			
PAD COLLECTION		METEOROLOGY	
SWEEP BRIGADES		THERMOCOUPLES	8
PHOTOGRAPHY		VANES	6
INFRARED IMAGING	2	ANEMOMETERS	5
MOVIES	2	SMOKE GENERATORS	1
		CAPTIVE BALLOONS	2
		FREE BALLOONS	

Table A.8. Test Conditions for Test No. 8

TRW TEST NO. 8 NWC TEST NO. 4 CTS TEST NO. _____

TEST SITE NWC

TEST SAMPLE Barrel, Carbon Composite, AS/APCO 2434 Fiber/Resin System.
2 ft dia x 3 ft barrel cut up into 12 segments

TYPE OF BURN	Hot propane	EXPLODE MODE	Delayed
BURN DURATION	20 minutes/burn	CONFIGURATION	1 ea 2 oz C-4
BURN LOCATION	Ground Zero		
BURN DATE	3-6-78, 3-7-78	EXPLODE LOCATION	Ground Zero
TIME OF BURN		EXPLODE DATE	3-8-78
		TIME OF EXPLODE	0757

PASSIVE INSTRUMENTATION		ACTIVE INSTRUMENTATION	
SP STANDS	90	LED	20
SP STRIPS	222	MICROWAVE	5
SP ROLLS		BALL	9
TUNA CANS	226	LADAR	1
BV VUGRAPHS	44	TC IN SAMPLE	
BV FRAMES	30	TC IN FLAME	1
BV LADDER		VELOCIMETER	
MILLIPORES			
PAD COLLECTION	1	METEOROLOGY	
SWEEP BRIGADES		THERMOCOUPLES	8
PHOTOGRAPHY		VANES	6
INFRARED IMAGING	2	ANEMOMETERS	6
MOVIES	2	SMOKE GENERATORS	
		CAPTIVE BALLOONS	3
		FREE BALLOONS	

Table A.9. Test Conditions for Test No. 9

TRW TEST NO. 9 NWC TEST NO. 5 CTS TEST NO. _____

TEST SITE NWC

TEST SAMPLE Half Barrel, carbon composite AS/APCO 2434 fiber/resin system
2 ft dia x 3 ft

TYPE OF BURN	JP-5 3 lbs Mg & Al	EXPLODE MODE	None
BURN DURATION	1st 3 min, 2nd 6 min	CONFIGURATION	
BURN LOCATION	See Text		
BURN DATE	3-23-78	EXPLODE LOCATION	
TIME OF BURN	1st 1126, 2nd 1336	EXPLODE DATE	
		TIME OF EXPLODE	

PASSIVE INSTRUMENTATION		ACTIVE INSTRUMENTATION	
SP STANDS	90	LED	
SP STRIPS	222	MICROWAVE	
SP ROLLS		BALL	
TUNA CANS		LADAR	
BV VUGRAPHS		TC IN SAMPLE	1
BV FRAMES	30	TC IN FLAME	1
BV LADDER		VELOCIMETER	
MILLIPORES			
PAD COLLECTION	1	METEOROLOGY	
SWEEP BRIGADES		THERMOCOUPLES	8
PHOTOGRAPHY		VANES	6
INFRARED IMAGING	2	ANEMOMETERS	6
MOVIES	2	SMOKE GENERATORS	
		CAPTIVE BALLOONS	3
		FREE BALLOONS	10-20

Table A.10. Test Conditions for Test No. 10

TRW TEST NO. 10 NWC TEST NO. 6 CTS TEST NO. _____

TEST SITE NWC

TEST SAMPLE Half Barrel, carbon composite, AS/APCO 2434 fiber/resin system plus half barrel debris from Test 9 (NWC 5)

TYPE OF BURN	JP-5	EXPLODE MODE	Explode in Plume
BURN DURATION	5 minutes	CONFIGURATION	1 ea 2 oz C-4
BURN LOCATION	See Text		
BURN DATE	3-24-78	EXPLODE LOCATION	See Text
TIME OF BURN	1601	EXPLODE DATE	3-24-78
		TIME OF EXPLODE	1605

PASSIVE INSTRUMENTATION		ACTIVE INSTRUMENTATION	
SP STANDS	90	LED	
SP STRIPS	222	MICROWAVE	
SP ROLLS		BALL	
TUNA CANS		LADAR	
BV VUGRAPHS		TC IN SAMPLE	
BV FRAMES	30	TC IN FLAME	
BV LADDER		VELOCIMETER	
MILLIPORES			
PAD COLLECTION	1	METEOROLOGY	
SWEEP BRIGADES	2	THERMOCOUPLES	8
PHOTOGRAPHY		VANES	6
INFRARED IMAGING	2	ANEMOMETERS	6
MOVIES	2	SMOKE GENERATORS	
		CAPTIVE BALLOONS	3
		FREE BALLOONS	10-20

Table A.11. Test Conditions for Test No. 11

TRW TEST NO. 11 NWC TEST NO. 11A CTS TEST NO. _____

TEST SITE NWC

TEST SAMPLE Spoilers (3 ea), T300/5209 composite skins (originally identified incorrectly as AS/3501), aluminum fittings and honeycomb inner structure.

TYPE OF BURN	JP-5	EXPLODE MODE	None
BURN DURATION	4 minutes	CONFIGURATION	
BURN LOCATION	See Text		
BURN DATE	5-3-78	EXPLODE LOCATION	
TIME OF BURN	1045	EXPLODE DATE	
		TIME OF EXPLODE	

PASSIVE INSTRUMENTATION		ACTIVE INSTRUMENTATION	
SP STANDS	90	LED	20
SP STRIPS	262	MICROWAVE	4
SP ROLLS		BALL	8
TUNA CANS		LADAR	1
BV VUGRAPHS	10	TC IN SAMPLE	3
BV FRAMES	30	TC IN FLAME	2
BV LADDER	342	VELOCIMETER	1
MILLIPORES			
PAD COLLECTION	1	METEOROLOGY	
SWEEP BRIGADES	4	THERMOCOUPLES	5
PHOTOGRAPHY		VANES	3
INFRARED IMAGING	2	ANEMOMETERS	3
MOVIES	2	SMOKE GENERATORS	
		CAPTIVE BALLOONS	3
		FREE BALLOONS	10-20

Table A.12. Test Conditions for Test No. 12

TRW TEST NO. 12 NWC TEST NO. 11B CTS TEST NO. _____

TEST SITE NWC

TEST SAMPLE Spoilers (3 ea) debris from Test 11A (T300/5209 composite skins (originally identified incorrectly as AS/3501), aluminum fittings and honeycomb inner structure.

TYPE OF BURN	JP-5	EXPLODE MODE	Explode in Plume
BURN DURATION	7 minutes	CONFIGURATION	1 ea 2 oz C-4
BURN LOCATION	See Text		
BURN DATE	5-4-78	EXPLODE LOCATION	Ground Zero
TIME OF BURN	1234	EXPLODE DATE	5-4-78
		TIME OF EXPLODE	1236.5

PASSIVE INSTRUMENTATION		ACTIVE INSTRUMENTATION	
SP STANDS	90	LED	20
SP STRIPS	262	MICROWAVE	4
SP ROLLS		BALL	8
TUNA CANS		LADAR	1
BV VUGRAPHS		TC IN SAMPLE	
BV FRAMES	30	TC IN FLAME	
BV LADDER	342	VELOCIMETER	1
MILLIPORES			
PAD COLLECTION	1	METEOROLOGY	
SWEEP BRIGADES		THERMOCOUPLES	5
PHOTOGRAPHY		VANES	3
INFRARED IMAGING	2	ANEMOMETERS	3
MOVIES	2	SMOKE GENERATORS	
		CAPTIVE BALLOONS	3
		FREE BALLOONS	10-20

Table A.13. Test Conditions for Test No. 13

TRW TEST NO. 13 NWC TEST NO. 12A CTS TEST NO. _____

TEST SITE NWC

TEST SAMPLE F-16 Cockpit, partially fabricated of carbon fiber composite material

TYPE OF BURN	JP-5	EXPLODE MODE	None
BURN DURATION	6 minutes	CONFIGURATION	
BURN LOCATION	See Text		
BURN DATE	5-5-78	EXPLODE LOCATION	
TIME OF BURN	1145	EXPLODE DATE	
		TIME OF EXPLODE	

PASSIVE INSTRUMENTATION		ACTIVE INSTRUMENTATION	
SP STANDS	90	LED	20
SP STRIPS	262	MICROWAVE	4
SP ROLLS		BALL	8
TUNA CANS		LADAR	1
BV VUGRAPHS		TC IN SAMPLE	3
BV FRAMES	30	TC IN FLAME	2
BV LADDER	342	VELOCIMETER	1
MILLIPORES			
PAD COLLECTION	1	METEOROLOGY	
SWEEP BRIGADES	2	THERMOCOUPLES	5
PHOTOGRAPHY		VANES	3
INFRARED IMAGING	2	ANEMOMETERS	3
MOVIES	2	SMOKE GENERATORS	
		CAPTIVE BALLOONS	3
		FREE BALLOONS	10-20

Table A.14. Test Conditions for Test No. 14

TRW TEST NO. 14 NWC TEST NO. 12B CTS TEST NO. _____

TEST SITE NWC

TEST SAMPLE Flat Plate, Thornel 300/Narmco 5208
1 ft x 1 ft x 1/4 in

TYPE OF BURN	Hot Propane	EXPLODE MODE	Delayed
BURN DURATION	20 minutes	CONFIGURATION	1 ea 2 oz C-4
BURN LOCATION			
BURN DATE	5-8-78	EXPLODE LOCATION	Ground Zero
TIME OF BURN	1615	EXPLODE DATE	5-9-78
		TIME OF EXPLODE	0835

PASSIVE INSTRUMENTATION		ACTIVE INSTRUMENTATION	
SP STANDS	90	LED	
SP STRIPS	142	MICROWAVE	
SP ROLLS		BALL	
TUNA CANS		LADAR	
BV VUGRAPHS		TC IN SAMPLE	3
BV FRAMES		TC IN FLAME	1
BV LADDER	342	VELOCIMETER	
MILLIPORES			
PAD COLLECTION	1	METEOROLOGY	
SWEEP BRIGADES		THERMOCOUPLES	5
PHOTOGRAPHY		VANES	3
INFRARED IMAGING		ANEMOMETERS	3
MOVIES		SMOKE GENERATORS	
		CAPTIVE BALLOONS	3
		FREE BALLOONS	

Table A.15. Test Conditions for Test No. 15

TRW TEST NO. 15 NWC TEST NO. 13A CTS TEST NO. _____

TEST SITE NWC

TEST SAMPLE Flat Plate, Thornel 300/Narmco 5208
1 ft x 1 ft x 1/4 in

TYPE OF BURN	Hot Propane	EXPLODE MODE	Delayed
BURN DURATION	20 minutes	CONFIGURATION	1 ea 2 oz C-4
BURN LOCATION			
BURN DATE	5-9-78	EXPLODE LOCATION	Ground Zero
TIME OF BURN	0821	EXPLODE DATE	5-9-78
		TIME OF EXPLODE	1259

PASSIVE INSTRUMENTATION		ACTIVE INSTRUMENTATION	
SP STANDS	90	LED	
SP STRIPS	142	MICROWAVE	
SP ROLLS		BALL	
TUNA CANS		LADAR	
BV VUGRAPHS		TC IN SAMPLE	3
BV FRAMES		TC IN FLAME	1
BV LADDER	342	VELOCIMETER	
MILLIPORES			
PAD COLLECTION	1	METEOROLOGY	
SWEEP BRIGADES		THERMOCOUPLES	5
PHOTOGRAPHY		VANES	3
INFRARED IMAGING		ANEMOMETERS	3
MOVIES		SMOKE GENERATORS	
		CAPTIVE BALLOONS	3
		FREE BALLOONS	

REFERENCES

1. Chovit, A. R.; Lieberman, P; and Sussholz, B: Review of Carbon Fiber Composite Hazards Test Program. Report RADC/TRW-78.2, 78.4730.RADC-2. 1 September 1978. Distribution limited to U.S. Government.

2. Archibald, G. W.: Thermal Properties of Graphite Fiber. Air Force Materials Laboratory, AFML-TR-77-228.

3. Radcliffe, S. W.; and Appleton, J. P.: Soot Oxidation Rates in Gas Turbine Engines. Combustion Science and Technology, 1979, pp 171-175.

4. DeMarrais, G. A.: Atmospheric Stability Class Determinations on a 481-Meter Tower in Oklahoma. Atmospheric Environment, 1978, pp 1957-1964.

5. Church, H. W.: Cloud Pulse From The Detonation. Sandia Lab., 1969, SC-RR-68-903.